Conference Proceedings

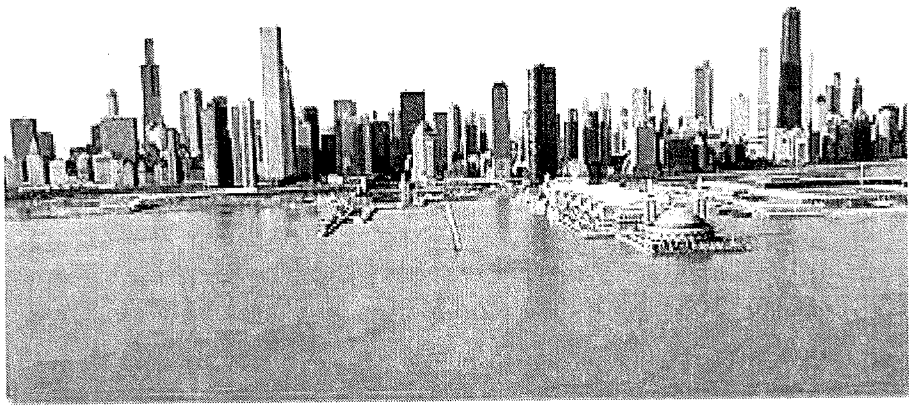

Twenty-Fourth Annual Meeting of the American Society of Biomechanics

University of Illinois at Chicago

July 19-22, 2000

American Society of Biomechanics founded 1977

UIC University of Illinois at Chicago

RUSH

Department of Orthopedics

The Whitaker Foundation

Brown

In Deo Speramus

Department of Orthopaedics

The Local Organizing Committee of the 24th Annual Meeting of the American Society of Biomechanics gratefully acknowledges the generous support of:

The Whitaker Foundation

The WHITAKER Foundation

University of Illinois at Chicago

UIC University of Illinois at Chicago

Department of Orthopedic Surgery
Rush-Presbyterian-St.Luke's Medical Center

RUSH
Department of Orthopedics

Department of Orthopaedics
Brown University

Department of Orthopaedics

Committees

ASB Executive Board Members

M. Melissa Gross - President
R. Bruce Martin
James Ashton-Miller
Robert Shapiro
J.J. Trey Crisco
Walter Herzog
Scott L. Delp
Julianne Abendroth-Smith
Gerald Smith
Joseph E. Hale
Kathleen Costa

Local Organizing Committee

Raghu N. Natarajan - Chair
Steve Lavender
Jamie Ryan

Program Committee

J.J. Trey Crisco - Chair
Steve Arnoczky
John Chow
Walter Herzog
Richard Hughes
Irene McClay
Tom Oxland

Awards Committee

R. Bruce Martin- Chair
Doris Miller
Don Chaffin
Bob Gregor
Neil Sharkey
Tom Buchanan
Ron Zernicke
Maury Nussbaum
Ted Gross
Mark Grabiner

Exhibitors

Bertec Corp.
HMA Technlogy, Inc.
Innovative Sports Training
Measurand, Inc.
Motion Analysis
Noraxon Inc.
Northern Digital, Inc.
Peak Performance Technologies Inc.
Redlake Imaging Corporation
Run Technologies, Inc.
SIMI Reality Motion System GmbH.
Tekscan, Inc.

ASB Information

General Information

The American Society of Biomechanics (ASB) was founded in October 1977. The purpose of the Society is to provide a forum for the exchange of information and ideas among researchers in biomechanics. The term biomechanics is used here to mean the study of the structure and function of biological systems using the methods of mechanics.

ASB Membership

Applications for membership can be made by completing the Membership Application Form located at the Registration Desk and mailing it to the Chairperson of the Membership Committee. PLEASE DO NOT MAIL DUES with your application form. Upon receiving a letter of acceptance from the Chairperson, you will be instructed where to send membership dues. Membership includes a subscription to the Journal of Biomechanics (although student members can opt not to receive the journal). In addition, special offers for the journals from Elsevier Science Ltd. and Human Kinetics are available to members. Applications for membership are considered quarterly by the Membership Committee. Further information concerning application for membership can be obtained by writing or emailing the Chairperson of the Membership Committee:

Scott L. Delp, Ph.D.
Mechanical Engineering Department
Stanford University
Stanford, CA 94305-3030
email: delp@leland.stanford.edu

General Information

Chicago Circle Center (CCC)

Located on the corner of HalstedSt. (main entrance) and Harrison St., with in the campus of University of Illinois (UIC), the Chicago Circle Center (CCC) offers a wide variety of retail and dining facuilities. There are several brand name food areas in the dining facilities. CCC has a number of lounges in which to relax, snack, read, listen to music, watch TV, or just talk or take a nap. The CCC also houses conference facilities with large meeting halls, and the latest in multimedia presentation capabilities. Conference sessions will be held on the 3rd floor of this building. The location of podium, poster and exhibition rooms are on pages 28 and 29 of this book.

A block north of UIC, on Halsted Street is Greek Island – famous, of course, for Greek food. On the south of the campus, on Taylor Street is the Italian Village. Both these places are within walking distance from UIC campus residence and CCC. CTA trains, CTA buses and Taxis are readily available at UIC to go to downtown Chicago.

Registration Desk

The conference registration desk is located in the lobby of the 3rd floor in CCC. The hours it will be open are:

Wednesday, July 19	2:00 P.M. to 8:00 P.M.
Thursday, July 20	7:00 A.M. to 5:00 P.M.
Friday, July 21	7:00 A.M. to 3:00 P.M.
Saturday, July 22	7:00 A.M. to 9:00 A.M.

Please check in at the desk prior to attending any events to pick up your conference materials.

Conference Name Badges

Every attendee of the ASB conference is required to wear their name badge for entrance to all ASB activities including social events and functions. All Local Organizing Committee Members and Volunteers will be wearing name badges. Please do not hesitate to ask any Local Organizing Committee Member or Volunteer for assistance.

Awards

Giovanni Borelli Award

The Borelli Award, the most prestigious honor given by the American Society of Biomechanics, recognizes outstanding career accomplishment and is awarded annually to an investigator who has conducted exemplary research in any area of biomechanics. This award is open to all scientists, including non-ASB members, but excluding ASB officers and members of the Awards Committee. Candidates may be self-nominated or nominated by others including non-ASB members. Selection is based on originality, quality, and depth of the research and its relevance to the field of biomechanics. A letter of nomination, a comprehensive curriculum vitae and five publications on a single topic or theme must be submitted. The awardee is expected to attend the 2000 Annual Meeting of the American Society of Biomechanics and to deliver the Borelli Lecture. The award consists of a $1,500 check and an engraved plaque. Congratulations to **Clint Rubin, Ph.D.,** this year's winner.

Young Scientist Awards

These awards recognize early achievement for promising young scientists, and are awarded annually to one pre-doctoral student and one post-doctoral scientist. Nominees for these awards must be current or pending members of ASB and may be self-nominated or nominated by an ASB member. For both the pre-doctoral and post-doctoral awards, submitted materials must include a letter of support or nomination letter, a curriculum vitae, copies of published manuscripts and/or manuscripts submitted for publication, and an abstract of original research for presentation at the 2000 Annual Meeting having the nominee as first or sole author. These awards include a $200 check, a certificate, and a waiver of conference fees for the 2000 Annual Meeting.

Post-Doctoral Young Scientist Award Winner: John Wu, University of Calgary

Pre-Doctoral Young Scientist Award Winner: Stefan Duma, University of Virginia

Journal of Biomechanics Award

This award, sponsored by Elsevier Science Ltd., publishers of the Journal of Biomechanics, recognizes substantive and conceptually novel mechanics approaches explaining the function of biological systems. Nominees must be members of ASB and submit a cover letter and a copy of the abstract of original research submitted for presentation at the 2000 Annual Meeting having the nominee as first or sole author, to both the Chairperson of the Awards Committee and Program Chairperson.

Journal of Biomechanics Award Winner: Shirazi-Adl, Ecole Polytechnique, Montreal

Clinical Biomechanics Award

This award recognizes outstanding new biomechanics research targeting a contemporary clinical problem and is co-sponsored by Elsevier Science Ltd., publishers of Clinical Biomechanics. Nominees must be members of ASB and must submit a cover letter specifying the candidate's interest in being considered for the Clinical Biomechanics Award and a copy of the abstract of original research submitted for presentation at the 2000 Annual Meeting having the nominee as first or sole author, to the Chairperson of the Awards Committee and to the Program Chairperson. The award includes a $250 cash prize and an engraved plaque.

Clinical Biomechanics Award Winner: Louis F. Draganich, University of Chicago

Student Travel Awards

These awards, generally around $250, are available only to ASB student members and are intended to offset the cost of travel to the annual meeting. Student members can apply for these awards after receiving notification of their abstracts being accepted for presentation. A copy of the accepted abstract, acceptance letter, and a letter from the student's advisor indicating a need for assistance should be submitted to the Chairperson of the Awards Committee.

Student Travel Award Winners: Kathleen Costa, University of Southern California
Alicia Koontz, University of Pittsburgh
Akinori Nagano, Arizona State University
James Funk, University of Virginia
Stefan Duma, University of Virginia
Witaya Mathiyakom, University of Southern California

Travel Award

A travel award is offered to foster collaborative research and interaction among scientists by helping to offset the cost of travel to a host institution.

Travel Award Winners: Don Andersson, University of Minnisota

Presentations

Speaker Ready Rooms

The speaker ready room is 605 of the Chicago Circle Center. To reach this room take the elevators located on north low-rise part on second/third floor of CCC (refer to the map). The room will have carousels and projectors for loading and checking slide presentations, a computer for transferring and checking computer presentations. Load the slides on the carousels and give it to the student volunteer. He will take it to the appropriate podium presentation room. No body, other than the designated student volunteer, will be allowed to take the carousels outside the speaker ready room. The speaker ready room will be staffed (open) as follows:

Wednesday, July 19: 3:00 PM to 9:00 PM
Thursday, July 20: 7:00 AM - 6:00 PM
Friday, July 21: 7:00 AM - 5:00 PM
Saturday, July 22: 7:00 AM - 3:00 PM

Podium Presentation Audio-Visual Requirements:

Oral presenters at the 2000 American Society of Biomechanics meeting must be prepared to present their research using overhead transparencies, 35 mm slides (dual projection will be available), or direct computer projection. Details for each media are provided below. All oral presenters will be asked to *confirm their media type at the time of registration, so* that the projectionists will be prepared to provide smooth transitions between presentations.

For overhead transparencies, presenters may simply bring their transparencies to the session in which they will present, and check-in with the projectionist and session chairs.

For 35 mm slide presentations, presenters should go to the speaker ready room and load their slides in the provided carousels *at least an hour before* the scheduled *start of the session* in which they will present. Authors are responsible to label the carousel(s) with the correct time and session. For dual projection, carousels should also be labeled left and right (from the audience perspective). After loading please check the slide order and orientation, and return the loaded carousel to the ready room desk. The slides will be available for pickup in the ready room, shortly after each session.

For computer projection (PowerPoint), only presentations using Microsoft PowerPoint 97 (PC) or higher will be accepted. All PowerPoint presentations will be preloaded on a dedicated computer in the presentation room. The presenter will have use of a remote mouse to control the presentation. Because of the potential for difficulties in file transfer, file compatibility, font availability, etc., presenters using computer projection *must transfer their presentation in the speaker ready room by 4:00 pm the day before their presentation.* Acceptable transfer media include 3.5 inch floppy, Zip100, and CD. If special fonts are used, they should be saved with the presentation to avoid font substitution.

All oral presenters are asked to check-in with the session chairs *at least 10 minutes before* **the scheduled start of the session in which they will present! Please confirm that the projectionist has your slides or computer presentation.**

Chairpersons for Podium Presentations:

Please arrive in the presentation room at least 15 minutes before the session is scheduled to begin, in order to introduce yourself to the presenters and the projectionist. Please introduce the presenter, their affiliation, and the title of the presentation. Session chairs are responsible for keeping the sessions on schedule. Please carefully keep track of time, ensure that each presentation starts and ends on time, and ensure that questions and discussion do not exceed the allotted time. This will allow participants to hear preceding or following presentations in the other presentation room.

Poster Presentations : ALL POSTERS are to be put up no later than 7:30 am, Thursday, July 20. ALL POSTERS will remain up for the duration of the conference. Posters can be attached to the poster boards with push-pins (not provided). The maximum outer poster dimensions are 44" x 44". Posters should remain till 1:00 P.M. on Saturday, July 22. All posters should be removed by 3:00 P.M. on Saturday, July 22. Poster boards will be removed from the rooms after 3:00 P.M. on Saturday, July 22. Poster session room assignments are listed below (Refer to the Map):

<u>Thematic Poster Sessions</u>

Gait	Posters 1 – 6	Room: 329
Aging	Posters 25 – 30	Room: 322
Posture	Posters 19 – 24	Room: 329
Assistive Devices	Posters 37 – 42	Room: 322

<u>Main Poster Sessions</u>

Odd numbered posters	Posters	7 – 79	Rooms: 322 and 329
Even numbered posters	Posters	8 – 78	Rooms: 322 and 329

TABLE OF CONTENTS

9:15 a.m. - 10:30 a.m. Podium Session 2 Room: 323
TISSUE MECHANICS Moderator: *Tom Brown Ph.D.*, University of Iowa

10:30 a.m. - 12:15 p.m. Odd Numbered Posters Rooms: 321/322/329

5:00 p.m. - 6:00 p.m. Even Numbered Posters / Wine & Cheese
Rooms: 321/322/329

FRIDAY, JULY 21, 2000

8:00 a.m. – 9:00 a.m. Keynote Lecture 2 Room: 323/324

9:15 a.m. – 10:45 a.m. Symposium 1 Room: 324

Cell stress: how do they manage it?
Moderator: *Annaliese Heiner Ph.D.*, University of Iowa

11:15 a.m. – 11:50 a.m. Thematic Poster Session 4 Room: 322
ASSISTIVE DEVICES Moderator: *Mark Redfern Ph.D.*, University of Pittsburgh

12:00 Noon – 1:45 p.m. Lunch

1:45 p.m. - 3:00 p.m. Borelli Lecture Rooms: 323/324

5:00 p.m. – 6:00 p.m. ASB Business Meeting Rooms: 323/324

6:00 p.m. Bus to Shed Aquarium

7:00 p.m. – 10:00 p.m. Banquet

SATURDAY, JULY 22, 2000

8:00 a.m. – 9:30 a.m. Symposium 3 Room: 324
Computing the Past : The modeling of Dinosaurs
Moderator: *Joseph J. Crisco Ph.D.*, Brown University

8:00 a.m. – 9:30 a.m. Symposium 4 Room: 323
The heart of the matter is in the neck: Biomechanics of the proximal femur
Moderator: *Mark D. Grabiner Ph.D.*, The Cleveland Clinic Foundation

1:30 p.m. - 2:45 p.m. Podium Session 12 Room: 323
MODELING Moderator: *Tom Buchanan Ph.D.*, University of Delaware

3:15 p.m. – 4:30 p.m. Awards Session Room: 323
Moderator: *Bruce Martin Ph.D.*, University of California, Davis

Tutorials

Tutorial # 1 **Room 605 CCC**
Wednesday, July 19, 2000 **1:00 p.m. – 4:00 p.m.**

Singing along with Louie, Louie, chossing cutoff frequencies for smoothing data, and other things of which we aren't quite sure: A tutorial on digital filtering.

Peter Vint, Ph.D.,
Research Integrations, Inc. Tempe, Arizona

The filtering tutorial will focus primarily on methods for establishing cutoff frequencies for the different types of digital filters being used. For those of you who attended Scott Tashman's tutorial on filtering at the 1996 annual meeting in Georgia, this year's tutorial will build on the information presented there. After a brief review of the general characteristics of filters and general filter types, example applications in biomechanics will be discussed. Then, the methods for determining automatic cutoff frequencies for digital filters will be emphasized, including Wells & Winter's residual analysis, Jackson/Hinrichs knee method, Challis' autocorrelation-based procedure, Yu's empirical method, Hatze's optimallu regularized Fourier series, and Woltring's GCVQS.

Tutorial # 2 **Room 605 CCC**
Wednesday, July 19, 2000 **7:00 p.m. – 10:00 p.m.**

The 'whys' and 'hows' of single subject analysis

Barry T Bates, Ph.D. University of Oregon
Janet S. Dufek, Ph.D. Human Performance & Wellness, Inc. Oregon
John A. Mercer, Ph.D. University of Nevada-Las Vegas, Las Vegas
Nicholas Stergiou, Ph.D. University of Nebraska-Omaha, Omaha

The single subject tutorial is designed to give researchers an understanding of the rationale behind this research approach and its importance to human movement research. The tutorial will emphasize the person as a legitimate unit of analysis for theory-driven research. Issues to be discussed include variability, aggregation and generalization. The most common criticisms of normality, independence and lack of generalizability will also be addressed. Comparisons between group designs and single subject designs and person-by-treatment interactions will be discussed using numerous examples for both parametric and non-parametric tests along with limitations.

Keynote Lectures

Keynote Lecture 1
Thursday, July 20, 2000

Room :323/324
8:00 a.m. – 9:00 a.m.

2001 is Almost Here:

Challenges to Human Exploration of Mars, and the Reality of Artificial Gravity

Laurence R. Young, Sc.D.

Director, National Space Biomedical Research Institute
Baylor College of Medicine

Apollo Program Professor of Astronautics
Massachusetts Institute of Technology
77 Massachusetts Avenue, Bldg. 37-219
Cambridge, MA 02139-4307
(P) 617-253-7759/7805; (F) 617-258-8111
Email: lry@mit.edu

The last big step in space left a footprint on the moon. Many hope that the next step will be on the red soil of Mars, but before that happens a number of serious obstacles to human interplanetary flight must be overcome. This lecture examines the threats to human health created by long space flights, and their relationship to health problems here on earth. It examines the use of spinning devices, from small centrifuges to rotating the entire spacecraft, as means of overcoming those problems by providing artificial gravity.

Keynote Lecture 2
Friday, July 21, 2000

Room: 323/324
8:00 a.m. – 9:00 a.m.

Motile Behavior Of Bacteria

Howard C. Berg, Ph.D.
Professor of Molecular & Cellular Biology and Physics, Harvard University

The bacterium *Escherichia coli* (*E. coli*, for short) is the best understood living thing. It resides in aqueous environments, including your gut. It swims through water some 30 diameters per second. This is not fast on an absolute scale, because the cell is only 1 micrometer across by about 2 micrometers long. A cell swims by rotating several thin helical filaments, called flagella. Each is driven at its base by a rotary motor, which can spin clockwise or counter-clockwise. The probability of turning one way or the other is determined by a sensory system sensitive to the concentrations of a variety of simple chemicals in the cell's environment. By changing the directions of rotation of its engines in response to what it tastes, the cell is able to migrate toward regions that it finds more favorable. My talk will focus on the biomechanics of rotary motors and flagellar filaments.

Symposiums

Symposium 1 **Room : 324**
Friday, July 21, 2000 **9:15 a.m. – 10:45 a.m.**

CELL STRESS: HOW DO THEY MANAGE IT?

Moderator: ***Annaliese Heiner*** *Ph.D.*, University of Iowa

CYTOMECHANICS IN ARTICULAR CARTILAGE ENGINEERING

Kyriacos Athanasiou
Department of Bioengineering, Rice University, Houston, Texas
e-mail: athanasiou@rice.edu

Regulation of the biomechanical environment is a powerful modulator in tissue engineering of articular cartilage. The application of extrinsic mechanical forces can have a profound effect on chondrocyte function and cartilage regeneration. Although the precise signaling pathways that are involved in mediation of mechanostimuli are not completely understood, evidence suggests that certain types of forces are desirable for cartilage synthesis and modeling.

Under static conditions, articular chondrocytes synthesize a material that is fibrous in nature, has poor tissue organization, and few lacunae.[1] Thus, since static culture conditions appear to be inadequate, the application of various mechanical stimuli has been studied extensively. The genesis of cartilaginous material in bioreactors has proven to be successful and is one of the best means to obtain reproducible tissue.[1,2] These bioreactors were used to test for biosynthesis and organization of neocartilage when chondrocytes were seeded on polyglycolic acid scaffolds. The bioreactors promoted deposition of cartilage extracellular matrix components, including glycosaminoglycans and collagen. For comparison, cells seeded on polyglycolic acid scaffolds and maintained statically exhibited less matrix integrity, suggesting that the mechanical stimulus conveyed by fluid flow greatly influenced synthesis of a cartilage matrix. In general, the composition, morphology, and mechanical properties of cartilage synthesized in a bioreactor appear better than cartilage grown under static conditions.[3] The decrease in proteoglycan synthesis from cartilage cells in static cultures is consistent with a number of previous studies demonstrating that static culture conditions reduce proteoglycan synthesis.[4] Moreover, application of a dynamic compressive loading was shown to increase chondrocyte proliferation.[5] Over short periods of time, cyclic loading inhibits cell division[6] and increases the synthesis of sulfated glycosaminoglycans and other cartilaginous components.[7] The effects of load were also shown to affect cartilage synthesis in vivo significantly, such that cyclic load was shown to cause mesenchymal tissue to differentiate into cartilage.[8] Microgravity has also been used to study the effects of mechanical forces on chondrocytes.[9] Scaffolds composed of polyglycolic acid were used as vehicles to support cell attachment, proliferation, and synthesis of an extracellular matrix on the Mir space station. It was shown that under the space station conditions, there was a reduction in glycosaminoglycan deposition within the matrix and an inferior aggregate modulus when compared to values for constructs on earth.

In general, it is known that static conditions have negative effects and that agitation or stirring is positive. The most potent biomechanical stimulator appears to be shear stress. Fluid flow-induced shear appears to have a direct effect on cell metabolism and extracellular matrix synthesis. Hydrostatic pressure, on the other hand, affects cytoskeletal organization, but is not potent in terms of matrix synthesis. Unlike intermittent or cyclic stress, static compression inhibits synthesis and cell division. Recognizing the value of the biomechanical environment in engineering articular cartilage ex vivo, bioreactors are routinely used to modulate fluid shear.

As it has become obvious that forces influence cell function and the eventual outcome of tissue engineering processes in cartilage, the next major issue to address is the actual stress-strain field that individual cells experience and translate into a biochemical action. This information will allow us to further optimize the use of mechanical forces in bioreactors. Also, it is essential to quantify the stress-strain fields experienced by individual cells attached on scaffolds to understand how mechanical stimuli affect cellular mechanotransduction. To this end, we have designed and used biomechanical instruments that allow us to obtain the intrinsic material properties of individual cells,[10] as well as to quantify the mechanical adhesiveness of cells as a function of surface modifiers (Fig. 1).[11]

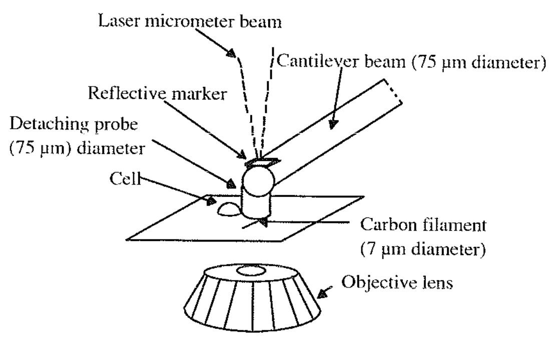

Fig. 1: The cytodetacher is used to evaluate the attachment capabilities of cells on various natural or synthetic substrata.

REFERENCES

1) Dunkelman et al.: Biotech Bioeng. 46:299, 1995.
2) Freed et al.: Exp Cell Res. 240:58, 1998.
3) Vunjak-Novakovic et al.: J Orthop Res. 17:130, 1999.
4) Jones et al.: Clin Orthop. 283, 1982.
5) Lee & Bader: J Bone Jt Surg. 15:181, 1997.
6) van Kampen et al.: Arth & Rheum. 28:419-424, 1985.
7) Veldhuijzen et al.: Conn Tis Res. 16:187, 1987.
8) Tagil & Aspenberg: J Orthop Res. 17:200, 1999.
9) Freed & Vunjak-Nokakovic: In Vitro Cell. Dev. Biol.-Animal. 33:381, 1997.
10) Shin & Athanasiou: J Orthop Res. 17:880, 1999.
11) Athanasiou et al.: Biomaterials. 20:2405, 1999.

TENDON DIFFERENTIATION IS RELATED TO LOAD.

Kathryn Vogel, **Ph.D.,**
Professor, Dept. of Biology
The University of New Mexico
Albuquerque, NM
kgvogel@unm.edu

Adult mammalian tendon is not a uniform tissue. Regions of tendon that serve under purely tensile conditions appear as dense linear bundles of collagen. However, a fibrocartilaginous tissue is found at the contact point where this tendon wraps under the bones of a joint (1). Characterized by rounded cells, higher water content, criss-crossing collagen fibrils, mRNA for type II collagen, and abundant amounts of the proteoglycan aggrecan, this cartilage-like tissue provides compressive strength at points where the tendon is subjected to transverse load.

Similarly, tissue further from bony contact is marked by expanded endotenon containing aggrecan. This may provide slip planes allowing collagen fiber bundles to move relative to one another when the tendon is bent. Neither of these features is found in the tensile regions of tendon. Both in vitro and in vivo loading experiments suggest that development of these different regions in tendon is regulated by the mechanical loading of the post-natal tissue. Type I collagen mRNA is highly expressed in fetal tendon, as would be expected for a rapidly-growing tissue. Interestingly, mRNA for collagen type IIA is also expressed throughout fetal tendon (2). This expression has been found in other fetal tissues that become cartilage and is considered a marker of pre-chondrocytes. In tendon, collagen type IIA expression was found not only in the locations that will eventually become fibrocartilage but also throughout tendon that will experience only tensile loading when the animal walks. This observation indicates developmental similarities for tendon and cartilage and further suggests that tendon develops its region-specific material properties as a cellular response to load.

References:

1. Vogel, K.G., S.P. Evanko and J.R. Robbins (1999) What proteoglycan content says about the mechanical history of tendon. In: "Biology of the Synovial Joint" Archer, Caterson, Benjamin and Ralphs, Eds. Harwood Academic publishers, The Netherlands, pp301-313.
2. Perez-Castro, A.V. and K.G. Vogel (1999) In situ expression of collagen and proteoglycan genes during developm,ent of fibrocartilage in bovine deep flexor tendon. J. Orthop. Res. 17:139-148.

***Ning Wang**, Ph.D.*,
Harvard School of Public Health

Symposium 2
Friday, July 21, 2000

Room : 323
9:15 a.m. – 10:45 a.m.

PREVENTING INJURIES THAT RESULT FROM LIFTING: TAKING SCIENCE BEHIND SPINE BIOMECHANICS INTO INDUSTRY

Moderators: ***Steve Lavender*** Ph.D., Rush-Presbyterian-St. Luke's Medical Center
Gunnar B.J. Andersson, M.D., Ph.D., Rush-Presbyterian-St. Luke's Medical Center

Participants:
Gary Allread, Ph.D. – Institute for Ergonomics, The Ohio State University
Kevin Granata, Ph.D. –Orthopedic Surgery, University of Virginia
Robert Andres, Ph.D. – Ergonomic Engineering, Inc.

This session will review what has been learned from epidemiological studies of low back pain as related to manual lifting, current thinking in terms of spine biomechanical models, the challenges of assessing low back injury risk in occupational settings, different type of workplace interventions designed to address the biomechanical issues, and the effectiveness of training people to protect themselves through improved lifting techniques.

Symposium 3 **Room : 324**

Saturday, July 22, 2000 **8:00 a.m. – 9:30 a.m.**

COMPUTING THE PAST : THE MODELING OF DINOSAURS

Moderator: ***Joseph J. Crisco*** Ph.D., Brown University

ANALYZING THE BIOMECHANICS OF DINOSAURS: THE ROLE OF TECHNOLOGY IN OVERCOMING THE PROBLEMS ENCOUNTERED IN STUDYING VERY LARGE EXTINCT ORGANISMS.

CHAPMAN, Ralph E.
Applied Morphometrics Laboratory
ADP/NHB, NMNH, Smithsonian Institution
Washington, DC 20560-0136

ANDERSEN, Arthur
Virtual Surfaces, Inc.
832 East Rand Rd., Suite 16
Mt. Prospect, IL 60056

SNYDER, Rebecca A.
Applied Morphometrics Laboratory
ADP/NHB, NMNH, Smithsonian Institution
Washington, DC 20560-0136

Dinosaurs and other large extinct organisms present many problems to those researchers attempting to work out the biomechanics of their skeletons. These problems make the progression from fossilized bones to useful and believable models of these animals as functioning organisms very difficult. The problems start with the fossilization process (taphonomic factors) which not only can distort the shape of the bones, but also can remove many of the elements, or significant portions of them. It also, except in very exceptional cases, removes any direct indication of the soft-parts (e.g. muscles, cartilage, most ligaments, and skin). Since dinosaurs also tend to be rare, better-preserved elements of the same bone often are not available from other specimens. Further, the bones collected by paleontologists generally are very fragile, heavy, and, for many species, much too large to be used directly in detailed studies of articulations. Thankfully, modern technology has provided the means to overcome many of these difficulties and we will discuss examples, especially from the Smithsonian's *Triceratops* project, of how paleontologists have applied three-dimensional scanning and modeling to help determine how dinosaurs worked biomechanically. The key is to scan the bones using CT- and/or surface scanning technology and then develop three-dimensional virtual models of the bones, which then can be re-assembled in virtual space in their appropriate positions. The final product is a whole, virtual model of the animal's skeleton. The models of individual bones that have been taphonomically distorted can be re-inflated or un-distorted virtually. Missing parts can be added by using analogous parts of other elements and pasting them into the missing areas.

Many missing bones can be generated either by mirror-imaging equivalent bones using the bilateral symmetry of the animal, or duplicating serial elements such as vertebrae. This allows prototyped versions of the bone to be generated at a more usable scale (done at 1/6 scale for *Triceratops*), the joint articulations studied using these smaller prototypes, and the movement apparent at these joints built into animations of the virtual skeleton. These virtual skeletons can then be used for standard biomechanical analyses and, of course, eventually fleshed out with muscles and skin using muscle scars and modern analogs as guides.

ROBOSAURS: MATHEMATICAL AND COMPUTATIONAL MODELING OF LOCOMOTION IN EXTINCT ANIMALS.

Donald M. Henderson Ph.D., Johns Hopkins University

Using only knowledge of living animals, our attempts to understand bizarre extinct organisms are often poorly constrained. Some extreme examples include flying pterosaurs with wing spans of up to 12m, or strictly bipedal dinosaurs that weighed up to 7,000kg. To investigate the mechanics and kinematics of terrestrial locomotion of pterosaurs and bipedal dinosaurs a series of mathematical and computational models were developed.

The models incorporate the geometry of fossil bones to produce both simple 'stick' representations and 3D bone shapes. Sets of 2^{nd}-order, ordinary differential equations were derived and solved by numerical approximations to control the motions of the 'stick' limbs through 3D space. The shapes and dimensions of the 3D bone forms, and their inferred articulations, were used to constrain the ranges of motions of the joints. Masses and centers of mass (CM) of the bodies of the modeled animals were also computed. Mass is used to estimate tendon and bone stresses, while the CM is used to locate balance points, to estimate load distribution between limbs, and determine the phase relationships between limbs and limb pairs. Gait aspects such as stride lengths and pace angulations were also constrained by information from preserved trackways that record actual walk sequences of pterosaurs and dinosaurs.

Given a model with a proposed limb configuration and hypothesized gait, a partial list of the information that can be extracted from a walking model includes: estimates of the bending and compressive stress that acted on limb bones throughout a proposed gait sequence; changes in lever arms and amount of stretching experienced by muscles; visual inspection of the correlation between synthetic trackways and fossil ones, and visual inspection of the stability of the model.

RECONSTRUCTING THEROPOD DINOSAUR LIMB FUNCTION USING 3-D COMPUTER-ANIMATED TRACK SIMULATION

Stephen M. Gatesy, Department of Ecology and Evolutionary Biology, Brown University, Providence, RI 02912 USA.

The hind limbs of theropod dinosaurs are composed of bones forming 17 linked segments that undergo cyclical movements during locomotion. This morphological, spatial, and temporal complexity is well suited to the tools of 3-D animation, which permit a model's kinematics to be freely manipulated. A NURBS model foot skeleton of a primitive theropod (Coelophysis) was created and animated using Studio 8.5 software by Alias|Wavefront. Metatarsal and phalangeal models were linked to a 3-D kinematic skeleton, creating a "puppet" limb controlled by six inverse kinematic constraints.

A preliminary stride was keyframed by rotoscoping the Coelophysis limb onto video of a walking turkey. This avian pattern was then modified based on Late Triassic footprints from East Greenland. Many Greenlandic theropods sank to considerable depth, allowing the substrate to intercept and preserve movements that normally occurred above the surface. Footprints were simulated in Studio using particles, which were emitted as the foot passed through a volume of "sediment" of variable depth. Substrate properties were not modeled. The relationship between foot movement and track shape was explored by changing translation, rotation, and timing variables during the reconstructed stance phase. Simulations confirm that Triassic theropod feet underwent toe convergence as in the turkey, but differed from this bird in hallucal orientation and the timing of metatarsal rotation. 3-D animation is a powerful technique for analyzing complex movements, which are difficult to create, compare, and communicate using static 2-D images. Supported by NSF and Alias|Wavefront.

Symposium 4 **Room : 323**

Saturday, July 22, 2000 **8:00 a.m. – 9:30 a.m.**

THE HEART OF THE MATTER IS IN THE NECK: BIOMECHANICS OF THE PROXIMAL FEMUR.

Moderator: ***Mark D. Grabiner*** Ph.D., The Cleveland Clinic Foundation

LOADING AND BONE CHANGES: DO THEY CONTRIBUTE TO EARLY HIP DEGENERATION?

Debra E. Hurwitz, Ph.D.
Assistant Professor, Department of Orthopedic Surgery
Rush-Presbyterian St. Luke's Medical Center
Chicago IL

Despite its vast economic and social impact, osteoarthritis remains poorly understood, especially the early asymptomatic phase of the disease. Bone and mechanical factors are interrelated and both may play a role in the progression of hip osteoarthritis. The main topics of this presentation are:

- How is the proximal femoral bone mineral density related to the dynamic hip joint loads during gait.
- What is the potential role of proximal femoral bone and dynamic hip joint loads during gait in the development of early hip osteoarthritis.

Z. Maria Oden, PhD, University of Texas Health Sciences Center at Houston

CAN EXERCISE REDUCE HIP FRACTURE RISK?

Christine M. Snow, Ph.D., FACSM
Director, Bone Research Laboratory
Oregon State University
Corvallis, OR 97331

Osteoporosis-related fractures are related to significant morbidity, mortality and economic cost. There are over 340,000 hip fractures annually in this country that carry health care costs of more than $9 billion. Specific exercise reduces risk of osteoporosis-related fractures by increasing peak bone mass, slowing age-related bone loss and reducing fall risk. Changes in these variables reduce the factor of risk, a ratio that reflects the interaction between applied forces (eg. falls) and skeletal fragility (bone mineral density, BMD). If the factor of risk is $<< 1$, fracture is unlikely but if > 1, fracture is probable. **Increasing peak bone mass:** In a randomized controlled trial, we demonstrated that, in 89 prepubescent boys and girls, bone mass at the hip (femoral neck) and spine increased by 4.6% and 3.5%, respectively, from 7 months of jumping at high magnitude and loading rate. Gains in jumpers were maintained after 7 months of detraining, a result that indicates the protocol enhanced bone growth and thus provide a means of increasing bone during skeletal maturation. **Increasing bone mass and reducing fall risk in adults:** In mature premenopausal women, specific exercise increases hip bone mass and reduces fall risk. After 12 months of weighted vest exercise that included jumping, women (30-45 yrs) demonstrated an increase of 2.6% in trochanteric and 1.5% in femoral neck BMD that were significantly greater than controls of similar age, body weight and BMD. This group also gained muscle mass, strength, power and balance. Six months of detraining in the exercisers reversed the gains in bone and muscle strength, power and body composition. In a similar exercise trial, postmenopausal women (>60 yrs) involved in weighted vest exercise for 9 months increased muscle strength, mass power and balance but not hip bone mass. However, after 5 years of continued exercise, bone loss at the hip was prevented at all regions of the hip (femoral neck BMD = +1.5% vs. –4.43%). These data demonstrate that specific types of exercise increase and/or preserve bone mass across the lifespan and also reduce risk factors for falling. Altering both the numerator and denominator of the factor of risk should result in a significant reduction in osteoporotic-related fractures.

Borelli Lecture

SEARCHING FOR WOLFF'S LAW: DO SPECIFIC MECHANICAL SIGNALS INFLUENCE BONE ADAPTATION?

Clinton T. Rubin, Ph.D.
Musculo-Skeletal Research Laboratory
Program in Biomedical Engineering
State University of New York at Stony Brook 11794-2580

The principal responsibility of the skeleton is to support the loads and moments which arise during activity, resulting in mechanical strain in the bone tissue. The skeleton's ability to adapt to these functional signals was recognized well over a century ago and is now referred to as Wolff's Law. The premise of this "law" is that bone strives toward an optimized structure which caters to an individual's level of activity. Thus, each individual would tune the mass and morphology of their skeleton such that it could safely withstand the extremes of functional loading. While mechanical signals are, in general, recognized as strongly anabolic, identifying those specific components which drive the osteogenic response has proven difficult.

There is increasing evidence that extremely low magnitude (<100 microstrain) mechanical signals can be strongly osteogenic if applied at a high frequency (15 to 60 Hz). Such high frequency low magnitude strains comprise a dominant component of a bone's strain history, indicating that these mechanical events represent a significant determinant of bone morphology. With this in mind, we have been examining if small perturbations in high frequency loading will stimulate an increase in bone mass without sacrificing bone quality. Extremely low-level strains (80$\mu\varepsilon$), if induced at 20Hz, promote osseointegration. Small displacements (25μ) across a 3mm fracture gap accelerate fracture healing. And long term animal studies (one year), have shown that low level mechanical loading, inducing cortical strains on the order of 5 microstrain, can increase cancellous bone volume fraction, thicken trabeculae, and increase trabecular number. Considering these strain levels are far below (<1/1000th) those which may cause damage to the tissue, we believe these signals hold great potential as a mechanical prophylaxis for osteoporosis.

Testing this hypothesis in the human, sixty-two healthy women, 3-8 years past the menopause, enrolled in a double-blind, placebo controlled pilot study. 32 women underwent mechanical loading of the lower appendicular and axial skeleton for two ten-minute periods per day, through floor mounted devices that produced a 0.2g mechanical stimulus at 30Hz (TX). 32 women received placebo devices (PL) and underwent daily treatment for the same period of time. When DEXA measurements were normalized for body weight, linear regression shows a -3.3% (± 0.83) loss of BMD in the spine of the placebo group. Treatment reduces this loss to -0.8% (± 0.82), reflecting a net benefit of 2.5% (p=0.03). The trochanter of the femur shows a 2.9% (± 1.2) loss of BMD in the placebo group, while treatment stimulates a +0.4% (± 1.2) gain, reflecting a net benefit of 3.3% of treatment (p=0.03).

Evidence in both animals and humans shows that short exposure to extremely low-magnitude, high frequency loads are osteogenic. Such a biomechanical intervention is self-targeting, endogenous to bone tissue, and auto-regulated. In essence, these studies lay the groundwork for a unique, non-pharmacogenic intervention for osteoporosis, based purely on the premise of "form follows function" in the skeleton.

This work was kindly funded by NIH grants AR39278 & 43498, NASA NAG5-3950, and Exogen, Inc.

The effects of antidepressants on obstructed and unobstructed gait in the healthy elderly

LF Draganich[1], PhD, J Zacny[2], PhD, J Klafta[2], MD, and T Karrison[3], PhD

1. Section of Orthopaedic Surgery and Rehabilitation Medicine, Department of Surgery
2. Department of Anesthesiology and Critical Care, 3. Department of Health Studies
The University of Chicago, Chicago, Illinois 60637

INTRODUCTION

Falls are the leading cause of death from injury in people 65 years or more of age. Most falls by elderly persons occur during activities such as walking or changing position, and tripping or tripping over an obstacle is among the most reported causes of falls. Antidepressants have been found to be associated with falling. We hypothesized that single doses of amitriptyline, a tertiary-amine tricyclic antidepressant, desipramine, a secondary-amine tricyclic antidepressant, and paroxetine, a selective serotonin reuptake inhibitor, would affect temporal-distance variables and the kinematics of the trailing limb when stepping over obstacles.

METHODS

Twelve healthy subjects, 10 male and 2 female, were tested. Their mean (SD) age was 66.9 yr (3.0 yr), their mean height was 170.0 cm (14.0 cm) and their mean weight was 761 N (12.4 N). Inclusion in the study required that each subject be 65 to 75 years of age, report being able to walk several blocks without rest, and be able to successfully step over an 8-inch high obstacle. A medical history was obtained and a physical (including neurologic) examination was conducted to exclude the presence of poor uncorrected vision or chronic conditions, including a history of heart disease, hip fracture, active cancer, or stroke, as these have been reported to be associated with loss of mobility. Subjects also passed a psychiatric symptomatology test, a psychiatric screening interview, an alcoholism screening test, and a resting 12-lead EKG. Subjects reported that they did not use central nervous system-active drugs within 30 days of their participation. The University of Chicago Institutional Review Board approved the protocol and informed consent was obtained.

Subjects arrived for testing by livery service at approximately 0615 h. At 0630 h subjects were given a baseline resting EKG. At 0715 h subjects were given a standardized breakfast adjusted for body weight. Drugs were administered with 100 cc to 200 cc of water at 0800 h. Doses of paroxetine 20 mg, amitriptyline 50 mg, desipramine 50 mg, or placebo were tested in a four-period, double blind, crossover design. Treatment orders were randomly assigned from those residing in three, 4×4 Latin squares. The washout periods between treatments were at least 6 days. Drug and placebo capsules were identical in size, weight, and appearance. The randomization schedule was generated by the project statistician at the beginning of the study and given to the pharmacist. The pharmacist placed the appropriate capsule in a white envelope with the subject number and trial number noted on it and gave it to the nurse who administered the drug to the subject on the morning of the gait tests. The treatment team was blind to treatment assignment. Gait testing began at 1200 h, four hours after the drug had been ingested and when drug plasma levels were predicted to be at or close to peak levels.

The motion analysis laboratory included a 9.5

meter walkway. The kinematic parameters were measured using the Watsmart (Northern Digital, Inc., Waterloo, Ontario, Canada) optical electronic three-dimensional digitizing and analysis system which detected the positions of infrared light-emitting diodes. Rigid segments of infra-red light emitting diodes were attached using elastic straps to the foot, shank, thigh, and pelvis of the left lower extremities of the subjects. Three sets of experiments were performed. Subjects first performed several practice trials. In experiment 1, the subject was asked to walk on the walkway, without encountering obstacles, in a self-selected manner. In experiment 2, the subject was asked to walk on the walkway, step over an obstacle (a white plastic dowel, 6 mm in diameter, placed across an aluminum frame) positioned 102, 153, or 204 mm high in a self-selected manner and continue walking to the end of the walkway. Trials for the three heights were in a random order.

The variables investigated for unobstructed gait consisted of velocity, stride length (normalized to lower limb length), cadence, maximum hip, knee, and ankle flexion and extension. Those for obstructed gait consisted of those temporal distance variables listed above, toe-obstacle clearance for the trailing limb (limb crossing obstacle last), angular velocity of hip, knee, and ankle flexion, and hip, knee, and ankle flexion when the toe of the trailing limb was directly over the obstacle.

All variables were separately analyzed by repeated measures analysis of variance (ANOVA). P levels ≤ 0.05 were regarded as statistically significant. The Greenhouse-Geiser adjustment to the degrees of freedom was used in assessing significance levels based on the overall F-test. If the overall F-test was significant, pairwise comparisons among treatment means were performed using paired t tests for the variables of gait, and Tukey tests for the variables of psychomotor function and

RESULTS

None of the subjects fell during any of the experiments. None of the subjects tripped during unobstructed gait. Compared with placebo, amitriptyline reduced maximum knee flexion during the swing phase of gait by 4.2%. This was marginally significant ($p = 0.051$). None of the drugs were found to have other statistically significant effects on unobstructed gait. None of the subjects tripped when stepping over obstacles in a self-selected manner. Compared with placebo, amitriptyline significantly affected four dependent variables, reducing velocity by 8.0%, cadence by 4.9%, angular velocity of hip flexion by 10.0%, and angular velocity of knee flexion by 8.0% when stepping over obstacles ($p \leq 0.028$).

DISCUSSION

To our knowledge, this is the first placebo-controlled study of the effects of antidepressants on the gait of the healthy elderly. The data confirm our hypothesis on amitriptyline, demonstrating causal effects on the temporal-distance measures and on the kinematics of the trailing limb when stepping over obstacles. These abnormalities may result in falling. However, neither desipramine nor paroxetine had deleterious effects on gait, suggesting that these latter drugs may be safer to use with regard to gait.

Acknowledgements

General Clinical Research Center grant M01 RR00055 and Home Health Care Committee grant from the University of Chicago. Thanks to Gary Piotrowski for performing gait tests and processing the data and to Debra Janiszewski for preparing the session materials, data entry, and analysis.

INVESTIGATION OF FRICTION FOLLOWING OBSTACLE CLEARANCE DURING WALKING

Jeremy Houser[1], Nick Stergiou[2], Shane D. Scholten[2], John Noble[2], Gregory M. Karst[3], and Charles S. Layne[1]

[1]Motor Control and Coordination Lab, University of Houston, Houston, Texas
[2]Biomechanics Lab, University of Nebraska at Omaha, Omaha, Nebraska
[3]Physical Therapy Education, University of Nebraska Medical Center, Omaha, Nebraska
Email: jjhouser@bayou.uh.edu Web: www.coe.uh.edu/~clayne/

INTRODUCTION

Obstacles and low friction conditions are two types of perturbations that could potentially cause instability during walking. Numerous studies (Begg et al, 1998; Chen et al, 1994; Chou & Draganich, 1997; Patla et al, 1991; Patla & Rietdyk, 1993) have investigated the effect of obstacle perturbation during walking. This research has focused on the approach to an obstacle by collecting gait data of the trailing limb while negotiating the obstacle. These studies have attempted to elucidate factors associated with tripping while navigating the obstacle. Several studies (Begg et al, 1998; Patla et al, 1991) have used GRF parameters associated with the landing of the leading limb following obstacle clearance. Slipping after obstacle clearance has received limited attention (Patla & Rietdyk, 1993) but may be an important factor in the loss of dynamic postural stability while traversing a cluttered environment. The purpose of this study was to investigate the effects of shoe traction and obstacle height on friction during walking to better understand the process of slippage avoidance following obstacle clearance.

PROCEDURES

Ten male subjects walked at a self-selected pace during eight different conditions: four obstacle height conditions (0%, 10%, 20%, & 40% of limb length) and two friction conditions. The obstacle was a one meter wide hurdle formed by two graduated supports and a thin wooden dowel. Friction was manipulated by wearing two different pairs of shoes (high and low traction). The high traction shoes had a dynamic COF of 0.7 and a static COF of 0.8. The low traction shoes had a dynamic COF of 0.3 and a static COF of 0.35). Frictional forces of the leading leg after it cleared the obstacle were calculated from the ground reaction forces (GRF), obtained using a Kistler force plate at 960 Hz. The force ratio (F_y/F_z) trace illustrates friction in-vivo (Figure 1).

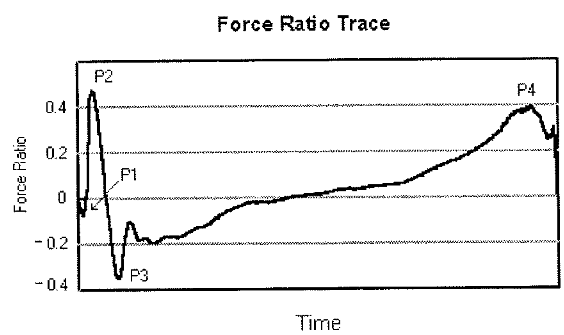

Figure 1: Force ratio trace.

Parameters analyzed were peak 2 (P2), peak 3 (P3), and peak 4 (P4) from the force ratio trace, and time of the braking phase (TB), time of the propulsive phase (TP), and time of stance (TS). Peak 1 (P1) was discarded from the analysis due to its inconsistencies. P1 was difficult to discern and was irregular in its occurrence. Perkins (1978) also stated that P1 was very inconsistent in its appearance. P1 is the first maximum negative peak on the force ratio trace, indicative of a high possibility of a forward slip. P2 is the first maximum positive peak indicative of a slight possibility of a backward slip. P3 is the second maximum negative peak indicative of a high possibility of forward slip. P4 is the second maximum positive peak indicative of a high possibility of relatively safe backward slip. Slippage may occur when the absolute peak force ratio exceeds the COF of a particular shoe. TB and TP were calculated from the F_Y curve. Two-way repeated measures ANOVAs (obstacle x shoe traction) were performed on the subject means for all parameters. Tukey's *post-hoc* comparisons were performed when there was a significant main effect ($p<0.05$).

RESULTS AND DISCUSSION

P2, P3, P4, and TS revealed statistical significance for both factors (height and traction) and their interaction. The values of all the peaks were similar as in Perkins (1978). All peaks showed significant increases from the low to the high traction shoe. In addition, all peaks significantly increased with increases in obstacle height. P2 and P3 significantly increased from the no obstacle to the obstacle conditions for both shoes. For P4 the obstacle height had no effect regarding the low traction shoe. Inconsequential slippage repeatedly occurred during push off (P4). However, for the high traction shoe P4 showed similar results as in the other two peaks. TS values were significantly shorter for the low traction shoe. Due to the decreased stability of the situation, subjects may have reduced TS in order to increase their dynamic stability. TB differences were significant only regarding obstacle height. The time required to overcome the obstacle allowed the center of gravity (COG) to travel further forward with respect to the foot, thus shortening TB. Placement of the COG over the foot at heel strike decreases the probability of a dangerous anterior slip. Presence of an obstacle may decrease the chance of slippage, due to the change in vector direction prior to heel strike.

SUMMARY

Peaks 2, 3, and 4 increased with increases in obstacle height. However, slippage did not occur because peak values never exceeded the COF of the corresponding shoes. The low traction shoes yielded smaller peaks than the high traction shoes. Increases in the obstacle height allowed for the subjects to position the center of gravity more anteriorly over the leading leg at foot contact. This lead to shorter TB with increased obstacle height, and the shift from braking to propulsion occurred sooner. These compensations appear to reduce the risk to the subject when confronted with an environment characterized by low traction and high obstacles.

REFERENCES

Begg, R.K. et al. (1998). *Gait Posture*, **7**, 99-109.

Chen, H.C. et al. (1994). *Gait Posture*, **2**, 139-146.

Chou, L.S., Draganich, L.F. (1997). *J. Biomech*, **30**, 331-337.

Patla, A.E. et al. (1991). *J. of Exp Psych: Hum Perc Perf*, **17**, 603-634.

Patla, A.E., Rietdyk, S. (1993). *Gait Posture*, **1**, 45-60.

Perkins, P.J. (1983). In *Walkway surfaces: measurement of slip resistance*, Philadelphia, PA: ASTM.

FOOT PLACEMENT SPECIFIES THE RESISTANCE ARM OF THE GROUND REACTION FORCE DURING PUSH-OFF IN GAIT INITIATION

A. Erdemir[1,2] and S. J. Piazza[1,2,3]

[1]The Center for Locomotion Studies and Departments of [2]Kinesiology and [3]Mechanical & Nuclear Engineering, Penn State University, University Park, PA

Email: sjp12@psu.edu Web: www.celos.psu.edu

INTRODUCTION

The foot may be considered to be a simple lever with its fulcrum at the ankle (Carrier *et al.*, 1994). The moment of the Achilles' tendon force about the ankle is resisted by the moment of the ground reaction force (GRF); the nature of this opposition determines how loads are transmitted between the musculoskeletal system and the ground. Gage (1993) suggested that gait deformities that involve abnormal foot rotations reduce the moment arm of the GRF, resulting in "lever arm deficiencies" that are potentially destabilizing.

Anatomical and geometrical analyses performed by Bojsen-Møller (1978) suggested that the GRF lever arm depends on selection of a rotation axis at the metatarsophalangeal joint during push-off. Two such axes were defined: a transverse axis passing through the first and second metatarsal heads, and an oblique axis through the second and fifth metatarsal heads. Bojsen-Møller (1978) theorized that an internally-rotated foot placement results in rotation about the oblique axis, giving the GRF a lower resistance arm, which is useful during high-load, low-speed activities, but this has not yet been demonstrated experimentally.

Viale *et al.* (1997) examined the changes in ankle kinematics and foot loading that occur with natural variation in foot orientation. Foot placement was found not to affect resistance lever arm, but this study lacked a controlled change of foot orientation and only considered running, a high-speed activity for which only large lever arms would be expected. Carrier *et al.* (1994) measured resistance arms during two activities, steady-state running and acceleration from a standing start. The authors found smaller late push-off resistance arms during the standing start activity. Whether resistance arms can be manipulated by foot placement, however, was not addressed.

The purpose of this study was to investigate whether internal/external rotation of the foot determines the resistance arm of the GRF during push-off. Selection of walking initiation as the activity to be studied permitted foot orientation to be precisely controlled. We hypothesized that an internally-rotated foot placement would result in smaller resistance arms than those found for an externally-rotated placement.

METHODS

Kinematic data, GRF, and center of pressure (COP) location were measured during the walking initiations of ten healthy, barefoot subjects (5 m, 5 f; 23-29 yr) using a six-camera motion analysis system (Vicon 370; Oxford Metrics Ltd.) and a force plate (Kistler Inst. Corp.). Reflective marker clusters were placed on the left foot and shank to record motions of these segments during the push-off period, defined to begin at the onset of plantarflexion and end at toe-off.

The left foot of each subject was placed such that an axis determined by the second toe and the posterior aspect of the heel was aligned with markings on the force plate (Figure 1). The right foot was placed in neutral position. Subjects began each trial standing in this manner, then walked several steps forward, leading with the right foot. Each subject completed ten trials with each of two foot placements: 20° internally rotated and 30° externally rotated.

The resistance arm of the GRF was determined by calculating the distance from the talocrural joint axis to the line of action of the GRF. The talocrural joint axis was determined using the optimization technique proposed by Bogert *et al.* (1994). A two-way repeated-measures ANOVA followed by pairwise comparisons was used to test the effects of foot placement (internally and externally rotated) and time (25 levels; every 4% of push-off).

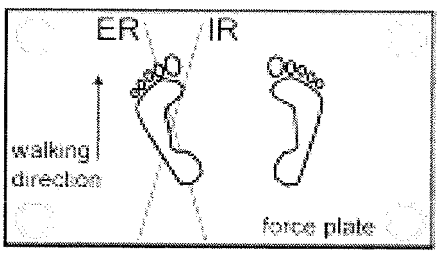

Figure 1: Initial placement of the feet on the force plate.

RESULTS AND DISCUSSION

Externally-rotated foot placement produced larger GRF resistance arms in late push-off (Figure 2). ANOVA revealed an interaction between foot placement and time of push-off; significant resistance arm differences were found between foot placement conditions only from 76%-100% of push-off (p-values <= 0.038). Advancement of the talocrural joint axis toward the GRF vector decreased the resistance arm of the GRF when the foot was internally rotated (Figure 3). Resistance arm was maintained in the externally rotated case, however, as the COP moved anteriorly under the head of the first metatarsal and the large toe.

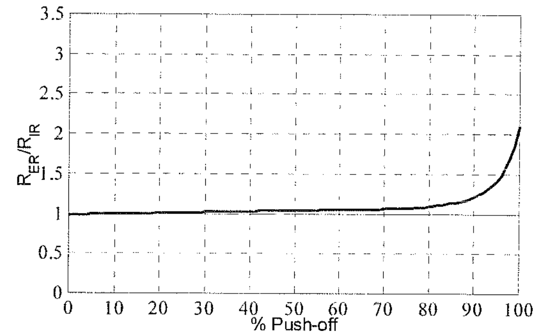

Figure 2: Ratio of resistance arms during push-off, averaged over ten subjects (ER: externally rotated, IR: internally rotated).

This study demonstrates that internal rotation of the foot reduces the resistance arm of the GRF during push-off in gait initiation. Future studies will determine whether foot placement is used to achieve favorable mechanical advantage during activities such as uphill walking, and will quantify changes in lever arm associated with pathological conditions such as internal rotation gait.

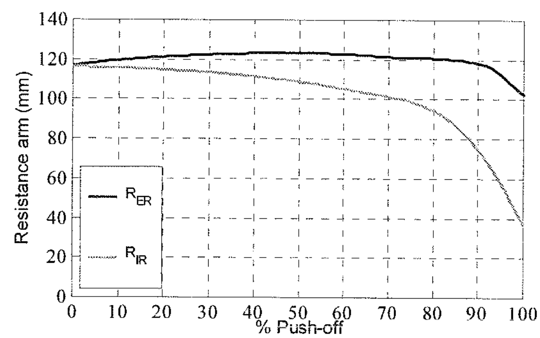

Figure 3: Resistance arms during push-off for a single subject, averaged over 10 trials.

REFERENCES

Bogert, T van den, *et al.* (1992), *J. Biomech*, **27**, 1477.
Bojsen-Møller, F (1978), *Biomech V*, 261.
Carrier, DR *et al.* (1994), *Science*, **265**, 651.
Gage, JR (1993) *Clin Orthop*, **288**, 126.
Viale, F *et al.* (1997), *Foot Ankle*, **18**, 157.

KNEE KINETICS DURING THE DEEP SQUAT

Chris O. Dyrby and Thomas P. Andriacchi

Stanford Biomotion Laboratory, Stanford University, Stanford California

Email: cdyrby@stanford.edu **Web**: www.stanford.edu/group/biomotion

INTRODUCTION

A large portion of the world population performs deep squatting as part of normal activities of daily living (ADL). Past studies(Dyrby, 1998) have tried to quantify the rotational components of motion in the knee during dynamic ADL's. These ADL's include walking, stair climbing and performing a deep squat. Recent studies (Stiehl et al., 1995) have reported that the knee lifts off during squatting. However, these studies are based on planar fluoroscopic measurements and did not measure if forces are present to produce liftoff. The purpose of this paper is to quantify the forces and moments about the knee during the deep squat. In particular, this study focused on net adduction moment, net quadriceps moment, anterior shear force and medial and lateral knee contact forces applied to the tibia.

MATERIALS AND METHODS

Eleven adults (5 female, 6 male) with no musculoskeletal impairments were studied. The subjects (28±8 yrs., 169±8 cm., 635±115 N) performed walking and deep squat activities. Measurements were obtained using an optoelectronic system for motion analysis (CFTC) and forceplate (Bertec) (Andriacchi et al., 1997). External knee flexion and adduction moments and net anterior knee force were obtained using an inverse dynamics approach (Andriacchi et al. 1997). Medial and lateral compartment knee forces were obtained using a statically determinate knee model (Schipplein and Andriacchi, 1991). Student's t-test were used at a significance level of $\alpha = 0.05$.

RESULTS AND DISCUSSION

The knee flexion moment during the squat was almost three times as large as that seen during walking ($p < 0.001$, Table 1, Figure 1). Conversely the adduction moment during squatting was significantly lower ($p=0.02$, Table 1) than during level walking. This combination of changes in the external loading produced a more uniform balance between the force on the medial and lateral compartments than during level walking (Table 1). Walking produced significant differences in the medial and lateral compartment loading ($p < 0.001$) while the deep squat showed no difference.

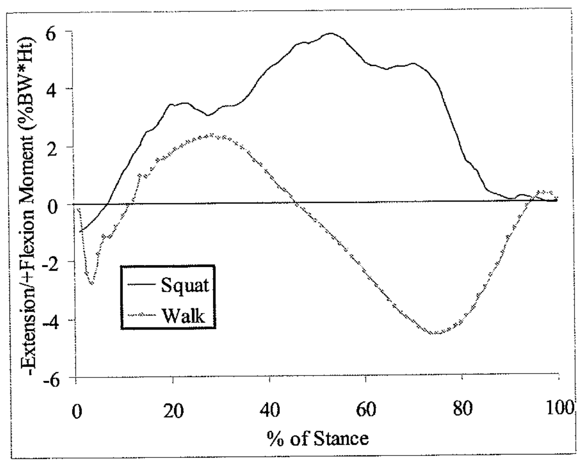

Figure 1: External knee flexion extension moments. The maximum knee flexion moment for the squat is nearly times that of walking.

Comparison of net anterior shear forces demonstrated an increase for the deep squat though this result was not significant (p = 0.06, Table 1).

DISCUSSION

This study demonstrated that there was an increase in the net quadriceps moment and a decrease in the adduction moment during the squat relative to level walking. This external loading is more likely to load the knee more uniformly (medial to lateral) than during level walking. Thus, it is less likely that liftoff would occur during squatting than during level walking. This finding is in contrast to the study reported by Stiehl et al. (1995) that described liftoff in subjects performing deep squatting. Given the stabilizing influence by the larger force generated by the quadriceps muscles and the lower adduction moment, it is not likely that the knee would experience liftoff during squatting.

This study also demonstrates an increase in the anterior shear force during squatting. This force would be sustained by the posterior cruciate ligament (PCL) or it's substitute. This shear force would be added to the substantial force generated by the quadriceps in deep flexion that must be sustained by the PCL, since in deep flexion the patellar tendon pulls the tibia posteriorly. Designs that incorporate any mechanical constraints on motion, i.e. a cam to substitute for a sacrificed PCL should consider the high net anterior shear forces sustained during the deep squat.

REFERENCES

Andriacchi, T.P., et al. (1997). in *Basic Ortho. Biomech.*, 2nd Ed. Lippincott-Raven, 37-68.

Dyrby, C.O. (1998) Masters Thesis, University of Illinois at Chicago.

Schipplein, O.D. and T.P. Andriacchi (1991). *JOR* **9**(1): 113-119.

Stiehl, J.B., et al. (1995) *JBJS* **77B**(6): 884-889.

ACKNOWLEDGEMENTS

This study was conducted in the Gait Analysis Laboratory at Rush-Presbyterian St. Luke's Medical Center, Chicago, IL. NIH Grant # AR20702 and Zimmer, Japan. The authors would also like to thank the Stanford Biomotion Laboratory.

Table 1: Comparison of the deep squat and walking.

	Deep Squat	Walking	p-value
Knee Flexion Moment (%BW*Ht)	**6.6 (1.2)**	**2.3 (1.2)**	**<0.001**
Knee Adduction Moment (%BW*Ht)	**1.4 (0.8)**	**2.3 (0.6)**	**0.01**
Peak Lateral Compartment Knee Force (N)	**1417 (616)**	**772 (279)**	**0.002**
Peak Medial Compartment Knee Force (N)	1468 (405)	1343 (247)	0.27
Peak Net Anterior Shear Force (%BW)	42.8 (6.7)	36.6 (5.7)	0.06

Note: **Bold** indicate significant differences. Standard deviation in parenthesis.

THE EFFECT OF TIBIAL TORSION ON SOLEUS FUNCTION

Michael Schwartz[1,2] and Gaio Lakin[3]

[1] Gillette Children's Specialty Healthcare, St. Paul, MN
[2] University of Minnesota, Minneapolis, MN
[3] Children's Health System, Birmingham, AL
Email: schwa021@tc.umn.edu

INTRODUCTION

The purpose of this study is to use induced acceleration analysis (IAA) to determine the effect of tibial torsion on the ability of the soleus to support and propel the body during gait. The IAA approach is well-suited for this study because it allows soleus action to be quantified in the presence of varying amounts of tibial torsion, while other factors such as body configuration and muscle activation are held constant [Kepple, Lakin].

The plantarflexors are important in stabilizing the knee and preventing crouch during gait [Gage, Sutherland]. External tibial torsion can be expected to increase crouch and valgus stresses at the knee [Gage]. In support of this hypothesis, excessive external tibial torsion was found to increase valgus stress at the knee in children with myelomeningocele [Lim].

It seems clear that a tibial derotational osteotomy has the potential to benefit a patient with excessive external tibial torsion. However, it has been difficult to isolate the effects of tibial derotation from those of concomitant treatments. The IAA model helps to identify and quantify the benefit of a tibial derotational osteotomy.

METHODS

The body is modeled as a 15-segment three-dimensional linkage system with appropriate mass properties. The dynamic equations of motion for the model are derived and converted into a FORTRAN program using SD/FAST (Symbolic Dynamics).

The model is configured for an individual subject based on joint angular positions and the center of pressure (COP) derived from computerized gait analysis (Oxford Metrics). Foot floor contact is modeled as a ball-and-socket joint located at the center of pressure. Segmental angular velocities are ignored in order to separate the effects of muscles from those of segment inertia.

The soleus is treated as a two-point, straight-line muscle [Delp]. A contraction of the soleus is modeled by the application of equal and opposite point forces at the muscle's origin and insertion, directed along the line of action of the muscle.

Tibial torsion is modeled as a continuous, linearly varying, twist of the bone. Thus a point on the tibia is rotated about the bone's long axis by an amount proportional to the point's distance from the knee joint. The ankle flexion axis, foot and COP are also rotated. The path of the COP relative to the foot is not altered.

RESULTS AND DISCUSSION

The inverse dynamics solution is used to validate the model [Kepple, Lakin]. The computed joint moments for the subject are applied and the predicted ground reaction force (GRF) is compared to the force plate data. Mean GRF errors are 1%, 6% and 2% of the total range for the anterior-posterior, medial-lateral and vertical components respectively.

The knee joint accelerations induced by a 1N soleus force during the typical period of soleus activation are found for varying amounts of tibial torsion [Table 1].

Table 1: Induced knee joint accelerations

Joint Acceleration [rad/s^2]	Tibial Torsion		10°	30°	50°
	Flexion (+) Extens. (-)	Ave	-.05	-.01	.02
		Max	.02	.09	.13
		Min	-.09	-.09	-.07
	Varus (+) Valgus (-)	Ave	-.04	-.21	-.34
		Max	-.02	-.17	-.29
		Min	-.05	-.31	-.49
	Int. Rot. (+) Ext. Rot. (-)	Ave	.31	.17	.00
		Max	.32	.18	.02
		Min	.31	.16	-.02

The induced knee joint accelerations shift toward flexion, valgus and external rotation as excess tibial torsion increases. This heightens the demand for knee extensor activation and collateral structure support. If this demand goes unmet, knee motion towards flexion, valgus and external rotation will occur. If the demand is met, the potential for damage to ligaments and cartilage may be increased due to acute and chronic overloading. The accelerations are based on unit soleus force. Peak soleus forces may be as large as 500 N. Thus it is clear that significant accelerations, stresses and motions can result from bony torsion.

The IAA model is also used to quantify the effect of tibial torsion on the forward propulsion and vertical support produced by the soleus. The average body center of mass (COM) acceleration induced by a 1N soleus force during the typical period of soleus activation is computed for varying amounts of tibial torsion [Table 2].

Excess external tibial torsion markedly diminishes the forward and upward accelerations of the body. This implies that increased muscle force is needed to maintain progression and prevent crouch.

Table 2: Induced COM accelerations

Acc [m/s^2]	Tibial Torsion		10°	30°	50°
	Propulsion	Peak	.12	.08	.02
		Ave	.00	-.05	-.08
	Support	Peak	.60	.55	.40
		Ave	.35	.29	.19

SUMMARY

Important deleterious effects of excess tibial torsion are quantified in terms of induced knee and COM accelerations. The acceleration changes are due to both the relocation of the COP (external levers) and the alteration of the soleus' line of action (internal levers). The model supports the concept that bony mal-alignment can lead to "Lever Arm Dysfunction" — significant gait pathology in the absence of a neuromuscular disorder. The objective data correlate with previous clinical observations related to valgus stress, crouch and the role of the soleus in level walking. The IAA model provides a tool for examining various aspects of abnormal gait independently and quantitatively.

REFERENCES

Kepple TM, *et al.* (1998). *Gait and Posture,* **6**: 1-8.

Lakin G and Schwartz MH (1999). *Gait and Posture,* **9**: 117.

Delp SL, *et al.* (1990). *IEEE Transactions on Biomedical Engineering* **37**: 757-767.

Lim R, *et al.* (1998). *Journal of Pediatric Orthopaedics* **18**: 428-433.

Sutherland DH, *et al.* (1980). Journal of Bone and Joint Surgery **62-A**(3): 354-363.

Gage JR, (1991). *Gait Analysis in Cerebral Palsy.* New York, NY: MacKeith Press.

STRESS RELAXATION OF DECALCIFIED BOVINE CORTICAL BONE IS FLOW INDEPENDENT

D. P. Fyhrie[1], G. Gibson[1], J. Kimura[1], D. Vashishth[2]

[1]**Bone and Joint Center, Henry Ford Hospital, Detroit, MI**
[2]**Dept. of Biomedical Engineering, Rensselaer Polytechnic Institute, Troy, New York**

INTRODUCTION

Creep and stress relaxation in biological materials are modeled as fluid flow independent (Fung, 1993), fluid flow dependent (Mow et al, 1980) or as a combination of the two (Setton et al, 1993). While each approach is theoretically distinct it can be difficult in practice to determine which is more appropriate for a particular tissue. For decalcified cortical bone our experimental data support the conclusion that stress relaxation is fluid flow independent.

THEORETICAL METHODS

An equation often used to model uniaxial stress relaxation is:

$$\sigma(t) = \sigma_{eq} + \Delta\sigma_0 \phi(t)$$

where, σ_{eq} is the equilibrium stress, $\Delta\sigma_0$, is the difference between the stress at time zero and at equilibrium and $\phi(t)$ is the relaxation function that describes the time dependence of stress, $\sigma(t)$.

The uniaxial equilibrium (aggregate) modulus H_A of a material is defined as the ratio of the equilibrium stress to the equilibrium strain of the material. A signature feature of the well known biphasic (flow dependent) theory of poroelasticity is that the characteristic time constant T of the relaxation function $\phi(t)$ is proportional to the ratio of the drag force of fluid flowing through the matrix to the aggregate modulus, H_A (Mow et al, 1980). Consequently, differences in the aggregate modulus H_A between specimens result in differences in the characteristic time T of the stress relaxation process. (For uniaxial confined compression T is proportional to $1/(H_A k)$, k is the tissue permeability.)

We exploited the characteristic dependence of T on H_A in the biphasic theory by incubating bone specimens in ribose solution to increase the crosslinking in the specimen and, consequently, increase the equilibrium modulus of the collagenous matrix. If stress relaxation in this material is governed by fluid flow the relaxation time constant will vary with H_A.

EXPERIMENTAL METHODS

Five mm diameter cylindrical specimens of bovine cortical bone were subjected to *in vitro* ribosylation by incubating in 100 mg/ml of ribose in Hanks buffer/ 1.3 mM $CaCl_2$ at 37°C with 100 µl/10 ml of toluene and chloroform and 5 mg/10 ml of gentamicin to prevent bacterial growth. The specimens were demineralized in formic acid sodium citrate solution (1M sodium citrate in 45% formic acid) for a period of eight weeks. Fifteen specimens (6 control and 9 ribosylated for 3, 8, 11, 17, 29 and 38 days) were used for unconfined stress relaxation compression tests. Each demineralized bone cylinder was loaded to a strain of 50% followed by a hold period under strain control. Stress was measured as a function of time and equilibrium modulus calculated as the ratio of equilibrium stress and strain.

The specimens were papain digested (0.4 mg/ml papain in 0.1M sodium acetate buffer, ph 6.0, 16hrs, 65^0C. Ribosylation (AGE products) was determined from fluorescence using 370nm excitation and 440nm emission wavelength standardized against a quinine sulphate solution (Knott et al, 1995). Collagen was determined from hydroxyproline content (Stegemann and Stalder, 1967).

RESULTS

The time dependence of stress was well fit by the equation,

$$\sigma(t)=\sigma_{eq}+\Delta\sigma_0 e^{-\sqrt{t/\tau}}$$

with τ the characteristic time of relaxation, analogous to T of the biphasic theory. (Adjusted r^2 was >0.99 for eleven specimens and was 0.97 and 0.66 for two).

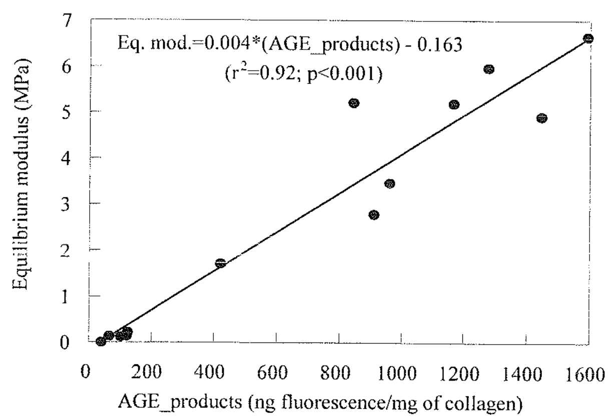

Statistical analyses (t-tests) of the data indicated that coefficients σ_{eq}, $\Delta\sigma_o$ and H_A were significantly different ($p < 0.0001$) between the ribosylated and control specimens while coefficient 'τ' was not ($p = 0.20$). These results were unchanged after adjustment for incubation time. Equilibrium modulus was strongly dependent upon the extent of ribosylation (Figure), however, the time constant τ was not dependent upon equilibrium modulus ($1/\tau = 0.0011H_A$, $r^2 = -0.42$). Note that r^2 negative means the linear statistical model motivated by biphasic theory is worse than assuming τ is constant.

CONCLUSION

Ribosylation of calcified bone significantly increased the equilibrium modulus of the collagenous matrix in direct relationship to the degree of ribosylation. This increase was expected as ribosylation increases the number of crosslinks in the tissue. Against expectation, the characteristic time constant of stress relaxation was not significantly affected by ribosylation. This strongly suggests that the viscous mechanisms of this material are not dependent on equilibrium modulus. As a result, we conclude that fluid flow is not the primary dissipative mechanism in decalcified bone matrix.

Fung YC (1993) *Biomechanics,* Springer-Verlag.

Knott L. et al (1995) *Biochem. J.* 310: 1045-1051.

Mow VC et al, *J Biomech Eng,* 102: 73-84.

Setton L et al (1993), *J Biomech,* 26:581-592.

Stegemann and Stalder (1967) *Clin. Chim. Acta* 18: 267-273.

David P. Fyhrie
Head, Section of Biomechanics
Bone and Joint Center
2799 W. Grand Blvd.
Detroit, MI 48202

fyhrie@bjc.hfh.edu

CORRELATIONS BETWEEN OSTEOCALCIN CONTENT, DEGREE OF MINERALIZATION, AND MECHANICAL PROPERTIES OF *C. CARPIO* RIB BONE

M. E. Roy[1], S. K. Nishimoto[2], J.-Y. Rho[1], S. K. Bhattacharya[3], and G. M. Pharr[4]

[1]Department of Biomedical Engineering, The University of Memphis, Memphis, TN
[2]Department of Biochemistry, The University of Tennessee, Memphis, TN
[3]Department of Surgery, The University of Tennessee, Memphis, TN
[4]Department of Materials Science, The University of Tennessee, Knoxville, TN; and Metals and Ceramics Division, Oak Ridge National Laboratory, Oak Ridge, TN
E-mail: jrho@cc.memphis.edu Web: memphis.mecca.org/BME/

INTRODUCTION Osteocalcin (OC), also known as γ-carboxyglutamic acid-containing protein or BGP, is one of the most abundant noncollagenous proteins found in bone matrix. It has a strong affinity for hydroxyapatite (HA), but not for amorphous calcium phosphate, and is a potent inhibitor of HA formation (Price et al., 1976). OC is a biochemical marker of bone metabolism or turnover (Price et al., 1980), but its exact role is unclear. The hypotheses of the current study were that the concentration of osteocalcin along the length of a bone is reflected in both its Ca/P ratio, an indicator of the degree of mineralization present, and in its microstructural properties.

METHODS The first, third, and fifth pairs of ribs were harvested from a fresh frozen *Cyprinus carpio* specimen. *C. carpio* rib bone was chosen for study primarily because of its unusually high content (~60%) of OC relative to other extractable proteins, like bluegill rib bone (Nishimoto et al., 1992). Each of the three pairs of ribs were cut into 14 pieces of approximately 5 mm each, producing segments of bone each representing about 6% of the overall length. Specimens were divided up such that alternating pieces were used for different tests for seven levels of discretization along the length of the rib. Specimens used for assays were prepared by extracting their mineral content with 10% formic acid over a period of 24 hours. Extracts of the specimen supernatants were used in all subsequent assays. The osteocalcin content was determined in triplicate by a radioimmunoassay specific for carp osteocalcin. Phosphate assays were performed in duplicate spectrophotometrically (Sigma Diagnostics, procedure 360-UV). Calcium assays were performed via atomic absorption spectrophotometry. Raw assay data were normalized to the initial sample weight. Specimens for nanoindentation were prepared by mounting in epoxy resin and polishing, and were tested using the Nano Indenter® II at Oak Ridge National Laboratory. The parametric, linear dependence between pairs of variables was determined by computing their correlation coefficient, with a significance level of 95%.

RESULTS The parametric correlation tests revealed a positive linear relationship between OC concentration and molar Ca/P ratio ($p < 0.05$; n = 19). No significant relationship was found between OC and the concentrations of calcium or phosphate. A significant negative correlation ($p < 0.05$; n = 21) was found between OC concentration and the microstructural elastic modulus in the longitudinal direction (E_L) (Figure 1). Finally, significant correlations were found between E_L and both the phosphate concentration ($p < 0.05$; n = 20) and the molar Ca/P ratio ($p < 0.05$; n = 19).

DISCUSSION In this research a significant positive correlation was found between the concentration of OC and the degree of mineralization, as measured by the molar Ca/P ratio. Ducy et al. (1996) have shown OC-deficient transgenic mice to have increased bone formation without impairing bone resorption or affecting mineral content, suggesting osteocalcin prevents excessive bone formation. A significant positive correlation between the Ca/P ratio of OC-deficient and wild-type mice has also been reported by Boskey et al. (1998). In addition, a significant negative correlation between OC and the microstructural mechanical properties of bone was found in the current study. Ducy et al. (1996) found an increase in bending failure load in OC-deficient mice, which was attributed to the increase in bone mass, but found no differences in yield energy and stiffness. A negative correlation between OC concentration and the elastic modulus of bone has also recently been reported in core samples from the inferior region of the anterior/posterior axis of the human femoral head (Brown et al., 1999).

REFERENCES Ducy, P. et al. (1996). *Nature* 382, 448-452; Boskey, A.L. et al. (1998). *Bone* 23, 187-196; Brown, S. J. et al. (1999). *J Bone Mineral Res* 14(S1), S327; Nishimoto, S.K. et al. (1992). *J Biol Chem* 267, 11600-11605; Price, P.A. et al. (1976). *Proc Natl Acad Sci USA* 73, 1447-1451; Price, P.A. et al (1980). *J Clin Invest* 66, 878-883.

ACKNOWLEDGMENTS Portions of this research were sponsored by the Whitaker Foundation, a junior faculty research fellowship from the Oak Ridge Institute for Science and Technology, and NIH grant #AR45297 (JYR). The AAS facilities at the Surgical Research Laboratories of The University of Tennessee, Memphis was supported in part by grants to SKB from NIH (#R01-AR-38540) and the UT-CAN-DO Laboratory research fund. Analytical instrumentation for nanoindentation testing was provided by the Division of Materials Sciences, U.S. Department of Energy, under contract DE-AC05-96OR22464 with Lockheed Martin Energy Research Corp. and through the SHaRE Program under contract DE-AC05-76OR00033 between the U.S. Department of Energy and Oak Ridge Associated Universities.

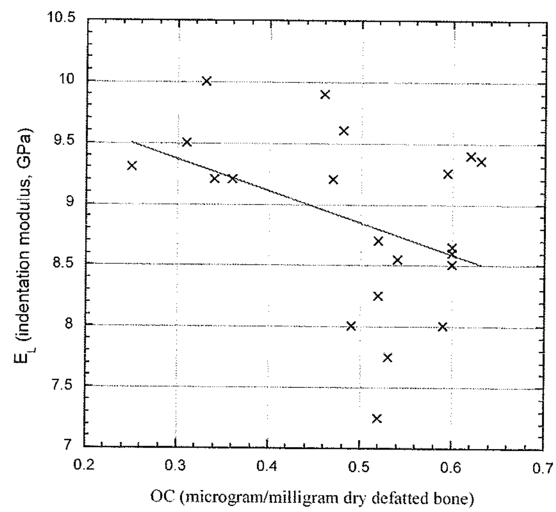

Figure 1. Indentation elastic modulus in the longitudinal direction as a function of osteocalcin concentration.

THE TRIAXIAL COMPRESSION VESSEL: A NOVEL MECHANICALLY ACTIVE CULTURE SYSTEM FOR CARTILAGE EXPLANTS

A. D. Heiner and J. A. Martin

Department of Orthopaedic Surgery, University of Iowa, Iowa City, Iowa

Email: anneliese-heiner@uiowa.edu

INTRODUCTION

Joint loading imposes complex stress states on articular cartilage, involving simultaneous solid matrix distortion, fluid flow, and hydrostatic compression. It is well established that loading regulates cartilage matrix biosynthesis (Steinmeyer et al., 1999; Quinn et al., 1998), suggesting that optimal stress conditions might promote cartilage stability and repair *in vivo*. Unfortunately, most *in vitro* models used to investigate cartilage responses to stress have used simple devices that either exaggerate distortion and fluid flow (unconfined axial compression) or minimize these effects (hydrostatic compression), thus creating mechanical conditions unlike those found *in vivo*. To address this issue, we developed a culture device capable of more closely simulating complex *in vivo* stress states. The device, termed the triaxial compression vessel (Figure 1), achieves this goal by permitting simultaneous and independent control of both axial and transverse compression. The cartilage explant is located in a cartilage housing, which holds the explant in position and keeps it chemically isolated. The lower chamber of the vessel applies transverse compression to the cartilage through a liquid pump. The upper chamber contains a piston which applies axial compression to the cartilage upon application of external air pressure. Culture nutrient medium is pumped to the cartilage through the platens, which are porous.

We are currently using this device to compare matrix synthesis in cartilage explants exposed to axial compression alone, versus equal axial plus transverse compression. We hypothesize that while the high shear stress produced by axial compression alone suppresses synthesis (Wong et al., 1999), the minimal shear stress produced by equal axial plus transverse compression does not.

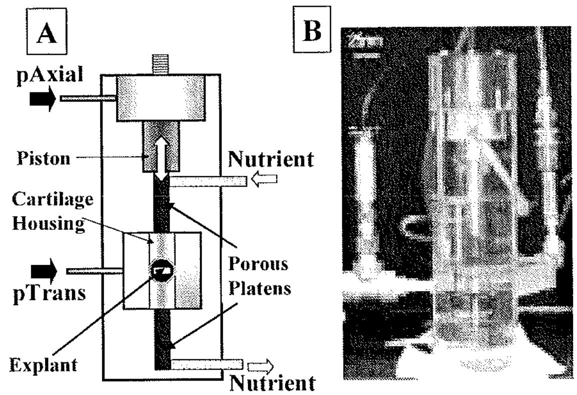

Figure 1. (A) Schematic and (B) physical appearance of triaxial compression vessel.

METHODS

Tibial plateau cartilage explants from three osteoarthritic human donors were cultured for 1 hour under one of three conditions: (a) 2 MPa axial compression at 1 Hz cyclic loading (axial alone), (b) 2 MPa axial plus 2 MPa transverse compression at 1 Hz cyclic loading (axial+transverse), or (c) not loaded (control). The explants were then incubated an additional 4 hours in growth medium containing 50 µCi/ml $^{35}SO_4$, to measure matrix (proteoglycan) synthesis. The $^{35}SO_4$-

labeled explants were washed, embedded and cryosectioned. Sections were collected and digested with papain. DNA content (fluoroscopic assay) and $^{35}SO_4$ content (scintillation counter) were determined.

RESULTS AND DISCUSSION

The matrix synthesis data ($^{35}SO_4$ incorporation/μg DNA) demonstrated high intrinsic donor-to-donor variability (Figure 2A). However, for all 3 donors, axial compression alone suppressed matrix synthesis. When the effects of donor variability were minimized by normalizing to controls within each experiment (CPM per μg for stressed explants/CPM per μg for controls), the axial alone group differed significantly from the axial+transverse group (2-tailed t-test, $p = 0.023$) (Fig. 2B).

The suppression of matrix synthesis by pure axial compression, which caused shear stress (equal to ½ of the applied axial stress), solid matrix distortion, and fluid flow, contrasted sharply with the minimal effects of equal axial+transverse compression, which caused little or no shear stress (theoretically zero, for pure hydrostatic stress). Future studies will explore this relationship in greater detail by varying the balance between axial and transverse compression to achieve intermediate shear stress states. We expect these studies will help to determine which stress conditions are likely to optimize cartilage matrix synthesis. These data may then serve as a basis for manipulating stress conditions *in vivo* to promote cartilage repair.

SUMMARY

We have developed a triaxial compression vessel capable of applying simultaneous axial and transverse compression to cartilage explants. Axial compression alone suppressed matrix synthesis, while equal levels of axial and transverse compression had a much smaller effect.

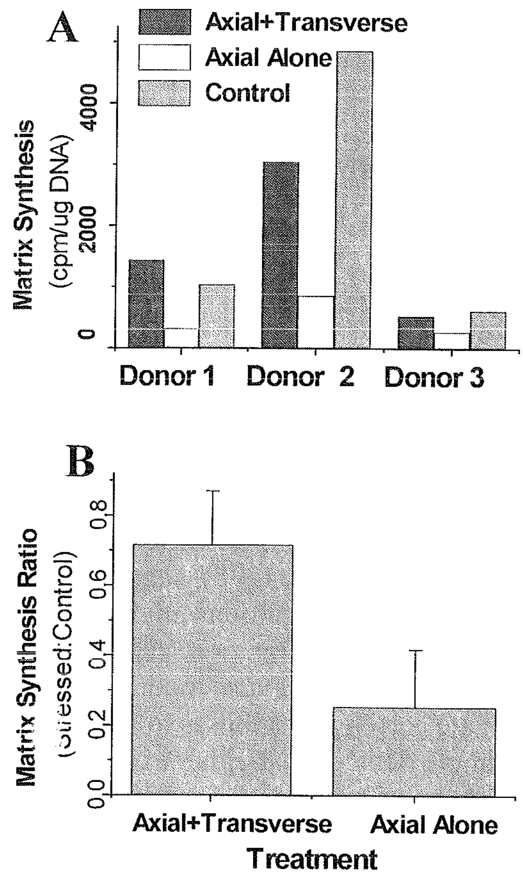

Figure 2. Stress effects on cartilage matrix synthesis. (A) $^{35}SO_4$ incorporation (CPM per μg DNA). (B) Ratio of stressed/control values. Bars indicate 1 std. dev. These groups are significantly different ($p=0.023$).

REFERENCES

Quinn, T.M. et al. (1998) *J Cell Science* **111**, 573-583.

Steinmeyer, J. et al. (1999) *Osteoarthritis Cartilage* 7, 155-164.

Wong, M. et al. (1999) *Matrix Biology* **18**, 391-399.

ACKNOWLEDGEMENTS

This research was funded by the University of Iowa Central Investment Fund for Research Enhancement.

A PIEZOELECTRICALLY-ACTUATED CELL STRETCHING DEVICE

William W. Clark[1] and James Wang[2]

[1]Mechanical Engineering Department, University of Pittsburgh
[2]Department of Orthopaedic Surgery, University of Pittsburgh Medical Center
Email: wclark@engrng.pitt.edu

INTRODUCTION

A number of systems have been designed to subject cells to mechanical loading in the laboratory and thereby simulate the micromechanical environment seen by many different types of cells (Schaffer, et. al., 1994). In most systems the cells are adhered to an elastic membrane that is deformed mechanically, thereby transferring the deformation to the cells.

The current methods commonly used for cell deformation primarily utilize vacuum actuation on the membrane or cam and follower mechanisms that load the membrane. Producing repeatable strains at levels below 1% can be impractical with these devices. A recent study by Tanaka (1999) presented a piezoelectric device for mechanically stimulating cells. The actuator was a piezoelectric bimorph which was attached to a collagen block containing cells. Achievable strains of 0.02% to 4% were reported, although only strains of 2% were verified.

The objective of this project was to design a new cell stretching mechanism that can produce repeatable membrane strains of less than 1%, at frequencies ranging from 0.5 to 5 Hz. A piezoelectric actuator was chosen to be the prime mover in the mechanism, because its displacement and force range is ideally suited to this application. In addition, one can easily achieve a wide range of position vs. time functions from the piezoelectric actuator.

DESIGN OF THE DEVICE

A schematic of the cell stretching device is shown in Fig. 1. Two silicone membranes (7.6 cm x 2.5 cm) are supported in a polystyrene frame. One end of each membrane is fixed to the frame, while the other end is attached to a linkage that is free to rotate, thus stretching the membranes. The cell culture will adhere to the membranes, so that mechanical strain imparted to the membranes will be transferred to the cells. The frame is housed in a 20.3 cm diameter petri dish which contains growth media. The linkage is driven by a piezoelectric Thunder actuator (model TH-7R, Face International Corporation). Since the toxicity of the actuator materials are unknown, the actuator is separated from the media with a lever arm.

A Thunder actuator is a thin (~0.6 mm) curved piezoelectric transducer consisting of a stainless steel backing and a piezoceramic wafer bonded together by a polyimide. The piezoceramic has electrodes on the top and bottom (across its thin dimension). When a voltage is applied, the piezoelectric effect causes the ceramic to contract or expand along its length. Because the ceramic is bonded to and constrained by the stainless steel, these very small strains are amplified

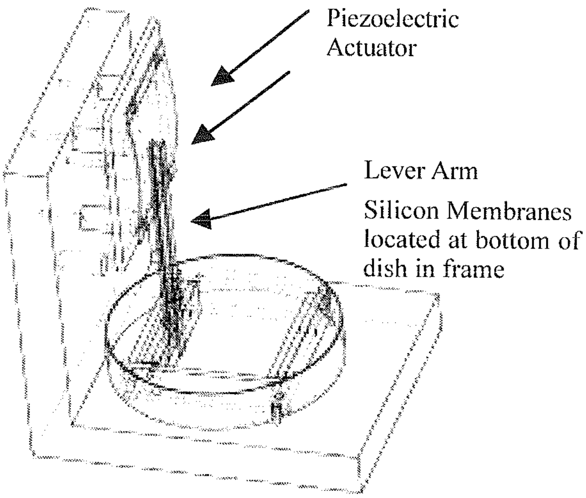

Figure 1: Schematic of piezoelectrically actuated cell stretching mechanism.

by relatively large changes in actuator curvature or dome height. This dome motion is imparted to the lever arm, and therefore to the membrane.

RESULTS

The Thunder actuator used in this design is capable of producing motions of approximately 1 mm under static loading of the membrane in the mechanism. At a frequency of 5 Hz, the peak-to-peak displacement is reduced to approximately 0.75 mm. These deflections are for a 180 V excitation applied to the actuator. If applied directly to the membrane, these deflections correspond to strains of 1.3% and 1%, respectively. By moving the actuator further away from the fulcrum of the lever, the displacement ratio is reduced by as much as six times. So, at its farthest location, the same actuator deflections correspond to strains of 0.22% and 0.16%. Of course, the excitation can be reduced for even lower strain in the membrane.

Actual strain in the membrane was measured for a series of static deflections of the lever arm to ensure that the device was imparting the expected strain levels. Strain was determined optically by tracking the membrane. An example of strain data is shown in Fig. 2 for two sets of markers placed 1 mm apart in the center of the membrane. Sets A & B are 20 and 40 mm, respectively, from the fixed end. Measured and expected strains are plotted, where expected strain is calculated from the deflections imparted to the lever arm by a dial caliper. Since the resolution of the optical system is very coarse for this application (strain resolution was limited to only ~0.35% corresponding to one pixel of motion), the data only serves to show that the correct trend is followed as the membrane elongation is increased.

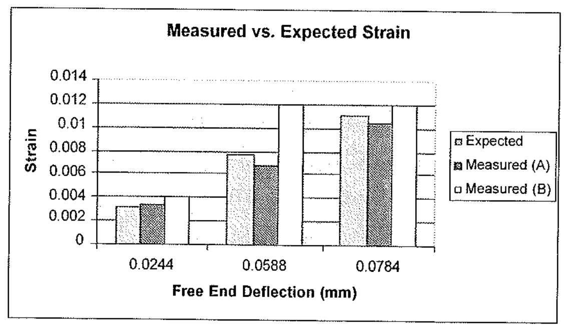

Figure 2. Strain in membrane for known lever arm deflections.

REFERENCES

Schaffer J.L. et al. (1994). "Device for the Application of a Dynamic Biaxially Uniform and Isotropic Strain to a Flexible Cell Culture Membrane", *Journal of Orthopaedic Research*, **12**, 709-719.

Tanaka, S. M. (1999). "A new mechanical stimulator for cultured bone cells using piezoelectric actuator," *Journal of Biomechanics*. **32**, 427-430.

Gender Differences in Knee Kinematics and Kinetics during Stair Climbing And Level Walking in Adults with Osteoarthritis of the Knee

C.A. Hughes, K.R. Kaufman, B.F. Morrey, M.A. Morrey and K.N. An
Orthopedic Biomechanics Laboratory, Mayo Clinic/Foundation, Rochester, Minnesota
Email: kaufman.kenton@mayo.edu

INTRODUCTION

Osteoarthritis (OA) of the knee is a common condition and a frequent cause of pain and disability in older people. Risk factors consistently associated with the disease in cross-sectional studies include older age, female gender, and being overweight. Symptoms of OA include pain, stiffness, and decreased range of motion of the joints. Female gender is a significant risk factor for OA. Felson et al. determined that women have a 1.8 times greater risk of developing OA than men. Adams and Marano concluded that arthritis is more prevalent among women than men at all ages, but the exact etiology for this difference in prevalence is unknown. These gender differences are most prominent when OA affects the knee. One of the common complaints of an individual suffering from OA of the knee joint is pain while climbing stairs. Therefore, this study was performed to quantify and compare gait characteristics of females and males with OA of the knee while walking on a level surface, and ascending and descending stairs.

METHODS

Knee kinematics and kinetics were measured during stair ascent, descent and level walking from 142 adults, 94 females and 48 males, diagnosed with Grade II osteoarthritis of the knee. Females had a mean age of 58 years and males 55 years. Mean weight of the females was 80 kg (±17), and the males 92 kg (±15). All of the OA subjects reported having pain in one or both knees on most days and showed radiographic signs of OA, including hypertrophic changes, marginal spur formation, subchondral sclerosis or cyst formation, or nonuniform joint space narrowing. A set of 24 reflective markers (Helen Hayes marker set) were placed on bony landmarks of each subject. A six camera ExpertVision system was used to collect 3-D marker trajectories at 60 Hz. Stairs consisted of four steps, each with a rise of 18 cm and a run of 25 cm. Handrails were not used by the subjects. A BERTEC force plate was positioned at ground level to measure initial reaction forces. The first and second stairs were independently attached to two separate KISTLER force plates. Kinetic data was collected during stair ascent and descent as previously described (Yu et al.). Joint moments were calculated using Orthotrak 4.0 gait analysis software (Motion Analysis Co, Santa Rosa, CA). Results were calculated from the average of three walking trials. The Shapiro-Wilk W test was used to determine the normality of the data within the subjects. If the data was normally distributed, a two sample t-test was used. If the data was not normally distributed, a Wilcoxon signed rank test was performed.

RESULTS AND DISCUSSION

During both stair ascent and descent, the female subjects (ascending 96.5°, descending 89.9°) had a 6 to 8 degree greater peak knee flexion angle than males (ascending 88.5°; descending 83.5°) ($p=0.001$, figure 1). The females (55.7°) also had a significantly greater peak knee flexion angle during level walking than men (51.6°)(p=.0159, figure 1). The difference in peak knee flexion is most likely due to a significant difference (p=0.001) in height between the female and male subjects. The female subjects had a mean height of 162 cm (±6) while the male subjects averaged 177 cm (±8). Similarly, the female subjects (0.24 Nm/Kg ±0.19) generated a greater maximum internal knee extension moment than men (0.18 Nm/Kg ±0.16) for all conditions, with only stair ascent demonstrating a significant difference (p=.0325, figure 2).

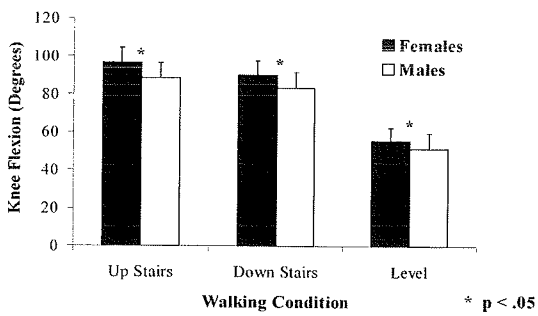

Figure 1: Maximum Knee Flexion Angle

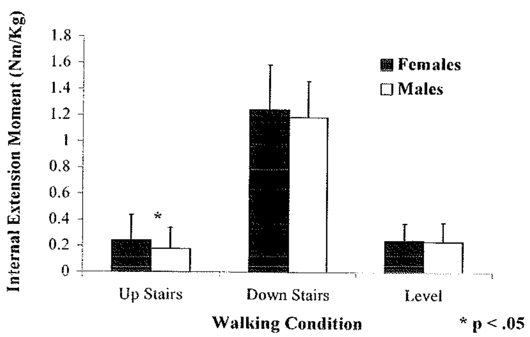

Figure 2: Maximum Internal Knee Extension Moment

SUMMARY

Gender differences are identified in the figures shown (Figures 1 and 2). This gender difference may partially explain the increased prevalence of osteoarthritis in females. Most tests of osteoarthritis treatments are assessed by criteria that do not reflect functional activities. This study demonstrates that quantified analysis of stair climbing can be used to document locomotor changes in patients with osteoarthritis. To better understand the effect of knee OA on activities of daily living, such as stair ascent and descent, it is important to examine the kinetics of the affected joint. This information may allow us to identify the potential biomechanical effects of OA of the knee. For all grades of radiographic severity of OA, more women than men report knee pain. Among those over age 60 years, women are twice as likely to have symptomatic arthritis than men. The female subjects with OA in this study needed to flex their knees to a significantly greater degree for all conditions of stair climbing and level walking. This resulted in a greater maximum internal knee extension moment being generated by the female subjects. This increased knee loading may be partially responsible for the increased prevalence of OA in females.

REFERENCES

Yu, B. et al. (1996). *J. Biomechanics*, **29**, 1625-1628.
Yu, B. et al. (1997). *Journal of Orthopaedic Research*, **15**, 348-352.
Felson, D.T. et al. (1997). *Arthritis & Rheumatism*, **40**, 728-733.
Adams, P.F. and Marano, M.A. (1995). *Vital & Health Statistics-Series10: Data From the National Health Survey*, **193**, 83-84.
Brandt, K.D. (1995). *Archives of Family Medicine*, **4**, 1057-1064.

ACKNOWLEDGEMENTS

Funding provided by American Home Products. The assistance of A. Walker, D. Hansen, B. Kotajarvi, D. Padgett and D. Morrow is greatly appreciated.

A RESPONSE SURFACE MODEL APPROACH TO PREDICT STRATEGIES FOR ADJUSTING JOINT STIFFNESS DURING LOCOMOTION

M.J. Kurz[1], J. Porter[1], and J.P.H. Steele[2]
[1]Peak Performance Technologies, Inc., Englewood, Colorado
[2] Colorado School of Mines, Golden, Colorado

INTRODUCTION

Response surface methodology (RSM) is a technique to explore the interaction of several response variables (Myers, 1992). RSM utilizes regression modeling to provide a conclusion for optimal interactions of the response variables of a system. The purpose of this study was to utilize response surface methodology to investigate joint stiffness strategies utilized by humans to accommodate leg stiffness while hopping.

REVIEW AND THEORY

Lower extremity strategies while running and hopping have been modeled using a simple spring-mass model (Farley et al., 1991; McMahan et al., 1990). Stiffness of the leg-spring system has been suggested as an indication of neuromuscular adaptations during locomotion. Stiffness of the leg-spring is dependent on the torsional stiffness of the individual joints that comprise the lower extremity. Farley et al. (1999) has suggested that ankle stiffness may be the primary mechanism for adjusting leg stiffness.

RSM attempts to find optimum interaction between response variables for a given system. RSM fits a complete second-order regression model to representative data to determine the interaction of the response variables. By evaluating the second partial derivatives of the fitted model, the behavior of the individual components of the system can be evaluated. Potentially, RSM may provide evidence of joint stiffness strategies utilized by the lower extremity during locomotion. In the present study we utilized a RSM to predict joint stiffness strategies while hopping.

PROCEDURES

Four healthy subjects (three males and one female; Height = 1.75 $\pm$ .06; Body mass = 63.6 $\pm$ 9.8) were instructed to perform continuous two-legged hopping for 20 seconds. Simultaneous, kinetic (600 Hz) and kinematic (120 Hz) data was collected for each condition: preferred hopping height, and maximal hopping height. A self-selected continuous hopping frequency was used for each condition. Ground reaction force data was generated via a force platform (AMTI, Inc., Newton, MA), and three-dimensional kinematic data were collected with four real-time cameras interfaced to a desktop computer (Peak Performance Technologies, Inc., Englewood, CO). Reflective markers were placed on the right lower extremity segments to establish local coordinate systems for the thigh, shank, and foot. Positional coordinates were smoothed using a Butterworth Low-pass Filter with a selective cut-off algorithm (Jackson, 1979). From the 20 seconds of continuous hopping data collected, 15 consecutive hops from each condition were selected for evaluation. Inverse dynamics were utilized to determine the joint moments at the hip, knee, and ankle. Kinematic and kinetic data calculated from each trial were normalized to 100 and 200 points respectively.

In order to normalize the peak vertical force values, the force data was represented as body weights. Leg stiffness (Kleg) was calculated from the ratio of peak body weight (PBW) to the leg compression (ΔL) during the contact phase (Figure 1).

$$Kleg = PBW / \Delta L \qquad (1).$$

Leg compression was equal to change in leg length from initial ground contact to maximal leg compression. Joint moments for each of the respective joints were normalized to body mass by dividing the joint moment by the subject's body mass. The stiffness at each joint (Kjoint) was determined by the ratio of the change in the joint moment (ΔMjoint) to the angular displacement ($\Delta\Theta$joint) from initial ground contact to maximal leg compression (Figure 2).

$$Kjoint = \Delta\, Mjoint / \Delta\Theta joint \qquad (2).$$

A least squares method was utilized to fit a complete second-order regression model to the respective data from all the subjects (120 trials total). To determine the joint stiffness strategies used while hopping, the second partial derivatives were calculated from the fitted regression model.

RESULTS

The coefficient of determination indicated that the fitted model was able to describe the interaction of joint stiffness at each of the respective joints well ($R^2 = .89$). Figure 3 details the fitted regression model, where Q= Kleg, x= ankle stiffness, y= knee stiffness, z= hip stiffness.

$$Q = .84x - 1.05y + .78z - .01xy - .01xz + .17zy + .007x^2 - .441y^2 - .011z^2 + 2.82 \qquad (3).$$

The slope values from the second partial derivatives of the ankle, knee, and hip joint stiffness were .014, -.881, and -.021 respectively. The response surface suggested that the behavior of the lower extremity is to minimize ankle joint stiffness, while maximizing knee and hip joint stiffness. Furthermore, the slope values indicate that knee stiffness is adjusted at a greater rate than at the other two joints.

DISCUSSION

The surface model suggests that adjustments in knee stiffness may be the strategy for adjustment of leg stiffness. Hip stiffness also increased but had less of an impact on total leg stiffness. The ankle had less joint stiffness. Potentially, the ankle joint may play a greater role in dissipation of energy during ground contact to prevent an injurous situation.

REFERENCES

Farley, et al. (1999). *JOB*, **32(3)**, 267-273.
Farley, et al. (1991)., *Am. J. Phys. Soc.* **71(6)**, 2127-2132.
Jackson, K.M. (1979). *IEEE Trans. Biomed. Eng.*, **26**:515-521.
McMahon, et al. (1990). *JOB*, **23**:65-78.
Myers, R.H. et al. (1992). *Stats*, **8**, 3-7.

Ground Reaction Force Variables as Predictors of Lower Extremity Shock in Forefoot and Rearfoot Strike Patterns

Carrie Laughton[1] and Irene McClay[1,2]

[1] Motion Analysis Lab, University of Delaware, Newark, Delaware
[2]Joyner Sportsmedicine Institute, Harrisburg, Pennsylvania
Email: laughton@udel.edu

INTRODUCTION

Ground reaction force (GRF) parameters have been used to predict tibial shock in rearfoot strike patterns (Hennig & Lafortune, 1991). However, forefoot strike (FFS) runners have significantly different GRF parameters when compared to rearfoot strike (RFS) runners (Williams, D.S., et al., in press). A typical FFS running pattern results in significantly lower vertical GRF loading rates (ZLR) and greater peak vertical GRFs (PZ) when compared to a RFS pattern. Force plate data is used as a way to indirectly measure both the magnitude and the rate of external loading on the lower extremity during running, while tibial acceleration attempts to measure the resulting shock to the lower leg which is directly influenced by GRFs. Predicting shock from GRF parameters would potentially eliminate the need for measuring tibial accelerations.

The relationships between selected GRF parameters and peak positive acceleration (PPA) have been previously investigated (Hennig & Lafortune, 1991; Hennig et al., 1993). These studies indicate that ZLR and PAP contribute significantly to skeletal shock in RFS runners. Due to differences in shock attenuating mechanisms between RFS and FFS patterns, the GRF components contributing the most to PPA may be different for the FFS pattern. Therefore, the purpose of this study is to investigate the relationships between selected GRF variables and PPA of a FFS pattern.

METHODS

Fifteen RFS runners with no lower extremity abnormalities or injuries will participate in this study. Thus far, GRF and tibial accelerometry data have been collected on six subjects during five running trials at a 3.7 m/s pace in both a FFS and RFS pattern.

The accelerometer (PCB Pieziotronics, Depew, NY), was protected by a machined aluminum casing and was mounted on a piece of lightweight thermoplastic material (3.28 g total weight) and was fastened to the leg in alignment with the longitudinal axis of the tibia on the distal, anteromedial aspect. This location was chosen to reduce the effects of angular accelerations resulting from rotational movement at the ankle. Elastikon (Johnson & Johnson) tape was tightly fastened around the leg and accelerometer to the subject's tolerance. A signal conditioner was strapped around the subject's waist with a belt.

A vertical GRF threshold of 10 N was used to determine heel strike and toe-off. GRF data were filtered at 50 Hz with a second order low pass Butterworth filter. All GRF variables were standardized to body weight. RFS pattern GRF vertical loading rates (ZLR), measured in body weights per second (bw/s), were determined from the time series GRF data as 20-80% of the amplitude from heel strike to the first peak (P1). FFS pattern ZLRs were determined as 20-80% of the amplitude to the average P1 in the RFS pattern. Braking load rates

(APLR) were determined as 20-80% of the slope to the first peak braking force (Fig 1).

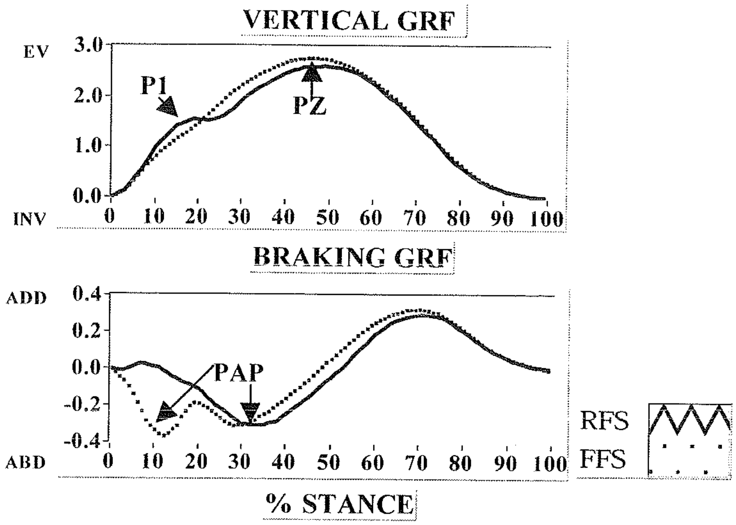

RESULTS and DISCUSSION

In general, PPA is higher in the RFS pattern as was ZLR. There were greater peak vertical GRFs (PZ), PAPs and braking load rates (APLR) in the FFS pattern (Table 1).

Table 1. Means for FFS and RFS

	FFS	RFS
PPA (g)	3.90 (1.92)	4.79 (1.82)
PZ (bw)	2.76 (0.21)	2.51 (0.27)
PZLR (bw/s)	34.75 (8.26)	50.99 (9.79)
PAP (bw)	0.36 (0.03)	0.35 (0.03)
APLR (bw/s)	17.83 (4.91)	6.33 (1.50)

In the FFS pattern PZ and ZLR are most highly correlated with PPA while ZLR and PAP are most highly correlated with PPA in the RFS pattern (Table 2). RFS GRF variables were not correlated with each other, while FFS pattern PAP and PZ were correlated with an r of 0.75.

Table 2. Correlations between peak tibial acceleration and selected GRF variables.

	FFS PPA	RFS PPA
PZ	0.72	0.01
ZLR	0.72	0.49
PAP	0.63	0.82
APLR	0.45	0.25

The two most highly correlated GRF variables to PPA were used to develop two separate regression equations to predict PPA for the RFS and the FFS pattern.

Figure 2: Forefoot Strike PPA (g) = -16.42 + 5.56 **PZ** (bw) + 0.14 **ZLR** (bw/s) **R^2 = .89**

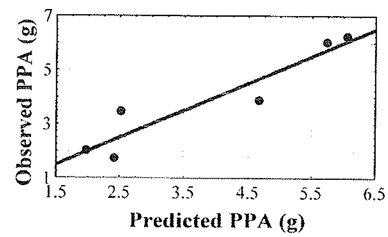

Figure 3: Rearfoot Strike PPA (g) = -16.31 + 49.70 **PAP** (bw) + 0.07 **ZLR** (bw/s) **R^2 = .84**

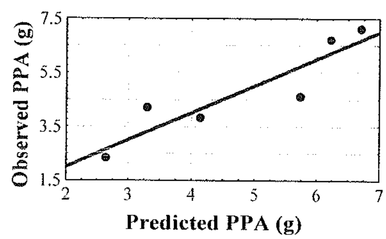

SUMMARY

The regression analysis for the RFS strike pattern in these preliminary data is consistent with previous findings that PPA can be predicted from ZLR and PAP (Hennig & Lafortune, 1991). However, in the FFS pattern, PPA was predicted using ZLR as well as PZ indicating that the GRF parameters contributing to tibial shock in FFS patterns are different from those of RFS patterns.

If peak accelerations can be accurately predicted using ground reaction forces, tibial accelerometry can be replaced by simpler methods of ground reaction force data collection.

REFERENCES

Hennig, E.M. et al. (1993). *J. Applied Biomech.* **9**, 306-314.

Hennig, E.M., & Lafortune, M.A., (1991). *Int. J. Sport Biomech.* 7, 303-309.

Williams, D.S., et al. (in press). *J. Applied Biomech.*

FOOT FORCE PATH LINEARITY IN THE FRONTAL-PLANE DURING PUSHES ON STATIONARY AND MOVING PEDALS

Kreg G. Gruben[1,2] and Citlali López-Ortiz[1]

Departments of Kinesiology[1], Mechanical Engineering[2], and Biomedical Engineering[2]
University of Wisconsin-Madison, Madison, Wisconsin
Email: gruben@education.wisc.edu

INTRODUCTION

The seat and pedal kinematically constrain lower limb motion during cycling such that the force of the foot on the pedal (foot force) can change its orientation through a wide range and still accomplish the objective of performing net work on the crank. Despite this latitude in force orientation, it has been shown that when humans push in the 'most comfortable manner' on a stationary or moving pedal, force orientation is tightly coupled to force magnitude (Gruben & López-Ortiz 2000). This coupling results in the head of the foot force vector tracing a straight line in the sagittal-plane. Thus, without a directional target, humans prefer to generate increases in sagittal-plane foot force through the addition of force vectors with invariant direction. These results prompted us to investigate frontal-plane foot force in order to evaluate the applicability of this mechanism to the control of three-dimensional foot force.

During kinematically constrained limb motion the forces exerted by the limb on its environment result from intersegmental joint moments, gravity, and limb dynamics (segmental masses and accelerations). Use of foot force to study motor control requires separating the effects of joint moments from the effects of gravity and limb accelerations. We can accomplish this separation by having subjects push against a stationary or pedal moving at a constant speed. In the stationary case the effect of acceleration is small and the effect of gravity is constant. In the dynamic pedaling case, if pedal speed is constant then every time the pedal passes through a specific position, the limb's posture and acceleration should be the same. Thus, changes in foot force reflect only changes in joint moments due to muscular forces. Using this technique, we can empirically determine the effect of neural control on foot force during both stationary and moving pedal conditions.

METHODS

Seated healthy human subjects (n = 11) pushed against a stationary pedal and pedaled a cycle ergometer at constant angular velocities of 10, 20, 40, and 60 rpm. Crank velocity was regulated with a feedback controlled motor. A pedal, instrumented to measure three axes of force, provided measurements of the frontal-plane components of the right foot force ($F_{medial\text{-}lateral}$, $F_{vertical}$). Digital encoders measured pedal and crank angles. All data was digitized at 200 Hz and stored on magnetic disk.

During stationary pushes the crank angle (θ_{crank}) was locked at 60, 30, 0, -30, -60° (θ_{crank}=0° corresponds to the middle of the down-stroke). These same angles are analyzed for the moving pedaling condition. For both stationary and moving conditions the subject attempted to match peak force magnitude to a target level using graphical visual feedback. For the moving pedal condition, the force magnitude target was only reached briefly during the pedal down-stroke. The target force level was sequentially set to 10 values (200, 250, 300, ..., 650 N) in random order. At each target force value, 3 s of data were acquired once the subject was comfortable achieving the target force (±10%). Foot force path in the frontal-plane was evaluated for linearity by propagating empirically-determined measurement error and considering pushes with < 2% curvature to be linear (see Gruben & López-Ortiz 2000). Force path orientation was determined using principal component analysis.

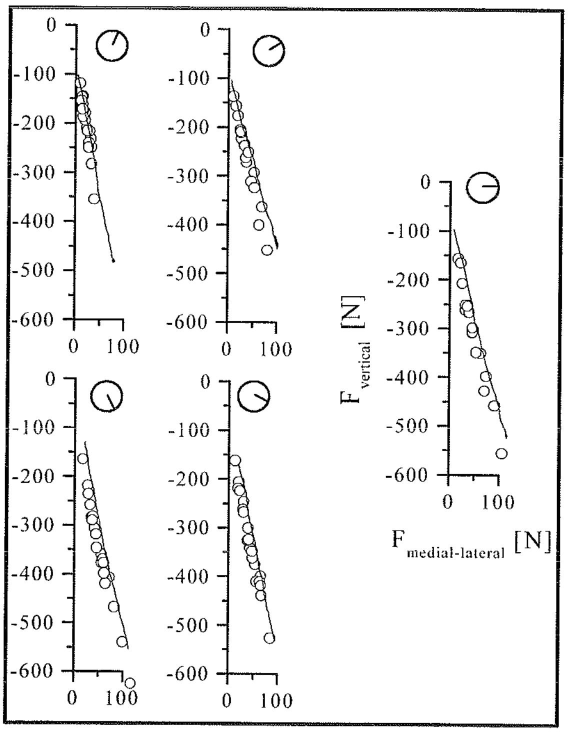

Figure 1 Sample data of frontal-plane force paths for a single subject. Each panel represents the data for a specific pedal axis location as indicated at the top of each panel. The crank rotated clockwise. $F_{medial\text{-}lateral}$ is positive in the lateral direction. Force path data for a single push against a stationary pedal is shown by the line in each panel. A force path constructed from a set of pushes against a moving pedal (40 rpm) is shown by the circles in each panel.

RESULTS and DISCUSSION

The relationship between $F_{medial\text{-}lateral}$ and $F_{vertical}$ was linear for 99% (544 of 550) of the stationary pedal pushes and 79% (171 of 216) of the moving pedal conditions (Fig. 1). The increased non-linearity for the moving pedal condition is likely due to these force paths being constructed from force generated during a series of pushes and thus includes some variability across push efforts that is not present in the stationary pedal push linearity assessment.

At a given pedal axis position, the orientation of the force paths is similar across pedal motion conditions (parallel nature of data in Fig. 1). This suggests that a similar motor control strategy may be used to generate increases in foot force despite the differences in muscle shortening velocities and limb dynamics. Offset between the force paths of Fig. 1 is due to inertial effects present in the moving but not stationary pedal conditions.

SUMMARY

Humans generate increases in three-dimensional foot force through the addition of directionally invariant force vectors. This requires precise coordination of force in several muscles and suggests that three-dimensional foot force path linearity is an invariant characteristic of motor control.

REFERENCES

Gruben, K.G., López-Ortiz, C. (2000). *J. Motor Behavior*, in press.

Gruben, K.G. (1999). *Proceedings of Progress in Motor Control II*, 84-85.

AKNOWLEDGEMENTS

This work was supported in part by the Virginia Horne Henry Fund for Women's Physical Education Issues.

PATELLOFEMORAL JOINT STRESS DURING STAIR ASCENT AND DESCENT: A COMPARISON OF PERSONS WITH AND WITHOUT PATELLOFEMORAL PAIN

J.G. Heino Brechter[1,2], Christopher M. Powers[1]

[1]**Department of Biokinesiology and Physical Therapy, University of Southern California, Los Angeles, California**

[2]**Department of Physical Therapy, Chapman University, Orange, California**

Email: brechter@chapman.edu

INTRODUCTION

Patellofemoral pain (PFP) is one of the most common knee disorders encountered in clincical practice. Patients with PFP typically complain of retropatellar pain that is aggravated by activities such as stair ascent and descent, running, and squatting. Although the cause of patellofemoral joint pathology is believed to be related to elevated joint stress (force per unit area), this hypothesis has not been adequately tested. Using an individualized biomechanical model of the patellofemoral joint which takes into consideration the inherent variability in patellofemoral joint contact area between individuals, the purpose of this study was to compare joint kinetics and patellofemoral joint stress (PFJS) in persons with PFP and pain-free controls during stair ascent and descent. It was hypothesized that subjects with PFP would demonstrate increased PFJS compared to a control group.

METHODS

Ten subjects with a diagnosis of PFP and ten pain-free individuals participated in this study. Lower extremity kinematics (Vicon) were obtained as subjects ascended and descended a portable four step staircase at a self-selected velocity. A raised forceplate (AMTI) permitted the collection of ground reaction forces from the first step. Kinematic and kinetic data were collected simultaneously.

Individualized patellofemoral joint contact area was obtained at multiple knee flexion angles using a previoulsy described MRI technique.(Heino et al., 1999) The knee joint angle and knee extensor moment (inverse dynamics approach) obtained during stair ambulation were used as input variables into a biomechanical model, (Heino & Powers, 1999) which was used to derive patellofemoral joint reaction force (PFJRF). PFJS was then calculated as the PFJRF/patellofemoral joint contact area and reported as a function of the stance phase of gait. Independent t-tests using trimmed means were used to compare walking velocity, peak knee extensor moment, peak PFJRF, PFJRF-time integral, peak PFJS, PFJS-time integral, and utilized patellofemoral joint contact area between groups.

RESULTS AND DISCUSSION

During stair ascent and descent, there were no significant differences peak PFJS, stress-time integral, or average utilized contact area between groups (Figs. 1-2). During stair ascent however, the PFP subjects demonstrated significantly lower peak knee extensor moments (0.805 vs. 1.16 Nm /kg; p=.04), peak PFJRF's (24.98 vs. 37.31 N/kg; p=.02; Fig.2), PFJRF-time integral (288.2 vs. 501.9 N/kg; p=.01; Fig. 2) compared to the controls. The same trend was observed during stair descent, however there were no statistically significant differences in these variables.

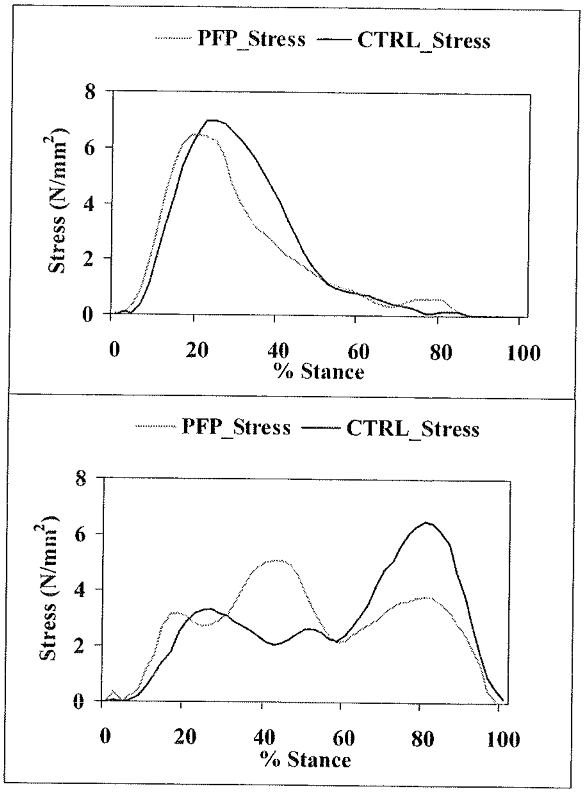

Figure 1. Mean patellofemoral joint stress in subjects with PFP and control subjects during stair ascent (top) and stair descent (bottom).

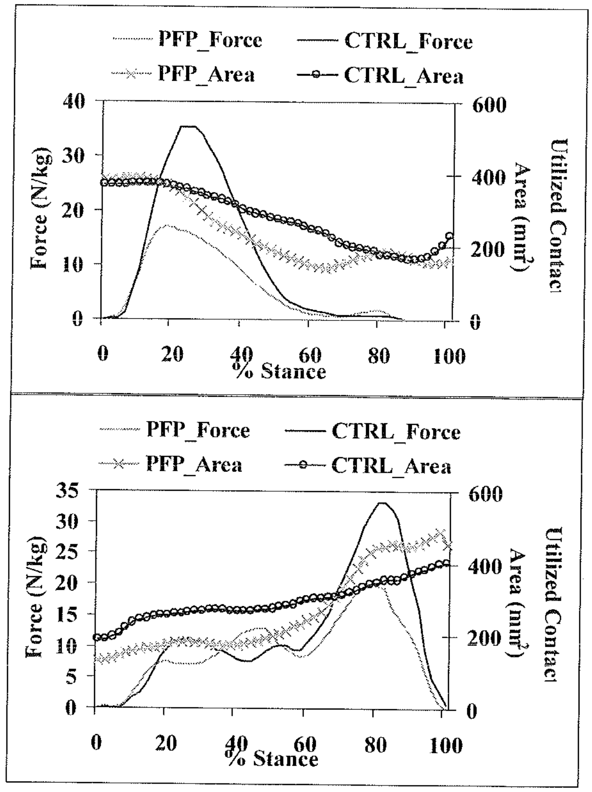

Figure 2. Mean patellofemoral joint reaction force and utilized contact area in subjects with PFP and control subjects during stair ascent (top) and stair descent (bottom).

The results of this study do not support the hypothesis that individuals with PFP exhibit excessive PFJS during stair ambulation. Joint stress in the PFP group appeared to be modulated through a reduction in the knee extensor moment and the PFJRF. The reduction in the knee extensor moment and PFJRF was likely the result of a slower velocity which was evident in the PFP group during both stair ascent (1.48 vs.1.98 m/min; p=.04) and stair descent (1.52 vs. 2.57 m/min; p=.008).

SUMMARY

1. Individuals with PFP did not exhibit excessive PFJS during stair ambulation.
2. The reduction in the knee extensor moments and PFJRF's in the PFP group appeared to be a compensatory strategy aimed at keeping joint stress within acceptable limits. This was accomplished through a reduced walking speed.

REFERENCES

Heino et al.(1999), *Trans ORS.*

Heino & Powers, (1999), *Gait & Posture*, 8(2).

ACKNOWLEDGEMENTS

This work was supported in part by the Foundation for Physical Therapy.

INCREASED VENTILATION AND INJURY HISTORY APPEAR TO MODULATE SPINE STABILITY

S.G. Grenier, R.A. Preuss and S.M. McGill
Spine Biomechanics Lab, Dept. of Kinesiology, University of Waterloo, Waterloo, Ontario
Email: sggrenie@ahsmail.uwaterloo.ca

INTRODUCTION

Spine stiffness, and subsequent stability, during isometric holds is dependent upon symmetric and stable muscle activation levels (Cholewicki & McGill, 1996). In addition, during challenged breathing, the same muscles that create stability are used to assist in lung ventilation (McGill et al. 1995). A related phenomenon has been reported in monitor lizards, where the same muscles used to breathe, assist in lateral movement of the spine for running (Owerkowicz et al., 1999). Ventilation takes precedence over running speed and therefore is a limiting factor. Humans use the diaphragm to breathe together with the abdominals if necessary, but does ventilation take precedence over spine stability? It was hypothesized that those subjects with a prior history of spine troubles would be more likely to exhibit anomalous motor patterns in those muscles involved in achieving both spine stability and ventilation.

METHODS

Workers from physically demanding jobs (n=51) volunteered for this study. Their current spine health was documented together with their prior history for disabling spine troubles (sufficient for work absence).

EMG was recorded bilaterally at three different sites. Pairs of Ag Ag-Cl surface electrodes were placed 3 cm apart, center to center, over rectus abdominis (RA, 3 cm lateral to the umbilicus), external oblique (EO, 15 cm lateral to the umbilicus), and internal oblique (IO, halfway between the anterior iliac spine and the midline, just superior to the inguinal ligament. The EMG signals were A/D converted via a 12 bit, 16 channel A/D board, full wave rectified and low pass filtered (Butterworth - cutoff at 2.5 Hz). Signals were normalized to the subject's MVC effort at each muscle site. An ultrasonic flow meter, in-line with the mouthpiece, recorded ventilation variables.

Subjects performed two weight holding trials (22 kg); one of 60 sec duration while breathing ambient air and the other of 70 sec while breathing 10% CO_2. Their flexed trunks were held at 30^0 from vertical and their feet were stationary, shoulder width apart. On average this resulted in a compressive load on the L4/L5 joint of 2730N, well below the NIOSH action limit. The linear enveloped EMG from the abdominal muscles were evaluated for anomalous patterns.

RESULTS

Of 51 subjects, 11 showed an anomalous abdominal motor pattern. Of those eleven, eight reported having had work disabling back pain. Fisher's exact test confirmed a link between prior injury history and anomalous motor patterns in the back stabilizing musculature (P=0.056). One of the 3 that had not reported any pain was a 21 year old apprentice with six months experience. Another is a 25 year veteran who had reported back pain but which was not work disabling.
Motor anomalies were only observed in either the external or internal oblique muscles. Most showed a pattern of entrainment with ventilation but some showed dramatic asymmetries between right and left muscle pairs while others instead

showed evidence of panicked breathing and erratic abdominal activation.

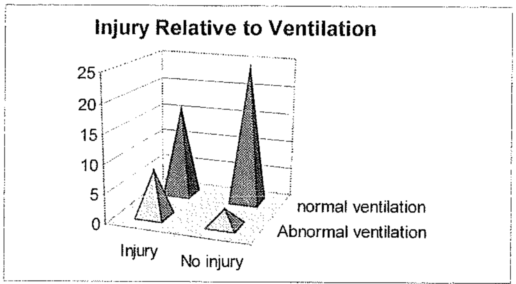

Figure 1: Those who exhibited motor anomalies were more likely to have a history of disabling low back troubles.

DISCUSSION

Although this initial investigation was not designed for statistical rigor, it appears that those with a previous injury history are more prone to experiencing inappropriate muscle activation to maintain sufficient spine stability. Cholewicki and McGill's (1996) analysis leads us to suspect that these anomalous motor patterns increase the risk of spine instability along with risk of injury. It is interesting to note that these anomalous motor patterns emerge even with light loads, as this phenomenon has been reported before with much heavier hand held loads (McGill et al. 1995).

Abdominal muscles appear to be important for achieving sufficient spine stability. Gardner-Morse and Stokes (1998) report that abdominal antagonistic co-activation increases spine stability. EO has the greatest effect but at the expense of increased muscle fatigue. IO was a more efficient stabilizer in their model. However, our data suggests that IO and/or EO also assist ventilation in abnormal subjects (even during light tasks), leading to increased risk due to muscle fatigue. In normal individuals IO and EO were activated at levels of 3% of MVC, or less, for the task. Cholewicki and McGill (1996) suggest this may be enough to stabilize the spine.

Hodges et al. (1997) report that the latency response of the abdominal muscles is affected by their respiratory activity. The response time is less when the muscle is prepared for expiration. This implies that in people who must use this muscle to breathe the risk of injury increases while inspiring, when the muscle may not be active.

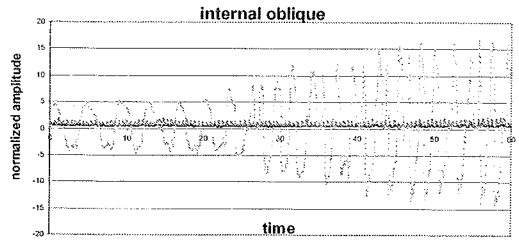

Figure 2: Despite the obvious increase in ventilation amplitude and frequency there is no evidence of entrainment in this normal subject's internal oblique.

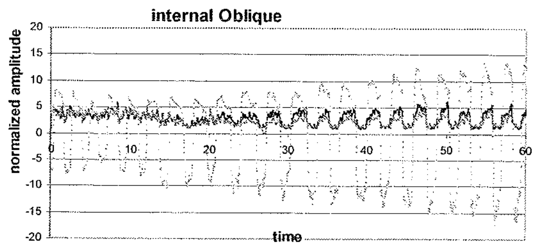

Figure 3: The entrainment of internal oblique with the ventilation is evident following the transition from normal to challenged breathing. Anomalous patterns are seen during the transition.

Given that 73% of those with anomalous abdominal recruitment had a history of back troubles, the question arises; does the motor control anomaly lead to injury or does the compromised motor response result from injury? A longitudinal is underway to assess this question.

Acknowledgement: Funding for this project was provided by the Worker Safety and Insurance Board of Ontario.

References:
Gardner-Morse & Stokes (1998). *Spine*, **23**(1):86-92.
Hodges et al. (1997). *J. Appl. Phys.*, **83**(3):753.
McGill et al. (1995). *Ergonomics*, **39**(9):1772.
McGill & Cholewicki (1996). *Clin. Biomech.*, **11**(1):1-15.
Owerkowicz et al. (1999). *Science*. **284**:1661.

Effects of Body Mass Index on Seat Interface Pressures of Elderly that were Institutionalized

Thomas W. Kernozek[1,2], Alissa Amundson[1], Jennifer Hummer[1], Patricia Wilder[1]
[1]Physical Therapy Department, University of Wisconsin – La Crosse, La Crosse, WI
[2]Gundersen Lutheran Sports Medicine, La Crosse, WI
E-mail: kernozek.thom@uwlax.edu

INTRODUCTION

Over 600,000 elderly individuals in nursing homes that are regular wheelchair users (Redford, 1993). Brandeis et al. (1990) reported that 17.4 % of patients had pressure ulcers upon admission to a nursing home. Ulcer development within the first year after admittance was 9.5-13.2 % and by two years was 20.4-21.6%. There was greater re-hospitalization rate and death rate of residents that developed a pressure ulcer after their admission. The ischial tuberosities constituted 15% of the overall ulcer locations, while the most common site for pressure ulcer development was under the sacrum or coccyx with prolonged bed rest (Smith, 1995)

Multiple factors influence the development of pressure ulcers and there is no consensus as to the primary predisposing factors (Pang & Wong, 1998). However, several studies indicate that pressure, shear, friction, and moisture as the four main causative factors, with the magnitude and duration of pressure as the key factor among these four (Smith, 1995; Pang & Wong, 1998). Intervention efforts that have attempted to decrease the seat interface pressures of the elderly that have been institutionalized, but few objective criteria identify individuals with increased seat interface pressures. Due to the relationship between peak pressure and pressure ulcer development, it may be important to provide objective characteristics of those with high peak seat interface pressures. Garber and Krouskop (1982) was the only investigation that examined the effects of body build on seat interface pressures. The majority of participants in this study had spinal cord injuries, all with a history of pressure ulcers. Participants were divided into three categories: thin (< 90% ideal body weight), average, and obese (>110% ideal body weight). There was a trend between body build and peak seat interface pressures. Greater peak seat interface pressures were reported under the bony prominences among the thin population compared to those classified as obese.

The purpose of this study was to determine if there were differences in peak seat interface pressures of elderly who are institutionalized elderly based on their body mass index (BMI).

METHODS

Seventy five individuals aged 65-95 residing in several skilled nursing facilities in small urban area volunteered to participate. Residents whose primary diagnosis was CVA or lower extremity amputation were excluded secondary to the likelihood of producing asymmetrical peak seat interface pressures. Residents who were no longer responsible for their own health care decisions were excluded. Each participant's age, gender, body weight, and height were obtained from their current medical chart.

The Novel Pliance™ seat pressure-mapping system was used to collect seat interface pressure data. This system comprises 1024, 1.5 cm^2 capacitive sensors, enclosed in a flexible mat that is 2mm thick. This pressure mat was connected analog to digital electronics and interfaced to a personal computer. The system contains an 8-bit analog to digital converter and sensor data was captured at 15 Hz. Weekly, the sensor mat was checked for accuracy in a pressure chamber. If sensor readings were inaccurate by greater that $\pm$ 1 kPa the sensor mat was recalibrated.

The pressure mat was placed in a standard folding wheelchair with a sling-type seat. Participants were asked to sit with their hands resting in their lap (not on the armrests), sitting as far back in the wheelchair as comfortable with both feet resting on the footrests. Footrests were adjusted to position the femur parallel to the floor. Seat interface pressures were collected for 30 seconds. Test-retest reliability of peak seat interface pressures of a group of 10 residents yielded an intraclass correlation coefficient of 0.84. This reliability reflects the reproducibility of the participant positioning as well as the peak seat interface pressure measurements. BMI was calculated by dividing the residents body weight in kilograms by their height in meters squared (Kenney et al., 1995). BMI values were classified by the ACSM as follows: 20-24.9 kg/m^2—desirable range for adult men and women, 25-29.9 kg/m^2—grade 1 obesity, 30-39.9 kg/m^2—grade 2 obesity, and > 40 kg/m^2—grade 3 obesity (morbid obesity). A thin category was added to the BMI groupings by the investigators. This was defined as a BMI value of less than 20 kg/m^2. No data from residents in the grade 3 obesity category were obtained.

A one-way ANOVA ($p<0.05$) was used to compare peak seat interface pressures between the BMI groups (thin, desirable range, grade 1 obesity, and grade 2 obesity). Pair wise, post- hoc comparisons were performed using the Bonferoni procedure.

RESULTS

Peak seat interface pressures were different based on BMI groups ($p=0.00$). Post- hoc comparisons demonstrated differences in peak seat interface pressures between the thin, desirable range, grade 1 obesity, and grade 2 obesity groups (p=0.00, p=0.00, p=0.00, p=0.00, respectively). Differences in peak seat interface pressures diminished as BMI increased (see Figure 1). Peak seat interface pressures were different between the desirable range and the thin group (p=0.00) but no differences were between the desirable range and other groups. Differences in peak seat interface pressures were found between the grade 1 obesity and the thin group (p=0.00) but no other differences between other groups. Peak seat interface pressures were different between the grade 2 obesity group and the thin group (p=0.00) with no other differences between other groups.

DISCUSSION

Peak seat interface pressures were greatest in the thin elderly group with the lowest BMI of the groups examined. Differences in peak seat interface pressures were less as the BMI increased. Garber and Krouskop (1982) reported a similar relationship between body build and peak seat interface pressure in individuals with spinal cord injuries. The relationship between body build and peak seat interface pressures is further supported by the differences in BMI and peak seat interface pressures in the present study. An explanation for these findings may be the reduction in subcutaneous tissue. This may result in the bony prominences being less protected against localized loads (Shannon & Lehman, 1996; Maklebust, 1997).

REFERENCES

1. Redford JB. *Arch Phys Med Rehabil* 1993;74:877-85.
2. Smith DM. *Ann Intern Med* 1995; 123: 433-442.
3. Brandeis GH, Morris JN, Nash DJ, Lipsitz LA. *JAMA* 1990;264:2905-9.
4. Pang SM, Wong TK. *Nursing Research* 1998;47(3):147-53.
5. Maklebust J. *Geriatric Nurs* 1997;18:250-4.
6. Shannon ML, Lehman CA. *Critical Care Nursing Clin North Am* 1996;8(1):17-28.
7. Garber SL, Krouskop TA. *Arch Phys Med Rehabil* 1982;63:17-20.

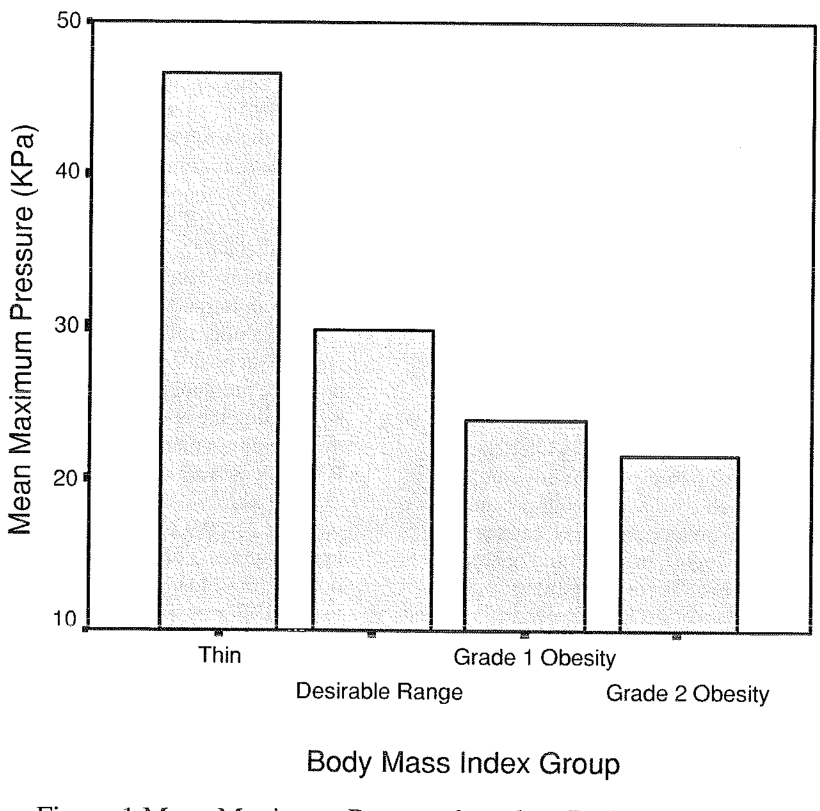

Figure 1 Mean Maximum Pressure based on Body Mass Index

MECHANICS OF SELF INJURIOUS BEHAVIOR IN PROFOUNDLY RETARDED ADULTS

Rhonda L. Boros[1], James W. Bodfish[3], Karl M. Newell[2], and John H. Challis[1]

[1]Biomechanics Laboratory, [2]Department of Kinesiology, The Pennsylvania State University, University Park, Pennsylvania
[3]Western Carolina Center, Morganton, North Carolina
Email: rlb248@psu.edu

INTRODUCTION

Self-injurious behavior (SIB) is a potentially harmful characteristic observed in a portion of the mentally retarded population. SIB has been studied for many years, drawing attention to the severe implications for the patients, family, and direct care givers. Not only is SIB a severe emotional and care task for the family and caregivers, but treatment and pharmaceutical options are very expensive. Estimates of over $100,000 a year per case, and over $3.5 billion nationally have been made (NIH, 1991). Several psychological theories have been proposed to explain SIB, yet no single or compound factor has been identified as making a direct contribution to SIB.

Behavior characterization of SIB has relied on assessment of the frequency of self-injurious occurrences, and the general nature of the injury (blows to face, pinches to arms, scratching of face, etc.). Direct estimates of the impact forces, as yet, have not been made. The purpose of this study was to utilize inverse dynamics to assess the impact forces realized by profoundly retarded SIB patients demonstrating blows to the head.

PROCEDURES

SIB patients are routinely videotaped as part of their normal monitoring; SIB trials were selected from available tape. Videotaped trials from three profoundly retarded patients were selected based on: 1) observed repeated blows to the head, 2) length of the repetitive SIB trial sequence (> 2 blows), and 3) potential for available data for both single and double arm blows. Subject details are presented in table 1.

The movements recorded on the videotapes were manually digitized using a Peak Motus digitizing system. A number of body landmarks were used to define body segment locations. A three-segment rigid body kinematic chain was used to represent the arm and hand. Points digitized on the head permitted determination of head kinematics. Body segment inertial parameters were determined using the equations of Zatsiorsky et al., (1990). Data were filtered and differentiated using the procedure of Challis (1999). The principle of conservation of momentum was used to estimate mean impact forces of the hand on the head. This approach avoided the need to calculate second derivatives, which are inherently noisy. Comparing video-derived estimates of mean impact forces with those measured using a load cell (Newell et al., 1998) served as validation of this approach. Mean forces were estimated to within 10% using this approach. The directly measured forces implied that peak forces were at least twice as large as the mean forces, although peak forces were not directly observable in this study.

RESULTS

Mean impact forces of over 200 N were observed in this study. Results indicated a high degree of variation in the impact forces both between subjects and for consecutive blows from the same subject. Summary data for impact forces are presented in Table 1. Table 2 compares peak impact forces of SIB with those of boxing.

Table 1: Impact forces of the repeat trials and mean (SD) impact force values for SIB subjects.

Subj.	Age (y)	Height (m)	Mass (kg)	Maximum Force (N)	Mean (SD) Force (N)
1	37	1.37	60.8	202.0	81.6 (70.8)
2	44	1.63	45.4	220.6	100.4 (62.1)
3	44	1.73	77.6	69.6	38.3 (22.5)

Table 2: Estimated peak impact forces for SIB subjects and boxing.

Condition	Peak Impact Force (N) as % body mass	Source
Subject 1	67.8	Present study
Subject 2	99.0	Present study
Subject 3	18.2	Present study
Boxing Jab	54-88	Hodgson
Boxing Cross	76-118	Hodgson
Boxing Max	300	Hodgson
Heavyweight Boxing Max	397.5	Atha, et al.

DISCUSSION

The SIB subjects showed large variations in the mean impact force between trials. Comparison of the forces produced by these subjects with those produced by boxers demonstrated that the peak impact forces normalized with respect to body mass were low. These low forces should be considered in the context that the SIB patients without restraint can have spells when they strike themselves upwards of 30 times in a minute. Although one blow may not be sufficient to cause much damage the repetitive nature of the impacts can lead to cumulative stress (Hof et al., 1991).

Results of this study indicated that SIB patients might be causing brain injury by repeated blows to the head. Methods utilized in this study are practical in that interference with subject movement was minimized. Researchers in the area have sought a quantitative and reliable measure of the force of impact of SIB.

REFERENCES

Atha, J., et al. (1985). *Br. Med. J.*, **291**, 1756-1757.

Challis, J.H. (1999). *J. Applied Biomechanics*, **15**, 303-317.

Hodgson, V.R. (1987). *Report to USA Amateur Boxing Federation, Inc.*

Hof, P.R., et al. (1991) *Acta Neuropathol.* **82**, 321-326.

National Institutes of Health (1989). *Treatment of destructive behaviors.* Beshesda, MD.

Newell, K.M., et al. (1998). *Am. J. Ment. Retard.*, **104**, 11-21.

Zatsiorsky, V.M., et al. (1990). In *Biomechanics on human movement: Applications in rehabilitation, sports and ergonomics*, pp. 186-202. Bertec Corporation.

PRELIMINARY EVALUATION OF A SHOULDER CAPSULAR STRETCHING BRACE FOR ADHESIVE CAPSULITIS

Paula M. Ludewig,[1] Donald D. Anderson,[2] and Carlos A. Guanche[2]

[1] Dept. of Physical Medicine & Rehabilitation, University of Minnesota, Minneapolis, MN
[2] Biomechanics Laboratory, Minneapolis Sports Medicine Center, Minneapolis, MN
Email: danders6@fairview.org Web: www.msmc.org

INTRODUCTION

Adhesive capsulitis is a disabling condition marked by shoulder pain and extreme limitations in shoulder motion. Patients are often unable to perform basic activities of daily living. A number of treatments have been proposed, ranging from physical therapy to open surgical release, but none has been shown to greatly influence the rate of recovery of range of motion and strength.

A shoulder capsular stretching brace based on the idea that extended gradual stretching will accelerate recovery compared to limited duration, more aggressive stretching has been built. The brace allows a number of arm positions to be maintained for extended periods of time. The weight of the brace plus arm are focused on stretching the capsule. A patient is intended to wear the brace for a period of time each day while carrying out some simple stretching exercises.

This pilot study tests the hypothesis that the shoulder capsular stretching brace, worn in a prescribed protocol, results in greater range of motion after it is worn than before.

MATERIALS AND METHODS

Five adhesive capsulitis patients have been evaluated to date. Before patients received any prescribed physical therapy, the experimental brace was worn as tolerated up to 30 minutes in the laboratory. Active range of motion was assessed in subjects before and after brace-wearing using a magnetic tracking technique which measures dynamic three-dimensional position and orientation of the humerus relative to the scapula and relative to the thorax across a range of functional shoulder positions (An et al., 1988; Ludewig et al., 1996). The accuracy of the specific technique used has been well characterized previously (Ludewig, 2000).

While subjects stood with their arms relaxed at their side, anatomical landmarks were palpated and digitized. This allowed transfer of data from a local sensor coordinate system to anatomic based reference frames for describing clinically relevant motions of the humerus. All subjects were tested for motion of the arm relative to the trunk and relative to the scapula for a minimum of 3 trials before and after wearing and exercising in the shoulder stretching brace. Motions included abduction (Abd); forward flexion (Flex); scapular plane abduction (Sab); external rotation with the arm in 0° of abduction (ER/0); and external rotation (ER/90) and internal rotation (IR/90) with the arm in 90° of abduction.

Each plane of motion was considered separately. As the data have been collected from a small sample size, statistical analyses have not yet been performed.

Each patient was asked to subjectively evaluate their shoulder pain. Pain ratings are represented on a 0-10 scale with 0 being no pain and 10 being the most pain imaginable.

Subjects rated their pain at rest and when abducting their arm before wearing the brace, immediately after wearing the brace, and ~48 hours after wearing the brace.

RESULTS AND DISCUSSION

Changes in humeral motion relative to the scapula (+ = increased, - = decreased) after a single brace wearing are shown in Figure 1. Peak (highest obtained) range of motion values across 3 trials are compared pre and post-brace. Only differences of $\geq 5°$ are considered meaningful. The most consistent motion improvements were internal rotation and scapular plane abduction. Three of five subjects showed total changes across motions of 15° or more. The remaining two had less positive changes and some motions showing decreases after wearing the brace.

All subjects reported decreased pain either immediately after or ~48 hours after bracing. The average rest pain was 2.3/10 before, 1.5 immediately after, and 0.8 ~48 hours after bracing. The average pain with abduction was 6.7/10 before, 5 immediately after, and 4.1 ~ 48 hours after bracing. No subjects reported any adverse effects.

Limitations of this study include the small sample size and lack of a control group. Future testing will involve a larger sample size and statistical analysis.

REFERENCES

An, K.N. et al. (1988). *J. Biomechanics*, **21**:613-20.

Ludewig, P.M. et al. (1996). *J. Orthopaedic & Sports Physical Therapy*, **24**:57-65.

Ludewig, P.M. (2000). *Physical Therapy*, **80(3)**, In Press.

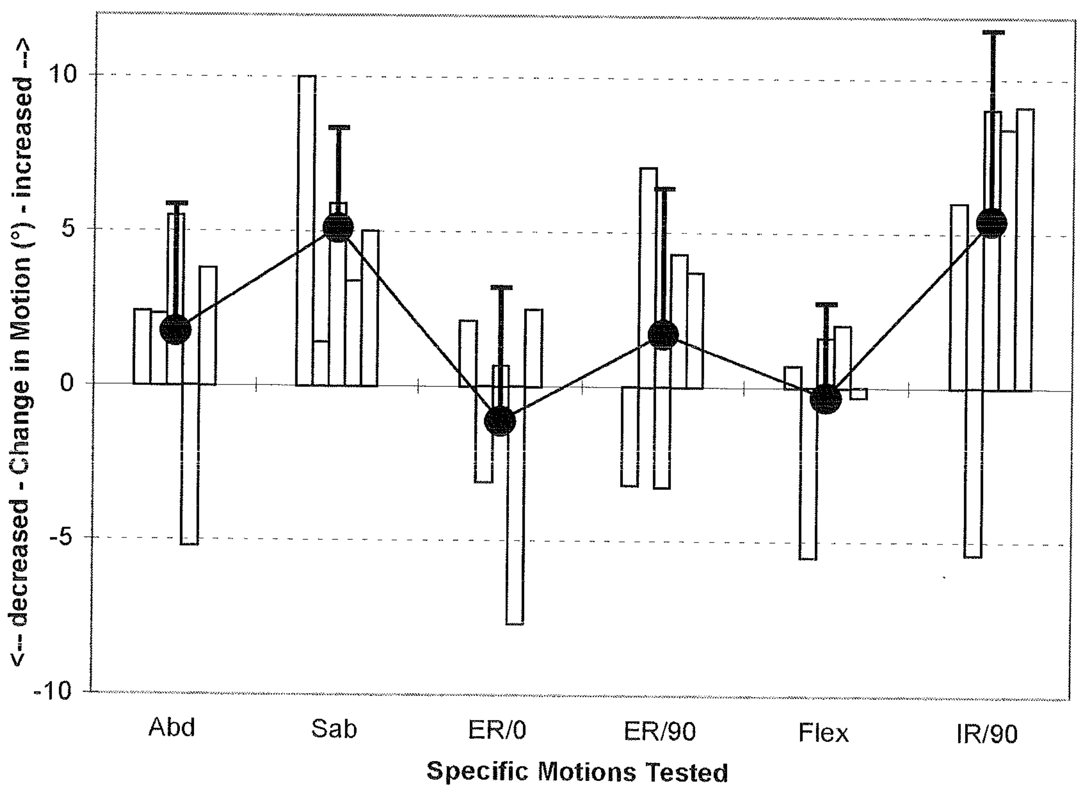

Figure 1. Peak to peak changes in motion after wearing the brace. Columns show individual data; a line connects averages across 5 subjects, with error bar showing standard deviation.

DETERMINATION OF KINEMATICS OF THE UPPER EXTREMITY.

George Rab M.D., Kyria Petuskey, M.S., Anita Bagley, Ph.D.

Motion Analysis Laboratory, Shriners Hospitals for Children, Northern California, Sacramento, California, U.S.A.

E-Mail: abagley@shrinenet.org

Introduction

Technical and conceptual issues make measurements of 3D upper limb motion difficult to collect and interpret. Modeling of the wrist and elbow can be simplified using two degree-of-freedom joints. The shoulder complex, however, has two separate articulations, scapulothoracic and glenohumeral, and a simple, non-invasive way of locating the scapula is lacking. We suggest that measurement of upper arm position relative to the trunk is a practical approach to model shoulder motion.

There is no consensus on local coordinate systems or on the sequence of movement to describe upper limb position. We describe a 3D system of upper extremity analysis utilizing retroreflective skin markers that follows philosophical and computational principles borrowed from lower extremity kinematic analysis. Its advantages are ease of use, reproducibility, and familiarity to clinicians.

Materials and Methods

The biomechanical model consists of ten segments whose local coordinate systems are used to calculate upper extremity motion relative to anatomical reference planes. All joints are assumed to have fixed centers of rotation. The wrist joint allows flex/ext and ulnar/radial deviation. The elbow joint is a flex/ext hinge with a pronation/supination axis along the forearm. The shoulder joint is modeled as a ball and socket joint between the humerus and the trunk, with the joint center at the geometric center of the humeral head. Scapular contribution to shoulder motion is ignored.

We used a standard 3D video-based technique with retroreflective markers over prominent bony landmarks (Fig. 1). Joint positions were calculated as displacement offsets from selected surface markers, expressed as a fraction of segment lengths. Segments were defined by proximal and distal joint centers, and a third non-colinear point. Rotation sequence was flexion-abduction-axial rotation.

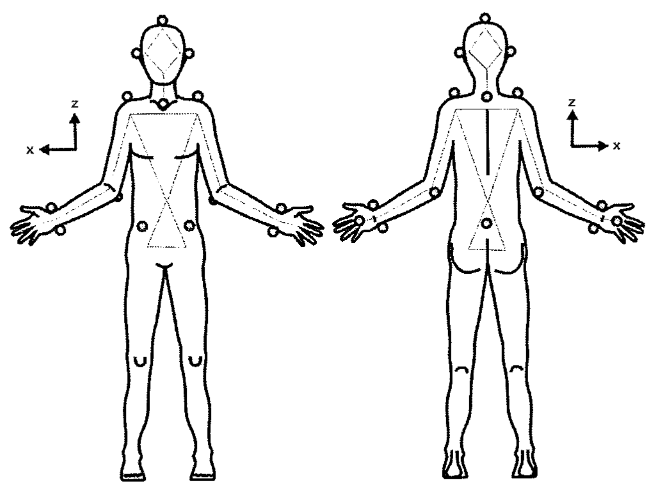

Figure 1: Surface markers and calculated segment joint centers (fine line).

Results

Accuracy of measurement was tested using an articulated rigid aluminum model of the shoulder girdle and upper extremity. Calculated and measured angular displacements were equal, with maximum standard deviations less than 1°. Sensitivity analysis demonstrated that shoulder angle measures were not significantly affected by perturbation of the shoulder joint center.

We have recorded 3D upper extremity movement during a variety of daily living activities on over 30 subjects, and routinely perform pre- and post-operative studies on children with abnormal movement patterns secondary to brachial plexus birth palsy. The method is practical and flexible for subjects with a wide range of height, weight, and ability to cooperate with data collection.

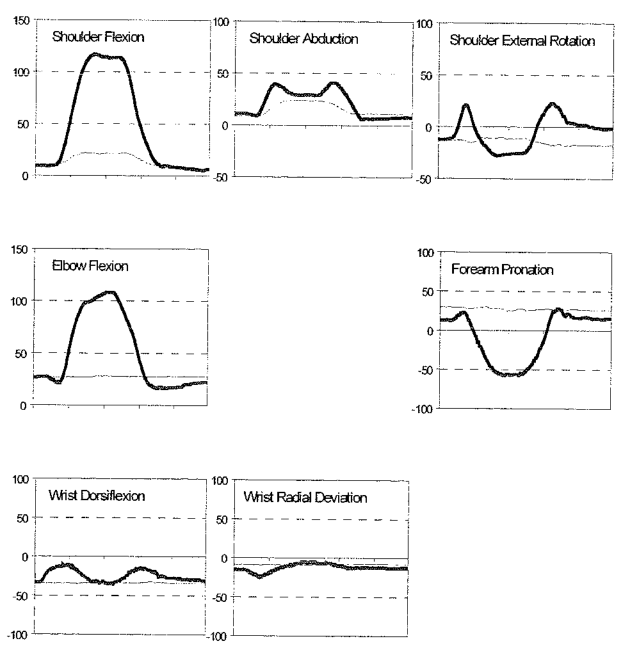

Figure 2: 3D data collected from a normal 40-year-old subject placing hand on head and returning arm to the side (thick line).

Summary

A method of three-dimensional kinematic analysis of the upper extremity is presented, using surface markers and current video data collection techniques. The rotation sequence is similar to methods used in lower extremity movement analysis, and is logical and easy to remember. It is our hope that a trend toward standardization of analytic techniques leads to an increase in communication and learning about upper extremity kinematics. The minimum requirement for reporting should be a clear description of axes (preferably with pictures), rotation sequences, and model assumptions.

Acknowledgement

The authors wish to express their appreciation to Larry Lamoreux for his help with the aluminum frame shoulder model

References

An K-N, Browne AO, Korinek S, Tanaka S, Morrey BF. (1991). *J Orthop Res* 9:143-149.

Nigg BM, Measuring Techniques. *In* Nigg, B. M., and Herzog, W. (Eds.). Biomechanics of the Musculo-Skeletal System. New York, John Wiley & Sons, 1994, pp. 268-278.

Sheehan FT, Mitiguy, P. (1999). *J Biomechanics* 32:1135-1139.

Wu G, Cavanagh PR. (1995). *J Biomechanics* 28:1257-1261.

INVERSE DYNAMICS ANALYSIS OF HEAD STABILITY DURING PREDICTABLE AND UNPREDICTABLE TRUNK PERTURBATION

M. Simoneau[1], S. W. Tinker[2], T.C. Hain[3] and W. A. Lee[1]
[1] Department of Physical Therapy and Human Movement Science, Northwestern University Medical School, Chicago, Illinois
[2] Biomedical Engineering, Northwestern University
[3] Otolaryngology, Northwestern University

INTRODUCTION

As the head provides a reference frame for detecting and controlling motion via the visual and vestibular systems, it is desirable to keep it stable in space. While much is known about reflex and mechanical factors, little is known about *predictive* control. To determine the contribution of prediction to head stability in space (HSS) we asked two question. First, is HSS better for a perturbation applied at a known rather than unknown time? Second, is predictive control, represented by muscle torque at the neck, greater for a perturbation applied at known than an unknown time?

METHODS

Ten healthy subjects were tested. A harness was fitted around the shoulders and chest. An inelastic cable clipped to the harness at the lower sternum was run anteriorly through a pulley to a load. Each trial began with the subject in a standardized posture. They were told to remain as well-balanced as possible. At the onset of the trial an electromagnet supported the load. Activation of a hand-held switch, operated either by the subject (predictable) or the experimenter (unpredictable), released the load and transferred it to the pulley, inducing a forward acceleration of the trunk.

Each subject performed 60 trials under two protocols (predictable and unpredictable) and two load (2% and 4% body weight). Trials were presented in blocks of 15, with the protocol and load fixed for a given block. The order of blocks was varied across subjects to minimize effects of experience.

Head and trunk kinematics were recorded using an optical system (Elite, BTS Inc.), with markers on the tragus (ear), the temple, the neck at C3-C4, and the anterior iliac crest. The trajectories of head center of mass (CoM) and center of rotation (CoR) were calculated from the head markers. An angular velocity sensor (Watson, Inc), on a headband, provided supplementary high-resolution measures of head velocity.

We treated the atlanto-occipital and C1-C2 articulations as a pin joint. The following expression was derived for head angular acceleration:

$$J_h\ddot{\theta}_h = m_h r_h(\ddot{x}\cos\theta_h + (\ddot{y} + g)\sin\theta_h) + Tmus$$

where θ_h is head angle in space; m_h the mass of the head; J_h the head moment of inertia about CoR; r_h the distance from the CoR to the CoM; $\ddot{x}$ and $\ddot{y}$ respectively are the linear accelerations of the CoR. "Net" torque (Tnet) is defined by the left-hand term of the equation and Tgi is the gravito-interactive torque. The torque from the neck muscles, Tmus, is Tnet – Tgi (Bedford et al, in press).

We computed peak head and trunk angular velocities for the first 600 ms after load onset and Tgi and Tmus integrals for the first 60 ms after load onset, when effects of predictive control should be most evident.

RESULTS AND DISCUSSION

Overall, the head and trunk were better stabilized (had lower peak angular velocities) in space when the subject voluntarily initiated the loading and hence knew its onset time, than when the load was imposed at an unknown time.

Table 1. Mean peak head and trunk angular velocities (deg/sec)

	Unpredictable		Predictable	
	2%	4%	2%	4%
Head	32.4	52.3	28.9	44.3
Trunk	2.81	5.91	1.99	3.36

Table 1 shows that the head and trunk were more stable in the predictable than unpredictable protocol. Also, head and trunk angular velocity increased with load. ANOVA showed significant effects of protocol and load for the head and trunk (respectively, Head: $P<0.05$ and $P< 0.001$; Trunk: $P<0.05$ and $P<0.0$).

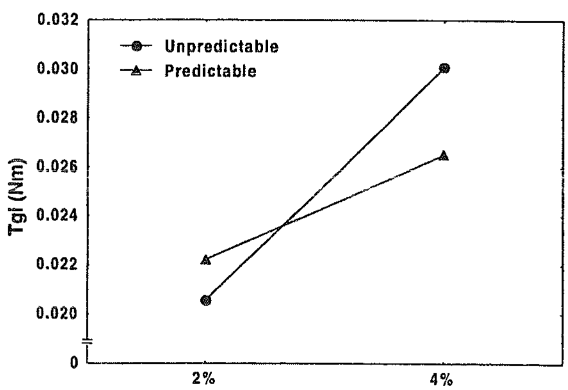

Fig. 1 shows Tgi for by protocol and load. There was no significant effect of either protocol or load on Tgi. In a simple mechanical system, Tgi would scale with load. The fact that it did not suggests that subjects actively controlled trunk motion, the primary source of Tgi, for the 4% load.

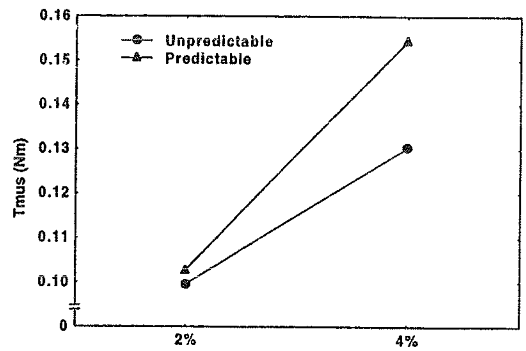

Fig. 2 shows Tmus by protocol and load. Tmus was significantly greater when the load was predictable for the 4% load only. That increase in Tmus was not due to larger trunk perturbation, because Tgi was similar both protocols. Thus the higher Tmus in the predictable, 4% condition must be due to predictive control.

SUMMARY

Both head and trunk are better stabilized if people can predict when a perturbation will occur. The higher Tmus in the predictable, 4% condition showed that subjects used predictive control of the head. For the 2% loads, predictive control of the head did not occur. Passive mechanics may be adequate to stabilize the head in space for small loads. These data suggest that trunk as well as neck control must be considered in understanding mechanisms of head stabilization.

REFERENCES

[1] Bedford, D.F., Steege, J.W., & Lee, W.A. *Neuroscience Letters*. (in press).

Supported by NINDS RO1 NS38286-02

KINEMATIC AND EMG VARIABILITY WHILE PRACTICING A MAXIMAL EFFORT TASK

David A. Gabriel

Biomechanics Lab, Brock University, St. Catharines, ON L2S 3A1

E-mail: dgabriel@arnie.pec.brocku.ca

INTRODUCTION

This paper explores changes in the variability of surface electromyographic (EMG) activity and kinematics associated with practicing a maximal performance task. The variability of muscle force-impulses producing movement is proportional to the mean size of the impulse (Schmidt et al. 1979). Since increases in limb speed require larger accelerative and decelerative force-impulses, movement variability increases due to an increase in the variability of the muscle force-impulses. If, however, antagonist muscle activity can compensate for variations in agonist muscle activity, movement variability does not necessarily increase (Darling and Cooke, 1987). This paper determined how changes in the variability of EMG activity result in a decrease in kinematic variability subsequent to practicing a maximal performance task.

METHODS

Eight subjects (aged 25 to 30 years) gave their permission to participate in this study. With the elbow in full extension, subjects rotated their forearm as fast as possible to reach a target corresponding to 80° of elbow flexion. The target area was ± 1.5° around the specified joint position. Subjects monitored elbow flexion angle relative to the target area on an oscilloscope. All movements were performed in the horizontal plane on a manipulandum. One hundred trials were completed on each of four practice sessions. The data were collected for the first five (1-5) and the last five (96-100) trials of each practice session.

Angular displacement and EMG activity of the biceps and triceps (lateral head) brachii were monitored concurrently. The EMG activity was amplified (5000×) and band-passed (3-1000 Hz) with a Grass P-511. All signals were digitized at 2 kHz, and stored on a hard disk for off-line processing. The EMG was then low-passed at 60 Hz with a zero-phase second-order Butterworth digital filter. The displacement signal was similarly low-pass filtered at 10 Hz.

Three measures were calculated for the first five (1-5) and last five (96-100) trials of each practice session. Peak velocity was obtained from the differentiated displacement curve. Trajectory (velocity versus position) variability was calculated from the area of ellipses with radii equal to one standard deviation in velocity and position at each point (SD^2). The coefficient of variation in biceps and triceps brachii EMG magnitude. A repeated measures analysis of variance was used to evaluate any change in these measures. Post-hoc testing was accomplished using Tukey's (HSD) test.

RESULTS

The data presented in Figure 1 is organized so that Block 1 is the mean of the first five (1-5) trials and Block 2 is the mean of the last five (96-100) trials of Session 1. This continues so that Block 8 is the last five (96-100) trials of Session 4 for a total of four hundred trials.

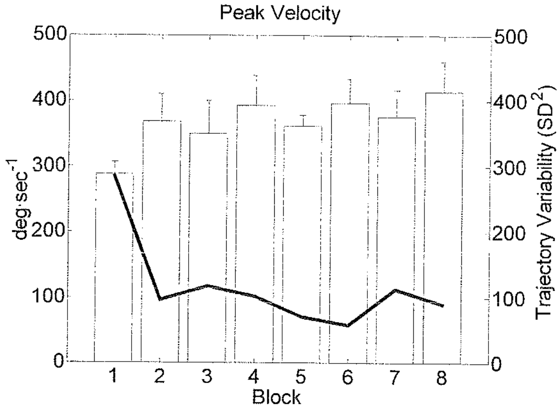

Figure 1. Peak velocity (bar: left y-axis) and trajectory variability (line: right y-axis).

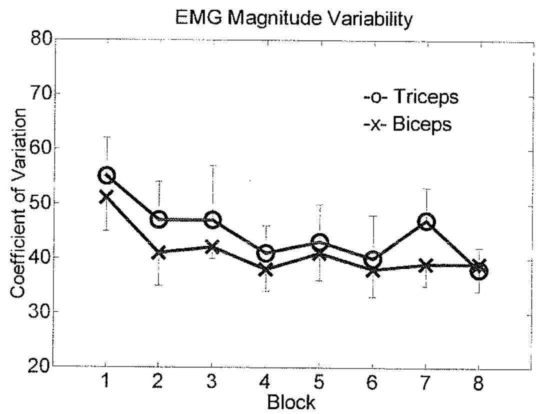

Figure 2. The coefficient of variation in biceps and triceps EMG magnitude.

Peak velocity increased 127-deg·sec^{-1} (44%) across the four practice sessions ($p<0.05$). There was a dramatic decrease ($p<0.05$) in trajectory variability of 186 SD^2 (66%) between the first five (1-5) and last (96-100) trials of Session 1, but it remained stable thereafter. The relative variability of the individual EMG bursts also decreased. Figure 2 shows that the coefficient of variation in biceps and triceps EMG magnitude exhibited a total decrease of 31 and 23%, respectively ($p<0.05$). Similar to trajectory variability, most of the change occurred early in the measurement schedule.

DISCUSSION

Kinematic variability decreased, but not because of a linkage between agonist and antagonist activity as suggested Darling and Cooke (1987). Rather, there was a decrease in the variability of muscle activity. Since angular acceleration is proportional to joint torque in single-joint movements, there should be a clear relationship between kinematics and EMG activity. A reduction in the variability of EMG magnitude should therefore result in a decrease in trajectory variability.

Decreased variability is a property of programmed movements (Georgopolous et al. 1981). The EMG and trajectory data suggest that practice resulted in greater central nervous system control over both the spatial-temporal aspects of movement and the magnitude of the biceps and triceps muscle force-impulses. This supports Moore and Marteniuk (1986) who also reported a decrease in EMG variability following practice. The authors suggested that practice shifted the generation of EMG activity to a higher level in the motion planning hierarchy though it is still subordinate to kinematics.

REFERENCES

Darling, W.G., Cooke, J.D. (1987). movements. *J. Motor Behavior*, **19**, 311-331.

Georgopolous, A.P. et al. (1981). *J. Neurophysiology*, **46**, 752-743.

Moore, S.P., Marteniuk, R.G. (1986). *J. Motor Behavior*, **18**, 397-426.

Schmidt, R.A. et al. (1979). *Psychological Review*, **86**, 415-451.

TOWARD AN OBJECTIVE MEASURE OF FRACTURE COMMINUTION SEVERITY

Christina L. Beardsley[1], Eric A. Brandser[3], J. Lawrence Marsh[2], Thomas D. Brown[1,2]

Departments of [1]Biomedical Engineering, [2]Orthopaedic Surgery, and [3]Radiology
University of Iowa, Iowa City, IA
Email: tom-brown@uiowa.edu

INTRODUCTION

Orthopaedists rely on fracture classification systems for establishing treatment protocol. Yet, high-energy injuries are insufficiently discriminated by current classifications, partly due to the subjectivity inherent in assessing comminution severity as a categorical variable [1]. Because area of fracture surface created is proportional to the energy absorbed in crack propagation, and since CT provides the capability for quantitative analysis, there is attraction in exploring interfragmentary surface area measurement as a continuous variable to describe fracture severity. Image analysis procedures are here reported to assess the accuracy with which the surface area of a bone surrogate can typically be measured.

PROCEDURES

Four rectangular prisms, machined to known sizes out of a specially designed polyetherurethane foam (a radiographic and fragmentation surrogate for cortical bone), were suspended in the center of a Plexiglas tube using a radiolucent expanding foam. During a helical scan, 132 tomographic slices of this construct were collected, at millimeter intervals. Each slice was 2 mm thick, and was collected at 135 KVp and 200 mAs. An extra-small field of view with additional magnification was employed. This produced a high-resolution slice (0.17 mm pixels). The 16-bit raw data file was wrapped into serial 8-bit 'tiff' images, scaling intensities appropriately.

Since fragment vs. background signal intensity is highly variable among individual fragments and among patients, conventional thresholding is inadequate. A special algorithm for quantitative analysis of the sections was thus developed utilizing PVWave (Visual Numerics, Inc., Boulder, CO). Based upon the graylevel intensity at a manually-selected seed point, and at the point's immediate neighbors, a region is initially grown. Points at its periphery are tested for satisfying inclusion criteria. As new points are annexed, their gray values are compared against a driving grayscale difference. The base of this driving grayscale difference is updated periodically, using a logarithmic weighted function. The effect of driving grayscale difference on final region size was explored parametrically. The (empirically) optimal driving difference is that above which further increment will produce an abrupt increase in perceived region size.

Once the fragment is grown, a binary map of the image is created, such that pixels are either 'on' or 'off' based on whether or not they have been incorporated into the region. This mapping is then high-pass filtered to identify edge points. Border points are ordered, and pixel-to-pixel Euclidean distances are summed around the border. Multiplication of the perimeter and the slice thickness yields (sectional) fragment surface area.

RESULTS AND DISCUSSION

Aggregating pixels into a common region followed the distinct pattern evidenced in the sigmoid curves for individual fragments (A,B,C,D) in Fig. 1.There was a sharp step at the onset where fragment pixels far from the edge were easily registered as part of the region. Approaching the margins of the object, plots of grayscale difference vs. region size tended to plateau. However, the length and slope of this plateau differed from fragment to fragment, with plateau characteristics also depending upon how the seed gray was updated. Finally, there was a takeoff point, after which it became obvious that driving threshold difference was too high and that the "fragment" region had spilled into background or into another fragment. Surface areas measured from representative CT sections of the four prisms are reported in Table I, along with known dimensions. Returned values tended to be highly reproducible (s.d. = 3.7%), despite differences in grayscale of the initial seed point. Not surprisingly, the larger the fragment, the higher the relative accuracy of surface area measurement.

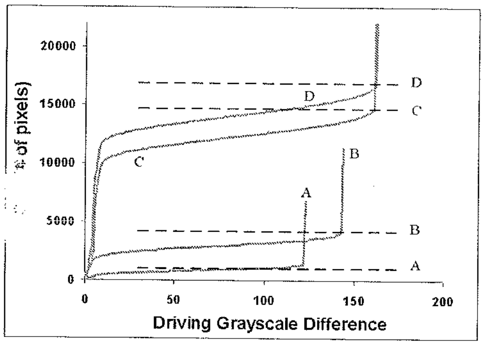

Figure 1. Effect of driving grayscale difference on region size. Dashed lines indicate true size.

Margin discrimination is of key importance in any edge detection scheme aimed at quantitative measurement. Heretofore, most fracture edge discernment has been targeted at visualization and volume rendering, not at perimeter measurement, so the present application represents an unusually rigorous demand for edge detection accuracy. "Fuzzy" edges due to partial volume effects, merely a nuisance to sharp rendition for visualization purposes, are the major source of error in fragment surface area calculations. Error in surface area measurement averaged only 5.2%. This of course is for idealized slices containing discrete objects with relatively simple shape. In an actual clinical CT slice, due to the complexity of configuration of multiple fragments, driving grayscale differences that work well at some sites may cause other sites of adjacent fragments to become confluent. The degree of accuracy that will be necessary to usefully distinguish between clinically distinct pathologies remains to be seen. Fig. 2 illustrates this automated edge delineation procedure applied to a typical bone fragment in a clinical tibial pilon fracture case.

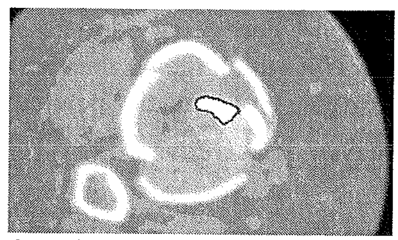

Figure 2. A bone fragment perimeter automatically identified in a tibial pilon fracture CT.

REFERENCE

[1]Swiontkowski et al (1997), *J Orthop Trauma*, 11(7):462-470

ACKNOWLEDGEMENT

Financial support provided by EBI, Inc.

Table I. Surface area (sides only) measured by edge detection for 2-mm thick foam cross sections of various sizes.

Actual Size (mm^3)	Actual Surface Area (mm^2)	Measured Surface Area (in mm^2, n=8)	Mean % Error
5.08 x 5.84 x 2	43.688	47.734 ± 3.415	9.26
9.17 x 12.50 x 2	86.665	80.984 ± 2.224	6.55
18.24 x 19.56 x 2	164.694	169.421 ± 4.447	2.87
22.61 x 21.56 x 2	176.682	179.357 ± 4.758	1.94

EMERGENT NON-INVASIVE REDUCTION OF PELVIC RING DISRUPTIONS

M. Bottlang[1], J. Sigg[1], T. Simpson[2], J. C. Krieg[1], S. M. Madey[1]

[1] Biomechanics Laboratory, Legacy Health System, Portland, Oregon
[2] Oregon Health Science University, Portland, Oregon
Email: mbottlan@lhs.org

INTRODUCTION

Pelvic reduction and stabilization in the early post-injury phase of pelvic ring disruptions is a potentially life saving intervention. It constitutes the most effective means to control pelvic venous bleeding [Burgess, AR et al., 1990]. However, no device for emergent, non-invasive pelvic reduction and stabilization at the accident site is available to date. Several invasive devices for pelvic reduction and stabilization have been introduced, but their application demands an operating room scenario. Most recently, the use of a circumferential sheet for stabilization of pelvic fractures has been reported [Routt, MLC et al., 1995]. While this technique is non-invasive and applicable at the emergency site, no data are available describing the efficacy and safety of circumferential pelvic compression.
This research provides a parametric investigation on the efficacy of a non-invasive 'pelvic sling' to induce pelvic reduction by means of circumferential compression. Furthermore, an optimal sling position and the required reduction force have been determined in a cadaveric study.

PROCEDURES

Seven fresh frozen whole-body cadaveric specimens were instrumented with a peritoneal pressure sensors (HP 78534, Hewlett Packard, Englewood, CO), a motion tracking system (pcBird, Ascension Tech. Corp., Burlington, VT) to trace spatial location of the pelvic wings, and a custom symphysis pubis sensor to detect symphysis contact (Fig. 1). A partially stable 'open book' pelvic fracture (symphysis gap=50 mm, monolateral disruption of anterior sacroiliac joint) and subsequently an unstable pelvic fracture (symphysis gap=100 mm, complete monolateral sacroiliac joint disruption) were created by forced external rotation of each hemipelvis after symphysiotomy. A prototype pelvic sling was designed, consisting of a 50 mm wide, flexible, non-elastic reinforced rubber belt. This belt circumvents the pelvis and is guided anteriorly over rollers contained in a belt buckle. Application of tension F_T to the ends of the belt gradually induces circumferential pelvic compression. Two sensors are integrated into the sling to continuously monitor sling tension (ELFS-500N, Entran, Fairfield, NJ) and lateral sling-skin interface pressure (HP 78534). This sling was applied in three distinct transverse plane levels, extending from the symphysis pubis to the iliac crest (Fig. 1), to first reduce the partially stable and then the unstable pelvic ring disruptions.

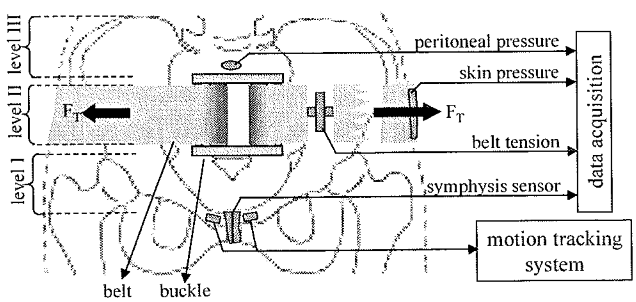

Fig. 1: Transverse view, instrumented pelvis.

Sling tension was applied manually and resulting sling tension, sling-skin pressure and spatial motion of the pelvic wings relative to each other were continuously monitored until symphysis contact was detected.

For each specimen, inlet and outlet radiographs of the pelvis before and after reduction were obtained to document the fracture pattern and quality of reduction. Finally, computer tomographic scans of one specimen were obtained before and after reduction of an unstable pelvic ring fracture to allow for computation of reduction-induced changes in true and false pelvic volume (V_{true}, V_{false}).

RESULTS AND DISCUSSION

Fracture patterns consistent with clinically relevant partially stable and unstable 'open book' pelvic fractures were achieved in all specimens, as documented by the inlet and outlet radiographs. Symphysis contact due to sling application at level I was achieved by $F_T = 177 \pm 44$ N and $F_T = 180 \pm 50$ N for reduction of the partially stable and unstable pelvis, respectively (Fig. 2). Sling application at levels II and III consistently required a significantly higher sling tension to achieve symphysis contact as compared to sling application on level I (two-tailed T-test, α=0.05).

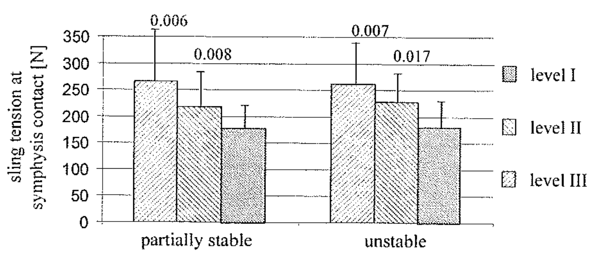

Fig. 2: Sling tension required for reduction.

Reduction of the unstable pelvis (i.e., symphysis contact) due to sling application on level I resulted in a peritoneal pressure increase of 10.1 ± 8.5 mmHg and induced an average sling-skin interface pressure of 24 mmHg, as measured at the lateral aspect of the pelvic soft tissue envelope.
Reduction of the partially stable and unstable pelvis (level I, F_T=200 N) yielded in a residual displacement vector at the symphysis of 5.1±2.0 mm and 11.3±5.3 mm magnitude, respectively.

Three-dimensional rendering of the true and false pelvic volume from computer tomographic scans yielded values of V_{true}= 1520 cm^3 and V_{false}= 1880 cm^3 for the unstable pelvis and V_{true}= 1230 cm^3 and V_{false}= 1820 cm^3 for the reduced pelvis.

Application of circumferential compression to the pelvic soft tissue envelope by means of a pelvic sling demonstrated to be an efficient, non-invasive means for controlled reduction of 'open book' type pelvic fractures (Fig. 3). This study quantified the sling tension required to achieve pelvic reduction and determined an optimal sling position at which the required sling tension is minimal. These findings are essential to minimize adverse effects such as peritoneal pressure increase and sling-skin interface pressure. Further investigations are necessary to address the effects of sling application to alternative fracture models, such as pelvic lateral compression fractures.

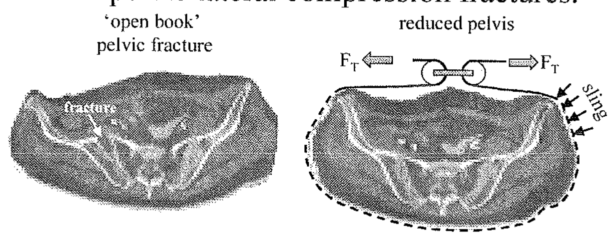

Fig. 3: CT scan, sling-induced reduction.

SUMMARY

The presented research constitutes a quantitative evaluation of the efficacy of circumferential compression to reduce pelvic ring disruptions. It provides results that are directly applicable to advance a potentially life-saving, non-invasive emergent care procedure.

REFERENCES

Burgess, A.R., et al., (1990), J Trauma, **30**:848-856.
Routt, M.L.C., et al., (1995), Clin Orthop Rel Res, **318**, 61-74.

ACKNOWLEDGEMENTS

Supported by Legacy Research Services.

ESTIMATION OF KNEE JOINT SURFACE ROLLING/GLIDING KINEMATICS VIA INSTANT CENTER OF ROTATION MEASUREMENT

John H. Hollman[1], Robert H. Deusinger[1], Dequan Zou[1], and Matthew J. Matava[2]

[1]**Prog. Phys. Therapy and** [2]**Dept. of Orthopedics, Washington University, St. Louis, MO**
Email: jhollman@clarke.edu

INTRODUCTION

One approach to assessing sagittal plane intrinsic knee joint kinematics has been through application of the concept of the path of instant centers of rotation (PICR) (Frankel et. al., 1971; Smidt, 1973). Rolling/gliding kinematics have been inferred from such studies. When a great amount of rolling relative to gliding occurs between joint surfaces, the PICR is located in close approximation to the point of contact. Conversely, when a lesser amount of rolling relative to gliding occurs, the PICR is located further from the point of contact. Such studies, however, have failed to quantify a relationship between PICR and intrinsic joint surface rolling and gliding. Moreover, these studies analyzed only non-weight bearing (NWB) knee extension; it is not known whether PICR and rolling/gliding kinematics are identical for NWB and weight bearing (WB) movement conditions.

The purposes of this study were to (1) describe a 2-dimensional analytic knee model for estimating joint surface rolling and gliding based on PICR measurements, and (2) quantify and compare knee joint surface rolling kinematics in normal subjects for NWB and WB movement conditions.

METHODS

11 adults (6 male, 5 female) without history of right knee injury or surgery participated in this study. Reflective markers were taped 10 cm distal to the greater trochanter, 5 cm proximal to the lateral femoral epicondyle, at the fibular head and lateral malleolus. NWB and WB knee extension movements were recorded and processed at 60 Hz with Ariel Performance Analysis System software (APAS99, rev. 3.5). A local reference system at the lateral femoral epicondyle was defined. Instant center of rotation (ICR) locations were calculated in a manner similar to methods described elsewhere (Hollman & Deusinger, 1999).

A planar knee model was developed to calculate joint surface contact points and to quantify rolling/gliding kinematics relative to selected ICR locations. The distal end of the femur was configured from previous anatomical research (Nuno-Siebrecht & Ahmed, 1998) to incorporate sagittal plane geometry using two discs, each having a distinct radius of curvature (2 cm posteriorly and 4 cm anteriorly). The proximal tibia was modeled as a flat surface. Femoral contact points were calculated at 10^{O} intervals based on the relationship $s = r\,\theta$, where s represents the arc length between contact points, r represents the radius of curvature, and θ represents a constant angular displacement of 10^{O} (0.175 radians). Based on these selected femoral contact point locations and ICR data obtained experimentally, the relative proportion of rolling to gliding was calculated via the *slip ratio* (O'Connor & Zavatsky, 1990), which is defined by the ratio s_m / s_f where s_m is the displacement (arc length) from an initial contact point to the next contact point on the convex surface and s_f is the displacement from an initial contact point to the next contact point on a flat surface. For a joint modeled in 2-D as a disc on a flat surface, s_m and s_f are given by

$$s_m = r_m\,\theta$$
and
$$s_f = (r_m - r_{icr})\,\theta$$

where r_m is the radius of the convex surface segment, r_{icr} is the radius from the ICR location to the femoral contact point, and θ is angular displacement of the convex surface, expressed in radians.

A two-factor repeated-measures ANOVA was used to test the null hypothesis that no difference in rolling kinematics existed between movement conditions at any knee angle ($\alpha = 0.05$).

RESULTS AND DISCUSSION

Graphic representation of NWB and WB PICR patterns is presented in the Figure. Repeated measures ANOVA revealed that the movement condition by knee angle interaction was significant ($F = 6.50$, $p < .01$) and subsequent residual interaction effects testing revealed that differences in joint surface rolling occurred between movement conditions in the terminal 20^O of knee extension. The table presents % rolling results obtained through terminal extension.

Results suggest knee joint rolling/gliding kinematics may differ between movement conditions. A greater proportion of joint surface rolling occurred in the terminal 20^O of WB knee extension than NWB knee extension.

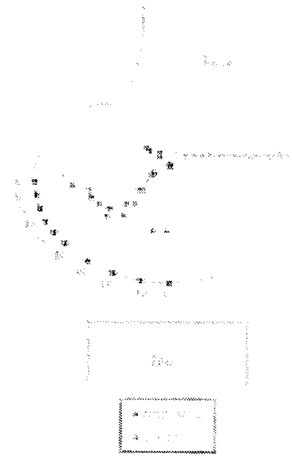

Figure. *NWB and WB PICR patterns.*

Table. % Rolling values obtained for each movement condition.

KneeAngle	% Rolling NWB	% Rolling WB
30	56.2	59.5
20	55.0	58.6
10	53.6	70.8
0	53.5	68.9

REFERENCES

Frankel VH et al. (1971). *J Bone Joint Surg*, **53-A**, 945-962.

Hollman JH, Deusinger RH. (1999). *JOSPT*, **29**, 463-469.

Nuno-Siebrecht N, Ahmed AM. (1998). *Proceedings of NACOB '98.*

O'Connor JJ, Zavatsky A. (1990). *Biomechanics of Diarthrodial Joints, Volume II.* Springer-Verlag.

Smidt GL. (1973). *J Biomech*, **6**, 79-92.

ACKNOWLEDGMENTS

This project was funded in part by the NIH-NCMRR training grant 5T32HDO743405.

A MODEL TO EVALUATE IMPINGEMENT FATIGUE PERFORMANCE OF ACETABULAR COMPONENTS

Aaron Bailey, Charlie Parduhn, and Janet Krevolin
Sulzer Orthopedics, Austin, Texas
Email: aaron.bailey@sous.com

INTRODUCTION:

Total hip replacement range of motion is potentially limited by impingement of the femoral neck with the acetabular liner. Impingement can occur *in-vivo* at extreme ranges of motion. Prosthetic impingement may lead to many different failure mechanisms, two of which are: 1) dislodgment of the liner 2) cracking of the liner. The authors have not found a published laboratory impingement tests in the literature. Therefore, a laboratory impingement model for the evaluation of acetabular liners was developed. The motivation for developing the model was to evaluate acetabular liners comprised of the new highly cross-linked polyethylene, Durasul™.

METHODS:

The fatigue apparatus for testing the acetabular liners is illustrated in Figure 1. The acetabular assembly is placed into the fixture with the maximum screw hole density positioned below the femoral head and in line with the load line. This orientation creates the maximum amount of unsupported PE. Each assembly is submerged in Ringer's solution at 37°C (98.6°F). The acetabular component is held at a 40° angle from horizontal. Although inverted, this orientation corresponds to the shell at 40° abduction and 20° of anteversion. A neck facsimile is assembled with a head and the assembly is positioned to impinge (Figures 1 and 2).

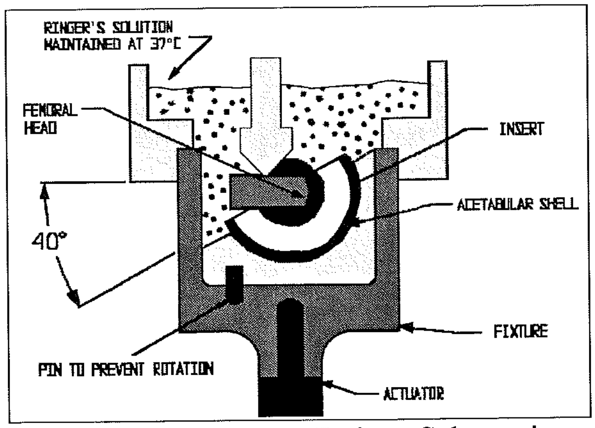

Figure 1: Impingement Fatigue Schematic

A 10,000 N-mm (88 in-lb) moment (Scifert *et al* 1997) is applied to the assembly by machining a notch in the neck, through which a load is applied. For example, for a 28 mm head a 10 mm (0.394 in) offset combined with a 1,000 N (225 lb) load creates the required 10,000 N-mm moment. The load is applied using a sine wave with R=0.1. This moment simulates *in vivo* impingement forces on the acetabular liner. Because impingement is rare during daily activity, the required cycle count (typically 5-10 million for fatigue tests) is reduced to 2 million cycles.

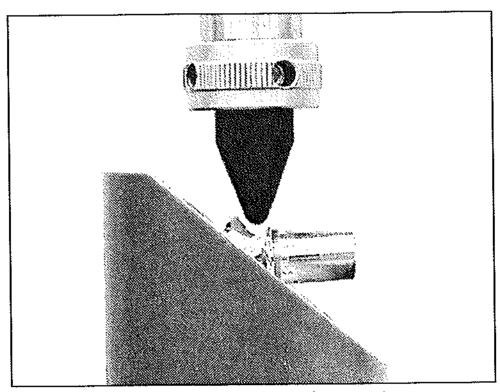

Figure 2: Impingement Fatigue Apparatus

MATERIALS:

This model was applied to six Durasul and six control liners. In-order to simulate a worst case scenario, size 49 x 28 mm and size 39 x 22 mm acetabular components were tested, because they possess minimal PE thickness. Acetabular shells with the maximum number of screwholes were selected. The femoral heads (28mm+8mm, 22mm+0mm) that created the worst impingement scenario were selected. Skirts on the femoral heads strongly effected the size selection.

Post-Test Evaluation

After testing, each acetabular system is inspected under a microscope and then disassembled. Freezing the liners with liquid nitrogen produced enough shrinkage of the PE to allow the liner to be removed with ease. Gross creep, gross wear, or penetration of the head/neck assembly into the liner that is visible to the naked eye, is evaluated. The liners are inspected for cracking under a microscope, particularly at the liner's rim where the PE is thin.

RESULTS:

A model for impingement was defined and evaluated by testing six Durasul™ Inter-Op™ liners (Sulzer Orthopedics) and six controls (Inter-Op UHMWPE liners packaged without oxygen). All acetabular assemblies, Durasul and Controls survived 2 million cycles with no adverse effects. All liners remained firmly attached to their respective shells. Small localized indentations from the femoral skirts were discovered in the PE liners (Durasul and Controls, size 49 mm and 39 mm) at the region of impingement. There was no other evidence of gross PE creep, wear, or penetration at any location. No PE cracking was detected.

DISCUSSION:

This test was successful in creating an impingement model in the laboratory. The physiological loads and angles represent femoral head/neck and acetabular liner impingement. The impingement model allowed a side-by side comparison of the two PEs. This test found the highly cross-linked Durasul and the Controls to perform equally. Aside from localized indentations, neither PE experienced gross creep, gross wear, cracking, or any other adverse effects when exposed to physiological impingement loads for 2 million cycles.

REFERENCES:

Scifert CF, Brown TD, Pederson DR, Callaghan JJ: The Effects of Cup Tilt and Anteversion on Dislocation Propensity in THA: *Orthopedic Research Society*, 1997.

THE NANOINDENTATION PROPERTIES OF INTRAMUSCULAR HERRING BONE RELATED TO MICROSTRUCTURE

Jae-Young Rho, Departments of Biomedical Engineering,
The University of Memphis, Memphis, TN 38152-6582
jrho@cc.memphis.edu
George M. Pharr, Department of Materials Science,
The University of Tennessee, Knoxville, TN and Metals and Ceramics Division, Oak Ridge National Laboraotry, Oak Ridge, TN
pharrgm@ornl.gov

INTRODUCTION It has long been known that variations in the microstructure of bone have a profound effect on the mechanical properties of the tissue and that these properties vary significantly between and within the cortices of bones. However, the microstructural basis and the functional significance of such variation remains poorly understood. One reason for this is the difficulty in acquiring large enough samples of a material comprised only of that particular structural type of interest for mechanical testing [1]. The availability of depth-sensing nanoindentation instruments with capabilities for measuring displacements on the order of nanometers makes it possible to measure the properties of the small microstructural features in bone. The primary aim of this research was to investigate the relationship between microstructure and nanoindentation properties of intramuscular herring bones.

MATERIALS AND METHODS

Intramuscular herring bones, which have a simple microstructure: collagen fibrils that are believed to have a single orientation (longitudinal) with a variation in mineralization along the length, have been used [2]. The apex region represents bone tissue at the earliest stages of calcification. The end nearest the backbone is fully mineralized. Nanoindentation properties were measured both at the longitudinal direction in the transverse section and at the transverse direction in the longitudinal section along the length.

The crystal orientation was examined with high-intensity synchrotron x-ray radiation at the National Synchrotron Light Source (Brookhaven National Laboratory). The coherence length and angle spread were measured to confirm that the crystals were aligned in the same orientation along the entire length of the bone so that the mechanical data could be ascribed to structural features. The coherence length (CL) represents the average distance between imperfections in specific crystallographic directions. The angle spread (AS) characterizes the degree of misalignment between perfectly coherent domains [3]. To confirm the correlation between nanoindentation properties, the coherence length, and the angular spreads, linear regressions were performed.

RESULTS The elastic modulus in the fully mineralized regions was approximately 20 GPa and 13 GPa in the longitudinal and transverse directions, respectively. The elastic modulus decreased as moving toward the apex region of the earliest stages of mineralization in the both longitudinal and transverse directions was approximately 5 GPa (Figure 1). The anisotropic ratio ($E_{longitudinal}/E_{transverse}$) was decreased from 1.5 to 1.0 as moving toward the apex region of the earliest stages of calcification. The properties at the early stages of mineralization demonstrated isotropic.

The variation in elastic modulus with orientation of the specimen axis to the long axis of the bone at the fully mineralized regions was between 20 GPa and 13 GPa and decreased montonically. The coherence length in the longitudinal direction progressively increased with full mineralization from 28 nm to 32 nm. However, crystal size could not be measured in the other directions because angular spread was wide. Nanoindentation properties was positively correlated with coherence length (r=0.85, p=0.03).

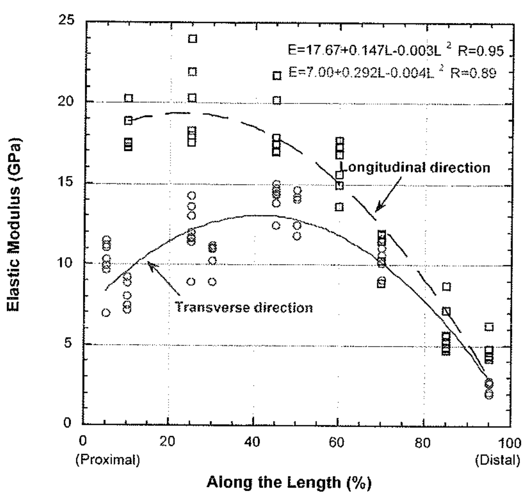

Figure 1. Elastic modulus of intramuscular herring bones in the both longitudinal and transverse direction along the length (degree of mineralization).

DISCUSSION In lamellar bone, a broad distribution of the fiber axis for collagen has been observed due to the local meandering, kink, and twisting of collagen fibers in the bone matrix. However, it has been shown that the ultrastructure of intramuscular herring bones was relatively simple microstructure, having collagen fibril aligned in the long axis [2]. Because it has long been assumed that collagen orientation directly influences the orientation of the minerals nucleated within the hole zone of the collagen, it is interesting to see if crystal orientation is aligned with that of collagen fibril. Indeed, the crystal and collagen were all aligned in the same orientation along the entire length of the bone.

At the earliest stages of calcification, the angular spreads were isotropic in different crystallographic directions. In the course of maturation, the angular spreads showed a tendency toward anisotropy. The higher degree of mineralization was due to the larger crystal size, which enhanced the stiffness of the tissue. Both the size and orientation of the bone mineral crystals were measured and identified as determinant factors for the mechanical properties of bone.

ACKNOWLEDGEMENT This research was sponored in part by the NIH AR45297. Instrumentation for the nanoindentation work was provided by the Division of Materials Science, U.S. Department of Energy, under Contract DE-AC05-96OR22464 with Lockheed martin Energy Corp., and through the ShaRE Program under Contract DE-AC05-76OR00033 between the U.S. Department of Energy and Oak Ridge Associated Universities. X-ray diffraction was carried out at the National Synchrotron Light Source, Brookhaven National Laboratory, which is supported by the U.S. Department of Energy, Division of Materials Sciences (Jianming Bai and Kisup Chung).

REFERENCES

[1] Weiner S, Wagner HD (1998) Annu Rev Mater Sci 28, 271-298.
[2] Lee DD, Glimcher MJ (1991) J Mol Biol 217, 487-501.
[3] Aizenberg J, Hanson J, Koetzle TF, Weiner S, Addadi L (1997) J Am Chem Soc 119, 881-886.

EFFECT OF FATIGUE ON THE BONE ORGANIC

S.P. Kotha[1,2] and N. Guzelsu[1,2]

[1] **Biomedical Engineering, Rutgers University, Piscataway, NJ 08854**
[2] **Biomechanics, Tr# 4, 675 Hoes Lane-UMDNJ, Piscataway, NJ 08854**
Email: guzelsu@umdnj.edu

INTRODUCTION

The origin of damage at the ultrastructural level is not known. It is hypothesized that damage at the ultrastructural level is caused by the cracking of bone mineral crystallites, debonding at the mineral organic interface or by the shear between and within the collagen fibrils. The objective of this study is to investigate if mechanical testing of decalcified bone samples that were previously fatigued might provide some insight into the damage mechanisms in the matrix phase when intact bone is loaded past yield.

METHODS

Bovine plexiform femoral bone from 12 to 18 month old steer were obtained from a local slaughterhouse (MOPAC, Souderton, PA). The lateral and medial quadrants were machined into dumbbell shaped mechanical test specimens (Kotha et al., 1998). Some specimens were loaded in tensile fatigue for 8 cycles in order to damage them and the remaining were taken as control samples. Tensile fatigue tests were conducted on an Instron Universal Testing Machine (Model 1321) using a triangular waveform and a strain rate of 0.0005 s^{-1}. Strain was recorded by an extensometer with a gage length of 12.5mm. The distance between the grips was 34mm. The stroke was set to 0.3 mm for the fatigue experiments. The stroke value chosen is such that the bone in the gage length of the specimen was loaded past yield. This is confirmed by the load-deformation curves that were recorded.

Control and fatigued bone samples were decalcified. The ends of the samples to be decalcified were coated with paraffin wax, before being put into 0.5M EDTA solutions at pH =8.3 and 4 °C for a period of ten days (Bowman et al., 1996). Each sample was treated in a separate container and the solution was changed every two days. Tensile testing to failure of decalcified bone was done under stroke control at a strain rate of 0.001 s^{-1}. The spacing between the grips was 12.5 mm. Load-deformation curves were obtained from which the mechanical properties were obtained. The cross-sectional area of the bone specimen before its decalcification was used to obtain the mechanical properties of decalcified bone samples. The elastic modulus of the decalcified samples was taken from the linear portion (30% - 60% of maximum stress) and yield portion (60% - 90% of maximum stress) of the stress-strain curve.

RESULTS

The elastic moduli obtained from the linear and yield portion of the stress-strain curves and the ultimate stresses of decalcified fatigued and control bones are similar (Table 1). The elastic modulus of the yield portion (60% - 90% of maximum stress) is higher than those of the linear portion (30% to 60% of maximum stress) in both the groups. The ultimate strain of decalcified fatigued bone is 28% higher than that of the control decalcified bones (Table 1).

DISCUSSION

The ultimate stresses and the two elastic modulus values corresponding to the linear and the yield portion of the stress-strain curves of decalcified bone are similar. This indicates that the strain in the toe region is increased. The two damage mechanisms that would account for this increase in strain are that the collagen fibrils cracked or that they had more crimps in them. If the increase in strain was due to cracking of the collagen fibrils, the elastic modulus values in the linear and yield region would also have decreased. As this is not the case, we hypothesize that the fatigued decalcified bone has a higher crimp than that of control decalcified bone.

In tendons elongated into the yield region, a new small period crimp within the collagen microfibril is superimposed on the original crimp after removal of load (Kasteilic and Brear, 1980). When tendon loaded past yield is unloaded, the length of the tendon is smaller than its initial length. This was due to the increased crimping within the collagen fibrils. We assume the same for fatigued decalcified bone. When the damaged decalcified bone is loaded, the added crimp that led to the shortening of the decalcified bone has to be straightened, which causes the strain in the toe region to increase. It is to be noted that this implies that some of the mineralized collagen fibrils in intact bone are being loaded in the yield zone when intact bone is loaded in tension past its yield point. At the end of the toe region, the deformation due to the added crimp is straightened and does not contribute to the deformation within the collagen fibrils. The linear portion of the stress-strain curve of decalcified bone is due to the elongation of the collagen fibrils. The elongation of the collagen fibrils is a combination of the elongation of the collagen molecules and shear between the collagen molecules. Since few collagen fibrils break in this study, the deformation due to the presence of cracks is minimal compared with the elongation of collagen fibrils. In the yield region, fibril disintegration occurs due to a shear slip mechanism. In tendon loaded into the yield region, ultimate strength was preserved due to "persistent or quickly re-formed lateral bonding forces at a low level of organization" namely between the collagen molecules within the microfibril (Kastelic and Brear, 1980). For the same reason, we believe that the ultimate stresses for fatigued decalcified bone and control decalcified bone are similar. In summary, it is noted that damage in fatigued bone occurs within the collagen fibrils of the organic matrix of bone.

REFERENCES

1) Bowman, S.M. et al. (1996). *J. Biomech.* 29(11):1497-1501.

2) Kotha, S.P. et al. (1998). *Biomed. Mat. Engnrg.* 8:321-34.

3) Kastelic, J. and Baer, E. (1980). *The Mechanical properties of Biological Materials.* Cambridge University Press.

ACKNOWLEDGEMENTS

NSF: BCS-9210253

Table 1: Mechanical properties of Control and Damaged decalcified bone (mean ± SD).

	Ultimate Strain %	Elastic Modulus (30 %- 60 %) GPa	Elastic Modulus (60 % – 90 %) GPa	Ultimate Stress MPa
Control	11.1 ± 1.13[a]	0.26 ± 0.05[a]	0.27 ± 0.06[a]	18.03 ± 3.56[a]
Damaged	14.23 ± 1.16[b]	0.24 ± 0.09[a]	0.24 ± 0.09[a]	21.74 ± 9.98[a]

IN-VITRO FLUORIDE ION TREATMENTS AS A TOOL TO INVESTIGATE THE MECHANICAL BEHAVIOR OF BONE WITH REDUCED BONE MINERAL CONTENT

S.P. Kotha[1,2] and N. Guzelsu[1,2]

[1] Biomedical Engineering, Rutgers University, Piscataway, NJ 08854
[2] Biomechanics, Tr# 4, 675 Hoes Lane-UMDNJ, Piscataway, NJ 08854
Email: guzelsu@umdnj.edu

INTRODUCTION

In-vitro fluoride ion treatments have been used to decrease the mineral content of bone (Kotha, et al., 1998). The mechanical behavior of bone with different mineral contents has been studied to understand the composite behavior of bone (Currey, 1990). The extent of mineral dissolution due to extended periods of immersion of bone in *in-vitro* fluoride ion solutions and its effects on the tensile behavior of bone are investigated in this study.

METHODS

Bovine plexiform femoral bone from 12 to 18 month old steer were obtained from a local slaughterhouse (MOPAC, Souderton, PA). The lateral and medial quadrants machined into dumbbell shaped mechanical test specimens (Kotha et al., 1998). The samples were treated in a non-ionic detergent (0.25 % Brij 56) for one day to remove some of the barriers to the diffusion of the fluoride ions. Some of the samples were placed in individual containers containing 1M potassium fluoride solutions for periods of 3 and 12 days while others were immersed in physiologic saline for a period of 12 days to serve as controls. Tensile tests to failure were conducted on an Instron Universal Testing Machine (Model 1321) at a strain rate of 0.0005 s^{-1}. Strain was recorded by an extensometer with a gage length of 12.5mm. The distance between the grips was 34mm. To determine the extent of dissolution due to fluoride ion treatments, some rectangular bars were treated in the same solutions. A decrease in the carbonate content with respect to control bone samples was taken to indicate the extent of dissolution. Carbonate content in the mineral was measured by fourier transform infrared spectroscopy (FTIR). A stir bar and a small aliquot of bone powder (about 25 mg) were placed in a petri-dish that was kept in a 10-cm gas cell. The gas cell was sealed after introducing 3ml of 3M hydrochloric acid into the petri-dish to dissolve the bone powder. After 10 minutes of stirring in the gas cell absorbance at 2360 cm^{-1} was measured. The amount of carbon dioxide in the sample was determined relative to the absorbance of carbon dioxide standards at 2360 cm^{-1}.

RESULTS

Carbonate content decreased by 20% in the 3 day fluoride treated and 32% in the 12 day fluoride treated bone when compared with controls. The representative stress-strain curves for control and fluoride treated bone are shown in Figure 1. The elastic modulus of the 3 day and 12 day fluoride treated bone decreased by 30% and 50% respectively with respect to controls. The yield and ultimate stresses decreased while ultimate strain increased with increased immersion times in fluoride ion solutions.

DISCUSSION

When bone is treated with high concentrations of fluoride ion solutions, the principal reaction is the dissolution of bone mineral leading to the precipitation of calcium fluoride or fluoroapatite like material (Lin, et al., 1981). This precipitate is assumed not to contribute to the mechanical properties of bone and acts like a filler material. Some of the fluoride exchanges with the hydroxyl ions or type A carbonate ions. This exchange mechanism leads to a decrease in the carbonate content. Therefore, a decrease in carbonate ion contents gives the upper limit of the bone mineral dissolution.

The composite behavior of bone with different bone mineral contents has been investigated (Currey, 1990). Bone from different organs and species was used in the study. The mechanical properties and volume fraction of the organic would be different in the tissue studied. In this study, we have taken bovine plexiform bone and altered its bone mineral content using *in- vitro* fluoride ion treatments. We study the composite behavior of bone where the volume fractions of the organic as well as its mechanical properties are not altered. This study like the one conducted by Currey (1990) shows that the elastic modulus, yield and ultimate stresses are reduced while the ultimate strains are increased by the reduced mineral content. This indicates that the mechanical properties of the organic are changed by a decrease in the bone mineral content. This is most likely due to an increased sliding between the collagen molecules due to a reduction in the bone mineral reinforcements.

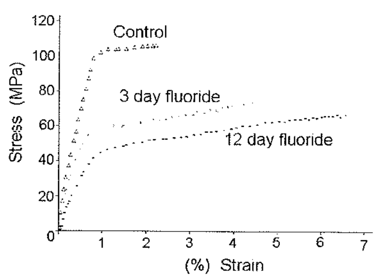

Figure 1: This graph shows representative stress-strain curves for Control, 3 and 12 day fluoride treated bone.

REFERENCES

1) Currey, J.D. (1990). *J. Biomech.* 23(8):837-844.

2) Kotha, S.P. et al. (1998). *Biomed. Mat. Engnrg.* 8:321-34.

3) Lin, J. et al. (1981) *Colloids and Surfaces.* 3:357-370.

ACKNOWLEDGEMENTS

NSF: BCS-9210253

Table 1: Mechanical properties and carbonate contents (mean ± SD).

	Elastic Modulus (GPa)	Yield Stress (MPa)	Ultimate Stress (MPa)	Ultimate Strain (%)	Carbonate Content (%)
12 day Control	19.0 ± 2.5[a]	97.0 ± 17.0[a]	101.1 ± 18.8[a]	2.87 ± 1.33[a]	5.0 ± 0.2[a]
3 day Fluoride	13.2 ± [illegible]2[b]	62.6 ± 10.1[b]	75.6 ± 12.0[b]	4.54 ± 1.18[b]	4.0 ± 0.3[b]
12 day Fluoride	9.6 ± [illegible]	42.4 ± 7.0[c]	68.0 ± 13.8[b]	6.58 ± 1.42[c]	3.4 ± 0.2[c]

Lower Extremity Stiffness in Runners with Different Foot Types

D. Williams[1], I. McClay[1,2], J. Scholz[1], T. Buchanan[3] and J. Hamill[4]

[1]Motion Analysis Laboratory, University of Delaware, Newark, DE 19716
[2]Joyner Sportsmedicine Institute, Harrisburg, PA 17111
[3]Department of Mechanical Engineering, University of Delaware, Newark, DE 19716
[4]Department of Exercise Science, University of Massachusetts, Amherst, MA 01003
e-mail: blaise@udel.edu

INTRODUCTION

The foot is the interface with the ground during gait. Therefore, differences in foot structures may result in differences in lower extremity mechanics. It is often suggested that low arch (LA) feet are flexible while high arch (HA) feet are more rigid in nature (Subotnick, 1981). Decreased flexibility at the foot is often associated with decreased overall lower extremity flexibility. This decreased compliance may result in a functionally stiffer gait pattern.

Stiffness during gait has been defined as the amount of vertical deflection of the body's center of mass for a given ground reaction force (McMahon and Cheng, 1990). Stiffness has recently been found to differ in individuals with different foot orientations during running (Viale et al, 1998). However, arch height was not characterized in this study. Running on stiffer surfaces results in greater initial peak ground reaction forces and vertical loading rates (VLR) (McMahon and Greene, 1979). It is therefore likely that a stiffer foot resulting in a stiffer gait will lead to a higher VLR. Finally, support moment (sum of the extensor moments of the hip, knee and ankle) may act to produce a stiffer landing.

Therefore, the purpose of this study was to compare lower extremity stiffness between HA and LA runners. It was hypothesized that HA runners would exhibit increased lower extremity stiffness associated with greater vertical loading rates and increased support moments.

PROCEDURES

The study included 20 HA and 20 LA with no lower extremity injury at the time of the experiment. Subjects were screened for inclusion in the HA or LA group using an arch ratio (Williams et al, in review). The arch ratio was defined as the height to the dorsum of the foot from the floor at 50% of the foot length divided by the individual's truncated foot length. Arch ratio values fell at or outside 1.5 standard deviations of the mean DORS/TFL ratio measurement based on a sample of 102 feet. Retroreflective markers were placed unilaterally on the segments of the rearfoot, shank, thigh and pelvis. The subjects ran along a 25 m. runway at a speed of 3.35 m/s +/- 5%. Kinematic data were collected at 120 Hz using 6 camera VICON motion analysis system (Oxford Metrics Limited, UK and force data (BERTEC, Worthington, OH) were recorded at 960 Hz. Ten footstrikes were collected and averaged for each subject. The kinematic and force data were combined to calculate joint moments through inverse dynamics.

Stiffness was estimated dynamically using the mathematical model presented by McMahon and Cheng (1990). Support moment was analyzed at the time of initial peak VGRF (SMFZ), peak knee flexion angle (SMKF) and peak A-P propulsive ground reaction force (SMAP). Finally, VLR was determined by calculating the rate of rise of the heel strike transient of the vertical ground reaction force over the interval spanning 20% to 80% of this peak. Comparison between HA and LA subjects were made using a one-tailed student's t-test ($p \leq 0.05$) to determine whether differences in stiffness existed between these groups. A backwards multiple regression was employed on support moment and loading rate variables.

RESULTS and DISCUSSION

Table 1. Stiffness Characteristics

	HA	LA
Stiffness(N/m)	7.2(1.2)	6.5(1.0)*
Support time (s)	0.26(0.02)	0.27(0.02)*
Vert Disp (m)	0.07(0.01)	0.08(0.01)*
VLR (N/s)	62.5(13.6)	52.1(10.8)*

N=Newtons, m=meters, s=seconds, *$p \leq 0.05$.

HA individuals showed no difference in support moment parameters. There was a significant relationship between loading rate and SMFZ and lower extremity stiffness ($R=0.558$, $p=0.000$). VLR and SMFZ explained 27.8% of the variance present in lower extremity stiffness ($R=0.563$, $p=0.001$).

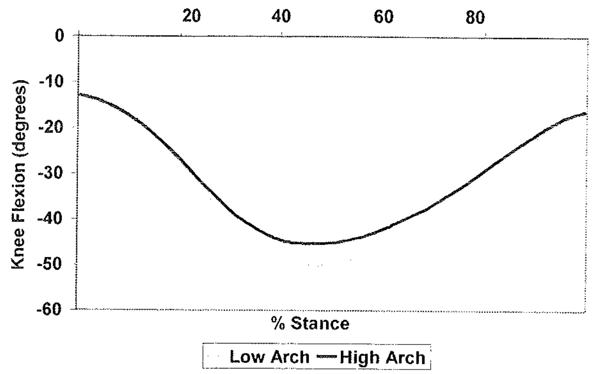

Figure 1. Knee Flexion Excursion During Stance

The results of this study supported the hypothesis that HA runners exhibited greater lower extremity stiffness. Stiffness has been shown to be related to speed in the past (McMahon and Cheng, 1990). However, both groups in the current study ran at the same forward velocity. Therefore, differences in stiffness can be attributed to factors other than forward velocity. HA runners exhibited shorter contact times and less vertical displacement of the center of mass, which would account for the increased stiffness. Although decreases in joint excursions of hip flexion, knee flexion and ankle dorsiflexion could account for a decreased COM excursion, only knee flexion excursion was significantly lower ($p=0.007$) in the HA group by 4.2 degrees when compared to the LA group. The decrease in contact times in the HA group may be due to smaller COM and knee joint excursion resulting in a more efficient stretch-shortening cycle and a quicker return of energy (McMahon and Greene, 1979).

Loading rate was the primary predictor of lower extremity stiffness. The decreased vertical displacement of the COM combined with shorter contact times in the HA runners likely resulted in faster loading and higher lower extremity stiffness. Vertical loading rate has previously been suggested to increase the risk of stress-related injuries to the lower extremity (Radin, 1991). Therefore, HA runners may benefit from training techniques to increase COM excursion, thus decreasing vertical loading rate and lower extremity stiffness during running.

SUMMARY

Based on the results of this study, it appears that there is a greater lower extremity stiffness in individuals with a HA foot structure when compared to those with a LA foot structure. This difference appears to be the result of a decreased COM excursion and a decreased foot contact time. The COM excursion appears to be regulated primarily by the control of knee flexion excursion. This stiffer limb leads to a quicker loading rate, which may increase the risk of stress injuries to the lower extremity.

REFERENCES

McMahon and Cheng, ***J. Biomech*** 1990
McMahon and Greene, ***J. Biomech*** 1979
Radin, ***J. Orthop Res*** 1991
Subotnick, ***Phys Sports Med*** 1991
Viale et al, ***Foot Ankle Int*** 1998

LOWER EXTREMITY POWER GENERATION STRATEGIES SPECIFIC TO TASK CONSTRAINTS

Kathleen E. Costa, J.L. McNitt-Gray, W. Mathiyakom, P. Requejo, and J. Eagle

Department of Exercise Science, University of Southern California, Los Angeles, California
Email: kcosta@usc.edu

INTRODUCTION

Previous research indicates divers performing forward and backward dives (Mathiyakom et al., 1998) and gymnasts performing landings of forward and backward rotating somersaults (McNitt-Gray et al., 1995) utilize different lower extremity mechanics to generate and control total body momentum. As with divers and gymnasts, heptathletes must successfully perform multiple events that require power generation in different directions. During the unseating phase of the shot-put and the take-off phase of the hurdle, hepathletes must generate horizontal momentum while limiting vertical momentum. During the take-off phase of the hurdle horizontal momentum must be generated in the forward direction, where as in the unseating phase of the shot-put, horizontal momentum must be generated in the backward direction. The purpose of this investigation was to test the hypothesis that multi-event athletes distribute power generation across the lower extremity in a different manner when generating horizontal momentum in forward versus backward directions. Identification of similarities and differences in power generation mechanics between events performed by multi-event athletes is necessary for improvement in designing sport specific training regimes for multi-event athletes.

PROCEDURES

Members of the USA Women's Heptathlon team (n=4) performed a series of hurdle take-offs (H) on a track and shot-put throws (SP) in a pit under the direction of their coach as part of a training camp. Ground reaction forces (GRF) during H and SP were quantified using a force plate mounted in the track and in the shot pit (600Hz, Kistler) and sagittal plane kinematics were simultaneously videotaped (60 fps). Kinematic and reaction force data were synchronized at force plate contact during H and at force plate departure during SP, data were processed as previously described (Costa & McNitt-Gray, 1999), and kinetic variables of the support leg were determined during the propulsion phase of each task using Newtonian mechanics. The propulsion phase was defined as the time at which all joints of the support leg were extending until ground departure. Net joint moment work (NJMW) of the ankle, knee, and hip was determined by integrating the net joint moment power (NJMP), defined as the product of net joint moment (NJM) and joint angular velocity (ω_j), during the propulsion phase. Within-subject, between-task comparisons were performed to determine differences in power generation strategies used to generate horizontal momentum in the forward and backward direction.

RESULTS AND DISCUSSION

Heptathletes demonstrated significant differences in power generation strategies when generating momentum in the forward as compared to the backward direction (Figure 1a and b). Heptathletes generated more positive NJMW at the hip when generating momentum in the backward direction as compared to the forward direction. Differences in NJMW at the hip between tasks were attributed to greater hip extensor NJM magnitudes and longer duration of propulsion phase during the SP as compared to the H (Figure 1c). No significant differences in hip angular velocity were observed between tasks during the propulsion phase, however, hip velocity was largely created by trunk motion during the SP task and by thigh motion during the H task.

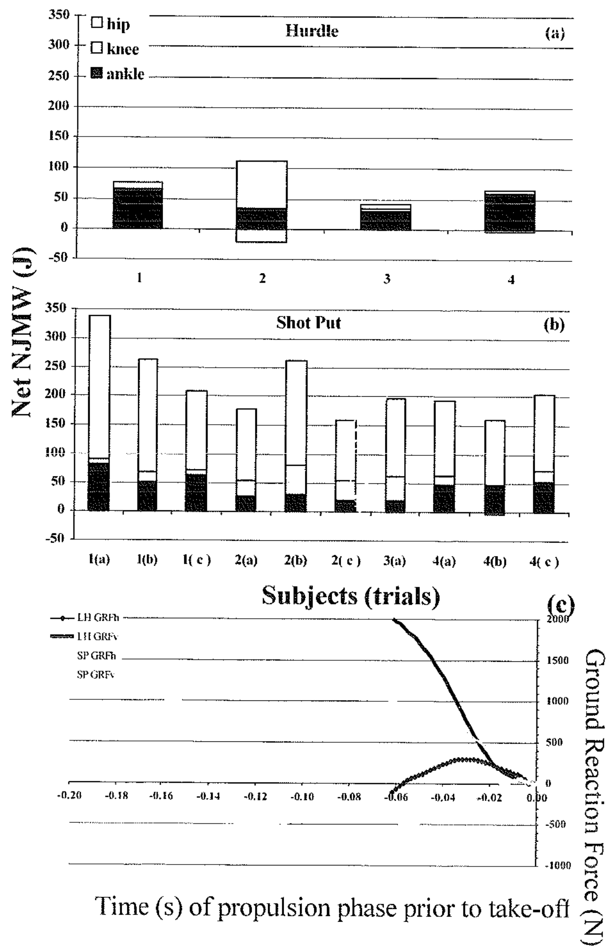

Figure 1. Net NJMW of ankle knee and hip for each subject (1-4) during propulsion phase of H (a) and SP (b), (c) vertical and horizontal GRFs during the propulsion phase of the H and SP for an exemplar subject (#4).

Although the absolute NJMW at the ankle were not significantly different between tasks, the relative contribution of the ankle NJMW to the total lower extremity work was significantly less during the SP task than the H task. The lower degree of ankle contribution to the total lower extremity work during the SP task may have been limited as a result of ankledorsiflexion observed prior to take-off.

In conclusion, significant differences in distribution of power generation between tasks may reflect task specific differences in momentum direction, propulsion phase duration, and/or kinematic constraints imposed by the task.

REFERENCES

Costa, K. & McNitt-Gray, J.L., (1999). *ISB 99* , 170.

Mathiyakom, W. et al., (1998). *NACOB '98,* 439-440.

McNitt-Gray, J.L. et al., (1995). ASB 95, 199-200.

THE BIOMECHANICS OF PORCINE CORNEAS

T.A. Newson[1] and I. MacPherson[1]

[1]The Department of Civil Engineering, University of Dundee, Scotland, DD1 4HN, United Kingdom. [email: t.a.newson@dundee.ac.uk]

INTRODUCTION

The anterior corneal surface accounts for over two-thirds of the optical power of the eye. Ninety percent of the corneal thickness is formed by the stroma. This is assumed to control the majority of the biomechanical behaviour of the cornea and mainly consists of water (78%) and layered protein fibres (16%), which provide strength, elasticity and form.

The stroma is divided into 300-500 sheets of collagenous material, *the stromal lamellae*, lying parallel to the corneal surface. Each lamella is composed of long collagen fibrils, which are embedded in a jelly-like ground substance. Thus the cornea can be thought of as a composite structure. The collagen fibrils have a Young's modulus (E) of the order of 1.0 GPa, along the fibril direction. However, the Young's modulus and the shear modulus of the ground substance are only in the order of 10^{-5} GPa. Therefore the stroma offers very little resistance to shear forces due to the properties of the ground substance and the orientation of the fibrils.

The overall aim of this research was to develop a finite element computer model of the human cornea, to assess the effects of keratorefractive surgery and corneal thinning disease. As part of the evolution of this model, techniques were developed for testing the biomechanical response of porcine cornea. This study is described in further detail below.

METHODS

Testing was conducted on fresh enucleated porcine eyes. A pressurised chamber filled with buffered saline solution was used to inflate corneal buttons (including an outer 5mm ring of sceral tissue) to determine the pressure-deformation response. The chamber was mounted into a modified Orbscan® unit to provide continuous topographic and pachymetric data on the specimens (accurate to 1-2μm). Testing was conducted in a temperature and humidity controlled environment. Three different types of test were carried out on a number of porcine corneal samples: load, unload and cyclic. The changes in corneal topography and pachymetry with pressure were measured.

RESULTS AND DISCUSSION

A typical cyclic loading test is shown in Figure 1, where three cycles of pressure

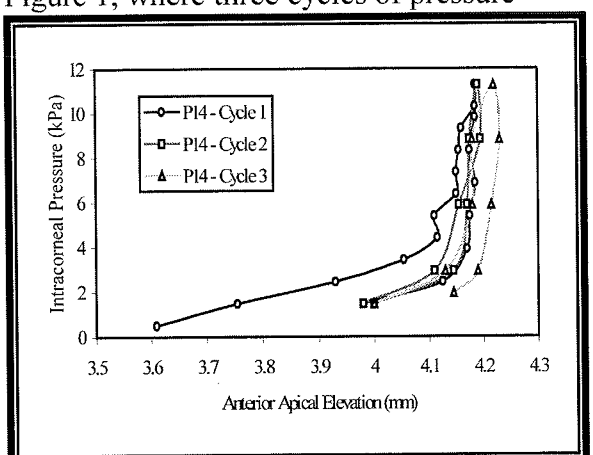

loading and unloading were performed.

Figure 1: Typical corneal pressure-deformation data for a porcine specimen The curves show considerable non-linearity, indicating a material that increases in stiffness with increasing pressure. The curve from the first cycle shows a rapid change in gradient between 2 and 4 kPa, which is in the region of the normal intra-ocular pressure of the porcine eye. During unloading, the curve follows a different path. The cornea does not fully recover the deformation created by the loading process. The second and third pressure cycles cause further deformation and the pressure-deformation curves are seen to shift to the right. If this process were to be repeated indefinitely, the difference between successive cycles would decrease and eventually disappear.

The porcine cornea had diameters of approximately 16 mm. The pachymetry at the centre of the cornea was 0.55 mm and 0.74 mm at the periphery. The corneal pachymetry was found to change under increased pressures. Measurements showed an 8% decrease in thickness due to the applied pressure. At low pressures, the rate of reduction in corneal thickness was large, but this reduces as the pressure increases.

After a loading and unloading cycle the cornea appeared to become opaque. Since the transparency of the cornea is dependent upon the regular distribution of the collagen fibrils, this suggests internal disruption of the structure had occurred. The load-deformation data shows a distinct change in behaviour between 2-4 kPa. At low stresses the corneal structure remains intact, with the collagen fibrils taking much of the load. Thus low-pressure cycles produce non-linear elastic loading paths with very limited hysteresis. At higher pressures, the collagen is no longer able to accommodate the required strains and relative sliding occurs between fibrils, which leads to permanent deformation on unloading (although a large amount of elastic recoverable deformation occurs, due to the collagen). Repeated cycling will eventually lead to structure where no further change occurs with cycling routine and this is therefore a preconditioned state. These structural changes need to be confirmed by techniques such as SEM.

One of the shortcomings of previous attempts to model corneal bio-mechanical behaviour has been related to the constitutive laws adopted. These have been inappropriate to accurately describe the behaviour, e.g. isotropic linear elasticity or empirical constitutive laws have been used, with insufficient validation (e.g. Pinsky and Datye, 1991). Consequently, a number of important material characteristics have yet to be modelled correctly, e.g. load-unload hysteresis, relaxation at constant strain and pre-conditioning during repeated load-unload cycles. This study has provided valuable data that enables validation of new more appropriate constitutive models.

SUMMARY

Testing showed the cornea to be non-linear elastic, with increasing stiffness with pressure and displaying preconditioning and permanent deformations over threshold pressure. Thinning of structure occurred during loading and behaviour was attributed to structural changes in stroma.

REFERENCES

Pinsky, P.M. and Datye, D.V. (1991). A micro-structurally based finite element model of the incised human cornea. *J. Biomechanics*, 24, 907-922.

AN EVALUATION OF MUSCLE MODEL PARAMETERS DETERMINED BY AN OPTIMAL FIT TO A STATIC STRENGTH CURVE

Zachary Domire and John H. Challis

Biomechanics Laboratory, The Pennsylvania State University, University Park, Pennsylvania
Email: zjd100@psu.edu

INTRODUCTION

For musculo-skeletal simulation the determination of model parameters is an important step. In order to characterize the muscular portion of the simulation model, several parameters must be determined. To determine muscle's static moment producing capability, it is necessary to know for each of the contributing muscles: degree of activation, moment arm, fiber length, tendon length, and the force-length properties.

Hatze (1981) presented a technique to determine the value of several of these parameters when given joint moments for a range of joint angles. Such an approach is attractive, particularly if a subject specific model is to be developed. However, to the best of our knowledge a careful evaluation of this method has never been performed. The purpose of this study was to determine the effectiveness of this approach in reproducing joint moment profiles of individual muscles.

PROCEDURES

The three major elbow flexors were chosen to evaluate the technique. Two different muscle models were developed. The first model was used to produce theoretical data where the individual muscle moment profiles were known. Given the data from the first model, parameters were determined for the second model.

Model one consisted of the force-length model of Hatze (1981), and a non-linear model spring representing the tendon. The parameters for the three muscles in model one were obtained from the literature (Hatze, 1981; Challis and Kerwin (1994). The muscle lengths were taken from van Zuylen (1988), and the moment arms were from Pigeon (1996).

Model one was then used to produce moment-angle curves for each of the three modeled muscles. The data were then summed to produce the net moment-angle curve for the elbow. To make the data more realistic random error was then added to this data. The distribution of random errors was estimated from a series of maximum efforts obtained from four subjects over the course of several weeks.

Given the noisy data from model one the task was to estimate the parameters for model two. To do this a static optimization algorithm was used, where the task was to find the muscle model parameters for model two so that a good fit was obtained to the moment-angle curve produced by model one. Multiple seeding of initial parameters estimates were required to guarantee optimization convergence.

The second model differed from the first in that the tendons in the second model were assumed to have a linear stress-strain curve, and a different model of the force-length curves of the fibers was used.

The net joint moment and the individual muscles moment-angle curves from model one were compared with those estimated by model two. The comparisons were numerically quantified using percentage root mean squared difference (%RMSD).

RESULTS

The model was able to fit the total moment angle curve very well. Typically %RMSD was less than one percent. The individual moment angle curves varied between two and 35 percent. Figure 1 shows a typical set of fits.

DISCUSSION

The evaluations run assumed that the moment arms and muscle lengths were known for each of the elbow flexors. It was also assumed that the maximum isometric forces were known. Although this may not seem realistic, all of the variables can be determined from MRI.

The evaluation used two different muscle models to evaluate the technique for determining model parameters. This approach is required because there is no other source of criterion data. This evaluation could be considered a best case scenario.

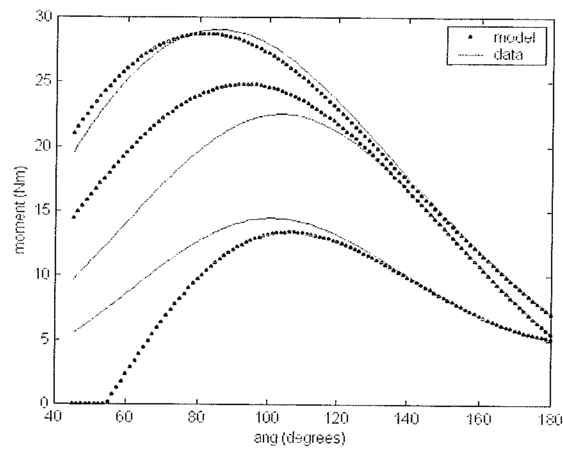

Figure 1: Top - biceps 2.6 %RMSD. Middle - brachialis 17.3 %RMSD. Bottom - brachioradialis 27.6 %RMSD.

Using optimization to determine muscle model parameters can accurately reproduce the total joint strength curve. In many investigations this may be sufficient. However, some cases, such as the modeling of surgical interventions, require the role of individual muscles to be determined. This technique can be fairly effective in these applications if the number of parameters to be determined is kept to a minimum.

REFERENCES

Challis, J.H., Kerwin, D.G. (1994). *Human Movement Sci,* **13**, 29-61.

Hatze, H. (1981). *Eur. J. App. Physio.*, **46**, 325-338.

Pigeon, P., et al. (1996) *J. Biomechanics*, **29**, 1365-1370

van Zuylen, E., et al. (1988). *J.Biomechanics,* **21**, 183-190.

STIFFNESS AND VISCOUS DAMPING OF THE HUMAN LEG

Li-Qun Zhang [1-4], Dali Xu [1,2], Mohsen Makhsous [1,2], and Fang Lin [1,2]

[1]Sensory-Motor Performance Program, Rehabilitation Institute of Chicago
Departments of [2]Physical Medicine & Rehabilitation, [3]Orthopaedic Surgery, and
[4]Biomedical Engineering, Northwestern University Chicago, Illinois
Email: l-zhang@nwu.edu

INTRODUCTION

Mass and spring model has been used in various studies to characterize the biomechanical features of the human leg and body[1,2]. Since human legs have inherent damping as well as stiffness properties[3], the body does not bounce like an undamped spring and mass in many cases. Viscous damping plays an important role in the functioning of the leg and body and helps absorb shocks and maintain stability. Compared with leg stiffness, much less work has been done to study the leg viscous damping property of human subjects. The purpose of this study was to quantify and study the viscous damping as well as stiffness of the leg and body through in vivo experiment on human subjects.

METHODS

Three subjects participated in the study. The subjects stood with both feet on an AMTI force platform. The body center of mass (COM) was moved up and down in small amplitude and random pattern by lifting the trunk through a harness and rope-pulley which flexed the knees, ankles, and hips slightly. The feet were stationary during the body movement. An Optotrak system was used to measure the movement with markers placed at the fifth metatarsal, heel, lateral malleolus, mid-leg, lateral epicondyle of the femur, greater trochanter, ASIS, and the acromion, and they were used to construct the stick figure (Fig. 1(b)). The subjects squatted slightly and the trunk was vertical.

The vertical movement of the marker on the ASIS was taken as the vertical movement of the body COM. Ground reaction force and lifting force were displayed on a computer monitor in real-time to help generate the small-amplitude random vertical movement.

The leg and body were modeled by a spring with stiffness (k), a dashpot with viscous damping (c), and a mass (m) (Fig. 1(a)).

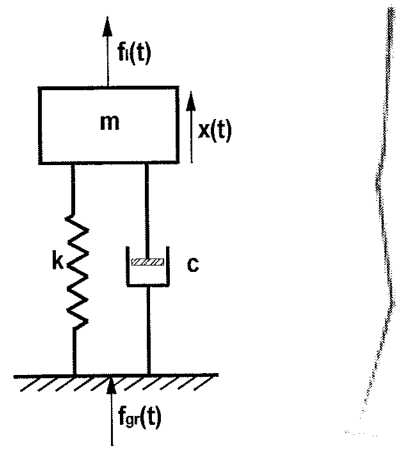

Figure 1: (a) A dashpot (c), spring (k) and mass (m) model of the human leg and body. (b) Stick figure during the COM movement trial.

The system was assumed linear time-invariant during the small-amplitude movement, and the vertical COM displacement x(t) was related to the vertical lifting force $f_l(t)$ as follows:

$$m\frac{d^2x(t)}{dt^2}+c\frac{dx(t)}{dt}+k\Delta x(t)=\Delta f_l(t)+e(t)$$

where Δx (t) and $\Delta f_l(t)$ represented the deviations of the vertical COM displacement and the vertical lifting force from their initial values, respectively. The gravitational force was assumed constant during the movement and thus did not appear in the above equation. e(t) was the modeling error.

System identification approach was used to estimate the model parameters from the measured body COM displacement and lifting force[4]. Since the body mass (m) could be measured separately, only the stiffness (k) and viscous damping (c) need to be estimated. The estimation was done over every 2-second long data with two consecutive segments overlap by 50%. The estimated parameters were averaged over the multiple segments. The variance accounted for (VAF), defined as VAF=$(1-\sigma_e^2/\sigma_s^2)*100\%$ (σ_s^2 and σ_e^2 were the variances of signal and simulation error respectively), was used to evaluate the modeling result.

RESULTS AND DISCUSSION

For a subject with a body mass of 78 kg, the body COM moved up and down in a range of about 7 mm and the corresponding lifting force varied about 200 N. The estimated viscous damping (c) was 950 N•s/m and the leg stiffness (k) was 28,500 N/m. The simulated and measured forces matched well with a typical VAF of 90%. Stick figure showed that the knee, hip, and ankle joints flexed slightly and contributed to the leg stiffness and viscous damping (Fig. 1(b)).

Viscous damping plays an important role in biomechanical movement. The estimated leg stiffness and viscous damping parameters were used to simulate body COM movement with a step input (a suddenly applied lifting force of 100 N to the body). With the damping ratio $\zeta = d/2/\sqrt{mk}$ =0.55, the body COM quickly reached its steady position of about 3.5 mm (Fig. 2). In contrast, with ζ=0 (no viscous damping), the body COM would oscillate infinitely between 0 and 7.0 mm.

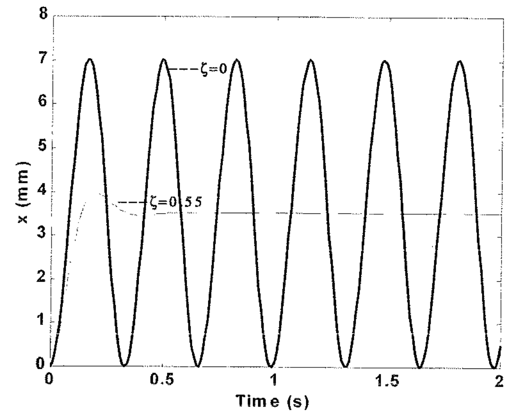

Figure 2: Simulation of COM vertical movement with a suddenly applied lifting force of 100 N (at time=0). Natural undamped frequency $\omega_n = \sqrt{k/m}$ =19 rad/sec and leg stiffness k = 28,500 N/m were used.

SUMMARY

Viscous damping helps absorb shock and maintain stability in functional tasks of various biomechanical systems. A better understanding of the viscous damping facilitated by in vivo estimation of the relevant parameters help us to gain insights into the control of biomechanical systems.

REFERENCES

1. McMahon, T.A. & Cheng, G.C. *J. Biomechanics* **23**, 65-78 (1990).
2. Farley, C.T. et al. (1998). *J. Appl. Physiol.* **85**, 1044-1055.
3. McMahon, T.A. & Greene, P.R. *J. Biomechanics* **12**, 893-904 (1979).
4. Zhang, L.-Q. et al., *J. Biomech.* **31**, 71-76 (1998).

ACKNOWLEDGEMENTS

The authors would like to acknowledge the support of the NIH and Falk medical Research Trust.

A TECHNIQUE TO ENLARGE THE 3D CONTROL VOLUME USING MULTIPLE CALIBRATION FRAMES AND THE DLT THEORY

Deborah King, Owen Murphy, and Meris Johnson

Biomechanics Lab, Montana State University, Bozeman, Montana
Email: dking@montana.edu

INTRODUCTION

The direct linear transformation theory (DLT) is one of the most widely accepted methods for determining three-dimensional coordinates for human movement analysis. The DLT theory allows for a relatively simple and flexible camera set-up and can produce accurate 3D reconstruction (Challis & Kerwin, 1992; Chen et al., 1994). However, for many activities, the spatial requirements of the control object can limit the use of the DLT theory.

Sports such as pole vault and figure skating involve large volumes of space. While control objects of sufficient size to encompass these activities can be constructed, several difficulties may arise: 1) maintaining accuracy due to structural distortion and flex, 2) assembling the object in limited time, and 3) maneuvering the object. Survey poles avoid the structural problems, but take time to survey and require surveying equipment. Pan and tilt video methodology solves the need for large control objects and allows large image sizes to be maintained, but requires specialized equipment and/or software. The purpose of this paper is to introduce a technique by which multiple control objects can be used with the DLT theory to calibrate an enlarged volume.

METHODS

By overlapping two calibration frames (Figure 1), it is possible to enlarge the space that could be calibrated using only one frame. Neither the location of the two frames, nor the control points of either frame need to be measured or surveyed during or after set-up.

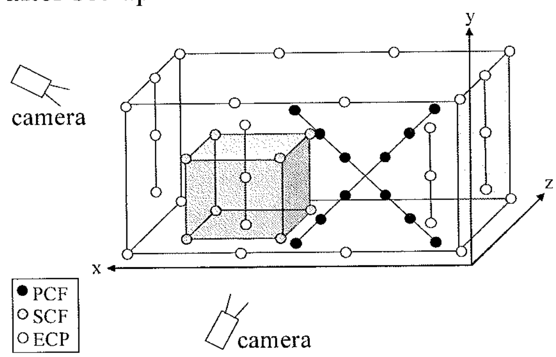

Figure 1. Calibration set-up. PCF = primary control frame, SCF = secondary control frame, and ECP = experimental control points. Not all points shown, NTS.

Step 1 - digitize the primary calibration frame (PCF, Figure 1) from each camera view and use the DLT theory to develop the DLT equations to predict 3D coordinates from the 2D coordinates.
Step 2 – digitize three points of the secondary calibration frame (SCF, Figure 1) that overlap with the PCF and determine their 3D coordinates using the DLT equations determined in step 1.
Step 3 – perform a coordinate transformation to calculate the coordinates of the SCF relative to the PCF based on the 3D coordinates of the overlapping points.
Step 4 – digitize the PCF and SCF in each camera view and use the DLT theory to determine the DLT equations based on the known locations of the PCF and the calculated locations of the SCF.

Table 1. RMS errors for re-predicting PCF and SCF points and for predicting ECPs for selected SCF positions.

	RMS Error (meters)					
	Re-predicted SCF and PCF points			Predicted ECPs		
SCF Position	*X-Axis*	*Y-Axis*	*Z-Axis*	*X-Axis*	*Y-Axis*	*Z-Axis*
0.1 m overlap	0.003	0.005	0.01	0.011	0.019	0.036
0.3 m gap	0.006	0.007	0.007	0.013	0.027	0.038
0.6 m gap	0.006	0.005	0.008	0.019	0.037	0.033
0.9 m gap	0.004	0.006	0.006	0.017	0.038	0.022

To test the accuracy of this technique, a set of experimental control points (ECPs, Figure 1) was constructed to encompass the calibrated volume. The total volume, with the PCF, SCF, and ECPs in place, was video taped with two normal speed video cameras. A Peak Motus system was used to perform the 4-step calibration along with a coordinate transformation program written in VisualBASIC. The root mean square (RMS) differences for re-predicting the PCF and SCF points and predicting the ECPs were determined along the x, y, and z-axes. Additionally, the SCF was moved from its overlapping position with the PCF in 0.1 m increments to determine if the PCF and SCF could be separated to further enlarge the volume while maintaining an accurate 3D reconstruction.

RESULTS AND DISCUSSION

The RMS errors for re-predicted the PCF and SCF points were 0.01 m or less along all axes, even with the PCF and SCF separated by 0.9 m (Table 1). Along the x-axis, the RMS errors for predicting the ECPs remained under 0.024 m (0.5% of the length of the volume) and showed no relationship to separation distance between the two frames (Table 1). The errors along the y and z-axes were larger, up to 0.038 m (1.7% of height and width) and did vary as the control frames were separated. However, the SCF was actually lower in height and narrower in width than the PCF and some of the ECPs were outside the calibrated volume, which influences accuracy (Wood & Marshall, 1986). Using only ECPs within the calibrated volume the errors were reduced to less than 0.5% of the height and width for all positions of the SCF.

SUMMARY

Using two overlapping or adjacent calibration frames to enlarge the 3D volume appears to provide accurate results. Errors for predicting points, were less than 0.5% of the calibrated volume along each axis if the predicted points were within the volume. Errors increased dramatically for predicting points outside the volume and thus care must be taken when using this technique to ensure that the enlarged volume fully encompasses the activity to be analyzed.

REFERENCES

Challis, J.H., Kerwin, D.G. (1992). *J. Biomech*, **25**, 1053-1058.

Chen et al. (1994). *J. Biomech*, **27**, 493-500.

Wood, G.A., Marshall, R.N. (1986). *J. Biomech*, **19**, 781-785.

EFFECTS OF PROLONGED ACTIVITY ON VERTICAL JUMP PERFORMANCE

Jill S. Carson, Jonathan E. Frank, and Robert Shapiro

Biodynamics Lab, University of Kentucky, Lexington, Kentucky
Email: rshap01@ pop.uky.edu Web: uky.edu/Education/khphead.html

INTRODUCTION

Many research projects investigate the effects of peripheral fatigue on certain activities such as walking, jumping, and cutting (Viitasalo et. al.,1993, Nyland et. al.,1994). Typically subjects undergo a prolonged activity protocol to induce peripheral fatigue and then perform selected trials of a specified skill. It is not clear however, how long the effects of prolonged activity last. When subjects are peripherally fatigued prior to testing, the level of fatigue varies greatly among the testing trials as more time passes from the fatiguing bout. Several different fatigue protocols have been utilized, including the use of treadmills, isokinetic dynamometers, and intensive exercise bouts. For isokinetic protocols, typically a decrease in torque production is measured. Once the subject is fatigued (as defined by the investigators) the subjects have to get out of the apparatus, move to the testing area, and wait for the investigators to prepare for testing before testing actually begins. By this time significant recovery may have occurred, and it is unknown as to how much the subject has recovered. As each trial goes by, more time passes, and more recovery takes place. Few have studied recovery rates of lower extremity peripheral muscle fatigue (Robinson et.al.,1990, Milner-Brown et.al.,1986). The purpose of this investigation was to determine how long the effects of peripheral fatigue last using a lower extremity peripheral fatigue protocol to enable investigators to more efficiently design experiments.

METHODS

Six male and 3 female healthy, volunteers were tested. The subjects were 26.9 (±5.3) years of age, 172.5 (±8.6) cm tall, and weighed 754.5 (±180.2) N. Subjects did not have any injuries within the past three years. Informed consent was obtained from each participant.

Each subject warmed up by walking on a treadmill for 5-10 minutes followed by light stretching. Reach height was measured. All height measurements were made to the nearest inch using a home made device for measuring jump height. The subjects performed five maximal vertical jumps, the highest jump defined the maximum jump height (MJH). Each subject performed six trials consisting of the following procedures: Subjects maximally jumped at a rate of 1 jump every 2 seconds until 3 consecutive jumps fell below 50% of the MJH (fatigue level)(prolonged activity protocol). They were then randomly assigned a resting period. After resting, the subjects performed 3 more maximum jumps; the heights were recorded (recovery height). The subjects then rested for two-minutes before starting the prolonged activity protocol again. This protocol was be done for resting periods of 15, 30, and 45 seconds, 1, 2, and 3 minutes for a total of 6 trials. The assignment of resting periods was randomized.

Vertical jump height was determined by subtracting reach height from MJH. The three recovery jump heights recorded after each rest interval were averaged. All average recovery jump heights were normalized (NRJH) to the MJHs.

NRJH = 100+[(avg. recovery ht. – MJH)/vertical jump ht. *100].

Repeated measures ANOVA were run to test significance between NRJH and the MJH, NRJH and 50% MJH, and NRJH and 75% MJH ($p<0.05$). SPSS was used for statistical analysis.

RESULTS

Figure 1 shows the recovery jump height as a percentage of MJH. As the rest interval increases, the recovery jump height becomes closer to the MJH. All recovery jump heights were significantly less than MJH. All recovery jump heights were also significantly greater than 50% of the MJH. When compared to 75% of MJH, the 15, 30, and 45-second rest intervals were not significantly different. These results show that between 15 and 45 seconds subjects have already begun to recover from the fatigue level and are at approximately 75% of MJH. Between one and three minutes, subjects are not fully recovered, however, their levels of performance were greater than 75% of their MJH.

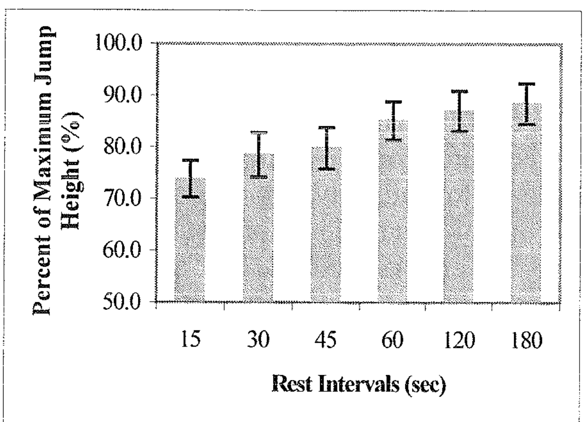

Figure 1: Recovery jump heights as a percentage of maximum jump height.

DISCUSSION

This study investigated how effective a peripheral fatiguing protocol would be in causing a prolonged decrement in performance. This investigation can assist investigators in planning protocols incorporating local fatigue conditions. It appears, based on these data, that subjects must be "re-fatigued" between trials, and investigators must keep the time between reaching "fatigue" and data collection to a minimum, under 15 seconds, if possible.

REFERENCES

Robinson, L.R., Mustovic E.H., et.al. (1990). *Archives of Physical Medicine and Rehabilitation*, **71**, 901-904.

Milner-brown, H.S., Mellenthin, M., et.al. (1986). *Archives of Physical Medicine and Rehabilitation*, **67**, 530-535.

Viitasalo, J.T., Hamalainen, K., et.al. (1993). *J. Sports Science*, **11**, 503-509.

Nyland, J.A., Shapiro, R., et.al. (1994). *J. Orthopaedic and Sports Physical Therapy*, **20**, 132-137.

ACKNOWLEDGEMENTS

Lexington Clinic Research Foundation

DEFORMATION CONTOUR MEASUREMENT WITH FIBER-OPTIC SENSOR TECHNOLOGY

J. T. Butcher, C.R. Bass[1], and L. Danisch[2]

[1]Automobile Safety Lab, University of Virginia, Charlottesville, Virginia
[2]Measurand, Inc. Fredericton, New Brunswick, Canada
Email: jtb2n@Virginia.edu

INTRODUCTION

Many applications in biomechanical research desire to monitor the changing shape of a locally deforming contour. Current contour measuring devices, such as the External Peripheral Instrument for Deformation Measurement (EPIDM), or chestband, uses an array of strain gauge bridges to measure local curvature at discrete intervals (Eppinger, 1989). These curvatures are then integrated to determine local contours in an impact environment. Though widely used to monitor thoracic contours during a frontal crash test, this instrument is bulky and has limited durability and accuracy in severe impact situations (Bass et al, 2000; Shaw et al, 2000).

Alternative measurement technology has been developed to address these issues. Shape Tape, designed by Measurand Inc., relies on fiber optic sensing loops, which are treated to lose light proportional to bending. These loops are arranged in sensor pairs, which are adhered to the top and bottom surface of a metal substrate. The prototype band contains eight sensors, each spaced an inch apart. This array is enclosed in a protective metal casing, shown in figure 1.

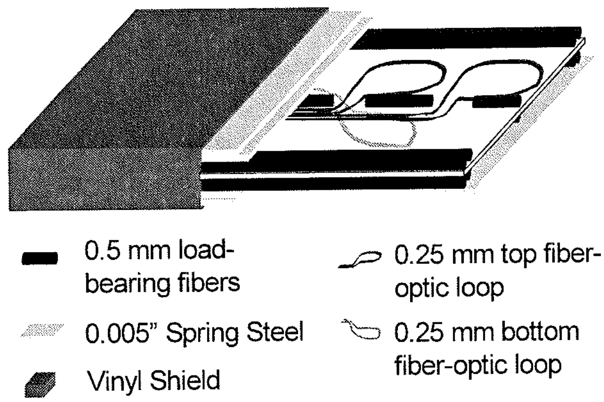

Figure 1: Shape tape Components

EVALUATION METHODS

Several tests were conducted to evaluate the effectiveness of Shape Tape. A calibration test was performed to investigate the linearity of the sensors. The band was wrapped around mandrels of varying diameters. The recorded signal voltages were compared to the mandrel curvatures to determine their relationship. The repeatability and durability of the sensor band was determined by adhering it to a linkage system driven by a motor. This cycled the band in a serpentine fashion for approximately 1000 cycles. Data was taken with the band lying flat just prior to, and immediately after this experiment. Pressure tests were conducted by subjecting the tape to a compressive load in a Tinius-Olsen Universal Testing Machine. Loads up to 1000 N were applied locally and uniformly on the band while sensor data were continually recorded. The band was also heated from 22C to 86C to determine its sensitivity to environmental temperature changes.

RESULTS AND DISCUSSION

Calibration results showed that the sensor pairs were linear, with R^2 values of 0.995 or better. A representative signal performance is shown in figure 2. This compares favorably to the chestband, which has a

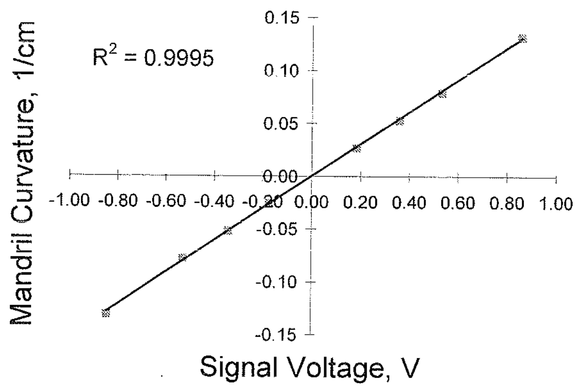

Figure 2: Representative signal calibration performance (signal pair 2)

typical linearity to about 3 percent of the full-scale measurement of 0.4 1/cm. The sensor values were repeatable to within 2 percent of full scale after 1000 cycles. The fiber-optic signals changed less than 2 percent of full scale. Localized pressure produced signal differences less than 9 percent of full scale. This resulting apparent radius of curvature, approximately 33 cm, is likely the result of the shape tape conforming locally to the underlying aluminum beam. The rounded edges of the indentor most likely caused the unloaded portions of the band to bend locally, resulting in additional curvature at these sensor locations. The pressure sensitivity test results are shown in figure 3. Signal changes to temperature changes were approximately negligible (0.5% of full scale).

CONCLUSIONS

Shape Tape measurement accuracy is comparable to that of the predominantly

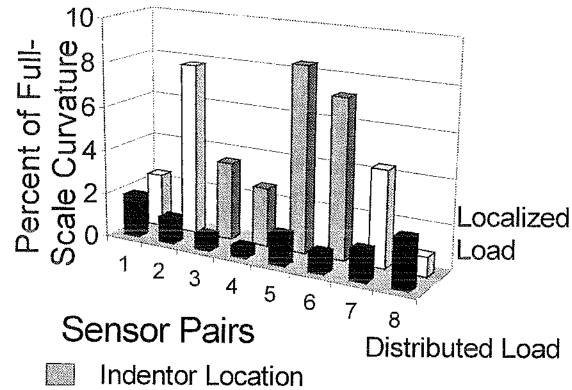

Figure 3: Shape tape pressure sensitivity

used chestband technology, but the Shape Tape has distinct advantages. Its small size (1.4 cm x 0.3 cm) enables it to be used in many testing situations for which other similar instruments would be poorly suited, such as determining local ribcage contours beneath subcutaneous tissue in thoracic impact experiments. Further testing will confirm its performance in characterizing dynamic deformation contours in controlled impact tests.

REFERENCES

Bass, C.R. et al. (2000). *SAE Technical Paper Series.* Paper No. 2000-01-0054.

Eppinger, R.H. (1989). *Proceedings of 33rd Stapp Car Crash Conference.* SAE No. 892426.

Shaw, C. et al. (2000). Presentation at 2000 SAE Conference. Detroit, MI.

A QUASILINEAR VISCOELASTIC MODEL FOR BRAIN TISSUE

Kurosh K. Darvish and Jeff R. Crandall

Department of Mechanical and Aerospace Engineering, University of Virginia
Email: kurosh@virginia.edu Web: cinderella.mech.virginia.edu

INTRODUCTION

The nonlinear viscoelastic behavior of brain tissue that was observed in oscillatory shear tests was modeled with a quasilinear viscoelastic constitutive relation. The dynamic viscoelastic behavior of brain tissue has been previously modeled with only linear models. The reader is referred to Darvish (2000) for a review of the previous models. Studies on live neural tissue (Thibault *et al.*, 1990) and physical head models with brain surrogate (Margulies, 1987) indicate that brain undergoes finite deformation prior to traumatic injuries. Therefore, it is necessary to use the nonlinear theories to model its mechanical behavior in injurious loading conditions. Recently, the nonlinear viscoelastic behavior of brain tissue at finite strains has been characterized using the results of stress-relaxation tests (Prange *et al.*, 1998). These models, due to the limitations of the test procedure, are not valid for short-time loadings (below 60 ms) that are observed in the events that might lead to traumatic brain injury, e.g., automotive crashes and ballistic injuries. Using the forced vibration method, the brain constitutive model can be improved by broadening its range of validity at the lower end down to about 1-ms (Darvish *et al.*, 1998).

METHODS

Four disc-shaped samples (15 to 20 mm diameter, 4.75 mm thickness) of cerebral white matter, extracted from two fresh bovine brains (two from each), were tested in oscillatory shear deformation using a computer controlled electromagnetic vibration system (Darvish, 2000). Samples were kept moist and warm (37°C) throughout the test using a physiological saline solution with chemical composition close to that of the cerebrospinal fluid. Samples were assumed to be homogeneous, isotropic, and incompressible. To account for moderate nonlinearity in shear, a third-order quasilinear viscoelastic constitutive relation was considered. In this model, the instantaneous elastic response was assumed to be a polynomial of the strain, containing the first and the third powers to ensure a symmetric shear response. The linear and the third-order complex moduli were determined in the range of 0.5 to 200 Hz by applying simple, double, and triple harmonic strain inputs with up to 20% maximum peak Lagrangian shear strain. A discrete spectrum approximation was assumed for the relaxation function in the form of Prony Series.

RESULTS AND DISCUSSION

The Lissajous curves of shear stress versus shear strain (Figure 1) showed significant nonlinear viscoelasticity for brain tissue in shear. The linear complex moduli were modeled with three different exponential decay rates and a constant term in the time domain. Parameter identification of the model was made in the frequency domain by curve fitting the magnitude and phase of the linear complex moduli with trial and error. The proposed average relaxation function can be written in kPa as:

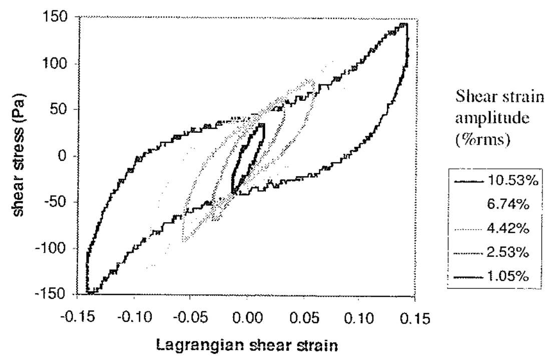

Figure 1: Lissajous curves of a brain sample at 5 Hz.

$$\psi(t) = 0.42 + 0.09 \exp(-10t) + 0.01 \exp(-100t) + 31.5 \exp(-5500t) \quad (1)$$

The last term in equation (1) was an indication of a significant transition at about 100 Hz. The average third-order quasilinear complex modulus was determined by trial and error as:

$$E_3(\omega_1, \omega_2, \omega_3) = 10.5\, E_1(\omega_1 + \omega_2 + \omega_3) \quad (2)$$

The capability of the proposed quasilinear modulus in predicting the magnitude of the third-order experimental results was significantly better at lower frequencies (below 40 Hz). The variation of the phase of the quasilinear modulus with frequency was always lower than the experimental results. The trend of the observed nonlinearity in the instantaneous elastic response (Figure 2) was significantly different from what was predicted by the model proposed by Prange *et al.* (1998). Our results indicated a stiffening shear modulus from about 5% shear strain while their model predicted a softening shear modulus from about 15% shear strain.

The results of this study showed that a third-order quasilinear viscoelastic model was a good predictor of the magnitude of the nonlinear shear stresses generated in brain tissue for up to 20% shear strain and frequencies below 40 Hz. This model however was a poor predictor of the phase of the nonlinear response.

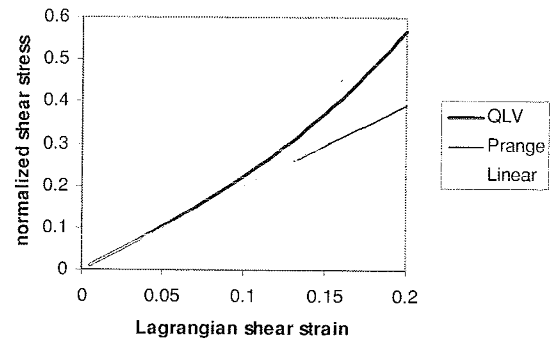

Figure 2: Normalized instantaneous elastic responses of the proposed model, the Prange *et al.* (1998) model, and the linear model.

REFERENCES

Darvish, K. K., *Characterization of Nonlinear Viscoelastic Properties of Brain Tissue Using Forced Vibrations*, Ph.D. Dissertation, University of Virginia, 2000.

Darvish, K., Takhounts, E. G., and Crandall, J. R. "A Dynamic Method to Develop Nonlinear Viscoelastic Model of Brain Tissue", *Advances in Bioeng.*, ASME, BED-VOL. 39, 1998.

Margulies, S. S., "Biomechanics of Traumatic Coma in the Primate," Ph.D. Dissertation in Bioengineering, University of Pennsylvania, 1987.

Prange M. T., Meany, D. F., and Marguiles, S. S., "Directional Properties of Gray and White Brain Tissue Undergoing Large Deformation", *Advances in Bioeng.*, ASME, BED-VOL. 39, pp. 151-152, 1998.

Thibault, L. E., Gennarelli, T. A., Margulies, S., Marcus, J., and Eppinger, R., "The strain dependent pathological consequences of inertial loading on central nervous system tissue," in: *Proc. IRCOBI conf.*, 1990.

A CHAOTIC ANALYSIS OF GAIT PARAMETERS IN DIFFERENT AGE GROUPS

Nick Stergiou[1], Ugo H. Buzzi[1], Patricia A. Hageman[2] and Jack Heidel[3]

[1]Biomechanics Lab, University of Nebraska at Omaha, Omaha, Nebraska
[2]Physical Therapy Education, University of Nebraska Medical Center, Omaha, Nebraska
[3]Dept. of Mathematics, University of Nebraska at Omaha, Omaha, Nebraska
Email: Nick_Stergiou@unomaha.edu Web: www.unocoe.unomaha.edu/hper/hper.htm

INTRODUCTION

Functional neuromuscular variability can be described as the normal variations that occur in motor performance across multiple repetitions of a task. Variability is inherent within all biological systems and recently has also been linked to the health of biological systems. Goldberger et al. (1986) observed different variability patterns in heart rhythms among healthy and diseased patients and suggested that a healthy system has a certain amount of innate variability. This healthy variability is not random or uncontrolled but has order and can be well characterized via chaotic mathematical descriptors. Pool (1989) speculated that chaotic variability may provide a healthy flexibility to the heart, brain, and other parts of the body. Conversely, many ailments may be associated with a loss of this chaotic flexibility. Thus, the mathematical theory of chaos and its methods may be beneficial in describing variability and subsequently, identifying health status. Thus, the purpose of this study was to use tools from the chaos theory to examine variability of certain gait parameters in two different age groups.

PROCEDURES

Twenty females (10 women age 20-37, 10 women age 71-79) participated in the study. Kinematic data from 30 continuous footfalls were collected at 60 Hz from the right lower extremity, while the subjects walked on a treadmill at their self-selected pace. The time series from the hip, knee, and ankle marker unfiltered Y-coordinates were analyzed using the Chaos Data Analyzer software (Sprott, 1992). The lyapunov exponents (LE), the correlation dimensions (COD), and the capacity dimensions (CAD) were calculated. LE is a measure of the stability of a dynamical system and its dependence on initial conditions. CAD and COD describe the geometric dimension of a dynamical system and often closely resemble each other. However, COD have been found to be more accurate for smaller data sets as they weigh more heavily on areas of the embedding space that actually contain data. All calculations were performed using 5 embedded dimensions. The embedded dimension, a description of the number of dimensions needed to unfold the structure of a given dynamical system, was calculated from a Global False Nearest Neighbor (GFNN) analysis (Abarbanel, 1996). Mean group values were calculated for LE, COD, and CAD and analyzed statistically using independent t-tests ($p<0.05$).

RESULTS AND DISCUSSION

The results showed that all LE were positive (Table 1). These results are in agreement with LE from walking data reported by Dingwell et al. (1999). This may indicate that the system is behaving chaotically. However, a time series consisting of random or noisy data can also produce positive LE. Thus, to assist in our evaluations we processed time series from periodic data (sine wave), from randomly generated data, and from known chaotic data (Lorenz attractor). Based on these data, we can see that our results are more chaotic than noisy. It is also evident in all chaotic tools used, that values increase in the system from the ankle and towards the hip. This may indicate an increase in variability in the system which can be due to the ground restriction at the lower end and the decrease in the available degrees of freedom. Significant differences were found in the knee and the ankle LE, and the COD for all parameters. No significant differences were found in CAD of any of the joints. Furthermore, in all significant differences identified, the elderly group had higher values than the young. This may indicate that the system may become more variable but also more noisy due to aging and lack of necessary control.

SUMMARY

Until recently time series were analyzed with linear methods and, variability in human movement was characterized as noise. Chaos theory challenges this approach and provide us with methods to analyze complicated nonlinear systems such as the human. With the methods used in this study we were able to identify differences between two age groups. It is possible that these methods can evolve into powerful diagnostic tools.

REFERENCES

Dingwell, J.B., et. al. (1999) Proceedings of ASB'99, 58-59.

Abarbanel, H.D.I. (1996). *Analysis of Observed Chaotic Data*, Springer-Verlag.

Goldberger, A., et al. (1986). *Physica*, **19**, 282-289.

Pool, R. (1989). *Science*, **243**, 604-607.

Sprott, J., Rowlands, G. (1992). *Chaos Data Analyzer*. American Institute of Physics.

ACKNOWLEDGMENTS

Supported by the University Committee on Research of the University of Nebraska at Omaha.

Table 1: Chaotic parameters evaluated for both groups (mean ± SD).

Variables:	Lyapunov Exponent	Correlation Dimension	Capacity Dimension
Periodic data:	-0.001 ± 0.032	1.167 ± 0.334	1.222 ± 0.271
Chaotic data:	0.100 ± 0.035	1.941 ± 0.110	1.663 ± 0.368
Random data:	0.469 ± 0.037	4.723 ± 0.723	3.257 ± 0.721
Hip – Young:	0.216 ± 0.033	3.012 ± 0.353*	2.245 ± 0.443
Hip – Elderly:	0.227 ± 0.024	3.437 ± 0.259*	1.938 ± 0.525
Knee – Young:	0.144 ± 0.030*	2.939 ± 0.268*	1.376 ± 0.698
Knee – Elderly:	0.169 ± 0.022*	3.542 ± 0.484*	1.450 ± 0.550
Ankle – Young:	0.078 ± 0.014*	2.886 ± 0.243*	1.821 ± 0.142
Ankle – Elderly:	0.108 ± 0.300*	3.346 ± 0.346*	1.914 ± 0.234

* $p<0.05$

SLIP POTENTIALS DURING LOAD CARRYING

Rakié Cham [1], M.S. and Mark S. Redfern [1,2], Ph.D.
Departments of [1]Bioengineering and [2]Otolaryngology - University of Pittsburgh
Email: chamr@msx.upmc.edu

INTRODUCTION

The ratio of shear to normal foot forces described by Strandberg and Lanshammar (1981) as the instantaneous "friction used," may also be thought of, on dry surfaces, as the "required" coefficient of friction (RCOF) (McVay and Redfern, 1994). The peak RCOF has been used to assess the frictional requirements of walking and related to slip potential (Hanson and Redfern, 1999). Although carrying loads is a common industrial task, few studies have investigated the effect of external loads on gait biomechanics (Myung and Smith, 1997). Holbein and Redfern (1997) suggested that carrying symmetrically might increase postural stability. However, if a slip occurs during load carrying, the chance of recovery might decrease compared to walking with no load. The first aim of this study was to investigate the effect of load carrying on the RCOF during walking. Second, for a given carrying task, the relationship between RCOF and body height was examined, along with a comparison of the results between men and women.

METHODS

Ten healthy young adults divided equally by gender participated. A previously built ramp instrumented with a force platform (FP) was used (Redfern and Dipasquale, 1997). An Optotrak-3020 motion measurement system was used to record body and foot movements. Both motion and foot forces were recorded at 350 Hz. The data describing ground reaction forces are reported here. The independent variables included 2 ramp angles (0^{o} and 10^{o}) and 3 load conditions (0, 2.3 and 6.8 kg). A total of 235 dry trials were recorded on a dry vinyl-flooring surface. The same polyvinyl chloride (PVC) hard-soled shoes were used for all trials. After informed consent was given, subjects were equipped with a safety harness, handed the appropriate load to carry and instructed to walk down the ramp at a comfortable pace while looking straight ahead on the wall.

RESULTS

Peak values of the RCOF time series were found for each trial. A repeated measures ANOVA on the RCOF values was performed with the independent variables being subject, ramp angle, load level and all first and second order interaction terms. All of the independent variables except load had a statistically significant effect ($p < 0.001$) on the RCOF (r^2=0.96). For the no load carrying condition, the RCOF increased from 0.183±0.040 for level walking to 0.329±0.027 when descending a 10^{o} ramp.

The specific relationship among ramp angle, load and RCOF was further investigated with an analysis of within-subject differences from the no load condition (Table 1). For level walking (0^{o}), there was no significant effect of load on the peak RCOF. However, for the 10^{o} ramp, significant differences were noted in the peak RCOF among the load carrying levels. More specifically, post-hoc Tukey comparisons showed a significant decrease in the peak RCOF when carrying a load compared to the control condition (0 kg) (Figure 1). There were no significant differences between the 2.3 and 6.8 kg load conditions.

Table 1: p-values for peak RCOF

Angle →	0°		10°	
Variable ↓	*p*	r^2	*p*	r^2
Subject	<0.001		<0.001	
Load	0.537	0.83	<0.001	0.76
Subject x Load	<0.001		<0.001	

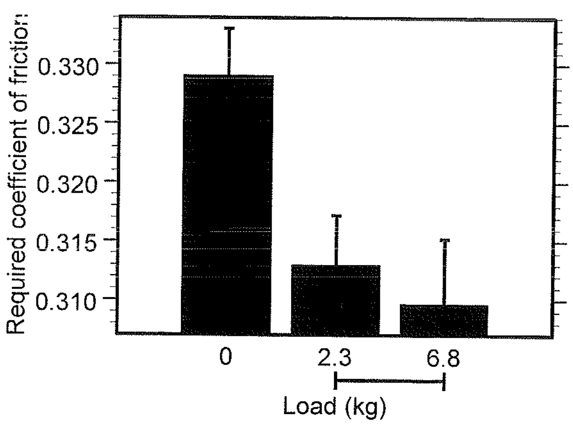

Figure 1: Peak RCOF for the 10° ramp condition during load carrying averaged across all subjects (mean ± S.E.M.)

Gender and height effects on RCOF values were investigated using a linear regression model with the independent variables being load, gender, height and second order interaction terms of these variables. For level walking, only gender was a significant factor. However, for a 10° degree ramp, all effects were statistically significant. Women had generally higher peak RCOFs compared to men (Figure 2). Load carrying effects found in Figure 1 still apply for both genders. For the 10° ramp, body height and RCOF were inversely related with peak RCOF decreasing with increased subject stature.

In summary, carrying a load affected the ratio of shear to normal foot force when descending a 10° ramp, but not for level walking. This finding was more evident for women than men. This study suggests that people adapt their gait for sloped surfaces when carrying to reduce slip potentials. These findings are part of a larger study that investigated gait kinematics and kinetics on different surfaces of varying inclination and slipperiness to fully understand the biomechanics of slips and falls toward their prevention.

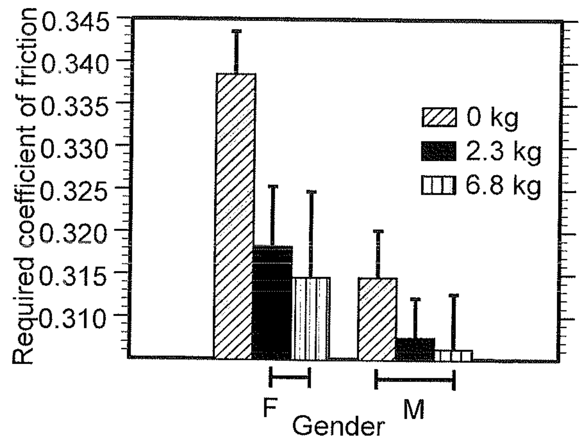

Figure 2: Load carrying effect on the RCOF compared between men and women (10°)

REFERENCES

Hanson, J.P., Redfern, M.S. (1999). *Ergonomics* ***42***, 1619-1633.

Holbein, M.A., Redfern, M.S. (1997). *Int J Ind Ergon* ***19***, 387-395.

McVay, E., Redfern, M.S. (1994). *AIHA J* ***55***, 626-634.

Myung, R., Smith, J.L. (1997). *Ergonomics* ***40***, 235-246.

Redfern, M.S., DiPasquale, J. (1997). *Gait and Posture* ***6***, 119-125.

Strandberg, L., Lanshammar, H. (1981). *J Occup Acc* ***3***, 153-162.

AKNOWLEDGEMENTS

This study was supported by NIOSH 5 R03 OH03621-02.

LEG SPRING MODEL PROPERTIES OF CHILDREN

G.D. Heise and G. Bachman

School of Kines. and Phys. Educ., University of Northern Colorado, Greeley, CO 80639
Email: gheise@hhs.unco.edu

INTRODUCTION

Investigators have examined the dynamics of running by applying a center of mass-based, leg spring model developed by McMahon and colleagues (Ferris et al., 1999; He et al., 1991; McMahon & Cheng, 1990). In this model, the leg and body are represented as a simple linear spring and a point mass, respectively (Fig. 1).

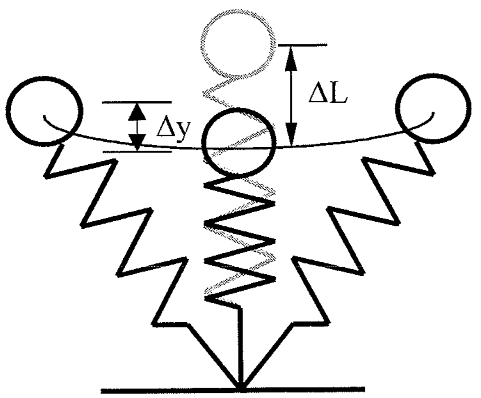

Fig 1: Leg spring model (adapted from McMahon & Cheng, 1990).

Leg spring stiffness (k_{leg}), the ratio of maximum vertical force during foot contact to ΔL, remains constant as humans run faster (He et al., 1991) and as various species of animals trot and hop faster (Farley et al., 1993). In addition, Farley and colleagues found k_{leg} and the effective vertical stiffness of the leg spring (k_{vert}) to increase with body mass when considering animals ranging from a 0.1 kg rat to 140 kg horse.

Human running and hopping are usually examined with adult samples. The invariance of k_{leg} across running speeds and the symmetry between legs, for example, were shown in samples of university students (Bachman et al., 1999) and adult amputee runners (Heise et al., 1999). Changes in body mass and leg length that accompany physical maturation are influences that have not been examined from the perspective of the leg spring model.

The purpose of the present study was to examine the properties of the leg spring model (k_{leg}, k_{vert}) in a sample of children. Specifically, the relationships of spring coefficients to running speed and body mass were investigated. The findings of the present investigation may have implications in the design and prescription of prosthetic limbs for children.

METHODS

Ten healthy children (4 girls, 6 boys) between the ages of 5 and 10 yr participated in the study (mean ± SE: age = 8.0 ± 0.6 yr; body mass = 27.5 ± 2.9 kg; leg length = 56.9 ± 2.5 cm). None of the subjects exhibited asymmetrical leg length discrepancies. Each subject attended one test session. At first, they practiced striking a force plate in the middle of a 20 m gymnasium during a 15-min warm-up. Subjects were then instructed to run at a slow or fast speed, however, speed was not imposed or controlled. Attempts were made to collect data for 8 trials (2 slow, 2 fast for each leg). Good trials were selected based on foot contact with the force plate and no apparent aberrations in running gait. Vertical ground reaction force data were collected and 2 camcorders recorded sagittal plane motion (one for forward velocity calculations and one for leg length at foot contact). For each satisfactory trial, k_{leg} and k_{vert} were calculated using the approach of McMahon and Cheng (1990) and normalized by multiplying them by the ratio of leg length to body weight (K_{leg}, K_{vert}).

RESULTS AND DISCUSSION

Data are presented from right foot contacts only. Left foot contacts resulted in similar leg spring measures. Stiffness coefficient values (mean k_{leg} = 3.88 kN/m; see Fig. 2 for K_{leg}, K_{vert}) were much lower than adult data reported previously (Bachman et al., 1999; He et al., 1991; Heise et al., 1999).

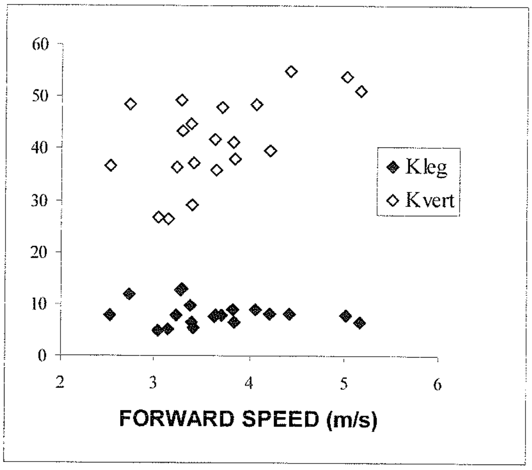

Fig 2: Normalized stiffness coefficients for 10 subjects (2 speeds each).

As expected, K_{leg} was independent of running speed (r = -.17), whereas K_{vert} showed a significant positive relationship with forward speed (r = .56, $p < .02$).

A regression analysis (Fig. 3) showed that body mass (M) significantly influenced k_{leg}: $k_{leg} = .1065(M) + .95$, $R^2 = .57$, $p < .001$
It is difficult to compare this relationship with the work of Farley et al. (1993) because their subjects were mostly animals and the range of body mass in their work greatly exceeded that of the present study.

He et al. (1991) suggested a constant k_{leg} across running speeds may simplify the fabrication of prosthetic legs. However, the results from the present investigation show that body mass influences leg spring stiffness in children when running and the fit of prosthetic legs may not be as simple as suggested.

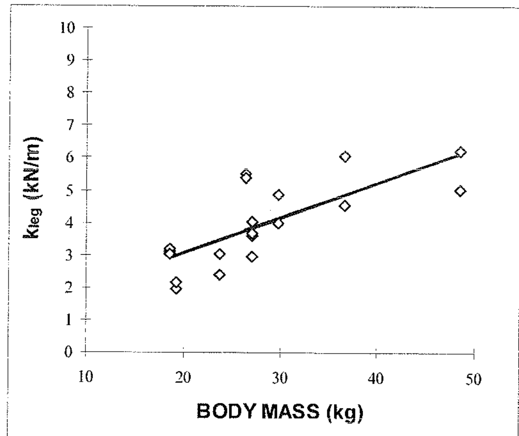

Fig 3: Leg spring stiffness as a function of body mass in 10 subjects (2 speeds each). Solid line is regression (see text for equation).

REFERENCES

Bachman, G. et al. (1999). Proceedings of 23rd ASB Meeting, p. 222.
Farley, C.T., et al. (1993). J. Exp. Biol., 185, 71-86.
Ferris, D.P. et al. (1999). J. of Biomech., 32, 787-794.
He, J. et al. (1991). J. Appl. Physiol., 71, 863-870.
Heise, G.D. (1999). Proceedings of XVIIth ISB Congress, p. 537.
McMahon, T.A. & Cheng, G.C. (1990). J. Biomech., 23(Supp), 65-7

DIFFERENT LEG INERTIAL PROPERTIES YIELD SIMILAR STRIDE TIMES

Todd D. Royer [1] and Philip E. Martin [2]

[1] **Dept of Exercise and Sport Sciences, Tulane University, New Orleans, Louisiana**
[2] **Exercise and Sport Research Institute, Arizona State University, Tempe, Arizona**
Email: todd.royer@tulane.edu

INTRODUCTION

Unilateral lower-extremity amputees have asymmetrical gait (Mattes et al., 2000). The prosthetic limb typically has a smaller mass and moment of inertia than the intact limb resulting in a lower extremity inertial asymmetry that may impact gait symmetry. Mattes and colleagues (2000) attempted to improve gait symmetry by eliminating the inertial asymmetry; however, this manipulation exacerbated the asymmetrical gait cycle.

Holt and colleagues (1990) added loads to both feet of non-pathological subjects and reported an increase in walking stride time. Furthermore, they were able to predict stride time using a model of a force driven harmonic oscillator (FDHO):

$$T = 2\pi\sqrt{\frac{I_{axis}}{2mgd}}$$

Specifically, the model incorporates gravitational acceleration (g), total leg mass (m), the leg's moment of inertia about a transverse axis through the hip joint (I_{axis}), and the distance from the leg center of mass to the hip axis of rotation (d) as inputs to predict stride time (T).

In theory, it is possible for limbs to have a different mass and moment of inertia while having the same FDHO predicted stride period, which may have implications for addressing the asymmetrical gait of unilateral amputees. We hypothesized that symmetrical and asymmetrical loading of the lower extremities such that the FDHO predicted stride period for both limbs match that of an unloaded limb results in equivalent temporal features of gait.

METHODS

To control for the additional confounds associated with amputation, non-pathological subjects were tested. Fourteen males and females ($M_{age} = 27.8 \pm 4.2$ yrs; $M_{height} = 170.2 \pm 6.9$ cm; $M_{mass} = 69.4 \pm 11.7$ kg) were videotaped while walking on a treadmill at 1.5 m/s. Lower extremity position data and body segment parameter equations (de Leva, 1996) were used to estimate the appropriate limb inertial characteristics input into the FDHO model to calculate predicted stride period. Two load conditions were modeled in which FDHO predicted stride time was held constant; one having no load (zero load) affixed to the limb and a second having load equivalent to 20% of the entire leg's mass distributed on the proximal and distal shank.

Subjects then walked under four randomly ordered conditions to quantify the left leg's temporal response to symmetrical (both legs were simultaneously loaded or unloaded) and asymmetrical (left leg was loaded while the right leg was unloaded, and vise versa) loads. Loads were affixed to the proximal (mean=2.4 kg) and distal (mean=0.4 kg) aspects of the shank with elastic bandages and tape. Total mass (subject mass plus added load) was held constant by carrying all unused leg loads in a waist pouch. Footswitches affixed to the heel and toe of the shoe sole were sampled at 1000 Hz to calculate stride, swing, and stance times.

RESULTS AND DISCUSSION

Results in Figure 1 indicate experimentally measured stride time remained stable across load conditions. Specifically, stride time increased only 1% with load distributed on the proximal (2.4 kg) and distal (0.4 kg) shank. Previous research has shown that temporal gait features are quite sensitive to load distribution. Holt and colleagues (1990) reported a 6% stride time increase for 2.2 kg foot loads while Royer et al. (1997) reported a 3% increase with 1 kg foot loading, consistent with the FDHO model's prediction for distal limb loading.

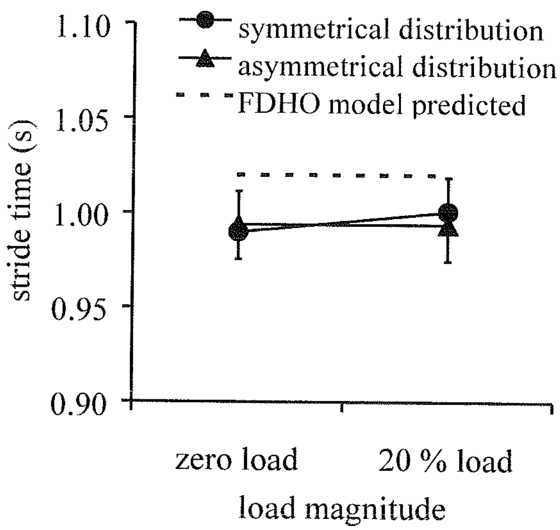

Figure 1: Experimentally measured stride time was consistent with the modeling goal of maintaining a constant stride time across load conditions; however, the FDHO model overestimated the actual stride time by 2%.

Swing time increased 2% when load was affixed to the limb (Table 1), regardless of whether symmetrical or asymmetrical loads were used, which is smaller than other values reported in the literature. Royer et al. (1997) reported a 7% increase in swing time and Skinner and Barrack (1990) reported a 3% increase with 1-2 kg foot loads. This suggests that swing time may reflect the limb's increased inertial characteristics per se, rather than the stride time trend predicted by the FDHO model. Stance time (Table 1) was not different for the symmetrical load distributions but was significantly longer for the unloaded leg when load was distributed asymmetrically. Thus, the longer swing time of the loaded leg was coupled with a longer stance time for the unloaded leg.

Table 1: Swing and stance times.

Load Condition	Swing Time	Stance Time
zero load on leg		
symmetrical	0.389 (0.02)	0.601 (0.03)
asymmetrical	0.387 (0.02)	0.607 (0.03)
20% load on leg		
symmetrical	0.395 (0.02)	0.605 (0.03)
asymmetrical	0.395 (0.02)	0.598 (0.03)

values represent the mean (sd) in seconds.

SUMMARY

It was hypothesized that symmetrical and asymmetrical loading of the lower extremities such that the FDHO predicted stride time for both limbs match that of an unloaded limb results in equivalent temporal gait features. Stride time was similar across load conditions; however swing and stance times differed. This suggests the FDHO model may be a useful tool for researchers and clinicians in efforts to improve gait symmetry for unilateral amputees.

REFERENCES

de Leva, P. (1996). *J Biomech*, **29**, 1223-30.

Holt, KG et al (1990) *Hum Mov Sc*, **9**, 55-68

Mattes, SJ et al (2000) *Arch Phys Med Rehab*, in press.

Royer, TD et al. (1997). *MSSE*, **29**, S113.

Skinner, HB, Barrack, RL (1990). *Arch Phys Med Rehab*, **71**, 112-5.

ACKNOWLEDGEMENTS

Support from the American Society of Biomechanics Graduate Student Grant-In-Aid is acknowledged.

SEGMENTAL INTERACTIONS DURING RUNNING OVER OBSTACLES OF INCREASING HEIGHT

Nick Stergiou, Shane D. Scholten, Jeremy Houser, Tracy Dierks and Daniel Blanke
Biomechanics Lab, University of Nebraska at Omaha, Omaha, Nebraska
Email: Nick_Stergiou@unomaha.edu Web: www.unocoe.unomaha.edu/hper/hper.htm

INTRODUCTION

Much research has been produced on behavioral transitions such as the walk-to-run or the run-to-sprint. However, limited research exists on running over high enough obstacles to cause a change of the landing strategy. Previous research has indicated that during running over obstacles of increasing height, most heel-strike runners change their contact strategy to a forefoot landing pattern (Scholten et al., 1999). Recently, behavioral transitions have been examined using the Dynamical Systems Theory (DST). In DST, the interacting components are examined while scaling up a control parameter to elicit new patterns of coordination (Clark & Phillips, 1993). The purpose of this study was to examine the different landing strategies used during running over obstacles of increasing height. By using DST, we investigated the interacting segments, while scaling up a control parameter (obstacle height).

PROCEDURES

Ten heel-strike subjects ran at a self-selected pace under seven conditions: a level surface and over obstacles of six different heights (10%, 12.5%, 15%, 17.5%, 20%, and 22.5% of their standing height). Sagittal view kinematics were collected (180 Hz) from the right lower extremity using a Peak Performance system. To examine segmental interactions, the phase portraits from segmental angular positions and velocities were used to calculate phase angles (Scholtz, 1990). Relative phase (RP) curves were calculated for two segmental relationships [foot-shank (F-S) and shank-thigh (S-T)] by subtracting the phase angle of the proximal segment from the distal segment. Mean ensemble RP curves were calculated for all conditions. From these curves two parameters were evaluated: a) mean relative phasing (MRP), and b) deviation phasing (DP). MRP and DP were calculated by averaging the absolute values and the standard deviations, respectively, of all points of the mean ensemble RP curve. MRP and DP were calculated for two intervals, a pre-landing period (from the obstacle to ground contact) and stance. One-way repeated measures ANOVAs were performed on MRP and DP for each segmental relationship and for each interval. A Tukey test was performed in comparisons that resulted in a significant F-ratio ($p<0.05$).

RESULTS AND DISCUSSION

Group results are presented in Table 1. The F-S MRP significantly increased in both periods, indicating that the F-S relationship becomes more out-of-phase with increases in obstacle height. An out-of-phase relationship means more independence in the actions of the two segments. No significant differences were found for the S-T MRP, indicating that the changing obstacle height did not affect the S-T segmental relationship. The DP results revealed significant differences for both F-S and S-T but only for the pre-landing period. The F-S DP increased with obstacle height, while the S-T DP decreased with the introduction of the obstacle. Increases in DP reveal an unstable system, while decreases are associated with a fixed and rigid system. Thus, the F-S relationship is unstable because it changes to more out-of-phase. On the contrary, the S-T relationship doesn't change and becomes even more rigid and inflexible. The fact that no significant changes were observed for DP during stance indicated that the system was stable in this period. Thus, it is possible that the system conducted all the necessary accommodations prior to contact.

A further examination of Table 1 reveals that the larger differences in F-S MRP for both periods were observed from 0% to 10% and from 12.5% to 15%. That was also the case for the pre-landing F-S DP. Therefore, the introduction of the obstacle caused behavioral changes, but the 15% condition was probably the height with the greatest effect. These results are in agreement with Scholten et al. (1999). In that study, it was mentioned that the 15% height condition is the height in which the landing strategy has been shown to change from heel-strike to forefoot strike.

SUMMARY

Introducing an obstacle and increasing the obstacle height elicited behavioral changes. These changes were different for the interacting segments at the ankle and at the knee. While the foot and the shank became more independent in their actions, the shank and the thigh strengthened even more their stable relationship. The 15% height seems to be a critical height for the observed changes.

REFERENCES

Clark, J.E., Phillips, S.J. (1993). *Child Dev*, **64**, 1143-1157.

Scholten, et al. (1999). *Proceedings of ASB'99*, 220-221.

Scholtz, J.P. (1990). *Phys Ther*, **70**, 827-843.

ACKNOWLEDGMENTS

Supported by the University Committee on Research of the University of Nebraska at Omaha.

Table 1: Parameters evaluated with superscripts indicating post-hoc differences ($p<0.05$). All values are in degrees.

Variables	0%	10%	12.50%	15%	17.50%	20%	22.5%
PRE MRP	$10.4^{15\%-22.5\%}$	$19.8^{20\%-22.5\%}$	$18.9^{15\%-22.5\%}$	$30.6^{22.5\%}$	$30.6^{22.5\%}$	39.2	43.6
Foot-shank	±1.7	±11.1	±7.9	±13.9	±11.2	±15.6	±14.4
PRE MRP	88.8	93.8	91.8	92.5	90.0	87.3	85.9
Shank-thigh	±7.8	±19.6	±20.1	±19.7	±20.3	±19.8	±18.8
PRE DP	$6.1^{17.5\%-22.5\%}$	10.1	11.3	15.3	17.4	17.8	16.8
Foot-shank	±2.7	±5.9	±7.0	±6.6	±9.1	±6.2	±4.7
PRE DP	$16.9^{10\%,15\%}$	10.1	10.9	10.2	11.2	11.1	12.3
Shank-thigh	±8.7	±2.0	±4.1	±3.3	±3.3	±3.6	±4.7
STANCE MRP	$37.8^{12.5\%-22.5\%}$	$44.8^{20\%-22.5\%}$	45.8	50.9	51.2	52.9	53.2
Foot-shank	±5.6	±11.4	±10.6	±12.8	±11.5	±11.0	±12.3
STANCE MRP	48.7	48.6	47.8	46.8	48.1	45.9	43.4
Shank-thigh	8.1	7.1	6.5	10.3	10.6	10.7	12.7
STANCE DP	9.4	11.3	13.0	14.3	15.5	17.4	15.9
Foot-shank	±6.9	±5.3	±7.2	±4.4	±6.6	±9.5	±6.8
STANCE DP	10.9	11.4	12.7	14.3	15.5	17.4	15.9
Shank-thigh	±7.7	±3.6	±4.7	±5.8	±5.3	±8.1	±3.9

INDEPENDENT CONTRIBUTIONS OF LOWER EXTREMITY STRENGTH AND COORDINATION TO MAXIMUM VERTICAL JUMP HEIGHT

Masao Tomioka, David Lord, Tammy M. Owings, Mark D. Grabiner
Department of Biomedical Engineering, The Cleveland Clinic Foundation, Cleveland, OH
Email: grabiner@bem.ri.ccf.org

INTRODUCTION

Decreased muscle strength, particularly of the lower extremities, has often been implicated as a factor underlying the increased incidence of falls by older adults. Recently, a comprehensive battery of lower extremity strength and power measurements in older adults did not uniquely discriminate older adults who fell after a large forward-directed postural perturbation from those older adults who did not fall.[1] This suggests that increased resistance to falls, *per se*, may not be generally assumed to be among the many benefits to be gained by older adults through strength training.

A minimum level of lower extremity strength is likely requisite for successful execution of a recovery task. However, the time-critical and multiarticular nature of the recovery task suggests that lower extremity coordination can play an important role in recovery. The present study was conducted to test the strength of this premise by determining the extent to which lower extremity strength and coordination independently contribute to maximum vertical jump height.

METHODS

Thirteen healthy young adults participated in the study consisting of two protocols. In one protocol, the subjects performed a minimum of five maximum countermovement vertical jump trials. A video-based motion capture system was used to record the motion of markers placed bilaterally on the lower extremities and on the trunk. A force plate was used to record the ground reactions beneath the right foot during the jumping and landing phases. Hip and knee kinematics were derived from the recorded motion of the reflective markers. Maximum jump height, normalized to body height, was derived using force plate data.

In the second protocol, maximum voluntary contractions of the right knee extensor muscles were measured during isometric contractions and isokinetic contractions performed at speeds of 60, 150, 240 deg/s. For each condition, the maximum measured force was converted to a moment and normalized to body weight•body height. The maximum rate of change of force was converted to a power value and similarly normalized.

A measure of knee-hip coordination was derived using phase angle relationships.[2] The relative phase angle was used to characterize the phase lag between the knee and the hip during the countermovement and propulsion phases of the vertical jump. The average value of the relative phase angle was used as the dependent variable in the subsequent regression analyses.

Correlation analysis was used to determine the strength, power and average relative phase variables that best correlated with jump height. Forward stepwise regression was used to determine the variables that best predicted jump height. Inclusion in the stepwise model reflected the independence of the variables. The magnitude of the standardized regression coefficients of the variables in the model were used as indices reflecting the strength of the contribution to the maximum vertical jump height.

RESULTS AND DISCUSSION

As a group, the mean±standard deviation of the maximum vertical jump height was 0.41±0.056 percent body height (range=.35 to .57 percent body height). The mean±standard deviation of the maximum normalized strength measured at 60 deg/s was 1.31±0.34 body weight•body height.

The maximum normalized strength measured at 60 deg/s and its quadratic term demonstrated the strongest correlations to normalized jump height (r=.71 and .76, respectively, p=.01).

The average relative phase angle during the propulsion phase of the vertical jump and its quadratic component were strongly correlated to normalized jump height (-.64 and .71, respectively).

The correlations between the linear and quadratic terms of the average relative phase angle during the propulsion phase of the vertical jump and the maximum normalized strength measured at 60 deg/s were weak and failed to achieve significance (all $r<.33$, $p>.05$).

Two variables satisfied the criterion of the stepwise regression for inclusion in the final model. The variables were the quadratic term of the normalized maximum knee extension strength at 60 deg/s and the quadratic term of the average relative phase angle during the propulsion phase of the maximum vertical jump. The adjusted R^2 of the regression was 0.77 (p=.001). The standardized regression coefficients, β, of the two terms were .59 and .52, respectively (p=.004 and .008, respectively).
The β coefficients demonstrate that for the subjects in this study, the measure of knee extension strength and hip-knee coordination during the propulsion phase of the maximum vertical jump were reasonably similar with respect to the extent of their contributions to maximum vertical jump height.

The similarity of the β coefficients raises the issue of the influence of improved strength and coordination on the maximum vertical jump height. If coordination was unaffected, a one standard deviation increase in maximum normalized knee extension strength, 0.34 body weight•body height (about a 25% increase), would be expected to result in an increase in maximum vertical jump height of 0.056 percent body height. This would be about a 13 percent increase in maximum vertical jump height. If strength remained unaffected, a one standard deviation increase in coordination, 6.28 (about a 46% increase), would be expected to result in the same increase in maximum vertical jump height. A question arises regarding the relative difficulty of affecting each of these functional changes.

Lower extremity strength and coordination independently contribute to vertical jump height of young adults.

REFERENCES

Pavol MP (1999) Unpublished Dissertation, Ohio State University.

Burgess-Limerick et al. (1996) Relative phase quantifies interjoint coordination. *J Biomechanics*, **26**, 91-94.

ACKNOWLEDGEMENTS

Funded, in part, by NIH-AG10557.

THE EFFECT OF AGING ON MULTI-FINGER FORCE PRODUCTION

Frederic Danion, Mark Latash, and Vladimir Zatsiorsky

Department of Kinesiology and Biomechanics laboratory,
Penn State University, University Park, PA
Email: mll11@psu.edu

INTRODUCTION

The reduction of muscular strength and power associated with aging is rather well documented. Some studies focussed on the hand, one of our most common effector, using hand-gripping tasks. In particular changes in motor unit properties have been documented with selective atrophy of high threshold motor units (Owing, Grabiner, 1998). However, these tasks do not provide information about changes in finger coordination with aging.

In a previous series of studies (Li et al., 1998), we investigated finger coordination during maximal force production (MVC) by a set of finger. Those studies demonstrated the following features. MVC by several fingers acting in parallel was shown to be smaller than the sum of MVCs of these fingers in single-finger force production tasks (force deficit). Force production by one finger was accompanied by involuntary force production by other fingers (enslaving). The total force was shared in a specific manner (sharing pattern).

The goal of this study was to provide a preliminary set of data to address changes in finger coordination associated with aging as reflected in such indices as force deficit, enslaving, and sharing pattern.

METHOD

Two groups of subjects were tested. The first group (OLD) included five elderly subjects (72 ± 2.4 years). The second group (CONT) was composed of 14 subjects (28.2 ± 8.7 years). In all trials, subjects were asked to press as strongly as possible (MVC) with a particular finger combination: either with one finger (index, middle, ring or little finger), or with all four fingers. These five combinations were proposed is a pseudo-ramdomized sequence. During single-finger tasks, subjects were asked to pay no attention to forces produced by the others fingers (slave fingers). Two sites of force generation were used 1) at the distal phalanges, and 2) at the proximal phalanges. Based on the anatomy of the tendon attachment, we assumed that in the first case, extrinsic and intrinsic muscles were activated, while in the second case, only intrinsic muscles produced force. T-tests were used to compare indices as MVC, enslaving, and force deficit. MANOVAs were used to compare force sharing patterns.

RESULTS

1) As expected, MVCs were lower for the OLD group. MVCs with four fingers dropped by 28% at the distal site (115 versus 83 N), and by 51% at the proximal site (163 versus 83 N).

2) The comparison between 4-fingers and 1-finger exercises, revealed larger force deficit for elderly subjects. At the distal site, force deficit was 9% for the CONT group and 21% for the OLD group. At the proximal site, these values were respectively 11% and 26% for the CONT and OLD groups.

3) Because of the significant differences in the MVCs between the groups, enslaving was expressed in terms of the average percentage of MVC exhibited by each slave finger. No difference in enslaving was found at the distal site (17%). By contrast at the proximal site, enslaving was smaller for the elderly subjects (17% versus 23%).

4) During the four-finger tasks, the sharing pattern of the total force across fingers was the same for both groups, independently of the site of force production (I=29%, M=32%, R=22%, L=17%).

DISCUSSION

The data suggest several effects of aging on finger coordination.

The disproportional reduction in MVC produced by the OLD group at the proximal phalanges suggests that aging may be associated with selective impairment of intrinsic hand muscles. Note that a change in the properties of some of the elements involved in a multi-finger synergy is likely to lead to a rearrangement of the whole synergy. In particular, some of the changes seen in the elderly are similar to those seen in healthy subjects under finger fatigue (Danion et al., 2000) that have been shown to lead to a central reorganization.

The increased force deficit in the OLD group also suggests an involvement of a central reorganization. The force deficit may be viewed as consequence of an inability to recruit certain high-threshold motor units. However, these motor units are the ones to show atrophy with age (Owing, Grabiner, 1998). Therefore, an increase in force deficit is probably a reflection of a central reorganization.

The smaller indices of enslaving in the OLD group are unexpected. They mean that elderly subjects had better control over individual finger forces, in contrast to the predominant view that aging is associated with a degradation in different aspects of motor performance.

The same sharing pattern in the two groups suggest that despite the many peripheral and central changes associated with aging, the central nervous system is still able to preserve the basic multi-finger synergy that defines force distribution among fingers.

SUMMARY

We investigated the effect of aging on finger coordination during maximal force production by one or several fingers acting in parallel. The results suggest 1) a greater impairment of the intrinsic hand muscles, and 2) a lower ability to recruit the maximum force of individual finger during multi-finger tasks. Despite these changes, the synergy that defines force distribution among fingers is preserved.

REFERENCES

Danion, F. et al. (2000). *J. Physiology (Lond)*, in press.

Owing T.M., Grabiner, M.D. (1998). *J. Gerontol. A Biol. Sci. & Med. Sci*, **53,** B425-429.

Li, Z.M., et al. (1998). *Exp. Brain Research*, **119**, 276-286.

ACKNOWLEDGEMENTS

The study was in part supported by a NIH grant NS-35032.

THE EFFECTS OF LATERAL LOADING ON INTRALIMB COORDINATION DURING WALKING ON YOUNG AND ELDERLY FEMALES

Jennifer E. Byrne[1], Nick Stergiou[1], Patricia A. Hageman[2], Daniel Blanke[1] and Ugo H. Buzzi[1]
[1]Biomechanics Lab, University of Nebraska at Omaha, Omaha, Nebraska
[2]Physical Therapy Education, University of Nebraska Medical Center, Omaha, Nebraska
Email: Nick_Stergiou@unomaha.edu Web: www.unocoe.unomaha.edu/hper/hper.htm

INTRODUCTION

Previous research has indicated that older adults adapt their gait towards that of a safer and more stable pattern (Judge et al., 1996); however, every year many elderly individuals find themselves victims of falls during walking. Proper coordination of the limb segments is necessary to generate a safe gait pattern. The majority of gait studies of healthy elderly focus on kinematic changes associated with aging, with less attention directed toward the study of coordination. The purpose of this study was to examine elements of coordination during the gait patterns of young and elderly women during free selected and perturbed walking. We challenged the coordination of our subjects by adding an ankle weight to one limb. In this way, the walking task becomes more difficult, as subjects have to adapt to a new walking strategy to compensate for the added weight. To examine walking strategies we used the Dynamical Systems Theory (DST). In DST, the interacting components are examined while manipulating a control parameter to elicit new patterns of coordination (Clark & Phillips, 1993). By using DST, we investigated the interacting segments in the same limb (intralimb coordination), while manipulating a control parameter (added weight).

PROCEDURES

Twenty females (10 women age 20-30 yrs, 10 women age 67+ yrs) walked at a self-selected pace with and without a weight (5% of their body weight) attached on their right ankle. Sagittal view kinematics were collected (60 Hz) from the leg carrying the weight using the Peak Performance system. To examine intralimb coordination, the phase portraits from segmental angular positions and velocities were used to calculate phase angles (Scholtz, 1990). Relative phase (RP) curves were calculated for two segmental relationships [foot-shank (F-S) and shank-thigh (S-T)] by subtracting the phase angle of the proximal segment from the distal segment. Mean ensemble RP curves were calculated for all conditions. From these curves two parameters were evaluated: a) mean relative phasing (MRP), and b) deviation phasing (DP). MRP and DP were calculated by averaging the absolute values and the standard deviations, respectively, of all points of the mean ensemble RP curve. MRP and DP were calculated for two intervals of the stance period: braking and propulsion. Two-way mixed ANOVAs (weight by age) with repeated measures on the weight factor were performed on MRP and DP for each segmental relationship and for each interval ($p<0.05$).

RESULTS AND DISCUSSION

The group results are presented in Table 1. For the young group, the added weight resulted in significant increases for the S-T MRP in both periods. This indicated a more out-of-phase relationship or more independence in the actions of the two segments. No differences were found for the F-S MRP. For the elderly group, the added weight had a significant effect only during the braking period and for both S-T and F-S. This effect was opposite for the two segmental relationships. The S-T MRP increased and became more out-of-phase, while the F-S decreased and became more in-phase. No differences were found during the propulsion period. Furthermore, no differences were found between the two age groups, except for S-T MRP during the braking period and without the weight. The DP results, revealed a significant increase for S-T in the elderly group and during the braking period. Even though no other DP comparisons were significant, the added weight always increased DP. Increases in DP reveal an unstable system, while decreases are associated with a fixed and rigid system. Finally, the results revealed no significant interactions.

SUMMARY

In this study we simulated an imbalance between the lower limbs by adding an ankle weight. This resulted in behavioral changes that were different between the two groups. While the young addressed the added weight with compensations throughout the stance only at the knee, the elderly also incorporated changes at the ankle. The changes in the elderly group occurred only during the braking period. Thus, it seems that this period is more crucial for the elderly than the young females. In conclusion, the differences identified between the two groups suggest that changes in intralimb coordination may take place with the aging process. The parameters identified in this study can be used in future research to determine if these coordinative changes have a direct effect on an individual's risk of falling.

REFERENCES

Clark, J.E., Phillips, S.J. (1993). *Child Dev*, **64**, 1143-1157.

Judge, J.O. et al. (1996). *J. Gerontol Med Sci*, **51**, M303-M312.

Scholtz, J.P. (1990). *Phys Ther*, **70**, 827-843.

Table 1: Parameters evaluated for both groups (mean ± SD). All values are in degrees.

	Young Females		Older Females	
	No weight	Weighted	No weight	Weighted
Braking S-T MRP	18.9♦♣ ± 3.9	21.1 ± 3.2	15.1♦ ± 2.6	18.1 ± 3.6
Braking F-S MRP	22.7 ± 2.3	22.2 ± 2.2	25.4♦ ± 2.9	23.6 ± 2.6
Propulsion S-T MRP	59.0♦ ± 5.0	63.0 ± 4.0	57.6 ± 5.3	58.2 ± 6.1
Propulsion F-S MRP	11.5 ± 2.8	12.2 ± 2.3	13.8 ± 3.3	13.2 ± 3.3
Braking S-T DP	5.2 ± 1.5	5.8 ± 3.1	5.5♦ ± 1.5	6.6 ± 2.2
Braking F-S DP	4.1 ± 0.9	4.3 ± 1.2	3.7 ± 1.5	4.1 ± 0.8
Propulsion S-T DP	9.7 ± 5.5	10.3 ± 8.8	7.5 ± 1.6	9.9 ± 2.4
Propulsion F-S DP	2.7 ± 0.9	2.9 ± 0.9	3.0 ± 0.8	3.5 ± 0.8

♦ significant differences between weight conditions for the same group
♣ significant differences between age groups for the same weight condition

EFFECT OF TAICHI EXERCISE ON ISOKINETIC MUSCLE STRENGTH AND POSTURAL STABILITY DURING QUIET STANCE

Ge Wu*, Fang Zhao, Xinglong Zhou, Liu Wei

*Department of Physical Therapy, University of Vermont, Burlington, VT, 05401
Biomechanical Teacher Section, Beijing University of Physical Education, Beijing, China, 100084

INTRODUCTION

The frequency of falls and fall-related injuries increases with age [Sullivan, 1993]. There is increasing evidence that exercise in the form of Tai Chi (TC) does reduce the incidence of falls in the elderly [Wolf et al., 1997]. We hypothesize that TC enhances eccentric muscle strength which is the critical element in enhancing individual's postural stability. This is supported by the fact that muscular atrophy in normal aging occurs primarily in type II fibers [Larsson et al., 1978], which results in decreased force production during high velocity movements and functional abilities, and increased risk for falling [Tanaka et al., 1998].

The aim of this study was to examine whether or not there are differences in muscle strength and postural stability measures among old adults who had and had not practiced TC in the past years.

METHODS

Two groups of old adults (>55 yrs) were tested: control group (N=20) who had never practiced TC in the past, and experimental group (N=21) who practiced TC on a regular basis for a minimum of 5 yrs.

The biomechanical measurement included knee flexor and extensor concentric strength at 60 deg/s, and eccentric strength at 60 and 120 deg/s, respectively, and the center of pressure (COP) displacement during quiet stance with eyes open and closed, respectively.

The means and standard deviations of the peak strengths and the maximum excursion in the m-l and a-p directions were calculated and compared between the two groups using Student-t test.

RESULTS

The experimental group showed significantly higher knee extensor strength at all three speeds tested than the control group($p < 0.06$). Their knee flexor strength, however, was not significantly different, although higher, than that of the control group ($p > 0.32$) (see Fig. 1).

The experimental group had significantly smaller excursion of the COP in both directions with eyes open than the control group ($p < 0.05$). With eyes closed, however, the experimental group showed smaller COP excursion in the m-l direction only than the control group. There was no significant difference in the a-p COP excursion between the two groups (Fig. 2).

The correlation between the COP excursion and muscle strength was calculated. It was found that the COP excursion in the a-p direction was most correlated with the eccentric strength of the quadriceps muscle at 120deg/s (cc=-0.5) (Fig. 3). The negative correlation coefficient indicated that the stronger the muscle the less COP excursion.

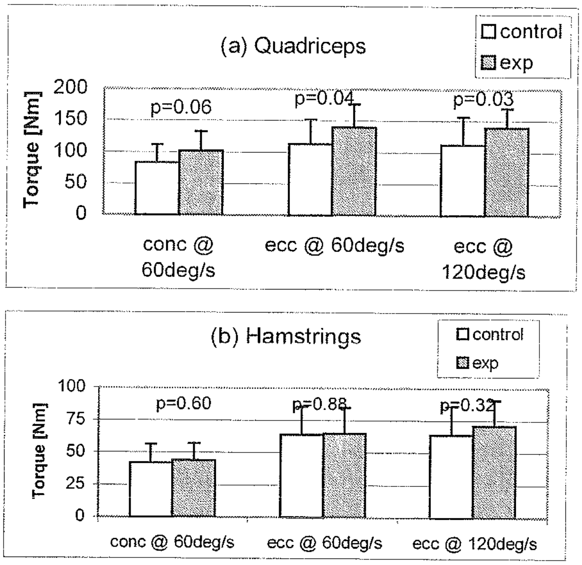

Fig 1. Muscle strength

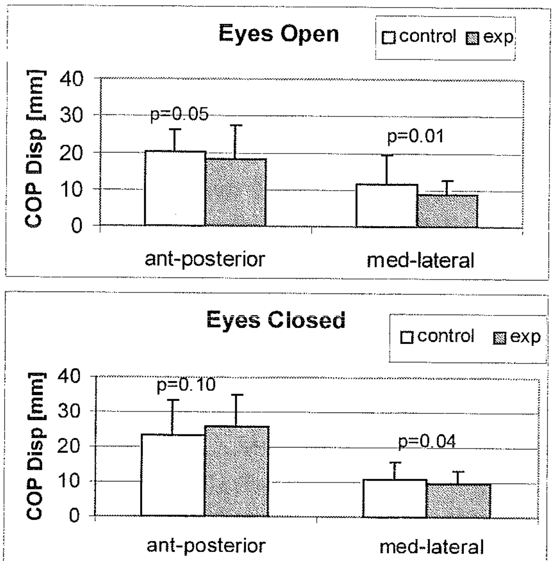

Fig 2. COP excursions

DISCUSSIONS

There have been limited studies on the effect of eccentric exercise on postural stability. This study provided quantitative data on muscle strength difference between people who either have or have not participated in TC exercise, a form of exercise that involves eccentric contraction of postural muscles. In addition, these strength data were correlated with the COP excursion during quiet stance, an indicator of postural stability.

The results showed that people who practice TC had higher concentric and eccentric strengths of the quadriceps at high speed, and lower COP excursions during quiet stance. In addition, the results showed a good correlation between the A-P COP excursion and the eccentric strength at 120deg/s. This suggested that the maintenance of eccentric strength of postural muscles at high speed is beneficial for maintaining good postural stability.

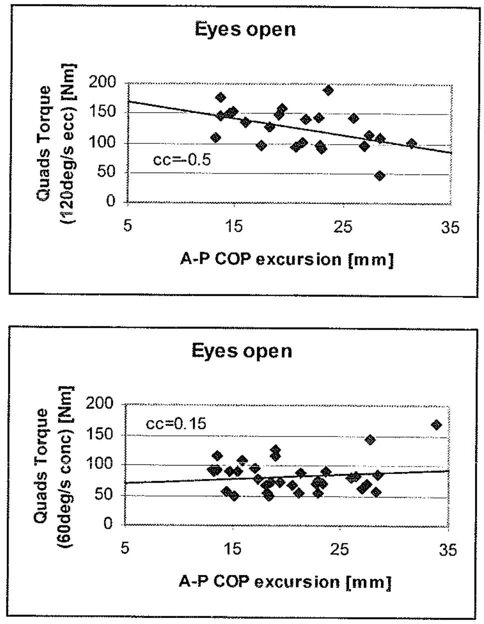

Fig 3. Correlation between COP and strength

ACKNOWLEDGEMENT

This work was supported by NIH grant No.1R29AG11602.

REFERENCES

Larsson et al., Acta Physiol Scand. 103:31-39, 1978

Sullivan, Geriatric Physical Therapy. St. Louis, Mo: CV Mosby Co, 1993

Tanaka et al., Am J. Phy Med and Rehab, 77(2):122-127, 1998

Wolf et al., Physical Therapy.77(4):371-81; 1997

STEPPING OVER AN OBSTACLE CHALLENGES DYNAMIC STABILITY IN THE ELDERLY ADULTS

Li-Shan Chou[1], Kenton R. Kaufman[1], Robert H. Brey[2]

[1]Orthopedic Biomechanics Laboratory, Department of Orthopedic Surgery
[2]Vestibular/Balance Laboratory, Department of Otorhinolaryngology
Mayo Clinic, Rochester, MN 55905
Email: chou.lishan@mayo.edu

INTRODUCTION

Falling to the side has been found to be an important risk factor for hip fracture (Greenspan et al., 1998). Imbalance and tripping over obstacles during gait were reported as two of the most common causes of falls in the elderly (Tinetti et al., 1989). Imbalance of the whole body during obstacle crossing may cause inappropriate movement of the lower extremities or misplacement of the swing foot, which will consequently lead to a foot-obstacle contact and result in a fall. Greater motion of body segments will result in greater excursion of the whole body's center of mass (COM). Furthermore, the greater swing time required for the limb when stepping over a higher obstacle also implies a longer duration of single stance for the supporting limb. It is, therefore, reasonable to expect that maintaining dynamic balance of the whole body during obstacle crossing is a more challenging task than during unobstructed level walking.

In a recent study (Kaya et al., 1998) demonstrated that excessive lateral momentum of the whole body during gait was observed in the elderly with bilateral vestibular hypofunction. However, there is a lack of knowledge about how dynamic stability of the whole body is maintained during balance-challenging ambulatory tasks, such as obstacle crossing. The purpose of this study was to investigate the effect of obstacle height on the motion of the COM while negotiating obstacles in different subject groups.

METHODS

Eighteen subjects, including six healthy young adults (mean age, 30.2 years), six healthy elderly adults (mean age, 70 years) and six elderly patients with imbalance (mean age, 75.7 years), were recruited for this study. Gait analysis was performed on each subject during unobstructed level walking and when stepping over an obstacle of height corresponding to 2.5%, 5%, 10%, or 15% of the subject's height. All trials were conducted at a comfortable self-selected walking speed while barefoot. The order of obstacle height was randomly selected.

A 13-link biomechanical model of the human body was used to compute the kinematics of the whole body's COM. The 3-D trajectory of the whole body's COM was computed from the weighted sum of the COM from each body segment. The linear velocities of the whole body's COM were computed using the GCVSPL algorithm (Woltring, 1986). Effects of the subject group and the obstacle height on the gait parameters were assessed with a two-way ANOVA with repeated measures.

RESULTS

Total displacement of the COM in all three orthogonal directions increased linearly ($p \leq 0.036$) with obstacle height. Significant group differences were found in both the anterior/posterior (A/P) and medial/lateral (M/L) directions ($p=0.021$ and 0.05, respectively). All subject groups maintained a similar magnitude of M/L displacement of the COM during unobstructed walking. However, when stepping over higher obstacles, the elderly demonstrated greater M/L displacements of the COM than the young adults. Elderly patients demonstrated the greatest M/L displacement of the COM during the crossing stride (Figure 1). Peak forward velocities of the COM of all subjects decreased linearly ($p<0.001$) as obstacle height increased. Significant group differences were identified for the peak forward velocity of the COM ($p=0.025$). Peak M/L velocities of the COM increased linearly ($p=0.002$) as obstacle height increased (Figure 2). Although no significant group differences were found in peak M/L velocities of the COM, elderly patients demonstrated the greatest M/L velocity during all of the testing conditions. Both peak upward and downward velocities of the COM increased linearly ($p<0.001$) with obstacle height. No significant group differences were identified for the maximum upward and downward velocities of the COM.

DISCUSSION AND SUMMARY

Investigating the effect of obstacle height on the motion of the COM while negotiating obstacles in different groups of subjects will enhance our understanding of the increasing incidence of falls with aging and provide recommendations for the development of strategies aimed at reducing falls.

The results of this investigation have shown that elderly patients with imbalance demonstrated the largest and fastest movement of the COM in the M/L direction when stepping over an obstacle. This may explain the propensity to fall sideways in the elderly population, which has been shown to be the most likely cause of hip fractures (Hayes et al., 1996; Greenspan, 1998).

REFERENCES

Greenspan SL et al. (1998) *Am J. Med* **104**:539-45.

Hayes WC et al. (1996) *Bone* **18**:77S-86S.

Kaya, BK et al. (1998) *J. of Gerontology* **53A**: M126-134.

Tinetti ME et al. (1989) *N Engl J Med* **302**: 1055-1059.

Woltring, HJ (1986) *Adv Eng Software* **8**: 104-113

ACKNOWLEDGMENTS

Supported by NIH grants (HD07447 &AG05770) and the Mayo Foundation.

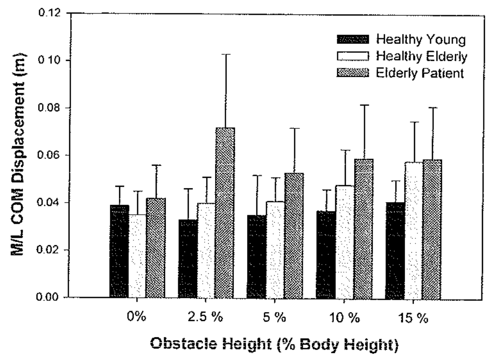

Figure 1. M/L COM displacements

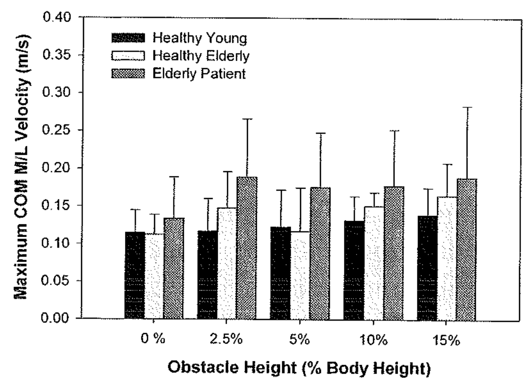

Figure 2. Maximum M/L COM velocities

DIRECT DYNAMICS SIMULATION OF STEPPING TO RECOVER BALANCE

Darryl G. Thelen and Dana R. Burd

Engineering Program; Hope College; Holland, MI 49423
Email: thelen@hope.edu

INTRODUCTION

Recovering balance during an impending fall often involves taking rapid step(s) in order to move the base of support (BOS) safely under the center of mass (COM). Experimental studies of balance recovery have documented that healthy older adults demonstrate significant age-related differences in stepping strategy (Luchies et al. 1994, McIlroy and Maki 1996) and abilities to recover from large perturbations of balance (Thelen et al. 1997, Wojcik et al. 1999). However, it is difficult to determine the underlying causes of these differences in an experimental paradigm, where many physical, psychological and environmental factors contribute to the movement observed.
The objective of this study was to develop a direct dynamics simulation of a person stepping to recover balance during a forward fall. The model was then used to predict how variations in muscle mechanics properties and latency time affect stepping performance.

METHODS

A seven linked-segment model of a person included the feet, shanks, thighs and head-arms-trunk. Thirty musculo-tendon actuators, acting about the ankle, knee and hip joints, were driven by eighteen independent muscle excitation signals. A general Hill-type model was used to represent musculo-tendon contraction dynamics (Zajac 1989). This model incorporated the force-length and force-velocity relationships of muscle, and the stress-strain relationship of tendon. Parameters of the musculo-tendon model included maximum isometric muscle stress (σ_{max}) and maximum contraction velocity (V_{max}). Four muscle-specific parameters (fiber pennation angle, physiological cross-sectional area, optimal fiber length and tendon slack length) were used to scale the general musculo-tendon model for each actuator (Zajac 1989, Delp 1990). A dynamic simulation package (ADAMS, Mechanical Dynamics Inc.) was used to conduct all modeling and analyses.

The simulations conducted were that of a young adult male using a single step to recover balance upon release from a 30° forward lean (Figure 1). The biomechanics and muscle activities of this task have been described previously (Thelen et al. 1997, 2000). In the model, muscle excitations were represented by a double-step function, with muscles fully activated and de-activated at prescribed switch times following an initial latency period. Myoelectric signals were used to estimate the latencies and switch times for individual muscles (Thelen et al. 2000).

After obtaining a simulation that reasonably reproduced the kinematics and kinetics of the task, model parameters were varied one at a time and the effect on stepping performance determined. Stepping performance was characterized by relative step length, which was defined as the distance between the whole body COM and foot COM at landing (Feuerbach and Grabiner 1994).

RESULTS

The simulated step length was 1.15 m, with the foot landing 430 ms after release, which was comparable to experimental observations (Thelen et al. 1997). The relative step length was 0.28 m. Simulated joint torque-time histories were comparable to those obtained through inverse dynamics analysis (Figure 2). Varying muscle strength (σ_{max}) and maximum contraction velocity (V_{max}) had substantial effects on stepping performance, with 10% reductions shortening the relative step length by 0.18 and 0.11 m, respectively. In comparison, increasing the response latency by 10 ms shortened the relative step length by less than 0.02 m.

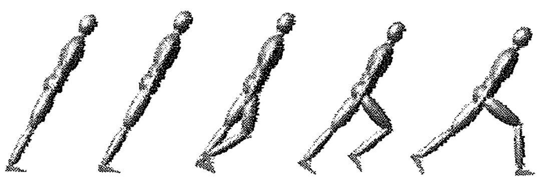

Figure 1: Simulation of stepping following release from a forward lean.

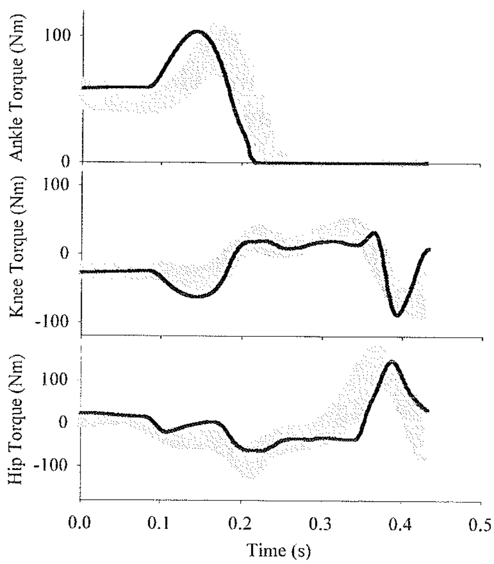

Figure 2: Simulated (solid line) and experimental (shaded, avg. ±1 S.D.) joint torques in step leg. Positive values represent extension.

DISCUSSION

Numerous studies have documented changes in the mechanical output of skeletal muscles with age. These changes include a substantial loss of isometric strength (~30% by age 70) and slowed contractions (as reviewed by Doherty et al. 1993). How such changes in muscle impact movement, and in particular balance-recovery abilities, are less well understood. Previous experimental studies of the forward stepping task found healthy old adults were able to initiate a stepping response as quickly as young, but were unable to recover from as large of forward leans and generated slower step velocities (Thelen et al. 1997, Wojcik et al. 1999). The model results suggest that these observed differences in stepping performance could come about from age-related changes in muscle strength and speed.

REFERENCES

Delp S.L. et al. (1990) *IEEE Trans Biomed Eng*, **37**, 757-67.

Doherty T.J. et al. (1993) *Can J Appl Physiol*, **18**, 331-358.

Feuerbach J.W. and Grabiner M.D. (1994) *Proceedings of 18th Annual Meeting of ASB.*

Luchies C.W. et al. (1994) *J Am Geriatrs Soc*, **42**, 506-512.

McIlroy W.E., Maki B.E. (1996). *J Gerontol Med Sci*, **51**, M289-M296.

Thelen D.G. et al. (1997) *J Gerontol Med Sci* **52A**, M8-M13.

Thelen D.G. et al. (2000) *J Electromyogr Kinesiol*, in press.

Wojcik L.W. et al. (1999) *J Gerontol Med Sci* **54**, M44-50.

Zajac F.E. (1989), *Crit Rev Biomed Eng*, **17**, 359-411.

ACKNOWLEDGEMENTS

Supported by NSF CAREER Grant BES-9702275.

LOWER EXTREMITY MUSCLE STRENGTH DOES NOT INDEPENDENTLY PREDICT BONE MINERAL DENSITY OF THE PROXIMAL FEMUR IN HEALTHY OLDER ADULTS

Tammy M. Owings [1], Michael J. Pavol [1,2], and Mark D. Grabiner [1]

[1] Department of Biomedical Engineering, The Cleveland Clinic Foundation, Cleveland, OH
[2] Programs in Physical Therapy, Northwestern University Medical School, Chicago, IL
Email: owings@bme.ri.ccf.org

INTRODUCTION

Direct relationships between muscle strength and bone mineral density (BMD) have been widely documented (Nordström et al. 1997, Alfredson et al. 1997). However, there is a general influence of body size on both BMD and muscular strength. Therefore, a question arises as to the extent to which the relationship between BMD and muscle strength is independent of body size.

The purpose of the present study was to determine the extent to which lower extremity muscular strength is an independent predictor of proximal femur BMD in healthy older adults. It was hypothesized that the BMD of the proximal femur in older adults would not be related to the maximum voluntary isometric strength of the hip, knee, and ankle muscles after adjusting for the influence of body weight and height.

METHODS

The present analysis was performed retrospectively on data compiled from a larger study. Fifty women and 29 men (age: 72±5 years; height: 1.64±0.09 meters; mass: 76.0±14.0 kg) participated. These older adults were healthy, independent, community dwellers who, prior to entry into the study, were examined for the presence of exclusionary factors such as cardiovascular, musculoskeletal, or neurological disorders. Because of the strenuous nature of some of the tasks performed in the larger study, subjects were required to have a minimum BMD value of 0.65 $g \cdot cm^{-2}$ for entrance into the study. BMD of the right femoral neck was assessed using DXA.

The maximum voluntary isometric strength of the hip, knee, and ankle at multiple joint angles were determined using a Kin-Com isokinetic dynamometer. Flexion and extension strength were measured at each joint. Compensating for passive moments and inertial effects, forces were converted to moments and low-pass filtered at 10 Hz. The maximum angle-specific moment was determined based on a scaled quadratic regression equation that was fit to the population moment-angle data.

An allometric scaling process was used to determine if maximum isometric strength should be scaled, i.e. normalized, due to the influence of body weight and height. Pearson correlations were used to determine the relationship between proximal femoral BMD and isometric strength.

RESULTS

The BMD values of two subjects were greater than four standard deviations above the mean of the sample, thus their data were excluded from the analysis.

The allometric scaling process revealed that it was appropriate to normalize the maximum voluntary isometric hip, knee, and ankle joint moments in each direction of exertion to body weight • height. The relationship between lower extremity strength and the BMD of the proximal femur were reliant on the normalization process. The magnitudes of most (5 of 6) of the correlation coefficients between the non-normalized isometric strength measures and the BMD of the proximal femur were statistically significant ($p<0.05$, Table 1). However, the magnitudes of the correlation coefficients between the normalized isometric strength measures and the BMD of the proximal femur had a substantially diminished magnitude and failed to achieve significance ($p>0.05$, Table 1).

The correlation between the subject's body weight • height and BMD of the proximal femur was significant ($p<0.01$) with the coefficient of determination (r^2) accounting for 25 percent of the shared variation. Furthermore, the correlation coefficient between the subjects' body weight • height and each of the measures of non-normalized isometric strength were significant ($p<0.01$).

DISCUSSION

Caution should be used when comparing biological variables (i.e., muscle strength and BMD) such that the influence of anthropometric variables (i.e., body weight and height) does not bias results allowing for misinterpretation of causal relationships. After adjusting muscular strength for the influence of body weight and height, the relationship between BMD and muscular strength was diminished. Thus, the results suggest that lower extremity muscular strength does not independently predict BMD in the proximal femur in healthy older adults.

Table 1: Pearson correlation coefficients between the bone mineral density of the proximal femur and the (A) non-normalized and (B) normalized maximum voluntary isometric strength measures (n=77).

	(A)	(B)
Plantarflexion	0.203	-0.150
Dorsiflexion	0.381‡	0.080
Knee extension	0.395‡	-0.005
Knee flexion	0.353‡	0.060
Hip extension	0.252†	-0.063
Hip flexion	0.368‡	0.016

† $p<0.05$; ‡ $p<0.01$

REFERENCES

Nordström, P. et al. (1997) *Calcified Tissue International*, **60**, 332-337.

Alfredson, H. et al. (1997) *Calcified Tissue International*, **60**, 338-342.

ACKNOWLEDGMENTS

This work was supported by NIH-R01AG10557 (MDG).

THE INFLUENCE OF SHAPE AND SLIDING DISTANCE OF MOVEMENT LOCI OF THE FEMORAL HEAD ON THE WEAR OF THE ACETABULAR CUP

D. Bennett[1], J. F. Orr[1], and R. Baker[2]

[1]Department of Mechanical and Manufacturing Engineering, The Queens University of Belfast, Belfast, Northern Ireland.

[2]Musgrave Park Hospital, Belfast, Northern Ireland.

Email: d.b.bennett@qub.ac.uk

INTRODUCTION

Wear and the generation of ultra high molecular weight polyethylene (UHMWPE) particles is now considered the most important cause of long term failure in total arthroplasty. The importance of multidirectional motion in the wear process of the components used as bearing surfaces in total hip and knee arthroplasties has recently been emphasised (Wang et al., (1997), Bragdon et al., (1996)). This study determines the trajectory of specified points on the femoral head of a total hip replacement (THR) for individual THR patients and the distances traversed by these points. The shape and distance traversed by these trajectories were correlated with radiographic wear measurements.

METHODS

Twenty points were selected on the surface of the femoral head of a right custom hip implant. A computer program was designed to utilise gait data from THR patients to simulate the motion of these points. Gait analysis was performed on 19 THR patients at a period of 5 years post-operation. Gait analysis was performed using a 6 camera VICON 370 motion analysis system (Oxford Metrics, Oxford, England). Angular motions of the points were determined by a program written specifically for this project (MATLAB, Mathworks Inc., Natick, MA). The loci of the points were plotted on the developed surface of the femoral head. The shape of the loci were quantified by determining the aspect ratio (length/width = L/F in Figures 1 and 2) of each.

Wear measurements were made of serial radiographs using a development of Livermore's technique of concentric circles (Livermore et al., 1990).

RESULTS AND DISCUSSION

The size, shape and direction of the loci of the points differed widely between subjects and included oblong, quasi-elliptical, figure-8 and longitudinal paths. The largest average sliding distance traversed by the 20 points for a THR patient was 140% greater than the lowest average distance traversed. The average sliding distance of the points for THR patients was 18.06mm (ranging from 10.08 to 24.41mm).

The average aspect ratio of the loci varied between subjects from 2.49 to 9.21. Lower aspect ratios signified wider loci, while higher aspect ratios signified thinner loci. Figure 1 shows the locus of a point for Subject A, which was wider than that for Subject B (Figure 2), which tended to be longitudinal in shape. Thin, longitudinal wear paths closely resemble those paths

produced under conditions of unidirectional motion (Barbour et al. (1999)). Conversely, wider paths resemble those wear paths produced under conditions of multidirectional motion at the hip joint.
Furthermore as a wider locus will cross more paths than a slender one, this would suggest that the wider path will also cause more wear on a molecular level.

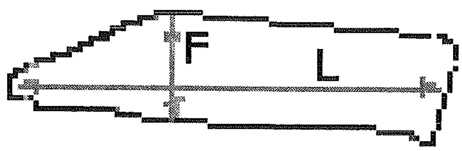

Figure 1. Locus of point for Subject A.

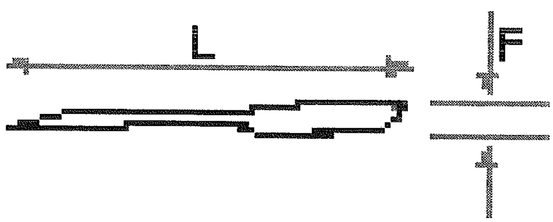

Figure 2. Locus of point for Subject B.

UHMWPE under unidirectional wear conditions experiences orientation hardening and displays higher wear resistance. Wear tests have shown the wear rate of UHMWPE to be significantly greater for conditions of multidirectional wear than for conditions of unidirectional wear (Wang et al., (1997), Endo et al., (1999)).

The average wear rate of the acetabular cup was 0.21mm/year (range: 0.06-0.47 mm/year). Individual wear rates showed positive correlation with the average sliding distance for the twenty points and improved positive correlation with the product of sliding distance and inverted aspect ratio (Figure 3).

SUMMARY

An understanding of the paths taken by points on the femoral head may inform studies of wear mechanisms and shear forces acting on the polymer. Shorter, longitudinal paths tend to cause less wear than larger, wider paths.

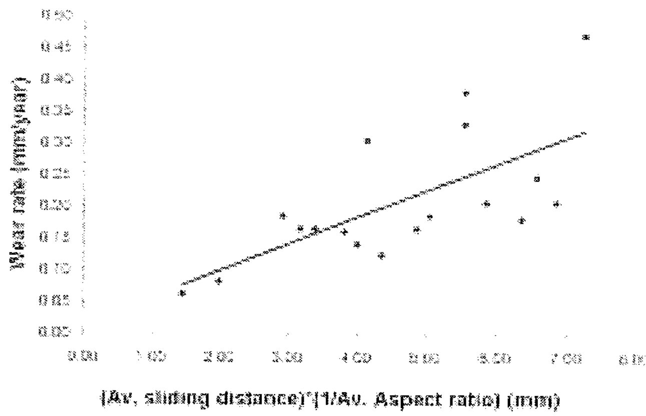

Figure 3. Plot of Wear rate against the product of the average sliding distance and the inverse of the average aspect ratio of the loci.

REFERENCES

Barbour P. S. M. et al., (1999). *Proc. Institute Mechanical Engineers., Part H: J. Engineering in Medicine,* **213**, 455-467.

Bragdon C. R., et al. (1996). *Proc. Institute Mechanical Engineers., Part H: J. Engineering in Medicine,* **210**, 157-166.

Endo M. M. et al. (1999). *Bio-Medical Materials and Engineering*, **9**, 13-20.

Livermore J., (1990). *J. Bone and Joint Surgery,* **72-A**, 518-528.

Wang, A. et al. (1997). *Wear*, **203-204**, 230-241.

EFFECT OF FEMORAL COMPONENT MALROTATION ON CONTACT STRESS IN TOTAL KNEE REPLACEMENTS

Benjamin J. Fregly

Computational Biomechanics Lab, University of Florida, Gainesville, Florida
E-mail: fregly@aero.ufl.edu **Web:** www.aero.ufl.edu/~fregly

INTRODUCTION

Proper internal/external rotational alignment of the femoral component is essential to the success of total knee replacements. In particular, femoral component external rotation has been found to reduce patellofemoral complications, currently the number one cause for revision (Berger *et al.*, 1998). Since slight femoral external rotation may also reduce the need for lateral retinacular release, some surgeons routinely aim for 3º to 5º of such rotation (Agaki *et al.*, 1999).

In addition to its effect on patellar tracking, femoral component rotational alignment may also affect the contact stresses exerted on the polyethylene tibial insert, thereby influencing wear. However, to our knowledge, no studies have investigated this effect over a large range of flexion angles.

This study uses computer simulation to predict how femoral component malrotation affects tibial insert contact stresses. A novel approach combines rigid body dynamics with elastic contact to study contact stresses during movement. The results suggest that a adding a small amount of femoral component external rotation to improve patellar tracking will not increase polyethylene contact stresses and consequently wear.

MODEL DEVELOPMENT

A hybrid rigid-deformable multibody dynamics model of the tibial and femoral components of a total knee replacement was created for this study. The femoral component was treated as a rigid body possessing six degrees of freedom relative to the fixed tibial component, with the medial and lateral contact surfaces being treated as deformable. Five radii of curvature (three for the femoral and two for the tibial component) were used to describe the surface geometry.

Two elastic half-space contact models were used to calculate tibiofemoral contact forces and stresses based on the interpenetration of the undeformed surfaces and their material properties (Johnson, 1985). The first was a Hertz model which assumed locally quadratic surface profiles in the region of contact. The second was a half-space boundary element model which made no assumptions about the contacting geometry by discretizing the contact region into elements. Checks were developed to ensure that the amount of penetration and conformity between the contacting surfaces remained small enough to warrant the use of elastic half-space theory. The entire multibody dynamics model was implemented in the commercial software Pro/MECHANICA MOTION.

The model was used to perform a one-second dynamic simulation of a 90° knee flexion motion. This was achieved by prescribing a sinusoidal sagittal plane rotation of the femur relative to the tibia, with the motion of the remaining five degrees of freedom being predicted by dynamic simulation. In addition to elastic contact forces, the motion was influenced by the major knee joint ligaments (minus the ACL) modeled as one or more bundles of nonlinear elastic springs (Blankevoort and Huiskes, 1996). Articular contact was maintained by a fixed downward vertical load of 1500 N applied at the midpoint between the posterior femoral condyles. Because the patella and limb segments were excluded in this initial study, all inertia in the model was from the femoral component alone.

Once a nominal dynamic simulation was developed, the femoral component was rotated about the long axis of the femur by ±10° to simulate the effects of internal/ external rotational malalignment.

RESULTS AND DISCUSSION

The nominal dynamic simulation predicted larger contact forces and stresses in the medial than in the lateral compartment, with the maximum stresses occurring near 90° of flexion (t = 0.5 sec; Fig. 1). A dramatic jump in contact stress occurred at a flexion angle of 17° (t = 0.15 and 0.85 sec) when the anterior-posterior curvature discontinuity in the femoral component was traversed. Although such discontinuities have been associated with excessive wear in industrial cam mechanisms, surface finishing of the femoral component may diminish this effect. Since the contact surfaces were quadratic by construction, stress results from both elastic contact models were nearly identical.

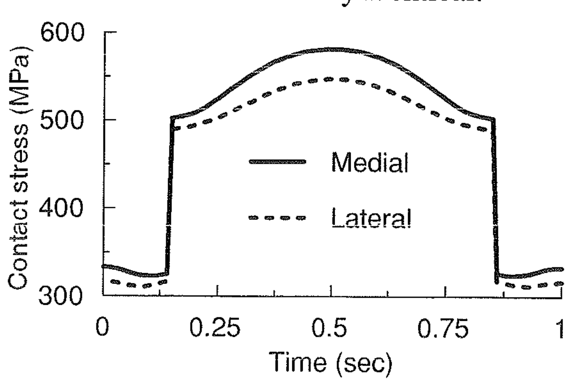

Figure 1: Average contact stresses for the nominal dynamic simulation.

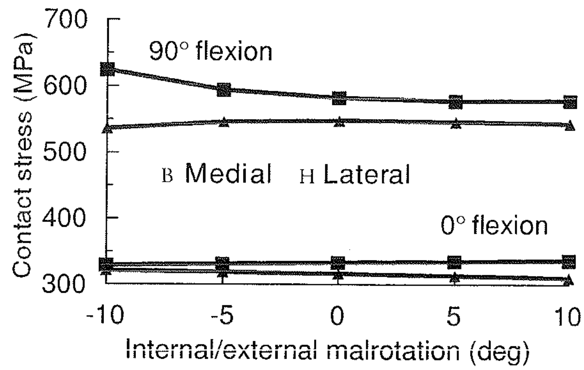

Figure 2: Sensitivity of contact stresses to femoral component malrotation.

The simulations with femoral component malrotation predicted contact stress sensitivity only for internal (i.e., negative) malrotation and only in highly flexed positions (Fig. 2). Even then, the magnitude of the sensitivity (+7% medially for 10° internal rotation) was small. The lack of appreciable sensitivity in extension agrees with published *in vitro* test results (Liau *et al.*, 1999).

These simulation results suggest that for this implant geometry, adding a small amount of femoral component external rotation to improve patellar tracking will not come at the expense of increased tibial insert contact stresses and wear. A more complete dynamic simulation validated against video fluoroscopic movement data and including the patella, limb segments, and muscles is being developed to confirm these findings.

REFERENCES

Akagi, M. *et al.* (1999) *Clin Orthop* **366**, 155-163.

Berger, R.A. *et al.* (1998) *Clin Orthop* **356**, 144-153.

Blankevoort, L. and Huiskes, R. (1996) *J Biomechanics* **29**, 955-961.

Johnson, K.L. (1985) *Contact Mechanics.* Cambridge University Press.

Liau, J.-J. *et al.* (1999) *Clin Biomechanics* **14**, 717-721.

STATIC ALIGNMENT AND DYNAMIC JOINT LOADS DURING GAIT AMONG SUBJECTS WITH KNEE OA

Adam B. Ryals[1,2] Debra E. Hurwitz[1] Ali Karrar[3] Thomas P. Andriacchi[4]

[1]Department of Orthopedic surgery, Rush-Presbyterian-St. Luke's Medical Center, Chicago, IL
[2] Department of Bioengineering, University of Illinois at Chicago
[3] Department of Rheumatology, Rush-Presbyterian-St. Luke's Medical Center
[4] Department of Mechanical Eng./Functional Restoration, Stanford University, Stanford, Ca.
Email: aryals1@uic.edu

INTRODUCTION

Medial compartment osteoarthritis (OA) is the most common form of knee OA. Increased loading may be one pathogenic factor leading to the progression of OA. The external adduction moment has been shown to be the primary determinant of the load distribution between the medial and lateral compartments of the knee during walking. Furthermore, it has been shown that the external knee adduction moment in an OA population is greater than that observed in normals (Baliunas et al., 1999). Additionally, the radiographic disease severity as assessed by Kellgren and Lawrence (KL) grade was correlated with the external adduction moment (Sharma et all, 1998). Therefore, analyzing factors which contribute to higher magnitudes of the external adduction moment may lead to a greater understanding of the development and progression of medial compartment OA.

In a previous study by Andrews et al., (1996) the mechanical axis and toe-out angle were predictive of the external adduction moment in normal subjects. However, Prodromos et al. (1985) found no correlation between the mechanical axis and the adduction moment in a population of preoperative high tibial osteotomy candidates. In a follow up study it was suggested that toe-out angle was a mechanism to decrease the external adduction moment (Wang et.al, 1990). Yet to be determined are the combined abilities of mechanical axis, toe-out angle and KL grade in predicting the external adduction moment in subjects with knee OA. The first objective of this study is to test which of these factors (mechanical axis, toe-out angle or KL grade) best predicts the external adduction moment. The second objective is to test whether, in the presence of each other, these individual factors all still make a significant contribution to the variance in the adduction moment.

METHODS

This study is based on a subset of 62 subjects (average age 62 $\pm$ 10 years) with radiographic evidence of knee OA and no other significant joint involvement who participated in a double blind study on the effects of nonsteroidals on knee joint loads. The subjects underwent gait testing after a two-week drug washout period. Inclusion into the present study was based on having a standing full-length radiograph and a KL grade of at least 1. The mechanical axis ranged from -9^{o} valgus to 15^{o} varus ($5^{o}\pm5^{o}$). Ten subjects had a KL score of 1, 23 had a score of 2, 22 had a score of 3, and 7 had a score of 4.

Kinematic and kinetic gait parameters were obtained using an optoelectronic camera system and force plate (Andriacchi et al., 1995). Inverse dynamics were used to calculate three-dimensional external moments which were normalized to % body weight times height (%BW*Ht). Subjects walked at self-selected speeds of slow, normal and fast. A representative walking trial at a speed of about 1 m/s was chosen for the analysis.

Pearson correlations as well as a multivariate linear regression model were used to test if the mechanical alignment, toe-out angle and KL grades were predictive of the external adduction moment (α =.05). The adduction moment typically consists of two peaks the first of which occurs in early stance and the second in late stance. Both peak adduction moments were analyzed in this study.

RESULTS

The mechanical axis was the best predictor of both the first and second peak adduction moments (Table I, Fig. 1). While KL grade was also predictive of the first and second peak adduction moments, once the effects of mechanical axis were accounted for, KL grade no longer made a significant contribution to the variance in either peak adduction moment.

Table I: External Knee Adduction Moment

	First peak	Second peak
Mean ± SD (% BW*Ht)	3.49 ± 1.08	2.53 ± 1.07
	Correlation Coefficients	
Mechanical Axis	R= 0.76, p<.001	R=0.75, p<.001
Toe-out angle	R= -0.23, p=.075	R= -0.45, p<.001
KL grade	R= 0.31, p=.015	R= 0.27, p=.037

Toe-out angle was negatively correlated with the second peak adduction moment. However, it only accounted for 10% of the variability of the adduction moment after accounting for the effects of the mechanical axis.

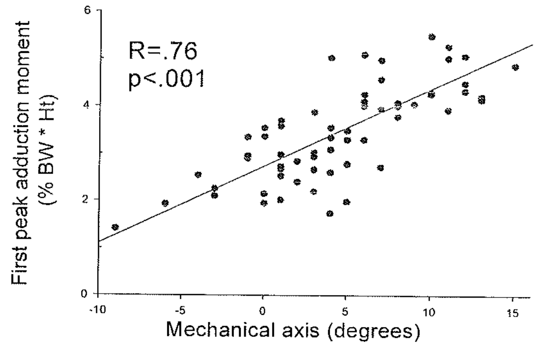

Fig 1: The mechanical axis was the best predictor of the adduction moment

DISCUSSION

Among these subjects with knee OA, the static alignment and not the disease severity as assessed by the KL grade is the primary determinant of the peak adduction moment. Furthermore, this study indicates that alterations to gait such as increasing toe-out angle only partially compensate for the effects of a varus deformity. The correlation between the knee adduction moment and mechanical axis was not found by Prodromos et al. (1985), possibly because the subjects in the Prodromos study were more disabled, had a greater varus deformity and probably at a later stage in the disease process than those in the present study. Understanding relationships between the adduction moment and mechanical axis may lead to a greater understanding of the progression of OA.

REFERENCES

Andrews M, et al.: *JOR*, 14(2), 1996.
Andriacchi et al.: *Basic Orthopedic. Biomechanics* 37-67, 1995.
Baliunas et al.: *46th ORS,* 2000 (in press).
Prodromos CC., et al.: *JBJS AM,* 67, 1985.
Sharma L., et al.: *Arthritis Rhum,* 41 1998.
Wang, et al.: *JBJS* 72(6) 1990.

Acknowledgements: NIH/NIAMS SCOR Grant AR39239

GLENOID INCLINATION IS ASSOCIATED WITH FULL-THICKNESS ROTATOR CUFF TEARS

Richard Hughes, Jason Wening, Laurie Huston, James Carpenter, and John Kuhn

Orthopaedic Research Lab, Department of Surgery, University of Michigan, Ann Arbor, MI
Email: rehughes@umich.edu

INTRODUCTION

Factors associated rotator cuff pathology include repetitive overhead arm activities, age, and scapular morphology. The best known anatomic association is the "hooked acromion" identified by Bigliani *et al.*, (1986). There may be other morphologic parameters that are associated with rotator cuff pathology. We hypothesized that the angle of the glenoid in the plane of the scapula ("glenoid inclination") may also be associated with rotator cuff tendon pathology. The rationale for this theory is that the tendency of the humeral head to migrate superiorly, which may impinge the supraspinatus tendon between the humeral head and acromion, depends on the direction of the net muscular and gravitational forces acting on the humerus. If the net force is directed into the glenoid, superior migration should not occur. If the net force is directed too superiorly, the force transmitted to the humerus through the articular surface may insufficient to prevent superior migration of the humeral head. The net force acting on the humeral head can be decomposed into shear and compression. As glenoid inclination angle increases, the superior shear component increases. According to this theory, less deltoid force would be required to produce superior humeral head migration in a shoulder having greater glenoid inclination angle. The objective of this study was to test the hypothesis that glenoid inclination angle play a role in rotator cuff pathology. Two strategies were used to address this hypothesis: (1) an anatomic study was conducted to compare glenoid inclination angles in shoulders with full-thickness rotator cuff tears and normal shoulders; and (2) a computational model was developed to analyze the effect of glenoid inclination on superior humeral head migration. We hypothesized that glenoid inclination angles would be greater in shoulders with rotator cuff tears.

MATERIALS AND METHODS

Measurement accuracy. A pilot study was conducted to assess the accuracy of measuring glenoid inclination from radiographs. The glenoid angle of four cadaver shoulders was measured radiographically and by three-dimensional digitization. Each shoulder was disarticulated from the torso. Soft tissue was dissected down to the rotator cuff. 600 micron lead beads were glued at the intersection of the spine and medial border of the scapula. Each scapula was placed on a x-ray cassette and an exposure made. The scapula was oriented so that it was parallel to the film.

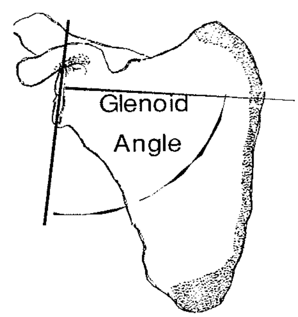

Figure 1. Glenoid inclination angle.

Radiographs were digitized using NIH Image. Four points were identified: (1) lead bead on medial border, (2) spinoglenoid notch, (3) superior glenoid tubercle, and (4) inferior glenoid tubercle. Lines were constructed between points 1 and 2 and between 3 and 4. Glenoid inclination angle was the angle between these two lines (Figure 1). Glenoid inclination was also computed using points digitized in three dimensions directly from the specimens. A Flock of Birds electromagnetic tracking system equipped with a plastic digitizing stylus was used for digitizing landmarks. Glenoid inclination was computed from the digitized locations and compared to the radiographic measurements.

Anatomic study. Eight pairs of cadaver shoulders were tested (mean age 77; S.D. 10). One shoulder from each pair had a full-thickness rotator cuff tear, while the contralateral shoulder did not. Glenoid inclination angles were computed using the radiographic method. Differences in glenoid inclination angle between shoulder with tears and shoulders without tears were evaluated using a non-parametric sign test.

Mathematical model. An analytic model was developed to relate glenoid inclination angle with the minimum deltoid force necessary to produce superior migration of the humeral head. A planar model was constructed, and it assumed that (1) the glenohumeral joint reaction force acts perpendicular to the articular surface, (2) the glenohumeral joint has negligible friction, (3) superior humeral head migration does not occur when the net reaction force on the humerus can be represented as a non-negative linear combination of vectors normal to the glenoid articular surface. The radius of the glenoid articular surface was assumed to be 26.3 mm, and the distance from inferior to superior glenoid was 39 mm (Iannotti *et al.*, 1992). Rotator cuff forces were taken from electromyographic estimates of muscle force during the initiation of arm abduction (Laursen *et al.*, 1998). The line of action of the deltoid was assumed to be perpendicular to that of the supraspinatus. The lines of action of the infraspinatus and subscapularis were assumed to be 45° below the supraspinatus. The minimum deltoid force necessary to produce humeral head migration was computed at each glenoid inclination angle. All programming was done in MATLAB.

RESULTS

Measurement accuracy. The radiographic technique for measuring glenoid inclination was validated by three-dimensional digitization. The average difference between glenoid inclination angles measured radiographically and by three-dimensional digitization was –0.17° (S.D. 3.5°).

Anatomic study. The average glenoid inclination angle measured in shoulders with full-thickness rotator cuff tears was 98.6° (5.6° S.D.); the mean glenoid inclination angle in normal shoulders was 91.0° (4.7° S.D). The difference was found to be statistically significant (P=0.008).

Mathematical model. An increase in inclination angle from 90 to 98.6 decreases the predicted minimum deltoid force necessary to superiorly sublux the humeral head by 51%.

DISCUSSION

Glenoid inclination angle appears to be associated with the existence of full-thickness rotator cuff tears, and there is a mechanical explanation for this phenomenon.
The mathematical model shows that glenoid inclination angle can significantly affect whether an imbalance of superior and inferior forces acting on the humerus will lead to superior migration of the humeral head. Theoretically, shoulders with a larger inclination angle would be more prone to subacromial impingement of the supraspinatus tendon. If subacromial impingement is related to the development of full-thickness rotator cuff tears, then the anatomic results are consistent with the theory.

This study cannot determine causality. Prospective studies will be required to determine whether the inclination causes the cuff tear or the cuff tear causes the inclination.

REFERENCES

Bigliani, L.U. (1986) *Orthop. Trans*, **10**, 228.
Ianotti, J.P. *et al.* (1992) *Journal of Bone and Joint Surgery*, **74-A**, 491-500.
Laursen, B. *et al.* (1998) *J. Biomechanics*, **31**, 731-739.

CEMENT PENETRATION ASSOCIATED WITH PRESSURIZATION OF THE GLENOID IN TOTAL SHOULDER ARTHROPLASTY

J. E. Hale,[1] T. J. Panek,[2] C. A. Guanche,[1,2] D. D. Anderson,[1,2] and D. D. Buss[1,2]

[1] Biomechanics Laboratory, Minneapolis Sports Medicine Center, Minneapolis, MN
[2] Dept. of Orthopaedic Surgery, University of Minnesota, Minneapolis, MN
Email: jhale1@fairview.org Web: www.msmc.org

INTRODUCTION

Prosthetic replacement of the glenohumeral (shoulder) joint provides pain relief and improved function in patients with disabling arthritis. Premature implant loosening is a significant clinical concern with the glenoid at greatest risk. Most total shoulder replacement (TSR) designs have glenoid components that are cemented in place.

A stable cement-bone interface is derived from mechanical interdigitation of cement with the surrounding cancellous bone. The strength of that interface increases linearly with cement penetration depth (Askew et al. (1984)). Increased pressure during cement/implant insertion has been suggested as a means to facilitate cement penetration (Harris (1994)). Improved cementing techniques for total hip arthroplasty, including cement pressurization, are credited for increased survival rates compared with historical cementing techniques (Harris (1994)). We believe that similar results are attainable in the shoulder. The objective of this study is to analyze the effects of pressurizing cement into the glenoid cavity.

MATERIALS AND METHODS

The effect of pressurization on cement penetration was evaluated in three matched pairs of fresh-frozen cadaveric shoulders, age 60 and greater. This age range was chosen to represent typical TSR patients.

Glenoid components were implanted using standard TSR surgical techniques. For each matched pair of shoulders, one received a component cemented in place using finger packing. On the opposite side, cement was injected under pressure using an instrument similar to a caulking gun. The type of cement (Howmedica Simplex P, low viscosity) and mixing technique were the same for both sides/treatments. Following cement insertion, a polyethylene glenoid component (Intermedics) with a keeled design was implanted in each shoulder.

A low speed saw was used to create a series of five slices through the bone and cement surrounding the polyethylene implant. Both surfaces of each slice were scanned and digitally analyzed to determine the cement penetration. Alizarin red biological stain was used to enhance contrast between bone and cement. Absolute penetration (P) and relative penetration (P*), as defined by Panjabi et al. (1983), were computed using the following equations:

$$P = (A2 - A1)\ \text{mm}^2$$

$$P^* = (A2 - A1)/(A3 - A1) \times 100\ \%$$

where A1 = cross-sectional area of the glenoid component, A2 = cross-sectional area occupied by the cement, including A1, and A3 = cross-sectional area within the cortical-cancellous bone boundary. Scanned images from paired shoulder specimens, depicting the influence of cement

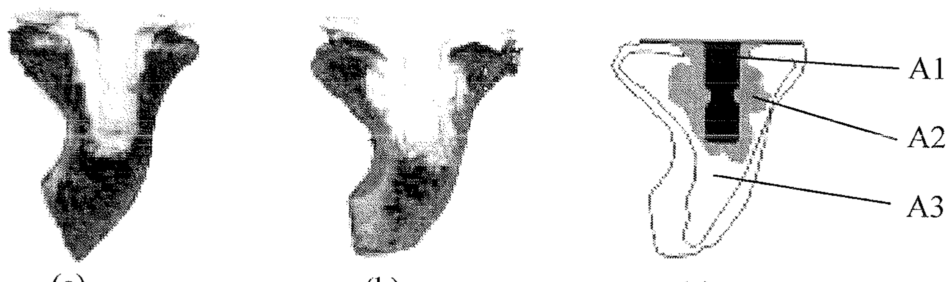

(a) (b) (c)

Figure 1. Representative sections through specimens with the glenoid component implanted using (a) finger-packed and (b) pressurized cementing technique. Schematic diagram (c) illustrates the boundaries of the areas corresponding to A1, A2, and A3.

pressurization as well as the basis for area calculations, are shown in Figure 1.

RESULTS AND DISCUSSION

The highest values for absolute and relative penetration occurred in the pressurized specimens (P > 100 mm^2, P* > 50%). An overall measure of the relative penetration for each specimen was obtained by calculating the mean and standard deviation of the individual slices (Table 1).

Table 1. Mean and standard deviation for relative cement penetration in %.

Specimen number	finger-packed	pressurized
1	28.9 ± 14.3	42.2 ± 6.2
2	30.8 ± 6.6	46.2 ± 4.5
3	25.6 ± 5.8	21.5 ± 5.7

In two of three matched pairs of shoulders, the mean penetration for the pressurized case was greater than that for the non-pressurized case, but it was slightly less in the third pair. Although both techniques exhibited considerable variability, smaller standard deviations for the pressurized case suggest a more uniform distribution of cement in these specimens. Comparison of absolute penetration values for matched pairs followed a trend similar to that for relative penetration.

Differences in penetration between pressurized and non-pressurized cementing techniques were evaluated as an indicator of implant stability. Overall, the effect of pressurization on cement penetration tended to be as good or better than the traditional non-pressurized approach. In the one case where penetration for the non-pressurized side exceeded that for the pressurized side, the posterior cortex was violated during pressurization. This complication, clearly undesirable, likely counteracted any positive effects of pressurization. Future testing will involve a larger sample size and statistical analysis.

REFERENCES

Askew, M.J. et al. (1984). *J. Orthopaedic Research* **1**:412-20.

Harris, W.H. (1994). Instructional Course Lectures, Michael Schafer, ed., AAOS Press, Chicago, **43**:367-72.

Panjabi, M.M. et al. (1983). *J Biomechanics* **16(7)**:473-80.

ACKNOWLEDGMENTS

This research was funded by the Minnesota Chapter of the Arthritis Foundation. Glenoid implants were provided by Intermedics.

INTERNAL PRESSURE IN HUMAN LUMBAR VERTEBRA

Ruth S. Ochia [1] and Randal P. Ching [2]

[1] Department of Bioengineering, University of Washington, Seattle, WA

[2] Department of Orthopaedics, University of Washington, Seattle, WA

Email: rso10@psu.edu

INTRODUCTION

In Roaf's theory of burst fracture formation, he described an axial compressive load on a vertebra, which induced endplate failure from the nucleus pulposus being pushed into the vertebral body. This resulted in an increase in vertebral internal pressure that would cause the body to explode with retropulsion of bony fragments into the canal space (Roaf 1960). This aspect of Roaf's burst fracture theory (internal vertebral pressurization) has not been previously tested under destructive impact conditions.

The current research measures changes in internal pressure of lumbar spinal segments under high- and slow-speed axial-compressive loads to determine whether an internal pressure rise is associated with burst fracture formation.

PROCEDURES

Specimen Preparation: Twenty-one human cadaveric thoracolumbar 3-body spinal segments were used (sections T12-L2, T11-L1, and L1-L2). They were randomly divided into two groups: high- and slow-speed with mean ages of 73.7 ± 8.8 and 67.4 ± 12.0 years, respectively. These specimens were determined to be free of pre-existing pathologies and fractures using visual and radiographic inspections. Bone mineral density (BMD) was determined for each specimen using dual x-ray absorptiometry (DXA) (Hologic Inc., Waltham, MA).

Internal Pressure System: The internal pressure (IP) measurement system consisted of a pressure transducer (Model 4503, Eaton Lebow, Troy, MI), a 90° brass elbow, and a 3/16-inch brass tube.

Mechanical Testing: The internal pressure system was degassed with a vacuum pump while submerged in distilled water bath. It was not removed from the bath for the remainder of the test.

The upper and lower vertebrae were potted in dental cement (Labstone Buff, Miles Dental Products), so only the middle vertebra and its adjacent discs would be exposed to axial compressive loading. While the specimen was submerged, a hole in the pedicle of the middle vertebra was made to a depth of 1/2 inch. The 3/16-inch brass tube was removed from the rest of the IP system, but it was kept submerged. The 3/16-inch brass tube fitted with a 1/8-inch brass rod insert was pressed into the undersized pedicle hole. The brass rod was used to keep the tube clear of bone debris. This rod was removed and the rest of the internal pressure system (elbow and pressure transducer) was reattached to the secured metal tube. The potted specimen was secured to the water tank with a metal bracket. The tank was bolted to a load cell (MTS, Minneapolis, MN) (Figure 1). The water was then heated to 37°C and the specimen remained at that temperature for at least 1/2 hour.

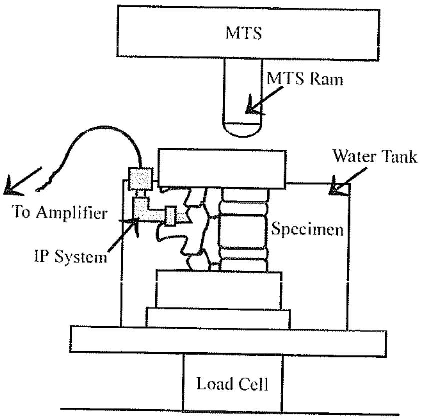

Figure 1: Schematic of IP system in a specimen with the water tank.

The specimens were then subjected to axial compressive loading at 10mm/sec and 2500mm/sec, slow- and high-speed, respectively under displacement controlled testing. The maximum displacement for each specimen was limited to 1/4 the middle vertebral height plus 1/2 the heights of both discs, as measured from lateral radiographs.

Analysis: An ANOVA was used to determine the differences in measured internal pressure, failure load and energy absorption, based on a significance level of 0.05. Clinical fracture type was determined from post-injury lateral radiographs by an orthopaedic surgeon.

RESULTS AND DISSCUSSION

The measured initial peak internal pressure was 6.23 ± 3.97 kPa and 2.38 ± 1.56 kPa for slow- and high-speed, respectively. Internal pressure decreased significantly from the slow to high speed tests ($p < 0.01$), while neither failure load or energy absorption were significantly different (Figure 2).

All of the slow-speed specimens resulted in compression fractures. The high-speed specimens had 3 burst, 3 compression with burst elements, 3 compression with disc herniation, and 2 compression fractures.

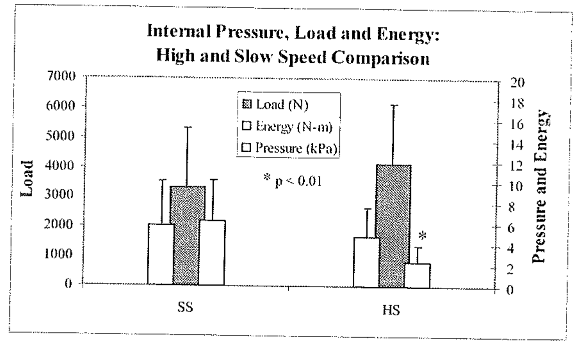

Figure 2: Comparison of slow speed (SS) and high speed (HS) internal pressure, failure load and energy absorption.

Roaf's theory of burst fracture formation described an internal pressure rise, which resulted in vertebral explosion and bony retropulsion into the canal space. The current research does not support this theory in that there was no measured increase in internal pressure at high speed and burst fractures were still produced. In conclusion, a possible modification to Roaf's theory could be that entry of the nucleus into the vertebral body does not cause an internal pressure rise, but instead acts as a wedge, which splits the vertebral body apart and then pushes bony fragments into the canal space.

REFERENCES

Roaf, R. (1960). *Journal of Bone and Joint Surgery,* **42 B,** 810-823.

ACKNOWLEDGMENTS

This research was supported by AO Foundation, Berne, Switzerland and UW Graduate School. The authors wish to thank Russell Scott of UW Roosevelt Radiology Clinic for performing the DXA scans.

RELATIONSHIP BETWEEN RATE OF LOADING AND DYNAMIC RESPONSE INCLUDING FAILURE INITIATION IN A LUMBAR MOTION SEGMENT

Jamie L Ryan, Raghu N. Natarajan and G.B.J. Andersson
Department of Orthopedic Surgery, Rush-Presbyterian-St.Luke's Medical Center, Chicago.
E-mail: rnataraj@rush.edu

INTRODUCTION

Mechanical failures of the motion segment are believed to contribute to back injuries, back pain and disc degeneration. In order to begin to understand the failure progression in a disc due to cyclically applied sudden loads, a model study has been conducted on the stress distribution in a disc due to an impact load applied over varying time periods. The hypothesis of the current study is that the faster the load is applied to the lumbar motion segment, a larger volume of the disc is subjected to stresses beyond its failure state. It is also hypothesized that as the rate of loading increases, the disc becomes stiffer.

METHODS

A three-dimensional validated non-linear finite element model of L3-L4 was used for this study (Natarajan, 1999). The disc components were modeled as poro-elastic. Permeability values for the nucleus, annulus, endplate, cancellous bone and cortical bone were taken from the literature (Argoubi, 1996). A parameter that relates the ratio between the outward flux of fluid and the variation in the skeletal volume (equivalent to porosity of the component) was defined for nucleus and endplate as 0.8 while the corresponding parameter for annulus was assumed to be 0.7. A much smaller value for this parameter was assumed for cancellous (0.27) and cortical bones (0.02). Another parameter that relates the ratio between the outward flux of fluid and the variation in the fluid pressure (similar to 1/bulk modulus of the material) was assumed as 1.0E-6 for all components. The drained elastic moduli and poisson's ratios for all the disc components were also taken from literature (Argoubi, 1996). The disc was assumed to have an initial pressure of 1 MPa. Stress levels at which failure initiates in endplate, annulus and cancellous bone were taken from literature. The static loading response of the L3-L4 disc to 3000 N axial compression was found to agree with values available in literature.

The inferior surface of the L4 vertebra was fixed in all directions while a surface pressure (equivalent to 3000 Newton) was applied on to the superior surface of the L3 vertebra. The load was applied , instantaneously, in 2.5 s,10 s and 20 s. A general-purpose finite element program ADINA was used for the analyses.

RESULTS

A static load of 3000 N produced a maximum disc compression of 2.5 mm. This increased to 3.9 mm when the compressive load was applied instantaneously. As the time required to apply the full load increased, the maximum disc compression also increased. A disc compression of 3.8 mm was observed when the load achieved its full value in 2.5 s (Figure). The disc compression increased to 5.3 mm when the full load was applied in 20 seconds.

Both under static compression loading conditions as well as under dynamic compression loading modes, initial failure was always observed in the endplates. A static compressive load of 3000 N produced a larger volume of superior endplate failure than failure in the inferior endplate. Twelve percent of the superior endplate volume was above the failure stress level while only six percent of the inferior endplate volume was above the failure stress level. An instantaneously applied compressive load produced failure only in 2 percent of the total endplate volume (Figure). The compressive load of 3000 N when applied in 10 seconds produced fissures in only 1 percent of the total endplate volume. The percentage of endplate fissure volume decreased further to 0.3 when the total load was applied over a longer time period of 20 seconds.

During dynamic load application, when the total compressive load of 3000 N was applied instantaneously, maximum equivalent stress in the endplate was 5.7 MPa. This maximum stress value was reduced to 5.1 MPa when the total load was applied in 20 seconds. Thus as the time taken to apply the load increased, the maximum stress in the endplate decreased.

DISCUSSION

A non-linear finite element model including fluid flow between the disc and the surrounding tissues showed that when a compressive load was applied suddenly the disc became stiffer as compared to when the load was applied slowly. At the same time the stresses in the disc components increased producing larger volume of fissures in endplates. Endplate fissure volume decreased exponentially as the load was applied more slowly. The current study showed that when a single cycle of compressive load (3000N) was applied suddenly, failure occurred in 2% of the endplate volume. Conversely, the failure was reduced to an insignificant amount of endplate failure volume (0.3%) when the full load was applied in 20 seconds. The current study thus shows that if lumbar discs are subjected to a suddenly applied load, endplate failure can occur and if this type of sudden loading is repeated the endplate fissure volume may increase which can lead to the ultimate failure of the disc.

Increased flexibility of the motion segment was observed due to dynamic loading when fluid flow was included in the model. The current study showed that the disc under suddenly applied load became 55% more flexible as compared to a disc in which the fluid flow was not considered. This increase in flexibility is due to the flow of fluid from the disc into the surrounding tissues. With this increased flexibility the disc is therefore capable of adjusting to suddenly applied loads.

Rate of loading also had an effect on the deformation of the disc. As the time taken to apply the full dynamic load increased, the disc became more flexible. The dynamic stiffness decreased by 38% when the full load was applied in 20 seconds as compared to the stiffness of a disc in which the load was suddenly applied. This means when the load was slowly applied there was enough time for the fluid to flow through to the surrounding tissues that this produced larger deformation.

In conclusion the current study showed that the faster the load is applied on to the lumbar motion segment, the larger the volume of fissures occurring in the endplates. This study also showed that increases in rate of loading increases the stiffness of the motion segment (figure).

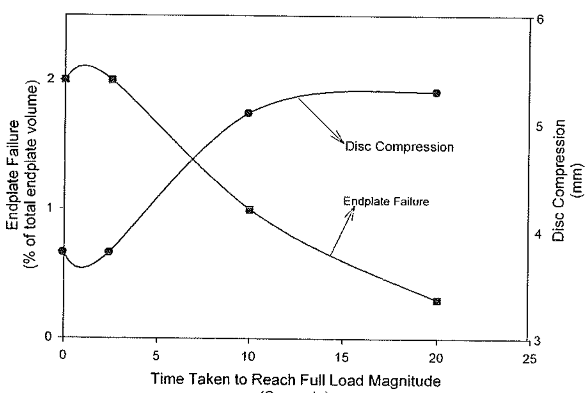

DYNAMIC RESPONSE IN A LUMBAR MOTION SEGMENT FOR VARIOUS RATES OF LOADING

REFERENCES

(1) Natarajan RN & Andersson GBJ, (1999), *SPINE*:24, 1873-1881.

(2) Argoubi M and Shirazi-Adl, (1996), *J. Biomechanics*, 29, 1331-1339.

BIOMECHANICAL EVALUATION OF DIAGONAL TRANSFIXATION IN PEDICLE SCREW INSTRUMENTATION

Tae-Hong Lim, Jesse Kim, Timothy Yoon, Atsushi Fujiwara and Howard S. An

Dept Orthopedic Surgery, Rush-Presbyterian-St. Luke's Medical Center, Chicago, IL, USA

INTRODUCTION

In pedicle screw instrumentation, it is common to use one or more transfixators that crosslink the longitudinal rods horizontally. Such a horizontal transfixation (HTF) of the longitudinal rods was shown to provide an additional stability in axial rotation and lateral bending but not in flexion extension. Most significant contribution of HTF was noted in axial rotational stability because the torsional instability appeared to be most difficult to prevent using pedicle screw fixation. Recently, diagonal transfixation (DTF) has been suggested as a way to improve the overall biomechanical rigidity of the pedicle screw systems. However, the construct stiffness changes due to DTF has not been well investigated yet. The purpose of this study was to investigate biomechanical advantages of DTF compared with the HTF using flexibility tests and finite element (FE) analyses.

METHODS

Nondestructive flexibility tests were performed using 10 calf lumbar spines (L2-L5). L2 and L5 vertebrae were used to attach the loading and base frames, respectively. Pure moments were applied to the loading frame in flexion (FLX), extension (EXT), lateral bending (LB) and axial rotation (AR) up to 8.2 Nm. Resulting motions of L3 and L4 vertebrae were measured using a 3-D motion analysis system. The flexibility tests were repeated on the following cases: 1) intact; 2) pedicle screw instrumentation without TF after total removal of L3-4 disc; 3) pedicle screw instrumentation with DTF; and 4) pedicle screw instrumentation with HTF. Diapason spinal fixation system (Stryker, Allendale, NJ) was used for instrumentation, and the transfixator was connected to the end of the pedicle screws. For HTF, the transfixator was connected to the superior left screw and to the inferior right screw.

3-D FE models of the tested constructs were developed to investigate the effect of diagonal and horizontal transfixation on the construct stability and the corresponding stress changes in the pedicle screws. 3-D beam elements were used to model the 6.5 mm pedicle screws, 6 mm longitudinal rods, and 6 mm transfixator. The vertebra was modeled as a rigid beam connecting the screws. The posterior elements, preserved in flexibility tests, were not included in FE models to simulate the pedicles screw fixation of the most unstable spine. A rigid connection at the rod-screw, bone-screw, and rod-transfixator was assumed in all model. Nodes representing the bone-screw interface and vertebral body within the inferior vertebra were constrained not to move in any direction. Rotational moments of 8.2 Nm in FLX, EXT, LB and AR were applied for analyses. The resultant displacements of the nodes in the elements for the screw and vertebral body were predicted and used to evaluate the stabilizing effect of DTF as compared with HTF. Moments acting on each screw and their percentages changes due to HTF and DTF were also predicted to estimate the stresses in the screws. The percentage moment changes from the model with no transfixator were used to represent the rate of stress changes due to DTF and HTF.

RESULTS

Mean (± SD) rotational angles of the L3 vertebra with respect to the L4 vertebra in response to the maximum moment of 8.4 Nm are listed in Table. As compared with the intact case, the pedicle screw instrumentation without TF significantly reduced the motion in FLX (37.5%), EXT (23.7%), and LB (83.4%), but it failed to significantly reduce the AR motion (14.4%, $p>0.1$). When compared with no TF case, HTF significantly improve the LB and AR stability by 15.7% and 13.9%, respectively, while no improvement of stability was found in FLX and EXT. In contrast, DTF significantly improved the FLX and EXT stability by 12% and 10.7%, respectively, but not the LB and AR stability as compared with no TF case. Comparison between HTF and DTF cases showed that the stabilizing effect of DTF was greater in FLX and EXT (13% and 11%; $p<0.01$) than that of HTF, but smaller in LB (11%, $p<0.05$) and AR (6.6%, $p>0.1$).

Finite element model predictions of the motion changes were similar to those observed in flexibility tests. In HTF case, the magnitudes of the moment applied on both right and left pedicle screws were identical, while the load changes, as compared with the no TF case, were 0.02% increase in FLX/EXT, 27.5% increase in LB, and 58% decrease in AR. In the case of DTF achieved by connecting the left superior screw and the right inferior screw , however, the loads in the left screw were increased by 11.5% in FLX/EXT, 43.6% in LB, and 7.9% in AR, whereas the load changes in the right screw were 10.9% decrease in FLX/EXT, 0.06% increase in LB, and 18.1% decrease in AR.

DISCUSSION

The results of this study showed that DTF provides more rigid fixation in FLX/EXT but less in LB and AR as compared to HTF. These changes in the construct stability may not be desirable since the pedicle instrumentation was known to provide excellent stabilization in FLX, EXT and LB but not restore the AR stability beyond the intact level. Furthermore, model predictions of the total load on the pedicle screws showed that the pedicle screws may experience greater stresses in the DTF construct than in the HTF construct. Such an increases in the total load should result in higher stresses in the pedicle screws and may cause the screw breakage. These limitations of the diagonal transfixation should be considered for clinical application.

ACKNOWLEDGMENT
This study was supported by Stryker Inc. (Allendale, NJ).

Table (Unit: degrees).

Case	FLX	EXT	LB	AR
Intact	5.66 ± 2.43	4.26 ± 0.90	7.02 ± 1.69	2.16 ± 0.56
no TF	3.18 ± 0.68	3.16 ± 0.38	1.11 ± 0.21	1.78 ± 0.43
HTF	3.22 ± 0.63	3.17 ± 0.55	0.94 ± 0.22	1.53 ± 0.46
DTF	2.79 ± 0.63	2.82 ± 0.38	1.05 ± 0.25	1.66 ± 0.49

no TF = pedicle screw fixation only without using a transfixator; HTF = horizontal transfixation; DTF = diagonal transfixation.

ON EVALUATION OF MUSCLE FORCES AND SPINAL PASSIVE-ACTIVE SYNERGY IN COMPRESSION

A. Shirazi-Adl [1], M. Parnianpour [2], S. Sadouk [3]

[1] **Dept of Mechanical Eng, École Polytechnique, Montréal, Québec**
[2] **IWSE Dept, The Ohio State University, Columbus, Ohio**
[3] **Senior Flexonics Inc, Burbank, California**
Email: **abshir@meca.polymtl.ca**

INTRODUCTION

The redundancy in the trunk active system can serve balancing the varying external moments along the spine, actively augmenting the stiffness of the system by adequate activation level, and controlling posture to minimize active muscle forces and tissue stresses/strains. A number of methods have been proposed to solve for the highly redundant problem of spinal active-passive load distribution. Due to the shortcomings in existing reduction, optimization and EMG-driven models, and combination thereof, a novel kinematics-based approach is introduced that utilizes the passive-active synergy. This is then applied for the analysis of load distribution of the lumbar spine in an optimal neutral posture under compression loads.

Our in vivo measurements of normal standing volunteers carrying up to 445 N loads in hands have shown that the pelvis rotates posteriorly and the lumbar flattens as loads increase. There was, however, negligible surface EMG activities in back superficial muscles (Parnianpour et al., 1994). Our recent model studies have demonstrated the substantial effect of changes in the lumbar lordosis and pelvic tilt on the passive-active load-sharing, system equilibrium/stability, and tissue stresses. It appears, therefore, that, for a given task, a posture is so adopted as to yield an optimal load configuration that requires minimum muscle exertion. In the current study, a solution technique for the redundant spinal system is described and applied to the analysis of an optimal posture obtained by varying the lordosis and pelvic tilt under a 2800 N axial compression.

METHODS

Two different models of the lumbar spine, a detailed realistic one and a simplified beam-rigid body one, are used. The latter model is constructed based on the former with equivalent overall geometry and nonlinear direction-dependent structural properties. An optimal postural solution is sought for changes in lordosis and pelvic tilt in order to minimize required moments at different levels. The total axial load of 2800N accounts for 245N of the upper body weight applied anteriorly at different levels and a concentrated load of 2555N applied 8mm anteriorly at the L1 simulating weight in hands + penalty of upper global muscles.

A novel kinematics-based muscle force evaluation algorithm coupled with optimization is employed for the redundant active-passive system to calculate unknown segmental muscle forces for the optimal posture using a muscle architecture with 46 local muscles. This approach uses a hybrid force-displacement method. At given applied compression loads, displacements (if all available) are prescribed at each lumbar level and corresponding loads are evaluated. These loads are fed into a separate algorithm that calculates the statically equivalent muscle forces at each level based on the current configuration and equilibrium conditions. The force penalties of these muscles are then fed back into the finite element module as additional updated external loads and the procedure is continued till a convergence is reached. If displacements at a level are insufficient to solve for unknown muscle forces at that level, then an optimization approach should also be used. In the current study, sagittal and lateral rotations were prescribed and optimization was employed. Cost functions of minimum total muscle forces/stresses, cubic power of muscle stresses, and shear forces were considered.

RESULTS AND DISCUSSION

Large moments are neede to equilibrate the total compression load of 2800 N. Pelvic tilt and flexion rotations substantially diminish these moments. An optimal posture can, thus, be found resulting in minimum segmental moments (<1 N-m) in order to support 2800 N compression load (Table 1). The effect of variation in lordosis and pelvic rotation in reducing the required moments is in accordance with our earlier studies (Shirazi-Adl and Parnianpour, 1996). The cost function of the sum of cubic power of muscle stresses activates more muscles (Table 2). In contrast, however, only one muscle is activated at each level when the other objective functions are employed. The solution simultaneously satisfies the kinematics and equilibrium requirements of the entire spine while performing a task. The passive-active synergy is, hence, accounted for by pro[illegible]nsideration of passive stiffness and required active muscle forces for a given posture and loading. The predicted minor activation level of muscles present considerable experimental challenge (i.e., relative activation may be very close to noise level of EMG signals). Hence, the role of realistic mathematical modeling cannot be overemphasized for the optimal design of postures; e.g., for safe lifting techniques.

Table 1: Rotations (+ve: ext) resulting in min equilibrium moments under 2800 N.

Level	Segmental Rotation °	Total Rotation °	Segmental Moment Nm
L1	-5.0	-10.82	0.69
L2	-3.07	-5.82	0.22
L3	-0.62	-2.75	0.18
L4	-2.02	-2.13	0.02
L5	-4.43	-0.11	-0.41
S1	4.32	4.32	30.72

Table 2: Muscle forces (N) on each side and their extension moment M for the cost function of minimum sum of cubed muscle stresses for the optimal posture in 2800N. IC: Iliocostalis, IP: Iliopsoas, LT: Longissimus thoracic pars lumborum, MF: Multifidus, QL: Quadratus Lumborum.

Level	IC	IP	LT	MF	QL	M Nm
L1	2.2	13.58	1.35	2.93	2.17	0.542
L2	1.14	3.83	0.49	1.63	0.64	0.172
L3	0.95	1.93	0.36	1.98	0.39	0.127
L4	0.44	0	0.17	1.32	0.2	0.105
L5	-	0	0.04	0.16	-	0.013

ACKNOWLEDGEMENTS
The work is supported by grants from the NSERC-Canada and IRSST-Québec.

REFERENCES

Parnianpour, M., Shirazi-Adl, A. et al. (1994). *Proceedings of IEA '94*, 119-121.

Shirazi-Adl, A., Parnianpour, M. (1996). *J Biomech Eng*, **118**:26-31.

PEDIATRIC TENSILE NECK STRENGTH CHARACTERISTICS USING A CAPRINE MODEL

Russell Mayer, Frank A. Pintar, Narayan Yoganandan

Department of Biomedical Engineering, Marquette University
Department of Neurosurgery, Medical College of Wisconsin
and V.A. Medical Center, Milwaukee, WI
Email: rmayer@mcw.edu Web: mcw.edu

INTRODUCTION

The introduction of passenger airbags has increased reports of injuries related to their deployment. While the majority of these injuries have been minor, the exposure of children to airbag deployment has resulted in more serious injuries (Winston). In many cases, adult occupants sustained little or no injury while child passenger injuries resulted in severe injury or death. The mechanism of the injuries has been primarily attributed to tensile loading as the airbag unfolds under the chin of the child.

Obtaining tolerance values for children of different age groups can help mitigate these injuries. Determination of these data for children is difficult because tissue for these tests is not readily available. Through the use of animal models, scaling factors determining the relationship between developmental age group strengths can be tested and related to human age group tolerance.

METHODS

The tensile neck strength and material characteristics of the pediatric cervical spine were studied using a caprine (goat) cadaveric animal model. The human age equivalent for one-year-old, three-year-old, six-year-old, twelve-year-old, and adult was determined using CT images to evaluate the skeletal equivalent maturation stage. Each specimen was initially tested under sub-failure loads in tension and load relaxation from the head to C6. The ligamentous spine was then sectioned into OC-C2, C3-C4, C5-C6, and C7-T1 motion segments. These segments were tested under several conditions including sub-failure in axial tension, load relaxation, pure moment bending in flexion-extension, lateral bending, and failure in axial tension.

The cervical sections were mounted by dissecting and embedding the desired vertebrae. Some muscle was left intact along with gauze soaked in Ringer's solution to preserve the fluid in the specimen and the integrity of the intervertebral joints. The segments were mounted by passing wires over the vertebrae pedicles and through the vertebral bodies. The vertebrae and wire composite were mounted in PMMA (dental acrylic), creating an interface for the piston and load cells.

Axial testing of the cervical spine was done with an electro-hydraulic piston (MTS, Minneapolis, MN). The computer-controlled system was programmed under force and displacement control. A bottom six-axis load cell, an upper load cell, and an

LVDT provided measurements for all reactions of the system under quasi-static loading rates.

Pure moment testing used a four-camera, three-dimensional motion analysis system (Motion Analysis Corp., Santa Rosa, CA). A pure moment was created with masses hung from a pulley system. This system applied torque to the top of the specimen preparation through load arms. A bottom six-axis load cell measured the reaction forces and moments of the specimen.

RESULTS AND DISCUSSION

From the caprine models, several individual scaled relationships were developed. Measurements of linear and rotational stiffness, load relaxation rate, and destructive failure force in tension were taken for comparison. Figure 1 shows the average overall tolerances scaled to the adult strengths in comparison to other currently used scale factors.

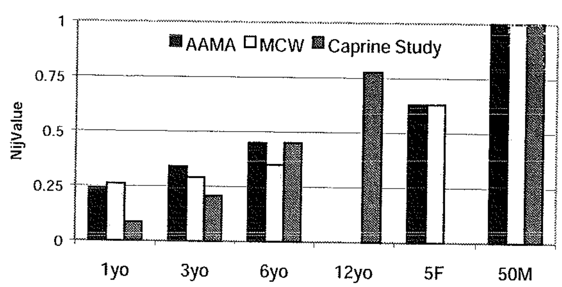

Figure 1: Two current scaling factors for cervical spine strength compared to caprine tests. Values are given for a 1-, 3-, 6-, and 12-year age groups as well as small female and mid-sized male.

Current tolerance levels for children and infants have been developed using several different methods. Most methods use the strength of lumbar ligaments, or different structure size and height comparisons (Yoganandan; Melvin). Very few tests have been done on young specimens to validate calculated tolerance factors.

The use of tolerance data in the configuration of child and infant crash test dummies can create a more realistic estimate of injury. Determination of injury probability can then lead to safer and stronger designs.

SUMMARY

Injuries induced in destructive testing such as endplate failure and ligament tears are consistent with clinical observations. Specimens demonstrated increased strength characteristics with age. Stiffness and tensile strength increase with cervical level and with age. Scaling relationships were developed with respect to the adult specimens. Results indicated that currently used scaling relationships may require more conservative strength limits for children of one and three years of age.

REFERENCES

Melvin J. (1995) SAE paper #950872 Warrendale, PA

Yoganandan N, Pintar FA, et al. (1996) *Med. Eng. Phys.* **18**: 4:289-294

Winston FK, Reed R. (1996) *40th Stapp Car Crash Conference* SAE paper #962438 Warrendale, PA

ACKNOWLEDGEMENTS

This study was supported in part by DOT NHTSA and the Department of Veterans Affairs Medical Research

FUNCTIONAL IMAGING OF THE NORMAL AND ARTHRITIC KNEE

Eugene J. Alexander, Thomas P. Andriacchi, and Philipp K. Lang

Stanford University, Stanford, CA

Email: gene.alexander@stanford.edu Web: www.stanford.edu/group/biomotion

INTRODUCTION

Osteoarthritis (OA) is the most common condition to affect the joints of humans and a frequent cause of pain and disability. The appropriate selection of treatment plans for OA is dependent on the development of better methods for the assessment of the disease process. Degenerative changes to articular cartilage can be described in biological, mechanical and morphological terms.

From a morphological viewpoint there has been substantial progress in our ability to study cartilage using MRI. From a mechanical viewpoint recent studies have demonstrated a relationship between the dynamic loads at the knee during gait and progression of knee OA (Prodromos 1985). The combination of imaging methods with functional kinematic information obtained during walking could greatly enhance our ability to study OA. The primary purpose of this work is to integrate cartilage imaging techniques with newly developed methods to study the functional kinematics of the knee joint.

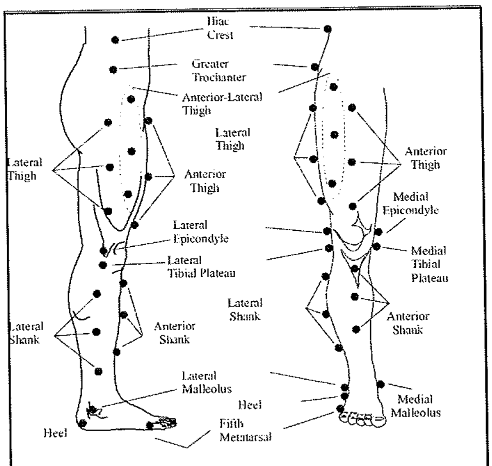

Fig. 1. Point cluster marker set.

MATERIALS AND METHODS

Kinematic measurements were obtained using a point cluster technique (Andriacchi et al. 1998) with interval deformation correction (Alexander et al. 1998) described elsewhere. These techniques seek to minimize the error associated with skin deformation relative to the bone. The marker set is shown in Figure 1. The medial markers are in place only during a reference data acquisition, with the subject standing still.

These markers are magnetically opaque; that is, they are designed to be observable by both the opto-electronic system and the MRI. Some of these markers, and their corresponding coordinate systems, are shown in Figure 2. By corresponding these external and internal markers, it is possible to animate high resolution 3D internal images, such as 3D cartilage thickness maps, with subject specific motion data.

A computational method for the calculation of the 3D cartilage thickness maps is based on a 3D Euclidian distance transformation (EDT) (Stammerberger 1999). For a given set of feature points in a binary volume, the EDT computes the distance to the closest feature point for each non-feature point of the volume. By using the points on the cartilage-bone interface (inner cartilage surface, ICS) as feature points, the EDT measures the distance to the closest voxel on the ICS for all other points, including the ones on the outer cartilage surface, resulting in a truly three-dimensional distance value determined normal to the ICS.

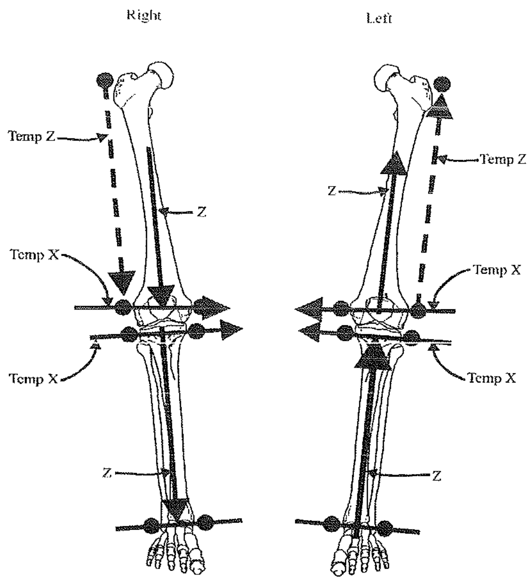

Fig. 2. Anatomic coordinate systems.

RESULTS

Figure 3 shows a three dimensional cartilage thickness map clearly showing a large defect on the medial femoral cartilage. Figure 4 show another result, three time steps of an animation of a healthy cartilage from an anterior and lateral point of view.

DISCUSSION

This methodology describes a technique

Fig. 3. A 3D cartilage thickness map.

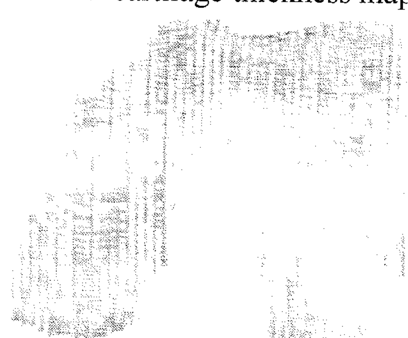

that combines medical images (MRI) of articular cartilage with dynamic measurement of human movement. Thus, for the first time the relative *in vivo* movement of cartilage in the weight bearing portion of the knee can be examined. Local defects can be identified and studied relative to the areas loaded during such activies as walking. This should allow us to be able to generate visualizations which detail the motion of the knee joint over lesion areas in the cartilage.

Fig 4.Healthy knee, leg extension, anterior(A-C) and lateral(D-F) views.

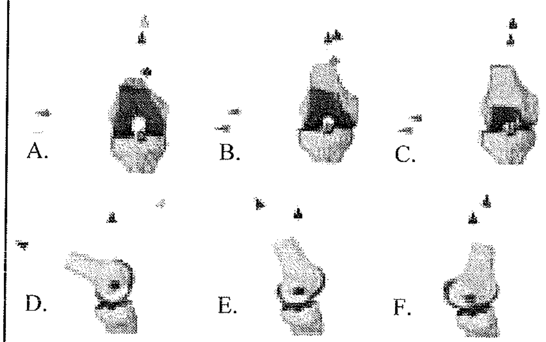

REFERENCES

Alexander, E.J, et al. (1998). Optimization Techniques for Skin Deformation Correction, *Int. Symp. on 3-D Human Movement*, Chattanooga, TN, 104-107.

Andriacchi, T.P., et al. (1998). A Point Cluster Method for In Vivo Motion Analysis: Applied to a Study of Knee Kinematics, *J. Biomech. Eng.*, **120(12)** 743-749.

Prodromos, C.C., et al.(1985) *J. Bone Joint Surg* **67A**, 1188-1194.

Stammberger T, et al. (1999) Determination of 3D cartilage thickness data from MR imaging: computational method and reproducibility in the living. *Mag Res Med*; **41**:529-536.

ACKNOWLEDGEMENTS

This work was supported in part by the NIH, AR20702-17, AR39421-8, and AR54327-01.

IN VIVO MEASUREMENT OF ARTICULAR SURFACE PROXIMITY

William J. Anderst and Scott Tashman
Bone and Joint Center, Henry Ford Hospital, Detroit, MI
Email: anderst@bjc.hfh.edu

INTRODUCTION

This paper describes a method to determine the proximity of articular surfaces during movement. This information may be useful in the study of osteoarthritis, in biomechanical modeling, and in identifying normal and pathological joint mechanics. As an example, the distances between the tibia and femur articular surfaces during canine gait before and after anterior cruciate ligament (ACL) transection are presented.

METHODS

Kinematic Data: Kinematic data was collected using a biplane radiographic system capable of tracking implanted radiopaque markers in 3D at a rate of 250 frames/s with a dynamic accuracy of $\pm$ 0.1mm (Tashman, 1995). Four 1.6mm tantalum spheres were implanted into the right tibia and femur of each dog at the beginning of the study. Data was acquired from 0.2s before to 0.3s after paw-strike for 3 trials of treadmill walking at 1.5m/s. 3D marker coordinates were determined using previously described techniques (Tashman, 1999). All animal procedures were approved by our institutional Care of Experimental Animals Committee.

Computed Tomgraphy Data: Computed tomography (CT) data was collected for each dog (1mm slices, 0.488mm x 0.488mm resolution). Custom designed software determined the surface points of each bone from the CT scans.

The relationship between the implanted tantalum markers and surface points was derived from the CT scans. This information was combined with the 3D kinematic data and allowed the surface points of each bone to be determined for every frame of 3D data collected. Minimum distances between bone surface points on the tibia and femur were then calculated at each instant.

Solid Figure Reconstruction: In order to visualize the results, the CT slices were reconstructed into 3D solid figures (Geiger, 1996). Custom designed software animated the solid figure bones according to the 3D kinematic data, and the articular surfaces were color coded according to the minimum distance to the other bone at each instant.

RESULTS

Figure 1 shows the color coded surface of the femur of a representative subject at sequential instants of the stance phase of gait. Each sphere on the surface of the femur represents a two-pixel by two-pixel region (0.976 mm^2). Pictures A, B and C display the minimum distance from the femur to tibia surface prior to ACL transection, while pictures D, E and F display the minimum distances between bone surfaces two years after ACL transection.

Figure 2 shows the same femur with india-ink staining. The india-ink stain is most prominent on areas of full-thickness cartilage loss.

DISCUSSION

There are two major findings to note in Figure 1. First, in both the ACL intact (A, B, C) and post-ACL transection (D, E, F) conditions, the largest area of close joint proximity during paw-strike was on the medial half of the femur. Furthermore, after ACL transection, the imbalance between the size of the areas of close proximity on the medial and lateral condyles had shifted even more toward the medial side. These results agree with the india-ink staining results (Figure 2) that show cartilage loss on the medial femoral condyle. The correspondence between the areas of closest joint proximity and the region of cartilage loss in Figures 1 and 2 was also present in other dogs that experienced cartilage damage two years after ACL transection.

The second feature to note in Figure 1 is the anterior shift in the areas of closest proximity at each corresponding time instant of weight-bearing. At times t=0.000s (paw-strike), t=0.100s, and t=0.200s, the region of close proximity between the femur and tibia was shifted in the anterior direction two years post ACL-transection, relative to ACL-intact. This result agrees with the previously reported finding of a rapid anterior tibial translation relative to the femur after paw-strike in ACL deficient dogs (Tashman, 1999).

These findings suggest that this method may provide useful information regarding *in vivo* articular surface contact areas during dynamic movements.

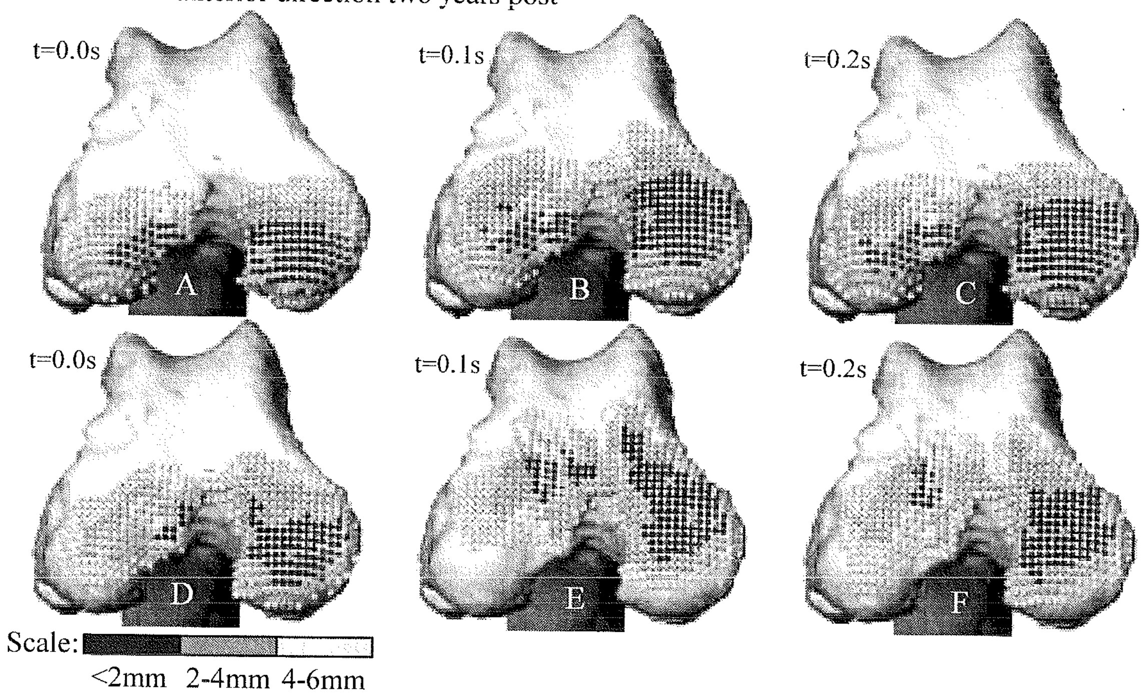

Figure 1: Minimum distance from femur surface to tibia surface. Femur regions closer to tibia are darker, while regions farther from tibia are lighter. A, B and C are ACL intact, while D, E, and F are two years after ACL transection. t is time in seconds after paw-strike.

Figure 2: Femur of dog 2 years post ACL transection with india-ink staining. Note regions of full-thickness cartilage loss on medial condyle.

REFERENCES

Geiger, B. (1996). *nuages software*, version 4.1.

Tashman, S. (1995). *Proc. Amer. Soc. Biomech.*, Stanford, CA.

Tashman, S., et al. (1999). *Proc. Orthop. Res. Soc.*, Anaheim, CA.

EVALUATION OF DYNAMIC JOINT LOADING DURING RISING AND DESCENDING TO A KNEELING POSITION

Takeo Nagura, Chris Dyrby, Ajit Chaudhari, John MacMahon, Eugene Alexander and Thomas Andriacchi

Stanford Biomotion Laboratory, Stanford University, Stanford, California
Email: tnagura@leland.stanford.edu Web: stanford.edu/group/biomotion

INTRODUCTION

Although kneeling is a common activity among many populations, there is almost no information about joint mechanics during this movement. Moreover, the ability to kneel is limited in patients who have had prosthetic surgery such as total knee arthroplasty (TKA). The limitation of range of motion (ROM) is one of the main reasons, however there is also no basis to support whether these prosthesis can permit this activity in terms of mechanical loading.
The purpose of this study was to quantify the mechanical loads and ROM on the lower-limb joints of healthy subjects during kneeling activity.

METHODS

Six healthy male volunteers (age 30.7±3.7, height 1.77±0.1m, weight 669±9 N) performed all the tasks related to standing from the kneeling position (Fig. 1), or returning to the kneeling position from erect posture, using one or two legs (Fig 2.). Four activities were analyzed:

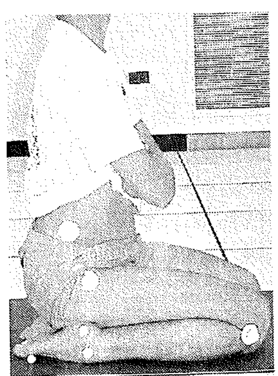

Figure 1. Kneeling position.

1) Single legged rise: lift hips and step on the force plate (Fig. 2A), then stand up using one leg.
2) Double legged rise: lift hips and set toes on the ground. With ankles in dorsi-flexion, lift the knees off the ground to the squat position (Fig. 2B), and then stand up using both legs.
3) Single legged kneel: reverse the motion of single legged rise from erect posture.
4) Double legged kneel: reverse the motion of double legged rise from erect posture.

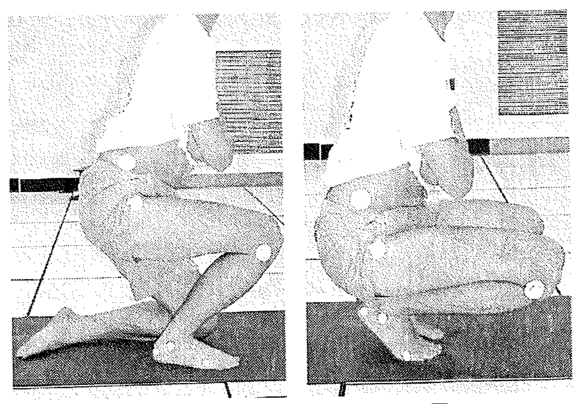

A B

Figure 2. Single legged (A) and Double legged (B) activity.

The motion was analyzed using 6 retro-reflective markers (CTFC), a four-camera system (Qualysis), and a force plate (Bertec). Each subject performed 3 trials of each activity bilaterally, with only the markered leg on the force plate. The kinematics and joint kinetics data were calculated for the hip, knee and ankle.

To compare the data with other activities, 10 healthy subjects were randomly chosen from previous studies for walking and stair-climbing. Two-sided Student's t-tests were used to test for significance ($\alpha<0.05$).

RESULTS

Average ROM of hip, knee, and ankle in all kneeling trials were 65.9±8.6, 149.7±7.4, and 88.6±9 degrees, respectively. ROM of these 3 joints was significantly wider than in walking or stair-climbing.

There were different, but highly reproducible patterns in flexion-extension moments for each activity (Fig. 3). Moreover, very similar patterns were seen between single legged rise and single legged kneel, or double legged rise and double legged kneel. The largest flexion moments were about the knee in double legged rise (14.1±1.7 %BW*Ht), while the moments about the hip were the largest in single legged rise (9.2±1.2 %BW*Ht). These two magnitudes were significantly larger than those in walking or stair-climbing.

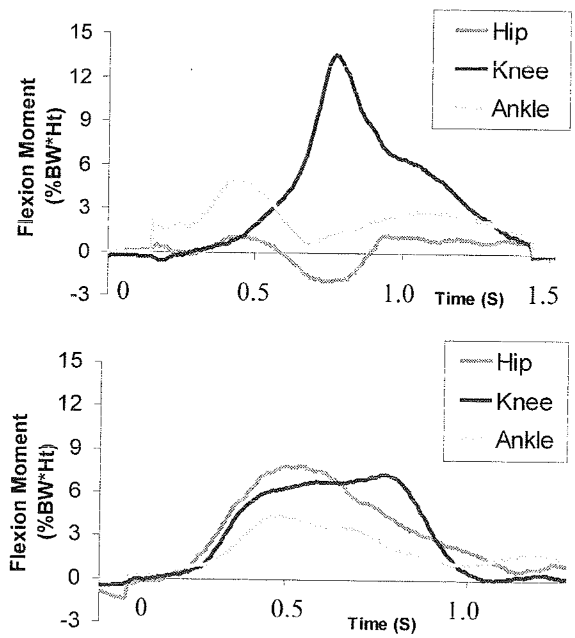

Figure 3. Typical flexion moments pattern in double legged rise (above) and in single legged rise (below).

Moments in other planes were small (below 3%BW* Ht) in all trials.

Maximum anterior-posterior joint loads reached over 60 %BW in each joint for most of the trials, which were significantly larger than those in walking or stair-climbing, except the loads on ankle in double legged rise and double legged kneel. Axial loads were similar in single legged motion, but significantly smaller in double legged motion, compared with the other two activities.

DISCUSSION

Kneeling requires a large ROM for each joint and large flexion moments about hip and knee. These results indicate that not only a high degree of joint flexibility, but also large net extensor muscle moments are needed to perform the tasks. The characteristics of the forces on each joint suggest that there are more anterior-posterior loads rather than axial loads in these activities. Moreover, these loads must result in greater joint reaction forces on each joint, associated with muscle contractions and ligament forces.

In conclusion, there seem to be very high mechanical loads in the lower-limb during kneeling activities. These magnitudes of the loads will be valuable indicators to create or assess new type of prostheses that permit kneeling.

REFERENCES

Andriacchi, T.P. et al. In Mow, V.C. & Hayes, W.C. (1997). *Basic Ortho. Biomech.* Lippincott -Raven Press.

Schipplein O. D., Andriacchi T.P.(1991). *J. Orthop. Res.* **9**, 113-119.

EXPERIMENTAL INVESTIGATION OF BEARING MOTION INITIATION IN A ROTATING PLATFORM TOTAL KNEE

J. K. Otto, T. D. Brown, J. J. Callaghan, and A. D. Heiner

Orthopaedic Biomechanics Laboratory, 2181 Westlawn Building,
University of Iowa, Iowa City, IA 52242
Email: tom-brown@uiowa.edu

INTRODUCTION

Although mobile bearing total knee replacements are growing in popularity, little is known about the mechanics at the 'mobile' interface. Recent *in vivo* fluoroscopic data suggest that these bearings in fact may not move as intended in a large subset (≈50%) of patients. If so, it is important to understand the factor(s) impeding motion.

METHOD

Rotating platform total knee components* (Figure 1) were potted with bone cement and secured to a custom made MTS testing fixture. This particular implant's tibial tray has a beveled hole that accepts the mating stem of the mobile polyethylene insert, thus providing the insert with rotational freedom about the superior/inferior axis. Fixturing allowed the tibial tray to undergo free mediolateral and anteroposterior translational and varus/valgus rotation. The MTS actuator controlled both the axial load and the internal/external rotation/torque applied to the femoral component.

The moment (torque) that resisted motion at the 'mobile' tibial tray/polyethylene (PE) interface was of particular interest. Two fundamentally different types of experiments were performed, termed 'static' and 'dynamic'. In the static tests, after loading the components, the level of internal/external torque was gradually increased until a maximum level resisting torque was produced, followed by a rapid rise in angular displacement (Figure 2). The dynamic tests differed in that a constant angular velocity of 10°/s was maintained throughout the range of endo/exorotation. An LVDT was configured so as to monitor rotation of the insert with respect to the femoral component. Experiments were performed at full extension at various levels of loading (1, 2, 3, 4 BW, 1 BW=686.5 N), motion (10° internal and external rotation), and medial/ lateral condyle weight distributions (50/50 and 60/40, respectively). All experiments were performed with the components submersed in 10% fetal bovine serum (Life Technologies, Gaithersburg, MD). Six replicate trials were done at each experimental parameter setting (order varied).

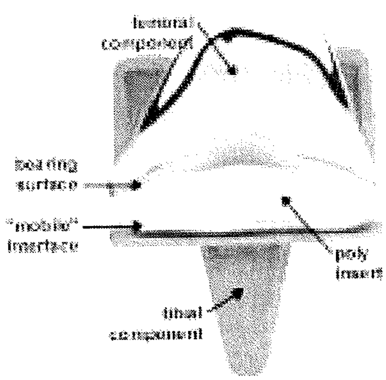

Figure 1: Rotating platform total knee (courtesy Depuy, Inc.).

RESULTS AND DISCUSSION

LVDT data showed that for all practical purposes, nearly all relative motion accommodating the imposed endo/exorotation occurred at the 'mobile' interface (Figure 2).

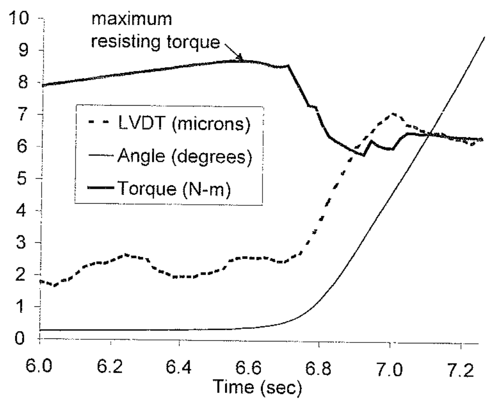

Figure 2: Resisting torque peaked just before PE slippage. The LVDT registered little motion between the PE insert and femoral component.

Dynamic experiments delivered a nearly constant torque level during the imposed motion, from which the series average was calculated. There was a nearly linear relationship between resisting torque and axial load for both static and dynamic cases (Figure 3 and Table 1). There was no statistically significant difference for behavior on internal vs. external rotation (p=0.64), nor on 50/50 vs. 60/40 (p=0.42) load cases, even though the prosthesis is left-right non-symmetrical. There was, however, a marginally significant difference (p=0.058) between torque values in the static and dynamic experiments. The static experiments produced a slightly higher level of resisting torque. This result was expected, considering that for Coulombic friction, the static coefficient is always slightly higher than the kinetic coefficient.

The maximum level of resisting torque reported here (≈6.5 N-m) extends into the range of peak torques developed in a TKA patient fitted with an instrumented prosthesis (Taylor, 1998). This lends strong credence to observations of bearing non-motion in about half of the patients studied by fluoroscopy (Stiehl, 1997).

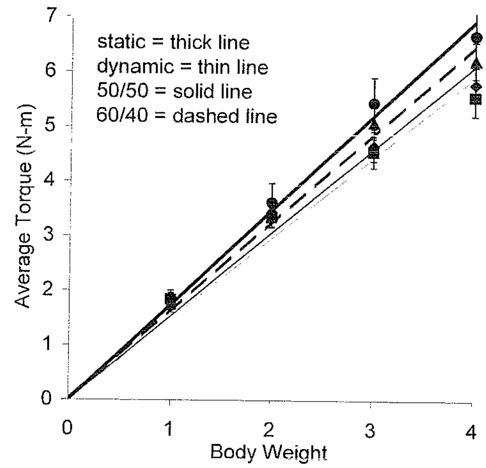

Figure 3: Near linear relationship between axial load and resisting torque for both static-dynamic and 50/50-60/40 cases.

Table 1: Linear relationship between resisting torque T (N-m), and axial load P (N), from the best fit lines in Figure 3.

	50/50	60/40
Static	T = 0.00253 P	T = 0.00236 P
Dynamic	T = 0.00223 P	T = 0.00215 P

*Depuy LCS cemented components, femoral: PS, Std+/Rt; tibial tray: rotating platform II, size 4; PE insert: PS, Std+, 10.0 mm thickness.

REFERENCES

Stiehl, *et al.* (1997). *CORR*, **345**, 60-6.
Taylor, *et al.* (1998). *J Arthroplasty*, **13**, 428-37.

ACKNOWLEDGEMENTS

Johnson & Johnson/Depuy provided financial assistance.

ACL ELONGATIONS DURING RUNNING AND SIDESTEPPING

S.G. McLean[1,2] and A.J. van den Bogert[2]

[1]Department of Human Movement, The University of Queensland, Australia
[2]Department of Biomedical Engineering, Cleveland Clinic Foundation, Cleveland OH
Email: mcleans@bme.ri.ccf.org

INTRODUCTION

Anterior cruciate ligament (ACL) injury is one of the most common and traumatic injuries of the human knee joint. Knowledge of the ligament's functional and mechanical loading during specific joint movements is essential if the mechanism of injury is to be identified. This information can provide the impetus for improved preventative, surgical repair and rehabilitation procedures. To date, research investigating ACL length changes under prescribed movement conditions has been predominantly experimental, adopting both *in vitro* and *in vivo* analysis procedures. A lack of active musculature and aging test specimens, has limited the application of *in vitro* data to ligament loads in young healthy individuals. Studies investigating ligament length changes *in vivo* have typically employed surgically implanted transducers (Beynnon et al., 1999), reducing the patient's ability to perform and/or tolerate dynamic and high-risk knee movements. If mechanisms of ACL injury are to be identified, then the ligament's mechanical behavior during such movements needs to be assessed. Analytic modeling techniques afford a non-restrictive, non-invasive approach to investigating complex knee movements. Their use to date in this area however appears limited. The purpose of the current study was to quantify *in vivo* ACL length changes during the stance phase of a sidestep cut, a complex knee movement previously linked to ligamentous injury, using a new combined experimental and mathematical modeling approach. Comparisons with similar data obtained for running were made in an attempt to provide insight into the associated mechanism of ACL injury.

METHODS

Changes in ACL length (right knee) during the stance phase of sidestep cutting and running were calculated for seven male (21.2 ± 1.3 yrs) subjects using combined 3D high-speed video and magnetic resonance (MR) techniques. For each subject, a relationship between external 3D skin marker coordinates and internal ligament geometry was defined by maintaining marker locations during kinematic data collection and ensuing MR scans (Figure 1). Ligament attachment sites were then described mathematically in local segment (femoral) coordinates, enabling straight-line ligament length to be calculated for each time-step during the dynamic movement.

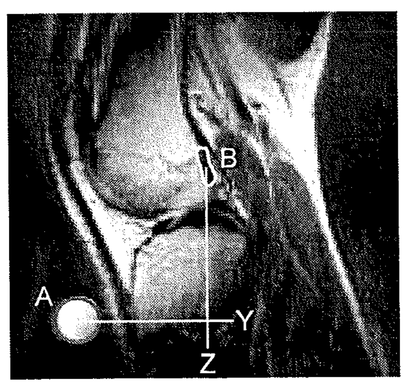

Figure 1. Sagittal image used to calculate 3D femoral attachment location (B) from external marker coordinates (A).

Static validation and error propagation analyses yielded satisfactory results. From the individual trial data, mean maximum length (L_{max}), maximum rate of length change (ΔL_{max}) and inter-trial variability for peak length (σ_L) and peak rate of length change ($\sigma_{\Delta L}$) were calculated and submitted to a one-way (gait) repeated measures (n=5) ANOVA (α=0.01).

RESULTS AND DISCUSSION

Figure 2 displays ACL length change comparisons between running and cutting as a function of stance for one subject. For all subjects, L_{max} was significantly greater during cutting compared to running. Similarly, ΔL_{max} during cutting was found to be greater statistically ($\alpha < 0.01$) than that observed for running (Table 1). Inter-trial variability in σ_L and $\sigma_{\Delta L}$ was evident for both running and cutting but not significantly different. These results are extremely useful in understanding the specific mechanisms of injury. Considering the mechanical properties of the ACL, peak elongation during cutting, occurring at 26.3 ± 5.2% of the stance phase may be of a great enough magnitude to compromise tissue integrity. This potential is further compounded by the fact that as a visco-elastic structure, the stresses developed within the ACL during cutting will similarly be large due to the extreme rates (up to 1100%/sec) of loading (Lydon et al., 1995). It has already been shown that execution of abnormal and potentially hazardous knee movements during sidestepping is common in some individuals (McLean et al., 1998). It is during these movements that elongation and resultant stress magnitudes that place the ACL at risk are likely. This statement appears feasible considering the inter-trial variability in ligament lengths observed for cutting.

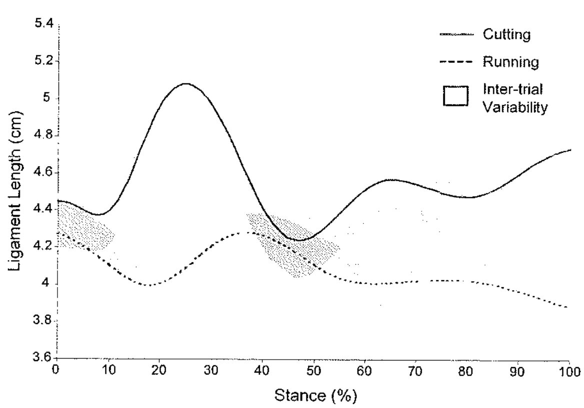

Figure 2. ACL length (mean ± SD trials) during the stance phase of running and sidestepping for a single subject.

Table 1. Comparisons of group mean data (N=7) between running and sidestep cutting.

DV	GAIT CONDITION	
	Cut ($\bar{x} \pm SD$)	Run ($\bar{x} \pm SD$)
L_{max} (cm)	5.39 ± 0.23	4.90 ± 0.37*
ΔL_{max} (cm/s)	52.6 ± 10.1	25.6 ± 11.5*
σ_L (cm)	0.12 ± 0.01	0.13 ± 0.01
$\sigma_{\Delta L}$ (cm/s)	6.09 ± 2.80	4.90 ± 2.51

* Denotes statistical difference (α = 0.01)

In the current project we have successfully quantified ACL length changes during the stance phase of running and sidestepping. Comparisons of these data have elucidated to a greater understanding of ACL rupture mechanisms linked to sidestep cutting. Increases in peak elongation and elongation rate displayed during cutting compared to running combined with the variability, appear to be the likely cause of injury. The research technique may be a useful tool in the evaluation and development of preventative, surgical and rehabilitation procedures in the future.

REFERENCES

Beynnon et al., (1999). *Am J Sports Med* **25**(6), 823-9.

Lydon, C. et al., (1995). *Clinical Biomechanics* **10**(8), 428-433.

McLean et al., (1998). *Bull Hosp Jt Dis* **57**(1), 30-38.

SHOULD THE SOURCE OF ELECTROMECHANICAL DELAY BE RECONSIDERED?

Peter F. Vint[1], Scott P. McLean[2] and Gregory M. Harron[3]

[1]Research Integrations, Inc., Tempe, AZ
[2]Iowa State University, Ames, IA
[3]University of North Carolina at Greensboro, Greensboro, NC
E-mail: Peter.Vint@ResearchIntegrations.com

INTRODUCTION

Electromechanical delay (EMD) has been defined as a temporal delay (26-131 ms) between the detected onset of muscular activity and the realization of force. It has been suggested that EMD is primarily attributable to "taking up slack" in the series elastic component (SEC) of the musculo-tendon (MT) actuator (e.g., Cavanagh & Komi, 1979; Viitasalo & Komi, 1981). However, if EMD were primarily attributable to an uptake of slack in the SEC, it could be argued that EMD should be manifest only at the beginning of an exertion initiated from rest. Once steady-state tension is developed by the MT, it would be expected that EMD be restricted to the short delays associated with depolarization of the muscle fiber and propagation of the action potential.

From the available literature, it is not possible to understand whether EMD exists beyond the initial stage of tension development because previous investigations involving EMD have been limited to the initiation of tension development from a resting state. Yet, some investigators have applied constant EMD values in an effort to temporally align EMG and force- or moment-time profiles during dynamic activities (e.g., Ingen Schenau et al., 1992). Inherent to this practice, however, is the assumption that EMD is manifest during pre-loaded MT states. This assumption appears to contradict the aforementioned association between EMD and the uptake of MT SEC slack.

Temporal shifts between changes in EMG and force initiated from a non-resting condition (i.e., a state of pre-tension) would suggest that EMD is not exclusively associated with SEC slack. Furthermore, varying the initial conditions would permit examination of whether EMD remains constant and thus test the validity of using a constant temporal offset. Therefore, the purposes of this study were 1) to test whether EMD is associated exclusively with the onset of tension from a resting state or if it is manifest continuously throughout a sustained submaximal isometric exertion; and 2) to test whether the duration of EMD remained constant regardless of initial tension.

METHODS

Twenty-four subjects (mean age 23.9 ± 5.4 years, mean height 171.7 ± 7.3 cm, and mean mass 72.9 ± 12.8 kg) performed isometric elbow flexion trials during which force data were obtained using a strain gauge device attached at one end to the subject's wrist using a padded leather cuff and at the other end to an immovable structure. Pre-amplified, bipolar electrodes were used to measure surface EMG activity from *m. biceps brachii*. All force and EMG data were obtained from the dominant arm.

Subjects completed three maximum effort isometric elbow flexion tasks in the transverse plane during which isometric force data were collected for 5 s at 1000 Hz. Subjects then completed a series of trials in which submaximal *pulse* forces of 25%, 50%, and 75% (expressed relative to maximal effort) were produced from a constant *baseline* force level of 0%, 25%, and 50%, respectively. Subjects produced baseline and pulse forces by matching a real-time display. After the baseline force was achieved, subjects received an audible cue at 1 s intervals during a 10 s period to produce the appropriate pulse force. Pulse forces were initiated and released as quickly as possible and were performed so that baseline intensity forces were maintained immediately prior to and following every intermittent pulse exertion. Subjects performed three trials for each condition that were presented in randomized across subjects. EMG and force data were collected for 10 s during these sustained baseline/intermittent pulse exertion trials.

Force and rectified EMG records were low-pass filtered at 5 Hz using a 4th-order, zero-lag Butterworth digital filter. Filtered force and EMG data were normalized by their respective instantaneous maximum values. For each trial, EMD was defined as the temporal shift, τ, that maximized a normalized cross-correlation function (Oda & Moritani, 1996).

RESULTS AND DISCUSSION

EMD between the activity of *m. biceps brachii* and isometric elbow flexion force ranged from 60.6 ± 16.6 ms (50% baseline-75% pulse) to 83.5 ± 12.9 ms (0% baseline-25% pulse). A 3×3 (condition×trial) repeated measures ANOVA revealed a significant condition effect ($p < .01$). Neither the trial effect ($p = .04$) nor the condition×trial interaction ($p = .30$) was significant (Figure 1). Post-hoc pairwise comparisons of mean condition values demonstrated that EMD values from the 0% baseline intensity were significantly longer than those from the 25% and 50% baseline intensities. Despite the trend, EMD values were not statistically different between the 25% and 50% baseline intensity conditions.

These data suggest that explanation of the EMD as a period used to remove slack from the SEC should be reconsidered. When muscle sustains a sub-maximal load a limited number of motor units are activated. It is possible that non-activated motor units retain slack associated with the SEC. This would help explain the existence of an EMD when tension was increased from a state of pre-tension. However, because the tendon represents the largest component of the SEC and would presumably have any slack removed prior to the initiation of any force, the magnitude of EMD when force was raised above a pre-tension state should be dramatically less. This is contrary to the appreciable EMD (60 ms) found when force was developed from 25% and 50% pre-tension. These data also suggest that the use of a constant temporal offset for correction of the EMD be reconsidered because the magnitude of EMD decreased as the level of pre-tension increased.

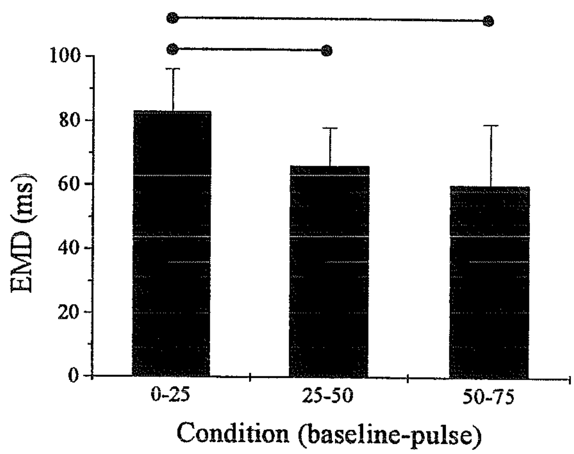

Figure 1. Mean EMD (±SD) during conditions of varying baseline intensities but similar relative pulse force intensities (n=24). Horizontal bars depict significantly different pairwise comparisons ($p < .01$).

REFERENCES

Cavanagh, P.R., & Komi, P.V. (1979). *Eur. J. Appl. Physiol.*, **42**, 159-163.

Ingen Schenau, G.J. van. et al. (1992). *Neuroscience*, **1**, 197-207.

Oda, S., & Moritani, T. (1996). *Eur. J. Appl. Physiol.*, **74**, 29-35.

Viitasalo, J.T., & Komi, P.V. (1981). *Acta Physiol. Scand.*, **111**, 97-103.

PROPERTIES OF FORCE DEPRESSION FOLLOWING SHORTENING CONTRACTIONS

Hae-Dong Lee[1] and Walter Herzog[1]

[1]Human Performance Lab, Faculty of Kinesiology, University of Calgary
Email: lee@kin.ucalgary.ca & walter@kin.ucalgary.ca

INTRODUCTION

The maximal isometric muscle force produced following shortening contractions is smaller than the corresponding force during purely isometric contractions (Abbott & Aubert, 1952). This phenomenon, referred to as force depression following shortening, has been observed in single fibres (Edman, *et al.*, 1993; Sugi and Tsuchiya, 1988), whole muscles (Maréchal & Plaghki, 1979; Herzog & Leonard, 1997) and human skeletal muscles (De Ruiter *et al.*, 1998; Lee, *et al.*, 1999). The amount of force depression following shortening is increased with increasing shortening distance (Abbott & Aubert, 1952; Herzog & Leonard, 1997; Maréchal & Plaghki, 1979; De Ruiter *et al.*, 1998); there are conflicting results about the influence of the speed of shortening on force depression.

In previous studies, force depression was assessed by comparing the steady-state isometric force produced following shortening to the corresponding steady-state isometric reference force. Possible force depressions during and immediately after the shortening phase have not been investigated systematically. Therefore, it is not known if force depression is just a phenomenon that occurs in the steady-state isometric situation or if force depression occurs during the dynamic shortening phase.

The purpose of this study was to investigate if force depression is a static and/or dynamic phenomenon.

METHODS

Force depression following shortening was investigated in cat soleus (n = 6). The surgical implantation of nerve cuffs and experimental set up has been described elsewhere (Herzog & Leonard, 1997).

The protocol was designed to test the effect of force depression as a function of the shortening distance. The muscle was allowed to contract isometrically first and then was released at a constant speed (4 mm/s) to a specific length; –4 mm. The starting lengths were +6, +4, +2, 0, -2, and –4 mm (Fig. 1), where 0 mm is the soleus reference length corresponding to included ankle angle of 80°. Stimulation of the soleus nerve was supramaximal (3 times the α-motoneuron threshold, 30 Hz, 0.1 ms pulse duration).

RESULTS

Steady-state force depression was increased with increasing amount of shortening, as had been shown previously (Herzog & Leonard, 1997: Fig. 1). Changes in muscle force during shortening showed two distinctive phases. In the initial phase, muscle force decreased almost linearly with a steep slope. The amount of decrease in force in the initial phase was increased with increasing amounts of shortening (Fig. 2). After the initial phase, the rate of change in force was decreased. In the final phase, force was decreasing in a linear fashion with a slope much smaller than that during the initial phase. In this final phase, the slopes of force decrease were virtually the same for all contractions independent of the amount of shortening (Fig. 3).

Following the shortening phase, force recovery was larger in muscles that had shortened more (Fig. 3), but the differences in force recovery were too small to change the order of force depression that had been established immediately following the shortening phase (Fig. 1).

Taken together , the results of this study indicate the following:

- The events causing force depression are dynamic; they occur during the shortening phase
- The amount of force depression observed immediately following shortening is

somewhat larger than the isometric steady-state force depression typically evaluated.

- Independent of the amount of shortening, the decrease in force during shortening showed two distinct phases; an initial fast phase of force decrease, and a final slow phase of force decrease.
- The slope of the force-time curves in the initial and final phases of force decrease are independent of the amount of shortening; however, the amount of force decrease in the initial phase is positively related to the amount of shortening.

CONCLUSIONS

From the results of this study, we suggest that force depression is a dynamic phenomenon that occurs during the shortening phase of muscle contraction and does not increase in the isometric recovery phase following shortening. Furthermore, the differences in force depression as a function of the amount of shortening are caused primarily by the amount of force decrease in the initial phase of shortening. In the final phase, force decreases occur at virtually identical rates independent of the amount of shortening. Since force depression is positively related to the amount of shortening on the ascending and descending limb of the force-length relation, it is unlikely that the initial isometric force influence the results. However, at present, we are unable to provide a satisfactory mechanism for the observed results.

REFERENCES

Abbott, B.C., Aubert, X.M. (1952). *J. Physiol. (Lond.)*, **117**, 77-86.

De Ruiter, C.J. *et al.* (1998). *J. Physiol.* **507.2**, 583-591.

Edman, K.A.P. *et al.* (1993) *J. Physiol. (Lond.)*, **466**, 535-552.

Herzog, W., Leonard, T.R. (1997). *J. Biomech.*, **30**, 865-872.

Lee, H.-D. *et al.* (1999) *J. Appl. Physiol.*, **87**, 1651-1655.

Maréchal, G., Plaghki, L. (1979). *J. Gen. Physiol.*, **73**, 453-467.

Sugi, H, Tsuchiya, T. (1988). *J. Physiol. (Lond.)*, **407**, 215-229.

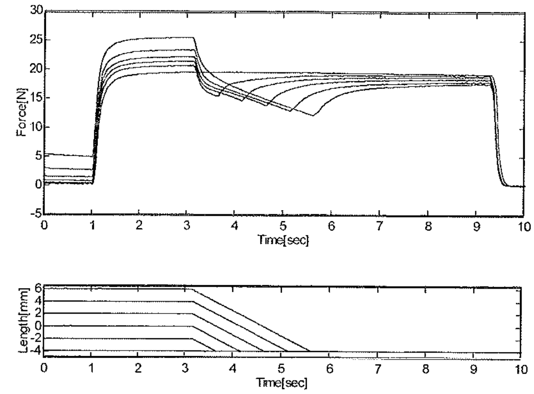

Figure 1. Representative data of force and length-time histories of the isometric reference contraction and the different shortening contractions.

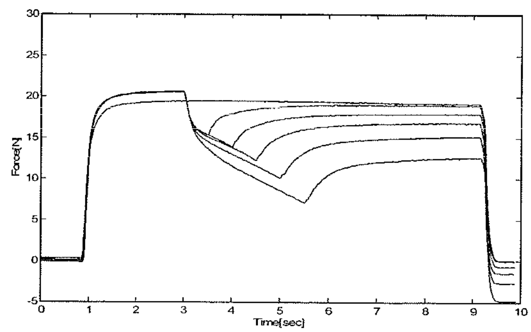

Figure 2. Representative data of force-time histories for isometric reference and shortening contractions normalised to the starting point of shortening for the contraction with the smallest amount of shortening.

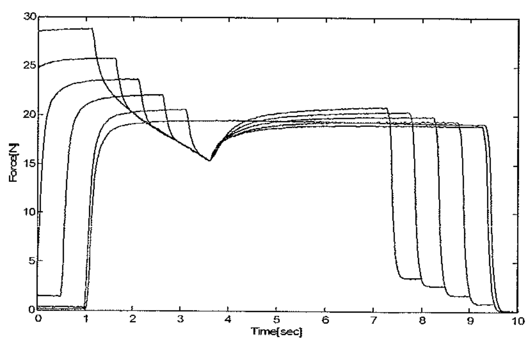

Figure 3. Representative data of force-time histories for isometric reference and shortening contractions normalised to the starting point of shortening for the contraction with the smallest amount of shortening.

ACKNOWLEDGEMENTS

NSERC of Canada.

ARCHITECTURE OF THE BICEPS BRACHII CHARACTERIZED WITH ULTRASOUND AND MRI

D. J. Asakawa[1,2], G. Pappas[1,2], S. L. Delp[1], and J. E. Drace[2]

[1]Biomechanical Engineering Division, Mechanical Engineering Dept., Stanford University
[2]Diagnostic Radiology Center, Palo Alto VA Health Care System, Palo Alto, California
Email: djasakawa@stanford.edu

INTRODUCTION

Cine phase contrast magnetic resonance imaging (cine-PC MRI) allows examination of muscle-tendon motion *in vivo* (Drace & Pelc, 1994). Relating changes in velocity and strain calculated from cine-PC MRI to the underlying muscle contraction mechanics requires detailed knowledge of a muscle's architecture and its effect on the trajectory of muscle tissue during contraction. Specifically, knowledge of the extent of tendon within the muscle must be known to interpret its effect on muscle motion. Also, orientation of the muscle fascicles with respect to the tendon, and the change in fascicle orientation with flexion, must be understood to calculate strain along a fascicle. These architectural characteristics have not been previously reported for the biceps brachii muscle. The purpose of this study, therefore, was to characterize (i) the extent of the biceps aponeurosis within the muscle, (ii) the orientation of the distal fascicles with respect to the tendon, (iii) the change in orientation of the fascicles with flexion of the elbow. Ultrasound imaging has been used effectively to study muscle architecture (Rutherford & Jones, 1992; Fukunaga et al., 1997). We used MRI and ultrasound imaging to characterize biceps brachii architecture and provide the basis for interpretation of *in vivo* measurements of muscle-tendon motion.

METHODS

Static axial MR images of the biceps brachii were acquired from 12 subjects (10 male, 2 female, age: 21 to 44 years, height: 5'3" to 6'2") with a 1.5T GE scanner. The extent of the aponeurosis within the muscle and the length of the biceps brachii long head muscle were measured from these images using GE image analysis software.

We acquired ultrasound images of the biceps brachii from the same subjects with the elbow extended and with the elbow flexed 90° while the subject resisted a load equal to 5% of their maximum voluntary contraction (MVC) strength. An Acuson Sequoia 512 Ultrasound System (Mountain View, CA) with a 52-mm, 15-MHz transducer was used to obtain the images. The transducer was oriented to produce a sagittal plane image of the biceps brachii with the distal aponeurosis evident (Fig. 1).

NIH Image software was used to quantify the angles between clearly evident fascicles and the aponeurosis. We recorded angles in the distal muscle in two separate regions: 0-2 cm, and 2-4 cm proximal to the point where the most distal fiber inserted into the tendon. We measured angles of fascicles anterior and posterior to the aponeurosis. Paired t-tests were performed to compare fascicle insertion angles with the elbow extended to fascicle insertion angles with the elbow flexed.

Figure 1: Ultrasound image of the distal biceps brachii ; the distal tendon (upper left) continues as an internal aponeurosis. Fascicles are visible inserting into the aponeurosis.

Table 1: Average Fascicle Insertion Angles for the Distal Biceps Brachii

Elbow Extended				Elbow Flexed 90° with 5% MVC			
Anterior		*Posterior*		*Anterior*		*Posterior*	
0-2cm	2-4cm	0-2cm	2-4cm	0-2cm	2-4cm	0-2cm	2-4cm
17°	14°	14°	12°	21°	18°	17°	15°

RESULTS

The central aponeurosis extended 34% of the length of the biceps brachii muscle on average. The average aponeurosis length was 7 ± 1 cm in the 12 subjects. The length of the entire biceps brachii long head muscle averaged 20 ± 2 cm with the arm flexed approximately 10°, consistent with An et al. (1981) and Murray (1997).

There was asymmetry between the anterior and posterior fascicle insertion angles. The average insertion angle for fascicles anterior to the aponeurosis was 17° for the distal 2 cm of the muscle with the elbow extended (Table 1). The posterior fascicles in this same region inserted at 14° with the elbow extended. Fascicles anterior to the aponeurosis inserted at a significantly greater (P • 0.05) angle than the fascicles posterior to the aponeurosis in both regions (0-2cm and 2-4cm) when the elbow was extended. With the elbow flexed, resisting 5% MVC, only fascicles within the distal 0-2 cm of the muscle showed a significant difference in anterior and posterior insertion angles.

Fascicle insertion angles with the elbow flexed and resisting 5% MVC were significantly higher (P • 0.05) than angles measured with the elbow extended for all regions of the muscle studied. For example, fascicle insertion angles anterior to the aponeurosis increased with elbow flexion from 17° to 21° in the distal 0-2 cm of the muscle and from 14° to 18° in the distal 2-4 cm of the muscle.

DISCUSSION

The biceps brachii is generally considered to be a parallel-fibered muscle, but distal fascicle insertion angles can influence muscle contraction mechanics such as change in fascicle length with flexion. We found that fascicle insertion angles at the distal end of the biceps brachii muscle were asymmetric with respect to the aponeurosis. Fascicle insertion angles increased 3-4° with a 90° change in joint angle accompanied by application of a 5% MVC load. This increase in fascicle insertion angle was small but consistent across subjects. In addition, the extensive aponeurosis has the potential to influence the motion of distal muscle tissue as well as muscle tissue along the longitudinal axis of the muscle.

We used this characterization of biceps brachii architecture to aid in the interpretation of muscle tissue velocity and strain calculated in the same subjects using cine-PC MRI. Detailed knowledge of muscle architecture is also useful when interpreting the effects of assumptions made in modeling muscle contraction mechanics for the biceps brachii.

REFERENCES

Drace, J.E., Pelc, N.J. (1994) *J. MRI*, **4**,157-163

Rutherford, O.M.. Jones, D.A. (1992) Eur. J. Applied Physiology, **65**, 433-437

Fukunaga,T. et al. (1997) J. Biomech, **30**,457-63

An,K.N. et al. (1981) J. Biomech **14**, 659-669

Murray, W.M (1997) PhD Thesis, Northwestern University, Evanston, IL

ACKNOWLEDGMENTS

Funding provided by NIH Grants HD31493 & HD33929, the Department of Veterans Affairs, and a Whitaker Foundation Graduate Fellowship.

ANTERIOR AND CENTERLINE STRAINS DIFFER IN THE BICEPS BRACHII DURING ACTIVE ELBOW FLEXION

G. Pappas[1,2], D.J. Asakawa[1,2], S.L. Delp[1], F.E. Zajac[1], and J.E. Drace[2]

[1]Biomechanical Engineering Division, Mechanical Engineering Dept., Stanford University
[2]Diagnostic Radiology Center, Palo Alto VA Health Care System, Palo Alto, California
Email: gpappas@stanford.edu

INTRODUCTION

Assumptions about the architecture and contractile properties of muscle are made in models of the musculoskeletal system. For example, the assumption that skeletal muscle shortens uniformly along its length is commonly made to facilitate modeling of muscle contraction mechanics.

In vivo data are required to test assumptions about muscle contraction, improve the accuracy of representations of muscle-tendon mechanics, and further our understanding of muscle function. Magnetic resonance imaging (MRI) and ultrasound imaging have been used to study muscle architecture and contraction mechanics *in vivo* (Drace & Pelc, 1994; Fukunaga et al., 1997). Strains estimated with cine phase contrast MRI have suggested that shortening of the biceps brachii along its centerline is not uniform (Pappas et al., in review). We hypothesized that the large central aponeurosis of the biceps brachii, which was included in the centerline strain measurements, was the principal source of non-uniform shortening.

The purpose of this study was to compare shortening along the anterior fascicles of the biceps brachii, which do not include tendon, with shortening along the centerline of the biceps brachii muscle-tendon complex. *In vivo* muscle-tendon strains were estimated at two different load levels to study the dependence of the strain measurements on load.

METHODS

Cine phase contrast MRI was used to measure *in vivo* biceps brachii tissue velocity over a mid-sagittal imaging plane during elbow flexion in 12 healthy subjects. Estimates of muscle-tendon displacement and strain were derived through integration of the quantitative three-dimensional velocity images (Zhu et al., 1996). Each subject performed cyclical elbow flexion and extension tasks over an 80° range of motion, from near full extension to approximately 90° flexion, within a 1.5T GE MR imager. Subjects performed elbow flexion against 5% and 15% of their measured maximum voluntary contraction (MVC) strength.

Displacement and strain in the biceps brachii during elbow flexion were determined by tracking the position of square (1cm x 1cm) tissue regions of interest (ROIs) over the entire motion cycle. Centerline strain was determined from the position trajectories of ROIs distributed along the longitudinal axis of the biceps brachii. Anterior strain was computed from ROIs located subcutaneously along the superficial boundary of the biceps (in the mid-sagittal plane). The strain distributions along the centerline axis and anterior boundary of the muscle were computed for the muscle in its most flexed state, relative to its state at extension. A negative strain indicated the distance between two tracked regions decreased and implied local muscle shortening as compared to the state of the muscle in an extended elbow position.

RESULTS

At maximum elbow flexion, the strain along the centerline of the biceps brachii was highly non-uniform (Fig. 1, top panel). Shortening along the centerline of the muscle-tendon complex was non-uniform for both loading conditions and was significantly lower in magnitude at the distal end of the muscle as compared to shortening at the midportion and proximal end of the muscle. Mean strain levels at the distal end of the muscle, within the aponeurosis region, were between zero and -5%. Shortening in the midportion and proximal end of the muscle was between 20-35%. The trends in the centerline strain distribution at maximum elbow flexion were similar across the two load levels and consistent with a previous study of centerline strain during elbow flexion with a 2-lb loading condition (Pappas et al., in review).

The strain along the anterior fascicles at maximum flexion was approximately constant over the entire length of the biceps (Fig. 1, bottom panel). The mean strains for the 5% and 15% MVC cases were both 21% and were not significantly different from each other.

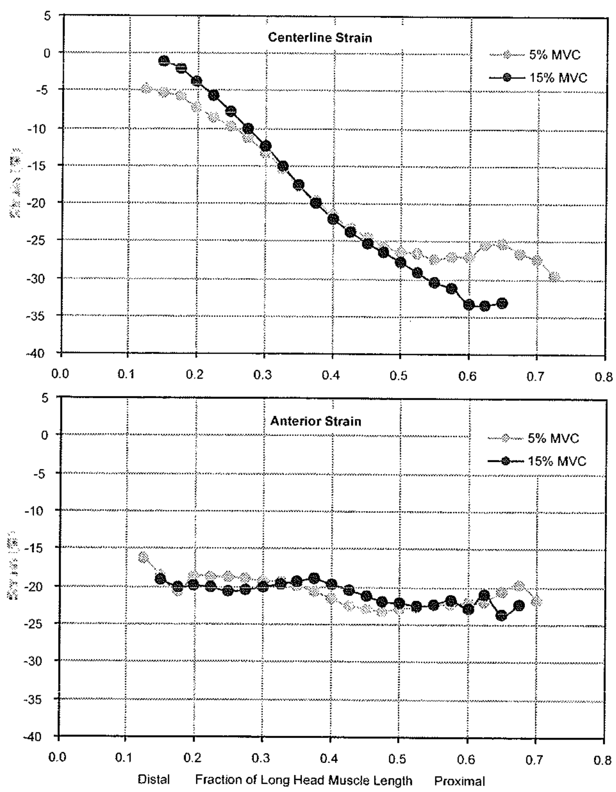

Figure 1. Centerline (top panel) and anterior (bottom panel) strain distributions in the biceps brachii for 5%, and 15% MVC loading conditions. Negative strains indicate local muscle shortening in elbow flexion as compared to extension.

DISCUSSION

Our results demonstrate a dramatic difference in the shortening between the centerline and anterior portions of the biceps brachii. Centerline strain at the distal end of the muscle was significantly lower in magnitude than strain at the midportion and proximal end of the muscle-tendon complex. Lower strain levels observed at the distal end of the muscle are likely due to the existence of a prominent internal aponeurosis, which spans the distal third of the muscle. In contrast, shortening along anterior fascicles was approximately constant under the two loading conditions, suggesting uniform muscle fiber shortening during active contraction. The fascicles in the anterior region of the muscle were specifically chosen to exclude the central tendon of the biceps brachii.

Our results support the hypothesis that non-uniform shortening along the centerline of the biceps brachii arises from the presence of the central aponeurosis in the distal third of the muscle. The architectural properties of the biceps brachii may lead to a distribution of fiber lengths and sarcomere lengths during contraction. Such length heterogeneity has important functional consequences, such as alteration of the muscle's force-length properties (Huijing,1995).

REFERENCES

Drace, J.E., Pelc, N.J. (1994). *J. MRI*, **4**,157-163

Fukunaga, T. et al. (1997). *J. Biomechanics*, **30**, 457-463.

Pappas, G. et al. (in review). *J. Biomechanics.*

Zhu, Y., et al. (1996). *Magn Reson Med,* **35**, 471-80.

Huijing, P.A. (1995). *Human Movement Science* **14**, 443-486.

ACKNOWLEDGMENTS

Support was provided by the Department of Veterans Affairs, NIH Grant HD31493, HD33929, and NIH Research Resource Grant P41 RR09784.

ECCENTRIC CONTRACTIONS OF THE QUADRICEPS FEMORIS MUSCLE HAVE GREATER MOTOR OUTPUT VARIABILITY THAN ISOMETRIC AND CONCENTRIC CONTRACTIONS

Evangelos A. Christou, M.S., A.T.C/L, Les G. Carlton, Ph.D.

Department of Kinesiology, University of Illinois at Urbana-Champaign
Email: christou@uiuc.edu Web: www.kines.uiuc.edu

INTRODUCTION

Eccentric contractions have been shown to be different in several neurophysiological and performance characteristics when compared to isometric and concentric contractions (Enoka, 1996). Results from a previous study in our lab (Christou & Carlton, 1999) have shown that eccentric contractions are more variable when compared to concentric contractions and supported the hypothesis that the central nervous system (CNS) might regulate gradation of muscle force by a unique strategy during eccentric contractions (Enoka, 1996). Direct comparisons of the three contraction types for motor output variability, however, is minimal in the literature. The aim of this study was to compare the ability of young adults to regulate force under rapid isometric, concentric and eccentric contractions of the knee extensor muscle group.

PROCEDURES

Twenty-four healthy young adults with no history of previous knee pathology were recruited for this study. To assess force production and motor output variability during a leg extension task, and to provide a near constant velocity of 25°/s throughout the range of motion, a KIN-COM 500H isokinetic dynamometer was used. Each participant attended two testing sessions and performed leg extensions that ranged from 90-100° of knee flexion (isometric at 90°). Six different parabolas were displayed on the monitor of the isokinetic dynamometer based on maximum voluntary contraction (MVC) (20, 35, 50, 65, 80 and 90% MVC) and with a time to peak force of 200ms. Each participant was instructed to match the parabola displayed by controlling the leg extension force. To familiarize the participants with the targeted parabolas, thirty practice trials were given for each target prior to the data collection. In addition to verbal feedback and encouragement, the first half of the practice trials received visual feedback. The remainder of the practice trials and the test trials were given visual feedback only after the trial was completed. All target parabolas were randomly assigned for each subject and were counterbalanced in order across subjects. Forty trials per contraction type (isometric, concentric and eccentric) were collected for each target parabola. A rest period of 120 seconds was given between data collection trials. Means, standard deviations (SD) and coefficient of variations (CofV) for variability in peak force (PF), impulse (IMP), time to peak force (TPF) and impulse duration (ID) were computed.

RESULTS AND DISCUSSION

No significant differences were found for the mean PF, IMP and TPF produced by isometric, concentric and eccentric contractions at each goal MVC ($p>0.05$). However, ID was significantly different between the three contractions ($p<0.01$).

Variability of PF, measured using SD, increased as the level of force increased for all contractions in a non-linear fashion. Differences among contractions were found only for IMP and ID with eccentric contractions being significantly more variable compared to isometric and concentric contractions ($p<0.05$). No significant interaction was found.

CofV, a measure of variability that normalizes variability (SD) to the amount of force or time produced, revealed significant differences for all examined parameters. CofV for PF revealed significant differences between the three contractions ($p<0.01$). Eccentric and concentric contractions were more variable compared to isometric contractions. CofV for IMP revealed both significant differences between the three contractions ($p<0.01$) and a contraction x %MVC interaction ($p<0.01$) (Figure 1).

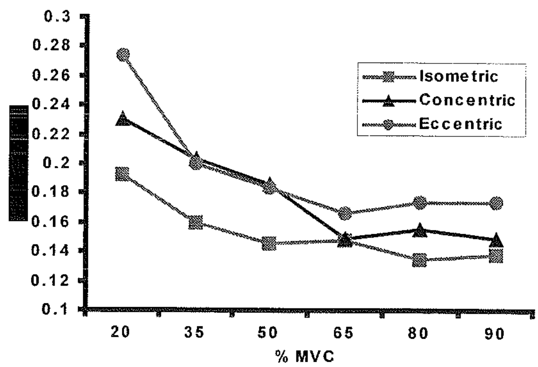

Figure 1. This graph illustrates the differences in the CofV for Impulse among the three contraction types.

CofV for TPF and ID also revealed significant differences between contractions ($p<0.01$). Eccentric contractions were more variable compared to isometric and concentric contractions. The results of this study indicate that eccentric contractions are relatively more variable in controlling different levels of force (peak force and impulse) when compared to isometric and concentric contractions. Control of the temporal characteristics (TPF and ID) of force production, were also more variable for eccentric contractions (Figure 2).

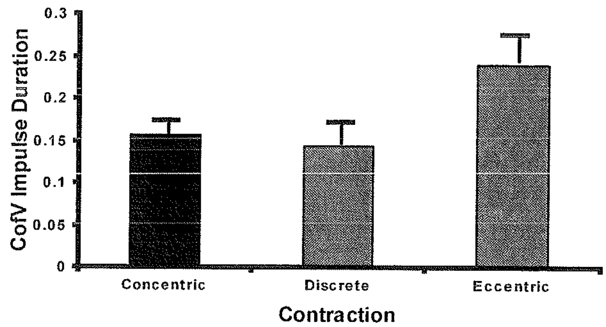

Figure 2. This graph illustrates that CofV for ID was higher during eccentric contractions.

SUMMARY

When comparisons between isometric, concentric and eccentric contractions were normalized to the mean force or time produced, eccentric contractions were found to be more variable. The findings of this study support previous results (Christou & Carlton, 1999) and suggest that eccentric contractions might be more variable due to an alternative recruitment of motor units, as suggested by Nardone et al. (1989). The results of this study, provide further evidence to the hypothesis that eccentric contractions might be uniquely controlled by the CNS (Enoka, 1996).

REFERENCES

Christou, E.A., & Carlton, L.G. (1999). *ASB Proceedings*, 122-123.

Enoka, R. (1996). *Journal of Applied Physiology*, 81, **6**, 2339-2346.

Nardone, A. et. al., (1989). *Journal of Physiology London,* 409, 451-471.

THE EFFECT OF STEP LENGTH AND CADENCE ON THE INSTANTANEOUS FORWARD VELOCITY OF WALKING

Steve C. Miff [1,2], Dudley S. Childress [1,2,3], and Steven A. Gard [2,3]

[1]**Department of Biomedical Engineering, Northwestern University, Chicago, Illinois**
[2]**VA Chicago Health Care System, Lakeside Division, Chicago, Illinois**
[3]**Northwestern University Rehabilitation Engineering Research Program, Chicago, Illinois**
Email: steve-miff@nwu.edu **Web:** www.repoc.nwu.edu

INTRODUCTION

Energy expenditure of walking is reduced by conserving mechanical energy through storage of kinetic energy and through exchange between potential energy of the trunk and a part of kinetic energy of forward progression. Understanding the behaviors of the vertical trunk movement and the instantaneous forward velocity under various walking conditions can provide insight into the energetics of walking.

In this study we analyze the behavior of the instantaneous forward velocity. We control step length and cadence such that various walking velocities are achieved. We investigate the influence of step length and cadence on the instantaneous forward velocity in order to understand peak-to-peak changes for various kinds of gait patterns.

METHODS

We measured the instantaneous forward velocity of walking in three able-bodied, adult male subjects. The subjects walked at speeds from about 0.8-2.2 m/sec under three testing conditions: (1) constant step length of 0.75m, (2) freely-selected cadence and step length, and (3) constant cadence of 110 steps/min. The constant step length and constant cadence values were chosen from parameter averages observed in the literature. (Drillis 1958)

We used a rocker-based inverted pendulum model (Fig. 1) to derive and analyze mathematical relationships between step length (S_l), cadence (f_{cad}), peak-to-peak forward velocity ($V_{max} - V_{min}$), and walking speed (V). (Childress and Gard, 1999; Gard and Childress, 2000) Results from our theoretical analysis were compared with the empirical measurements.

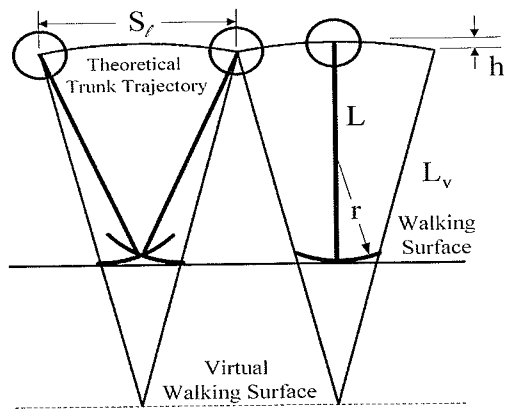

Figure 1 Rocker-based Inverted Pendulum

RESULTS

The rocker-based inverted pendulum model suggests that the leg length (L) is effectively increased by the foot rocker (Morawski and Wojcieszak, 1978) as shown in Equation (1):

$$L_v = \frac{L^2}{L - r} = L \cdot \frac{1}{1 - r/L} = L \cdot \rho \qquad (1)$$

where L_v is the virtual leg length, r is the radius of the foot rocker, and ρ is a dimensionless variable that we call the "roll factor" (approximately 1.8-1.9 for healthy adult male ambulators.) The model predicts that the vertical excursion, h, is a function of only L, ρ, and S_l:

$$h = \frac{S_l^2}{8L\rho} \qquad (2)$$

Setting the maximum change in potential energy equal to the maximum change in kinetic energy, we obtain Equation 3:

$$mgh = m\left(\frac{(V_{max} + V_{min})}{2}\right)(V_{max} - V_{min}) \qquad (3)$$

Assuming that $[V_{max} + V_{min}]/2$ is equal to V we obtain equation 4:

$$h \cong \left(\frac{V}{g}\right)(V_{max} - V_{min}) \qquad (4)$$

Combining equations (4) and (2) we obtain:

$$(V_{max} - V_{min}) \cong \left(\frac{S_l^2 \cdot g}{8 \cdot V \cdot L \cdot \rho}\right) \qquad (5)$$

Walking speed is equal to the product of step length and cadence: $V = S_l \cdot f_{cad}$. Assuming a linear relationship between S_l and f_{cad}, it can be shown that $(V_{max} - V_{min})$ is constant for freely selected gait over a range of walking speed. Our empirical data (Fig. 2) supports the analytical result. Statistical analysis of the data obtained from our research subjects indicates an average $(V_{max} - V_{min})$ value of about 0.33 m/sec.

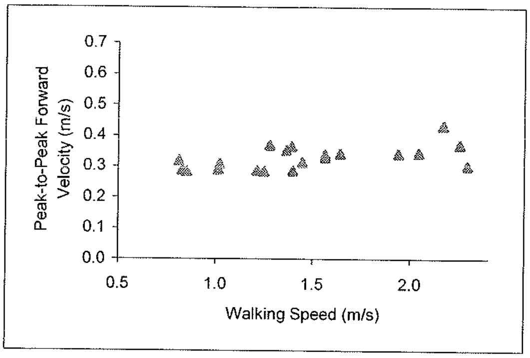

Figure 2 $(V_{max}-V_{min})$ for freely selected gait.

For constant step length gait, S_l is constant and thus equation 5 indicates that the peak-to-peak forward velocity is inversely related to walking speed, i.e. $[(V_{max}-V_{min}) \propto 1/V]$. Empirical data (Fig. 3) supports this relationship. A best fit performed by minimizing the sum of squares of the residuals indicates a hyperbolic relationship.

During fixed cadence gait (f_{cad} constant), the speed of walking is completely controlled by step length. Since velocity is proportional to step length, equation 5 indicates that the peak-to-peak forward velocity is proportional to the walking speed, i.e. $[(V_{max} - V_{min}) \propto V]$. Empirical data (Fig. 3) suggests a linear relationship between the two variables.

SUMMARY

The peak-to-peak forward velocity for steady-state walking is constant for freely selected gait. The peak-to-peak forward velocity, $(V_{max} - V_{min})$, is related to the change in momentum with each step. Thus, our results suggest that for freely selected gait the momentum change is constant over typical walking speeds, and $\Delta KE \cong \Delta PE$. We believe these conditions are necessary in order to achieve an efficient walking style. The conditions further imply a step-ratio constant, "a", such that $S_l = a \cdot f_{cad}$.

For constant step length walking, the model predicts that the peak-to-peak forward velocity is inversely related to walking speed, while for constant cadence gait the peak-to-peak forward velocity is proportional to walking speed. The empirical data closely resembles the analytical relationships.

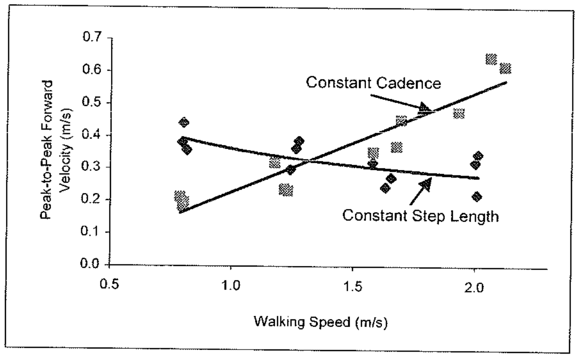

Figure 3 $(V_{max}-V_{min})$ for constant step length and constant cadence gait.

REFERENCES

Childress, D.S. and Gard, S.A. (1999). *ISB*, Calgary, Canada, August 8-13th.

Drillis, R. (1958). *Ann NY Acad Sci*, **74**, 86-109.

Gard, S.A. and Childress, D.S. (2000). *GSMAS*, Rochester, MN, April 12-15th.

Morawski J.M. and Wojcieszak, I. (1978). *J. Biomech*, **VI-A**, 445-451.

ACKNOWLEDGEMENTS

This work was funded by the National Institute on Disability and Rehabilitation Research (NIDRR) of the Department of Education under grant number H133E980023. The opinions contained in this publication are those of the grantee and do not necessarily reflect those of the Department of Education. The authors acknowledge the use of the VACMARL of the VA Chicago Health Care System, Lakeside Division, Chicago, IL.

KINEMATICS OF MANEUVERS COMMONLY RESPONSIBLE FOR HIP DISLOCATION

D. R. Pedersen[1], H. J. Yack[2], R. Wahi[2], J. J. Callaghan[1], T. D. Brown[1]
[1]Department of Orthopaedic Surgery, University of Iowa, Iowa City, Iowa
[2]Department of Physical Therapy, University of Iowa, Iowa City, Iowa
Email: doug-pedersen@uiowa.edu

INTRODUCTION

A significant minority of patients undergoing total hip arthroplasty (THA) experience prosthesis dislocation. Escape of the spherical femoral component head from the concave hemispherical acetabular component usually is associated with an untoward motion by the patient that causes impingement contact at an extraneous peri-articular site. One barrier to progress in avoiding this complication is the limited understanding of the predisposing biomechanical factors, including why certain maneuvers/postures are problematic. The objective of this study was to measure, for the first time, natural hip kinematics during activities suspected of inducing dislocations.

METHODS AND MATERIALS

Patient recollections of what specific physical maneuver they were performing at the time of THA dislocation commonly involve one of six actions: 1) sit-to-stand rise from a normal chair height (SSN);
2) sit-to-stand rise from a low seated position such as a toilet (SSL);
3) leg crossing in a seated position (XLG);
4) bending at the waist from a standing position, to retrieve an object lateral of the foot on the affected side (STOOP);
5) rolling over in bed with the hip extended (ROLL); and 6) planting the foot on the affected side and turning the entire body away (externally rotating the hip) while in an erect posture (PIVOT).

Three-dimensional kinematic data were collected on ten healthy middle-aged subjects (Table 1) using an Optotrak 3020 motion analysis system (Northern Digital, Waterloo, Ontario). Triads of non-collinear markers were attached to the foot, leg, thigh, and pelvis on the right side, to track the subject (dressed in shorts) performing each of the above maneuvers. A newly developed marker system for the distal thigh was used to enhance the accuracy of femoral rotation tracking (Houck et al. 1999). Kinematic data were filtered using a fourth-order Butterworth, zero-lag, low-pass filter at 6 Hz. Subject-specific marker position calibration data (digitized bony landmarks), captured with the subject standing at rest on the force plate, were used to define the transformation matrix between the external marker reference system and the principal axes of each of the five body segments. The hip joint center was calculated based on pelvic anthropometrics.

Table 1: Subject Demographics

Height [cm]	Weight [kg]	Age [years]	Gender
190	102.3	44	Male
173	63.6	49	Female
170	69.1	52	Male
165	95.5	49	Female
160	80.9	57	Female
173	74.1	47	Male
168.9	61.4	45	Male
161.3	62.5	49	Female
195.6	122.7	46	Male
149.9	40.9	59	Female

RESULTS

Rotations of the femoral segment (with respect to the pelvis) about each of the global anterior X, superior Y, and lateral Z directions (ad-/abduction, endo-/exorotation, flexion/extension, respectively) describe the hip motion paths for each of the activities. The intra-subject consistency of performance of each activity was good, making the 'average' motion path of each subject a meaningful measure. The inter-subject range of motion (ROM) was much more varied. During SSN, the subjects tended to adduct first and then extend, while for SSL they tended first to abduct and then extend their leg (Figure 1). Femoral adduction/endorotation as a function of hip flexion demonstrates a ROM path toward an anterior 'impingement' front for posterior dislocation maneuvers (SSN, SSL, XLG, STOOP). Whereas PIVOT and (to a lesser extent) ROLL involved exorotation extrema most suggestive of posterior-impingement-induced anterior dislocation (Figure 2).

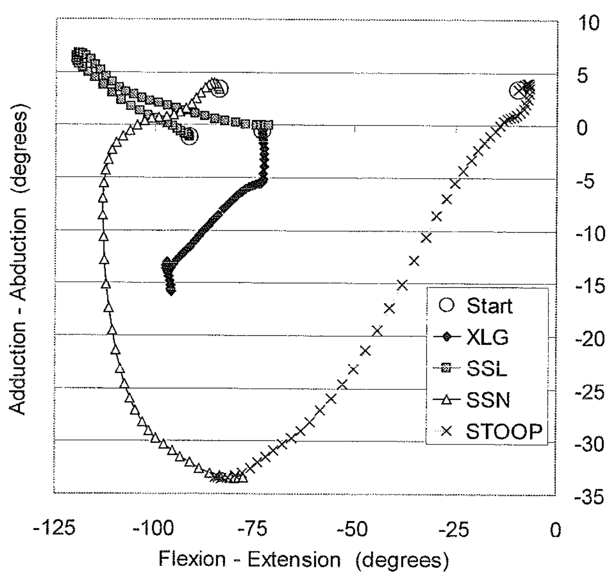

Figure 1: Abduction vs. flexion for one typical subject.

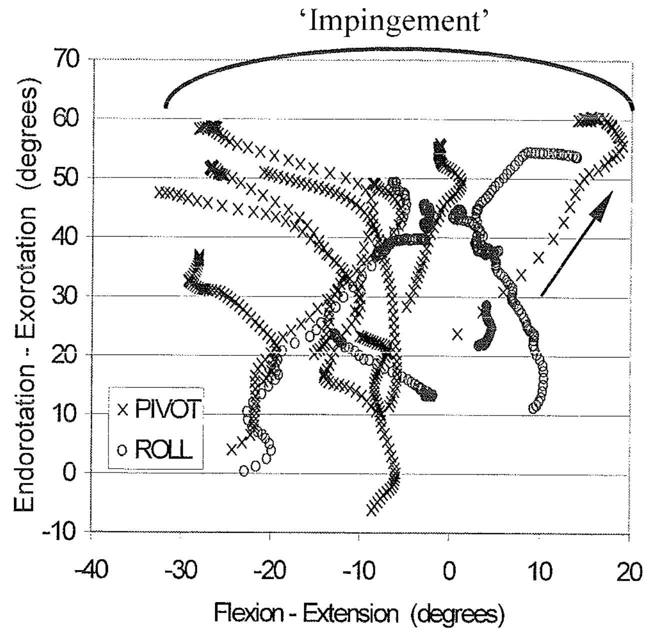

Figure 2: Femoral rotation vs. hip flexion for all subjects. The arrow indicates the direction of motion for one pivot maneuver.

CONCLUSIONS

The hip kinematic data here presented provide a measure of the path of natural hip motion during six activities suspected of being involved in THA dislocations. These normal-subject kinematic data of course are not *per se* predictive of THA dislocation, but they constitute key data necessary for rigorous finite element modeling of that phenomenon.

REFERENCES

Houck, J. et al. (1999). *Gait Posture*, **9**, Suppl 1, S52.

ACKNOWLEDGEMENTS

We appreciate the efforts of Jason Wilken and Mark Nadzadi, and the support of a VA Merit Grant (Iowa City VAMC).

LIMITATIONS OF INVERSE DYNAMICS IN IDENTIFYING QUADRICEPS AVOIDANCE

K. Manal and T.S. Buchanan
Center for Biomedical Engineering Research, University of Delaware
Email: manal@udel.edu

INTRODUCTION

Inverse dynamics are often used to estimate muscle forces during static and dynamic tasks. For example, quadriceps force required to extend the knee during a sit-to-stand task has been estimated from the knee extensor torque and effective moment arm of the quadriceps tendon (Ellis et al., 1984). This method of estimating muscle force will be referred to as an "inverse dynamics approach". Since the torque calculated using an inverse dynamics approach represents a *net* joint moment, quadriceps force estimated in this manner can underestimate the actual force generated by the muscle group. The degree of underestimation is related to the amount of muscular co-contraction between flexors and extensors and the relative ratio of their moment arms.

In this study, joint moments based on an inverse dynamics approach were interpreted with and without considering EMG activity of the quadriceps and hamstrings during a sit-to-stand task. The purpose of this paper is to demonstrate that EMGs need be considered when estimating muscle force and making side-to-side functional comparisons.

METHODS

One unilateral anterior cruciate ligament deficient (ACLd) subject participated in this study. High-speed video (60 Hz) was used to film the subject (mass = 80 kg) while performing a sit-to-stand task. The subject was instructed to rise from a seated to a standing position. Force data were sampled at 960 Hz using separate force platforms under each foot. In-house software was used to calculate sagittal plane kinematics and kinetics at the knee. Moment arms for the extensor and flexor muscle groups were determined according to Delp et al. (90) using SIMM (Software for Interactive Musculoskeletal Modeling). In addition, EMG data were collected from the vastus lateralis and biceps femoris longus. These muscles were considered to adequately represent muscular activity of the quadriceps and hamstring for the purposes of this study (Olney & Winter, 1985). EMG data were sampled at 960 Hz. The EMG data were normalized to maximum values determined during maximal isometric testing of each muscle group. EMGs were full-wave rectified and low pass filtered at a cut-off frequency of 4 Hz.

RESULTS AND DISCUSSION

Data reported in Figures 1 & 2 represent the average of 3 sit-to-stand trials. Standard deviations were not overlaid on the graphs for sake of clarity. Standard deviations followed the average curves closely suggesting the subject performed the sit-to-stand task in a repeatable manner. Knee extension torque for the intact and ACLd knees are plotted in Figure 1. Based on these data and moment arms determined from the SIMM model, peak quadriceps force for the intact and ACLd knees were approximately 2875N and 2300N respectively. These values were determined by dividing peak torque for each knee by the moment arm at which peak torque was generated. Smaller peak extension torque and force for the ACLd knee is consistent with the idea of "quadriceps avoidance" proposed by Berchuck and Andriacchi (1990). However, it is clear from the EMG data the subject did not "avoid" activating the quadriceps when rising from the chair. Normalized EMG for the representative quadriceps (vastus lateralis) and hamstrings (biceps femoris longus) are shown in Figure 2. EMG activity for the ACLd quadriceps was consistently greater than EMG activity for the intact knee during the ascent phase of the sit-to-stand task. EMG activity of the ACLd quadriceps was 5% - 10% of normalized EMG greater than for the uninvolved knee. It is unlikely this finding was an artifact of the normalization process since similar results were noted for the same subject when performing an identical task during an unrelated testing session.

SUMMARY

Interpreting the results of the extension moment based on the inverse dynamics approach alone might lead one to speculate the subject exhibited quadriceps avoidance of the ACLd knee during the sit-to-stand task. However, the EMG data do not support this conclusion. Use of the net joint moment to estimate muscle load and function can lead to erroneous conclusions when antagonistic muscle activity is present. Caution should therefore be exercised when interpreting the results of an inverse dynamics approach when EMG data are not considered.

ACKNOWLEDGMENTS

This work was supported in part by NIH AR46386.

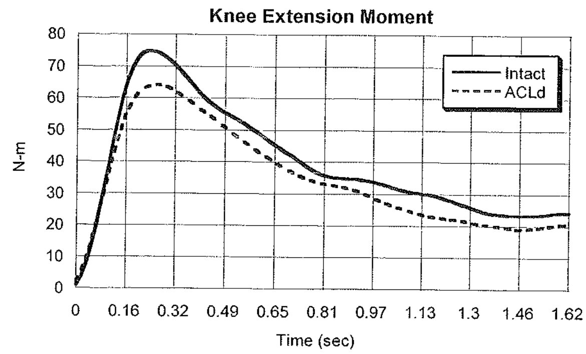

Figure 1. Average right knee net extension torque for the intact and ACLd knees during the sit-to-stand task. (positive torque = Extension). Note that the ACLd knee has a smaller net knee extension moment.

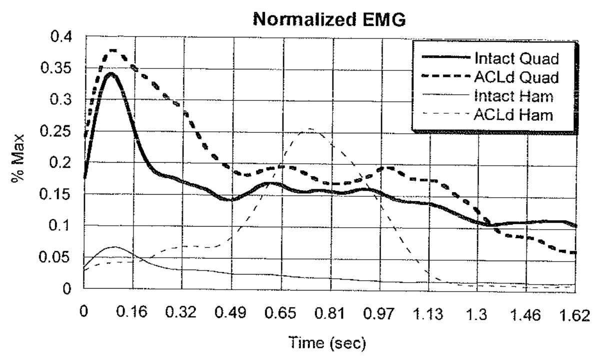

Figure2. Normalized EMG for the quadriceps and hamstrings of the intact and ACLd knees during the sit-to-stand task. Note that despite having a lower net extension moment, the ACLd knee had greater quadriceps activity.

REFERENCES

Berchuk, M., Andriacchi, T.P. (1990). JBJS(A) 72: 871-877.

Delp, S. et al. (1990). IEEE Trans Biomed Eng. 37(8):757-767.

Olney, S.J., Winter, D.A. (1985). Physiother Can. 37(4): 2111-2117.

Ellis, M.J. et al. (1984). J Biomed Eng. 6:113-120.

GAIT CHANGES IN PATIENTS WITH PROGRESSIVE MULTIPLE SCLEROSIS

Ann E. Walker[1], John H. Noseworthy[2], and Kenton R. Kaufman[1]

[1]Biomechanics Laboratory, Dept. of Orthopedics, [2]Dept. of Neurology
Mayo Clinic, Rochester, Minnesota
Email: kaufman.kenton@mayo.edu

INTRODUCTION

Multiple sclerosis (MS) is a chronic inflammatory disease of the central nervous system of unknown etiology. The clinical manifestations and presentations of MS are varied depending on the location and severity of pathologic injury. Its symptoms include muscle weakness, sensory disturbances, spasticity and gait ataxia. Clinical evaluation of gait is difficult because systems including muscle function, motor control and integration of movement may be affected by MS leading to subtle and obvious changes in locomotion capabilities. Identification of effective therapies for MS have been significantly hindered due to the largely unpredictable clinical course of the disease and the limited understanding of its etiology and pathogenesis. The purpose of this study is to determine if gait analysis can detect ambulation changes of patients with progressive MS.

PROCEDURES

Eighteen patients (7 women, 11 men, mean age 49 ± 8.5 years) with MS of differing levels of disability participated in this study. Each patient was evaluated by a neurologist to confirm the diagnosis of progressive MS. The Kurtzke Expanded Disability Status Scale (EDSS) was used to quantify the severity of the disease for each subject. EDSS scores were determined through a neurological examination with scores ranging from 0 (normal neurological exam) to 10 (death from MS). All subjects participated in five separate gait evaluations over the course of eighteen months (0, 1, 26, 52 and 78 weeks). A set of 21 reflective markers were placed on bony landmarks as described by Kadaba et al. (1989). Data from at least three complete gait cycles was collected for both the right and left side of the body. Gait analysis instrumentation included a six camera ExpertVision System (Motion Analysis Corporation, Santa Rosa, CA) which was used to collect three-dimensional trajectory data of the reflective markers at a sampling rate of 60 frames per second. Data analysis was performed using Analyze software (Meglan, 1991.) to obtain temporal-distance (TD) parameters. A one-way ANOVA with repeated measures was utilized for data analysis.

RESULTS AND DISCUSSION

Analysis of the TD parameters (Table 1) yielded several trends. On an absolute scale, all TD parameters, with the exception of step width, exhibited a decrease over time. Significant differences were found in the velocity between visits 3 and 4 ($p=0.07$) (Graph 1) and cadence between visits 4 and 5 ($p=0.04$) (Graph 2).

As compared to normal adults, the MS patients displayed significant differences in their ambulation characteristics. At the onset of the study, the MS patients had a mean cadence of 92.5 step/min which is approximately 19% slower than normal subjects reported by Perry and Kadaba et al. (112-115 step/min). At the conclusion of the study, MS patients demonstrated a decreased mean cadence 23% slower as compared to normal adults. Mean stride length values followed a similar pattern. MS patients had a 26% shorter stride length (102 cm) compared to normal adults (138 cm). As a result of decreased cadence and stride length, MS patient's velocity (81 cm/s) was 39% slower than normal (133 cm/s) (Perry, Kadaba et al.) which progressed to 45% slower (73 cm/s) at the conclusion of the study. EDSS scores worsened in seven of the eighteen patients (39%) with three patients experiencing scores that increased by more than 1.0 from their initial to final evaluation.

SUMMARY

Changes in TD parameters, with the exception of step width, were detected in the majority of the MS patients over the 18-month time period. Significant changes were noted in the patient's velocity and cadence parameters. Although the average step width of the MS patients was larger than adult normals, it's difficult to ascertain why this parameter remained relatively unchanged throughout the study. Most likely, the limitations in change are related to the subject's anthropometrics and stability requirements. Further clinical investigation of the relationship between changes in EDSS score and gait TD parameters will be undertaken.

Table 1: Comparison of gait parameters

Time (weeks)	Velocity (m/s)	Stride Length(m)	Step Width (m)	Cadence (step/min)
0	0.78(0.07)	0.99 (0.07)	0.15 (0.01)	90.25 (3.46)
1	0.81(0.07)	1.02 (0.07)	0.16 (0.01)	92.53 (3.91)
26	0.77 (0.07)	0.98 (0.06)	0.16 (0.01)	91.93 (3.05)
52	0.74 (0.07)	0.97 (0.07)	0.16 (0.01)	87.0 (3.82)
78	0.73 (0.08)	0.95 (0.07)	0.16 (0.01)	87.54 (4.13)

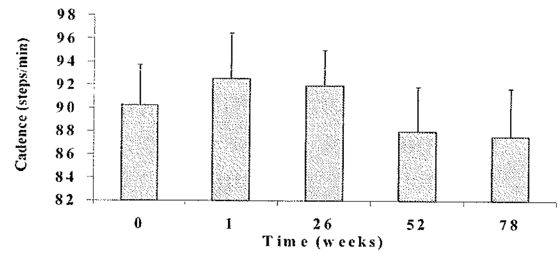

Graph 1: Mean cadence for MS patients

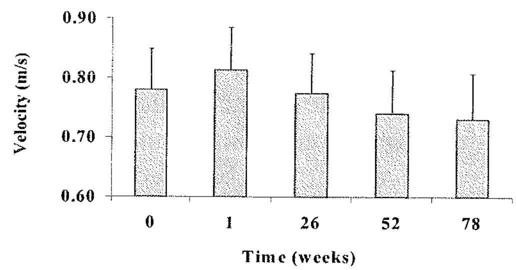

Graph 2: Mean velocity for MS patients

REFERENCES

Growney et al. (1997). *Gait and Posture*, **6**: 147-162.
Kadaba et al. (1990). *Journal of Orthopaedic Research*, **8**: 383-392.
Meglan, DA. PhD Dissertation, *Enhanced Analysis of Human Locomotion.* Ohio State University, 1991.
Perry, J. (1992). *Gait Analysis. NJ:* SLACK Incorporated.

ACKNOWLEDGEMENTS

Funding provided by the Mayo Foundation. The assistance of C. Hughes, D. Morrow, D. Hansen, B. Kotajarvi and D. Padgett is greatly appreciated.

ORIENTATION OF LINEAR FOOT FORCE PATH DEPENDS ON LIMB AXIS DURING HUMAN LOWER LIMB PUSHING EFFORTS

Pamela S. Barrett[1] and Kreg G. Gruben[1,2]

Department of Kinesiology[1], and Mechanical Engineering[2] and Biomedical Engineering[2], University of Wisconsin-Madison, Madison, Wisconsin
Email: pbarrett@education.wisc.edu

INTRODUCTION

This research investigates how humans push with their foot during lower limb exercise. Specifically, this study evaluates the effect of changes in limb axis on force path linearity and orientation during pushes against a stationary bicycle pedal. Limb axis is defined as the line intersecting the hip joint and pedal pivot.

During cycling, foot force patterns have been shown to be reproducible and consistent across subjects and different levels of experience (Sanderson). Despite this and considerable research efforts no model has yet been developed that can predict foot forces during cycling. Recently, Gruben and López-Ortiz found that humans increase force in a specific manner when pushing against both stationary and moving pedals (Gruben 1999, Gruben & López-Ortiz 2000). They report that increases in foot force are produced through addition of force vectors with directional invariance. This is observed as linearity of the path traced by the head of the foot force vector. This requires the coordinated control of several muscles and suggests a motor control strategy in which foot force path is a key variable. In addition, they found that the orientation (θ_L) of this linear force path is repeatable and varies systematically with changes in pedal axis position. Their data suggest that changes in limb posture for a given pedal axis position have limited affect on force path orientation. We hypothesize that limb axis may be important in determining this orientation.

METHODS

While seated, one healthy human subject performed pushing efforts against a translationally fixed pedal. The pedal was free to rotate about the transverse (horizontal) axis. The subject's right foot was securely fastened to a sole plate that was mounted on a custom pedal. The pedal was instrumented with a multi-axis force transducer. The pedal was constructed to allow adjustment of the pedal pivot location parallel to the sole plate without alteration in limb configuration (joint angles).

With the pedal pivot located under the 1st metatarsal head (1stMTH), subjects were instructed to push to 400N in "the most comfortable manner." This foot/pedal relationship was considered the subject's neutral position. Pedal angle was recorded and for subsequent pushing trials the subject was asked to maintain this same pedal angle. Repeated pushes were then performed for various pedal pivot positions ranging from 12 cm posterior, to 6 cm anterior to the 1stMTH.

Foot force and pedal angle were recorded for each pedal axis position. Sagittal-plane components of force were calculated to yield foot force path. These force paths were evaluated for linearity by propagation of measurement error and for orientation using principal components analysis (Gruben and López-Ortiz, 2000).

RESULTS AND DISCUSSION

Linear force paths were observed for all push efforts. Since force direction was not specified, the foot force direction could have a range of possible values as magnitude increased to the 400N goal. Despite this freedom of direction, foot force increased in a highly specific manner resulting in a linear force path. This suggests that a "preferred" motor strategy for lower limb pushing efforts increases foot force through the addition of directionally invariant forces independent of pedal axis position.

Orientation of the linear force path changed systematically with changes in limb axis

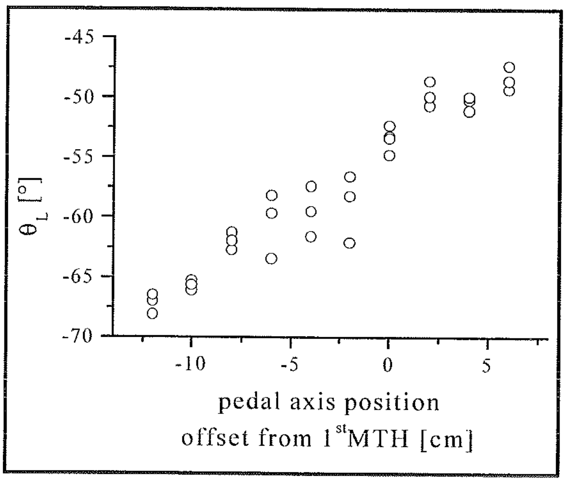

Figure 1 Orientation of foot force path relative to the horizontal plotted vs. pedal axis position. Pedal axis position of zero indicates the pedal axis is under the 1stMTH, while positive positions indicate the pedal axis is anterior of the 1stMTH.

(Figure 1). As the pedal pivot moved forward of the first metatarsal head, θ_L decreased. As the pedal pivot moves backward in relation to the first metatarsal head, θ_L increases. Since pedal axis location determines limb axis orientation, these results show that the orientation of the linear force path rotates in the same direction as the limb axis. As suggested by studies in cats, limb axis may play an important role in the control of foot force direction (Bosco & Poppele 1996)

SUMMARY

These results suggest that the motor control system employs a preferred pattern of force generation when pushing against a pedal in a "most comfortable manner." The orientation of this linear force path is dependent on limb axis.

REFERENCES

Bosco, G., Poppele, R.E. (1996). *J. Neurophysiology* 75(4):1647-1658.

Gruben, K.G., López-Ortiz, C. (2000). *J. Motor Behavior*, in press.

Gruben, K.G. (1999). *Proceedings of Progress in Motor Control II*, 84-85.

Sanderson D.J. (1991). *J. of Sports Science,* **9**(2), 191-203.

AKNOWLEDGEMENTS

This work was supported in part by the Virginia Horne Henry Fund for Women's Physical Education Issues.

ESTIMATION OF CENTER OF MASS DURING STANDING: SOME REMARKS ON INVERTED PENDULUM MODELS

Davide Lenzi , Lorenzo Chiari , Angelo Cappello

Department of Electronic, Computer Science and Systems, University of Bologna, Italy
Email: dlenzi@deis.unibo.it Web: http://www-bio.deis.unibo.it

INTRODUCTION

The center of mass (COM) and center of pressure (COP) are commonly investigated in the study of posture and balance in quiet stance. While the COP can be easily measured by a force plate, locating the COM is a more complicated problem. Several methods have been proposed in literature to estimate COM during walking (e.g. [1]) or standing [2], using kinematics and/or platform recordings. The aim of our study is to compare two common estimation techniques: the first is based on the direct measure of an anatomic site position by means of a motion analysis system [1]; the second is based on an inverted pendulum model of the body and uses inverse dynamics and time-to-frequency domain transformation techniques to estimate the instantaneous COM from COP data [2,3].

METHODS

In this preliminary study we examined one able-bodied male subject, aged 24 years, over six trials. He was requested to stand with eyes open on a force platform, FP, (Kistler) in a stationary (S) upright posture for the first three trials, and to oscillate using only the ankle (A) joint, both the hip and the ankle (HA) or any joint (HKA), respectively, for the last three trials. Kinematics of trunk, thigh and shank was recorded by means of a stereo-photogrammetric system, SPS, (Elite). Experimental set-up is shown in Fig.1. Each trial lasted 60 s and the sampling rate was 50 Hz. Anthropometric measures were taken in order to characterize the inertial properties of the body and of each segment. The instantaneous anterior-posterior displacement of the body COM (X_{COM}) was calculated using whole body kinematics and anthropometric data. This measure, assumed as the gold standard (GS) for any estimation, was compared with the results of two different methods:

1. *one-marker based* (OMB), anatomical COM. It assumes that COM location is fixed to a particular anatomic site, measured by SPS.
2. *inverted pendulum model* (IPM). It estimates COM displacements from the trajectories of COP measured by FP using a low-pass filter defined by an inverse dynamics approach [2] adapted to the biomechanical model proposed in [3]:

$$\frac{\phi_{com}}{\phi_{cop}} = \frac{\Omega_0^2}{\Omega^2 + \Omega_0^2}; \quad \Omega_0^2 = \frac{mgd}{I - mh^2}$$

   where Ω is the angular frequency and Ω_0^2 is a biomechanical constant depending on gravity and inertial properties of body segments; d is the distance of the COM from the ankle joint, I is the moment of inertia of the human body with respect to the ankle, h is the height of the ankle joint and m is the total body mass.

Finally, a sensitivity analysis was carried out on the IPM to assess the influence of the accuracy of model parameter estimates (anthropometric and inertial) on model outcome.

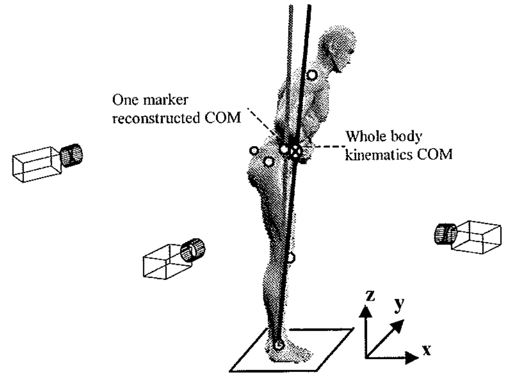

Figure 1 *Experimental set-up*

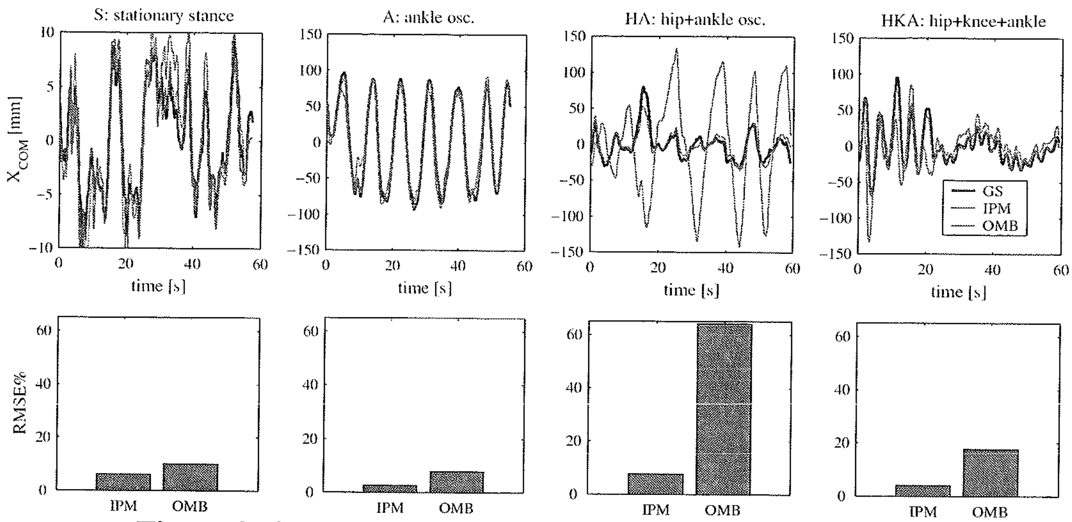

Figure 2 *Comparison of the two methods for X_{COM} estimation*

RESULTS

Fig. 2 compares the trajectories of X_{COM} estimated by OMB and IPM with the GS. The four upper panels report the trajectories obtained during S, A, HA and HKA trials, respectively. IPM provides a better fit than OMB, especially when the task becomes more complex. This observation is confirmed in the lower panels, where the discrepancy between OMB or IPM and GS is represented by the corresponding root mean square errors as percentage of the range (RMSE%). In particular, the result corresponding to the S trial is the mean of the three S trials performed. The RMSE% computed for IPM never exceeds 10% of the range while OMB reaches 65% (in the worst case: HA).
Fig. 3 reports the changes in RMSE% in the four testing conditions when parameters *I* and *d* are changed up to ±20%.

DISCUSSION AND CONCLUSIONS

The results showed that the inverse dynamics approach using an IPM and COP data, allows a better estimate of COM location than the simplest motion analysis method (OMB). This is probably due to the fact that the instantaneous COM location depends on the instantaneous body geometry and it cannot be associated to a particular anatomic site, even in quiet standing, although the movement of the COM is usually small. The low sensitivity of the IPM to the inertial measures (*I*) suggests that it is not necessary a particular accuracy on the estimation of such parameters, while more attention should be given to the estimation of anthropometrics (*d*), especially for ankle oscillation tests, when the IPM better reflects the real motion.

REFERENCES

[1] Saini, M. et al. (1998). *J. Biomech. Eng.* **120**, 133-139.
[2] Brenière, Y. (1996). *J. Mot. Behav.* **28**, 291-298.
[3] Karlsson, A., Lanshammar, H. (1997). *Gait & Posture* **5**, 198-203.

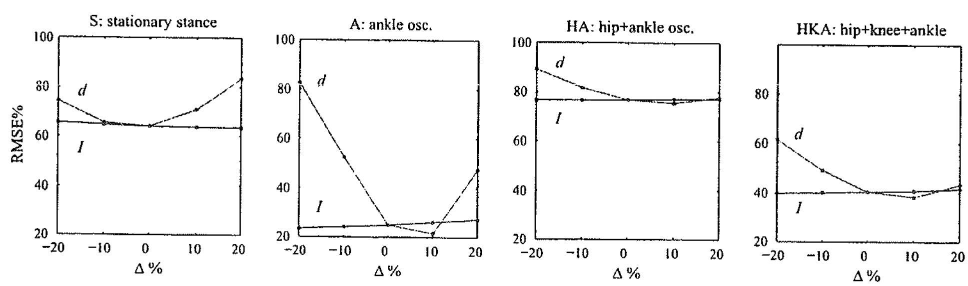

Figure 3 *Sensitivity analysis*

POSTURAL STABILITY IN YOUNG AND ELDERLY ADULTS: A COMPARISON BASED ON LIMITS OF STABILITY DURING STATIC AND DYNAMIC TASKS

Evangelos Christou, Brian Moss, Angela Boule, Pat Yoon, Joshua Evans, Karl Rosengren.

Department of Kinesiology, University of Illinois at Urbana-Champaign
Email: christou@uiuc.edu Web: www.kines.uiuc.edu

INTRODUCTION

Balance is defined as the ability to maintain the center of body mass (COM) within the limits of stability primarily determined by the base of support (BOS). Differences in postural sway and movement strategies between young and elderly adults have been shown using various visual and postural conditions (Woollacott & Shumway-Cook, 1996). Most studies, however, ignore the limits of stability, which are an integral part of balance. Several ways exist to estimate base of support in posture; in this experiment we used the geometric outline (Figure 1) of the base created by the performers feet during a normal upright relaxed stance (Slobounov et al., 1997). The aim of this study was to compare movement of center of pressure (COP) in anterior-posterior (AP), medial-lateral (ML), total area of movement created by COP (TAM) and the ratio of TAM to the base of support (TAM:BOS), in young and elderly adults, under different visual and postural constraints

PROCEDURES

Twenty healthy young adults (23∀5 years) and twenty healthy elderly individuals (65∀6 years) volunteered for this study. Postural stability was assessed using a force platform and each participant's predicted BOS (Figure 1). During each condition, participants stood barefooted within their predicted BOS, on the force platform, under different visual and postural constraints.

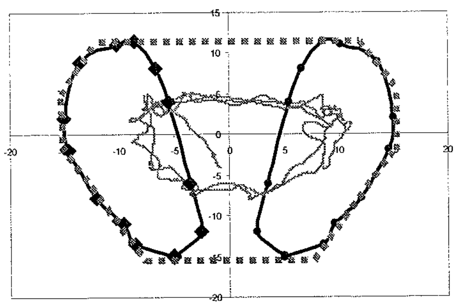

Figure 1. This graph illustrates the participant's feet and predicted BOS for dual and single leg stance, along with COP movement during the LS task.

The following conditions were used: 1) Quiet standing with eyes open (EO) and eyes closed (EC) for 30 s, 2) Single foot stance with both dominant and non-dominant feet (10 s each foot) and 3) A dynamic limits of stability (LS) test involving rotating around the base of support as far as possible without moving one's feet (for 20 s). Each condition was performed twice and each trial lasted either the indicated time length unless or until the participant lost his or her balance or changed postures. Performance on the force platform was measured by the range and standard deviation (SD) of movement of the COP in AP and ML direction, TAM and TAM:BOS.

RESULTS AND DISCUSSION

The predicted area for BOS was not significantly different between the two age groups ($p>0.05$). During the single foot stance task, both TAM and TAM:BOS, were significantly different for the two age groups ($p<0.01$). Furthermore, significant age x foot interactions were found for both TAM and TAM:BOS ($p<0.01$).

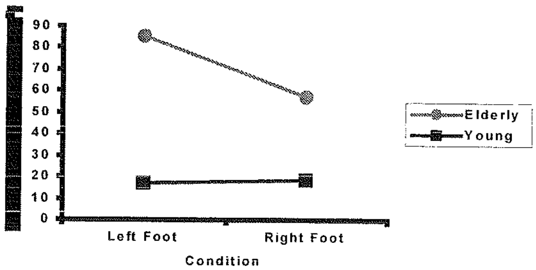

Figure 2. This graph illustrates the age x foot interaction found for TAM. Similar interaction was found for TAM:BOS.

Postural sway, during the single foot stance task, in AP direction revealed significant differences in SD and range of postural sway ($p<0.05$). Furthermore, there was an age x foot interaction ($p<0.01$). Postural sway in ML direction during the single foot stance also revealed differences in SD and range of postural sway ($p<0.05$). However, there was no significant age x foot interaction ($p>0.05$). During the dynamic limits of stability task, both for TAM and TAM:BOS, differences between the two age groups approached significance ($p=0.076$). Both TAM and TAM:BOS were higher in young participants. Range of movement of the COP in the AP direction, however, was significantly higher in young participants ($p<0.05$).

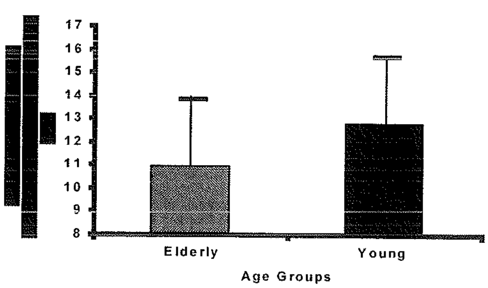

Figure 3. This graph illustrates that young participants produced greater movement of COP in AP direction compared to elderly participants during the LS task.

During the quiet standing task, both TAM and TAM:BOS, were significantly different for the two visual conditions ($p<0.01$). Movement of the COP was greater during the EC condition. There were no age related differences ($p>0.05$). Postural sway in AP direction during the quiet stance revealed differences in SD and range of postural sway ($p<0.05$) between visual conditions. Age related differences were found, furthermore, only for the SD, which had a significant age x visual condition interaction ($p<0.01$). There were no significant differences for postural sway in ML direction ($p>0.05$).

SUMMARY

Elderly, during the single foot stance, exhibited greater postural sway in AP direction, especially with the non-dominant foot. When the goal was to produce postural sway as close to the limits of BOS (LS task), however, elderly had significantly smaller postural sway in AP direction. Similar BOS was found for young and elderly participants in this study. During quiet standing, the two groups had similar performance.
Performance with EC produced significantly greater postural sway compared with EO. The overall results of this study, suggest that elderly might be less stable in AP direction. This might be due to weakness of the leg and back muscles, primarily controlling balance strategies during AP movement.

REFERENCES

Slobounov et al., 1997. Journal of Motor Behavior, 29, 3, 263-281.

Woollacott & Shumway-Cook, 1996. Journal of Aging and Physical Activity, 4, 214-233.

GRIP FORCE RESPONSES TO CHANGES IN THE PROVISION OF SUPPORT

Alexander S. Aruin

Rehabilitation Foundation, Inc., Wheaton, Illinois and Department of Physical Medicine and Rehabilitation, Rush-Presbyterian St. Luke's Medical Center, Chicago, Illinois
Email:aaruin@rush.edu Web: rfi.org/research/MOTION/MOTION/Malindex.htm

INTRODUCTION

Grip strength is an important prerequisite to good hand performance. Muscle weakness and impaired motor control are important factors in generating grip force. The impairment is often manifested in decreased ability to perform simple daily tasks such as pouring a drink or feeding. The procedures for testing grip forces are well documented and used in clinical practice to monitor progress during occupational and physical therapy, to assess potential for rehabilitation, or to monitor the likelihood of postoperative complications (Fess and Moran, 1981, Griffith et al, 1989). The usefulness of grip force assessments decreases when a patient cannot perform a simple task such as lifting an object with one hand and using the other arm for help. It is reasonable to assume that grip force is changed when assistance is provided. For example, a series of experiments with fingertip contact of surrounding objects provided a body of evidence that light touch contact is important in reducing postural sway while standing (Jeka, 1994). However, the effects of light touch and additional support on grip force while manipulating an object were not investigated. The purpose of the study is to determine whether there are adjustments in grip force as a result of additional support provided to the arm.

METHODS

Eight healthy subjects participated in the experiment while comfortably seated at an adjustable table. The total task involved grasping the cup located in the initial position, them lifting and transporting it to the final position. The cup was instrumented with two strain gauges; one was located on the side, and the second was set in the base of the cup (Scholtz, Latash, 1998). A cylindrical grasp involving an opposition of the thumb and the rest of the fingers was used. The subjects were required to lift the cup with the dominant arm, and transfer it without additional support, and then with additional support provided by the contra lateral arm. Provision of the contra lateral arm support included light touch of the index finger, and maximal or 50-percent support of the palm. In addition, an upper extremity skateboard was used as a movable support. Two different cup weights were used in the study: ¾lb and 2lb. The following parameters were measured: peak grip force, time required to reach peak force, and movement time. A PC computer with customized software based on the LabView-4 package was used to control the experiment, collect the data, and perform most of the analyses.

RESULTS

With no additional support, the subjects applied more than 50% of their maximal isometric grip force to lift and transfer the 2-lb cup. The grip force decreased when any of the studied supports were provided. The smallest grip force was recorded when 50-percent of the maximal force provided by the contra lateral arm was used. Similar grip forces were measured when maximal support by the contra lateral hand was provided and when a skateboard support was used. Light touch substantially decreased grip force when compared to conditions without additional support. Similar but smaller changes in grip force were seen with the lesser weight.

DISCUSSION

Lifting and transporting an object required the subjects to apply grip force higher that it was required to prevent the object from slipping. Any additional support decreased the force needed to securely hold the object. This suggests that the brain adjusts grip forces while performing the same task involving different provisions of support. The ability of the CNS to reduce grip force in conditions of light touch (in which the forces provided with the finger are too small to unload the arm), is the most intriguing. It is quite possible that light touch used as an additional reference point in stabilizing the extremity may result in eliminating muscle fatigue while performing different tasks.
One of the potential applications of light touch while lifting objects is in rehabilitation of individuals with weakness of muscles of one extremity.

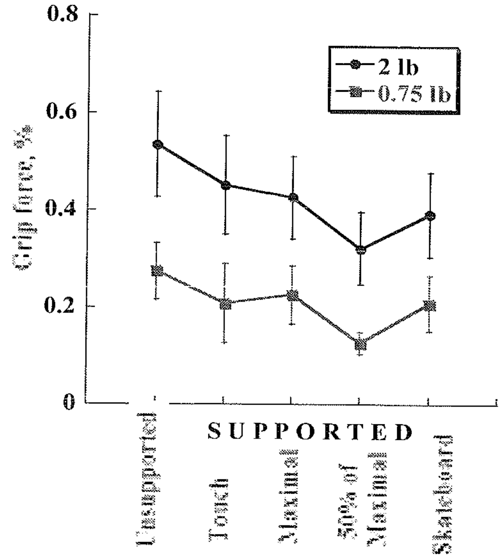

Figure 1. Grip force (normalized by the maximal isometric force) measured without additional support and with different provisions of support. Averaged data for 10 subjects are presented.

REFERENCES

Fess, I, Moran, C. (1981). *Clinical Assessment Recommendations.* Am. Society of Hand Therapists.

Griffith, J. et al. (1989) British J of Surgery, 76, 704-705

Jeka, J, Lackner, J. (1994) *Exp Brain Res*, 100, 495-502

Scholz, J., Latash, M. (1998) *Human Movement Science* 17, 753-779

ACKNOWLEDGEMENT

This study was in part supported by grant HD-30128 from the National Center for Medical Rehabilitation Research, NIH.

BIOMECHANICAL COMPENSATIONS DURING STAIR ASCENT AND DESCENT IN CHILDREN WITH HEMIPLEGIA UTILIZING THREE DIFFERENT ANKLE FOOT ORTHOSES (AFOS) CONFIGURATIONS

Susan Sienko Thomas, Cathleen E. Buckon, Sabrina Jakobson-Huston,
Michael D. Sussman, Michael D. Aiona

Shriners Hospitals for Children, Portland, Oregon Email: SST@SHCC.org

INTRODUCTION

For children with cerebral palsy, AFOs are prescribed to prevent deformity at the ankle, promote a stable base during locomotion and improve the dynamic efficiency of gait. Although AFOs have been found to improve locomotion, their limitation of ankle motion is thought to adversely affect the ability of the child with cerebral palsy to ascend and descend stairs. The purpose of this study was to determine whether a specific AFO configuration (hinged, posterior leaf spring (PLS), or solid) produced biomechanical compensations which inhibited the ability of the child with hemiplegia to ascend or descend stairs.

REVIEW AND THEORY

Stair locomotion is an important functional activity. In order to ascend and descend stairs the ankle requires 30-40 degrees of both plantar and dorsiflexion to control the forward progression of the body. Restriction of ankle motion by an AFO has been shown to produced compensatory movements at the pelvis and hip in children with normal neurological systems[2]. Children with cerebral palsy often have difficulty with stair ambulation due to poor motor control and balance, spasticity and contractures. Despite the difficulty posed by stairs, no information exists regarding the kinematics of stair locomotion in children with cerebral palsy and the subsequent biomechanical compensations required by the child when orthotic devices are utilized.

METHODS

Nineteen children with a diagnosis of spastic hemiplegia, cerebral palsy with a mean age of 9.3 years (range 6.3-15.3 years) were evaluated during stair ambulation. Each child participated in the study for one year which consisted of three months of no AFO wear followed by a randomized AFO sequence. Each AFO was worn for three months with assessments performed at the completion of each wearing period. Each child ascended and descended a series of four stairs using a reciprocal stepping pattern. Stair locomotion data were collected with a six camera motion measurement system (Vicon 370, Oxford Metrics) and analyzed using Vicon Clinical Manager (VCM). Only data from stairs 1 to 3 during ascent and 3 to 1 during descent for both the involved and noninvolved sides were used in the analysis. Velocity and single limb stance times were assessed during stair ascent and descent. Maximum and minimum values were evaluated at the pelvis over the entire cycle (sagittal, coronal, transverse planes), hip (sagittal, coronal planes) knee and ankle (sagittal plane) during stance and swing. Data were analyzed using univariate repeated measure ANOVAs with linear contrasts. P values ranged from .008-.025 using a Bonferonni correction.

RESULTS

During stair ascent on the involved side no differences were found at the pelvis or hip in any plane. Knee extension during stance was greater barefoot compared to hinged p=.003 AFO wear. Ankle motion during stance showed greater dorsiflexion when the hinged AFO was worn in comparison to barefoot p=.0001 and solid p=.0004 AFO wear. Velocity was fastest with the PLS AFO in comparison to barefoot p=.004 and solid p=.007 AFO wear. The involved limb showed increased single limb stance times during hinged p=.017 and PLS p=.006 AFO wear in comparison to barefoot. The only biomechanical compensation by the non involved limb at the ankle was a decrease in plantarflexion during stance when a hinged p=.008 AFO was worn on the contralateral side. No differences in gait parameters were found.

During stair descent, the involved side allowed greater plantarflexion during stance barefoot p=.0001 in comparison to all AFOs. During swing, the hip p=.0003 and knee p=.0026 showed an increase in flexion while the ankle had greater plantarflexion p=.0001 and less dorsiflexion p=.0001 during barefoot in comparison to AFO trials. No differences in gait parameters were found. On the non involved side, no kinematic compensations were seen at the pelvis, hip, knee and ankle during stance or swing. Single limb stance times were greater p=.016 when AFOs were worn in comparison to barefoot.

DISCUSSION

During ascent and descent, the majority of differences were seen at the ankle between barefoot and all AFOs with minimal differences occurring between the AFOs. During stair ascent the increase in dorsiflexion offered by the hinged AFO allowed for a smooth transition of the center of mass over the foot, improving single limb stability. During stair descent in the barefoot condition, children with hemiplegia chose to minimize pelvic obliquity on the involved side by increasing hip and knee flexion to clear the plantarflexed foot during swing. Velocity during stair locomotion was slower for children with hemiplegia barefoot and in all AFOs when compared to normal children wearing a unilateral solid AFO[2]. During stair locomotion on the non involved side, minimal kinematic compensations were seen resulting from the AFO configuration. Maximum and minimum angles at the hip, knee and ankle were found to be similar to those of Andriacchi et al.[1]. Despite claims that orthotic devices are detrimental for stair ambulation in children with cerebral palsy, kinematic evaluation reveals improved stability during stance on the involved limb while no compensations were made by the non involved limb. For children with hemiplegia the hinged and PLS AFOs offer motion and stability without significant compensations at proximal joints.

REFERENCES

1. Andriacchi, TP, Andersson, GBJ, Fermier, RW, Stern, D, Galante, JO (1980) A Study of Lower-limb Mechanics During Stair-Climbing. JBJS, 62-A, 749-757.

2. Nahorniak, MT, Gorton, GE, Gannotti, ME, Masso, PD (1999) Kinematic compensations as children reciprocally ascend and descend stairs with unilateral and bilateral solid AFOs. Gait and Posture, 9, 199-206.

ACKNOWLEDGEMENTS

Research was funded by the Shriners Hospitals for Children.

A NEW METHOD OF QUANTIFYING KINEMATIC INSTABILITY IN THE DISTAL RADIAL-ULNAR JOINT

Patricia G. Neale, Michael E. Hahn, Richard A. Berger and Kai-Nan An

Orthopedic Biomechanics Lab, Mayo Foundation, Rochester, Minnesota
Email: An.kainan@mayo.edu

INTRODUCTION

This study utilized a dynamic wrist simulator to study the forearm motions of pro/supination while under an active loading scheme. The wrist was examined in the intact state and then after several destabilizing procedures. The 3Space Fastrak electromagnetic system (Polhemus, Inc., Colchester, VT) was used to monitor bony motion, with sensors attached to the distal radius, distal ulna, and 3rd metacarpal. Traditional methods were selected to assess the differences in bony motion after the destabilizing procedures; however, these methods were not sensitive enough to detect repeatable differences. This summary will describe the various methods of data analysis used to study kinematics under these conditions, describing particularly the single method which best discerns the instability of the DRUJ.

ANALYSIS METHODS:

1) Basic Euler Angle Analysis. A spherical joint model is initially used to define the pronation/supination motion, which allows 3 DOF of rotation. Multiple bony landmarks were used to establish the anatomical coordinate system, with the center defined by the ulnar fovea. Motions captured by the sensors were transformed into motions of the bones with respect to one another. Differences in flexion/extension or radial-ulnar rotation were calculated as a function of the pronation-supination angle. Even though there was a significant amount of soft tissue destruction between the different phases of this study, this method of euler angle differentiation was not powerful enough to discern these differences.

2) Measuring global distances between bony landmarks. Once the points of interest (radial styloid and ulnar fovea) were transformed into the local anatomical coordinate system based on euler angle motions, differences in distances between these points could be measured. This distance can be expressed as a motion in the transverse plane, or as a total motion in three dimensions. This method, albeit sensitive, was not without shortcomings: if the DRUJ subluxed during motion, the distance between these bony landmarks repeatably increased; however, if it dislocated during motion, the distance could decrease, as the radius moved medially toward the ulna.

3) Measuring angular changes between bony landmarks: DRUJ index. In this method, we look at a line connecting the ulnar center of rotation and the calculated center of the sigmoid notch (R1) versus a line created between the radial styloid and the calculated center of the sigmoid notch (R2) (Fig. 1).

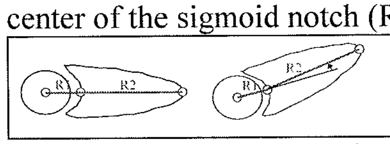

Figure 1: Description of the angular analysis method in neutral (left) and supination (right).

If no dislocation exists, then the radius will rotate freely around the ulna, and the angle between these two lines will be a function of the pronation-supination angle as well as the ligamentous constraints. However, if instability exists, this pattern is altered and is referred to as the DRUJ instability index.

a) Using Digitized Points. The anatomical landmark that best represents the distal center of rotation for the pronation-supination motion of the DRUJ is the ulnar fovea. During data collection, this point was estimated from the insertion of the DRUL, and was used to estimate the origin of vector R1. However, the digitized position of the ulna frequently did not replicate the anatomy's center of rotation (Fig 2). Therefore, R1 was not reliably calculated.

b) Using Screw Displacement Axis. Next, the intersection of the three-dimensional SDA with the plane of the distal ulna was used to define the center of rotation. The screw displacement axis of the radius was calculated from the sigmoid notch motion in an intact, unloaded condition. Next, the intersecion of this axis with the plane of the distal ulna was found.

Weaknesses of this method included the fact that the planar intersection of this axis varied quite a bit throughout the rotation motion, particularly at the end range of motion Due to variances in angulation of the SDA, the intersection of the axis with the plance of the distal ulna frequently was not located near the perceived center of rotation (Fig 2).

c) Using Planar Least Squares Circle Fit. Another method was implemented that uses a linear least squares fit to a circle by first finding the eigenvectors of an inertia matrix of the set of points describing the motion of the sigmoid notch. The largest eigenvector is the perpendicular to the circle, and a coordinate system transformation is applied, with this vector as the z axis. Then, a circle is fit to these points. The geometric center of this circle is defined as the joint center of rotation.

RESULTS

The planar least squares fit method was advantageous to find the center of rotation, as the circle-fit center of rotation more closely approximated the clinical center of rotation of the ulna (Fig 2). Therefore, the results were more repeatable between specimens.

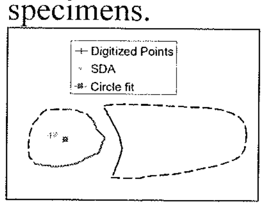

Figure 2: Comparison of the planar view for the 3 angular change methods attempted. Figure shows forearm in neutral position.

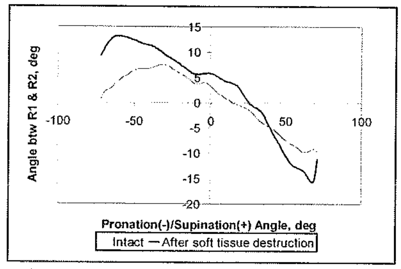

Figure 3: Example of data patterns using circle fit analysis through a pronating motion. Differences between the two conditions are easily discerned and repeatable.

DISCUSSION

For studies of kinematics of the DRUJ, one reliable method of anlyzing data is to look at the map of angular changes between bony landmarks, using planar least squares circle fit to establish the center of rotation.

ACKNOWLEDGEMENTS

This study was funded by NIH grant AR43622 and the Mayo Foundation. Acknowledgment to J.-R. Haugstvedt, T. Nakamura, and M. Fujita for assisting with data collection in this project.

A COORDINATE SYSTEM FOR VISUAL PERCEPTION OF MOTION DIRECTION

Warren G. Darling and Marc A. Pizzimenti
Department of Exercise Science, The University of Iowa, Iowa City, IA 52242
Email: warren-darling@uiowa.edu

INTRODUCTION

Programming reaches to visual targets is thought to involve transformation of information between visual and kinesthetic coordinate systems to specify an upper limb orientation for target acquisition (e.g., Flanders et al. 1992). For static visual perceptions, human subjects apparently use earth-fixed vertical and trunk-fixed a/p axis to specify orientations (Darling et al. 1996, 1997). Programming reaches to moving objects must involve specification of the direction of motion. Whether the coordinate system perceiving direction of motion is the same or different to that for static visual perceptions is the focus of this study.

PROCEDURES

Six young adults with no history of neuromuscular disorders participated. The subject sat in a dark room in front of a dim visual display with a white dot moving along an oblique axis presented on a black background. In one experiment, the subject aligned the axis of dot motion parallel to earth-fixed vertical (i.e., dot moving straight up/down), to head and trunk longitudinal axes and to an oblique white line presented on the display (vertical plane). Arrow keys were used to control axis of dot motion and another key was pressed when the perceived motion was aligned to the desired axis. In another experiment, the subject aligned the axis of dot motion parallel to head and trunk a/p axes and to an oblique white line presented on the display (horizontal plane). Orientation of the line and of the head and trunk were varied on different trials. Subjects performed 5 trials with the head and trunk in comfortable erect (standard) positions and 20 trials in each condition with head, trunk and line orientation varied in each experimental condition. Orientation (3D) of the head and trunk were measured with an electromagnetic system (Minibird – Ascension technologies). Axis of dot motion was computed from the specified pixels of the endpoints of dot motion. Errors for single trials were computed as the angular difference between axis of dot motion and the desired axis for that condition. Constant (mean of single trial errors), absolute constant (magnitude of constant error) and variable (s.d. of single trial errors) errors for each axis were computed for each subject and were submitted to two-way (axis, orientation) repeated measures ANOVAs for each experiment. Regression analyses were used to determine whether single trial errors were biased towards alternative axes in each subject.

RESULTS & DISCUSSION

Accuracy of aligning the axis of the moving dot to vertical was clearly better than to internal axes or to an external line. Single trial errors for aligning the dot motion to head and trunk axes often exceeded 0.2 rad while such errors rarely exceeded 0.1 rad when aligning to vertical. Absolute constant and variable errors were significantly lower when aligning the moving dot to earth-fixed vertical than to any of the other axes (Fig. 1A; $p < 0.05$ for post-hoc comparisons). Regression analyses showed that the single trial errors were not biased toward alternative axes (head or trunk) when aligning the moving dot to earth-fixed vertical ($p > 0.05$). These results strongly suggest that earth-fixed vertical provides one axis for visual perceptions of motion.

Accuracy of aligning the axis of the moving dot to horizontal head and trunk a/p axes provided less clear results. When head orientation was varied, subjects aligned the moving dot to the trunk-fixed a/p axis most accurately ($p < 0.05$). However, when trunk orientation was varied, errors were high when aligning the dot's motion to both head and trunk a/p axes (Fig. 1B). Aligning the dot's motion to the external line was quite accurate when both head and trunk orientations were varied (in a single condition). These data suggest that moving objects are perceived most accurately relative to external axes rather than body-fixed axes, if such axes are available. Otherwise, perceptions are accurate relative to the trunk a/p axis if its orientation is stable and not rotated about its longitudinal axes. Regression analysis did not show clear perceptual biases toward trunk or head a/p axes in any condition.

SUMMARY

These findings strongly suggest that the earth-fixed vertical is one axis used for visual perceptions of axis of motion of moving objects. This is consistent with previous findings concerning static visual perceptions. Such accurate visual perceptions of vertical presumably depend on inputs from the vestibular otoliths that specify head orientation relative to earth-fixed vertical. Perception of motion direction in the horizontal plane appears to be related best to external visual axes, if such axes are available, or to the trunk a/p axis if there is no trunk rotation. Previous work on static visual perceptions did not consider external visual axes for perceptions. Thus, additional study of use of such axes in perception is needed. Provision of external visual axes may be useful to assist visual and, perhaps, kinesthetic perceptions, and movement control in microgravity environments.

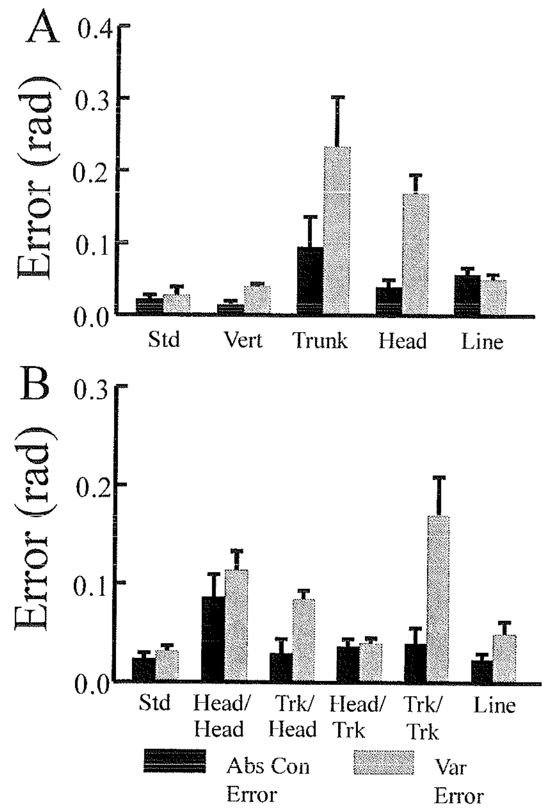

Figure 1: Perceptual errors in vertical (A) and horizontal (B) planes. Conditions on abscissae (segment moved/perceptual axis in B). Each bar is the mean error for six subjects. Error bars are 1 S.E.

References

Darling W.G., Butler A.J. and Williams T.E. (1996) Exp Brain Res, 112:127-34.
Darling W.G. and Hondzinski J.M. Exp Brain Res, 116 (1997) 485-92.
Flanders M, Tillery S.I.H., Soechting J.F. (1992) Behav & Brain Sci 15:309-320

Acknowledgements

Partially supported by US PHS grant NS34895.

FINGER COORDINATION IN MULTI-FINGER FORCE PRODUCTION TASKS INVOLVING FINGERS OF THE RIGHT AND/OR OF THE LEFT HAND

Sheng Li[1], Frederic Danion[1], Mark L. Latash[1],
Zong-Ming Li[2], Vladimir M. Zatsiorsky[1]

[1]Department of Kinesiology Penn State University, University Park, PA 16802
[2]Department of Physical Therapy, Walsh University, North Canton, OH 44720
E-mail: mll11@psu.edu

INTRODUCTION

Finger coordination within a hand during maximal voluntary force production (MVC) tasks in isometric conditions has been extensively studied as a model of the problem of motor redundancy (Li et al., 1998a). A number of characteristics have been introduced to describe finger interaction in such tasks, including: Sharing (total force is shared among the fingers in a certain pattern preserved over a range of total force; Li et al., 1998a,b); Deficit (peak force generated by a finger in a multi-finger MVC task is smaller than its peak force in a single-finger MVC task; Li et al., 1998a); and Enslaving (voluntary force production by a finger is accompanied by involuntary force generation by other fingers of the hand; Li et al., 1998a). Note that lower enslaving may be viewed as an index of better control of individual finger forces, i.e. as an index of higher dexterity. Some features of finger coordination such as force deficit resemble the well-known phenomenon of bilateral deficit (Oda & Moritani, 1995). One purpose of the present study has been to extend the results to finger coordination in the non-dominant hand. The other purpose was to compare the phenomena of force deficit during multi-finger tasks and of bilateral force deficit.

METHODS

Thirteen right-handed healthy subjects participated in this experiment. The experiment consisted of three major parts: (1) Force production by fingers of the right hand; (2) Force production by fingers of the left hand; and (3) Force production by fingers of two hands acting together. Within the first part, tasks included MVC force generation by each of the four fingers of the right hand (I - index, M - middle, R - ring, and L - little finger), by each pair of fingers (IM, IR, IL, MR, ML, and RL), and by all four fingers acting together (IMRL). The same tasks were included into the second part, but forces were generated by fingers of the left hand. Within the third part, subjects were asked to produce MVC force by the following finger combinations: ($IM_R + IM_L$) and ($IM_R + RL_L$), where subscripts R and L refer to the right and left hand respectively. Within each trial, the force value of each finger was measured at the moment when the maximal force value was reached for the explicit task.

RESULTS

Fingers of the left hand demonstrated lower peak force (on average, by 11.5%) and higher indices of finger enslaving. There were no differences in force deficit between the hands. During four-finger two-hand tasks, the symmetrical task ($IM_R + IM_L$) was associated with a small, statistically not significant additional drop in peak force produced by each of the IM-groups as compared to corresponding single-hand, two-finger tasks, IM_R and IM_L (between 2% and 2.5% of corresponding MVCs). In other words, no significant bilateral deficit effects were observed. During the asymmetrical task ($IM_R + RL_L$), the force deficit was higher as compared to IM_R task and RL_L task separately. The force of the left-hand RL-group dropped by 9.8% as compared to these fingers performing the two-finger task separately. These effects were not statistically significant. The force of the right-hand IM-group significantly dropped (by 15%) when they were acting together with the left hand RL-group. The force deficit calculated for the right hand IM-group when they acted together with the left hand RL-group was slightly higher (by about 3%, statistically not different) than during the four-finger task performed by the fingers of the right hand, $IMRL_R$. For the left hand, the force deficit of the RL-group when they acted together with the right hand IM-group was significantly smaller than during the four-finger task performed by the fingers of the left hand, $IMRL_L$. The magnitude of the moment about the body midline in bimanual tasks was significantly smaller than expected from peak finger forces generated in single-hand tasks, i.e. in the absence of bilateral effects. This difference was particularly strong for the ($IM_R + RL_L$) task, in which the expected moment was substantial.

DISCUSSION

The higher enslaving in the left hand may be viewed as an index of its lower dexterity, while similar indices of force deficit in the two hands suggest that an inability to recruit certain groups of motor units may not be the defining factor for this phenomenon. The earlier introduced principle of minimization of secondary moments (Li et al., 1998a) implies that sharing patterns during force production by four fingers of a hand are organized so as to minimize the total moment generated by all the fingers with respect to the longitudinal axis of the hand. Based on the results of the present study, it can be suggested that forces generated by fingers of the two hands are coordinated so that their total moment with respect to the midline of the body is minimized. This may be viewed as an attempt to avoid lateral trunk perturbations in the sitting subject. Our preliminary assessments of moments generated by master fingers in a frontal plane support this hypothesis. Experiments with simultaneous force generation by fingers of the two hands have demonstrated no bilateral effects when similar finger groups were involved in both hands. Bilateral effects were seen only during force generation by different fingers or finger groups in the two hands (asymmetrical tasks). These effects included an additional drop in finger forces, i.e. a bilateral force deficit. A generalization of the principle of minimization of secondary moments allows one to consider bilateral force deficit as a reflection of an optimization criterion and, therefore, as a task-dependent phenomenon.

REFERENCES

Li, Z.-M., Latash, M. L., Newell, K. M. & Zatsiorsky, V. M. (1998*a*). Motor redundancy during maximal voluntary contraction in four-finger tasks. *Exp Brain Res,* **122**, 71-78.

Li, Z.-M., Latash, M. L. & Zatsiorsky, V. M. (1998*b*). Force sharing among fingers as a model of the redundancy problem. *Exp Brain Res,* **119**, 276-286.

Oda, S. & Moritani, T. (1995). Movement-related cortical potentials during handgrip contractions with special reference to force and electromyogram bilateral deficit. *Eur J Appl Physiol*, **72**, 1-5

ACKNOWLEDGEMENTS
The study was in part supported by an NIH grant NS-35032.

STRENGTH EVALUATION OF SINGLE RADIUS TOTAL KNEE REPLACEMENT (A CASE STUDY)

He Wang[1], Kathy Simpson[1], Michael Ferrara[1], Samatchai Chamnongkich[1], Steve Casto[1] and Ormonde Mahoney[2]
[1] Department of Exercise Science, University of Georgia, Athens, Georgia
[2] Athens Orthopedic Clinic PA, Athens, Georgia
Email: hwang@coe.uga.edu Web: http://www.coe.uga.edu/exs/

INTRODUCTION

A successful total knee replacement (TKR) should allow normal knee function. Compared to previous multiaxis TKR designs, the Scorpio™ TKR (Osteonics, Inc.) utilizes one fixed flex/extension (F/E) axis, based on the premise that only one fixed F/E axis exists in intact knees (Elias, et al., 1990; Hollister at al., 1993). The location of the Scorpio F/E axis has been surmised to generate a longer moment arm of the patellar ligament than previous multiaxis designs. Hence, for our participants, would the maximum knee extensor torque of the TKR limb be similar to the non-TKR limb?

In addition, it was of interest to observe the effect of a posterior stabilized (PS) TKR design. Thus, would the stabilizing post provide the restraint to replace the posterior cruciate ligament or would the participants exhibit greater quadriceps activity during isolated knee flexion, when the quadriceps serve as an antagonist to assist in posterior displacement stabilization? Therefore, the objective of this case study was to compare the maximum knee F/E torques and the quadriceps co-contraction activity during antagonist actions of the TKR and the non-TKR (N-TKR) limb during isolated knee F/E movements.

METHODS

Two male participants (55-63 yr.) with a unilateral Scorpio™ PS TKR (P1 = 29 mo; P2 = 31 mo.) took part in this case study. Both were prescreened for health and functional status by the same surgeon who performed the operations. Two days of accommodation practice occurred prior to the actual strength testing.

The isometric strength (KIN-COM III™) of the quadriceps and hamstring were measured at 60° and 30° of knee flexion, respectively. During isokinetic concentric testing (60°/s), the range of motion was between 10° to 80° of knee flexion. For a given test, the trial exhibiting maximum torque was analyzed. An 8-channel BTS TELEMG™ system was used to collect quadriceps EMG activity. EMG window intervals of 167 ms were used for analysis. Integrated EMG (iEMG) intervals representing quadriceps co-contraction during the hamstring concentric test were normalized to their respective quadriceps concentric EMG interval. As this was a case study with only 2 participants, no statistical analyses were performed.

RESULTS

The TKR limb compared to the N-TKR limb demonstrated:

1. less maximum concentric (16% and 21% less for P1 and P2, respectively) and isometric (12% and 29%, respectively) quadriceps torque for both participants (Table 1).
2. 14% less maximum hamstrings concentric torque for P1 but 16% greater torque for P2. However, P1 had similar hamstring isometric peak torque for both knees.

3. less quadriceps co-contraction by P1 except for the VM at 10°-20° and 30°-50° range of knee flexion (Figure 1).

Table 1: Peak torque (Nm) of quadriceps and hamstring for participant 1(P1) and 2(P2)

		Concentric		Isometric	
		P1	P2	P1	P2
Quad	TKR	245.7	198.7	262.9	217.1
	N-TKR	291.6	252.8	298.9	306.2
Ham	TKR	118.0	127.7	144.2	143.2
	N-TKR	136.9	106.9	143.9	106.9

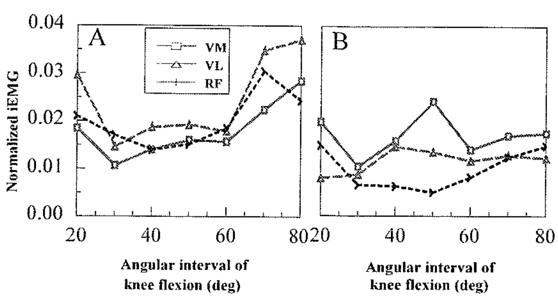

Figure 1: Normalized co-contraction iEMG of P1 quadriceps during knee flexion for A) N-TKR knee and B) TKR knee.

DISCUSSION

In this study, both participants exhibited TKR quadriceps torque deficits, even 2.5 years after their operations. However, one of the participants presented greater TKR compared to N-TRK hamstrings strength. This participant's results supported partially those of Berman et al. (1991), who indicated that the TKR limb quadriceps strength does not recover to that of the N-TKR quadriceps by 2 years post-surgery, but the TKR hamstring strength can attain strength levels of the N-TKR knee within 7 to 12 mo. after surgery. Interparticipant differences may account for our mixed findings, although the participants engaged in the same post-surgery rehabilitation and are currently physically active.

It was surprising that the N-TKR quadriceps exhibited greater co-contraction iEMG than the TKR quadriceps. In addition to the antero-posterior (A/P) conformity of the prosthesis, perhaps the posterior stabilizing post provided the A/P restraint necessary. Hence, more quadriceps co-contraction EMG activity of the TKR limb was not necessary. In addition, the TKR design may not have allowed as much A/P translation as the intact knee (Dennis et al., 1998; Mahoney et al., 1994), therefore, less quadriceps co-contraction was needed in the TKR vs. the N-TKR .

REFERENCES

Berman, A.T., et al. (1991). *Clin Orthop,* **(271)**, 106-113.

Dennis, D.A., et al. (1998). *J Arthroplasty,* **13(7)**, 748-752.

Elias, S.G., et al. (1990). *Clin Orthop,* **(260)**, 98-103.

Hollister, A.M., et al. (1993). *Clin Orthop,* **(290)**, 259-268.

Mahoney, O.M., et al. (1994). *J Arthroplasty,* **9(6),** 569-578.

ACKNOWLEDGEMENTS

Support for the case study comes from The Athens Orthopedic Clinic Foundation.

LINER STABILITY IN ACETABULAR COMPONENT FATIGUE PERFORMANCE

Aaron Bailey, Robert Radefeld, and Janet Krevolin
Sulzer Orthopedics, Austin, Texas
Email: aaron.bailey@sous.com

INTRODUCTION:

A model was developed to evaluate the stability of acetabular liners within their respective shells. Liner stability is important because instability could lead to the liner dislodging from the shell, increased micromotion, and increased backside wear. Debris from backside wear may cause osteolysis and lead to implant loosening. Stability is measured as a function of micromotion and lever-out performance characteristics, both before and after extensive fatigue cycling. This test model assesses the stability of acetabular systems by measuring changes in micromotion and lever-out strength over time. The motivation for creating this model was to evaluate acetabular inserts made from the new highly cross-linked polyethylene (PE), Durasul™.

METHODS:

<u>Micromotion</u>: The stability of the locking mechanism is first assessed by measuring relative motion between the shell and liner (micromotion). This micromotion study is modeled after a previous study (Wentz *et al* 1996) and evaluates the stability of the liner and shell over a period of physiological fatigue cycling. The micromotion measurements are conducted in three stages.

<u>Stage 1</u>: The specimens are axially loaded from 1335-45 N (300-10 lb ≈ 2 X body weight) via a femoral head, while rotating the head 0-35° at 0.5 Hz in air at room temperature. Five spring-loaded LVDTs are arranged in a fixture to measure rim axial, rotational, and polar axial micromotion (Figure 1). The initial measurements are conducted on virgin specimens (1-10 fatigue cycles).

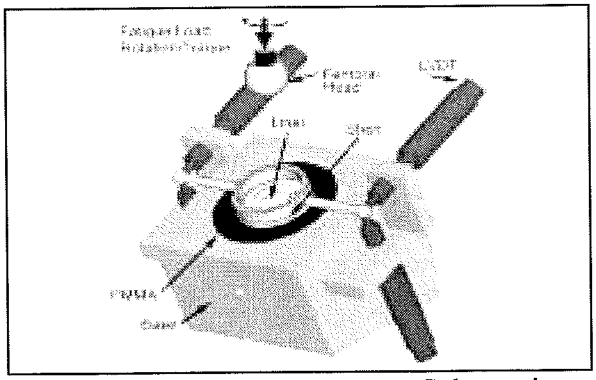

Figure 1: Motion Measurement Schematic:

<u>Stage 2</u>: A second set of micromotion measurements is conducted (as described in stage 1) on the specimens after a 1000 cycle break-in period (1001-1010 fatigue cycles).
<u>Stage 3</u>: The specimens are then fatigued for 10 million cycles submerged in Ringer's solution at 37°C (98.6°F) under sinusoidal physiological loads (3336-334 N [750-75 lb]) and torque (2.5-0.25 N-m [22-2.2 in-lb]). A 40° inferior-superior load angle is incorporated. The acetabular assembly is placed into the fixture with the maximum screw hole density positioned in line with the load line, to create the maximum amount of unsupported PE. The torque is applied through a glued femoral head at 6 Hz. After 10 million cycles, the final micromotion measurements are conducted (as described in stage 1) at 1335-45 N axial load and rotated 0-35° at 0.5 Hz in air at room temperature (10,000,001-10,000,010 fatigue cycles).

<u>Lever-out</u>: Stability is also measured as a function of pre and post fatigue snaplock

strength. (Figure 2). The pre-fatigue lever-out testing is conducted on six additional virgin liners (not fatigue tested) used as lever-out controls. Following fatigue and micromotion of the cycled specimens, a slot is machined into the inner diameter of the liners to accommodate a lever arm. The peak axial load required to lever the PE liner from its respective shell is recorded.

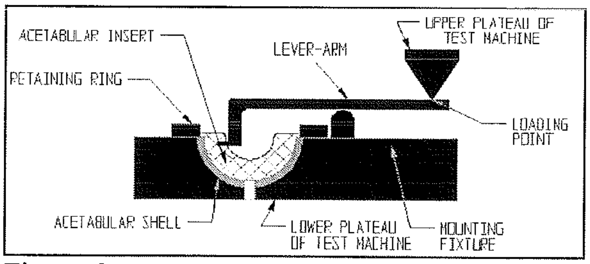

Figure 2: Lever-out Test Schematic

Post-Test Evaluation: After testing, each acetabular system is inspected under a microscope for gross creep, gross wear, and cracking, particularly at the liner's rim where the PE is thin.

RESULTS:

A model for stability was defined and evaluated by testing six highly cross-linked Durasul Inter-Op™ liners (Sulzer Orthopedics) under physiological fatigue loads and torque. Micromotion and lever-out tests were conducted on the same specimens. All acetabular assemblies survived 10 million cycles with no adverse effects. All liners remained firmly attached to their respective shells during fatigue. There was no evidence of gross PE creep into the screwholes, or at any other location. No PE cracking was observed at the liner's tabs, or in the liner's body.

Micromotion: Figure 3 illustrates the average motion of the PE in the acetabular shell at each stage of testing. The results indicate a substantial decrease in motion over time. The decrease in micromotion was found to be statistically significant for the polar and rotational data using a student's t-t-test ($p<0.05$).

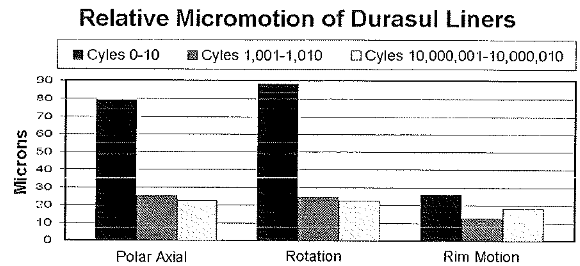

Figure 3: Change in Motion with Fatigue

Lever-out: The Durasul Inter-Op post fatigue lever-out strength (76.7±3.8 N-m [679±34 in-lb]) was statistically greater than the pre-fatigue lever-out strength (65.5±9.5 N-m [580±84 in-lb]) ($p<0.05$).

DISCUSSION:

The fatigue cycles experienced by the Durasul liners had a beneficial effect on the strength of the locking mechanism, relative to both the micromotion and lever-out performance characteristics.

CONCLUSION:

This test was successful in creating a stability model in the laboratory. The cyclic loads and torque did, in fact, effect snaplock stability. This effect was measured as a function of micromotion and snaplock strength, and found to be statistically significant.

REFERENCES:

Wentz MJ, Rubash HA, Shanbhag AS: Evaluation of Micromotion of the Inter-op Acetabular System, University of Pittsburgh, 1996.

OPEN BOOK PELVIC FRACTURES: EFFECT OF PELVIC REDUCTION AND HEMATOMA FORMATION ON RETROPERITONEAL PRESSURE

J. Sigg[1], M. Bottlang[1], T. Simpson[2], J. C. Krieg[1], S. M. Madey[1]

[1] Biomechanics Laboratory, Legacy Health System, Portland, Oregon
[2] Oregon Health Science University, Portland, Oregon
Email: mbottlan@lhs.org

INTRODUCTION

Open book pelvic fractures are frequently accompanied by life threatening blood loss in the retroperitoneal space (Ben Menachem, 1991). Reduction of the disrupted pelvis can induce a dramatic decrease in retroperitoneal bleeding (Failinger, M. et al., 1992). However, the mechanisms responsible for this potentially life saving intervention are controversially discussed. It has been hypothesized that pelvic reduction causes pressure-induced retroperitoneal tamponade due to the decrease in pelvic volume. This cadaveric study quantitatively characterizes the retroperitoneal pressure response on volume changes due to a) retroperitoneal hematoma formation, and b) reduction of a disrupted pelvis. Furthermore, the hypothesis will be tested, if reduction of an open book pelvic fracture causes sufficient retroperitoneal pressure increase to potentially induce pressure-tamponade of venous bleeding.

PROCEDURES

Seven fresh frozen whole-body cadaveric specimens were instrumented with retroperitoneal and peritoneal pressure sensors (HP 78534, Hewlett Packard, Englewood, CO)(Fig. 1). Two flexible membranous pouches were inserted into the retroperitoneal space of the false pelvis, adjacent to the superior margin of each sacroiliac joint. These inflatable pouches ensured reproducible simulation of hematoma formation on clinically relevant sites. Retroperitoneal hematomas were simulated up to a total volume of 1.5 l at a constant rate of 15 ml/s, utilizing an infusion pump (7000 MDX, Sarns Inc., St Paul, MN). Hematoma volume as well as retroperitoneal pressure ($\boldsymbol{P_{RP}}$) and peritoneal pressure ($\boldsymbol{P_P}$) were simultaneously sampled at a rate of 16 Hz (SCXI-1000, National Instruments, Austin, TX). A partially stable open book fracture (symphysis gap=50 mm, monolateral disruption of anterior sacroiliac joint) and an unstable open book fracture (symphysis gap=100 mm, complete monolateral sacroiliac joint disruption) were created by forced external rotation of each hemipelvis after symphysiotomy. Electromagnetic motion tracking sensors were affixed to each pelvic wing to monitor the extent of pelvic disruption.

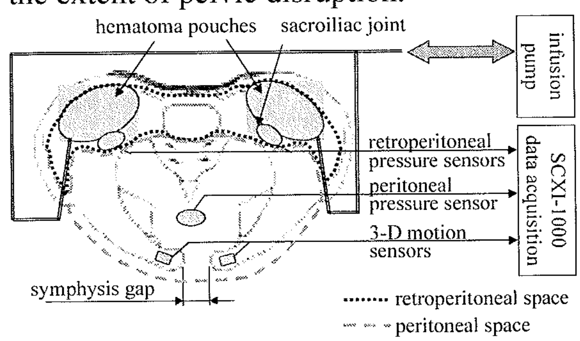

Fig. 1: Transverse view, instrumented pelvis

Changes of $\boldsymbol{P_{RP}}$ and $\boldsymbol{P_P}$ in response to hematoma formation were recorded, first for the intact pelvis and subsequently for the partially stable and unstable pelvis. Furthermore, the effect of pelvic reduction on $\boldsymbol{P_{RP}}$ was determined, first for reduction of the partially stable pelvis and then for reduction of the unstable pelvis. Each pelvic reduction experiment was performed with and without simulation of a 1.5 l hematoma. Finally, the $\boldsymbol{P_{RP}}$ response to hematoma formation in the unstable pelvis was recorded where a hematoma simulation fluid (Glycerol, 1480 cp) was directly infused into the disrupted retroperitoneum. This scenario simulated the effect of shock-induced coagulopathy, where blood traces throughout the retroperitoneal space without clotting.

RESULTS AND DISCUSSION

Hematoma formation in the intact pelvis induced a P_{RP} increase of 5±3 mmHg, 27±13 mmHg and 96±37 mmHg and a P_P increase of 0.4±0.7 mmHg, 3.6±2.2 mmHg, and 12±9 mmHg for hematoma volumes of 0.5 l, 1.0 l, and 1.5 l, respectively. Introducing an open book fracture caused a significant decrease in P_{RP} response on hematoma formation as compared to the intact pelvis (α=0.05) (Fig. 2). Simulation of a 1.5 l hematoma caused P_{RP} responses of 82±30 mmHg and 69±23 mmHg for the partially stable and unstable pelvis, respectively. These peak P_{RP} values decreased on average by 30.6%±4% over the first 100 s while the hematoma volume remained constant at 1.5 l. Infusing hematoma simulation fluid directly into the disrupted retroperitoneum of the unstable pelvis resulted in a drastically lower P_{RP} response (7±1.8 mmHg at 1.5 l).

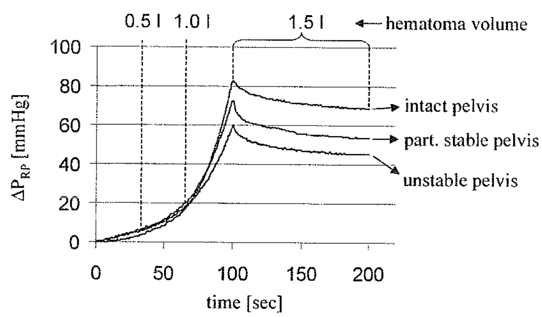

Fig. 2: P_{RP} response on hematoma formation

Reduction of the partially stable or unstable pelvis in the absence of a hematoma did not induce a statistically significant increase in P_{RP} (Fig. 3).

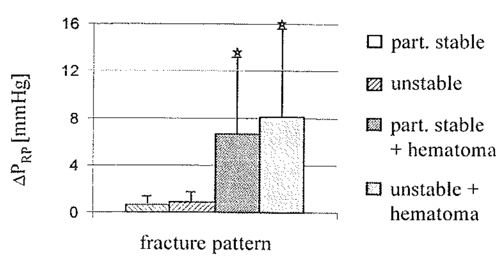

Fig. 3: P_{RP} response on pelvic reduction

Only in the presence of a 1.5 l hematoma a modest but statistically significant pressure increase was observed for reduction of the partially stable pelvis (6.7 mmHg) and unstable pelvis (7.4 mmHg).
These findings demonstrate that the potential space of the retroperitoneum maintains a high degree of inherent compliance even in case of severe pelvic disruption. Retroperitoneal hematoma formation can induce local pressure gradients sufficient for pressure-tamponade of venous bleeding. However, in the presence of coagulopathy, retroperitoneal hemorrhage is likely to onset a cascade, where deficient blood clotting prevents formation of a localized hematoma, which in turn prohibits pressure-tamponade mechanisms. Furthermore, it has been shown that pelvic reduction induces only a small P_{RP} increase. Reduction-induced pressure tamponade is therefore not likely a major contributor of the clinically observed decrease in pelvic hemorrhage after pelvic reduction. Instead, alternative mechanism such as reduction-induced congruity of bleeding surfaces and stabilization-induced protection of blood clot formation are likely to play the dominant roll in the control of retroperitoneal hemorrhage.

SUMMARY

The presented results do not support the hypothesis that retroperitoneal hemorrhage can be controlled by means of reduction-induced pressure tamponade. These findings advance the understanding of basic concepts in pelvic hemorrhage and suggest the need for emergent reduction and stabilization of open-book pelvic fractures.

REFERENCES

Ben-Menachem, Y., Coldwell, D.M. (1991). *AJR*, **157**, 1005-14.
Failinger, M. et al. (1992). *J. Bone Joint Surg,* **74-A**, 781-791.

ACKNOWLEDGEMENTS

Supported by Legacy Research Services

STABILITY OF THE FIRST METATARSAL BASE WEDGE OSTEOTOMY

Susan E. D'Andrea and Charles C. Southerland

Barry University, School of Graduate Medical Sciences, Miami Shores, Florida
Email: sdandrea@mail.barry.edu

INTRODUCTION

Base wedge osteotomies are a well-established surgical indication for patients presenting with hallux valgus deformities. Proximal osteotomies are indicated for severe deformities in cases when the intermetatarsal angle is greater than 15 degrees (Landsman and Vogel, 1992). Numerous base wedge procedures have been identified to correct hallux valgus deformity, all requiring internal fixation.

First metatarsal base wedge osteotomies are subject to instability due to their inability to resist bending from vertical ground reaction forces upon weight bearing. This results in dorsal elevation of the metatarsal head with progressive angulation at the fixation site (Fillinger et al., 1998). Previous studies have attempted to quantify the stability of proximal osteotomies (Campbell et al., 1998; Lian et al., 1992); however, most have concentrated on the fixation technique rather than the geometry of the osteotomy alone.

The purpose of the current study was to assess the strengths of various first metatarsal base wedge reduction methods. This will be accomplished by using a relative comparison of osteotomy fracture force to an intact bone. By using such a ratio, a clearer understanding of the most stable base wedge osteotomy can be ascertained.

METHODS

For the current analysis, thirty, first metatarsal Sawbone® bone models (Pacific Research Laboratories, Inc., Vashon Island, WA) were divided into five groups: (a) Intact bone, (b) Juvara osteotomy fixated with one screw, (c) Juvara osteotomy fixated with two screws, (d) Sglartto box hinge osteotomy and (e) Sglartto non-hinged box wire method. These osteotomies were chosen because it is believed that they represent the greatest degree of stability in base wedge procedures.

Each model was mounted in the base of Instron® Model 8521(Instron, Inc., Canton, MA) at a 15 degree angle to simulate the orientation of the bone during weight bearing (Figure 1). Force was applied to the bone through a block of PMMA molded to fit across the sesmoids under the metatarsal. The force transducer was advanced at a rate of 3 millimeters per second until fracture occurred. These parameters were chosen based on similar studies found in the literature (Fillinger et al., 1998).

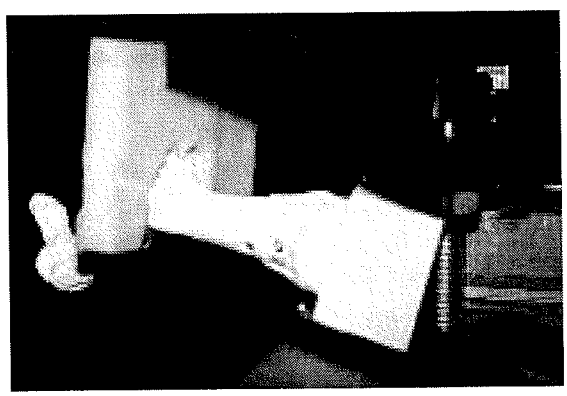

Figure 1: Experimental Set Up

Maximum force at fracture was recorded for each bone. Peak forces for the surgically prepared bones were divided by average force for the intact bone in order to create an index of stability for each osteotomy.

RESULTS

Results show considerably smaller loads throughout all osteotomy groups compared to that of the intact bone (Table 1).

Table 1: Fracture Load and Stability Index

Osteotomy Type	Average Force (N)	Stability Index (%)
Juvara Single (n=5)	35 (±22)	12.3
Juvara Double (n=5)	55 (±43)	19.4
Sglartto Hinge (n=5)	20 (± 3)	7.2
Sglartto Non-Hinge (n=4)	25 (±22)	8.9
Intact Bone (n=10)	282 (±71)	--

The stability index ranged from 7 to 20% with the Sglartto Non-Hinge Osteotomy being the least stable. Larger sample sizes are necessary to determine if these differences are statistically significant.

Failure modes were similar within a given osteotomy type. The Juvara type osteotomy showed an oblique fracture distal to fixation point. For the Sglartto type, stress risers were found at the insertion site of the wire fixation. In all cases, distal migration of the metatarsal head was noted (Figure 2).

DISCUSSION

This initial study utilized Sawbones® due to their isotropic nature. In this case, anticipated differences in the results could be interpreted to be a factor of the osteotomy geometry and its internal fixation alone. Future studies will include bilateral cadaveric metatarsals with one side being used as the control.

Results from these data should provide reliable measures of the stability of base wedge reduction procedures. As more types of osteotomies are introduced, it will become possible to objectively assess their stability and outcome in the surgical patient.

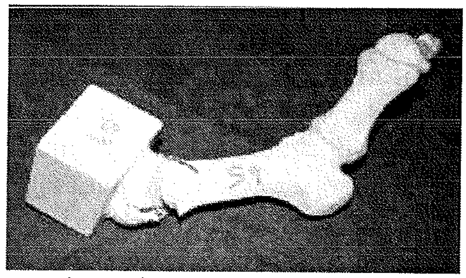

(a) Sglartto Osteotomy

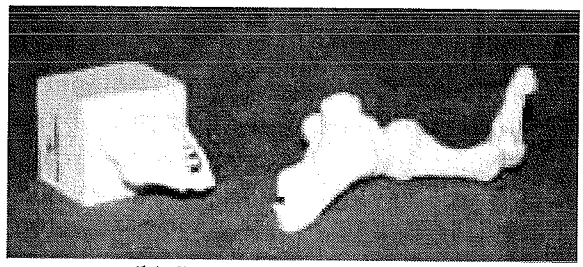

(b) Juvara Osteotomy

Figure 2: Failure Modes for Osteotommies

REFERENCES

Campbell, J.T. et al. (1998). Foot and Ankle International, 19(5): 293-299.

Fillinger, E.B. et al. (1998). J. of Foot and Ankle Surgery, 37(4): 292-302.

Landsman and Vogel (1992). J. of Foot Surgery, 31(3): 211-218.

Lian, G et al., (1992). Foot and Ankle, 13(9): 509-514.

ACKNOWLEDGEMENTS

The authors would like to acknowledge Dr. Scott Banks and the staff in the Orthopaedic Research Laboratory at Good Samaritan Medical Center, West Palm Beach, Florida for the use of their equipment and their assistance during data collection.

EFFECT OF FATIGUE ON THE BONE MINERAL

S.P. Kotha[1,2] and N. Guzelsu[1,2]

[1] Biomedical Engineering, Rutgers University, Piscataway, NJ 08854
[2] Biomechanics, Tr# 4, 675 Hoes Lane-UMDNJ, Piscataway, NJ 08854
Email: guzelsu@umdnj.edu

INTRODUCTION

At the ultrastructural level, debonding at the mineral organic interface was postulated to be the cause of damage in osteons (Ascenzi et al., 1998). It was shown that the bone mineral crystallites were more disoriented while the collagen fibrils were not affected by cyclic loading in which the final loading was the compression cycle. The objective of this study is to investigate if fatigue testing in tension of cortical bone samples would lead to a greater oreintation of the bone mineral crystallites in the direction of loading and if the interplanar spacing between the (002) planes of the bone mineral would change.

METHODS

Bovine plexiform femoral bone from 12 to 18 month old steer were obtained from a local slaughterhouse (MOPAC, Souderton, PA). The lateral and medial quadrants were machined into dumbbell shaped mechanical test specimens (Kotha et al., 1998). Some specimens were loaded in tensile fatigue for 8 cycles in order to damage them and the remaining were taken as control samples. The load- deformation curves that were recorded indicated that the fatigued bone samples were loaded past their yield point. Control and fatigued bone specimens were cut into five 2mm thick sections perpendicular to the length of the test specimen. After the samples were cut, the samples were left to dry in air for a day. X-Ray diffraction (XRD) was performed on these sections within four days of mechanical testing. The cut pieces were placed with their lengths perpendicular to the plane of the holder. Since most of the (002) planes of the bone mineral are oriented perpendicular to the long axis of bone, the (002) planes of the bone mineral are parallel to the plane of the holder. XRD was performed on a Philips Analytical X-Ray diffractometer (PW3050-MPD) using Ni-filtered Cu K_α radiation, divergent slit of 1° and a receiving slit of 0.05°, operating voltage of 40 kV and a current of 45 mA. The samples were scanned at a stepwidth of 0.02° two theta (2θ), with a measuring time of 10 seconds over a scan range from 23 to 28 degrees 2θ. Measurements of the background were taken for later subtraction. The scans were background corrected and were $K\alpha_2$ stripped to improve angular accuracy. No smoothing of the XRD profile was done. The position of the (002) peak and the full width at half maximum (FWHM) of the scans was obtained using the software provided with the diffractometer. The FWHM of the (002) peak was calculated by the equation:

$$\beta_{002} = (\beta^2_{\text{sample}} - \beta^2_{\text{standard}})^{1/2}$$

where β_{standard} is the instrumental broadening obtained from the powdered standard (SiO_2). The values for the unit cell parameters were calculated using Bragg's law: $\lambda = 2d \sin\theta$, where 'λ' is the wavelength of the incident beam, 'θ' is the bragg angle and 'd' is the value of the spacing between the (002) planes.

RESULTS

The FWHM of the 002 peak of fatigued bone is smaller compared to that of control bone (Table 1). The positions of the 002 peak are similar in both fatigued and control bone (Table 1). The interplanar spacing of the (002) planes is shown not to change with fatigue loading.

DISCUSSION

The results show that the FWHM of the 002 peak decreased due to fatigue testing (Table 1). This indicates that the bone mineral orients towards the direction of applied load. Since the position of the 002 peak of the bone mineral did not change due to fatigue loading, there is little change in crystallite strain due to fatigue loading. Therefore, the interplanar spacing between the (002) planes of the bone mineral does not change in the fatigued and control bones. The decrease in the FWHM of the 002 peak indicates that the increased number of bone mineral crystallites contributing to the diffraction process is more than the decrease in crystallite size along the c-axis of the bone mineral crystallite. This would indicate that few of the bone mineral crystallites break during fatigue loading. The presence of the organic in bone decreases the intensity of the diffracted x-rays. The intensity obtained by using a powder standard (SiO_2) is similar to the intensities obtained from the 002 peak of the bone mineral in intact bone pieces. This indicates that the broadening in the standard can represent the instrumental broadening in the 002 peak of the bone specimens ($\beta_{standard}$). Bone proteoglycan has been shown to change orientation by 5° while the collagen does not, due to compressive or torsional loading (Skerry et al., 1990). Assuming the bone proteoglycan to be associated with some of the bone mineral crystals, some of the bone mineral would change orientation due to tensile loading. Though the mode of loading as well as the ultrastructure of the bone used was different, we assume the results to apply to this study. This would indicate that some of the bone mineral crystals along with the associated non-collagenous bone matrix reorients between 3°- 4° towards the direction of applied load while the collagen fibrils do not change orientation. This leads to some bonding changes between the mineral with its associated non-collagenous organic and the remaining collagenous organic. It is shown that there is no change in the interplanar spacing of the (002) planes.

REFERENCES

1) Ascenzi, A. et al. (1998). *Calcif. Tissue Int.* 62(3):266-273.
2) Kotha, S.P. et al. (1998). *Biomed. Mat. Engnrg.* 8:321-34.
3) Skerry, T.M. et al (1990). *Calcif. Tissue Int.* 46:318-26.

ACKNOWLEDGEMENTS

NSF: BCS-9210253

Table 1: X-Ray Diffraction measurements (mean ± SD).

	Half-Width at Half Max (2θ°)	Peak Location (2θ°)	Interplanar Spacing A°
Control	0.267 ± 0.010^a	25.89 ± 0.03^a	6.699 ± 0.007^a
Damaged	0.220 ± 0.008^b	25.89 ± 0.02^a	6.698 ± 0.005^a

RELATIVE EFFECTS OF COLLAGEN FIBER ORIENTATION, MINERALIZATION, POROSITY, AND PERCENT AND POPULATION DENSITY OF OSTEONAL BONE ON EQUINE CORTICAL BONE MECHANICAL PROPERTIES IN MODE-SPECIFIC LOADING

J.G. Skedros[1], M.R. Dayton[1], and K.N. Bachus[2]

[1]Bone and Joint Research Laboratories, Veterans Affairs Medical Center, Salt Lake City, Utah
[2]Orthopedic Bioengineering Research Laboratory, University of Utah, Salt Lake City, Utah
Email: kent.bachus@hsc.utah.edu

INTRODUCTION

Predominant collagen fiber orientation (CFO) can significantly influence the mechanical properties of cortical bone (e.g., Martin and Ishida, 1989; Martin and Broadman, 1993; Riggs et al., 1993). Previous studies have demonstrated that CFO is a strong predictor of tensile, compressive, or bending strength. Few of these studies, however, have examined the relative effects of CFO, mineralization, and other microstructural variables in the context of the in vivo habitual loading mode ("mode-specific loading" e.g., *compression testing* specimens from a habitually *compressed* cortical region, or *tension testing* specimens from a habitually *tensed* cortical region) (Riggs et al., 1993). Evaluating mechanical influences of such histologic variables in the context of a habitual loading mode is important since: 1) in vivo studies have shown long bones of all animals studied receive directionally consistent bending during typical daily gait-related activities (Biewener, 1993), and 2) cortical bone is substantially stronger and stiffer, has different fatigue behavior, and likely has greater toughness in compression than in tension. Consequently, a long limb bone *must accommodate* regional strain-mode-related disparities in habitual loading. Analyses of bone in specific loading modes may demonstrate a rather different role for CFO than suggested by studies that have not evaluated mechanical properties in mode-specific loading. This study tested the hypothesis that CFO will more strongly correlate with energy absorption, a measure of toughness, than with elastic modulus, yield stress, or ultimate stress in compression-tested specimens from "compression" regions.

METHODS

Cubic specimens (5x5x5mm) were cut from "compression" cortices of 10 mature standard bred horse 3rd metacarpals at mid diaphysis (n: caudal = 20, cranial-medial = 10). Specimens were tested unrestrained to ultimate failure in axial compression at 0.002/sec (Riggs et al., 1993). Specimen fragments were evaluated for percent ash content (%ash; 550°C), predominant CFO using circularly polarized light, porosity, percent of osteonal (secondary) bone, and secondary osteon population density (OPD) (Skedros et al., 1996). Data were evaluated using Pearson correlations.

RESULTS

Energy density absorbed to yield stress (0.2%-offset criterion). CFO explained the greatest percentage of variance ($r = 0.411$, $p=0.03$) and was followed by percent osteonal bone ($r = 0.367$, $p=0.05$) and OPD ($r = 0.346$, $p=0.06$).
Total energy density absorbed to ultimate stress. CFO explained the greatest percentage of variance ($r = 0.565$, $p=0.002$). %Ash was the only other

parameter exhibiting a significant correlation ($r = 0.441$, $p=0.01$).

Ultimate stress. %Ash explained the greatest percentage of variance ($r = 0.508$, $p=0.004$) and was followed by OPD ($r = 0.364$, $p=0.05$), percent osteonal bone ($r = 0.330$, $p=0.07$), and porosity ($r = -0.312$, $p=0.09$)

Yield stress. %Ash explained the greatest percentage of variance ($r = 0.403$, $p=0.03$) and was followed by OPD ($r = 0.350$, $p=0.06$).

Elastic modulus. %Ash explained the greatest percentage of variance ($r = 0.451$, $p=0.01$). Porosity was the only other parameter approaching a significant correlation ($r = -0.310$, $p=0.09$).

Histologic correlates. The most strongly correlated parameters were percent secondary bone and OPD ($r = 0.897$, $p<0.00001$). Additional significant correlations included CFO with percent osteonal bone ($r = 0.667$, $p=0.0001$) and OPD ($r = 0.614$, $p=0.0006$).

DISCUSSION

These data demonstrate that CFO most strongly influences the elastic and total energy density absorbed. Martin and Ishida (1989) investigated the relative importance of CFO, porosity, density, and mineralization on tensile strength of bovine cortical bone. Linear regression analysis showed that CFO was consistently the single best predictor of tensile strength. Martin and Broadman (1993) demonstrated that among CFO, porosity, mineralization and histologic type (plexiform, mixed, or osteonal), CFO ranked highly as a predictor of bending properties. These data reflect conventional wisdom that the in vivo role for predominant CFO is primarily for affecting strength- or stiffness-related material properties. In contrast, the present data suggest that CFO may more strongly influence regional material "toughness" for in vivo mode-specific loading conditions. The probability that this is primarily achieved by *remodeling* is supported by the linked relationships of CFO with percent osteonal bone and population density of secondary osteons. It is therefore plausible that these linked relationships enable bone remodeling to affect post-yield properties (and possibly microdamage incidence) by "toughening" specific regions for locally prevalent habitual loading modes. There are data suggesting that such differential tissue organization would be beneficial since notable disparities in microdamage accumulation can occur in "compression" vs. "tension" cortical regions during physiologic loading (Reilly et al., 1997, 1999). This may be the mechanical explanation for regional ultrastructural and microstructural heterogeneities that have been reported in "tension" and "compression" cortices of various limb bones (Riggs et al., 1993; Skedros et al., 1996, 1997).

REFERENCES

Biewener, A.A. (1993). *Calcif. Tissue Int.*, **53(Suppl. 1)**:S68-S74.

Martin, R.B., and Ishida, J. (1989). *J. Biomech.*, **22**:419-426.

Martin, R.B., and Broadman, D.L. (1993). *J. Biomech.*, **26**:1047-1054.

Reilly, G.C., Currey, J.D., and Goodship, A.E. (1997). *J. Orthop. Res.*, **15**:862-868.

Reilly, G.C., and Currey, J.D. (1999). *J. Experimental Biol.*, **202**:543-552.

Riggs, C.M., et al. (1993). *Anatomy and Embryol.*, **187**: 239-248.

Skedros, J.G., et al. (1996). *The Anatomical Record*, **246**:47-63.

Skedros, J.G., Su, S.C., and Bloebaum, R.D. (1997). *The Anat. Rec.*, **249**:297-316.

BIOMECHANICS OF PITCHING WITH INJURY IMPLICATIONS

Naiquan Zheng, Glenn S. Fleisig, Steve B. Barrentine, James R. Andrews

American Sports Medicine Institute, 1313 13th Street South, Birmingham, AL 35205
Email: nigelz@asmi.org URL: http://www.asmi.org

INTRODUCTION

Shoulder and elbow are the two most commonly injured joints of baseball pitchers. Their injury mechanisms are still not known. Applications of biomechanics may provide some insights. An understanding and application of proper throwing mechanics may also improve performance and reduce the risk of injury. Motions, forces and torques at the shoulder and elbow during pitching are presented and discussed with related injuries.

METHODS

Twenty-nine healthy professional and college baseball pitchers were tested in an indoor laboratory as previously described (Fleisig et al, 1995). Fourteen reflective markers were placed on bony landmarks. Three-dimensional coordinates were determined with an automatic digitizing system (Motion Analysis Corporation, Santa Rosa, CA). Marker position data were filtered with a 13.4 Hz low-pass fourth-order Butterworth filter. Data were normalized in time, based upon the time of lead foot contact (0%) and ball release (100%) before averaging. Using inverse dynamics, shoulder kinetic parameters were calculated as the force and torque applied by the trunk to the upper arm (Fleisig *et al.*, 1995). Similarly, elbow kinetics was calculated as the force and torque applied by the upper arm to the forearm.

RESULTS

The ball speed was 38.1±0.7 m/s with the range of 37.1 to 40.2 m/s. The interval from foot contact to ball release for the group averaged 0.139±0.002 seconds. The axial rotation of the spine decreased during stride phase, reaching its minimum at foot contact (-51.4±9.6°). It reached neutral position (-0.9±0.2°) at ball release. The lateral bending of the spine at foot contact was 1.6±5.5°. The spine bent laterally 28.2±6.2° at ball release. The shoulder was abducted 94±9° and horizontally abducted 7±7° at ball release. The shoulder externally rotated about 50° at foot contact and reached 177±7° shortly before ball release (Fig. 1). The elbow angle was about 82° at foot contact and extended to 158±6° at ball release.

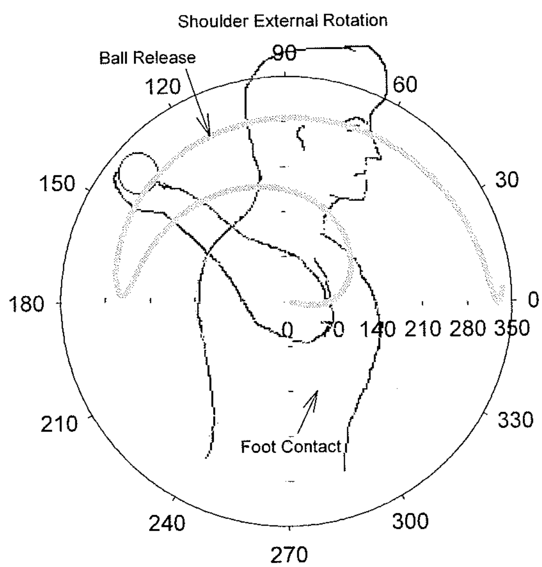

Fig. 1 Shoulder external rotation during pitching (the radius stands for time in millisecond, normalized from foot contact (140 ms) and ball release (279 ms)).

Based upon the force and torque at the shoulder and elbow, there were two critical instants. The first occurred near the maximum external rotation of the arm. At this instant a maximum varus toruqe of 64±12 Nm was generated at the elbow. In addition, a 16 Nm flexion torque, 300 N medial force, a 160 N anterior force and a 270 N proximal force were produced at the elbow. The second critical instant for the shoulder occurred immediately after ball release. At this instant, a maximum proximal force of 1070±120 N was generated. In addition, an anterior force of 80 N, an inferior force of 100 N, a 26 Nm adduction torque and a 44 Nm horizontal adduction torque were produced at the shoulder.

DISCUSSION

The UCL and articulation between the radial head and humeral capitellum withstood valgus torque applied by the forearm to the elbow. Fleisig et al (1995) reported that the load on the ulnar collateral ligament (UCL) during pitching is near its maximum capacity. The corresponding elbow injuries include UCL tear, muscle tears, avulsion fractures, lateral elbow compressive injury. The varus torque and rapid extension of the elbow explains the mechanism of olecranon impingement. The shoulder externally rotated about 180 degrees and internally rotated at 7000 deg/sec before ball release. As the abducted arm externally rotated at the shoulder, the humeral head translates anteriorly. At maximum external rotation, the posterior rotator cuff may become impinged between the glenoid labrum and the humeral head. This "over-rotation" injury can cause degeneration of both the superior labrum and the rotator cuff. Muscles and other soft tissues at the shoulder generate over 1000 N to stop the rapidly moving arm during arm deceleration. Such large proximal force plus internal rotation and horizontal adduction at the shoulder might be the cause of rotator cuff tear, impingement, and the labrum degeneration.

At ball release, the spine had little axial rotation and the shoulder had little horizontal adduction. Excessive spine axial rotation will result in the pitching arm being behind the ball release zone, which would require a pitcher to have significant shoulder horizontal adduction to compensate for the excessive spine rotation. Such shoulder horizontal adduction at ball release may shift the humeral head to the rim of the glenoid fossa, causing the humeral head to be reseated off-center and placing the labrum in jeopardy for injury. At ball release, the spine laterally bent about 28^{0} to raise the pitching arm. In order to keep the desired position of the forearm at ball release a pitcher may compensate for any loss of lateral bending by extra shoulder abduction. Such compensation may cause high stress and impingement of the shoulder.

SUMMARY

Baseball pitching is one of most demanding activities of the shoulder and elbow. The shoulder had about 180 degrees external rotation with internal rotation velocity of 7000 deg/sec. Two critical instants, one during arm cocking and the other after ball release, had high forces and torques at the shoulder and elbow. They were found related to the shoulder and elbow injuries.

More research is needed to identify factors related to these injuries. A biomechanical model of the shoulder with detailed structures may find direct relation of the force and torque at the shoulder to these injuries. Studies correlating kinematics and incidence of injury would also be helpful.

Reference:

Fleisig GS et al (1995): Am. J. Sports Med. 23: 233-239.

SCHLAGER FENCING BIOMECHANICS: DETERMINATES OF IMPACT FORCE

Anna Galea and Jack Dennerlein
BioRobotics Laboratory, Harvard University, Cambridge, MA
galea@hrl.harvard.edu jax@hsph.harvard.edu

INTRODUCTION

Schlager swords are used by a subset of fencers interested in reproducing fencing styles from before the 17th century. Anecdotally, it is easier to bruise an opponent inadvertently with excessive force during contact when using these heavier weapons than with the use of modern epees or foils. Sportsmanship in fencing dictates scoring without bruising one's opponent. Thus, minimizing the impact force is desirable and advantageous for the safety of the sport. It is hypothesized that the mechanics of the thrust, specifically, the independent variables of sword speed, vertical angle of attack, and roll, dictate the force of the hit. The aim of this study is to measure the impact force and correlate it with these independent variables.

EXPERIMENT

The sword used is a standard 86 cm schlager. It requires about 40 N of force for a 15 cm bend [1]. In order to study the three independent variables (speed, pitch, and roll) and their associated biomechanics independently, the types of hits asked for of the test fencer (one subject [2]) were as follows:

- Straight lunges of various speeds, to study the effect of velocity.
- Punches (hits imparted by arm extension with no body motion) to study why these blows tend to feel harder than lunges.

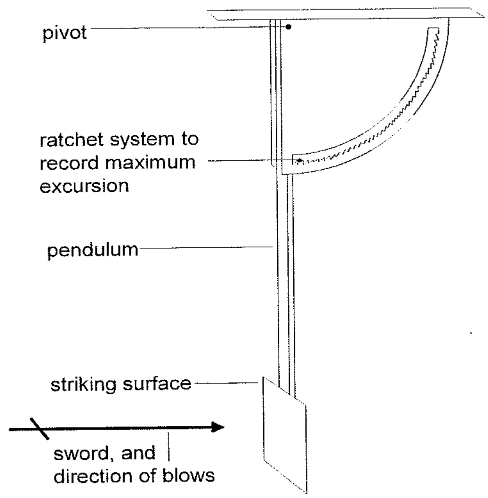

Figure 1.
Apparatus to measure impact force.

- Lunge-throughs, (a lunge aimed at a target a few inches beyond the striking surface).
- Corkscrew lunges and punches, where the sword is rolled as the hit is executed.
- Off-line shots with a negative pitch angle.

An innovative pendulum mechanism was developed to measure impact force (Fig. 1). Impact was made with an aluminum striking surface, which minimized friction between the metal sword tip and the pendulum and contact time. The impact would cause the pendulum to swing, whereby a simple ratchet would record the maximum excursion of the pendulum. This was correlated with the impact force.

To measure the sword speed, angle of attack and the sword roll, data was gathered from a frame-by-frame analysis of a standard 30 frames per second video recording of the experiment [3]. The last 3-8 frames before impact were analyzed for the velocity and roll rate, and the last frame before pendulum motion was analyzed for the static variables such as angle and roll.

RESULTS AND DISCUSSION

The straight lunges (Fig. 2) yielded a direct relationship between impact velocity and the force of impact. Higher force for a higher velocity was of course expected, and so this run sets up a baseline by which to determine what elements of a thrust increase the force.

Punches had a higher impact velocity than the lunges (including the lunge-throughs). For comparable speeds, however, the punches yield less impact force. Lunges included the movement of the whole body towards the target while punches only include the mass of the arm. Hence this less impact force is expected [4].

Lunge-throughs had a higher impact force and on average were faster than lunges. Experienced fencers "pull" or decelerate their lunges at the end of the elbow extension prior to impact. This process does not occur for lunge-throughs and is probable cause for the higher force.

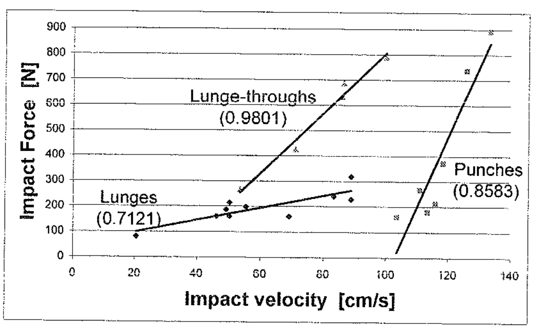

Figure 2. Comparison of impact velocity versus force for the three types of straight hits. (R^2 values indicated)

Off-line shots were found to produce almost identical force to lunges. The effect of pulling a shot, which is seen in lunges, is countered by force absorbed in bending of the wrist.

Corkscrew shots showed an overall slight increase in the force, due to their punching component (which was necessary to maintain a roll rate). Roll rate, however, affects force more so than velocity, based on the correlation between force and a linear combination of normalized roll rate and velocity.

SUMMARY

A direct relationship between impact velocity and the imparted force was realized, with a higher force imparted partway through a full lunge (i.e. lunge-throughs). Punches produced higher overall forces, but off-line shots are safely executed. Roll rate was found to correlate strongly to the imparted force, since the torque generated limits the bend of the sword and a higher force is translated. The conclusions gathered yield sound training protocols for practical schlager fencing.

REFERENCES

[1] Savian et al "Schlager Safety Testing": reported by J. Crouchet 1996

[2] Erdmann et al, *J. Biomech.* 30(7): 679-88, 1997

[3] Schmidt et al, *J. Biomech.* 32(6): 615-622, 1999

[4] Laursen et al, *J. Biomech.* 31(8): 731-740, 1998

ACKNOWLEDGEMENTS

The authors would like to acknowledge Fred Kutz and Garrett Stanley for their help and guidance with this study.

A PROSPECTIVE STUDY OF ILIOTIBIAL BAND FLEXIBILITY AND ABDUCTOR STRENGTH - IMPLICATIONS FOR MARATHON TRAINING SUCCESS

John M. MacMahon[1], Ajit M. Chaudhari[1], and Thomas P. Andriacchi[1]

[1]Stanford Biomotion Laboratory, Stanford University, Stanford, California
Email: dixiedog@stanford.edu **Web:** www.stanford.edu/group/biomotion

INTRODUCTION

Peak iliotibial band (ITB) flexibility and peak abductor strength were measured prospectively in a population of runners training for marathons. These two measures are considered strong indicators of lower limb flexibility and strength for marathon runners. It is hypothesized that increased ITB flexibility and abductor strength reduces injury rates while also increasing completion rates for marathon training.

METHODS

Runners were recruited from two marathon training programs. Each team engaged in a 5-month training schedule. The teams had similar schedules with respect to total mileage and total number of runs. The two teams differed with respect to their warm-up and cool-down regimens. Team A (initially N=21) was coached to warm-up and stretch together prior to runs and to jog cool-down laps after their runs while team B (initially N=20) did not. Inclusion in the study was based on the following criteria:

- Mileage – Initially <20 mi./wk
- Injuries - no reported surgeries or significant soft-tissue injuries of the lower limbs
- Experience - < 3 marathons

Early on in their training (~1 month)and again later in their training (~4.5 month) two measures were acquired from each runner.

Measure 1 - runners were asked to perform the standing ITB stretch 4 times (Fig. 1). Each stretch (4 trials) was held for 30 sec. (data collected over last 5 sec.) followed by rest (<1min.). Kinematics and kinetics of the stretch were analyzed using 7 retro-reflective markers, a four-camera system, and a force plate. Inverse dynamics were applied to determine hip abduction moments during the stretch.

It was assumed that increased adduction moments result in higher forces in the ITB. Increased forces in the ITB results in greater tissue relaxation and thus flexibility (Taylor et al. 1997).

Measure 2 - Abductor strength measures were acquired with a dynamometer contacting the runner just proximal to the lateral malleolus. The test stand was adjusted to 20° of abduction for each runner. (Fig. 1). Each test (4 trials) included 3 sec. of isometric force development, followed by rest (20 sec.).

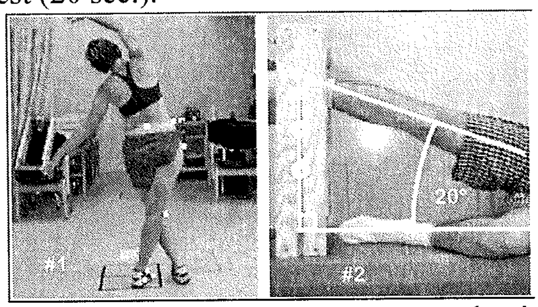

Figure 1: Measure 1- right ITB stretch with ipsilateral foot on force plate. Measure 2 – isometric strength test at 20° of abduction.

The runners were not coached during the tests. The forces were multiplied by the moment arm measured from the greater trochanter to the lateral malleolus to get hip abduction moments. These moments were then normalized by body weight and height (%BW*HT).

Pair-wise two-sided t-tests were used for all analyses between an individual's earlier measurements early and their later measures.

RESULTS

Both teams had no differences in peak normalized abductor strength or flexibility ~1 month into their training ($p>0.05$). However, just prior to race day team A had significant higher peak ITB flexibility ($p<0.05$) and peak abductor strength ($p<0.0001$) than team B (Figs. 2 & 3).

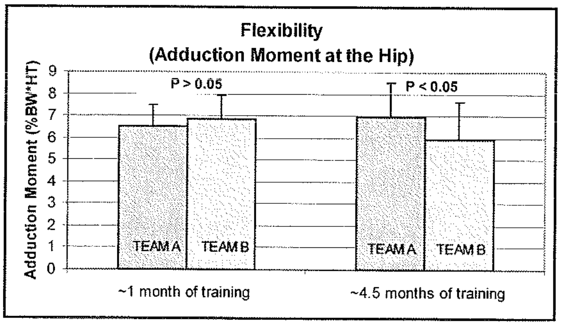

Figure 2:Flexibility: peak hip adduction moment, before and after training for runners who completed training on teams A (N=14) and B (N=6).

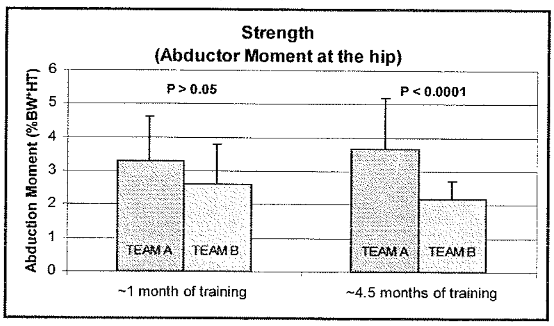

Figure 3:Strength: peak abductor strength before and after marathon training for runners who completed training on teams A (N=14) and B (N=6).

Also, team A had a higher percentage of runners complete their training (85% vs. 28%) and a lower percentage of drop outs due to injury (11% vs. 33%).

DISCUSSION

A training regimen incorporating stretching, warm-up and cool-down periods is implicated in increasing completion rates of marathon training and also implicated in reducing the potential for injury.

Unlike an interventional studies on recreational runners (e.g. Van Mechelen et al. 1993), this study chose marathon runners whose mileage was greatly increasing during the training. Increasing mileage is agreed upon as a major injury risk factor and may result in increasing the sensitivity to these training variables (Fredericson, 1998). Other coaching variables may also play a role in training success.

SUMMARY

Marathon training that includes an active component of warm-up, cool-down and stretching is implicated in a significant improvement of ITB flexibility and abductor strength. The subsequent physiological benefit decreases injury and/or drop-out rates occurring in marathon training.

REFERENCES

Fredericson, M.(1998).*Sp. Med.* **21**(1)49-72.
Taylor, D.C. et al. (1997). *Med. Sci. Sp. Ex.* **29**(12), 1619-1624.
Van Mechelen, W. et al. (1993). *AJSM* **21**(5), 711-719.

ACKNOWLEDGEMENTS

Stanford Motion and Gait Analysis Laboratory, Kevin Rennert, Rich Bragg, Chris Dyrby and Gene Alexander.

A NONLINEAR, MULTIPLE-SURFACE CONTACT FINITE ELEMENT MODEL OF A ROTATING PLATFORM TOTAL KNEE

J. K. Otto, T. D. Brown, and J. J. Callaghan

Orthopaedic Biomechanics Laboratory, 2181 Westlawn Building, University of Iowa, Iowa City, IA 52242
Email: tom-brown@uiowa.edu

INTRODUCTION

Although mobile bearing total knee replacements are growing in popularity, little is known about the mechanics at the 'mobile' interface. The finite element method provides an attractive means to investigate this interface in more detail than experimental testing would allow. We have developed a nonlinear, multi-contact-surface finite element model of a rotating platform total knee for the purpose of studying the mechanics at the mobile interface under physiologically relevant loading.

METHODS

A 3-D finite element model of a rotating platform total knee* was meshed with the Patran 8.5 pre-processor (Figure 1). Abaqus 5.8 was used to perform a nonlinear, large-displacement contact analysis. Since the CoCr elastic modulus (220 GPa) is over 300 times stiffer than UHMWPE, the femoral component and tibial tray were modeled as rigid Bezier surfaces (3-noded triangular elements). The PE insert (8-noded hexagonal elements) was treated as a nonlinear deformable body with a Poisson ratio of 0.45 and a tangent elastic modulus governed by a constitutive 4th-order relationship with von Mises stress (σ): $E(\sigma) = 634.92-12.31\sigma-3.61\sigma^2+0.199\sigma^3-0.00283\sigma^4$ MPa (Cripton, 1993). Unlike finite element models with prescribed bearing surface traction, this model used multiple-surface contact interactions (femoral component/PE and 'mobile' tibial tray/PE interfaces), which permitted a more realistic load transfer analysis.

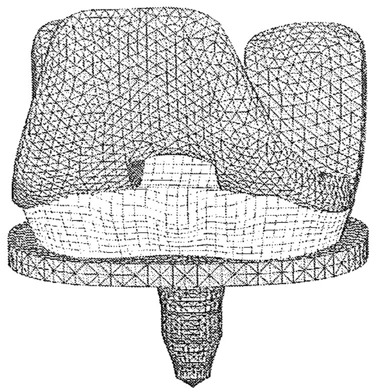

Figure 1: FEM of a rotating platform TKR.

The femoral component was given rotational freedom about the anteroposterior (A/P) axis, and full translational freedom in the A/P, mediolateral (M/L), and superior-inferior (S/I) directions. The metal tibial tray was given freedom only to rotate about the S/I axis. The PE insert, by contrast, had complete translational and rotational freedom, constrained only by contact with the femoral and tibial components.

Positioned in full extension with a 50/50 condyle weight distribution, the implant was given a pure vertical axial load of either 1, 2, 3 or 4 BW (1 BW=686.5 N). Then the tibial tray was internally rotated 10°. An experimentally derived friction coefficient of 0.072 was used at the interfaces. For comparison, a purely elastic PE model (E=634.92 MPa) was loaded to 4 BW and 10° of internal rotation.

RESULTS AND DISCUSSION

As would be expected in this doubly nonlinear system, peak stresses in the PE did not increase proportionally with each unit increase in axial load (Table 1). The simplified elastic model had a peak stress twice that of the nonlinear case. Besides additional recruitment of contact area with increasing axial load, the location of peak stress moved from being on the bearing surface before endorotation to being on the 'mobile' interface during rotation (Figure 2). Interestingly, the contact patches were concentrated on the medial and lateral peripheral edges of the PE insert, and moved centrally, towards the axis of rotation, with increasing axial load. There was a nearly linear relationship between axial load P (N) and resisting torque T (N-m), T=0.00175 P. During internal rotation of the tibial tray, the PE insert rotated less than 0.1° relative to the femoral component. Therefore, for all practical purposes, nearly all relative motion accommodating the imposed endorotation occurred at the 'mobile' interface, for full extension.

Table 1: Summary outcome measures (Before = no rotation, After = 10° rotation).

BW	Peak Stress (MPa) Before	Peak Stress (MPa) After	Contact Area (mm^2)	Average Torque (N-m)
1	15.9	16.7	515	1.37
2	16.4	19.6	717	2.52
3	16.9	20.2	867	3.62
4	17.3	20.6	1000	4.70
4*	34.4	75.0	1008	4.76

*elastic polyethylene model

The maximum levels of torque resisting bearing motion reported here approach the range of peak torques developed in a TKA patient fitted with an instrumented prosthesis (Taylor, 1998). This lends credence to observations of bearing non-motion in about half of the patients studied by fluoroscopy (Stiehl, 1997). Parametric FE studies hopefully will identify design changes that could reduce potentially problematic peripheral polyethylene stresses, and increase bearing mobility by reducing resisting torque.

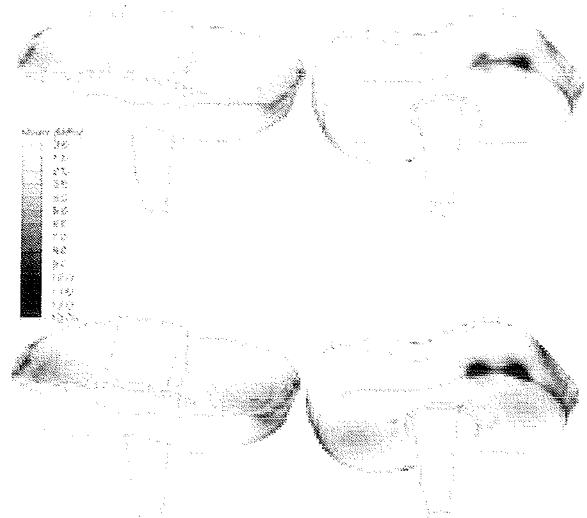

Figure 2: Stress distributions spread and move centrally with additional axial load. Top: 1 BW, bottom: 4 BW, left: no rotation, right: 10° internal rotation of the tibial tray.

*Depuy LCS cemented components, femoral: PS, Std+/Rt; tibial tray: rotating platform II, size 4; PE insert: PS, Std+, 10.0 mm thickness.

REFERENCES

Cripton, P.A. (1993). Thesis. Queen's University.

Stiehl, *et al.* (1997). *CORR*, **345**, 60-6.

Taylor, *et al.* (1998). *J Arthroplasty*, **13**, 428-37.

ACKNOWLEDGEMENTS

Johnson & Johnson/Depuy provided financial assistance. Andrew Dooris, Mark Nadzadi, and Doug Pedersen supplied valuable technical help.

POROELASTIC PARAMETER ESTIMATION OF INTERVERTEBRAL DISC: A FINITE ELEMENT AND EVOLUTIONARY BASED ALGORITHM

Hamid Katoozian [1], Neil Broom [1] and Peter Robertson [2]

[1] **Department of Mechanical Engineering, University of Auckland, Auckland, New Zealand**
[2] **Department of Orthopaedic Surgery, Auckland Hospital, Auckland, New Zealand**
Email: h.katoozian@auckland.ac.nz

INTRODUCTION

During the last two decades, a more realistic approach to the modelling of the intervertebral disc (IVD) has been used based on the theory of consolidation and poroelasticity (Simon et al, 1985). Together with these mathematical and numerical simulations, more sophisticated experimental studies based on the rate dependent and creep behaviour of the IVD have also been introduced (Martinez et al, 1997).

Finite element analysis (FEA) as a computational tool for numerical evaluation of stress, strain, and displacement in structural systems has become well known in biomechanics. The FEA technique has been used extensively to predict time dependent behaviour of the IVD under various loading schemes, kinematic boundary conditions, and material properties.

The accuracy of the FEA results is highly dependent on the correctness of the initial input values for material properties. In recent years there has been substantial application of classical identification methods to estimate the properties of materials. The traditional technique of parameter estimation for structures is formulated in an abstract setting in Hilbert spaces, and an optimization technique, e.g. least squares and feasible directions, is then used to solve the identification problem (Katoozian, 1999). The basic ideas is to discretize the model into a FEA mesh and then use an iterative identification task to estimate parameter values that minimize the error between the simulated FEA output and the experimental data.

Earlier optimal control approaches suffered from a major weakness of being trapped in local extremum. Although some initial parametric and sensitivity analyses would enable one to make a proper initial guess for unknown parameters, convergence to the global extremum is still not guaranteed. In this study a new approach based on the application of Genetic Algorithm (GA) to the biomechanical parameter estimation has been introduced.

Evolutionary Algorithms (EA) are powerful optimization techniques taking inspiration from genetics and natural selection. Unlike classical search methods, EAs with heuristic capability can effectively explore very large solution spaces.

METHODS

The commercial FEA code ABAQUS 5.8 for nonlinear poroelastic analysis has been used. The poroelastic FEA model in ABAQUS is based on multi-phase material using effective stress to describe the behaviour of the solid phase. This code employs principles of the theory of consolidation with emphasis on Darcy's law for low velocity fluid phase.

The genetic algorithm code, GAfortran 1.6.4 (Carol, 1997), was incorporated into the estimation process using an interface program. The GA code initializes a random sample of individuals with parameters to be optimized using evolution via 'survival of the fittest'. The selection scheme used is tournament selection with a shuffling technique for choosing random pairs for 'mating'. The routine includes binary coding for the individuals, jump mutation, creep mutation, and the option for single-point or uniform crossover.

Variation of nodal displacement at each load increment to be evaluated by FEA code is a function of IVD poroelastic properties (elastic modulus and permeability). In this problem, by using known values of displacement at the specific sensor sites, the error function was computed. This function (objective function to be minimized) was taken as the sum of the weighted errors at each load increment;

$$error = \sum_j \sum_i \left(w_i (u_i - u_{ei})^2 \right)_j$$

where $u_i = u_i(E_a, k_a, E_n, k_n)$ is the displacement field which is a function of poroelastic properties. E_a, k_a, E_n, k_n are elastic modulus and permeability of

annulus and nucleus respectively. Index i and j refer to nodal points at the sensor site and load increment during each step of loading. w is the weighting factor and u_{ie} is the experimental displacement data that was conducted using vertebral units obtained from tails of freshly slaughtered bovines (Race et al, 2000).
The parameter estimation process begins by incorporating some initial values for parameters using the GA technique, then performs an evolutionary search, and ends with final values of variables that minimize the error function.

RESULTS AND DISCUSSION

Figure 1 shows the axisymmetric FEA model of the IVD and Figure 2 presents the convergence history of the algorithm. The percent reduction in error estimator function during the computation was 80%. Final values of the poroelastic parameters are summarized in Table 1.

This study utilises the Evolutionary Algorithm technique to estimate the system characteristics such that the error between experimental data and model output is minimized. The numerical results indicate the effectiveness of the algorithm in estimating IVD characteristics. Following the considerable reduction in error estimator function (Figure 2) meaningful estimated poroelastic parameters were computed. In this kind of analysis there is always a compromise between the level of accuracy of estimation and the number of function calls (FEA runs), this being about 5000. This number is substantially greater than that required in classical optimisation techniques.

Further studies will be conducted using a 3-D model of the human spinal motion segment to obtain poroelastic parameter values. The effects of anisotropy and swelling should also be considered in order to determine more realistic characteristics.

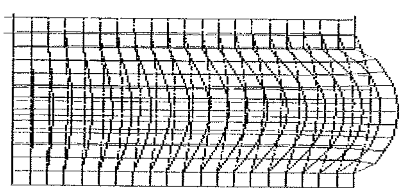

Figure 1: Deformed and Undeformed IVD mesh

Table 1: Estimation Results of Poroelastic Properties

Material	E (MPa)	k (m/s)
Nucleus	4.63	0.1E-10
Annulus	7.30	0.2E-11

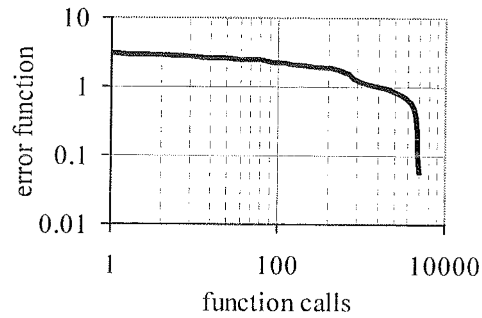

Figure 2: Convergence History

SUMMARY

An axisymmetric finite element model of the intervertebral disc of bovine tail was constructed and the load controlled experimental data of the same specimen was used. Two sets of poroelastic isotropic material properties for annulus and nucleus were determined by using the Genetic Algorithm technique to minimize the displacement error between the experimental data and the corresponding finite element results. Fairly meaningful values of elastic stiffness and permeability have been achieved after a considerable number of iterations.

REFERENCES

Carroll, D.L. (1997). *Univ.of Illinois, Mech.Eng.Dept., Urbana, IL, USA.*

Katoozian, H. (1999). *Proceedings of Int. Soc. Of Biomech.,* 846.

Martinez, J.B, Oloyede, V.O.A., Broom, N.D. (1997). *Med.Eng.Phys.*, **19**, 145-156.

Race, A., broom, N.D., Robertson, P. (2000): *SPINE*, in press.

Simon, B.R. et.al. (1985), *J.Biomech.Eng.*, **107**, 327-335.

ACKNOWLEDGEMENTS

The authors gratefully acknowledge the support of a project grant from the Health Research Council of New Zealand and the provision of computing facilities by the Department of Engineering Science, University of Auckland.

ESTIMATION OF THE FINITE CENTER OF ROTATION IN PLANAR MOVEMENTS

John H. Challis

Biomechanics Laboratory, The Pennsylvania State University, University Park, Pennsylvania
Email: jhc10@psu.edu

INTRODUCTION

Human movement is not generally two-dimensional in nature, despite this human movement is often analyzed in two-dimensions due to the relative simplicity of data collection, analysis, and interpretation in two-dimensions. The center of rotation for human joints in two-dimensions is a kinematic variable which is popular for the assessment of joint function. The center of rotation is normally represented by the finite center of rotation (FCR) which relates to a measure taken from a single finite displacement.

A number of different procedures have been advanced for the computation of the FCR. It was the purpose of this study to compare the accuracy of the procedure of Crisco et al. (1994) for estimating the FCR with a new procedure which uses least-squares principles.

METHOD

Two different procedures were used to compute the FCR, the procedures were,
Procedure A - the procedure of Crisco et al. (1994) who presented the formulae for determining the FCR for a rigid body undergoing a finite displacement.
Procedure B - this uses least-squares principles to determine rigid body attitude and position. The first step is to compute the mean position vectors,

$$\bar{x} = \frac{1}{n}\sum_{i=1}^{n} x_i \qquad \bar{y} = \frac{1}{n}\sum_{i=1}^{n} y_i$$

where x - position of a point measured on the body in a body fixed reference frame, y - position of the point measured in the inertial reference frame, and n is the number of points measured. The positions of the points are computed relative to the mean position vector

$$\hat{x}_i = x_i - \bar{x} \qquad \hat{y}_i = y_i - \bar{y}$$

The attitude angle (ϕ) of the body can then be estimated in a least-squares sense from

$$\phi = -tan^{-1}\left(P/Q\right)$$

Where $P = \sum_{i=1}^{n}\left(\hat{y}_{xi}\hat{x}_{yi} - \hat{y}_{yi}\hat{x}_{xi}\right)$,

$Q = \sum_{i=1}^{n}\left(\hat{y}_{xi}\hat{x}_{xi} + \hat{y}_{yi}\hat{x}_{yi}\right)$ and the subscripts x,y refer to the horizontal and vertical components of the vectors respectively. The position vector of the body v can be determined from the mean vectors

$$v = \bar{y} - [R(\phi)]\bar{x}$$

If the attitude and position are known at two instants (e.g. t_1, t_2), then it is possible to compute the FCR from

$$FCR = p + \left[2.tan\left(\tfrac{1}{2}\varphi\right)\right]^{-1}.\left[R\left(90^o\right)\right].\Delta v$$

Where $p = \frac{1}{2}\left(v(t_1) + v(t_2)\right)$, $\varphi = \phi(t_2) - \phi(t_1)$, $\left[R\left(90^o\right)\right]$ - matrix representing a 90° counter-clockwise rotation, and $\Delta v = v(t_2) - v(t_1)$.

Three different evaluations were made of the two procedures. In all cases the FCR had to be estimated, and was assumed to be the origin of the inertial reference system.

1) Two data points 60 mm apart aligned so that a line between them lies on the y axis, with the mid-point at the origin of the axis system. Noisy versions of these data points were rotated through angles from 4 to 24 degrees.

2) A set of similarly orientated data points but with the distance from the FCR to the mid-point of the pair varied from 0 to 180 mm, the rotation angle was fixed at 10 degrees.

3) Using the same data points as in evaluation 1, with a fixed rotation angle of 10 degrees, but with the standard deviation of the noise varying from 0.1 mm to 1.5 mm.

RESULTS

As the rotation angle was increased the accuracy in the estimation of the FCR increased for both procedures (figure 1).

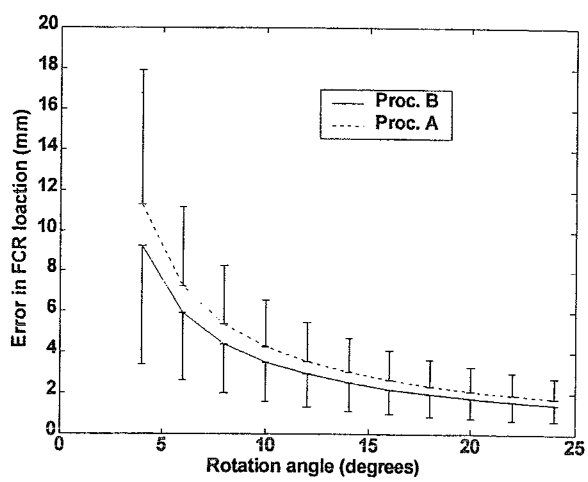

Figure 1 – Results for evaluation 1.

As the mean position of a pair of landmarks was moved further from the FCR the accuracy of its determination by both procedures decreased, with the better performance by procedure A. With increasing noise levels the accuracy with which the FCR was estimated decreased. Procedure A produced higher mean errors than procedure B (figure 2).

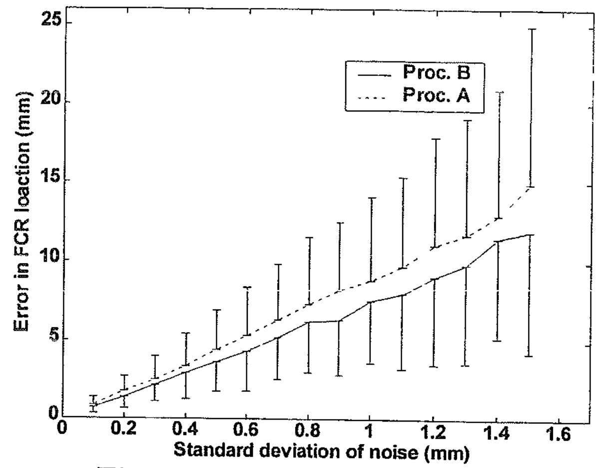

Figure 2 – Results for evaluation 3.

DISCUSSION

For the comparisons made of the two procedures, procedure B under all conditions was superior to procedure A, albeit by small amounts under certain conditions. Crisco et al. (1994) demonstrated that their procedure was more accurate than a number of available procedures (e.g. Reuleaux, 1875; Spiegelman. and Woo, 1987). Procedure B used least-squares principles to estimate the FCR, which removed some of the influence of noise in the position data, but could not account for all of it. Careful experimental protocols to reduce noise are important irrespective of which procedure is used.

REFERENCES

Crisco, J.J., et al. (1994) *J. Biom.* **27**, 1183-1187.

Reuleaux, F. (1875) *The Kinematics of Machinery: Outline of a Theory of Machines.* MacMillan, London.

Spiegelman, J.J. and Woo, S.L.Y. (1987) *J. Biom.* **20**, 715-721.

On Identifying Similarity and Difference of Bone Cement Mixing/Delivering Methods Using AE Techniques

Eng T. Ng and Gang Qi
Department of Mechanical Engineering, The University of Memphis, Memphis, TN 38152

Introduction: Hand mixing (HM) and vacuum mixing (VM) methods are the two major procedures in the practices of fixation of arthroplasties. VM method has been shown to be effective in reducing porosity generated in the mixing/delivering procedure[2,3] and therefore can significantly increase mechanical performance of bone cement. However, Hansen and Jensen[1] showed that the strength of Simplex brands and low-viscosity cements does not affected by VM methods. Moreover, Vila et. al.[4] found that the VM does not have significant effect on the fatigue crack propagation behavior of the cement. Apparently, the classical fracture mechanics approaches have limited capability to identify the mechanical behaviors between HM and VM methods. Therefore, the purpose of this paper is to introduce an approach which uses the acoustic emission (AE) technique to provide a view of various aspects of HM and VM and to distinguish the mechanical behaviors of them using Palacos R cement as an example. The hypotheses to be tested are: 1) the two mixing methods have similarity on the regression slope of crack growth rate; 2) the two methods exhibit difference between the features associated with non-material properties such as fabrication process and environment.

Materials and Methods: The Palacos R bone cement was used for this study. The cement blanks were made by both HM and VM methods and machined to standard compact tension specimens. Fatigue test were conducted in a servohyraudlic machine (Instron Model 8500) at a stress ratio R=0.1. The frequency used was from 2-10 Hz. The AE count growth rate, dn/dN, and the mode I stress intensity factor range, ΔK, were calculated based on AE counts, number of cycles, and specimen geometry empirically. The stress intensity factor range ΔK was given as:

$$\Delta K = \frac{\Delta P}{B\sqrt{W}} f(\alpha) \quad \ldots 1$$

where $f(\alpha)$ is the geometry factor . The AE count growth rate was plotted on the log-log based 10 scale as a function of ΔK. Then a linear regression was fit to the data to determine the coefficients of the relationship between the count growth rate and ΔK as shown below[2]:

$$\frac{dn}{dN} = \alpha(\Delta K)^{\beta} \quad \ldots 2$$

In the AE model, the parameters α and β are material constants and represents the slope β and intercept α of the above equation when the both side was plotted on a logarithmic scale. The crack propagation rate obtained from Paris Law is defined as below:

$$\frac{da}{dN} = \phi(\Delta K)^{\varphi} \quad \ldots 3$$

where ϕ and φ are material constants.

Results: The cumulative fatigue damage for maximum load of 180N for HM specimen is revealed by the integration of cumulative counts as shown in Fig. 1. As it can be seen, a short

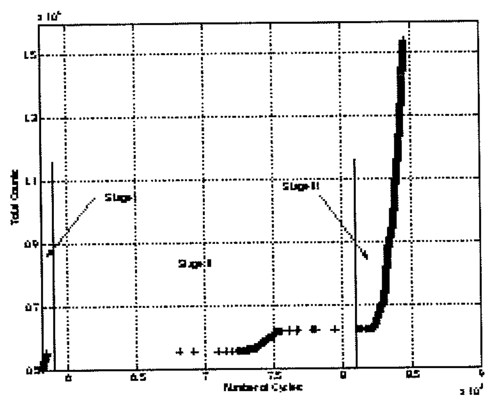

Figure 1. AE total counts at 180N for HM specimen during the fatigue.

period of high AE activities were followed by a stable prolong period. The rupture period was composed by a sudden exponential rise of AE counts. Similar trends for VM specimen at 180N was observed in Fig. 2. This figure revealed that the number of AE counts and the number of cycles to failure were much higher than those in HM specimen. The reason may be possible due to the presence of less microvoids in VM specimen as indicated in the existing publications[2,3]. Due to limitation space, the figures for maximum loads at 230N and 300N for VM specimens do not show in this paper.

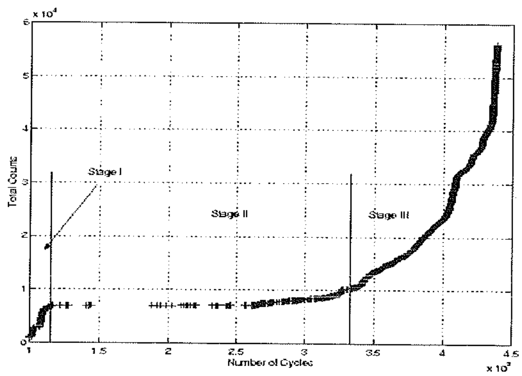

Figure 2. AE total counts at 180N for VM specimen during the fatigue.

The AE count growth rate, dn/dN, as a function of ΔK for each specimen at various loads was plotted in Fig. 3. In this figure, the top curve was the results of HM specimens whereas the bottom curve was the results of VM specimens. From this figure, it is noticed that the count rate in HM specimen was much higher than that of VM specimen. The coefficients of

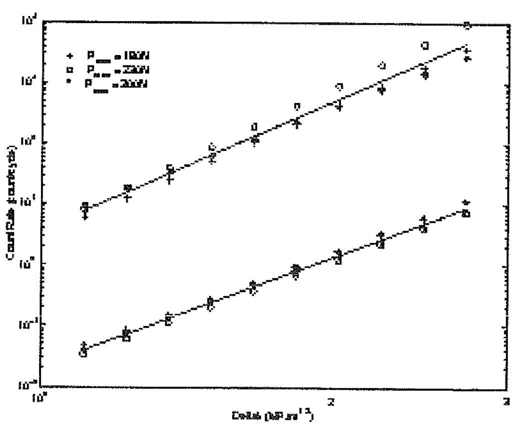

Figure 3 The total count rate data and associated regression line for bone cement.

AE model Eq. 2 were given in Table 1. From the table, it indicated that β is equal to $\varphi + 2$. A student t-test at 95% confidence with four degree of freedom is applied for comparative purpose. The results show that there was no significant difference between the count rate regression slope β for both specimens. This slope is a representative of material intrinsic property. This result shows consistency with that obtained by Villa[4]. However, there is a significant difference on the count rate regression intercept α between the two specimens. This intercept can be considered as an indicator of different fabrication process of the specimens. It is clearly shown that AE technique can distinguish the similarity and difference between HM and VM methods.

Table 1. Count Growth Rate Parameters.

Load (N)	HM Specimen		VM Specimen	
	β	α	β	α
180	7.0892	3.0092	5.6618	2.7×10^{-2}
230	7.8372	3.7558	6.0219	1.8×10^{-2}
300	6.3079	4.9530	6.3179	2.1×10^{-2}

Summary:

1. The similarity is a reflection of material property because both specimens were the same material. The results were statistically tested and show that there is no significant difference on count rate regression slope, β.
2. The difference is a reflection of fabrication process because different fabrication processes. The results show significant difference of α values between HM and VM specimens.
3. The correlation model between the acoustic emissions and ΔK was established.

References:

1. Hansen, D. and Jensen, J. (1992). *Acta Orthop Scand*, Vol.63, No.1, p13-18,
2. Lewis, G., (1999). *J. of Biomed. Mat. Res. (Appl. Biomat.)*, Vol.48, p143-149.
3. Vesnovsky, O., Topoleski, L.D. (1999). *Society For Biomaterials 25th Annual Meeting Trans.*, p.96.
4. Vila, M., et al. (1999). *J. of Biomed. Mat. Res. (Appl. Biomat.)*, Vol.48, p128-134.

COMPARISON OF ELECTROMAGNETIC TRACKING AND VIDEO MOTION ANALYSIS USING A DYNAMIC PENDULUM MOTION

K.J.McQuade[2], J. Parker[1], M. Rodgers [1,2]

[1]University of Maryland School of Medicine, Dept. of Physical Therapy,.[2]VA Maryland Health Care Center, Rehabilitation R&D, Baltimore, MD.
Email: kmcquade@som.umaryland.edu

Introduction

Electromagnetic tracking technology has become increasing popular in recent years (An et al 1988; Johnson and Anderson 1990; McQuade and Smidt 1998). In order to determine the performance of magnetic tracking compared to standard optical methods for motion analysis, it is important that measurements be made dynamically and be compared to some standard criteria. The purpose of this study was to develop a dynamic pendulum and record simultaneous pendulum motion with Ascension's Flock of Birds sensors and Motion Monitor software (Insport Inc. Chicago, Ill), and Peak Performance Motus video analysis system (Peak Performance Tech. Inc., Englewood, Co).

Methods

A pendulum was constructed (Figure 1) out of PCV pipe and acrylic. The axis of rotation of the pendulum was fixed to a 10K Ohm high precision rotary potentiometer (Spectrum +- 2% linearity). The potentiometer was excited with a 5 volt regulated power supply and calibrated with a static protractor through a range of 180 degrees in 10 degree increments. A machined plastic cube was mounted on the distal end of the pendulum to allow simultaneous mounting of up to four sensors in orthogonal orientations. The sensor cables were routed in a groove and up to the top of the pendulum. The entire apparatus was bolted to a wooden bench. An additional sensor was mounted to a fixed vertical reference bar. Round reflective markers (1.5cm diameter) were attached to the rod, and one reflective marker placed on the vertical reference bar.

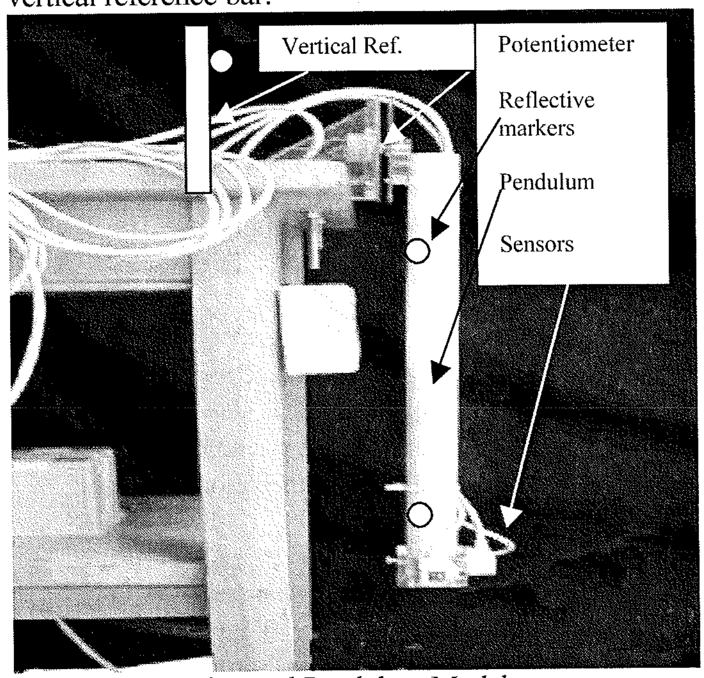

Figure 1: Experimental Pendulum Model.

The pendulum was lifted to approximately 90 degrees and dropped while recording simultaneous pendulum movements from the potentiometer, magnetic tracking sensors, and with 3 Peak cameras. The potentiometer signal was split and input into the A/D board used with motion monitor and the A/D board with Peak performance. All data acquisition was set to 60 hz.
The pendulum angular displacement was determined for all three measurement systems. Angles were zero offset adjusted for initial position.

Results and Discussion

Results are summarized in Figures 2-4. Figure 2 shows a comparison using raw unfiltered angular displacements.

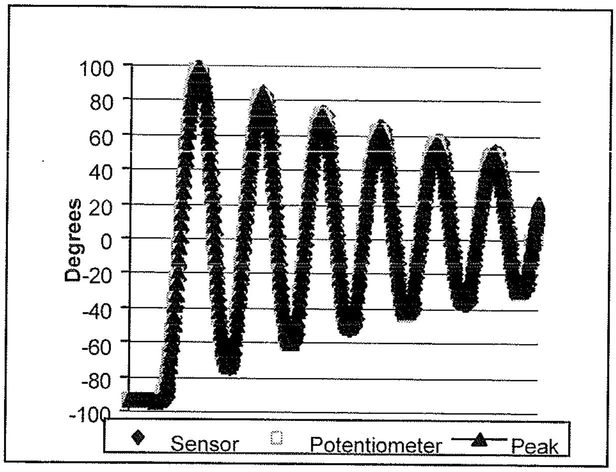

Figure 2 : Graph shows angular displacement comparisons for the potentiometer, the magnetic tracking sensor and the peak optical system.
The absolute angular differences of the magnetic tracker, the peak determined angles compared to the potentiometer angle varied as a function of the velocity of the pendulum.

The mean absolute angular deviation from the potentiometer was 5.9 degrees for Sensor and 1.47 degrees for the Peak system.

The segment length stability is presented in Figure 3. The magnetic sensors resulted in more stable segment length. The magnetic tracking sensor standard deviation 0.03 mm. The standard deviation of the peak sensor length was 6.33 mm.

All data comparisons were un-smoothed. Velocity calculations used the central differences formula for the Potentiometer and Peak, but were based Euler angles for the Magnetic tracking sensors.

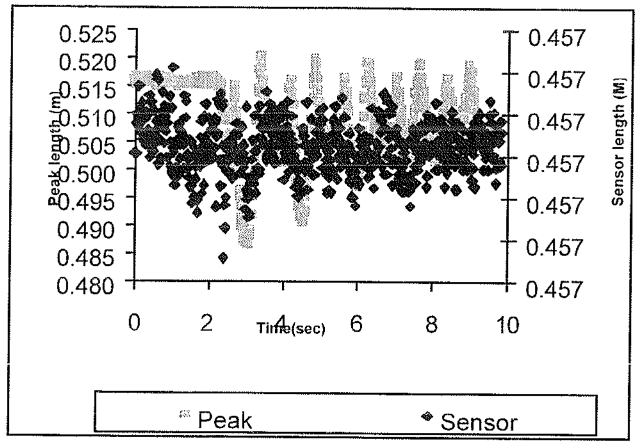

Figure 4: Variations in segment length throughout one pendulum swing cycle for optical and magnetic tracker system.

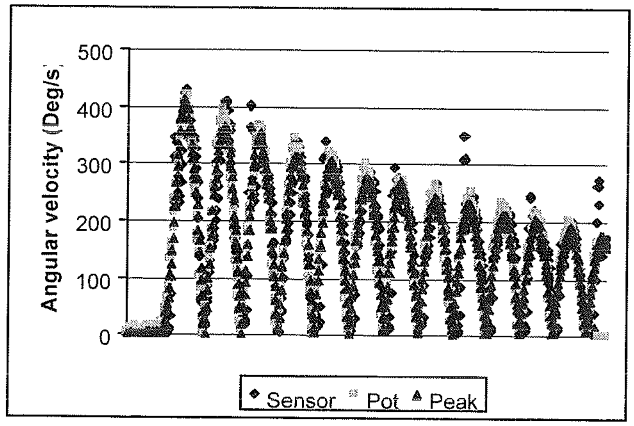

Figure 5: compares the Angular velocities determined by the potentiometer, Sensor and Optical recordings.

Summary
Pendulum dynamic motion provides a good dynamic model for comparing different measuring systems. while the sensor was more stable in segment lengths, it showed more variability in angular displacements and velocities

References

An KN, Jacobsen MC, Berglund LJ, Chao EYS (1988): *J. Biomechanics* 21:613-620.
Johnson GR, Anderson JM (1990):. *Clin. Biomechanics* 5:131-136.
McQuade K, Smidt G (1998): . *J. Orthop. and Sports Phys Ther* 27:125-133.

Acknowledgements

Veterans Affairs Rehab. R&D Merit Grant,B2168RA

A SIDE SUSPENSION DEVICE FOR SIMULATION OF LOCOMOTION IN MICRO-GRAVITY

[1,2]Marc M. Peterman, [1,3]Andrew J. Hamel, [1]David R. Lemmon,
[1,3]H. Joseph Sommer, III, and [1,2,4]Peter R. Cavanagh

[1]The Center for Locomotion Studies and the Departments of [2]Kinesiology; [3]Mechanical Engineering; [4]Biobehavioral Health, Medicine, Orthopaedics and Rehabilitation;
The Pennsylvania State University, University Park and Hershey, PA
Email: celos@psu.edu Web: www.celos.psu.edu

INTRODUCTION

A new micro-gravity simulator has been developed to allow minimally constrained locomotion in side suspension, where subject orientation is such that the gravity vector acts normal to the sagittal plane. Prior art consists of several supine and upright micro-gravity simulators (Davis and Cavanagh, 1993), and a side suspension system previously used for simulation of lunar gravity during the Apollo program (Hewes, 1969). The motivation for revisiting the side suspension configuration was to provide a ground-based means of verifying pitch axis performance of the NASA Treadmill Vibration Isolation and Stabilization system (TVIS) hardware for the International Space Station (ISS). Side suspension was required to align the pitch axis with the gravity vector, allowing gravity-free rotation about the pitch axis. The new side suspension device (SSD) may also prove useful in simulation of reduced gravity locomotion on Mars.

METHODS

The NASA TVIS system isolates the ISS exercise treadmill from the module superstructure, minimizing vibration transmission and providing stabilization of the active running surface in roll, pitch and yaw. During on-orbit verification testing on shuttle flight STS-81, a limit cycle pitch oscillation was observed under certain circumstances (McCrory, et al., 1999). Due to launch availability and cost constraints, a ground-based simulation was required to reproduce the pitch oscillation problem and explore stabilization solutions.

To approximate the on-orbit operational environment, both the TVIS system and subject were suspended in a sideways configuration from the ceiling of a tall test tower (Figure 1).

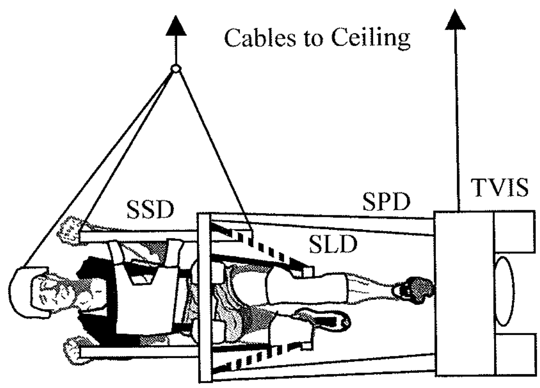

Fig. 1: Schematic of SSD supported runner and TVIS treadmill independently suspended from 30m cables.

The runner and treadmill were independently suspended from 30-meter cables to minimize pendulum effects of short suspension. Suspension of TVIS was straightforward; however, suspension of the runner required an elaborate harnessing and support system due to constraints imposed by the subject load devices (SLDs), subject positioning devices (SPDs), and lower limb motions. Also, the limb closest to the ground could not be supported from above because of interference with the motion of the other leg.

The primary design considerations for the SSD support system were subject comfort and realistic foot-fall on the treadmill belt. The latter constraint required unrestrained medial-lateral motion of the legs while simultaneously supporting the mass of the limb segments against the pull of gravity. This was accomplished using modified knee braces and zero free length springs (Streit, et al., 1993) incorporated into leg support struts. This system provided a constant supporting force over a limited range of operation in the coronal plane. A photo of the actual SSD and TVIS system is shown in Figure 2.

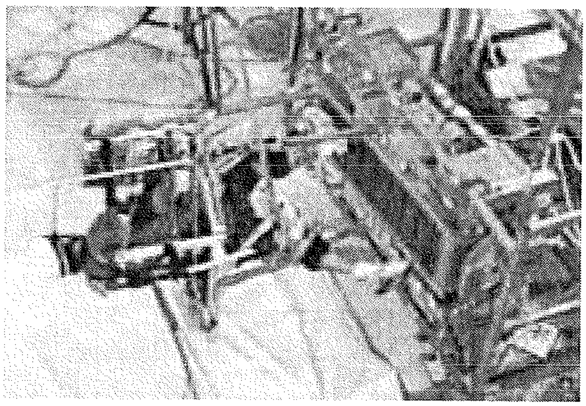

Fig. 2: Photo of SSD and TVIS testbed.

RESULTS

The SSD was delivered to the NASA subcontractor for TVIS (Wyle Laboratories, formerly Krug Life Sciences, Houston, TX) and was implemented as described above. The subcontractor successfully reproduced the STS-84 pitch oscillation problem and imposed corrective design changes to the TVIS in the form of SPDs. The SSD was then used to verify the efficacy of the SPD design iteration. A range of male and female subjects from Wyle and the astronaut corps participated in the TVIS testing and provided positive feedback.

Additional running data were gathered at the Center for Locomotion Studies (CELOS) to compare hip, knee, and ankle kinematics, and ground reaction forces to those collected using the CELOS supine micro-gravity simulator (McCrory, et al., 1999) and data from over-ground running.

DISCUSSSION

The current SSD design represents a considerable improvement over side suspension simulations conducted in the 1960s. In the current design, realistic running speeds are attainable with minimal discomfort from the supporting constraints. It has been observed, however, that running in the SSD and other simulators can be exhausting because, without the aid of gravity, additional effort is required during the swing phase. Additionally, the use of the SLDs and harnessing system can be tiring (McCrory, et al., 1999).

CONCLUSION

The device presented here represents a new approach to the simulation of micro-gravity locomotion. Running in an attitude where the body sagittal plane is perpendicular to the gravity vector is possible in a device which supports the lower limbs against gravity.

REFERENCES

Davis, B.L., Cavanagh, P.R. (1993) *Aviation, Space, and Environmental Medicine*, 64(6): 557-566.

Hewes, D.E. (1969) *Human Factors*, 11(5): 419-432.

McCrory, et.al. (1999) *Journal of Applied Biomechanics*, 15: 292-302.

Streit, D.A., Casalena, J., Paik, J. (1993) *Applied Mechanisms and Robotics Conference* AMR-93-016.

ACKNOWLEDGEMENTS

This work was supported by NASA contract 9-97029/D0-C9 through Wyle Laboratories (formerly Krug Life Science).

INFLUENCE OF ANTHROPOMETRIC MEASURES ON COP-BASED PARAMETERS OF BODY SWAY

Lorenzo Chiari, Laura Rocchi, Davide Lenzi, Angelo Cappello

Department of Electronics, Computer Science and Systems, University of Bologna, Italy
Email: lchiari@deis.unibo.it **Web: www-bio.deis.unibo.it**

INTRODUCTION

Nowadays measures of postural ability by dynamometric platform are very common in clinical practice. By this technique it is possible to calculate the displacement of the COP (Centre of Pressure, i.e. the application point of the foot-to-ground reaction force) during experiments with a variety of different set-ups. Several measures were proposed in literature for describing the COP motion. They can be either summary statistic scores directly computed from COP time-series *[1]* or new stochastic parameters recently proposed in literature *[2], [3]*.
The aim of our study is to investigate the influence of the main anthropometric measures on all such parameters during quiet standing.

METHODS

In this preliminary experimental session we considered data from 17 subjects (9 male and 8 female), aged 21-29 years (23.7 ± std 2.68). Normal-bodied subjects were selected in order to cover a sufficiently wide range of anthropometric properties (see Table below).

measure	*mean*	*std*	*range*
Weight (kg)	64.8	16.6	44.7-99.8
Stature (cm)	169.8	10.5	151-188
Trunk-height (cm)	50.8	4.3	43-58

Each subject was requested to stand on the dynamometric platform in a stationary upright stance, in the most comfortable way with free foot placement. Subjects were instructed to look at a small circular target (∅=3 cm), placed at eye height, about 1.5 m from the platform. Romberg test was performed, i.e. trials were carried out with both eyes open (*EO*) and eyes closed (*EC*).

Each experimental session was composed of four tests, two *EO* and two *EC*. During posturographic recordings, each consisting of a 50 s acquisition, COP coordinates were measured by a multi-component strain gage force platform (Bertec Corporation) and sampled at a frequency of 20 Hz. The list of measures and parameters follows.
Anthropometric measures (AM): 1) weight 2) stature 3) legs length (malleolus –greater trochanter) 4) trunk length (shoulder-greater trochanter) 5) chest circumference 6) waist circumference 7) hip circumference.
Foot placement measures (FPM): measured by footprint. For description see figure below.

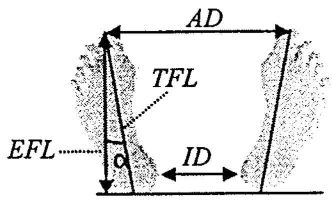

$$BOS = \frac{(AD+ID)\cdot EFL}{2}$$

$$\cos\alpha = \frac{EFL}{TFL}$$

COP-based parameters (CP): 1) summary statistic scores (*mdist, rdist, totex, range, mvelo, area_cc, area_ce, area_sw, mfreq, fd, fd_cc, fd_ce, prd, rd, f50, f95, cfreq, freqd*) *[1]*. 2) stochastic parameters adapted from Collins *et al.* (H_s, K_s, H_l, K_l) *[4]*. 3) sigmoid stochastic parameters (K, Δt_c) *[3]*.
The parameters were calculated from the bidimensional and one-dimensional time-series (Anterior-Posterior and Medial-Lateral COP displacement).
The first step was to look for the monotonic association between each possible couple of variables in terms of ranks (Spearman-rank correlation analysis). Afterwards, we tried to establish linear relationships among the *AM* and *FPM*, considered as independent variables, and all the *CP*, considered as dependent variables. In order to do that, a multiple linear regression model was used.

RESULTS AND DISCUSSION

First, only two independent measures into the anthropometric set are put in light. On the basis of a 0.8 threshold for r, stature and trunk length are considered uncorrelated. Actually it is not completely clear why the trunk length is poorly correlated with total height (r=0.68, p=0.02), but this could be investigated only with a greater population. It is verified that BOS and cos(α) are not correlated, either. Moreover none of the *CP* is significantly correlated with each of the *AM* and *FPM*. For this reason the multiple regression analysis is applied to test the dependence of any *CP* on subject characteristics. We consider that a multiple linear correlation exists when the squared correlation value is higher than 0.95. Overall results are shown in Table1. The parameters listed are those for which a multiple linear correlation is significant.
In this case, the joint use of stature and trunk length establishes several relationships with *CP*. This can lead to think that a two-segment model (hinged at the hip joint) can somehow describe and predict better than the one-segment model (total height) some instances of the postural behaviour of the body during upright stance. No significant differences are noticed between the *EO* and *EC* experiments. All the parameters correlated with the *AM* are correlated with the *FPM*, but not viceversa. In particular, *cfreq-ML* and *range-AP* and *planar* are correlated only with the *FPM*. This is an important point because it suggests that foot position can hardly influence the results of postural experiments if they are quantified by the *range* values, as it often happens.

SUMMARY

The present preliminary results show that some care should be taken, in perspective, when quantifying postural sway through *CP*, in order to address the dependence, that here comes to light, with *AM* and *FPM*. For this reason the choice of a standardized foot placement and the measurement of the main anthropometric features could help in data interpretation and comparison among different subjects. Moreover, the regression equations identified for 10 out of 18 summary statistics and 3 out of 6 stochastic parameters might become informative about what we actually measure by these parameters. Nevertheless, it is remarkable that the stochastic parameters proposed in *[3]* are unaffected by either *AM* and *FPM*.

REFERENCES

[1] Prieto, T.E. et al. (1996). *IEEE Trans. Biomed. Eng.* **43**, 956-966.
[2] Collins, J.J., De Luca, C.J. (1993). *Exp. Brain. Res.* **95**, 308-318.
[3] Chiari, L. et al. (1998). *Proc. Sat. 28th Meet. Soc. Neurosci.*, 33-34.
[4] Chiari, L. et al. (2000). *Gait & Posture* (accepted).

Table 1: Significant results obtained through multiple linear regression

Dependent parameter (R^2>0.95)	Components			Conditions		*AM* (stature, trunk length)	*FPM* (BOS, cos(α))
	Planar	*AP*	*ML*	*EO*	*EC*		
totex	✓	✓		✓	✓	*YES*	*YES*
mvelo	✓	✓		✓	✓	*YES*	*YES*
f50	✓	✓		✓	✓	*YES*	*YES*
f95	✓	✓	✓	✓	✓	*YES*	*YES*
freqd	✓	✓	✓	✓	✓	*YES*	*YES*
cfreq	✓	✓		✓	✓	*YES*	*YES*
cfreq			✓	✓	✓	NO	*YES*
fd	✓			✓	✓	*YES*	*YES*
fd cc	✓			✓	✓	*YES*	*YES*
fd ce	✓			✓	✓	*YES*	*YES*
range	✓	✓		✓		NO	*YES*
H_s	✓			✓	✓	*YES*	*YES*
K_s	✓			✓	✓	*YES*	*YES*
K_l	✓				✓	*YES*	*YES*

DYNAMIC BALANCE IN CHILDREN OF DIFFERENT DEVELOPEMENTAL LEVELS DURING REACHING TASKS

Jefferson W. Streepey and Rosa M. Angulo-Kinzler

Department of Movement Science, University of Michigan, Ann Arbor, MI 48109
Email:jstreepy@umich.edu

INTRODUCTION

The development of postural stability in children is critical for being able to engage and explore their surrounding environment. Previous studies have indicated a transition period between the ages of 6 and 10 years in which children begin to exhibit adult balance performance (Forssberg and Nashner, 1982; Shumway-Cook and Woollacott, 1985). These studies, however, have failed to fully explore the extent to which task demands can influence balance control .

The purpose of this study was to compare differences in the center of pressure (COP) excursions of two different age groups of children (4-5 yrs and 10-11 yrs) and adults during self-generated reaching movements in different directions and to different extents. It was hypothesized that by increasing the demands of the task older children would not necessarily exhibit balance control similar to adults. In addition, an interplay between balance control, task, and age would be observed.

PROCEDURES

Eighteen subjects (5 adult, 9 older children and 4 younger children) were asked to stand on a force plate while reaching in different directions (forward, mid-way, and to the side) toward a target placed at different distances (arm's length and maximum reach distance) from the subject. Reflective markers were placed on the right lateral malleolus and the third MCP joint of the right hand. Kinematic data were collected at 60 Hz and lowpass filtered at 3.4 Hz while force data were collected at 600 Hz and lowpass filtered at 7.4 Hz.

COP data were derived from the force plate, and the resultant COP was used to determine reach onset and offset. The first 300 ms prior to reach onset were averaged to calculate $UCOP_{ix}$. The onset and offset points were used to define the direction of the COP excursion. The coordinate system was then rotated to fit the COP direction as the x-axis. COP_x excursion was the distance between reach onset and offset along the transformed x-axis. COP_y excursion occurred perpendicularly to COP_x. Two measures of the base of support (BOS) were used to normalize COP_x and COP_y. Average COP_y amplitude was measured as the mean of peak-to-peak differences in COP_y from reach onset to offset. Reach distance was the difference, normalized by body height, between the third MCP marker and the ankle in the horizontal plane. COP_{ix}, the initial COP_x position in the rotated reference system, was determined again by averaging the first 300 ms of COP_x.

RESULTS

Adults, older, and younger children all differed in $UCOP_{ix}$ (0.45 ± 0.05, 0.39 ± 0.06, and 0.25 ± 0.09 respectively) for the forward arm's length reach. As the task requirements became more difficult older children and young children showed no difference in $UCOP_{ix}$. Adult $UCOP_{ix}$ continued to be higher than those of the young children, but, for reaches to the side, their $UCOP_{ix}$ was similar to that of the older children. When correcting for COP direction, significant differences in COP_{ix} existed between all three groups for all reaching tasks except for the maximum mid-way and side reaches in which adults and older children had greater COP_{ix} than the younger children.

COP_x excursions in young children were significantly higher than in the other two groups for the maximum mid-way reach (0.46 ± 0.15 versus 0.22 ± 0.10 and $0.24 \pm$

0.11 respectively). Average COP_y amplitude was similar among adults, older children and young children for all but two conditions. Young children had a higher average COP_y amplitude than the adults or the old children in the arm's length reach to the side. Adults showed significantly lower average COP_y amplitude than older and young children for the maximum forward reach.

Among the arm's length reaches, significant differences in reach distance were found only for the side reach between the adults (0.40 ± 0.09) and the older children (0.33 ± 0.07), though the young children (0.36 ± 0.17) were no different from either group. For the maximum reaches, adult reach distance was greater than either the young or older children for all directions but the forward reach where adults and young children reached similar distances (0.62± 0.06 and 0.60 ± 0.15).

DISCUSSION

Distinctions in $UCOP_{ix}$ between the three groups became less clear as the task difficulty increased. Older children and younger children differed only for the forward arm's length reach. Adults remained closer to the anterior edge of the BOS than the older and younger children but did not differ from either group for the side reaches. It is possible that this lack of group differences resulted from an anticipation of the task to be performed. A rotation of the initial COP by the direction of the COP excursion was used to control for this anticipation This correction produced distinct initial positions for each of the three groups for the majority of the tasks. Still, for the maximum midway and side reaches adult and older child exhibited similar COP_{ix}.

Although analysis of endpoint COP excursion did little to provide insight into balance control, examination of the average COP_y amplitude occurring between reach onset and offset suggested an interplay between task and group. The magnitude of the average COP_y may depend on both, difficulty of the task and age (i.e. the subject's experience performing the task) (Fig. 1). Reach distances also suggest an interplay between task difficulty and subject experience so that more experienced adults reach farther under the more difficult conditions despite having an average COP_y amplitude of the same magnitude as the other two groups.

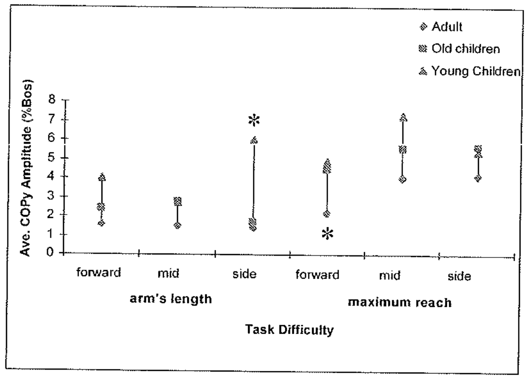

Fig 1. Average COP_y amplitudes were similar for all groups for the arm's length forward and midway reach. As the reaches became more difficult, the more experienced groups maintained a lower average COP_y amplitude until the tasks reached a level where all three groups were relatively inexperienced in performing the task. Asterisks denote significantly differences (p.<0.05).

REFERENCES

Forssberg, H., Nashner, L. (1982). *J. Neuroscience*, 2, 545-552.

Shumway-Cook, A., Wollacott, M.H. (1985). *J. Motor Behavior*, 17, 131-147.

SYNERGISTIC CONTROL OF POSTURAL AND FOCAL JOINTS IN GOAL-DIRECTED ARM MOVEMENTS WHEN UNCERTAINTY ON TARGET LOCATION

O. Martin[1], N. Teasdale[2], M. Simoneau[2], P. Corbeil[2] (Email: omartin@u-bourgogne.fr)
[1]Université de Bourgogne, UFRSTAPS, 21000 Dijon, France
[2] Université Laval, Faculté de Médecine, Division Kinésiologie, Québec, Canada G1K 7P4

INTRODUCTION

Voluntary focal movements are performed with postural anticipatory responses generated by the central nervous system in a feedforward manner and serve to prevent an upcoming mechanical perturbation resulting from the movement itself. For tasks in which the subject from an upright standing position has to point to a target with uncertainty on its final location, postural adjustments are integrated into the pointing responses. Little is known, however, as to how these postural and focal compensations during pointing are coordinated at joint level (i.e. elbow and hip).

To examine these joints interactions when there is an uncertainty on target location, a visual double-step perturbation requiring a reprogramming of the arm movement was introduced randomly. Trials directed towards the same spatial goal but differentiated only by the likeliness of a visual perturbation were compared.

METHODS

Seven volunteers aged 24 to 36 (all males and right-handed) participated on a voluntary basis. In the initial position, the right hand was in contact with the lower extremity of the sternum. The task required pointing with the right hand to one of two targets (LEDs) positioned along the sagittal axis. The two targets were 20 cm apart, 10 cm ahead and 10 cm beyond a distance corresponding to the length of the right arm extended in a pointing position (respectively within and beyond prehension space conditions). In the control condition (without uncertainty; n=20 trials), after a ready signal, one of the two targets was light up and the subject had to point as fast and as accurately as possible to the target. In a step-target condition (n=80 trials), a visual perturbation occurred randomly in 33% of the trials at hand movement onset, turning off the initial target and simultaneously lighting up the other one.

The elbow and hip joint angles for arm and postural movements analysis were obtained from a Selspot II system. Markers were placed on the right ankle, knee, both hips and shoulders, elbow, index and ear lobe. A two-way anova with repeated-measures factors (2 targets x 2 uncertainties) was used.

RESULTS AND DISCUSSION

The analyses focused on the specific effects of step-target uncertainty examined by comparing trials in the control condition (without uncertainty) vs. non-perturbed trials in the step-target condition (with uncertainty condition) for both targets, within and beyond prehension space.

Interaction between movement and posture at joint level.

The stick diagrams in Figure 1 show that the initial position before movement onset was not different across conditions. During arm movement, the forward bending of the trunk increases with uncertainty (right panels), particularly for movement beyond the prehension space (bottom panels).

The analysis of angles vs. time (Figures 2) shows that with uncertainty the hip angle decreases significantly from 200ms after pointing onset (near hand peak velocity) for both targets ($p<.008$) when elbow angle is

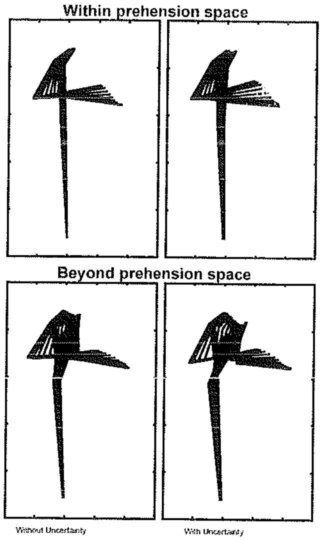

Figure 1: stick figures (sagittal plane) for one representative subject without and with uncertainty to targets located within and beyond the prehension space.

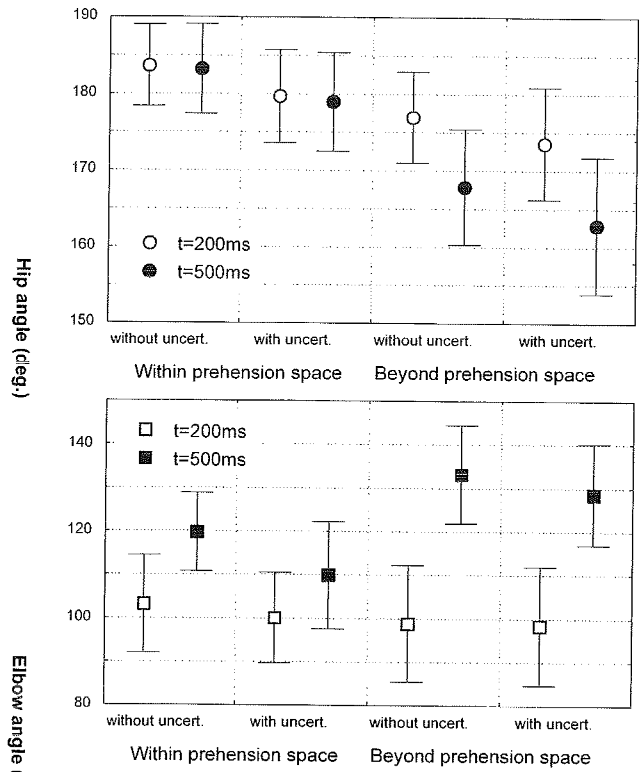

Figure 2. Mean value of the angles of elbow joint (top panel) and hip joint (bottom panel) calculated 200ms and 500ms after arm movement onset, within and beyond the prehension space (left and right frames respectively) in condition without and with uncertainty.

not yet modified at this time. On the other hand, at 500ms after pointing onset, corresponding to the end of the pointing movement, both elbow and hip angle have decrease significantly with uncertainty ($p<.001$ and $p<.016$ respectively).
These results indicate that uncertainty trials were characterized by a hip angle adaptation, which precedes changes observed at elbow level. After that, in the final part of the pointing, postural and focal commands seems to be closely synchronized and juxtaposed to reach the target. This modification of the temporal phasing of the hip and elbow joint activities indicates that posture precedes movement to integrate first the contextual uncertainty. The change observed in course of pointing, from the sequential adjustment of both joints to their parallel regulation in this specific "joint system", could allow a more effective multi-joint compensation by dissociating the control of multiple degrees of liberty for a while, when environmental constraints impose complex additional programming. Therefore, our results suggests that in condition of movement uncertainty, upright standing posture and goal-directed arm movement modify the joint control process when information is incomplete to program movements. The subsequent constraints require the dynamic adjustments of the joint angular coordinates, in a synergistic way, to allow an on-line interaction between movement and posture in critical situation.

SUMMARY

The effect of a likely perturbation regarding hand pointing upon the coordination between posture and movement suggests that with uncertainty, posture and movement modify synergically their specific joint control strategies.

REFERENCES

Massion J. (1992) Prog Neurobiol, **38**, 35-56
Martin O. et al. Neurosci Lett **281**, 53-56.
Acknowledgments. Study supported by NSERC-Canada, and FCAR-Québec.

INFLUENCE OF LOWER EXTREMITY STRENGTH ON THE OUTCOME OF AN INDUCED TRIP IN HEALTHY OLDER ADULTS

Michael J. Pavol[1,2], Tammy M. Owings[1], and Mark D. Grabiner[1]
[1]Dept. of Biomedical Engineering, Cleveland Clinic Foundation, Cleveland, Ohio
[2]Programs in Physical Therapy, Northwestern University Medical School, Chicago, Illinois
Email: m-pavol@nwu.edu

INTRODUCTION

Aging is associated with an increased incidence of falling and a decrease in lower extremity strength and power. The question arises whether the increased falling by older adults is due to decreased strength or power. We reported on 79 healthy older adults who were safely tripped during gait (Pavol et al., 1999a,b). Three groups of fallers emerged from the 9 falls and 39 recoveries recorded. Fallers employing a lowering strategy of the tripped foot included five "during-step" and three "after-step" fallers, who "fell" prior to and after recovery step ground contact, respectively. One "elevating" faller used an elevating strategy of the tripped foot. This study investigated whether lower extremity weakness contributed to these falls.

METHODS

Ankle, knee, and hip flexion and extension strength were measured in 79 older adults in whom trips were induced. Isometric strength was measured through a maximum voluntary exertion (MVE) at 3-4 joint angles. Concentric and eccentric isokinetic strength at 30°/s were each measured by two MVEs. Subjects were to generate their maximum moment as rapidly as possible, then exert maximally until told to relax. Arms were kept folded on the chest. Practice, verbal encouragement, and rest were provided. Ankle and hip strength were measured while supine, knee strength while seated. Joints were tested a week apart.

Active joint moments were computed from the strength data, compensating for inertial artifacts and the measured passive joint moments. Isometric active moments were standardized to a reference joint angle using the measured, population-average, moment-angle relationships. The mean of the two largest standardized moments defined isometric strength. Isokinetic strength was quantified by the maximum active moment generated at the midrange of the tested range of motion. Rates of moment increase were averaged over periods of 100 ms (150 ms at the hip). The maximum rate of increase was represented by the mean of the two largest values from separate MVEs. Measures were normalized to body weight times height.

The strength measures were subjected to a factor analysis, using principal component analysis for factor extraction and an oblique factor rotation. Factor scores, computed by the regression method, were compared between each group of fallers and those who recovered using a similar strategy. Mann-Whitney tests were used for the during- and after-step fallers (α=.05). One-sample t tests were used for the elevating faller (α=.002).

RESULTS AND DISCUSSION

Strength differed greatly between subjects, with coefficients of variation in isometric strength of 21-31%. Seven factors were identified, explaining 88.2% of the variance in measured strength. Unique factors were associated with strength in each of flexion and extension at the ankle (DF, PF), knee (KF, KE), and hip (HF, HE). A final factor (ROI) was associated with high rates of moment increase. Overall extension strength was quantified as the sum of factors PF, KE, and HE, overall flexion strength as the sum of factors DF, KF, and HF, and total strength as the sum of all seven factors. Scores for these derived factors were standardized to a mean of 0 and standard deviation of 1.

The during-step and elevating fallers were significantly stronger in several strength factors than were those who recovered (Table 1). Similar trends were seen in almost every factor. While a surprising result, increased strength in older adults has been related to increased walking speeds and a faster walking speed was identified as a primary contributor to the during-step and elevating falls (Pavol et al., 1999b).

The strength of the after-step fallers and those who recovered did not differ (Table 1). Nevertheless, except for factor PF, the after-step fallers' strength averaged 0.41 standard deviations below the mean of those who recovered. Total strength scores for the after-step fallers were in the 3rd, 16th, and 53rd percentiles. Also of note, the strength demands on the after-step fallers were likely among the highest, as they exhibited a lower hip height, more inclined trunk, and more forward-rotating center of mass at recovery step ground contact (Pavol et al., 1999a). As a result, the below-average strength of the after-step fallers may have been insufficient to effect a recovery. This conclusion is supported by the buckling observed in the fallers' recovery limb.

Thus, the strongest and the weakest older adults may be at greater risk of falling from a trip, although due to different mechanisms.

REFERENCES

Pavol, M.J., et al. (1999a). *Proc. of 23rd Annual Meeting of the ASB*. 238-239.

Pavol, M.J., et al. (1999b). *Proc. of 23rd Annual Meeting of the ASB*. 240-241.

ACKNOWLEDGMENTS

Funded by NIH-R01AG10557 (MDG).

Factor	Lowering Strategy			Elevating Strategy	
	Recovery (n = 19)	During-Step Fall (n = 5)	After-Step Fall (n = 3)	Recovery (n = 10)	Fall (n = 1)
DF	-.20 ± 1.17	-.14 ± 1.16	-.39 ± .81	.42 ± 1.23	-.49
PF	-.36 ± .83	.91 ± .69 *	-.22 ± 1.46	.36 ± 1.14	2.43 †
KF	-.31 ± .81	.60 ± .64 *	-.57 ± .27	.48 ± 1.06	.08
KE	-.09 ± 1.26	.39 ± .63	-.82 ± .91	.35 ± .63	.89
HF	-.40 ± 1.07	.28 ± .57	-.77 ± .76	.50 ± .91	1.19
HE	-.34 ± .90	.30 ± .90	-.72 ± .52	.40 ± 1.09	1.18
ROI	.02 ± .92	-.37 ± .58	-.46 ± 1.02	.20 ± 1.34	1.07
Extension	-.35 ± 1.06	.70 ± .44 *	-.76 ± .83	.48 ± 1.04	1.96 †
Flexion	-.38 ± 1.03	.31 ± .51	-.73 ± .57	.59 ± 1.12	.33
Total	-.36 ± 1.07	.42 ± .43	-.84 ± .79	.58 ± 1.10	1.36

Table 1: Comparison of strength scores (* $p<.05$, † $p<.002$ *vs.* corresponding Recovery group)

THE ROLE OF INITIAL CONDITIONS IN THE POSTURAL SWAY RESPONSE TO GALVANIC VESTIBULAR STIMULATION

L. Daniel Latt and Mark S. Redfern

Department of Bioengineering, University of Pittsburgh, Pittsburgh, PA
Email: lattld@msx.upmc.edu Web: balance.eei.upmc.edu

INTRODUCTION

The galvanic (electrical) vestibular stimulus (GVS) elicits postural sway in human subjects during stance. The stimulus is created by applying current to electrodes overlying the skin of the mastoid processes behind the ears. The current creates a small-localized electric field that alters the resting potential of the vestibular nerve. If the anode is placed at one mastoid and the cathode at the other (binaural – bipolar configuration), postural sway will be elicited in the frontal plane towards the anode (Redfern, 1994). The sway response is typically quantified by measuring either the displacement of the head or the center of pressure (COP).

The postural sway response to GVS has been used for many years to study the role of the vestibular system in postural control. The potential applications of this technique in the clinic diagnosis of vestibular system dysfunction are many (Cass, 1996). Unfortunately, the large between-trial variability in the responses has necessitated the collection of a large number of trials and has subsequently precluded its widespread clinical use. One of the potential sources of variability in the response is the postural initial condition. The goal of this study was to determine the effect of the initial conditions, initial position (IP) and initial velocity (IV), on the postural sway responses measured at the head and the center of pressure (COP).

METHODS

The subjects were 10 normal healthy young adults ages 22 to 31 years with no known history of otological disease. The stimulus consisted of a binaural-bipolar pulse of amplitude 0.5 mA and duration 5 sec. The displacement of the head was recorded by a magnetic position tracking system (Flock of Birds, Ascension Technologies). The displacement of the COP was calculated from the forces and moments that were obtained from a force plate (Bertech Corporation model 4060A). Each trial consisted of a random duration pre-stimulus period of up to 60 seconds, the 5 seconds of stimulation, and then a 5-second post-stimulus period. Each of the stimuli was presented 15 times as three sets of five stimuli. A quiet stance trial of 30 seconds was recorded before each set to determine the baseline position and velocity.

The IP and IV of the head and the COP were normalized using the baseline position and velocity for each experimental set to allow averaging across sets and subjects. The IP of each segment was calculated as the mean position during the one-second period preceding stimulus onset. This value was divided by the standard deviation of its corresponding baseline to obtain a normalized IP. Similarly, the normalized IV was calculated as the mean velocity during the one-second preceding the onset of the stimulus divided by the standard deviation of the baseline velocity. The distributions of IP and IV were broken into three groups by percentile, negative = 0% - 33%, low = 34% -66%, and positive = 67% - 100%. Each trial was assigned to an IP group and to an IV group.

RESULTS AND DISCUSSION

The ensemble-averaged displacements of the head and the COP are shown in Figure 1. The anticipated response is a rapid deviation of both the head and the COP to the left following the onset of the stimulus and a rightward deviation back to center following the termination of the stimulus. This response is seen in the displacement of the head at all three initial positions. However, it is apparent in this figure that the head displacement that is elicited by the stimulus (change in displacement during the trial) is much smaller than the displacements that occur spontaneously (the distance between the three curves before stimulus onset). The displacement response of the head following both positive and negative IV is larger than the responses elicited with zero IV.

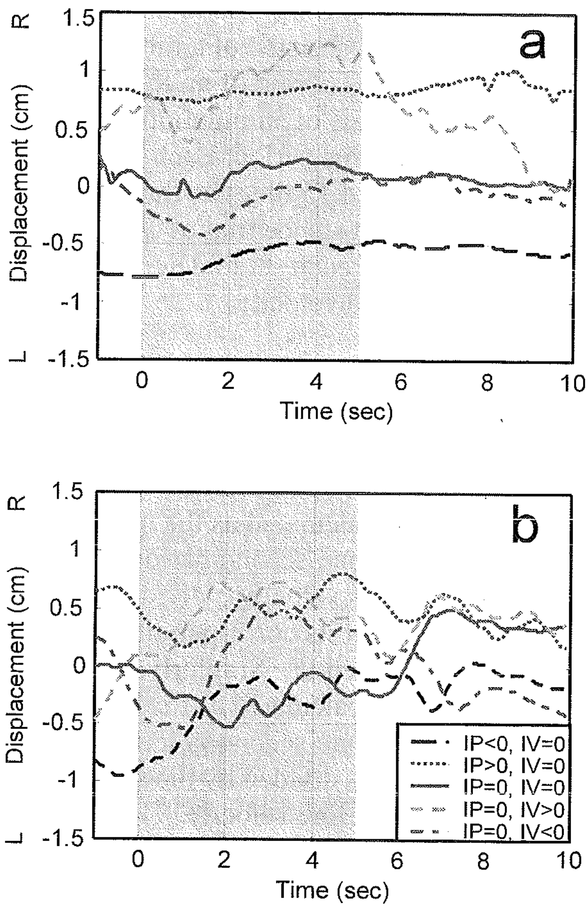

Figure 1: Ensemble-averaged displacements of the head (a) and the COP (b). The period during the stimulus is shown in gray. Each curve shows the response following one set of initial conditions.

The displacement of the COP shows results similar to that found for the head. There are responses in the initial position condition conditions, but they are difficult to interpret because the responses are either small relative to the initial displacement or the response appears to be in the wrong direction, or there is not an appropriate termination response. In contrast, both the positive and negative initial velocity conditions of COP displacement show large responses in the expected direction.

Both the displacements of the head and the COP were parameterized by calculating the peak magnitude of the response during the stimulus period. A multi-factorial ANOVA was used to determine significant sources of variation in the peak magnitude. Both IP and IV were found to have significant effects on the peak magnitude of the response. A post-hoc analysis revealed that when a subject assumed an initial position in the direction of the anticipated response, the subsequent response was substantially decreased. Initial positions centered over the base of support and opposite the direction of the anticipated response permitted, but did not enhance, the subsequent response. The effect of increasing the initial velocity was to increase the magnitude of the response, regardless of the direction of the initial velocity.

The implications of these findings for the use of GVS in the clinical diagnosis of vestibular disorders are: (1) the initial position and velocity should be recorded. These quantities can then help guide the interpretation of the response. (2) The number of trials necessary to obtain consistent responses can be greatly reduced by eliminating the postural initial conditions as a source of variability.

REFERENCES

Cass SP, Redfern MS, Furman JM, DiPasquale JJ. *Galvanic-induced postural movements as a test of vestibular function in humans.* Laryngoscope 1996; 106(4):423-30.

Redfern MS, Nicholas SC. *Kinematic response to galvanic stimulation in man.* Taguchi K , Igarashi M , Mori S , editors. Proceedings of the 12th International Symposium on Posture and Gait, Matsumoto, Japan, 1994.

INITIAL CENTER OF MASS STATE DOES NOT DETERMINE THE OUTCOME OF A NOVEL SLIP INDUCED DURING A SIT-TO-STAND

Michael J. Pavol, Eileen F. Runtz, Yi-Chung Pai

Programs in Physical Therapy, Northwestern University Medical School, Chicago, Illinois
Email: m-pavol@nwu.edu

INTRODUCTION

Slips are a major cause of falls and fall-related injury. The incidence of these falls may potentially be reduced through training an individual's response to a slip. One proposed training protocol involves inducing a slip during a sit-to-stand movement (Pai, 1999). The ability to recover from such sit-to-stand slips was found to increase with repeated exposure. It is probable that this increase in the ability to recover was accompanied by an alteration in body state at the time of slip initiation. This study tested the hypothesis that the balance recovery outcome of a novel slip during a sit-to-stand is determined by the state of the body's center of mass (COM) at the initiation of the slip.

METHODS

An unexpected slip was induced during a sit-to-stand in 45 healthy subjects. Slips were induced using a low-friction platform which, when released, would slide anteriorly by 29 cm. Subjects were informed that they would experience a simulated slip, but were unaware of the timing or mechanisms involved. A fall-arrest system was worn.

The slip was induced following several normal sit-to-stand trials. Subjects sat on a knee-height stool with their feet on the platform. They were instructed to stand up as quickly as possible without using their arms, then remain standing still. In the slipping trial, the platform was released when less than 5% of the subject's body weight was supported by the stool and the body's horizontal COM velocity exceeded 90% of the peak level in the normal sit-to-stand trials. No warning was given prior to the slip.

The motion of the torso and bilateral upper and lower limbs during the slip response was recorded using a motion capture system. The horizontal and vertical positions of the body COM (x_{com} and z_{com}) were calculated from the filtered kinematic data. x_{com} was measured anteriorly from the position of the most posterior heel. Corresponding body COM velocities ($\dot{x}_{com}$ and $\dot{z}_{com}$) were computed. Measures were normalized to one of foot length or body height (bh). Slip initiation was determined from the motion of a marker attached to the platform.

The outcome of a slip was classified as a fall if the body COM descended within 3%bh of its seated height. Outcomes in which the fall-arrest system was activated for less than 50 msec, or in which the force on this system averaged less than 4% body weight over a 1 second period starting at the first COM descent, were classified as recoveries. All other outcomes were classified as having been assisted by the fall-arrest system.

t-tests were used to compare the initial body COM states (*i.e.* at slip initiation) of the fallers to those who recovered from the slip. A backwards, stepwise, logistic regression analysis tested whether the probability of falling was a multivariable function of initial

COM state. All four body COM state variables were included in the initial logistic model, with the likelihood-ratio criterion used for variable elimination. A significance level of α=0.05 was used.

RESULTS AND DISCUSSION

The outcomes of the slips were 11 recoveries and 16 falls, with 18 subjects excluded because of possible fall-arrest system assistance. No measure of initial body COM state differed between fallers and those who recovered (p> .05; Table 1). The backwards logistic analysis excluded all of the body COM state variables from the final model. Thus, a multivariable relationship between initial body COMstate and slip outcome likely does not exist (Figure 1). It must be concluded that initial body COM state alone did not determine the balance recovery outcome of a novel slip during a sit-to-stand.

A possible reason for this result is that, in almost all instances, the response to the slip included a step. While body COMstate is critical to the ability to recover balance without stepping, balance recovery may depend to a greater extent on the neuromotor response when stepping is involved.

Table 1: Comparison of initial body COM states between slip outcome groups

Measure	Recover (n=11)	Fall (n=16)	p
x_{com} (%ft len)	19±8	12±15	.17
z_{com} (%bh)	42±4	43±4	.68
$\dot{x}_{com}$ (%bh/s)	20±10	21±11	.88
$\dot{z}_{com}$ (%bh/s)	37±10	35±17	.83

REFERENCES

Pai, Y.-C. (1999). *J. Biomechanics*, **32**, 1377-1382.

ACKNOWLEDGMENTS

Funded by NIH R01-AG16727-01

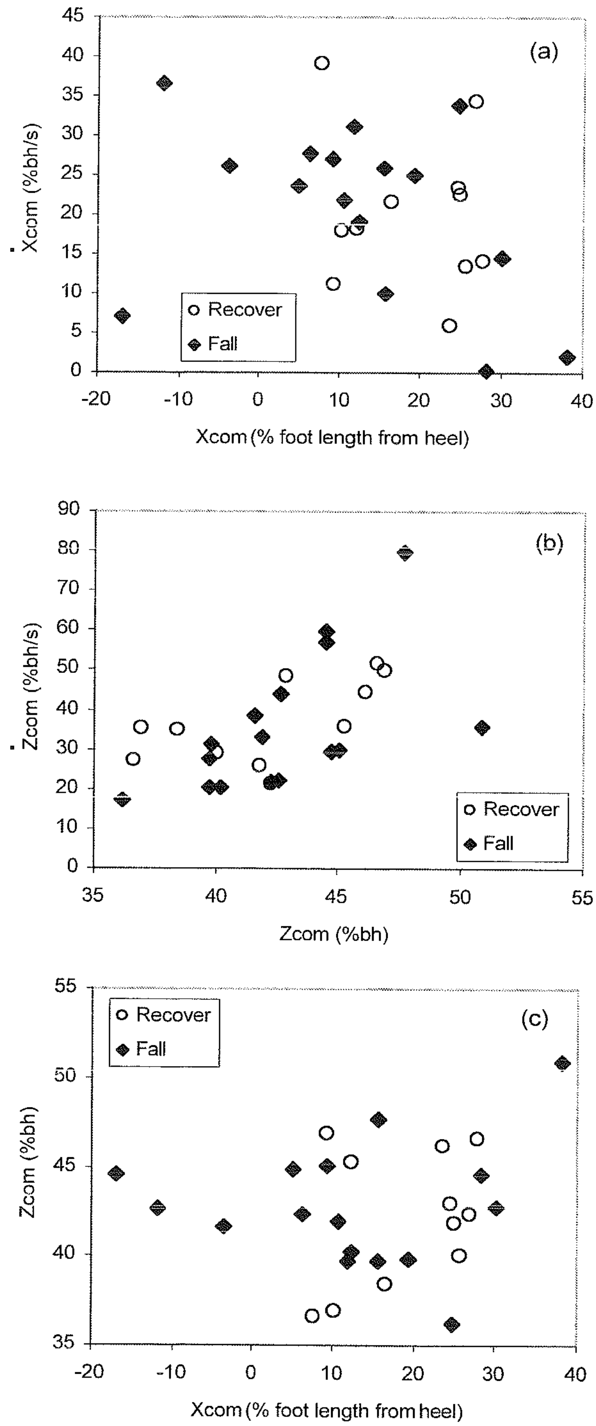

Figure 1: No relationship existed between initial body COM state and slip outcome.

SOME EFFECTS OF FOOT ORTHOSES ON JOINT MOTION AND MOMENTS, AND GROUND REACTION FORCES.

C. J. Nester, M. L. van der Linden, P. Bowker
School of Health Care Professions, University of Salford, England.
c.j.nester@salford.ac.uk

INTRODUCTION.

The biomechanical mechanisms through which foot orthoses derive their clinical benefit are not clearly understood, although changes in some characteristics of rearfoot and knee kinematics and kinetics have been reported. We have found no reports of the effects of foot orthoses on the hip or pelvis. The purpose of this study was to describe the effects of medially wedged foot orthoses (MWO) and laterally wedged foot orthoses (LWO) on joint kinematics and moments, and ground reaction forces.

METHOD.

Fifteen subjects were recruited into this study (8 male). Each subject performed 10 gait cycles in each of three conditions: shod; shod with MWO; and shod with LWO, walking at a controlled cadence of 108 steps/minute and wore their own footwear. The MWO comprised a 3mm base with a 10° wedge under the medial aspect of the insole, and an arch filler. The LWO comprised a 3mm base with a 10° wedge under the lateral aspect of the insole.

Kinematic data were acquired using the Kadaba et al (1989) marker set and five infra red cameras. Following calculation of joint centres and a local co-ordinate system for each segment, rotations at the pelvis, hip, knee and rearfoot complex were calculated using Euler angles.

Kinetic data were collected using two Kistler force plates. Calculated segment masses, moments of inertia, and segment velocities and accelerations were combined with the positions of the joint centres and the kinetic data, to derive the three dimensional moments at the rearfoot complex, knee and hip using inverse dynamics.

Data for each subject was derived by averaging the ten gait cycles. Discrete parameters describing the key characteristics of the joint and ground reaction force data were derived from each subject's data. The discrete data values were found to be suitable for parametric statistical testing, and were compared across the sample using standard paired t-tests (sig. level $p < 0.05$).

RESULTS.

The peaks in the transverse plane rearfoot complex motion and moment data were significantly affected by both orthoses ($p<0.01$) (Fig 1a). Changes in the knee kinematics were negligible (<1.3°). The peaks in the frontal and transverse plane knee moments were only affected by the MWO ($p<0.009$) (Fig 1b). All angular changes at the hip and pelvis were negligible (<1.2°) and hip moments were only minimally affected.

Both orthoses changed the initial peak in the lateral ground reaction force (Fig 1c) ($p=0.001$ in both cases) and the second peak of the medial ground reaction force ($p< 0.02$ for both).

DISCUSSION.

The greatest effect of the orthoses was on the rearfoot complex. The magnitude of the changes suggests that a wide range of structures within the foot will be affected by each orthosis, which may explain why such a wide range of foot pathology are successfully resolved using foot orthoses.

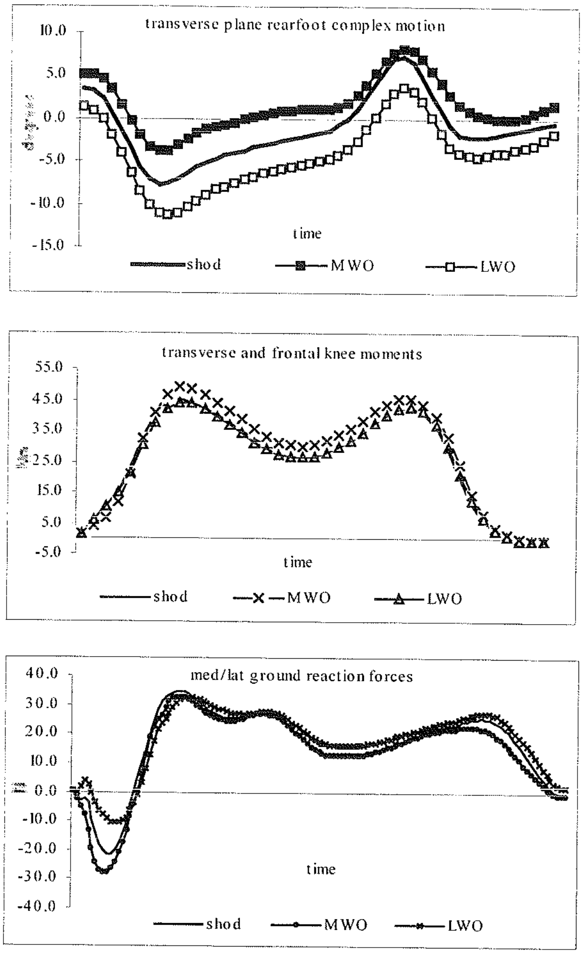

Figure 1. a)- rearfoot complex motion (+ve, supination)
b) frontal plane knee moments (+ve, varus)
c) med/lat ground reaction force data (+ve medial).

The minimal effect of the orthoses on knee kinematics is consistent with the conclusions of Lafortune et al (1994), although they studied running gait. However, their proposition that because the knee was not affected, compensation for the effects of the orthoses on the foot must occur at the hip is not supported by our results, since the effect on hip kinematics was also minimal. The increase in the knee varus moment with the MWO, may influence the distribution of load between the medial and lateral femoral-tibial compartments, and consequently the development of osteoarthritic changes.

If, as our results suggest, the kinematics of the pelvis, hip and knee are minimally affected by either orthosis, the question remains as to where within the limb the significant transverse plane angular changes at the rearfoot complex are referred. As opposed to producing significant changes in the kinematics of proximal joints, foot orthoses may act by altering the stresses within passive structures, or the action of musculature. Some muscular effects of foot orthoses have been reported (Nawoczenski and Ludewig 1999).

Changes in foot pronation/supination due to the orthoses would be expected to change the shock absorption capabilities of the foot. This perhaps explains the increase and decrease in the lateral force during the contact phase in the MWO and LWO conditions respectively (Fig 1c).

In conclusion, both the MWO and LWO had greatest effect on the kinematics and moments of the rearfoot complex, with some effects on the moments at the knee. The kinematics of the knee, hip and pelvis were minimally affected. It may be that the effects of foot orthoses that are extrinsic to the foot, occur in the passive and active soft tissues of the lower limb.

REFERENCES:

Kadaba .M., et al. (1990) *J.Orthop. Research.* 8:383 – 392.

Lafortune.M., et al. (1994) *J. Orthop. Res* 12:412-420.

Nawoczenski..D., Ludewig.P. (1999) *Arch. Phys. Med. Rehab.* 80:540 – 544

ACKNOWLEDGEMENTS:
This work was funded by the Arthritis Research Campaign (ARC)

GENDER DIFFERENCES IN THE KINETIC FEATURES OF MANUAL WHEELCHAIR PROPULSION

Brian T. Fay[1,2], Michael Boninger[1,2,3], Rory A. Cooper[1,2,3], Alicia M. Koontz[1,2]

1 - School of Health & Rehabilitation Science, University of Pittsburgh, Pittsburgh, PA 15260
2 - Human Engineering Research Laboratories, VA Pittsburgh Highland Medical Ctr, Pittsburgh, PA 15206
3 - University Pittsburgh Medical Center, Dept Physical Medicine & Rehabilitation, Pittsburgh, PA 15261
Email: bfay@pitt.edu

INTRODUCTION

Research into manual wheelchair propulsion (MWP) has documented resulting cumulative trauma and repetitive strain disorders in manual wheelchair users (MWU). Researchers have asserted such injuries can be reduced by proper wheelchair fit and propulsion technique. Such assertions are based on the opinion that better wheelchair fit and efficient propulsion technique improves MWP physiological and biomechanical efficiency. (1)

Most researchers, however, have not considered the gender of the MWU. Reasons for considering the gender of the MWU include differences in the anthropometrics (2) and kinematics of wheelchair propulsion (3). Fay, et al (2) has demonstrated significant difference between genders in linear and circumference measures, but similar proportions between genders when considering ratios of stature to linear measure and weight to circumference measure. A muscularity ratio demonstrated more muscular upper arms in males. Fay, et al (3) later demonstrated statistically significant differences in the joint angles for gender groups based on anthropometric percentile pairings and a high degree of difference for groups based on anthropometrically similar pairings. One postualted reason for greater difference between similar pairings versus percentile pairings was due to strength differences between females and males with similar linear anthropometrics. It was suggested that further investigation into differences in the force generated between these pairings may shed light on the kinematic observation.

METHODS

Nine female and eight male subjects were randomly selected from a database of 13 females and 31 males who had participated in the recording of velocity and bilateral three-dimensional pushrim forces and moments during manual wheelchair propulsion. Mean maximum force, rate of force application, moment and rate of moment application and number of propulsion cycles were evaluated under three speed conditions (2 mph, 4 mph, and start from rest). For the 2 and 4 mph trials, the subject was instructed to push the wheelchair at the indicated speed. Feedback of speed was provided via a bar graph appearing on a computer monitor positioned in front of the subject. For the last speed condition, the subject started from rest and accelerated as fast as possible to 4 mph. All trials last for 20 seconds.

Statistical analysis of the data was performed to determine the correlation between right and left sides; right and left variables with high corelation were averaged into one variable. An independent samples t-test to compare the randomly selected groups.

An effort was also undertaken to compare males and females of similar anthropometric measures. For this comparison, the male subjects' measures were subtracted from the females'. Two pairings were made between males and females whose anthropometric differences for upper extremity measures (circumference of the biceps, elbow wrist and length of upper and forearms) summed to less than 10 cm and upper extremity correlation coefficients exceeded 0.95. Analysis was performed for only the start up trial.

RESULTS AND DISCUSSION

Statistically significant differences between gender groups were found for all variables except the rate of resultant force application at 2 mph and 4 mph (Table 1). This demonstrates the females, in general, do not produce as much force tangental to the pushrim as do males. In addition, the rate of force application was significantly less. These effects were even more highly significant for the start up trials where subject started from rest. Considered alone, these results suggest the musculature of women, as a group, does produce the pushrim force and moment levels of men. This would further indicate that women require more propulsive cycles than do men to reach and maintain a specified speed. Evaluation of the number of propulsion cycles between groups did not show a statistically significant difference between genders, but results trended toward women having more cycles both at start up and while maintaining a specified speed. Statistical differences were less pronounced for the anthropometrically matched pairs during the start up trial (Table 2); however, males did produce higher forces and moments and the number of cycles required to reach the specified speed were less.

The observation of reduced force and moment production and rate of production for females in the randomly selected group tends to validate the observation made in [2] that smaller circumference measures and reduced muscularity ratio (circumference:limb length) are related. Conclusions of [3] found highly significant differences in the joint angles for groups based on anthropometrically similar pairings. It is interesting to note variation in force and moment levels for the second pairing in this study which could be the result of differing kinematics. However, the overiding conclusion is that differences were reduced when the anthropometrically similar parings were considered. This may indicate that with proper physical training and wheelchair setup, females may perform at levels similar to males.

Table 1: Force and Moment Comparison for randomly selected gender groups

Speed = 2mph

Quantity	Female avg	Male avg	p-value
Fr (N)	58.37 (18.50)	84.28 (28.49)	0.030
Fr ROR (N/s)	4.35 (1.65)	5.38 (2.30)	0.278
Ft (N)	30.98 (15.58)	50.02 (19.57)	0.031
Ft ROR (N/s)	1.459 (0.59)	3.26 (2.17)	0.016
Mz (N-m)	10.33 (5.19)	16.67 (6.52)	0.031
Mz ROR (N-m/s)	0.48 (0.20)	0.72 (0.20)	0.016

Speed = 4mph

Quantity	Female avg	Male avg	p-value
Fr (N)	83.023 (19.029)	121.880 (37.335)	0.018
Fr ROR (N/s)	6.704 (2.097)	10.396 (5.677)	0.104
Ft (N)	39.196 (19.592)	59.069 (17.360)	0.042
Ft ROR (N/s)	2.404 (0.863)	4.017 (1.216)	0.007
Mz (N-m)	13.064 (6.530)	19.687 (5.786)	0.042
Mz ROR (N-m/s)	0.801 (0.288)	1.339 (0.405)	0.007

Speed = Start Up

Quantity	Female avg	Male avg	p-value
Fr (N)	83.705 (14.452)	165.561 (41.047)	0.000
Fr ROR (N/s)	5.145 (1.162)	13.056 (5.411)	0.001
Ft (N)	52.245 (21.294)	88.233 (23.793)	0.004
Ft ROR (N/s)	2.856 (0.853)	5.876 (2.405)	0.003
Mz (N-m)	17.413 (7.097)	29.408 (7.930)	0.004
Mz ROR (N-m/s)	0.953 (0.284)	1.958 (0.802)	0.003

SUMMARY

Randomly selected groups of males and females who use manual wheelchairs were compared for the maximum average pushrim force, moment and number of propulsion cycles to attain and maintain a specified speed. Statistically significant differences were found via an independent samples t-test for total applied force, the rate of applied force, applied axle moment, rate of applied axle moment. Trends toward statistical significance were noted for the rate of resultant pushrim force at 2 and 4 mph and number of cycles to attain and maintain the specified speed. Upon considering anthropometrically matched gender pairs, the previously noted differences were reduced with only tangential pushrim force and axle moment significant. It is proposed that appropriate physical training and wheelchair setup may improve performance of females.

REFERENCES

[1] Burnham R (1994). "Upper extremity peripheral nerve entrapments among wheelchair athletes." Arch. Phys. Med. & Rehab. 75:518-24.

[2] Fay BT, Boninger ML, Cooper RA (2000). Gender-based anthropometric differences of manual wheelchair users. Proceedings of the 22nd Annual RESNA Conference. *In Press.*

[3] Fay BT, Boninger ML, Cooper RA (1999). Gender differences in the kinematics of manual wheelchair propulsion. Proceedings of the 22nd Annual RESNA Conference.

ACKNOWLEDGMENTS

This study was funded by the National Institute on Disability and Rehabilitation Research grant #H133P970013-98.

Table 2: Force and Moment Comparison for anthropometrically paired males and females

Pairing 1			
Quantity	Female avg	Male avg	p-value
Fr (N)	78.755	103.559	0.086
Fr ROR (N/s)	5.067	10.419	
Ft (N)	20.700	23.968	0.047
Ft ROR (N/s)	1.161	1.795	0.135
Mz (N-m)	6.898	7.988	0.047
Mz ROR (N-m/s)	0.387	0.598	0.135
Vmax (m/s)	1.537	1.926	0.071
V ROR (m/s-s)	0.0148	0.0165	0.033
Pairing 2			
Quantity	Female avg	Male avg	p-value
Fr (N)	95.016	103.589	0.027
Fr ROR (N/s)	5.191	10.419	0.206
Ft (N)	39.691	23.968	0.154
Ft ROR (N/s)	4.031	1.795	0.233
Mz (N-m)	13.229	7.988	0.154
Mz ROR (N-m/s)	1.343	0.598	0.232
Vmax (m/s)	1.624	1.926	0.054
V ROR (m/s-s)	0.014	0.016	0.052

RELATING SHOULDER JOINT FORCES AND RANGE OF MOTION DURING WHEELCHAIR PROPULSION

Alicia M. Koontz[1,2], Michael L. Boninger[1-3], Rory A. Cooper[1-3], Brian T. Fay[1,2]
[1]Dept. of Rehab. Science and Technology, University of Pittsburgh, Pittsburgh, PA 15261
[2]Center of Excellence in Wheelchairs & Related Technology, VAMC Highland Dr., Pittsburgh, PA
[3] Department of Physical Medicine and Rehabilitation, University of Pittsburgh, Pittsburgh, PA
Email: amkst63@pitt.edu

INTRODUCTION

Nearly one half of manual wheelchair users (MWUs) have shoulder pain and/or injury even after short periods of time in a wheelchair (Nichols, 1979). Repetitive loading on the shoulder joint and the large range of motion (ROM) that the shoulder passes through during wheelchair propulsion has been implicated as a causative factor of pain and injury among MWUs. At the start of a propulsion stroke, the shoulder is generally in extension, abducted and internally rotated (Cooper, 1999). As the stroke progresses, both internal rotation and abduction decreases and the shoulder is flexed. Shoulder angles are at their extremes at the beginning and end of the stroke. If the forces acting at the shoulder are also at their peak magnitudes, this may cause the arm to be more prone to injury. The purpose of this paper was to investigate the timing between peak shoulder angles and forces during wheelchair propulsion. The measures analyzed in this paper can be helpful in the prevention and treatment of shoulder pain and injury in MWUs.

PROCEDURES

Ten (5 men and 5 women) experienced MWUs with a spinal cord injury at the T-4 level or below provided written informed consent to participate in this study. The average age and years post injury was 34.6 $\pm$ 7.0 years and 11.4 $\pm$ 2.6 years, respectively. Subjects' own personal wheelchairs were fitted bilaterally with SMART^{Wheels}, force and torque sensing pushrims (VanSickle, (1995). Skin mounted markers of the OPTOTRAC motion analysis system (Northern Digital, Inc.) were attached to the following bony landmarks: acromion process, lateral epicondyle, olecranon, 3rd and 5th metacarpalphalangeal joints, radial and ulnar styloids. A rigid body made of carbon fiber composite was secured to the sternum to measure trunk movement. Wheelchairs were secured to a dynamometer with a resistance comparable to that of a tile floor. Participants were instructed to propel at a steady-state speed of 0.9 m/s (2mph) for about a minute during which 20 seconds of kinetic and kinematic data were collected.

Shoulder joint angles and forces were determined using a local coordinate system approach (Cooper *et al.*, 1999). The output variables of the biomechanical model include 3-D net joint forces acting at the glenohumeral joint (anterior/posterior, superior/inferior, and medial/lateral components) and shoulder angles expressed in anatomical terms (sagittal and horizontal flexion/extension, abduction/adduction, and internal/external rotation). The time at which maximum and minimum angles and forces occurred were determined using MATLAB (Mathworks, Inc.). The difference between each peak shoulder angle and peak force component was calculated for each stroke. Time differences were averaged across the first five strokes.

RESULTS AND DISCUSSION

The average times in between when the peak force component and peak angle occurred was shortest for the group of MWUs for several force component/angle combinations: superior force and maximum sagittal flexion angle, lateral force and minimum abduction angle, anterior force and maximum horizontal extension angle, and superior force and minimum abduction angle (see Table 1). For most subjects, each peak force/angle combination occurred at the end of the propulsion stroke with the exception of the horizontal extension angle and anterior force component which occurred at the beginning of the stroke. A representative plot showing the peaks of the superior force and sagittal flexion angle is shown in Figure 1.

Wheelchair propulsion requires the shoulder to move over a large ROM. At the extreme ends of its ROM, the shoulder was also found to be subjected to peak loading conditions. At the beginning of the push phase, an anteriorly directed force is acting at the same time the shoulder is maximally extended (in the horizontal plane). At the end of the push phase the force acting upward through the joint was at its peak when the shoulder was fully flexed (in the sagittal plane) and while minimally abducted. Both of these peak force and angle combinations may be causing the head of the humerus to be forced up further into the joint which can over time result in impingement under the acromioclavicular arch and subsequent inflammation. Distributing the propulsion forces more uniformly along the pushrim may help reduce the incidence of shoulder joint pain and injury in MWUs.

Table 1 –Time differences between peak shoulder force components and shoulder angles (Mean ± SD)

Peak Force Components	Peak Angle	Mean Time Difference (msec)
Superior	Max sagittal Flexion	45.7 ± 22.2
	Min abduction	18.6 ± 11.5
Lateral	Min abduction	51.8 ± 18.5
Anterior	Max horizontal extension	91.2 ± 50.7

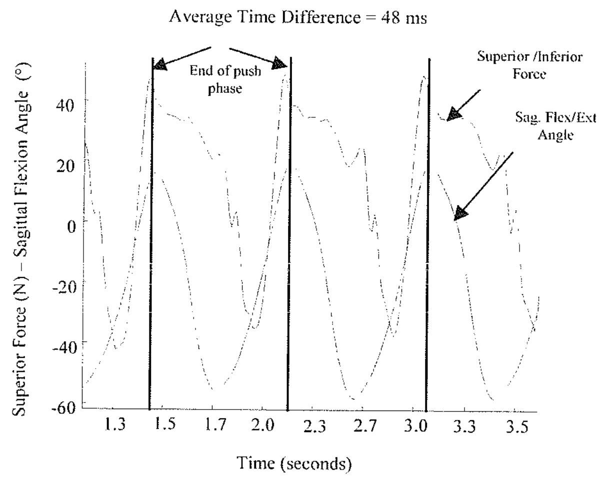

Figure 1: Superior/inferior shoulder force component and sagittal flexion/extension angle at 2 mph for a single subject

ACKNOWLEDGEMENTS

Partial funding was provided by the U.S. Dept. of VA Affairs (Project B689-RA), the National Institutes of Health (NIH K08 HD01122-01) and the PVA.

REFERENCES

Cooper R.A. et al. (1999). *Amer J of Phys Med & Rehabil,* **78**:435-446.

Nichols P.J. et al. (1979). *Scand J Rehabil Med,* **11**:29-32.

VanSickle, D.P. et al. (1995). *Proceedings 18th Annual RESNA Conference.* 352-354.

STRUCTURAL PROPERTIES AND VISCOELASTIC MODELING OF DYNAMIC ELASTIC RESPONSE PROSTHETIC FEET

Mark D. Geil

Health and Performance Sciences, Georgia Institute of Technology, Atlanta, Georgia
Email: mark.geil@oip.gatech.edu

INTRODUCTION

Dynamic Elastic Response (DER) prosthetic feet are designed to assist the lower-limb amputee by storing energy in the stance phase of gait and returning a portion of that energy at toe-off to assist in limb progression. Since the introduction of a very few DER designs in the mid-1980s, the number of manufacturers and designs has expanded rapidly.

Several articles compare kinematic, kinetic, and metabolic parameters of various DER feet in gait. Few articles compare material and structural properties. This project compared structural properties and employed a new viscoelastic modeling technique to objectively compare 11 different conventional and DER prosthetic feet independent of the amputee.

METHODS

Material tests of prosthetic feet were performed on an Instron (Canton, MA) 8521 Servohydraulic Material Testing Machine. The feet tested represent the majority of prosthetics prescriptions for prosthetic feet and included multiple samples of: Seattle Voyager and Lightfoot, College Park TruStep, Ohio Willow Wood Carbon Copy HP, Kingsley Steplite Flattie and Steplite Strider, Otto Bock Dynamic Plus, and the Flex Foot Variflex.

Sinusoidal cyclic loading tests were conducted at 1 Hz. Constant strain rate tests were conducted at strain rates of 0.1 mm/sec, 1 mm/sec, and 10 mm/sec. Stress-relaxation and creep tests were also conducted. Feet were tested to a maximum of 800 N, based on recommendations for fatigue testing by Toh, et al. (1993) and results for vertical propulsive force in Arya, et al. (1995).

Each foot was connected to the Instron machine using a custom-machined device with a standard inverted pyramid adapter. The tests were performed with each foot placed at the maximum plantarflexion allowed by the inverted pyramid. Two sheets of Teflon were placed on the testing surface to minimize friction.

Data were analyzed using a program previously developed by Geil et al. (1997) to determine the viscoelastic model coefficients. Each foot was modeled as a Standard Linear Solid (SLS) consisting of a series spring and damper connected in parallel with a second spring. Spring and damper coefficients were determined using differential equation solutions found in Wang et al. (1997). Data from creep, stress-relaxation, and constant strain rate tests were compared to predicted values from these equations, and the root mean square (RMS) error was calculated. Total RMS for each test was minimized by iteratively changing the SLS model coefficients.

RESULTS AND DISCUSSION

Tests revealed marked differences in structural properties of prosthetic feet both in stiffness and viscoelasticity. Each foot tested in cyclic loading revealed energy loss due to hysteresis. The feet varied in stiffness and required different testing amplitudes to achieve the 100 N minimum and 800 N maximum in the cyclic testing.

Energy was calculated as the integral of force versus displacement. The College Park feet showed the greatest loading and unloading energy, and the Flex foot showed the least. Hysteresis was calculated as the difference in loading energy (input energy) versus unloading energy and as a percentage of input energy. The College Park feet showed the largest percentage loss, and the Otto Bock and Kingsley feet showed the least (Fig. 1). Percentage loss and actual energy loss in Joules were generally correlated, but the Flex foot showed the fifth highest percentage loss with the lowest actual energy loss.

Average total RMS error for actual results versus predicted results was 0.0105. The most accurately modeled feet were the SACH (0.004341). The least accurate were the Flex foot (0.0281) and the College Park feet (0.0176). This indicates that the SLS model might not be as appropriate for the

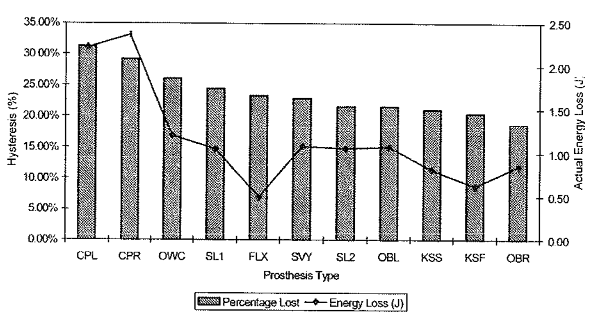

Figure 1: Amount of energy loss (J, line) and energy loss expressed as a percentage of input energy (vertical columns) for each foot under 1 Hz sinusoidal loading between 100 N and 800 N.

Flex and College Park feet. The highest parallel spring coefficient was found on the only pediatric foot tested, a Seattle Light (SL1). Only the Flex foot showed a higher series spring stiffness than parallel, suggesting again that this foot might require a different viscoelastic model. Although the College Park feet showed the greatest energy loss, they also showed the smallest damping coefficients, also indicating the possibility of an inappropriate model.

Amputees use the structural properties of DER feet differently in gait. The measured hysteresis and viscoelastic properties are independent of variations in loading rates, frequencies, and amounts and will be useful in evaluation of functional gait results to determine how much of the measured parameters might be due to inter- and intra-subject variation. Furthermore, analysis of such variation and its effects on the function of each foot will provide valuable design insight. These material and structural property results should be coupled with an extensive functional gait analysis of each foot.

REFERENCES

Arya, A. P., et al. (1995). *Prosth Orth Intl*, **19**, 37-45.

Geil, M. D., et al. (1997). *RESNA '97*, 555-557.

Toh, S. L., J. C. Goh, et al. (1993). *Prosth Orth Intl*, **17**(3), 180-188.

Wang, J. L., M. Parnianpour, et al. (1997). *Biomed Eng- Appl, Basis, & Comm*, **9**(1), 5-19.

ACKNOWLEDGMENTS

This work was supported by the Atlanta VA Rehab R&D Center. The generous donation of prostheses from each manufacturer is appreciated.

STABILITY ANALYSIS OF MANUAL WHEELCHAIR PROPULSION

K. Vrongistinos[1], Y. T. Wang[2], D. D. Pascoe[3], Y. S. Hwang[1], and D. B. Marghitu[3]

[1]Motor Behavior Lab, Southeastern Louisiana University, Hammond, Louisiana
[2]Biomechanics Lab, Georgia State University, Atlanta, Georgia
[3]Auburn University, Auburn, Alabama
Email: dvrongistinos@selu.edu

INTRODUCTION

Manual wheelchair propulsion (MWP) has been associated with cumulative trauma disorders. However there is only one study (Boninger, et al. 1997) that examined the stability of the movement during MWP. The purpose of this study is to develop an analytic technique to quantify stability during MWP based on Floquet theory. A technique that has been successfully used for gait analysis (Hurmuzlu & Basdogan, 1994).

THEORETICAL ANALYSIS

The analytical method to quantify the stability during MWP is based on Floquet theory, which is used to investigate the stability of periodic motions. One can apply the Floquet theory with numerical data with the help of Poincarè maps.

The motion of the system evolves in the six-dimensional space

$$\mathbf{s} = \{q_p, q_q, q_r, q'_p, q'_q, q'_r\} \quad (1)$$

where q_p, q_q, q_r are three generalized coordinates that dictate the motion, and q'_p, q'_q, q'_r are their first derivatives. Periodic motions are characterized by closed orbits or in the case of experimental data near-closed orbits. The Poincarè map for q_p is constructed at different times (t_1 through t_n) which are integer multipliers of period T.

The first return map for q_p is the plot of q_p with itself with a lag of one. The iteration points that are close together should be positioned near the 45° line because the motion is periodic, with identical successive trajectories coinciding on the 45° line.

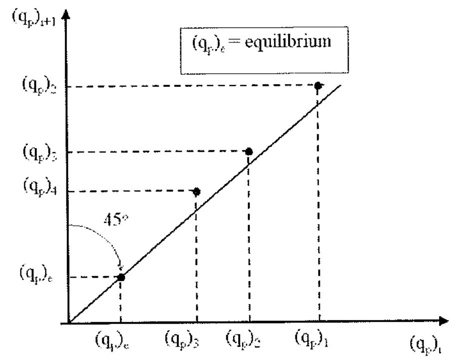

Figure 1: Equilibrium points and first return map for generalized coordinate q_p

The mathematical representation is

$$\mathbf{s}_{i+1} = \mathbf{f}(\mathbf{s}_i) \quad (2)$$

where s_i and s_{i+1} are the state space vector at two successive Poincarè sections. If we consider the equilibrium point s_e and define y_i as the perturbation vector then we have

$$\mathbf{s}_e + \mathbf{y}_{i+1} = \mathbf{f}(\mathbf{s}_e + \mathbf{y}_i) \quad (3)$$

$$\mathbf{y}_{i+1} = \mathbf{J}\,\mathbf{y}_i \quad (4)$$

by linearizing the map **f** about the equilibrium point and by retaining only the linear terms. Matrix **J** is a Jacobean matrix. The eigenvalues of this matrix are the Floquet multipliers that usually are complex numbers. A system is (a) stable when all eigenvalue are less than one, (b) marginally stable when at least one eigenvalue equals one, and (c) unstable when at least one eigenvalue equals more than one. In our case **J** is a 6x6 constant coefficient matrix and the return map is constructed where the trajectory intercepts a given plane.

METHODS

In order to validate the method a participant, experienced with wheelchair propulsion, pushed a common wheelchair on a stationary training roller two times for 36 s. One time he pushed at the 40% and another time at the 80% of his maximum speed that was previously measured with a 15s sprint test. Kinematics data were collected with a Watsmart system and the markers were placed on top of the second metacarpophalangeal joint (end effector), the ulnar styloid, lateral epicondyle, and greater tubercle.

The end effector's marker linear position and velocities where used for the analysis. The return map was reconstructed where the x coordinate intercepted into a plane vertical to the vector $v_p=[1,0,0]^T$ with origin at the mean value of x. Seven cycles from each trial between the 10s and 20s were used for each condition.

RESULTS AND DISCUSSION

The results showed that all the eigenvalues at the 40% speed condition where inside the unit circle (stable); whereas three eigenvalues at the 80% speed were outside the unit circle (unstable). The two maximum complex modulus for each condition were 0.8990 and 1.1916 respectively.

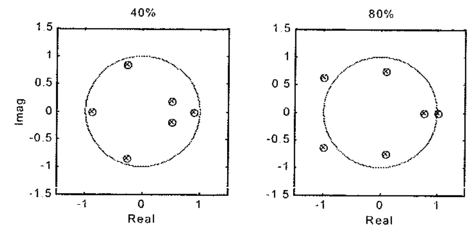

Figure 2: Left the 40% condition with all the eigenvalues within the unit circle and right the 80% condition with three eigenvalues outside the unit circle

The stability of the end effector is determined from both position consistency and velocity consistency. Theoretically the stability analysis in one section can be generalized for the whole cycle. Thus with this method it is possible to detect movement instabilities that maybe the result of an underling injury or deficiencies in technique.

SUMMARY

In this study we presented an analytical method to quantify movement stability during manual wheelchair propulsion based on Floquet theory.

REFERENCES

Hurmuzlu Y., & Basdogan C. (1994). On the measurement of dynamic stability of human locomotion. J. Biomech. Eng., 116(1), 30-36.

Boninger, et al. (1997). Three dimensional pushrim forces during two speeds of wheelchair propulsion. Am. J. of Phys. Med. Reh., 15, 420-427.

FINITE ELEMENT CALCULATION OF SEAT-INTERFACE PRESSURES FOR VARIOUS WHEELCHAIR CUSHION THICKNESSES

Mani Bidar[1], Robert Ragan[1], Tom Kernozek[2], and J.W. Matheson[2]
[1] Department of Physics
[2] Department of Physical Therapy
University of Wisconsin, LaCrosse, Wisconsin
Email: ragan.robe@uwlax.edu **Web: http://perth.uwlax.edu/faculty/ragan**

INTRODUCTION

Seat interface pressures are of interest to both researchers and clinicians since many patients with spinal cord injuries who use wheelchairs develop pressure ulcers. Pressure ulcers unquestionably result from a very complex set of risk factors, but the primary mechanism is sustained high pressure and the associated loss of circulation. The highest pressure occurs beneath the ischial tuberosities (IT) due to the concentration of localized forces. Wheelchair cushions reduce the pressure underneath these bony prominences by redistributing the forces over a larger area. The relatively recent advent of pressure sensitive mats with multiple sensors in a matrix have made it possible to measure seat interface pressures. Producers of cushions use seat interface pressures to assess the effectiveness of cushions in relieving high pressure. However, it is not clear whether the interface pressure provides enough information, since there is evidence that the highest pressures are interior (Reddy *et al.*, 1982) and that pressure ulcers develop internally and spread toward the surface.

Previous studies have used finite-element models of the buttocks and lower pelvis to investigate the interior pressures that occur in a seated human. Previous studies usually focused on isolated seating scenarios (Dabnichki *et al.*, 1994). The goal of the current study is to investigate, in a systematic fashion, the effect of the cushion thickness on these interior pressures.

METHODS

In order to study the interior pressures, a three-dimensional model of the buttocks and lower pelvis was developed using ANSYS® finite-element software. To reduce the computational requirements of the problem, an axisymmetric model was used. Each buttock were taken to be a horizontal circular slab of radius 16 cm and width 8 cm. The buttocks were considered to consist of nearly incompressible "soft" human tissue with a Young's modulus of 47 kPa and a Poisson's ratio of 0.49 (Todd and Thacker, 1994). Each IT was treated as a cylinder of radius 1.5 cm with a hemispherical point. The Young's modulus of the bone was taken to be 10^4 Pa and 0.31 was used for the Poisson's ratio. The minimum distance between the point of the IT and the skin was taken to be 2 cm before loading. Cushion thicknesses of 0 to 16 cm were studied. The elastic behavior of the urethane cushions are known to be highly nonlinear - exhibiting both linear and plastic response (Todd *et al.*, 1998). However, over the range of stresses encountered in this study (0.5 - 3.0 N/cm^2), the response was linear and the Young's modulus of the compressed foam was measured to be approximately 22 kPa with a Poisson's ratio of 0.1. The model mesh size varied from 0.5 cm on the axis of the model to 1.0 cm at the outer radius of the buttock. A no-slip constraint was used at the seat interface.

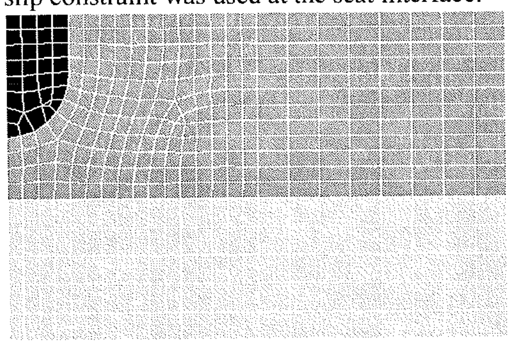

Figure 1 Cross section of the axisymmetric seat -interface model. (black=bone, dark gray=flesh, light gray=cushion)

The weight of the upper torso was divided into two loads; one applied to the top surface of the IT, and the other was applied as a uniform pressure on the top surface of the buttock. The values of these loads were found by fitting the results of the finite-element model to measured values obtained with a Novell Pliance™ pressure sensitive mat (1024 1.5 cm^2 capacitive sensors). Figure 2 shows the resulting fits for both hard seat and soft cushion with $P_{IT} = 4.56$ N/cm^2, and $P_{buttock} = 0.37$ N/cm^2. Surprisingly, the loads on the ITs were found to be a *small* fraction of the torso weight (15%), with the majority of the weight supported by the buttocks. This disagrees with other studies, where it was assumed that the total upper torso weight should be applied to the IT (Todd and Thacker, 1994). It remains unclear how the load should be distributed on the upper surface of these simple models.

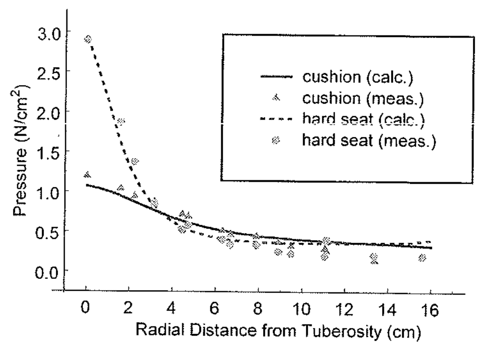

Figure 2 Measured (points) and calculated (lines) radial distribution of the seat-interface pressures for a soft cushion and a hard seat.

RESULTS AND DISCUSSION

Figure 3 shows some typical results for the interior pressures. Within the soft tissue, the area of highest stress is concentrated within a centimeter or two of the IT with the maximum compressive stress just below the bottom surface.

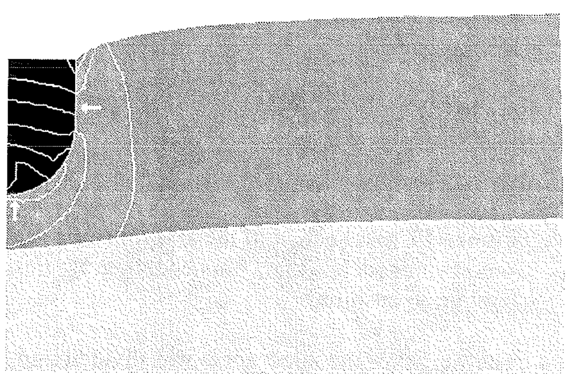

Figure 3 Contour plot of 3rd principal stress for a 16 cm cushion. The arrows indicate the areas of highest compressive (bottom arrow) and shear (top arrow) stress.

Figure 4 shows the dependence of the maximum interior stress, maximum seat interface pressure, and maximum shear stress. As expected, the pressures decrease with thicker cushions. However, almost all of the reduction is obtained with an 8 cm cushion where the maximum interior stress is reduced from 29.3 N/cm^2 for a hard seat to 16.0 N/cm^2. In fact, the shear stress *increases* slightly for thicker cushions. The maximum interior stress is indeed greater than the maximum interface pressure, but they are not in constant proportion. For a hard seat, the interface pressure is 79% of the maximum interior pressure, whereas for a 16cm seat it is 57%.

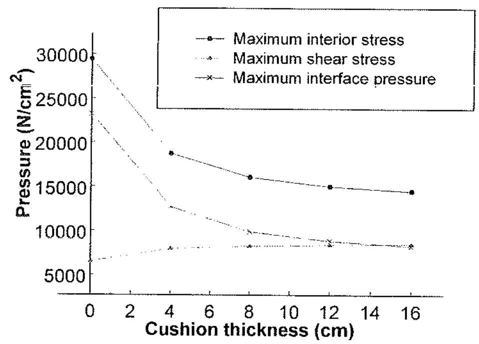

Figure 4 Maximum interior stress, interface pressure and shear stress for various cushion thicknesses.

SUMMARY

A finite element model of the buttocks and lower pelvis was developed to study the effects of cushion thickness on the distribution of stresses near the seat interface. It was found that urethane cushions did in fact reduce the maximum stress below the ischial tuberosity but that increasing the thickness beyond 8cm was ineffective in further reducing stress. It was also found that seat-interface pressures were a good but not a complete measure of internal stress reduction.

REFERENCES

Reddy NP, Patel H, Cochran GV, Brunski JB, *J Biomech*, 1982; 15: 493-504.

Dabnichki PA, Crocombe AD, Hughes SC, *J Engng in Medicine* H, 1994; 208: 9-17.

Todd BA, Thacker JG, *J Rehabil Res Dev* 1994; 31: 111-119.

Todd BA, Smith SL, Vongpaseuth T, *J Rehabil Res Dev* 1998; 35: 219-224.

ACKNOWLEDGMENTS

This work was funded by a UWL Faculty Research Grant.

BILATERAL MULTI-FINGER DEFICIT IN STATIC PRESSING TASKS

Z. M. Li, P. Jacob, K. Baker, C. Hurley
Department of Physical Therapy, Walsh University, OH 44720

INTRODUCTION

The phenomenon of bilateral deficit, i.e., decreased force-generating capacity in bilateral exertion as compared to unilateral exertion, has been investigated in a variety of tasks including leg extension (Vandervoort et al. 1984; Koh et al. 1993; Vint and Hinrichs 1996; Schantz et al. 1989), ankle plantarflexion (Kawakami et al. 1998), elbow flexion and extension (Ohtsuki 1983; Seki and Ohtsuki 1990; Oda and Moritani 1994), hand grip (Ohtsuki 1983), and wrist extension (Kroll 1965). The magnitude of bilateral deficit has been reported to be from non-significant to as high as 25%. Similar to bilateral deficit, individual fingers demonstrate decreases in force production when a set of fingers of one hand act in parallel as compared to the forces produced during single-finger tasks (multi-finger deficit, Ohtsuki 1981; Li et al. 1998). The multi-finger deficit of one hand was reported to be as high as 50% in four-finger force production tasks (Li et al. 1998). The purpose of this study was to investigate the deficit phenomenon using tasks that involved multiple fingers on both hands.

METHODS

Flexion forces produced by the index (I), middle (M), ring (R), and little (L) fingers, and electromyography (EMG) of extrinsic finger flexors of both hands were measured in 8 young right-handed normal subjects (Figure 1). The experimental tasks consisted of maximal voluntary contraction (MVC) tasks that included single- and multi-fingers: I, M, R, L, IM, IMR, and IMRL. The tasks were performed with (1) the right hand, (2) the left hand, and (3) two hands acting together. The EMG electrodes for extrinsic finger flexors were centered in the middle of the connection line between the medial epicondyle and the styloid process of the ulna (Basmajian and Blumenstein 1989).

Forces of individual fingers were determined at the instant of maximal total force production by eight fingers. EMG signals were full-wave rectified and smoothed using a fourth-order, zero phase shift low-pass Butterworth filter at a cutoff frequency of 6 Hz. EMG magnitudes from finger flexors of both hands were determined at the instant of the peak of the summed EMG signals.

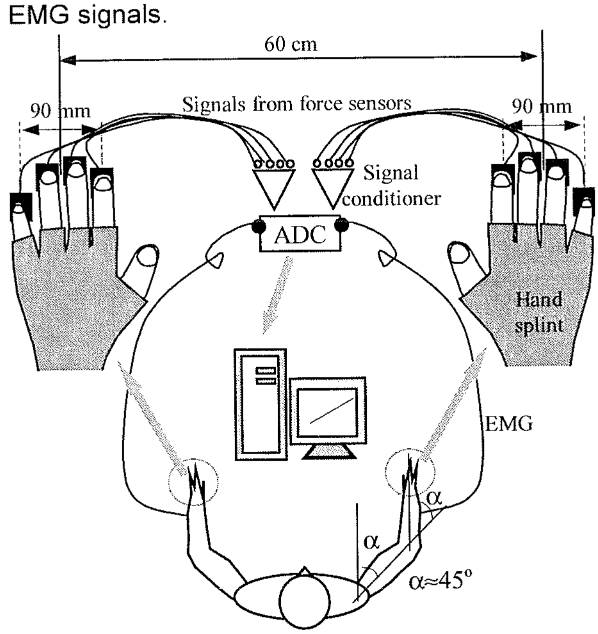

Figure 1. Experimental setup for finger force production and associated EMG signals of finger flexors.

RESULTS

In general, both force and EMG magnitudes were decreased in bilateral tasks as compared to unilateral tasks (Figure 2 and Figure 3). The force decrease during bilateral tasks ranged, on average, from 3.2% to 25.1%, depending on the involvement of specific fingers or the number of fingers. EMG magnitude decreased 3.9% to 30.6% during bilateral tasks. The utilization of an increased number of fingers was associated with increased bilateral force deficit. For example, the decreases in total force produced by the right hand were 10.0%, 13.4%, 19.3%, and 22.5% in bilateral I, IM, IMR, and IMRL tasks as compared to unilateral tasks.

Significant decreases in total force amount and EMG magnitude were shown in bilateral multi-finger tasks ($p<0.05$) in comparison with unilateral tasks. Individual fingers showed significant force deficit in unilateral multi-finger tasks as compared to unilateral single-finger tasks ($p<0.001$). Individual fingers showed additional force decreases in bilateral multi-finger tasks as compared to unilateral tasks of the same set of fingers. However, in some of the bilateral single-finger tasks, no-significant differences were found for force or EMG between bilateral and unilateral tasks. For example, the little fingers of both hands did not show significant decrease in bilateral force exertion. Likewise, EMG magnitude of the flexors of the right hand did not decrease when the right index finger (as well as ring, or little finger) flexed bilaterally together with left index finger, as compared to its unilateral flexion.

DISCUSSION

The current study investigated the phenomenon of bilateral deficit by measuring EMG activity and force production of single- and multi-finger(s) during unilateral and bilateral MVC tasks. The superimposition of bilateral deficit and multi-finger deficit support the "central ceiling" hypothesis (Li et al. 1998) of neural drive in maximal voluntary contraction, i.e., the more effectors are involved, the less amount of neural drive is allotted to each effector. The fact that no bilateral deficit was observed for some of the single-finger bilateral tasks indicates that the task performance might be limited in individual fingers due to peripheral anatomical / mechanical factors, i.e. local saturation with lower-than-maximum neural command. It appears that both central and peripheral mechanisms are responsible for the phenomenon of bilateral multi-finger deficit.

REFERENCES

[1] Basmajian JV & Blumenstein R (1989) William & Wilkins. p378 [2] Howard JD, Enoka RM (1991) J Appl Physiol. 70: 306-316. [3] Kawakami Y et al. (1998) Eur J Appl Physio 77:212-6. [4] Koh TJ et al. (1993) J Appl Physio 74:1200-5. [5] Kroll W (1965) Am J Phys Med 44:218-23. [6] Li ZM et al. (1998) Exp Brain Res 119:276-86. [7] Oda S, Moritani T (1994) Eur J Appl Physiol 69:240-3. [8] Ohtsuki T (1981) Ergonomics 24:21-36. [9] Ohtsuki T (1983) Behav Brain Res 7:165-78. [10] Seki T, Ohtsuki T (1990) Ergonomics 33:1131-42. [11] Schantz PG et al. (1989) Acta Physiol Scand 136:185-92. [12] Vint P, Hinrichs RN (1996) J Appl Biomech, 12:338-58. [13] Vandervoort AA et al. (1984) J Appl Physio 56:46-51

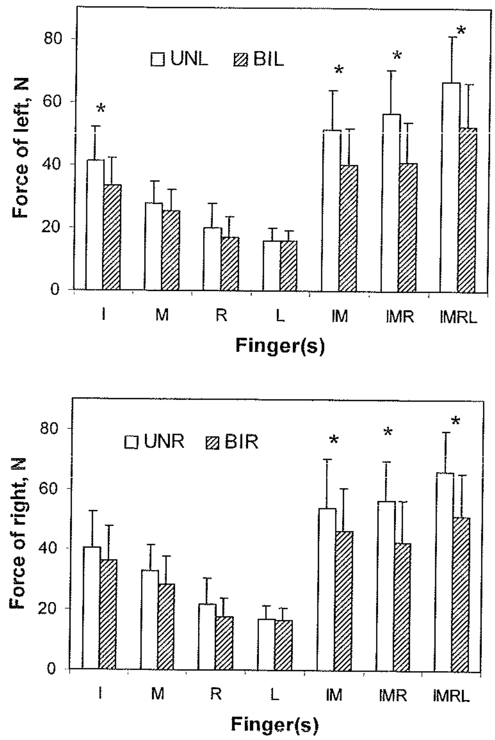

*Figure 2. Force of left and right hands in unilateral and bilateral tasks. * p < 0.05*

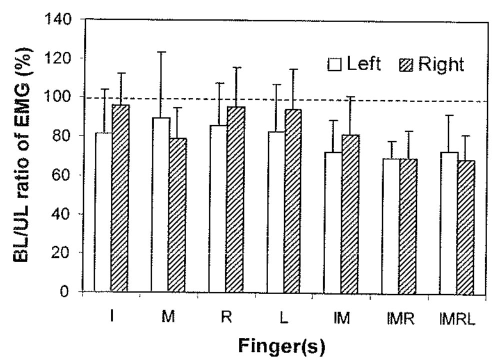

Figure 3. Bilateral to unilateral ratio of EMG of left and right hands

THE USE OF WEIGHTS IN ARTIFICIAL NEURAL NETWORK FOR STUDYING HUMAN POSTURAL CONTROL — QUANTIFYING CENTER OF PRESSURE AND LEG MUSCLE RELATIONS DURING QUIET STANCE IN THE YOUNG AND AGED

Ge Wu and Gongbing Shan
Department of Physical Therapy, University of Vermont, Burlington, VT, 05401

INTRODUCTION

A considerable amount of experiments has been done to understand the mechanism of human postural control [Wu and Chiang, 1997]. However, because of the complexity of the control system, the relations between the multiple inputs and the outputs of the control system have not been established [Lee, 1989]. In the previous paper, we have presented a variable called control potential (CP) to quantitatively determine the input-output relation in a complex system. CP is the product of the weights in both hidden and output layers in an ANN.

The purpose of this paper was to apply the CP concept to characterize the relation between the leg muscle activities and the center of pressure (COP) displacement during quiet stance in both young and aged people.

METHODS

Two groups of subjects were tested in this study: a young group (<22 yrs of age, N=7) and an aged group (>55 yrs of age, N=5). During the test, each subject was asked to stand quietly for 10 seconds, with either eyes open (EO) or closed (EC). The COP under the feet and eight leg muscle activities were measured simultaneously during the stance by an AMTI force plate [USA] and surface EMG electrodes [BTS, Italy], respectively. The eight muscles were bilateral tibialis anterior (TA), gastrocnemius (GAST), quadriceps (QUAD) and hamstring (HAMS). The measurement was repeated 5 times for each visual condition.

An ANN was constructed with 9 inputs, 2 outputs and 50 neurons in the hidden layer. The 9 inputs included 8 leg EMGs (normalized by the corresponding maximum voluntary contraction) and 1 vision (set to 1 for EO and 0 for EC conditions, respectively). The 2 outputs were the COP in the anterior-posterior (a-p) and medial-lateral (m-l) directions. There were 9×2 CP components representing the relations between the 9 inputs and the 2 outputs, respectively.

RESULTS

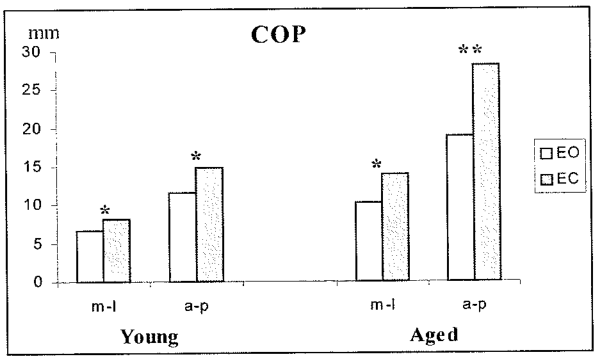

Fig.1. COP excursions in m-l and a-p directions (* $p<0.05$, ** $p<0.01$, comparison between visual conditions)

The COP excursions of the aged group were significantly larger ($p<0.05$) than that of the young group in both directions and for both visual conditions (Fig. 1). For both groups, the a-p COP was significantly larger than that of m-l direction ($p<0.01$). Moreover, the aged group showed a larger increase in a-p COP excursion when changing from EO to EC, which may suggest that the COP of the aged depended more on vision than that of the young.

The normalized RMS values of EMG of the aged group were much higher than that of the young group (Fig. 2). Furthermore, the RMS values of all EMG, except for right GAST, were not significantly different between the 2 visual conditions in the young group, but all, except for left HAMS, were significantly increased in the aged group ($p<0.05$). This indicated that the muscle activity of aged people also depended on vision.

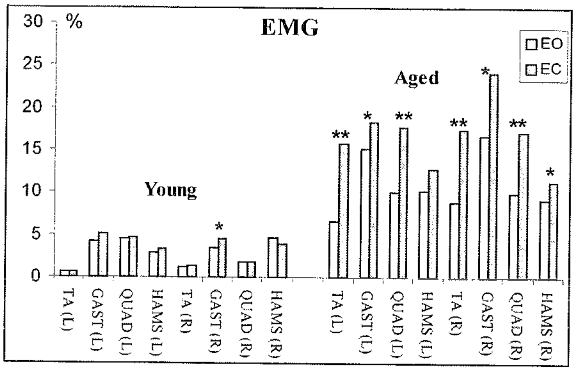

Fig.2 The mean RMS value of normalized EMG (* and ** are same as in Fig. 1)

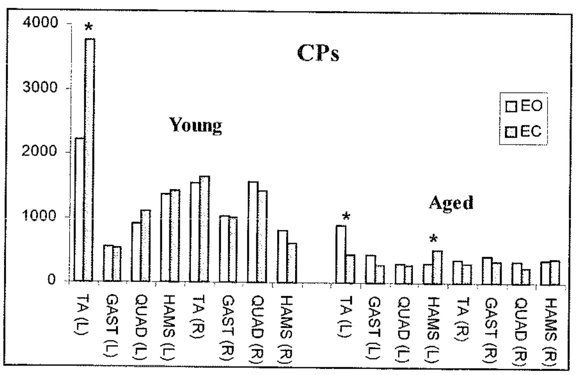

Fig.3 The absolute values of CPs between muscle and COP in both directions. (* and ** are same as in Fig. 1)

The CPs in the young group were significantly higher ($p<0.00$) than the corresponding ones in the aged group (Fig.3). With EO, the largest CP was for left TA in both groups, suggesting that the COP in both a-p and m-l directions was mostly related to the left TA activity. With EC, the CP relating to left TA was increased significantly in the young group, but decreased in the aged group. In addition, the CP relating to left HAMS increased significantly in the aged group.

DISCUSSIONS

The differences found in the CPs between the 2 age groups revealed different relations between the muscle activities and the COP displacement. First, the COP in young group was shown to be more related to the muscle activities than that in the aged group, even though the normalized muscle activities in the young group were significantly smaller than that in the aged group. Secondly, although the COP in the young group tended to relate most to TA, QUAD and HAMS played important roles as well. In the aged group, however, their COP tended to relate to TA only with EO. Thirdly, the COP-muscle relation did not seem to be affected by visual condition in the young group, but was modified in the aged group, suggesting that vision might play an important role in the control of COP by leg muscles. This is consistent with the findings by COP or EMG measures alone.

In conclusion, with the use of ANN and its weights, or CP components, we have quantitatively determined the relations between COP and muscle activities. These relations allow us to identify differences between the aged and young people, and to examine the role of vision in the control of COP displacements by the leg muscles.

REFERENCES

Wu and Chiang, Exp Brain Res 114, 1997

Lee. Am J Orthop Ther 43, 1989

ACKNOWLEDGEMENT

This work was supported by NIH grant No.1R29AG11602.

Gender Differences in Active Knee Joint Stiffness

Kevin P. Granata, PhD. and Sara E. Wilson, PhD
Motion Analysis and Motor Performance Laboratory
University of Virginia
E-Mail : KPG8n @ Virginia.edu

INTRODUCTION

Active female suffer 2 to 8 times the number of musculoskeletal injuries as equivalently trained men for both knee injury and low-back pain[1,2]. Research suggests these injuries may be related to biomechanical instability. One of the primary contributing components to stability during functional tasks is the mechanical stiffness of active muscles[3]. Research demonstrated that active co-contraction increases total joint stiffness, less in women than men, suggesting gender differences active muscle stiffness[4]. Gender differences in joint stiffness from active muscle contraction may cause decreased stability in women and contribute to the greater risk of musculoskeletal injury. As part of a larger study of biomechanical stability we measured the active knee stiffness as a function of gender in a controlled (non weight bearing) experiment.

METHODS

Sixteen male and fourteen female healthy volunteers between the ages of 21 and 39 participated following informed consent. Subject's thighs were securely fastened in to a isokinetic dynamometer with the lower leg free to move. Neutral ankle posture was maintained by means of a fixed ankle-foot orthosis (AFO). Subjects were required to support the lower leg and added weights of 0 kg, 6 kg and 20% max. at a knee flexion angle of 45^0. A sudden transient perturbation, i.e. a quick tap thrusting the leg downward (Figure 1), was applied to the angle. The resulting knee flexion / extension motions were recorded by an accelerometer attached to the heel of the orthosis. Subjects were asked to maintain a

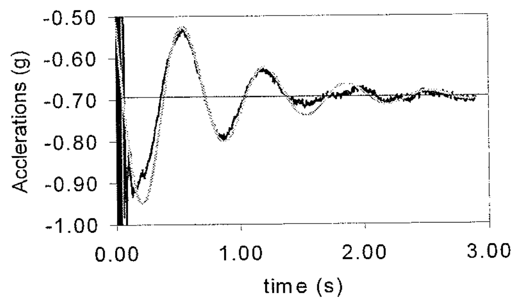

Figure1. Second-order damped harmonic model (gray) was fit to the acceleration data (black).

orthosis. Subjects were asked to maintain a constant muscle activity by monitoring an electromyographic display measured from bipolar surface electrodes over the belly of the biceps femoris (hamstring activity) and rectus femoris (quadriceps activity).

Flexion / extension oscillations of the knee were used to calculate stiffness. Fast Fourier transforms were performed to obtain the damped natural frequency, and peak-to-peak analyses recorded the exponential decay of the oscillation. These data were applied to a second order model of knee motion to determine active muscle stiffness and damping. Multiple regression and ANOVA were performed to assess the influence of gender, knee moment, and muscle (hamstring vs quadriceps) on active joint stiffness.

RESULTS

The model accurately represented the measured motion data explained 69% of the data variability with RMS error less than 5.9 % of the baseline acceleration of gravity. There was no performance difference as a function of gender.

The female subjects produced less than 57% of the active stiffness demonstrated by the male subjects, (K_{Female} [illegible]9.3 Nm/rad, K_{Male}=153.1 Nm/rad) ([illegible]re 2). As expected, stiffness increased with the knee moment. Multiple regression demonstrated much of the gender difference could be explained by moment (men supported heavier leg mass thereby applying greater total moment in the 0 kg and 6 kg conditions). However, even when accounting for total knee moment, strength and thigh length there continued to be a gender difference in active stiffness.

Active stiffness in the quadriceps was significantly greater than in the hamstrings (K_{Quad}=178.4 Nm/rad, K_{Ham}=113.6 Nm/rad). Due to the test protocol, the total knee moment during the quadriceps conditions was relatively lower than during the hamstrings tests. Despite lower knee moments the quadriceps continued to produce greater stiffness than the hamstrings. The ratio of quadriceps to hamstrings stiffness was not significantly different between genders.

It is known that antagonsitic co-contraction contributes to increased active joint stiffness[5]. Women were found to have significantly higher levels of agonist and antagonist activity suggesting these trials required a higher percentage of maximum strength. This is notable in that the females were performing at increased activation levels yet continued to demonstrate less biomechanical stiffness than the males. However, the ratio of antagonist to agonist activity was not significantly different between genders or between the hamstrings and quadriceps tests.

Reflex response also contributes to active joint stiffness. Although subjects were instructed to maintain a constant activation level throughout the transient motion, reflex responses were observable in the EMG data. Fourier analyses demonstrated that the frequency of the response was identical to the damped frequency of motion in both

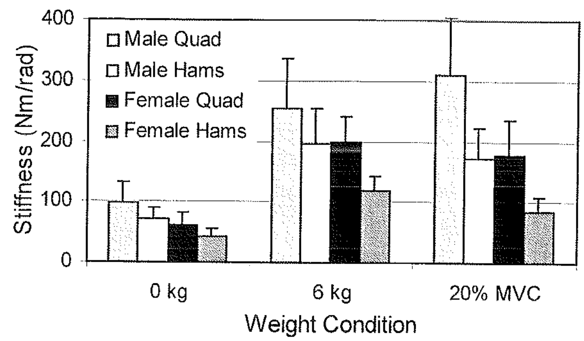

Figure 2. Active hamstring and quadricep stiffness was greater in males than females.

men and women. Further analyses concluded that no significant gender differences existed in the normalized amplitude of the reflex EMG at the damped frequency. Thus, reflex activation in response to the damped cyclic motion did not contribute to the gender difference in measured active stiffness.

SUMMARY

Biomechanical stability has been implicated as a factor in musculoskeletal injury and may contribute to gender bias in risk of injury. Factors that contribute to biomechanical stability include joint kinematics, load and stiffness. To initiate this investigation of gender factors in stability, we have begin by evaluating active stiffness, and concluded that females have reduced active stiffness compared to age matched males. Future analyses will require the investigation of factors that might contribute to this gender difference.

ACKNOWLEDGMENT

This research was supported in part by a grant R01 AR46111-02 from NIAMS/NIH. The authors wish to thank A. Massimini for her assistance in this effort.

REFERENCES

1. Hutchinson M, *Sports Med.* 1995;19:288-302.
2. Krause J, *Am. J. Epidem.*, 1997, 146 (8), 637-645
3. Nicholas J, *Jama.* 1970;212:2236-9
4. Wojtys E, *AOSSM*, 1998
5. Hogan N, *Adv. Bioeng*, 1980, 279-282
6. Sinkjaer T, *J. Neurophysiol*, 1988, 60, 110-121

ACTIVE KNEE STIFFNESS DECREASES AFTER FATIGUE

Sara E. Wilson, Ph.D. and Kevin P. Granata, Ph.D.

Motion Analysis and Motor Performance Laboratory
University of Virginia, Charlottesville, VA
Email: sew3k@virginia.edu

INTRODUCTION

Knee ligament injuries are a common problem with an estimated incidence of 60 knee ligament injuries for every 100,000 health plan members[1]. Instability of the knee joint during active running, cutting, and landing tasks contributes to knee injury. A component of joint stability is active muscle stiffness. This stiffness is a function of muscle activation, reflex behavior, and mechanical character of the musculature. It is known that fatigue can change the reflex behavior and proprioception of the knee joint. Functional measures of the force-by-displacement ratio indicate fatigue modifiers stiffness. However, these measures fail to discriminate between dynamic components of inertia, damping, dynamic contraction force and stiffness. The aim of this research was to investigate the effect of fatigue on active knee joint stiffness.

PROCEDURES

Sixteen men and fourteen women between the ages of 21 and 39 participated in this study after informed consent was obtained.

Active knee stiffness was assessed while subjects were seated with their lower leg flexed 45 degrees from horizontal and their thigh strapped to the seat. A fixed ankle-foot orthosis was used to prevent ankle motion and to attach weights to the lower leg. In this position the subjects supported the weight of their lower leg and an applied

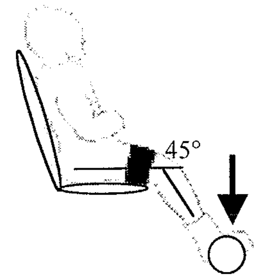

Figure 1. Stiffness was assessed by applying a vertical perturbation while the subjects supported a load.

load using the quadriceps muscles. An accelerometer was attached to the heel of the orthosis. Subjects were asked to isometrically hold weights of 0 kg, 6 kg, or 20% of maximum voluntary effort (MVE). A small force perturbation was applied to the orthosis. The stiffness was assessed before and after a fatigue exertion. Subjects performed fatiguing exertions of repeated maximal 90 °/s isokinetic extensions until maximum torque decline to 50% MVE.

Surface electromyography (EMG) electrodes were placed over the belly of the semimebranosus (hamstring activity) and rectus femoris (quadriceps activity). EMG data was rectified, integrated, and normalized to maximum voluntary effort. During the stiffness measurements, subjects were asked to maintain muscle tension using EMG feedback. Spectral analyses of the raw EMG were used to examine fatigue.

Stiffness was found using a rotational, second-order, damped model of the knee.

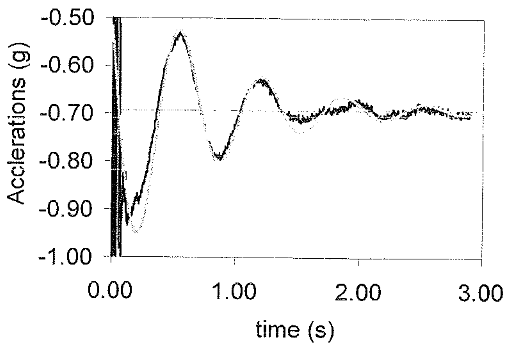

Figure 2. Second-order damped harmonic model (gray) was fit to the acceleration data (black).

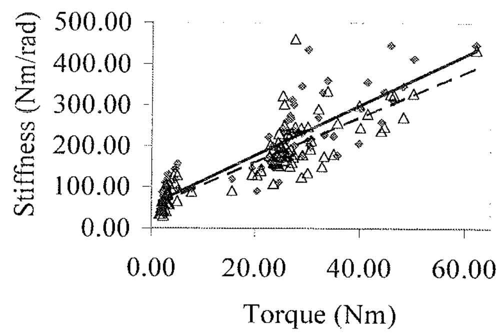

Figure 3. Pre-fatigue stiffness (solid markers and line) was greater than post-fatigue (triangles and dashed line).

RESULTS AND DISCUSSION

The model accurately represented the measured motion data ($r^2 = 0.69$). Stiffness increased linearly with supported torque ($r^2 = 0.75$). Analysis of variance with repeated measures showed a significant decrease in the stiffness and natural frequency after fatiguing exertions ($p<0.05$). The median raw EMG frequency during stiffness testing significantly decreased after fatigue exertions.

Rectus femoris electrical activity decreased significantly after fatigue although the loads supported were the same. This suggests that subjects recruited other muscles, such as the vastus medialis, vastus lateralis and vastus intermedius. This change in recruitment may account for the decreased stiffness characteristics.

Active joint stiffness in this model represents both the intrinsic and reflex stiffness. While attempts were made to minimize the contribution of voluntary response by asking subjects to maintain EMG levels via EMG feedback, it is also possible that changes in the response characteristics including an increase in reflex time, might play a role in the decreased frequency and stiffness after fatigue. Fatigue has been found by previous authors to alter the proprioception and increase reflex time[2,3]. Although subjects were instructed to maintain EMG at a constant level, some oscillation in the EMG was present. A median frequency for the integrated EMG of 1.05 Hz (the acceleration oscillated at a mean of 1.70 Hz) was observed. This median frequency decreased with fatigue, suggesting increases in reflex times.

SUMMARY

Active joint stiffness was found to be reduced after fatigue exertions. Decreased rectus femoris EMG activity suggests changes in the muscles recruited to support the same load. Decreased integrated EMG frequency also suggests changes in reflex response time. Future research will examine the influence of recruitment patterns and reflex behavior on active muscle stiffness.

REFERENCES

1. Miyasaka et al. *Amer. J. Knee Surg.* 1991;4:3-8. 2. Skinner et al. *J Orthop Res.* 1986;4:112-8. 3. Rozzi et al. *Journal of Athletic Training.* 1999;34:106-114.

ACKNOWLEDGEMENTS

This work was supported by a grant R01 AR46111-02 from the NIAMS of the National Institutes of Health. The authors wish to acknowledge the assistance of Ms. Amy Massimini.

BIMANUAL CONTROL OF THE UPPER EXTREMITIES: RESPONSES TO EXPECTED AND UNEXPECTED INERTIAL PERTURBATIONS

Philip E. Martin[1], Todd D. Royer[2], and George E. Stelmach[1]

[1]Exercise and Sport Research Institute, Arizona State University, Tempe, AZ
[2]Dept of Exercise and Sport Sciences, Tulane University, New Orleans, LA
email: philip.martin@asu.edu web: www.asu.edu/clas/espe/biomechlab

INTRODUCTION

Recent research on interlimb coordination has focused on temporal and spatial coupling of bimanual movements (e.g., Heuer et al., 1998; Kelso et al., 1979; Marteniuk et al., 1984; Sherwood, 1994; Steglich et al., 1999). Analyses of movement tasks that are either symmetrical or asymmetrical in target size, movement amplitude, movement speed, and/or movement direction are frequently limited to temporal and kinematic assessments. Inertial perturbation of the moving limbs is a less frequent approach when examining interlimb coupling. In addition, few studies have considered movement responses from joint kinetics and electromyography perspectives. In this investigation, we considered the extent to which temporal symmetry is retained in the presence of expected and unexpected inertial asymmetries. We hypothesized that temporal symmetry is sustained under asymmetrical inertial conditions. Further, net elbow torque and elbow flexor and extensor emg profiles are adapted asymmetrically to sustain temporal symmetry.

METHODS

Nine healthy young adults (M_{age} = 27.0±3.1 yrs) served as subjects. Each performed a simple bilateral elbow flexion task in a horizontal plane while seated. The arms were supported on instrumented, uniaxial manipulanda with the elbows aligned with manipulanda axes. The task required simultaneous elbow flexion through a 70 degree range to a 10 degree target in approximately 500 ms. The moment of inertia of the manipulandum and arm was altered by attaching cylinders of different mass (0, 1, or 2 kg) to the distal aspect of each manipulandum (~40 cm from the axis), creating three inertia conditions: light (L), medium (M), and heavy (H), respectively.

Surface EMG electrodes were positioned bilaterally over the biceps brachii and triceps brachii muscles. EMG and manipulandum potentiometer signals were sampled at 1000 Hz.

After 15 accommodation trials, subjects completed four blocks of 16 trials in which 75% of the trials were completed with manipulanda loaded symmetrically with 1 kg loads (medium-medium combination: MM). For the remaining 25% of the trials, the inertial properties of one manipulandum was altered without the subject's knowledge such that the cylinder load on that manipulandum was either 0 kg (light-medium combination: LM) or 2 kg (heavy-medium combination: HM). An additional four blocks of 8 trials were completed, utilizing the same inertial manipulations, except that subjects had knowledge of the specific load conditions for each trial.

Potentiometer data were digitally filtered and differentiated to generate angular velocity and acceleration data. Net elbow torque was computed using an inverse dynamics model.

Primary dependent variables included movement time, peak elbow torque, and peak biceps and triceps emg amplitudes.

RESULTS AND DISCUSSION

Results are highlighted in the series of figures at the bottom of the page. Movement time, peak elbow flexor torque, and peak biceps and triceps activation were all highly symmetrical under symmetrical load conditions (MM), regardless of whether the subjects knew in advance that the bilateral inertial properties were symmetrical. This is consistent with previous research that reflects highly symmetrical movement characteristics when task demands are symmetrical. In contrast to our prediction, movement time symmetry was disrupted under asymmetrical inertial conditions (LM and HM), but this disruption was more apparent when the subject did not know the inertial asymmetry was present. Thus, subjects did not alter temporal and kinematics characteristics of the movements sufficiently to ensure simultaneous target arrival, and thus temporal symmetry, for the two arms. Nevertheless, adaptation to asymmetrical loading at the level of the net elbow torque was apparent, which was consistent with our hypothesis. When an asymmetrical inertial manipulation was expected, subjects adapted elbow flexor torque asymmetrically by decreasing the torque for the L condition and increasing it for the H condition. A similar but smaller adaptation was observed for unexpected asymmetrical loading. A similar adaptation in response to expected and unexpected inertial asymmetries was not as apparent in the more variable and limited emg analyses.

CONCLUSIONS

In contrast to our hypothesis, temporal symmetry was not sustained under asymmetrical inertial conditions. Nevertheless, subjects adapted net elbow torque profiles in an apparent effort to sustain temporal symmetry.

REFERENCES

Heuer, H. et al. (1998). *Exp Brain Res*, **118**, 381-392.

Kelso, J.A.S. et al. (1979). *J Exp Psych Hum Percept Perform*, **5**, 229-238.

Marteniuk, R.G. et al. (1984). *Q J Exp Psychol*, **36A**, 335-365.

Sherwood, D.E. (1994). *Hum Movt Sci*, **13**, 841-860.

Steglich, C. et al. (1999). *Exp Brain Res*, **129**, 302-316.

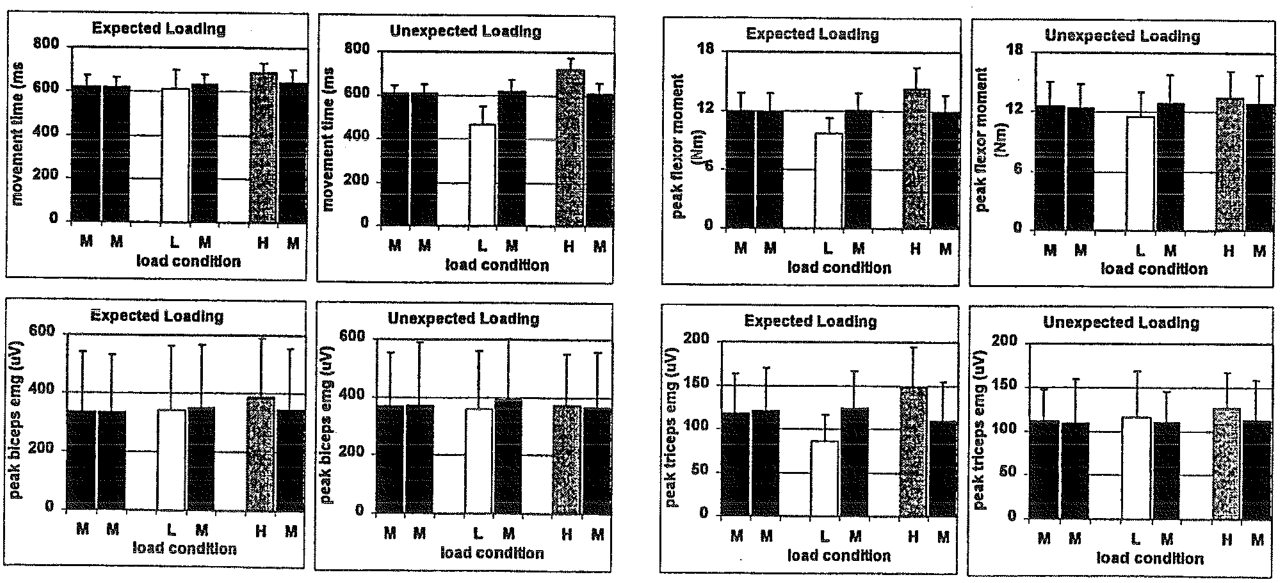

CAN PEAK IMPACT FORCES BE VOLITIONALLY REDUCED IN A FORWARD FALL ONTO THE HANDS ?

Kurt M. DeGoede and James A. Ashton-Miller

Biomechanics Research Laboratory, Department of Mechanical Engineering
University of Michigan, Ann Arbor, Michigan
Email: degoede@umich.edu

INTRODUCTION

The use of the arms to protect oneself during a fall is a natural and often used arrest strategy among untrained individuals (O'Neill 1994; Hsiao 1998). However, this can lead to distal radius fracture (Loder 1988). In fact, the distal forearm is the most common fracture site in the body with 213 such fractures occurring annually per 100,000 individuals (Donaldson 1990). Since risk of distal radius fracture has been linked to the magnitude of the impact load applied to the hands (i.e. Myers 1993), a strategy to reduce that load should lower fracture risk.

We tested the hypothesis that in a forward fall, healthy young males could learn to reduce the peak impact force involved in arresting the fall within four trials.

PROCEDURES

We tested five healthy young male volunteers aged between 22 and 28 years. None of the subjects had any previous falls training. The institutional review board approved all test procedures, and all subjects read and signed a written statement of informed consent.

The subjects stood on a force platform and leaned forward against a supporting tether attached at the waist. The subjects then flexed at the waist to the point at which the center of their shoulder joint was 1 m above the ground. Upon release, they were instructed to arrest their forward fall with their arms. No practice trials were given. The hands contacted the ground during the arrest on two AMTI force-plates, covered with 2.4 cm thick compact rubber foam.

The subjects performed three additional arrests without further instruction. Next, we asked the subjects to arrest two falls while keeping their head as far off the ground as possible, essentially 'stiff-arming' the fall arrest. Finally, the subjects were instructed to try to minimize the peak force of impact on their hands as much as possible over four trials.

In all trials, we measured the kinematics of the fall arrest at 200 Hz with 11 infrared markers using the Optotrak motion analysis system. The force plates were sampled at 2,000 Hz.

The kinematic data were low-pass filtered with a fourth-order Butterworth filter (Matlab) with a cutoff frequency of 100 Hz. The force-plate data were similarly filtered with a cutoff frequency of 300 Hz.

A repeated measures ANOVA was performed to compare the impact forces associated with each subject's first natural, worst-case stiff-arm, and best minimum impact trials.

RESULTS AND DISCUSSION

The largest impact forces (1098±134 N) were found during the stiff-arm impact

(Figure 1). The peak force was significantly affected by the landing strategy employed by the subjects (ANOVA, $p<0.001$). In fact, the force was 15 % lower in the first natural fall than in the worst-case stiff-arm landing at 929±85 N, and 55 % lower when the subjects volitionally minimized the peak force (511±104 N). The secondary rise in the reaction force was also significantly affected by the landing strategy used, with the magnitude of this force being 27 % lower for the minimal-impact arrest than for the stiff-arm landing ($p<0.001$). There were no significant between-subject effects for either body weight or height.

The biomechanics of the arrest of a fall to the ground has received some attention recently (Sabick 1999; Chiu 1998; Robinovitch 1998). One of these studies investigated a martial arts break-fall technique for a lateral fall, and the other two explored stiff-arm arrests of 1 - 5 cm forward falls. However, data from a ballistic pendulum-arm impact experiment with a biomechanical analysis of a fall indicated that the peak force applied to the distal forearm in a fall arrest could potentially be reduced by as much as 50 % by making modest adjustments to the initial elbow angle and the impact velocity of the hands (DeGoede 1999). In the current investigation, we found that young healthy males were indeed able to reduce the peak ground reaction by 50 % in actual forward falls arrested with the arms.

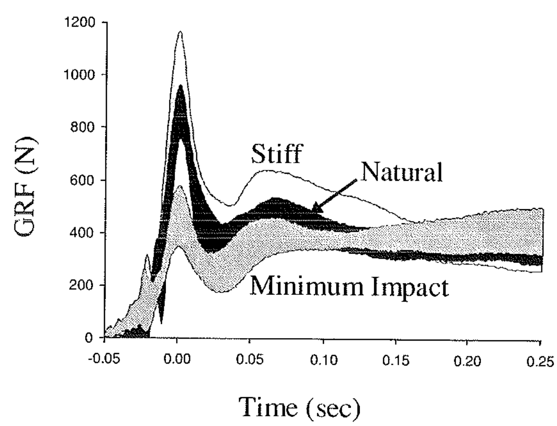

Figure 1: GRF at one hand during arrest of forward falls. Shaded regions indicate standard deviation envelopes for each of three different arrest strategies.

SUMMARY

This is the first demonstration that healthy young males can reduce the peak force applied to their hands by volitionally modifying their fall-arrest strategy. This may have implications for reducing the risk of wrist fracture in falls.

REFERENCES

Chiu, J., S.N. Robinovitch (1998). J Biomech **31**(12): 1169-76.

DeGoede, K.M., et al. (1999). J Biomech Eng, submitted.

Donaldson, L.J., et al. (1990). J Epidemiol Community Health **44**: 241-245.

Hsiao, E.T., S.N. Robinovitch (1998). J Biomech **31**(1): 1-9.

Loder, R.T., H.E. Mayhew (1988). Am Fam Physician **37**(2): 327-338.

Myers, E.R., et al. (1993). Calcif Tissue Int **52**: 199-204.

O'Neill, T.W., et al. (1994). Ann Rheum Dis **53**: 773-775.

Robinovitch, S.N., J. Chiu (1998). J Orthop Res **16**(3): 309-313.

Sabick, M.B., et al. (1999). J Biomech **32**(9): 993-8.

ACKNOWLEDGEMENTS

This work is supported by the NIH: P01 AG10542 and P30 AG08808. We would also like to thank Janet Grenier for her assistance with the data collection.

DYNAMIC vs. QUASI-STATIC COLLECTION OF CARPAL BONE KINEMATICS

Michael E. Hahn, Kok P. Looi, Min J. Park and Kai-Nan An

Orthopedic Biomechanics Lab, Mayo Foundation, Rochester, Minnesota
Email: An.kainan@mayo.edu

INTRODUCTION

Carpal bone kinematics have typically been collected in a quasi-static fashion using either biplanar radiography or electromagnetic tracking devices. While this allows for an intuitive collection setup, it has been suggested that the true nature of carpal kinematics may only be detected in dynamic collection (Short, et al., 1995), specifically when discrete instability is being investigated. Studies that have pursued dynamic collection have chosen Eulerian angles to describe carpal motion. This leaves the investigator without linear displacement data. The purpose of this study was to determine which components of carpal motion as described by screw displacement axes (SDA) were most affected by collection type. It was thought that a significant difference would exist between dynamic and quasi-static collection.

METHODS

Four fresh frozen cadaver forearms (mean age = 70.75 yrs) were dissected, leaving ligaments and tendons intact. The ECRL, ECRB, ECU, FCR, FCU, and APL were loaded according to physiological cross-section area (Brand, et al., 1981). Wrists were pre-conditioned for full flexion/extension (F/E) and radial/ulnar deviation (RUD) prior to data collection. The 3Space Fastrak electromagnetic system (Polhemus, Inc., Colchester, VT) was used to track the scaphoid, lunate and capitate. A local coordinate system was defined by the SDA describing the extreme ends of flexion/extension and radial/ulnar deviation. The X-axis was defined as the long axis of the forearm, the Y-axis described RUD and the Z-axis described F/E. Data was first collected with the wrist in static positions of rotation (Neutral, 40° flexion, 40° extension, 15° radial deviation, 30° ulnar deviation) as determined by planar fluoroscopic images. The capitate was assumed to indicate global hand position. Quasi-static kinematic data was then calculated as the motion from neutral to the four end positions.

Each wrist was then moved through a custom-made jig that allowed planar motion. Dynamic position and orientation data were collected at 30 Hz for all sensors. Kinematic data was calculated as the motion from neutral to each data point. A spline was fit to the raw data so that discrete points were selected where the global wrist angle value (based on the capitate position relative to the forearm) matched that of the desired quasi-static angle value.

Quasi-static and dynamic results were expressed using the concept of SDA and transformed into the local coordinate system. A one-way ANOVA and a Tukey-Kramer post-hoc test were used to determine significant differences between the collection techniques, for rotations about and linear displacement along the X, Y, and Z axes.

RESULTS

Linear displacement along the X and Z-axes proved to be significantly different between collection techniques (p=.006 and p=.019, respectively). No other measurements were found to be significantly different (α=.05). In X-axis translation, the static collection showed a greater translation than that shown by the dynamic collection, indicating a more proximal position (Fig. 1). In Z-axis translation, the static collection also showed a greater translation than that of the dynamic collection. This would indicate a greater ulnar shift of the carpus (Fig. 2).

DISCUSSION

These results support the theory that collecting carpal kinematics in a quasi-static fashion may limit the ability to detect subtle carpal instabilities, including subluxations of the scaphoid and/or lunate. When position of the carpal bones is recorded in a static orientation with muscles loaded, it is possible that the constant pull at the tendon attachment causes the individual bones to sublux from where they would be at a discrete point in the time-series of a dynamic collection. This indicates an inherent laxity in the wrist joint that is exacerbated when held in a static position with load applied. If conclusions are drawn from kinematic studies where the motion is quasi-static and the muscles are loaded, the authors feel that errors may be made in judging the degree of instability existing between the carpals. Furthermore, it can be assumed that the discrete point in a wrist's rotation where subluxation does occur will likely be missed in kinematic studies of quasi-static design. The present study has put forth a method for dynamic carpal kinematic collection that can determine the discrete point of instability and quantify the amount of instability in three dimensions.

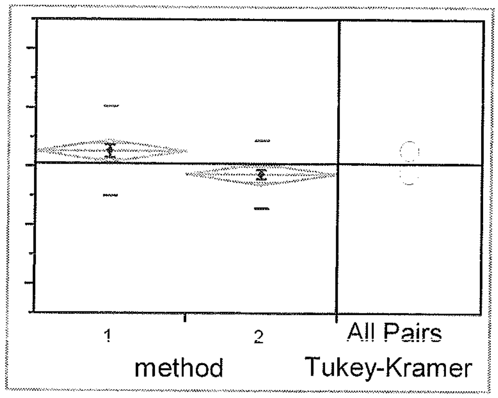

Figure 1. Significant difference in X-axis linear displacement. Methods 1 and 2 indicate the quasi-static and dynamic methods, respectively.

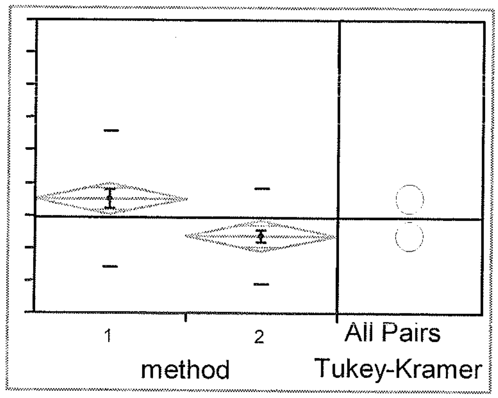

Figure 2. Significant difference in Z-axis linear displacement. Methods 1 and 2 indicate the quasi-static and dynamic methods, respectively.

REFERENCES

Brand, P.W., et al. J Hand Surgery, 1981

Short, W.H., et al. J Hand Surgery, 1995

ACKNOWLEDGEMENTS

This study was funded by the Mayo Foundation.

CARPAL BONE POSTURES AND MOTIONS ARE ABNORMAL IN BOTH WRISTS OF PATIENTS WITH UNILATERAL SCAPHOLUNATE INTEROSSEOUS LIGAMENT TEARS

S.L. Pike[1], D.L. Galvin[1], S.W. Wolfe[2], A-P.C. Weiss[1], E. Akelman[1], and J.J. Crisco[1]

[1]Department of Orthopaedics, Brown University, Providence, RI

[2]Department of Orthopaedics, Yale University, New Haven, CT

Email: joseph_crisco@brown.edu

INTRODUCTION

Motion of the human wrist is accomplished through complex kinematic patterns of the eight carpal bones, radius and ulna. Due to their small size, measuring the three-dimensional (3-D) kinematics of the carpal bones is a challenge, and has been achieved only in a small number of cadaveric (*in vitro*) studies. Kinematic analysis based on bone features and markerless registration is a potentially valuable tool for *in vivo* studies and clinical use, as it can accurately track joint motion without invasive markers [1,2].

Using one such markerless bone registration (MBR) method, we have studied normal healthy carpal motion in four directions of wrist motion. The purpose of this study was to determine if and how 3-D kinematics are altered *in vivo* when the scapholunate interosseous ligament (SLIL) is torn.

METHODS

Using computed tomography (CT)-based MBR, carpal bone postures and kinematics were determined for *both* wrists (defined as Injured and Uninjured) of 8 subjects with *unilateral* SLIL injuries (7 males, 1 female, avg. age: 38 [range: 20-54]). These values were compared to data from 20 healthy wrists defined as Normal (5 male, 5 female, avg. age: 26 [range: 21-47]).

Image Acquisition. After IRB approval and informed consent, both wrists were scanned simultaneously (voxel size: (0.2 to 0.9) x 1 mm^3) as patients held plastic grips aligned by protractors in neutral, 30° and 60° of flexion and extension, 20° and 40° of ulnar deviation, and 20° of radial deviation.

Bone Segmentation & Registration. Cortical surfaces of the carpal bones, radius, and ulna were segmented from the CT images. Left wrists were mathematically reflected into right wrists to simplify analyses. Bone postures and kinematics were calculated relative to the neutral position [2].

Data Analysis. Flexion(+)/extension(-) posture of a bone was defined as the angle between the sagittal plane projection of its principal inertia axis (I_1) and the long axis of the radius. Carpal bone motions were described using helical axis of motion (HAM) variables, consisting of a rotation about and translation along a unique axis, with respect to a coordinate system fixed in the distal radius. Bone rotations were plotted as a function of capitate rotation and fit with regression lines, for wrist flexion and extension. Capitate rotation was used as a measure of wrist rotation.

Statistics. A one-way ANOVA and Dunnett multiple comparison post-tests were used to compare postures of the bones in the neutral wrist position. Slopes of rotation regression lines for Injured and Uninjured wrists ($n = 8$), and Normal wrists ($n = 20$), were compared using Student's t-tests with a Bonferonni correction factor for multiple comparisons.

RESULTS AND DISCUSSION

Carpal Bone Neutral Postures. There were no significant differences between the neutral postures of the capitate bones in

Injured (-50° ± 19), Uninjured (-46° ± 23), and Normal subjects (-45° ± 9). This is important because all bone rotations were examined with respect to rotations of the capitate from its neutral posture.

Both the Injured (56° ± 13) and Uninjured (53° ± 7) lunates, however, were significantly less flexed ($p < 0.01$) than the lunate in Normal wrists (83° ± 8) in the neutral position (Figure 1). Both the Injured (34° ± 16) and Uninjured (27° ± 20) scaphoids were also significantly less flexed ($p < 0.05$) than Normal (49° ± 11).

Carpal Bone Rotations. In extension, Injured and Uninjured lunates rotated 35% and 26% as much as the capitate, respectively, each rotating significantly less ($p < 0.01$) than the Normal lunate, which rotated 69% as much as the capitate. They extended a similar amount to one another, however ($p = 0.77$). In flexion, the Injured and Uninjured scaphoids rotated 80% and 89% as much as the capitate, respectively, each rotating significantly more ($p < 0.01$) than the Normal scaphoid, which rotated 73% as much as the capitate. Again, their flexion was similar to one another ($p = 0.53$).

Varying bone rotations may be attributable to varying neutral bone postures, though the specific relation could not be proven in this study. For example, neutral Injured and Uninjured lunates were more extended than those of Normal subjects, leaving less range for further extension.

Remarkably, Feipel and Rooze have also recently reported abnormal bilateral kinematics in subjects with a variety of unilateral soft and hard tissue injuries, however they did not describe neutral posture differences [3]. Arkless, too, described a case for which a patient had post-traumatic unilateral wrist pain, but roentgenograms showed bilateral widening of the scapholunate joint [4]. The mechanism responsible for these bilateral differences has not yet been identified. In our study it is possible that aging affected wrist bone posture; mean injured subject age was 12 years greater than that of Normal subjects.

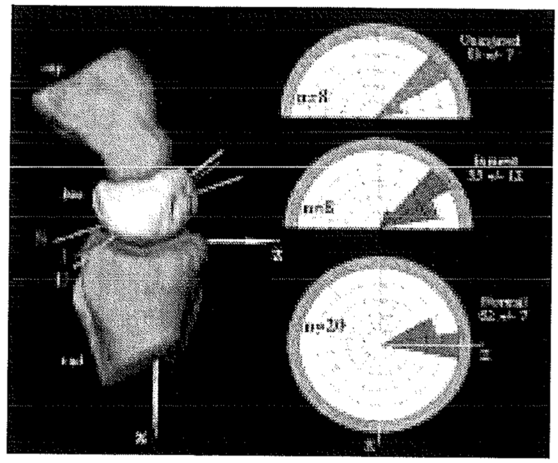

Figure 1: 3-D ulnar view of the neutral postures (I_1) of Injured, Uninjured, and Normal lunates. The capitate and radius are also rendered in dark grey. To the right are lunate posture angular histograms. Injured and Uninjured lunate postures were initially significantly less flexed than Normal, but similar to one another.

SUMMARY

Neutral postures of the scaphoid and lunate in wrists with SLIL tears were different from those of Normal subjects, though capitate postures, which were used as a measure of wrist position, were the same. Contralateral uninjured wrists were similar to the injured wrist and different from Normal. These postural differences may explain the abnormal bone rotations. Further research is needed to understand and confirm bilaterally abnormal wrist bone posture and kinematics in subjects with unilateral SLIL injuries.

REFERENCES

[1] Feipel & Rooze (1992) Surg Rad Anat 14: 341-8. [2]Crisco et al (1999) JOR 17(1): 96-100. [3] Feipel & Rooze (1999) Surg Rad Anat 21: 125-31. [4] Arkless (1966) Am J Roentgenol, Radium, Ther, Nucl Med 96(4): 837-44.

ACKNOWLEDGEMENTS

We thank C. Cobb & W. Smith for help in acquiring the CT images. Supported by NIH AR44005.

THE EFFECT OF EXTENSOR MECHANISM ON FINGER FLEXOR FORCE

[1]Z. M. Li, [2]V. M. Zatsiorsky, [2]M. L. Latash
[1]Department of Physical Therapy, Walsh University, OH 44720
[2]Department of Kinesiology, The Pennsylvania State University, PA 16802

INTRODUCTION

Several biomechanical models have been used in the literature to estimate muscle forces of individual fingers (Smith 1974; Ketchum et al. 1978; Harding et al. 1993). The purpose of this study was to compare two 2D biomechanical models in calculating hand muscle force in isometric tasks.

MEASUREMENT

The finger flexion forces were measured with the hand confined to 20° of wrist extension, 20° of flexion at the metacarpophalangeal (MCP) joint and full extension at the proximal and distal interphalangeal (PIP and DIP) joint. The measurements of force were performed at three anatomical locations: (a) at the middle of the distal phalanx of each finger (ExpDP), (b) at the DIP joint (ExpDIP), and (c) at the PIP joint (ExpPIP). Ten right-handed normal subjects participated the experiment. Subjects were instructed to press down vertically and maximally with: the index, middle, ring and little fingers on a pulling system (Li et al. 1998).

Table 1. Finger force production at different anatomical locations, mean (SD) from ten subjects), N

Location	Index	Middle	Ring	Little
ExpDP	46.5	40.4	28.1	23.2
	(12.7)	(11.9)	(6.4)	(5.1)
ExpDIP	47.4	44.9	28.9	21.3
	(9.0)	(15.5)	(6.3)	(3.9)
ExpPIP	53.7	52.5	40.1	34.5
	(26.3)	(23.5)	(10.8)	(9.8)

BIOMECHANICAL MODELING

Analysis included calculation of (a) the joint moments produced by the external forces as recorded in the experiment; (b) the internal muscular forces necessary to maintain equilibrium of the fingers in the static tasks.

Flexor model

In this model, it is assumed that (i) the flexor digitorum profundus (FDP) is the only flexor counterbalancing the external moment at the DIP joint, (ii) the FDP and flexor digitorum superficialis (FDS) maintain the equilibrium at the PIP joint, and (iii) the FDP, the FDS, and the intrinsic muscles (INT) maintain the equilibrium at the metacarpophalangeal (MCP) joint. In isometric conditions the phalanges are prevented from flexing, hence the phalanges can be considered a continuous rigid body. The moment equilibrium equations at the DIP, PIP, and MCP joints are:

$$\begin{aligned} &FDP\ b_{FDP,DIP} = M_{DIP} \\ &FDP\ b_{FDP,PIP} + FDS\ b_{FDS,PIP} = M_{PIP} \\ &FDP\ b_{FDP,MCP} + FDS\ b_{FDS,MCP} + LUM\ b_{LUM,MCP} \\ &+ UI\ b_{UI,MCP} + RI\ b_{RI,MCP} = M_{MCP} \end{aligned} \tag{1}$$

Extensor mechanism model

In this model, the effects of the intrinsic muscles on the extension of interphalangeal joints (extensor mechanism, Tubiana 1981) was modeled. The mechanism, without the activity of the extensor digitorum comunis (EDC), features the following: (a) The extensor hood surrounding the MCP joint receives tendinous fibers from the lumbricales and interossei. (b) The central tendon (extensor slip, ES) of EDC proceeds dorsally to attach to the middle phalanx, where tension from radial and ulnar bands (RB and UB) extends the PIP joint. (c) The RB and UB merge over the dorsum of the middle phalanx, forming the terminal extensor (TE) slip and inserting into the distal phalanx, where tension extends the DIP joint. (d) The lumbricale attaches proximally to the FDP tendon, and distally to the extensor mechanism; its activity increases passive tension in the extensor mechanism and decreases passive tension in FDP tendon's distal portion. The mechanical effects of the involved muscles/tendons at individual joints are listed in Table 2.

Table 2. Muscles/tendons involved in finger flexion and extension (adapted from Harding et al. 1993)

Joint	DIP	PIP	MCP
Muscle /tendon	FDP (+)*	FDP (+)*	FDP (+)*
	TE (−)	FDS (+)	FDS (+)
		ES (−)	RI (+)
		RB (−)	UI (+)
		UB (−)	LUM (+)

** Note that the FDP muscle force is reduced by lumbrical interaction at the DIP, PIP, and MCP joints. "+" indicates flexion force, "−" indicates extension force.*

With the extensor mechanism, the moment equilibrium equations at the DIP, PIP, and MCP joints are:

$$(FDP - LUM)\, b_{FDP,DIP} - TE\, b_{TE,DIP} = M_{DIP}$$
$$(FDP - LUM)\, b_{FDP,PIP} + FDS\, b_{FDS,PIP} - ES\, b_{ES,PIP} - RB\, b_{RB,PIP} - UB\, b_{UB,PIP} = M_{PIP}$$
$$(FDP - LUM)\, b_{FDP,MCP} + FDS\, b_{FDS,MCP} + LUM\, b_{LUM,MCP} + RI\, b_{RI,MCP} + UI\, b_{UI,MCP} = M_{MCP} \quad (2)$$

where $b_{i,j}$ is the moment arm of muscle i at joint j in Eq. (1) and (2) (adapted from An et al. 1979 with modification at the MCP joint according to standard kinematics method, Zatsiorsky, 1997). The following assumptions were made for the involved muscles and tendons (Smith 1974; Harding et al. 1993):

TE = 2/3 LUM + 1/3 UI
ES = 1/3 LUM + 1/3 RI + 1/3 UI
UB = 1/3 UI
RB = 2/3 LUM

The force generation capability of the intrinsic muscles was assumed to be proportional to the physiological cross-sectional area (Chao and An 1978) and represented as a lumped intrinsic muscle (INT), i.e., LUM = 0.083 INT, RI = 0.686 INT, UI = 0.23 INT

RESULTS

The force data of extrinsic and intrinsic muscle of individual fingers by the two models are shown in Table 3. The results suggest that when an external force was applied distally beyond the PIP joints, the extrinsic muscles are the major contributors in balancing the DIP, PIP, and MCP joints, and the simplified flexor model may be used to estimate the tension of the extrinsic muscles. However, the flexion model results in significant overestimation of the intrinsic muscle forces. If the external force was applied proximally beyond the PIP joint, the extensor mechanism has a large effect on force production of the extrinsic flexors, and it is unrealistic to employ the flexor model for the estimation of either extrinsic or intrinsic muscle forces.

References:

Smith (1974) Clin Orthop 104:92-111; Ketchum et al. (1978) J Hand surg 3(6):571-578; An et al. (1979) J Biomech 12:775-788; Chao and An (1978) J Engin Mech 104: 225-272; Harding et al. (1993) J Biomech 26(12):1403-1412; Zatsiorsky (1997) Kinematics of Human Motion. Human Kinetics. Li (1998) PhD Dissertation.

Table 3. Force produced by extrinsic muscles (FDP and FDS) and intrinsic muscle groups (INT) of individual fingers at different locations calculated by the flexor model (FM) and extensor mechanism model (EM)

		Index			Middle			Ring			Little		
		FDP	FDS	INT	FDP	FDS	INT	FDP	FDS	INT	FDP	FDS	INT
DP	FM	101.3	153.9	57.3	84.7	165.6	17.8	58.6	129.4	8.1	59.4	69	55.5
	EM	109.1	162	36.2	87.4	168.7	12.9	59.6	130.6	5.4	66.9	75.9	34.2
	%	-7.1%	-5.0%	58.3%	-3.1%	-1.8%	38.0%	-1.7%	-0.9%	50.0%	-11.2%	-9.1%	62.3%
DIP	FM	—	213.7	60.7	—	236.3	15.7	—	151.1	33.3	—	94.7	52.7
	EM	8.3	222.3	38.3	2.3	239	11.4	4.1	155.8	22.4	7.1	101.2	32.5
	%	—	-3.9%	58.5%	—	-1.1%	37.7%	—	-3.0%	48.7%	—	-6.4%	62.2%
PIP	FM	—	—	300.6	—	—	234.2	—	—	261.5	—	—	297.6
	EM	40.9	42.5	189.8	34.5	41.2	169.4	18.5	21.1	101.5	31.7	29	144.8
	%	—	—	58.4%	—		38.3%	—	—	157.6%	—	—	105.5%

THE EFFECT OF MIDSOLE PLUGS INSERTED INTO THERAPEUTIC FOOTWEAR FOR LOCALIZED PLANTAR PRESSURE RELIEF

[1,2]Jeffrey J. Saucerman, [1,5]Brian W. Loppnow, [1]David R. Lemmon, [1]John R. Smoluk and [1,3,4,5]Peter R. Cavanagh

[1]The Center for Locomotion Studies and the Departments of [2]Engineering Science and Mechanics; [3]Kinesiology; [4]Biobehavioral Health, Medicine, Orthopaedics and Rehabilitation; [5]Bioengineering Program
The Pennsylvania State University, University Park and Hershey, PA
Email: celos@psu.edu Web: www.celos.psu.edu

INTRODUCTION

Midsole plugs have been used in diabetic footwear to relieve focal areas of pressure under the foot (Brill et al., 1994). However, no current study in the literature has investigated the effects of midsole plugs to determine how well a plug may relieve plantar pressure. Additionally, there has been some debate on whether or not a plug intended for local pressure relief will redistribute stress by creating unwanted stress concentrations elsewhere. Through the use of both experimental methods and finite element (FE) models, the current research analyzes the effects of cylindrical midsole plugs made from soft foam. The FE model is then used to examine possible design modifications to plugs.

METHODS

Ten experimental conditions were examined in a single subject with elevated plantar pressure under the second metatarsal head (MTH). The experimental footwear consisted of an open sandal with a cloud crepe outsole, a cork midsole and an open-cell foam insole. Soft foam plugs of varied sizes were inserted into each midsole. Plug diameters of 19.0 and 25.4 mm were used, with plug depths of 3.2 and 9.6 mm. A high resolution Pliance pressure mat (Novel USA, Minneapolis MN) with 256 sensors in a 4 x 4 cm area was used to record plantar pressures from the subject during treadmill walking at a constant speed of 3.37 km/hr.

The subject's anatomical geometry was obtained from a sagittal plane ultrasound image, and a simplified two-dimensional plane strain FE model was created (see Figure 1). The model represents a second metatarsal embedded in homogeneous soft tissue. Footwear was added to the mesh using I-DEAS software (Structural Dynamics Research Corporation, Milford OH) to complete the model of the MTH2.

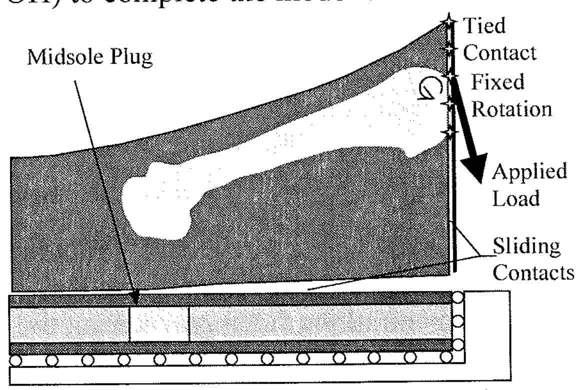

Figure 1: Schematic of the FE model.

Using material properties from the literature, soft tissue was characterized to be hyperelastic, while footwear materials utilized a hyperfoam model available in ABAQUS (Lemmon et al., 1997). Boundary conditions included a proximal restraint together with vertical and shear loading on the proximal end of the metatarsal. Footwear was constrained both vertically and horizontally.

To validate the FE model, custom code was used to convert a three-dimensional pressure distribution into a representative sagittal two-dimensional pressure distribution. Each experimental trial was compared to a matching FE model, and the difference in peak pressure was computed. A variation of the cylindrical midsole plug was prototyped using the FE model. By altering the material properties of elements in the midsole, a taper was introduced into the top of the plug. It was hypothesized that a taper may alleviate stress concentrations created by the plug.

RESULTS AND DISCUSSION

The FE model yielded results similar to the experimental pressure measurement. Model plantar pressure distributions were compared to experimental data, and peak pressures were generally found to be within 10% of experimental values. Both model and experiment demonstrated maximal pressure relief with a 6.4 mm insole, 25.4 mm plug diameter, and a plug depth of 9.6 mm. This combination allowed a pressure reduction at the control peak pressure site of 18.3% in experiments and 14.1% in the model compared to a 6.4 mm insole alone.

Analysis of the plantar pressure distributions from conditions with a plug showed that stress concentrations did appear during the propulsion phase of gait (see Figure 2). Although plantar pressure was relieved under the second metatarsal head, it was redistributed to the proximal edge of the midsole plug. These edge effects were sometimes even greater than the peak pressure seen in shoes with no plugs.

The prototype design of a tapered plug demonstrated the ease with which new designs may be tested in an FE model. The tapered plug caused a 20%, or 50 kPa,

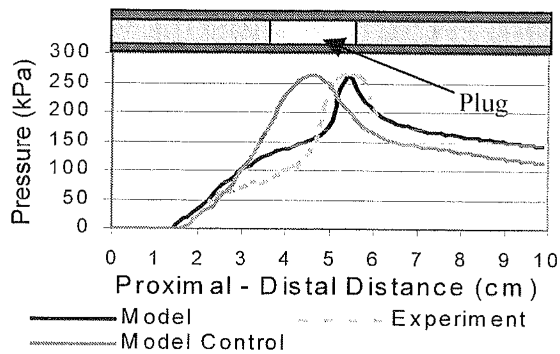

Figure 2: Typical comparison of model and experimental results. Note plug positioning with respect to the pressure distribution.

reduction in edge effect when compared to results for a cylindrical plug of the same plug size. The tapered plug was able to nearly eliminate all edge effects, while successfully reducing the pressure at the site of anatomical interest. The current research demonstrates that plugs should be used with caution, since they have been found to produce unintended edge effects. FEM may be an effective method for testing new footwear designs and reducing the number of experimental measurements.

SUMMARY

The therapeutic effect of midsole plugs in diabetic footwear has been analyzed using both experimental and computational approaches. Cylindrical plugs often cause stress concentrations, sometimes even higher than the original peak pressure. A prototype plug was designed using an FE model, which eliminates stress concentrations and reduces peak pressure.

REFERENCES

Brill, L.R. et al. (1994). *Prevention, protection and recurrence reduction of diabetic neuropathic foot ulcers.* Curative Technologies, Inc.

Lemmon, D.R. et al. (1997). *J. Biomechanics*, **30**, 615-620.

PRESSURE RELIEF AND LOAD REDISTRIBUTION BY A CUSTOM MOLDED INSOLE

Sicco A. Bus[1] and Peter R. Cavanagh[1,2,3,4,5]

[1]The Center for Locomotion Studies and the Departments of [2]Kinesiology; [3]Biobehavioral Health, [4]Medicine, [5]Orthopaedics and Rehabilitation; The Pennsylvania State University, University Park and Hershey, PA
Email: celos@psu.edu Web: www.celos.psu.edu

INTRODUCTION

Custom molded insoles (CMI) are routinely used in the care of diabetic patients with neuropathy. CMI are thought to relieve plantar pressures in regions 'at risk' for (re)ulceration by redistributing load to other regions of the foot. However, little quantitative evidence is available on the efficacy of CMI in achieving these goals. Therefore, the purpose of this study was to investigate the effect on pressure relief and load distribution of a CMI compared with a flat compliant insole in neuropathic diabetic patients with acquired foot deformity.

METHODS

Twenty diabetic patients (13 male, 7 female) with neuropathy and some degree of foot deformity participated in the study. Mean (± SD) age, height, and body mass was 64.4 ± 11.2 years, 1.73 ± 0.10 m, and 99.5 ± 15.7 kg, respectively. Using a first step approach, dynamic barefoot plantar pressures from each subject were recorded at 70 Hz with the Novel EMED-SF pressure platform. In-shoe plantar pressures from subjects wearing flat and custom molded insoles (Figure 1) were measured at 50 Hz with 99 element pressure sensing insoles (Novel PEDAR) that were placed between the sock and the insole of the shoe. A correction was made for sensor element size to allow barefoot and in-shoe pressure values to be compared. Approximately 30 mid-gait steps per foot per condition were collected as subjects walked at a preferred, and in subsequent trials, controlled walking speed along a 10m walkway.

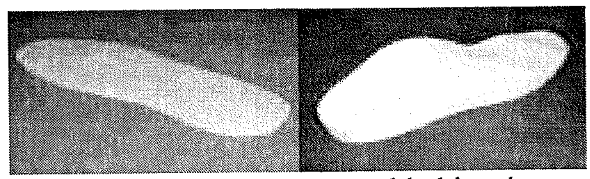

Figure 1. Flat and custom molded insole

All pressure data were analyzed with Novel Win, Ortho or Pedar Mobile software. The foot was divided into 10 anatomical regions as described by Cavanagh et al. (1987). For each region, mean (± SD) peak pressure (PP) and force-time integral (FTI) were calculated.

A sub-group of 21 feet was selected in which the first metatarsal head (MTH1) was the region of interest (ROI) based on either high barefoot pressure (>700 kPa) or prior plantar ulceration at this site.
A comparative regional analysis of PP and FTI between the two insoles was performed for these 21 feet by analysis of variance, ($p<0.01$). Load redistribution by the CMI compared to the flat insole was assessed using a new Load Transfer Algorithm (LTA) which, based on a series of assumptions, allows the direction and magnitude of inter-regional transfer of load within the foot to be determined. Since a metatarsal pad (MT) was incorporated into many of the CMIs a secondary analysis explored pressure relief and load distribution by metatarsal pads.

RESULTS

In-shoe PP was lower than barefoot pressure in all regions except the medial midfoot, 2nd toe and lateral toes regions (Table 1). Comparing insoles, PP and FTI were significantly decreased by the CMI in the lateral heel and 1st MTH and increased in the medial midfoot region. PP alone was significantly decreased in the medial heel and increased at the 2nd and lateral toes. FTI alone was significantly decreased at the lateral MTHs.

Table 1. Mean values for barefoot PP and in-shoe PP and FTI for all 21 feet with MTH1 as a region of interest in flat and CMI conditions.

	PP (kPa)			FTI (Ns)	
Region	**Bare**	**CMI**	**Flat**	**CMI**	**Flat**
Med. heel	409	236	305[a]	87	88
Lat. heel	323	236	311[a]	101	129[a]
Med. midf.	72	131	101[a]	65	26[a]
Lat. Midf.	162	133	123	76	72
1st MTH	892	314	373[a]	83	90[a]
2nd MTH	522	228	240	55	57
Lat. MTHs	454	189	186	77	85[a]
Hallux	477	303	297	30	32
2nd toe	150	195	169[a]	14	15
Lat. Toes	133	176	142[a]	18	16

[a] significantly different from CMI ($p<0.01$)

Individual analysis indicated that in 6 of the 21 feet, the CMI was successful in significantly reducing both PP and FTI at the 1st MTH when compared to the flat insole. In another 9 feet, either PP *or* FTI at MTH1 was significantly lower in CMI and this was considered moderately successful. In the remaining 6 feet, either PP or FTI were increased or unchanged in CMI and thus the intervention could not be considered to be successful.

The LTA revealed a large load transfer from the lateral heel region to the medial midfoot and a smaller transfer from the 1st MTH to the same midfoot region (Figure 2).

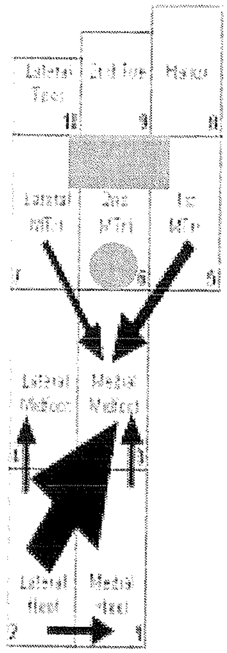

Figure 2. Load transfer (LT) between selected regions of interest (Size of arrow = amount of LT, values <3.0 Ns are discarded).

Table 2. Inter-regional LT (in absolute, % of Total load, and % of Regional load values)

Region	Ns	% T	% R
R2-R3	20.3 ±10.3	3.3	15.8
R5-R3	7.0 ±8.4	1.1	7.8

At the location of the MT pad (in figure 2), PP and FTI were significantly increased in 11 out of 14 feet analyzed when compared to the flat insole. At the effective area (in figure 2), load was decreased in all feet and PP in 9 feet.

DISCUSSION

Peak pressure and/or load at MTH1 were significantly reduced in 15/21 feet examined. These results demonstrate that an individual approach is required to the prescription and analysis of a CMI in a diabetic patient with neuropathy and acquired foot deformity. The data also show that 'cupping' of the heel in the CMI significantly reduced pressure and load in the lateral heel. The Load Transfer Algorithm offers a unique way to examine the mechanism of altered load distribution by a CMI.

REFERENCES

Cavanagh, P.R., Rodgers, M.M., Iiboshi, A. (1987). *Foot and Ankle*, 7, 262-276.

This work was supported by ConvaTec Inc.

ESTIMATION OF FIBULA LOAD-SHARING DURING DYNAMIC AXIAL LOADING OF THE LOWER EXTREMITY

James R. Funk, Lisa J. Tourret, and Jeff R. Crandall

Automobile Safety Laboratory, University of Virginia, Charlottesville, Virginia
Email: jrf4y@virginia.edu Web: http://cindarella.mech.virginia.edu/home.html

INTRODUCTION

Although many studies have investigated the role of the fibula in lower extremity axial load sharing, disagreement about its significance remains. Some studies have reported that the fibula bears less than 10% of the axial load of the leg (Segal et al., 1981; Takebe et al., 1984), while others have calculated fibula load sharing as high as 17% (Lambert, 1971; Wang et al., 1996). All previous studies have examined the role of the fibula quasistatically at relatively low loads. No prior research has attempted to quantify the magnitude of fibula load sharing dynamically at very high, potentially injurious axial load levels.

METHODOLOGY

Axial impact tests were conducted on twenty cadaver specimens in order to determine the injury tolerance of the foot/ankle complex to dynamic axial loading. Cadaver extremities were disarticulated at mid-femur and placed longitudinally in a test rig with the ankle in neutral position and the knee flexed 90° and constrained (Figure 1). The impact was delivered at 7 m/s by a pendulum which struck a transfer piston connected to the footplate. The test rig was instrumented with load cells and accelerometers at the footplate and knee block. A 5-axis load cell was implanted in the mid-diaphysis of the tibia with the fibula kept intact. Cubes equipped with triaxial magneto-hydrodynamic (MHD) angular rate sensors and accelerometers were mounted to the midfoot and tibia load cell assembly. After testing, specimens were x-rayed and dissected in order to evaluate injuries, and the foot and lower leg segment between the ankle and tibia load cell were weighed.

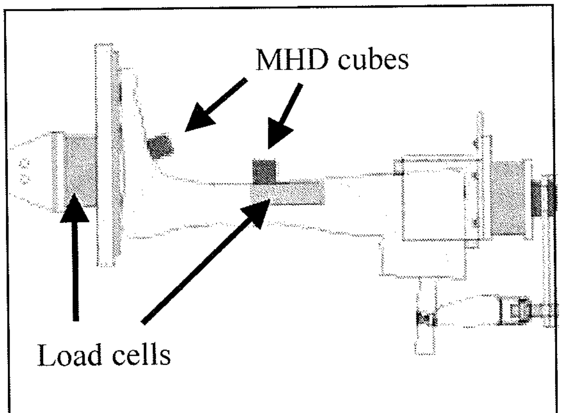

Figure 1. Schematic of test setup showing the location of key instrumentation.

The footplate axial load was inertially compensated for the mass of the footplate. Triaxial acceleration data were coordinate transformed to obtain the local axial accelerations of the foot and lower leg. Mid-shaft leg load was estimated by further inertially compensating the footplate load for the mass of the of the foot and lower leg using locally measured axial accelerations:

$$F_{leg} = F_{fp} - m_{foot}a_{foot} - m_{lowerleg}a_{lowerleg}$$

Fibula load sharing was estimated by comparing the peak inertially compensated total mid-shaft leg load to the peak locally measured mid-shaft tibia load:

$$\%Fibload = \frac{\left(F_{peakleg} - F_{peaktib}\right)}{F_{peakleg}}$$

RESULTS AND DISCUSSION

Peak calculated leg loads were higher than peak measured tibia loads in every case, indicating some amount of fibula load sharing (Figure 2). Injuries were produced in the foot and ankle region in 15 of the 20 limbs tested. The other 5 limbs either suffered no injury or more proximal fractures at the mid-shaft or tibia plateau.

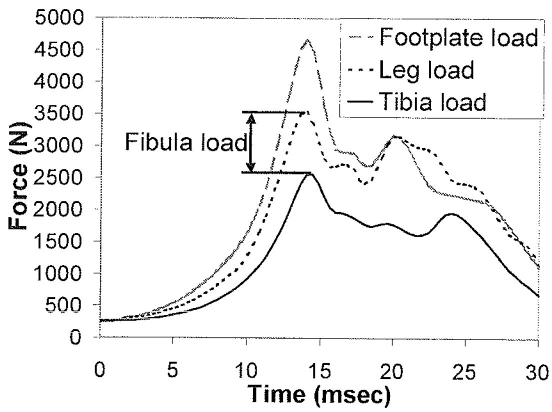

Figure 2. Sample time histories showing axial loads in the footplate, leg, and tibia.

It was found that the fibula bore significantly less relative load in specimens that suffered foot/ankle injuries compared to specimens that did not (Table 1). Fibula load sharing ranged from 6% to 28% in specimens with foot/ankle fractures and from 13% to 33% in specimens without foot/ankle fractures. The finding that the fibula bears 23% of the axial load in non-injured specimens is higher than any previously reported result.

However, this result is consistent with previous findings that relative fibula load sharing increases in eversion, and when the axial load increases (Takebe et al., 1984; Wang et al., 1996). Due to the geometry of the bones of the hindfoot, axial loading naturally induces eversion at the ankle. This eversion shifts the load path laterally. The very high fibula load sharing reported in this study may therefore be a consequence of the very high axial loads applied to the limb.

This hypothesis also explains why the fibula bears less relative load when there is injury to the foot/ankle complex. Injury disrupts the naturally occurring lateral load path, either directly by fracture of the lateral malleolus or distal fibula (5 of 15 injured specimens), or indirectly by fracture of the calcaneus or talus (14 of 15 injured specimens).

SUMMARY

This study is the first to quantify fibula load sharing during dynamic axial loading of the lower extremity. Inertial compensation was found to be a reasonable and repeatable technique for estimating mid-shaft leg loads. The fibula was found to bear significantly less relative load in specimens sustaining foot/ankle fracture. In specimens not suffering foot/ankle injury, it was estimated that 23% of the axial load was borne by the fibula, which is higher than anyone has reported previously.

REFERENCES

Lambert, K. L. (1971). *JBJS*, **53-A**, 507-513.
Segal, D. et al. (1981). *Foot & Ankle*, **2**, 25-29.
Takebe, K. et al. (1984). *CORR*, **184**, 289-292.
Wang, Q. et al. (1996). *CORR*, **330**, 261-270.

Table 1. Peak loads for injured and non-injured specimens (mean ± SD).

	Sample size	Footplate load	Tibia load	Leg load	% Fibula load*
Foot/ankle injury:	n=14	7.4 ± 1.8 kN	5.0 ± 1.4 kN	6.0 ± 1.6 kN	16.2 ± 7.4 %
No foot/ankle injury:	n=5	7.3 ± 0.5 kN	4.8 ± 1.2 kN	6.3 ± 1.4 kN	23.0 ± 7.6 %

*Significant difference between injured and non-injured specimens ($p < 0.05$)

FOOT BONE MOTION DURING MIDSTANCE

William Ledoux, [1,2] **Atsushi Kato,** [2] **Randal Ching,** [1,2] **and Bruce Sangeorzan,** [1,2]
[1] **RR&D Center for Excellence in Limb Loss Prevention and Prosthetic Engineering, VA Puget Sound, Seattle, WA**
[2] **Department of Orthopaedics, University of Washington, Seattle, WA**
Email: wrledoux@u.washington.edu **Web:** rehabctr.vamc.washington.edu

INTRODUCTION

Foot bone motion during weight-bearing is not completely understood. Previous research has employed X-ray photogrammetric techniques to describe the axes of foot joints (Lundberg et al., 1989a; Lundberg et al., 1989b; Lundberg et al., 1989c) or MR imaging to quantify nonweight-bearing motion (Udupa et al., 1998). Cadaveric models have been used to study weight-bearing conditions, although the motion of the individual bones of the foot was not quantified (Sharkey, 1998).

Our laboratory has developed a test protocol to simulate weight-bearing conditions on cadaveric feet (Ching et al., 1999; McCormack et al., 1998). Tests have been conducted to study well aligned, low arched (pes planus or flat foot) and high arched (pes cavus) feet.

This abstract will discuss bony rotations of well aligned feet for several loading conditions. Loads were applied to the tibia and Achilles tendon while the foot was in midstance position and the motions of the individual bones of the foot were measured.

METHODS

Ten fresh cadaver lower leg and foot specimens were obtained through the University of Washington Department of Biological Structure. Radiographic screening was performed to rule out pre-existing pathology. The soft tissue surrounding the tibial shaft was removed from each specimen, thereby exposing the extrinsic muscle tendons; only the Achilles tendon was used in the aspect of the study discussed here. Carbon fiber pins were placed into the tibia (ti), calcaneus (ca), talus (ta), navicular (na), cuboid (cu), first metatarsal (1m), and fifth metatarsal (5m). An acrylic rod was inserted into the intra-medullary canal of the tibia and cross-locked to allow for axial compressive loading of the foot. Each foot was then wrapped with moist towels and stored in plastic bags at -20°C until used.

For this study, only tibial and Achilles tendon loads were applied. A custom, acrylic foot-loading frame was fabricated. A pneumatic cylinder was used to load the foot via the tibial intramedullary rod, and a nylon cable and tendon clamp were used to connect the Achilles tendon to a second pneumatic cylinder. By adjusting the air pressure to each cylinder, the tibial compressive (T) and Achilles tendon tensile (A) loads could be controlled to generate the following loading conditions (in Newtons): T100-A0, T200-A0, T300-A0, T200-A100, T400-A200, and T600-A300. Since no other extrinsic muscles are included, these tests are only meant to simulate conditions that are on the order of physiologic loads.

Polhemus electromagnetic motion sensors (Fastrak 3-Space, Polhemus Inc., Colchester, VT) were used to record the 3-D motions of the foot bones. The sensors were attached via acrylic mounting blocks to the carbon fiber pins inserted in the seven bones of interest. Each sensor tracked the full six degree-of-freedom motion of the bone to which it was attached relative to a fixed transmitter. The motion data were recorded using a standard desktop personal computer. Positional and rotational accuracy of the sensors were verified to within 1-mm translation and 0.25-degree rotation.

RESULTS

The measured foot bone motions were similar, for the most part, to the motions expected due to bone morphology. As an example, the calcaneus plantar flexed under the applied loading conditions (Figure 1). Additionally, the relative bony rotations were expect. To demonstrate this concept, the rotation of all six bones for the T600-A300 loading condition in the three cardinal planes was given (Figures 2, 3 and 4). The tibia, although instrumented, was not included since the frame restricted its motion.

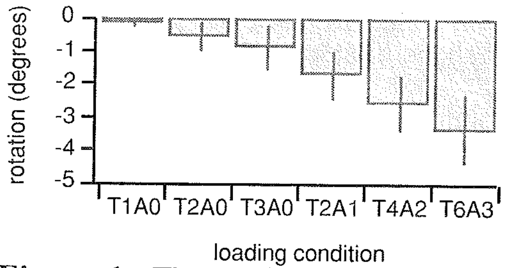

Figure 1: The rotation of the calcaneus in the sagittal plane (+ = dorsiflexion, - = plantar flexion) for the various conditions.

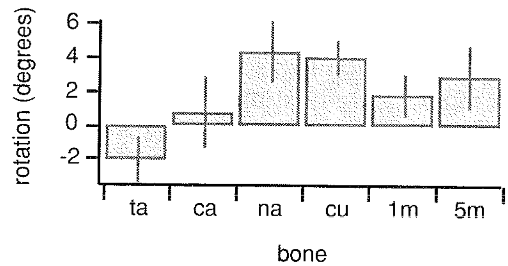

Figure 2: Rotation of the foot bones in the frontal plane (+ = eversion, - = inversion) for the T600-A300 condition.

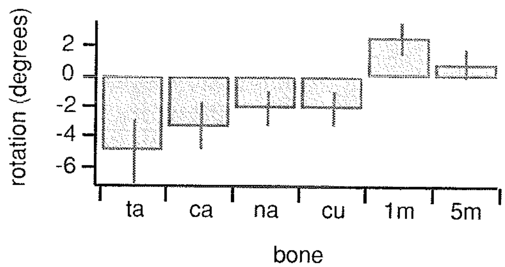

Figure 3: Rotation of the foot bones in the sagittal plane (+ = dorsiflexion, - = plantar flexion) for the T600-A300 condition.

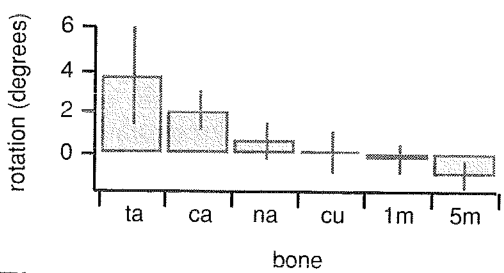

Figure 4: Rotation of the foot bones in the transverse plane (+ = internal, - = external) for the T600-A300 condition.

DISCUSSION

The bones of the foot demonstrated rotations that were mostly consistent with their bony morphology. Increased loading led to increased calcaneal motion in the sagittal plane. Note the effect of the Achilles tendon; the motion of the calcaneus increased when the tendon was loaded (compare T200-A0 to T200-A100 in Figure 1). The inversion of the talus was not expected, while the eversion of the remaining bones was (Figure 2). The plantar flexion of the talus, calcaneus, navicular and cuboid, and the dorsiflexion of the first and fifth metatarsal (Figure 3) demonstrated that the expected motion in response to loading the tibia and the Achilles tendon. The talus internally rotated more than the other bones (Figure 4), indicative of talar escape. The navicular and cuboid bones moved in very similarly in all planes, which was expected due to the tight ligamentous structures between them. Future work will involve physiologic loading simulations with all of the extrinsic muscles.

ACKNOWLEDGEMENT

This research was supported by Department of Veterans Affairs project number A0806C.

REFERENCES

Ching, R. P., et al. (1999). The effect of posterior tibial tendon rupture on hindfoot kinematics. In *Proceedings of the 17th Congress of the ISB* , Calgary, AB.

Lundberg, A., et al. (1989a). Kinematics of the ankle/foot complex: Plantarflexion and dorsiflexion. *Foot and Ankle*, **9**, 194-200.

Lundberg, A., et al. (1989b). Kinematics of the ankle/foot-Part 2: Pronation and supination. *Foot and Ankle*, **9**, 248-253.

Lundberg, A., et al. (1989c). Kinematics of the ankle /foot complex-Part 3: Influence of leg rotation. *Foot and Ankle*, **9**, 304-309.

McCormack, A. P., et al. (1998). Two reconstructive techniques for flatfoot deformity comparing contact characteristics of the hindfoot joints. *Foot Ankle Int*, **19**, 452-61.

Sharkey, N. A. (1998). High Fidelity Cadaveric Simulations. In *Proceedings of the 4th Annual Gait and Clinical Movement Analysis Meeting*, Dallas, TX.

Udupa, J. K., et al. (1998). Analysis of in vivo 3-D internal kinematics of the joints of the foot. *IEEE Trans Biomed Eng*, **45**, 1387-96.

COMPARISON OF RANGE OF MOTION, PERCEIVED PAIN, PLANTAR LOADING BEFORE AND AFTER SURGICAL CORRECTION USING THE AUSTIN PROCEDURE FOR HALLUX VALGUS - A 12 MONTH FOLLOW-UP

Kernozek, T.W., Ph.D. [1,2] , Sterikker, S. [3] ,Zimmer, K., [1] , Kopacz, J. [1]
[1] Physical Therapy Deparrtment, University of Wiscosin – La Crosse, La Crosse, WI;
[2] Gundersen Luthern Sports Medicine, La Crosse, WI
[3] Gundersen Hospital, La Crosse, WI
E-mail: kernozek.thom@uwlax.edu

INTRODUCTION

The hallux valgus (HV) deformity is an abnormality when there is lateral deviation of the distal end of the great toe accompanied with medial displacement of the distal end of the first metatarsal (Mann & Coughlin, 1981). The deformity is acquired, however, it has been suggested that a strong hereditary predisposition exists. The incidence ratio of females to males has been reported to be 8 or 9:1. Gender differences may be accounted for by combining the greater genetic predisposition and prolonged use of poor footwear. The etiology of this deformity remains unclear and is probably multifactorial (Scranton, 1983).

The goals of surgical intervention are to reduce the patients' level of discomfort, enhance the biomechanical alignment of the 1st. metatarsal and hallux, and improve cosmesis (Scranton, 1983). Numerous operative procedures are used to correct the HV deformity with no single procedure providing satisfactory postoperative results (Jahss, 1982).

Plantar loading patterns associated with a HV deformity seems to differ from those without the deformity. Blomgren et al. (1991) compared the pressure patterns of 66 patients with HV to 60 without the deformity. The HV group had greater maximum pressure in the small toe and tarsal regions, and less pressure in the 1st., 2nd., 3rd., and 4th. metatarsal and heel regions than controls. These results are similar to other studies where toe loading was reported to be lower with greater load on the lateral metatarsal heads for those with a HV deformity (Hutton & Dhanendran, 1981; Stokes et al. 1979). Both Grieve & Rashdi (1984) and Hutton & Dhanendran (1981) reported plantar load on the hallux decreased with an increased HV angle. Mitskewitch (1992) stated the greatest maximum pressure occurred in three locations depending on the severity of the deformity. The load distribution with HV was related to either pain under the lateral metatarsal phalangeal joints (Henry & Waugh, 1975) or pain associated with the lateral subluxation of the flexor mechanism and sesamoid complex caused by the deformity (Shereff, 1990).

The purpose of this study was to compare the perception of pain, range of motion (ROM) of the talocrural and first metatarsophalangeal joints, and plantar loading patterns before and after surgical correction for HV.

METHODS

Twenty five female participants with the diagnosis of a moderate or severe HV deformity were studied. All participants had an Austin osteotomy to correct their deformity. At the time of surgery, the mean HV angle was 31.7 ± 4.7°, while the mean intermetatarsal (IM) angle was 14.5 ± 1.7°. The primary surgeon performed all screening. The follow-up time was 12 ± 0.25 months. The mean age was 43 years (range 40 - 60 years).

The evaluation consisted of the participants completing an analog pain scale regarding their perceived pain during gait. Radiographs were then taken from dorsoplantar aspect in weight bearing and the HV and IM angles were measured. Seated talocrural joint and 1st. metatarsophalangeal joint ROM was measured using a goniometer. Pressure distribution measurements were performed barefoot for the involved limb on the second step. Data were collected using a capacitive pressure measurement platform (EMED SF Pedography Analyzer, Novel GMBH, Munich). The pressure platform consisted of a 32 X 62 sensor matrix with a resolution of 2 sensors/cm^2. The sampling frequency was fixed at 70 Hz. The platform was centered, flush within a walkway. Five trials were gathered for each participant. All procedures were repeated again 12 months after surgery.

Seven plantar regions on the foot were identified: 1 heel (HL) region, 1 midfoot (MF) region, 3 forefoot regions, and 2 toe regions. The 3 forefoot regions underneath the area of the metatarsal heads were divided into equal thirds. The medial forefoot (MFF) region was underneath the first metatarsal head, the central (CFF) region was underneath the 2nd. and 3rd. metatarsal heads, and the lateral (LFF) region was underneath the 4th. and 5th. metatarsal heads. The toe region was subdivided into 2 regions consisting of the hallux (MT) and the lesser toes (LT). The following variables were generated for each of the 7 plantar regions of the foot: peak force (PF) in %BW, force time integral (FTI) in %BW•s, peak pressure (PP) in kPa, pressure time integral (PTI) in kPa•s, and contact time (CT) in ms. A repeated measures multivariate analysis of variance (RM MANOVA) was used to detect differences in the loading parameters and range of motion measures before and after surgery ($p < 0.05$). Pain measures were compared with a dependent t-test.

RESULTS

Standing dorsoplanar radiographs were measured to determine HV angle and IM angle. The mean HV angle was $31.7 \pm 4.7°$ pre surgically and post surgically was $17.7 \pm 4.0°$. The average surgical correction was 14.0°. Pre surgical mean IM angle was $14.5 \pm 1.7°$ and $10.0 \pm 1.6°$ degrees postoperatively. The mean correction was 4.5 degrees. Significant changes were found in all radiographic measures.

Pre surgical and post surgical talocrural joint ROM and 1st. metatarsal phalangeal joint dorsiflexion ROM was unchanged. First metatarsal phalangeal joint plantar flexion ROM improved post surgically from 12.1° to 17.5°. Perceived pain during gait was reduced post surgically from 4.2 to 1.0.

No differences were found in any of the plantar loading parameters pre and post surgically in the HL, MF, MFF, LFF, and LT regions. The means and standard deviations for the forefoot and toe regions are located in Table 1. There were similar loading patterns in these plantar regions post surgically. Peak force and PP for the CFF increased post surgically. However, PTI, FTI and CT were unchanged in the CFF region. Peak force for the MT region was unchanged post surgically. Peak pressure, PTI, FTI and CT all decreased post surgically for the MT region.

Table 1: Regional plantar loading means and standard deviations pre and post surgically for Hallux Valgus.

Region	PF	FTI	PP	PTI	CT
MFF					
Pre	23.5 (6.1)	8.5 (2.7)	360.8 (156.8)	128.5 (55.2)	670.5 (93.1)
Post	25.2 (5.8)	8.6 (2.8)	436.2 (203.1)	149.4 (75.4)	631.1 (116.2)
CFF					
Pre	43.2* (6.1)	16.8 (3.3)	494.9* (186.3)	186.1 (73.3)	718.8 (99.5)
Post	47.4* (7.4)	17.6 (4.7)	619.8* (218.7)	168.7 (33.1)	676.0 (123.7)
LFF					
Pre	14.9 (4.5)	5.2 (1.8)	252.2 (171.5)	87.4 (49.6)	695.5 (104.2)
Post	14.9 (4.7)	5.4 (1.7)	265.6 (178.4)	83.9 (39.0)	649.1 (130.1)
MT					
Pre	12.4 (7.5)	3.8* (2.1)	439.3* (250.5)	120.9* (73.2)	602.0* (105.8)
Post	12.4 (6.2)	2.5* (1.6)	289.8* (169.4)	58.1* (38.9)	446.9* (138.3)
LT					
Pre	7.6 (4.4)	2.1 (1.2)	160.4 (79.7)	47.0 (25.0)	589.8 (113.9)
Post	9.1 (5.6)	2.1 (1.2)	202.3 (96.3)	58.1 (33.3)	582.8 (145.1)

DISCUSSION

Decreases in perceived pain during gait post surgically did not seem to increase plantar loading in the MFF or MT regions. First metatarsophalangeal joint plantar flexion improved post surgically, however this did not improve force production in the MT region. Henry et al. (1975) stated that accentuated loading under the CFF region is representative of the HV foot. Surgical intervention does not seem to change this characteristic but rather makes this CFF loading more pronounced based on PF and PP. Similar FTI, PTI and CT were observed pre and post surgically in the CFF region. Researchers have reported reduced loading under the MFF and MT compared to the non-pathological foot (Stokes et al, 1979; Hutton & Dhanendran, 1981; Grieve & Rashdi 1984). No changes in plantar loading were demonstrated in the MFF region in the present study. However, PF, FTI, PP, and PTI did increase slightly post surgically. Similar PF were found in the MT region but reduced FTI, PP, PTI and CT were found post surgically.

References

1. Blomgren, M., Turan, I., & Agadir, M. *J Foot Surg*, 30(1): 70-71, 1991.
2. Grieve, D.W. & Rashdi, T. *Ann Rheum Discuss*, 43: 816-818, 1984.
3. Henry, A.P.J. & Waugh, W. *J Bone Joint Surg*, 57-B(4): 478-481, 1975.
4. Hutton, W.C. & Dhanendran, M. *Clin Orthop*, 157: 7-13, 1981.
5. Jahss, M.H.: *Disorders of the foot*. WB Saunders, Philadelphia, 1982.
6. Mann, R.A. & Coughlin, M.J. *Clin Orthop Related Res*, 157: 31-40, 1981.
7. Mitskewitch, V. *Eur J Phys Med Rehab* 2(4): 4-10, 1992.
8. Scranton, P.E. *J Bone Joint Surg*, 65-A: 1026-1028, 1983.
9. Shereff, M.J. *Orthop*, 13(9): 939-945, 1990.
10. Stokes, I.A.F., Hutton, W.C. & Stott, J.R.R. *Clin Orthop*, 142: 64-72, 1979.

ACKNOWLEDGEMENTS

This project was supported by a UW-L Faculty Research Grant.

THE EFFECTS OF PHYSICAL ACTIVITY ON PREDICTED BONE DENSITY AND MICRODAMAGE ACCRETION OF THE FEMUR

Scott Hazelwood and Alesha Castillo

Orthopaedic Research Laboratories, University of California Davis, Sacramento, CA 95817
e-mail: sjhazelwood@ucdavis.edu

INTRODUCTION

An individual's physical activity level is thought to have a major influence on the density of load-bearing bones. For instance, significantly denser bone has been found in athletes compared to exercising and non-exercising controls (Nilsson and Westlin, 1971). Also, disuse studies have shown a severe amount of bone loss following bed rest or immobilization (Minaire et al., 1974; Whedon, 1984). Here, we used a bone remodeling simulation to study the effects of physical activity on bone density and damage accretion of the femur.

METHODS

A modified version of an internal bone remodeling simulation was used for this study (Fig 1, Hazelwood et al., 1997). In this model, bone density changes were determined by the amount of bone removed or added by active resorbing or refilling basic multicellular units (BMUs), respectively. Remodeling by BMUs was activated to remove damage and to eliminate bone in disuse. The mechanical stimulus, Φ, for remodeling was assumed to be proportional to the product of the strain range (s) raised to a power and the loading rate (R_L) from n different activities:

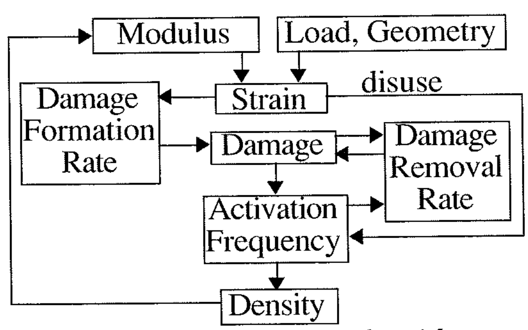

Figure 1. Bone remodeling algorithm.

$$\Phi = \sum_{i=1}^{n} s_i^q R_{Li}$$

The strain quantity, s, was assumed to be the principal strain with the maximum magnitude and the exponent, q, was set to 4. Disuse was defined as values of Φ below a set-point mechanical stimulus. Damage in bone was assumed to accrete at a rate proportional to the stimulus Φ. The damage removal rate was assumed to be proportional to the damage in the region, the BMU activation frequency, and the area resorbed by each BMU.

A 2-D finite element model (linearly elastic, isotropic), consisting of 4216 4-node quadrilateral elements, was created from a representative femur. A bony side plate was added to account for the out-of-plane cortical bone. Three load cases (single leg stance, abduction, and adduction), each consisting of joint reaction and abductor muscle forces, simulated the daily loading history for normal activity [equivalent to a femoral loading rate of 6000 cycles per day (cpd)]. Modulus-density relationships were determined from empirical data for both cortical and trabecular bone. The model's elements were initially assigned homogeneous material properties, and the modulus of each element was allowed to evolve over time.

A femur model for normal activity of an 800N person was run using ABAQUS 5.8 until the remodeling parameters achieved steady state. Using these results as the initial condition, remodeling was examined for an additional 1200 days for five different activity levels: (1) continued normal activity for the added period (baseline), (2) a 20% decrease in loading and activity, (3) a 20% increase in loading and activity, (4) a training schedule for runners varying between 25 and 40 miles per week (0 to 12 miles per day), and (5) daily running at 40 miles per week (an additional 3643cpd of loading on the femur).

Table 1. Predicted Femoral Density Results
[% increase (+) or decrease (-) of baseline]

activity	trochanter	prox. cortex	neck	head
20% decrease	-20.9	-22.2	-16.5	-18.6
20% increase	6.5	1.3	3.3	6.1
training sched.	3.0	-0.9	1.1	2.1
daily running	5.4	-3.1	0.7	5.4

RESULTS AND DISCUSSION

Inducing disuse by decreasing loading and activity by 20% had a substantial affect on femoral density compared to a 20% increase in loading and activity (Table 1). Bone loss in disuse was nearly equal in both cortical and trabecular bone regions, with most of the decrease in the cortical region found on the endosteal surface of the femoral shaft. When loading and activity were increased by 20%, density and damage increased slightly in the trabecular regions of the trochanter, neck, and head of the femur, with only minor increases observed in the cortical bone of the neck and proximal diaphysis.

Running according to a training schedule, with varying mileage and rest periods, produced smaller changes in the density of the femur than running performed on a daily basis, except in the neck region where density increases were approximately the same for both simulations (Table 1). Damage was 19 to 30% greater for daily running compared to the training schedule. Bone density decreases were observed in the proximal cortex for both running conditions. Modeling effects, which were not included in this simulation, may account for the net increase in bone density that has been observed in this region (Dalen and Olsson, 1974).

Although most stress fractures in athletes occur in the tibia, reports indicate that as many as 21% may occur in the femur (Johnson et al., 1994). These femoral fractures mainly appeared in the proximal cortex of the shaft and the inferior neck, locations which correspond to regions of high damage accretion in both running simulations (see Fig. 2 for daily running).

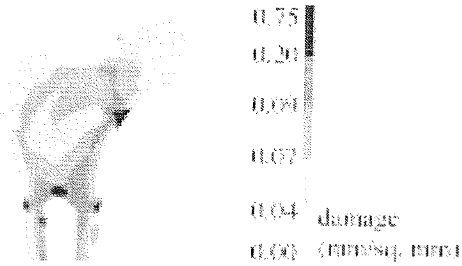

Figure 2. Increase in damage for the daily running condition at 40 miles per week compared to the baseline (normal) activity. Damage is defined as microcrack length per area bone.

SUMMARY

A simulation for internal bone remodeling was utilized to investigate the effects of physical activity on femoral bone density and damage accretion. While exercise may be useful in maintaining bone mass, disuse may lead to severe bone loss in the femur. A 20% decrease in loading and activity was observed to substantially reduce bone density in both cortical and trabecular bone. A 20% increase, on the other hand, produced only slight increases in density, primarily in the trabecular regions.

The training schedule reduced the femoral remodeling activity compared to the daily running schedule. The rest and varying mileage of the training schedule allowed the bone to more efficiently remove damage in all regions examined. Regions of high damage accretion for both running simulations correspond to observed locations of femoral stress fractures, indicating that the simulation may be useful in predicting fracture sites.

ACKNOWLEDGMENTS

Support provided by NIH grant AR41644.

REFERENCES

Dalen et al. (1974) *Acta Orthop Scan* 45:170.
Hazelwood et al. (1997) *Proc 21st ASB*, 256
Johnson et al. (1994) *Am J Sp Med* 22:248.
Nilsson, Westlin (1971) *Clin Orthop* 77:179.
Minaire et al. (1974) *Calcif Tiss Res* 17:57.
Whedon (1984) *Calcif Tiss Int* 36:S146.

FATIGUE CRACK GROWTH RATES IN EQUINE CORTICAL BONE

D.R. Shelton[1], J.C. Gibeling[1], R.B. Martin[2], S.M. Stover[3]

[1]Department of Chemical Engineering and Materials Science, College of Engineering
[2]Orthopaedic Research Laboratories, School of Medicine
[3]J.D. Wheat Orthopaedic Research Laboratory, School of Veterinary Medicine
University of California, Davis, CA 95616, email: rbmartin@ucdavis.edu

INTRODUCTION

Stress fractures are common in athletes, military recruits, and Thoroughbred racehorses, and may occur as hip fractures in the elderly. All of these injuries, to some extent, depend upon the propagation of fatigue cracks. Therefore, it is important to characterize the rates at which fatigue cracks grow and how microstructural differences found in cortical bone influence the crack growth rate. Mechanical and fatigue properties of equine third metacarpal (cannon) bone have been shown to vary with cortical region. Bend specimens taken from the lateral region were stronger and stiffer than those taken from the dorsal region under monotonic loading. However, dorsal specimens had a longer fatigue life (Gibson, et al., 1995). These results suggested that crack growth rates in different cortical regions might also differ.

For most engineering materials, a log-log plot of the rate of change of crack length (a) with number of cycles (N) versus the alternating stress intensity factor (ΔK) exhibits three distinct regions. At low ΔK, the crack growth rate data (da/dN) asymptotically decrease toward a threshold stress intensity factor. High ΔK values approach the fracture toughness of the material and result in fast fracture. This is manifest as an asymptotically increasing da/dN. Between these regions lies the Paris regime, which is commonly described by an equation of the form: $da/dN=C(\Delta K)^m$, where C is a constant and m is the Paris law exponent. Typically, the Paris law exponent has a value of 2 to 4 for metals and alloys, and 7 to 20 for ceramics (Suresh, 1991). To our knowledge, this type of curve has not been previously published for cortical bone. We tested the hypothesis that crack growth rate, and thus the Paris law exponent, differs within the lateral and dorsal cortices of equine cannon bone, tested in cyclic, Mode I loading.

METHODS

Six pairs of equine cannon bones were obtained fresh from Thoroughbred racehorses following necropsy. A bone saw was used to rough-cut two specimens from the mid-diaphysis of each bone, one from the lateral and one from the dorsal cortex. A mill was used to machine each rough-cut piece into a compact type (C(T)), specimen (Fig.1), measuring 25.4mm x 24.4mm x 5.0mm. The specimens were oriented such that the longitudinal axis of the bone was parallel to the loading direction. Side grooves were cut to a depth of 1 mm into each C(T) specimen (Norman, et al., 1992). The purpose of these grooves was to try to prevent the natural tendency of the crack to run longitudinally, parallel to the osteons.

The specimens were randomly assigned to a test matrix which determined the starting ΔK value for each test, ranging between 1.5-4.0 $MPa\sqrt{m}$. An MTS 810 servohydraulic test system was used first to precrack and then to fatigue crack the specimens in accordance with ASTM Standard E647-95. The control system was programmed to decrease ΔK with increasing a. Specimens were loaded at a frequency of 2 Hz.

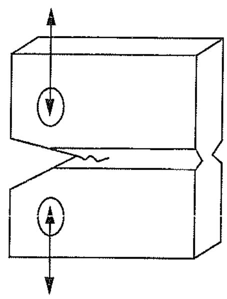

Figure 1 -Sketch of a C(T) specimen. Specimens were cyclically loaded in tension (as indicated by arrows) to propagate a transverse crack, perpendicular to the direction of loading.

During testing a drip system was used to keep the specimens wet and warm with calcium buffered normal (0.9%) saline (Gustafson, et al., 1996) containing an antimicrobial agent. The specimen temperature was maintained at 37 ± 2°C.

RESULTS

The alternating stress intensity factors and associated crack growth rates were plotted on a log-log plot for transverse crack propagation in dorsal specimens (Fig. 2). From this figure, assuming the threshold crack growth rate is 10^{-8} m/cycle, the threshold ΔK is 2.0 MPa$\sqrt{m}$ and the Paris law exponent is 10.2.

We were unable to obtain a similar plot for the lateral specimens since in all cases, in spite of the side grooves, the crack deviated from the desired path and ran longitudinally, thus invalidating the test. It should be noted that these results are not due to a failure of the test method, but reflect the dramatic differences in fatigue crack propagation resistance between the two regions.

DISCUSSION

The differences in crack growth behavior between the lateral and dorsal cortices appear to be another manifestation of regional property variations due, in part, to microstructural differences between regions.

We expect, based on previous studies (Martin et al., 1996 a,b), that histological evaluation of the test specimens will show that the dorsal region has greater porosity and smaller osteons than the lateral region. *In vivo,* the dorsal region of the equine cannon bone is loaded in tension and the lateral region is loaded in compression. It is likely that the observed variations in microstructure are due to the mechanical adaptation of these regions in response to the types of loading they experience.

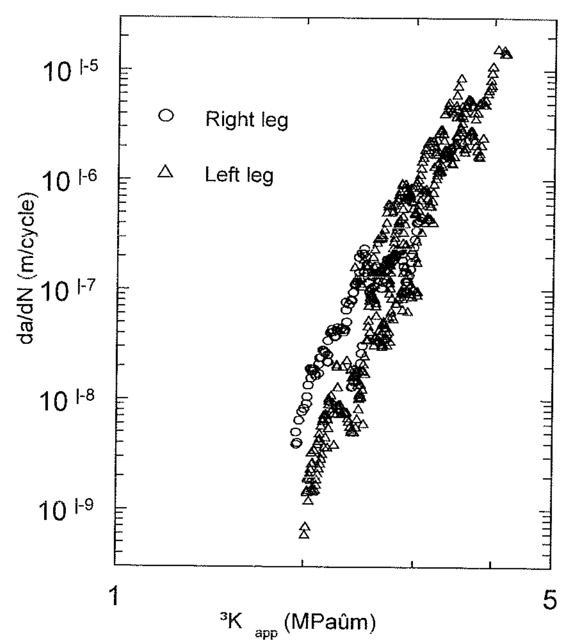

Figure 2 - Fatigue crack growth data for equine cannon bone, dorsal cortex.

REFERENCES

ASTM E647-95 (1995) ASTM, Philadelphia.
Gibson, et al. (1995) *J. Ortho. Res.* **13**:861-868.
Gustafson, et al. (1996) *J. Biomech.* **29**:1191-1194.
Martin, et al. (1996a) *Bone* **19**:165-171.
Martin, et al. (1996b) *J. Ortho. Res.* **14**:794-801.
Norman, et al. (1992) *J. Biomech.* **25**:1489-1492.
Suresh, S. (1991) *Fatigue of Materials.* Cambridge University Press.

ACKNOWLEDGMENTS

NSF Graduate Research Fellowship, NIH Grant AR41644, Hearst Foundation, Mr. & Mrs. A.J. Cooke, Calif. Horse Racing Board, Oak Tree Racing Assn., and the State of Calif. Satellite Wagering Fund.

ULTRASONIC CHARACTERSIZATION OF FATIGUE ACCUMULATION IN BOVINE CANCELLOUS BONE

Rho JY [1], Kankanla KR [1], Hoffmeister B [2], Gang Qi [3], and Zioupos P [4]

[1] Department of Biomedical Engineering, University of Memphis, Memphis, TN 38152
[2] Department of Physics, Rhodes College, Memphis, TN 38112
[3] Department of Mechanical Engineering, University of Memphis, Memphis, TN 38152
[4] Department of Materials and Medical Science, Cranfield University, Shrivenham SN6 8LA UK
E-mail: jrho@cc.memphis.edu Web: memphis.mecca.org/BME/

Introduction Ultrasound has been used as a powerful non-destructive tool in the field of composite materials to characterize the intrinsic changes in material properties at the microstructural level. Baste *et al.* (1996) reported that ultrasonic investigation detected all the microstructural changes in a ceramic matrix composite. The stiffening induced due to progressive closure of pre-existing prismatic pores was followed by degradation due to matrix transverse microcracking. The successful application of ultrasonic techniques in the fatigue testing of composite materials points to a possible use in similar studies on bone.

All fatigue testing done so far has been destructive in nature and have measured fatigue failure mechanism only in one direction, i.e., the direction of loading. For this reason, these studies cannot fully characterize the mode of failure in the other directions, which could yield valuable information pertaining to bone fatigue failure in vivo. The main objective of this study was to examine the ultrasound measurements to detect cyclic fatigue damage in the three orthogonal directions from cubic cancellous bone specimens. Secant modulus (determined by a servohydraulic cyclic loading system) and ultrasonic parameters (ultrasonic velocity and broadband ultrasound attenuation) were measured simultaneously.

Materials and Methods Seven specimens of trabecular bone were prepared from fresh frozen bovine proximal tibiae. The final specimens had flat and parallel surfaces with side lengths of 15 mm and were prepared using a low-speed saw with a diamond-wafering blade. Uniaxial compressive fatigue tests were performed on these specimens using a servohydraulic materials testing machine. Throughout the testing, the specimens were kept immersed in 0.9% saline solution in a custom-made irrigation chamber which was mounted on the actuator of the testing machine. Specimen were loaded at 2 Hz with a sinusoidal waveform under load control from 0 to 0.4 % compressive strain. The normalized secant modulus was determined from the load-displacement curve. At the end of each set of cycles, broadband ultrasound attenuation (BUA), longitudinal velocity (LUV) and apparent integrated backscatter (AIB) were determined.

Results The variation of the normalized secant modulus (Figure 1) and the ultrasound parameters is plotted over the number of cycles to fatigue failure for each specimen in all the measured directions. The normalized secant modulus was generally observed to remain constant during the initial period of fatigue loading. At higher number of cycles (> 10,000), there was a decrease in the modulus values. The BUA in all the directions was not changed during the initial stages of fatigue. However, the BUA in the A-P and S-I directions tended to increase during the final stages of fatigue. As the modulus values drop off rapidly at higher number of cycles, the BUA values in the A-P and S-I directions increase significantly, but that in the M-L direction shows less clear trends. The BUA in the S-I direction was the greatest, followed by those in the A-P and M-L directions, respectively.

The velocity values in all the three measured directions followed the path of the secant modulus degradation at higher number of cycles. A strong linear correlation was obtained between the secant modulus and the LUV in all three directions. However, unlike the indifferent trends observed for the BUA value in the M-L directions, the ultrasound velocities in these directions appeared to decrease consistently during the final stages of failure and also showed a good correlation with the secant modulus.

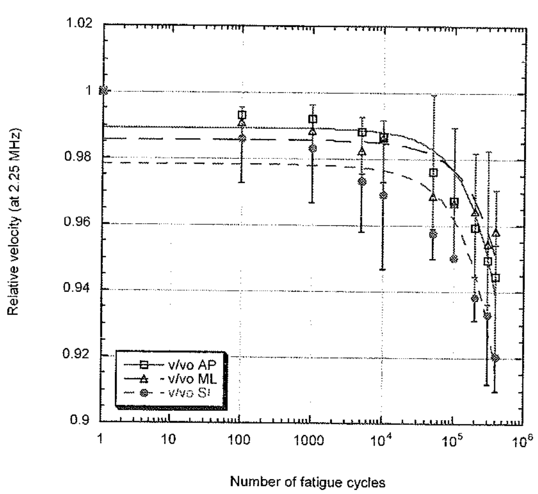

Figure 1. The longitudinal ultrasonic velocity (LUV) with fatigue in all three orthogonal directions in bovine cancellous bone.

Discussion The fatigue test results, in terms of the variation of the normalized secant modulus were followed with those obtained from earlier fatigue studies on bovine trabecular bone (Michel et al., 1993; Guo *et al.,* 1994). The variation of the BUA values depended on the direction of the measurements. By plotting the attenuation values in the A-P and S-I directions against the normalized secant modulus values during the latter stages of fatigue, a clear inverse linear correlations were shown. Williams *et al.* (1982) also found correlation between ultrasonic attenuation and fatigue in graphite/epoxy laminates. The correlation of microstructure and morphology with mechanical properties is an important aspect of ultrasonic evaluation.

The best ultrasonic parameter to indicate fatigue damage accumulation appears to be LUV, which correlated well with normalized secant modulus degradation. Also, this correlation was observed in each of the three orthogonal directions. As the bone specimens did not undergo any deformation at the structural level, this decrease in LUV could indicate the material property changes in the trabecular bone microstructure. The good inverse linear correlation between BUA (in the S-I direction) and normalized secant modulus supports the concept that ultrasonic attenuation possibly measures microstructural factors that govern stress wave propagation during microfailure events.

Reference Baste, S., El Bouzzaoui, R., 1996. Journal of Composite Materials 30, 282-308; Michel, M.C., Guo, X.E., Gibson, L.J., McMahon, T.A., Hayes, W.C., 1993. Journal of Biomechanics 26, 599-607; Guo, X.E., McMahon, T.A., Keaveny, T.M., Hayes, W.C., Gibson, L.J., 1994. J. Biomechanics 27, 145-155; Williams, J.H., Karagulle, H., Lee, S.S., 1982. Matl. Eval. 40, 655-662.

LONG BONES OF THE LOWER EXTREMITY EXPERIENCE SIMILAR STRAIN PROFILES DURING GAIT

Kelly J. Goodwin,[1,2] Marc M. Peterman,[1,2] Andrew J. Hamel,[1,3] and Neil A. Sharkey[1,2]

[1]The Center for Locomotion Studies, [2]Department of Kinesiology, and [3]Department of Mechanical Engineering, The Pennsylvania State University, University Park, PA
Email: celos@psu.edu Web: www.celos.psu.edu

INTRODUCTION

The primary mode of loading in most long bones is bending, with some superimposed axial compression. This bending and the resulting strains have been shown to be enhanced by the inherent curvature of long bones (Bertram and Biewener, 1988). It is also thought that bone curvature may serve to increase loading predictability and to achieve repeatable strain patterns during gait.

In addition to bone curvature, functional strains are influenced by other 'loading factors' that may include, but are not limited to, cross sectional geometry, tissue heterogeneity, and applied forces (muscle force, joint reaction force, ground reaction force (GRF)). The exact contribution of each of these factors will necessarily vary from one bone to the next.

The aim of this study was to determine if the different combination of loading factors acting on separate bones could conspire to produce similar strain distributions during functional loading. The study utilized a dynamic gait simulator (DGS) to characterize the strain distribution in the tibia and first metatarsal during the stance phase of gait. These bones were chosen because of their distinctly different structure and orientation within the lower extremity. Additionally, metatarsal curvature actually resists rather than enhances the naturally occurring bending moments due to the GRF.

METHODS

The DGS reproduces the kinematics and kinetics of the stance phase of gait (Sharkey and Hamel, 1998) while simulating the physiologic actions of the major extrinsic muscles of the foot. Five cadaver limbs were instrumented with strain gages, mounted in the DGS, and subjected to five trials under normal gait conditions.

The distal third of each tibia was instrumented with four stacked rosette strain gages (Micro-Measurements Group, Inc. WA-06-060WR-120) located on the anterior, medial, posterior, and lateral aspects of the bone within the same transverse plane. Rosettes were also affixed in the same manner to the dorsal, lateral, and plantar aspects of the mid-diaphysis of the first metatarsal. Strain data were collected simultaneously from both bones for the duration of each trial.

Principal strains and directions were calculated at each gage site. Axial strain gradients were calculated across the transverse section using the method of Rybicki et al. (1977).

RESULTS

The strain profiles of the two bones followed the magnitude of the vertical GRF (Figure 1). The tibia appears to be more affected by forces at heel strike than the metatarsal. However, both bones reach peak strains at toe-off. The magnitude of strains developed at the periosteal surface of the tibia was always greater than the first metatarsal strains. Throughout mid-stance, the average variation in principal axis direction was 9 (±3) degrees in the tibia and 32 (±18) degrees in the metatarsal.

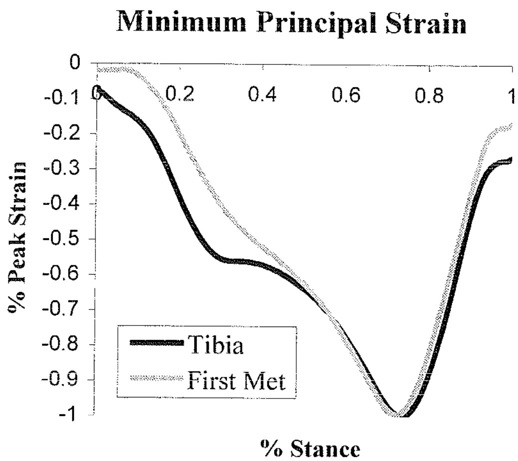

Figure 1: Normalized minimum principal strains of the posterior tibia and dorsal surface of the first metatarsal during stance. The plots represent average strains at each location over all five specimens.

DISCUSSION

Based on the structure and orientation of each bone, it is not necessarily intuitive that they would experience similar strain profiles during gait. Both the intrinsic (curvature, cross section geometry) and extrinsic loading factors in each bone resulted in a restricted strain environment that was consistent between the two bones and across specimens.

Of particular interest was the relationship between the direction of bone curvature and whether this curvature tended to resist or enhance bending of the bone. Bertram and Biewener have proposed that bone curvature serves to increase the loading predictability of bone while accentuating bending strains (1988). The first metatarsal is an exception to this case in that both the direction of curvature and the applied muscle forces act to *reduce* bending moments caused by the GRF.

It seems plausible therefore that the role of bone curvature is not necessarily to enhance bending strain, but is more suited to simply increase load predictability and provide a means to achieve a repeatable strain distribution. Strain magnitudes are then modulated by other extrinsic factors such as applied muscle forces and GRF. Loading predictability would appear to be especially critical in the metatarsals, where more variable external loading regimes occur, and curvature can serve to redirect variable forces into a repeatable loading pattern.

SUMMARY

Similar patterns of functional strain occur in the tibia and first metatarsal during normal gait even though different loading factors act on each bone. This finding suggests that strain profiles are not unique to a single bone, and loading predictability is important regardless of the tendency of bone curvature to either enhance or restrict bending strains.

REFERENCES

Bertram J., Biewener A.A. (1988). *J Theor Biol*, 131:75-92.
Rybicki E.F. et al. (1977). *J Biomech*, 10:701-795.
Sharkey N.A., Hamel A.J. (1998). *Clin Biomech*, 13:420-433.

ACKNOWLEDGEMENTS

The support of the Department of Kinesiology and the College of Health and Human Development is appreciated.

THE EFFECT OF UNILATERAL LIMB IMMOBILIZATION ON THE TIBIA AND FEMUR OF MOUSE

Timo Jämsä [1], Antti Koivukangas [1], Jorma Ryhänen [2], Pekka Jalovaara [1,2] and Juha Tuukkanen [1]

[1] University of Oulu, Oulu, Finland
[2] Oulu University Hospital, Oulu, Finland
Email: timo.jamsa@oulu.fi

INTRODUCTION

Mechanical stimuli are essential for the skeleton, and immobilization produces rapid bone loss in the weight-bearing bones (Peng et al. 1994). It is probable that a reduction of physical activity may also affect the involutional osteopenia seen in elderly people. Immobilization of a limb provides an experimental way to study mechanical influences on bone tissue without interfering with hormonal homeostasis. The present study was carried out to evaluate densitometric and mechanical changes in the tibia and femur during unilateral limb immobilization model in mouse (Jämsä et al. 1999).

MATERIALS & METHODS

The right hind legs of male NMRI mice were immobilized for three weeks against the abdomen by an elastic bandage with the hip joint in flexion and the knee and ankle joints in extension. Age-matched controls with no immobilization were used as controls. After sacrification, the tibiae and femora were dissected out.

The bones were scanned using a peripheral quantitative computed tomographic pQCT system (Norland Stratec XCT 960A) using a voxel size of 0.092 x 0.092 x 1.25 mm^2 and an attenuation threshold value of 0.93 cm^{-1} for cortical bone.

The tibial diaphysis was scanned at mid-shaft (Jämsä et al. 1998a) and at the proximal metaphysis, 3 mm from the proximal end of the bone. The femoral neck was scanned with the femoral neck in an axial direction (Jämsä et al. 1998b). Total and cortical bone mineral content (BMC), total and cortical bone mineral density (BMD), and cross-sectional area (CSA) were used for analyses.

The three-point bending strength of the tibial and femoral shaft and the strength of the femoral neck in axial and lateral loading configurations (Jämsä et al. 1998b) were measured (Fig. 1).

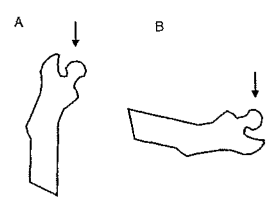

Figure 1: (A) Axial and (B) lateral loading of the femoral neck.

RESULTS AND DISCUSSION

Body weight decreased by 13.5% ($p < 0.001$) during the immobilization, indicating an overall decreased activity in this model. The pQCT analysis showed that CSA, BMC and BMD were significantly reduced at all three scan sites in both legs of the immobilized animals compared with the controls. However, with the exception of BMD of the tibial diaphysis, only the femoral neck showed a statistically significant difference between the immobilized and contralateral leg. The cortex was found to be a dominant discriminator at the femoral neck, which is in good agreement with the former findings that bone loss does not only occur in trabeculae but is accompanied by a decrease in cortical thickness (Weiss et al. 1991).

Mechanically, the tibia was a more sensitive indicator of bone loss in diaphyseal bending strength than the femur. The femoral neck also showed decreased strength, and the difference between the immobilized leg and the contralateral leg was most clearly seen in the lateral loading of the femoral neck. (Fig. 2)

SUMMARY

We conclude that three weeks of hind limb immobilization weakened the tibia and femur significantly compared to their contralateral counterparts. The reduction was more significantly seen in the mechanical bending strength than in the pQCT evaluation. The femoral neck showed more significant weakening than the diaphysis or the tibial metaphysis, and lateral loading was the most sensitive indicator of bone loss.

REFERENCES

Peng, Z., Tuukkanen, J., Zhang, H., Jämsä, T., Väänänen, H.K. (1994) *Bone* **15**, 523-532.

Jämsä, T., Koivukangas, A., Ryhänen, J., Jalovaara, P., Tuukkanen, J. (1999) *J. Bone Miner. Res.* **14**, 1708-1713.

Jämsä, T., Jalovaara, P., Peng, Z., Väänänen, H.K., Tuukkanen, J. (1998a) *Bone* **23**, 155-161.

Jämsä, T., Tuukkanen, J., Jalovaara, P. (1998b) *J. Biomech.* **31**, 723-729.

Weiss, A., Arbell, I., Steinhagen-Thiessen, E., Silbermann, M. (1991) *Bone* **12**, 165-172.

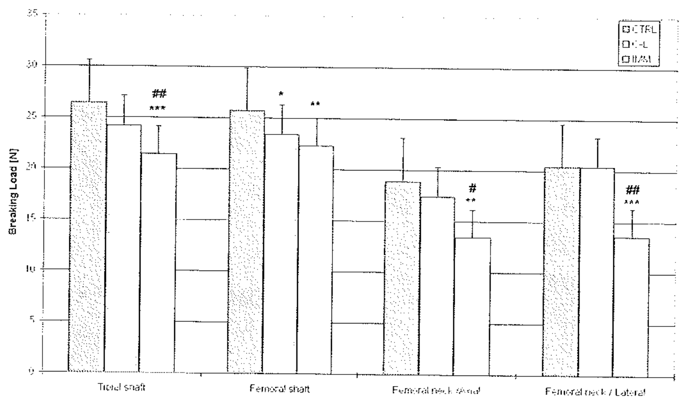

Figure 2: Breaking load of the bones of the immobilized (IMM) and contralateral (C-L) legs and controls (CTRL).

THE ONE-LEGGED AND TWO-LEGGED VERTICAL JUMPS: A KINETIC AND TEMPORAL ANALYSIS

Brandi Row[1,2] and Alan Hreljac[1,3]

[1]University of Oregon, Eugene, OR
[2]The Center for Locomotion Studies, The Pennsylvania State University, University Park, PA. [3]California State University, Sacramento, CA
Email: bsr7@psu.edu

INTRODUCTION

The one-legged and two-legged vertical jumps are used by athletes to propel themselves into the air in various athletic circumstances. In the one-legged technique, only one leg is in contact with the ground during the ground support time, appearing as a running jump, whereas the two-legged jump has both legs in contact with the ground during this time. The differences between the one-legged and two-legged squat and countermovement jumps have been investigated (van Soest et al., 1985), but there are few accounts of the differences in these conditions using a running approach (Vint & Hinrichs, 1996), as it is used in athletic competition.

Referring to the terminology of the deterministic model proposed by Hay (1993), these two jumping styles achieve the same reach height (Vint & Hinrichs, 1996), but there is a difference between the flight heights and take-off heights, with the flight heights being 0.09 m (16.7%) greater in the two-legged jump, and the take-off height being 0.10 m (8.1%) greater in the one-legged jump (Vint & Hinrichs, 1996).

The purpose of this study was to examine whether the overall jump height would be the same between the two conditions using a population of athletes trained in the two jumping techniques, and to investigate the temporal and kinetic differences.

METHODS

Eighteen female volleyball and basketball athletes were included in the study. The subjects had a mean age of 17.17 ± 1.58 years, standing height of 1.72 ± 0.068 m and mass of 65.8 ± 9.32 kg. The criteria for inclusion in the study were that the athlete was a part of a competitive volleyball or basketball team at the time of the study, was in training for her sport, and was familiar with the use of both the one-legged and two-legged vertical jumps.

Five maximum jump attempts in each condition where the feet landed appropriately on the force platform were collected. Only the trials that resulted in the maximum jump height were included in this analysis. The subjects were allowed a run-up of their preference during their jump, usually consisting of three steps. The approximated flight height, the difference between the reach of the fingers while standing flat-footed and at the top of the jump, was measured using a Vertec© vertical jump measuring device.

The movement was separated into an eccentric, or loading phase (the time between foot strike and maximum knee flexion) and a concentric, or propulsive phase (the time between maximum knee flexion and toe-off). Foot strike, toe-off and the kinetic data were determined from the vertical ground reaction force at 500 Hz.

Knee flexion was measured with an electrogoniome .

Statistical t-test. p<0.05) were performed on the intercondition approximated flight heights (H_{AF}), the total, eccentric and concentric ground support times (TOT, ECC and CON, respectively), the average vertical forces during the eccentric and concentric phases (FECC and FCON), the negative and propulsive impulses (IECC, ICON), the impact and active peaks (IPK, APK), and the impact loading rates (RTI).

RESULTS AND DISCUSSION

There was no difference in H_{AF} of the two conditions (Table 1). There were, however, differences in many of the other parameters (Table 1). TOT was greater for the two-legged jump, due to the longer ECC loading for that condition. IPK was greater for the one-legged condition, but APK was higher in the two-legged condition. Even while achieving the same height, the IECC and ICON, FCON were greater for the two-legged jumps.

The greater impulses and average concentric forces of the two-legged jump were not double those values of the one-legged jump, even with the addition of the second leg's musculature. The higher impact peak for the one-legged jump indicates a possible increase in muscle stiffness prior to the impact. An advantage of increased stiffness would be an increased ability to store elastic strain energy, and/or increase the capacity of the muscle to do positive work once the concentric contraction begins during the propulsive phase of the jump. The shorter time of eccentric loading during the one-legged jump may also have allowed for the reutilization of prestretch elastic energy.

SUMMARY

The one-legged and two-legged vertical jumps do not differ in jump height in a group of athletes accustomed to their use. The two-legged jump results in greater impulses and forces, and the one-legged jump utilizes a higher take-off height (Vint & Hinrichs, 1996) and potentially benefits from increased muscle stiffness on impact.

REFERENCES

Hay, J. (1993). *The Biomechanics of Sports Techniques, Fourth Edition.* London, England: Prentice-Hall.

Van Soest, A. et al. (1985). *Med Sci Sports Exerc,* **17**(6), 635-9.

Vint, P.; Hinrichs, R. (1996). *J Appl Biomech,* **12**, 338-58.

Table 1: Comparison of H_{AF}, temporal and kinetic parameters of both conditions (mean ± SD). * $p < 0.05$, ** $p < 0.001$

Variable	Condition	
	One-legged	**Two-legged**
H_{AF} (cm)	49.88 ± 4.40	49.23 ± 5.82
TOT (ms)	262 ± 31.68	339 ± 43.4**
ECC (ms)	137 ± 26.22	211 ± 41.21**
CON (ms)	126 ± 21.79	128 ± 18.97
IPK(BW)	2.28 ± 0.77*	1.76 ± 0.44
APK (BW)	2.98 ± 0.38	3.26 ± 0.37*
RTI (BW•s)	99.43 ± 40.6	78.92 ± 46.4
IECC (BW•s)	0.29 ± 0.06	0.43 ± 0.07**
ICON (BW•s)	0.25 ± 0.05	0.29 ± 0.05*
FECC (BW)	2.17 ± 0.40	2.04 ± 0.29
FCON (BW)	1.98 ± 0.17	2.23 ± 0.21

ADAPTATION OF RUNNING KINEMATICS TO SURFACE AND FOOTWEAR

E.C. Hardin[1], J. Hamill[1], and A.J. van den Bogert[2]
[1]Department of Exercise Science, University of Massachusetts, Amherst MA
[2]Department of Biomedical Engineering, Cleveland Clinic Foundation, Cleveland OH
E-mail: bogert@bme.ri.ccf.org

INTRODUCTION

Runners change their leg stiffness inversely to surface stiffness in order to maintain similar whole body movement on different surfaces (Ferris et al., 1998). It is generally thought that such adaptations mainly involve changes in knee joint angle, e.g. an increased knee flexion would lead to decreased leg stiffness (Frederick 1986; McMahon et al., 1987). Direct evidence of kinematic changes is scarce, however. This may be due to the fact that the changes are small (McNair and Marshall, 1994), though potentially important.

Running impact occurs at small flexion angles. The leg stiffness is therefore initially large and may be sensitive to changes in knee angle (McMahon et al., 1987). The purpose of our work was, then, to experimentally determine changes in sagittal plane kinematics during the stance phase of running as a function of shoe and surface and to interpret these changes as to their effect on overall leg stiffness.

METHODS

Twelve male subjects ran at a speed of 3.4 m s^{-1} on a treadmill with adjustable surface compliance. Six different combinations of surface and shoe stiffness were created and all measurements were done when the subjects were at metabolic steady state. Sagittal plane kinematic data were collected at 200 Hz with reflective markers placed on the humeral head, greater trochanter, femoral condyle, lateral malleolus, calcaneus and fifth metatarsal. Marker paths were digitally filtered at 12 Hz and hip, knee and ankle joint angles were calculated. Mean values were calculated from 10 randomly selected stance periods for joint angle at contact, maximum joint angle and peak joint velocity. A two-way repeated-measures ANOVA was used to test for surface and midsole differences ($p<0.05$).

A two-segment model (McMahon et al., 1987) was used to establish theoretical force-length relationships of the lower extremity. If the segments have length L, the knee joint has rotational stiffness k, and heel strike occurs at knee angle φ_0, the force F depends on the joint angle φ as follows:

$$F = \frac{k(\varphi - \varphi_0)}{L \sin \frac{\varphi}{2}}$$

Length change as a function of joint angle is:

$$\Delta = 2L\left(\cos\frac{\varphi_0}{2} - \cos\frac{\varphi}{2}\right),$$

resulting in nonlinear spring properties for the leg as shown in Fig. 1.

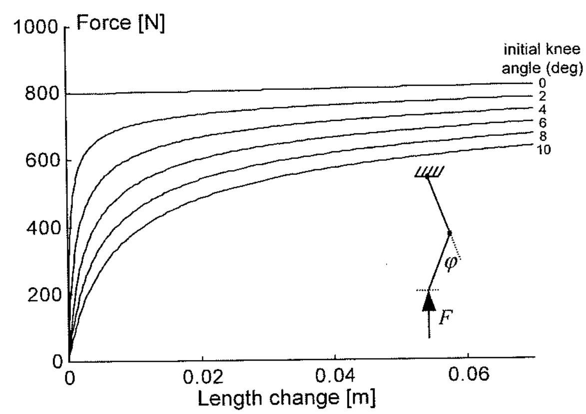

Figure 1: Force-length curves for the leg model with k=200 Nm/rad and L=0.5 m.

RESULTS AND DISCUSSION

Experimental results are presented in Table 1. As surface compliance increased, knee flexion at touchdown decreased ($p<0.05$), peak knee angle remained the same ($p>0.05$) and peak joint velocity of the hip, knee and ankle increased ($p<0.05$). Effects of midsole hardness were smaller.

"Increased knee flexion" has been proposed as a mechanism for adaptation to running on hard surfaces (Frederick, 1986; McMahon et al., 1987; Ferris et al., 1998) but it is unclear whether this term refers to flexion angle at impact, at midstance, or a larger change in angle between these two events. Our results clearly show that, for this range of surface stiffness, runners impacted with more extended knee on a harder surface while the peak flexion angle did not change. Consequently, knee flexion velocity increased with increasing surface stiffness. These results are consistent only with the third interpretation of "increased flexion."

The two-segment model qualitatively shows the effect of initial knee angle. When impacting with a more extended knee the short-range stiffness (slope of the force-length curve) quickly decreases, whereas an initially more flexed knee leads to a *greater* short-range stiffness at the same stage of leg deformation. This "buckling" behavior, when initial flexion angle is small, may regulate the magnitude of impact force. Limitations of the model are assumptions of constant joint stiffness and muscle activation. Both rise during knee flexion and would result in a larger force than predicted. However, the striking effect of geometry remains.

We conclude that runners modify their lower extremity geometry to adapt to surface stiffness. These adaptations may reflect adjustments in leg stiffness. Leg stiffness varies rapidly during impact, thus models with constant stiffness may not provide insight into impact-related questions.

REFERENCES

Frederick EC (1986) *J Sports Sci* **4**:169-184.
McMahon TA et al. (1987) *J Appl Physiol* **62**:2326-2337.
McNair PJ, Marshall RN (1994) *Br J Sports Med* **28**:256-260.
Ferris DP et al. (1998) *Proc R Soc B* **265**:989-994.

Table 1. Mean sagittal kinematic variables during running stance. Significant differences noted by a superscript: a = 100>200>350; b = 100 & 200 >350; c = 100<200<350; d = midsole effect.

	Midsole	40 Shore A			70 Shore A		
	Surface	100 $kN \cdot m^{-1}$	200 $kN \cdot m^{-1}$	350 $kN \cdot m^{-1}$	100 $kN \cdot m^{-1}$	200 $kN \cdot m^{-1}$	350 $kN \cdot m^{-1}$
Touchdown angle (°)	Hip[a]	22.5	20.0	14.7	23.7	20.4	15.5
	Knee[b]	9.8	8.2	4.6	10.9	8.4	4.4
	Ankle	-1.2	-3.2	-1.4	-2.4	-3.8	-2.3
Maximum flexion/ dorsiflexion (°)	Hip[b, d]	26.4	25.8	22.9	27.4	27.1	24.3
	Knee	41.0	41.7	42.3	42.1	42.6	42.5
	Ankle	21.0	19.5	22.0	20.5	19.2	21.0
Maximum flexion velocity ($° \cdot s^{-1}$)	Hip[c, d]	87.9	121.3	154.3	86.1	138.1	169.0
	Knee[c]	446.3	498.1	542.6	444.0	515.1	572.7
	Ankle[c, d]	351.7	394.5	414.2	378.3	415.8	470.1

MECHANISMS OF POWER GENERATION DURING THE TAKE-OFF PHASE OF DIVES ARE DIRECTION DEPENDENT

Witaya Mathiyakom[1], Jill L. McNitt-Gray[1], James Eagle[1] and Barry Munkasy[2]

[1] **Biomechanics Research Laboratory, Department of Exercise Science**
University of Southern California, Los Angeles, California
[2]**Department of Health and Kinesiology, Georgia Southern University, Statesboro, Georgia**
Email: mathiyak@usc.edu

INTRODUCTION

Generation of linear and angular impulse during the take-off phase of the backward (BACK) and reverse (REVERSE) dives is achieved by strategically timing the location of the total body center of mass (TBCM) relative to the reaction force associated with lower extremity joint extension (Miller et al., 1989; 1990). Despite differences in translation direction relative to the anatomical reference system, competitive divers performing the BACK and REVERSE dives have been shown to use extensor net joint moments (NJM) (Mathiyakom et al., 1998; 1999b) and similar lower extremity coordination patterns (Mathiyakom et al., 1999a) during the take-off phase. The differences in anatomical orientation and the timing of joint extension between tasks was hypothesized to contribute to differences in power generation mechanisms between dives. The purpose of this study was to test the hypothesis that the net joint moment power (NJMP) and generation of positive NJM work during the take-off phase would be different between BACK and REVERSE dives.

PROCEDURES

Five national level platform divers (3 females and 2 males) performed a series of platform dive take-off from a force plate onto a foam landing pit as part of a training session supervised by their coach. During the performance of each dive, reaction forces (600 Hz, Kistler, 0.6 x 0.9m force plate) experienced during the takeoff phase were recorded onto the video images (60 fps.) using the Real Time Kinetic Feedback System (USC Biomechanics Lab). Both kinematic and kinetic data were processed as previously described (Mathiyakom et al., 1998; 1999b). Take-off phase, defined from the final weight acceptance to plate departure, was divided into three phases (Land, Transition, Go) according to the movement of the lower extremity joints. Net joint moment work at the ankle, knee and hip was calculated for each phase of the take-off by integrating NJMP, defined as the product of NJM and joint angular velocity. Paired t-test was used to determined significant differences ($p<0.05$) in work done at each joint between dives.

RESULTS AND DISCUSSION

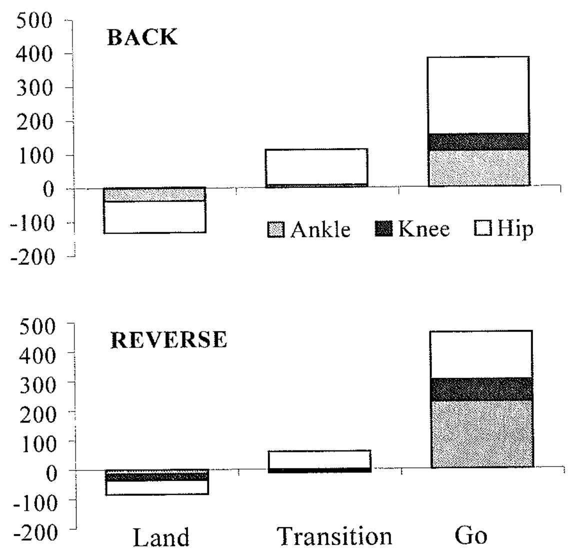

Figure 1. Significant between dive differences in support NJM work were observed during the Transition phase. Significant between dive differences in the relative ankle and knee NJM work were observed during the Go phase.

Despite differences in anatomical orientation relative to the direction of translation between dives, the divers were able to achieve similar horizontal and vertical TBCM velocity at plate departure (horizontal: BACK: -0.95 ± 0.12 m/s; REVERSE: 1.08 ± 0.21 m/s; vertical: BACK: 2.18 ± 0.32 m/s; REVERSE: 2.24 ± 0.24 m/s). Although no significant differences in NJM support work (sum of work done across joints) done across phases was observed between dives, significant differences in ankle, knee, and hip contributions to NJM work were observed between dives (Figure 2).

During the Go phase, significantly greater relative positive NJM work was done at the ankle during the REVERSE (47 ± 15%) as compared to the BACK (28 ± 4 %) dive (p = 0.04) (Figure 2). In contrast, significantly greater relative positive NJM work was done at the hip during the Go phase of the BACK (60 ± 13%) as compared to the REVERSE (36 ± 20%) dives (p = 0.03). The relative contribution of the knee NJM to the support work was relatively small and not significantly different between dives (BACK: 11 ± 15% and REVERSE 17 ± 8%). Source of these between dive differences in NJM work was attributed to differences hip NJM magnitude between dives.

Although minimal NJM work was observed at the ankle and knee during the Land and Transition phases, mechanical demand was imposed on muscles opposing dorsiflexion and knee flexion. The small degree of flexion at the ankle and knee suggests that together they served as a stable base that facilitated hip energy absorption and generation during these phases. Stabilization of the ankle and knee preceding the Go phase also allowed the diver to strategically orient the TBCM relative to the foot center of pressure prior to the initiation of lower extremity joint extension during the Go phase.

In conclusion, these results suggest that differences in anatomical orientation coupled with translation direction may not influence absolute power generation but may influence the distribution of power generation between the ankle and hip. This trade off between the ankle and hip has also been observed when landing gymnastics skills with different translation directions and anatomical orientations (McNitt-Gray et al., 1995). The mechanical objective of translation and rotation of the body specific to each dive may impose directional constraint (Ridderikhoff et al., 1999) on lower extremity power generation mechanisms.

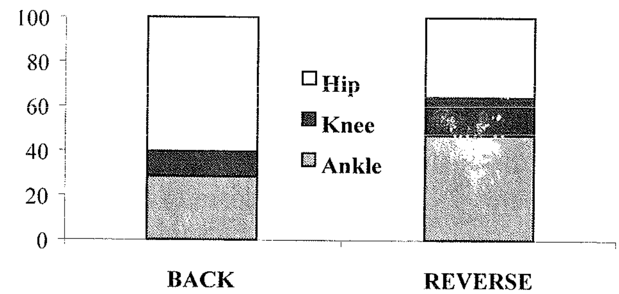

Figure 2. Relative NJM work distribution during Go phase of the BACK and REVERSE dives.

REFERENCES

Mathiyakom, W. et al. (1998). *NACOB'98*, 439-440.

Mathiyakom, W. et al. (1999a). *SCCB'99.*

Mathiyakom, W. et al (1999b). *ISB'99*, 167.

McNitt-Gray, J.L. et al. (1995). *ASB'95*, 199-200.

Miller, D.I. et al. (1989). *Int J Sport Biomech*, 5, 60-88.

Miller, D.I. et al. (1990). *Int J Sport Biomech*, 6, 283-308.

Ridderikhoff, A. et al. (1999). *Med Sci Sports Exerc*, 31, 1196-1204.

METAL BASEBALL BATS CAN OUT PERFORM WOOD BATS WITH A SIMILAR "SWEET SPOT"

J.J. Crisco and R.M. Greenwald

Department of Orthopaedics and Division of Engineering, Brown University, Providence, RI

National Institute for Sports Science and Safety, Providence, RI

Email: joseph_crisco@brown.edu

INTRODUCTION

Recent advances in metal and composite bat technologies have led to speculation that metal bats largely out perform wooden bats in baseball. With the potential rise in performance from metal baseball bats, used almost exclusively at the collegiate and high school level in the United States, questions arise as to the effects of metal bats on offensive-defensive balance and safety levels in baseball. Despite the amount of controversy generated, there are presently no available data describing the performance of metal and wood bats in the field. The purpose of this study was to compare the performance of wood and metal baseball bats swung by experienced players.

METHODS

Two wood and five metal baseball bat models (six bats of each model) were studied with 19 players in a batting cage facility. Pitched and batted ball velocities, as well as bat motion, impact location, and bat rotation axis were tracked in three-dimensional space using a commercially available system (four cameras at 500 Hz) and analyzed using specifically written computer code. Of the more than one thousand hits recorded, 538 were considered "line drives" and were included as a trial in the analysis. Automated algorithms and user interaction in Track 3D (Qualisys Inc., Glastonbury, CT) generated and exported files containing the 3D coordinates of markers identifying the ball and five positions along the bat. Data files were then processed using a series of custom programs written in Borland C (SPSS Corp, Chicago, IL) and Matlab (The MathWorks, Natick, MA).

The variables calculated and analyzed included: pitched and batted ball velocities, bat kinematics and impact location of the ball on the bat. To determine ball velocities, the pitched and batted segments of the ball path were defined separately by eliminating data within a 0.004 second window about the time of impact and also near the periphery of the field of view. Ball velocity was assumed to be constant over the pitched and batted segments of the ball path.

The variables describing bat motion were calculated using the two frames just prior to the time of impact, which was defined as the time at the end of the ball inbound segment. The motion of the bat was described using the helical axis of motion (HAM) for rigid bodies. The location of the impact (i.e. where the ball hit the bat) was determined as the intersection of two lines: the long axis of the bat and the path of the pitched ball. The estimate of the error was the shortest distance between these two lines. Once the location of the impact point on the bat was defined, its velocity was then calculated using rigid body transformations. Bat impact speed was defined as the magnitude of bat velocity at the location of the impact. The significance of the difference in the speeds of the batted ball between bat models was determined using an ANOVA and then t tests post hoc (Sigma Stat, SPSS, Chicago, IL).

Of special note is that we have reported all data in U.S. Customary Units because of their long tradition in baseball and the continued use of these units by the sports governing bodies, baseball ball and bat manufacturers, and fans alike.

RESULTS AND DISCUSSION

The results clearly indicated that metal bats can out perform wood bats (Figure 1). Of the five metal bat models, one bat model (model M2) statistically out performed all other models, while one metal bat model (not shown here) was most similar to the wood bats. The data suggest that maximum batted ball speed was generated from two primary components: bat swing speed and barrel efficiency ("trampoline effect"). Furthermore, how much each of these components contributed to batted ball speed varied with bat model.

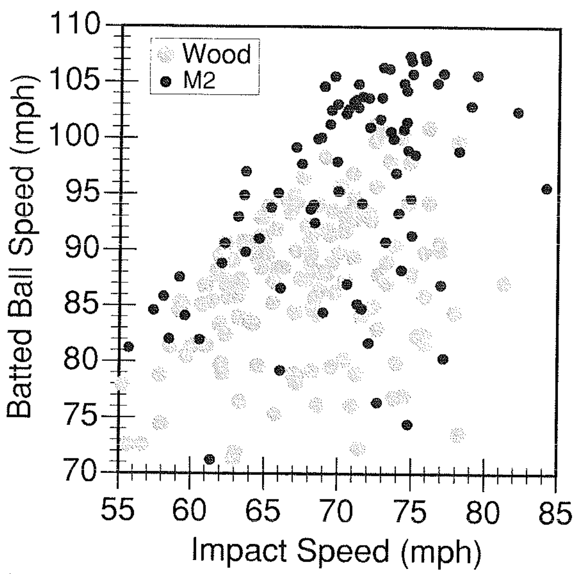

Figure 1. Batted ball speeds for the metal bat M2 exceeded the speeds of balls hit with wood bats (W). Plotting batted ball speeds as a function of bat impact speed accounts for different swing speeds, thus this data suggests that the existence of a "trampoline effect" contributed to the performance of bat M2.

Examination of batted ball speed as a function of impact location revealed a "sweet spot" region, which contrary to popular belief, was not different between metal and wood bat models (Figure 2). While the mechanisms and phenomenon found in this study are deemed valid, it should be noted that the absolute values of and differences in the variables (e.g. batted ball speed) are limited to the experimental environment, the specific bat models used in the study, and the specific players who were recruited. The findings of this study should dramatically increase our understanding of bat design and performance, and provide an extensive data base for future studies and for comparisons with laboratory test methods presently being proposed for the regulation of bat performance by the governing bodies of baseball.

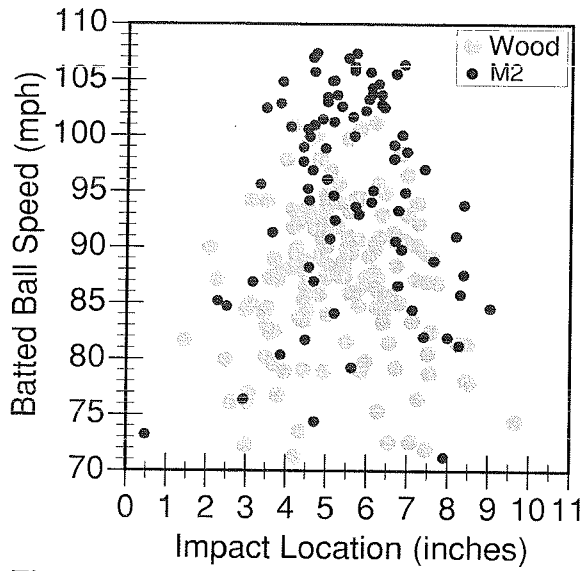

Figure 2. Batted ball speeds of wood (W) and a metal (M2) bats plotted for varying impact locations measured from the tip of the bat. The "sweet spot" was considered to be the length of the bat over which batted ball speeds were a maximum.

SUMMARY

Batted ball speeds, defined as a measure of bat performance, were determined in a novel study of wood and metal baseball bats. Some metal bats clearly outperformed wood bats, while other metal bats performed more similarly to wood. However, all models appeared to possess similar "sweet spots".

ACKNOWLEDGEMENTS. Funding for this work was provided by the Sporting Goods Manufacturers Association (SGMA), University Orthopaedics, Inc., and the Rhode Island Hospital Orthopaedic Foundation. We are indebted to Mike and Lynn Coutts of Frozen Ropes, Franklin, MA. for their assistance in this study and for making their facility available to us. We gratefully acknowledge the bat and baseball manufacturers who donated their products, and the players who participated in the study.

KINETIC COMPARISONS BETWEEN AMERICAN AND KOREAN PROFESSIONAL BASEBALL PITCHERS

Rafael F. Escamilla[1], Glenn S. Fleisig[2], Steven W. Barrentine[2], James R. Andrews[2], and Kevin P. Speer[1]

[1]Division of Orthopaedic Surgery, Duke University Medical Center, Durham, NC
[2]American Sports Medicine Institute, Birmingham, AL
Email: rescamil@duke.edu Web: http://msrbsgi1.mc.duke.edu/escamilla/

INTRODUCTION

With numerous professional baseball leagues throughout North America, South America, Asia, and Australia, pitching mechanics are likely to be taught differently according to cultural influences. Since several kinematic differences have previously been reported between American and Korean professional pitchers (Escamilla et al. 1999), it is hypothesized that kinetic differences may also exist. Fleisig et al. (Fleisig et al., 1995) have proposed several injury mechanisms that may be associated with baseball pitching kinetics. Therefore, the purpose of this study was to quantify and compare shoulder and elbow kinetic data between American and Korean professional pitchers, and provide possible injury implications for these two groups.

MATERIALS AND METHODS

Eighteen healthy professional baseball pitchers served as subjects. The American group (n=11) were born and raised in the United States and pitched for minor and major league teams. The Korean group (n=7) were born and raised in Korea, and pitched for the Korean Dolphins. The American group had a mean mass, height, and age of 83.4±5.2 kg, 1.81±0.10 m, and 22.6±3.5 y, respectively, while the Korean group had a mean mass, height, and age of 76.9±8.7 kg, 1.77±0.11 m, and 25.1±4.1 y, respectively. Reflective markers were attached bilaterally at the lateral malleoli, lateral femoral epicondyles, greater femoral trochanters, lateral superior tip of the acromions, lateral humeral epicondyles, and wrists. Shoulder and elbow joint center locations of the throwing arm were calculated in each time frame. Data were collected for 8-10 fastball pitches thrown with 100% effort from an indoor pitching mound towards a strike zone located at regulation distance. A Motion Analysis four-camera automatic digitizing system was used to collect 200 Hz video data. Eleven kinetic parameters were measured during the arm cocking (lead foot contact to maximum shoulder external rotation), arm acceleration (maximum shoulder external rotation to ball release), and arm deceleration (ball release to maximum shoulder internal rotation) phases of the pitch. Shoulder and elbow kinetics were calculated utilizing inverse dynamics. Kinetic data were averaged for the three fastball trials with the highest ball velocity and that were thrown for strikes. Unpaired t-tests were used to assess significant kinetic differences ($p<0.05$).

RESULTS AND DISCUSSION

Kinetic comparisons are shown in Table 1. Kinetic differences are probably due more to kinematic differences than anthropometric differences, since there were no significant differences in body weight and body height, but several kinematic differences were observed between the two groups (Escamilla et al., 1999). Kinetic differences may also help explain the 10% greater ball velocity by the American group (38±1 m/s vs. 35±1 m/s).

The 29% greater maximum shoulder internal rotation torque observed in the American group suggests that the shoulder internal rotators may be more active in this group. These muscles contract eccentrically during the arm-cocking phase in order to control the rate of shoulder external rotation (DiGiovine et al., 1992). Elbow varus torque reached its maximum value during the arm-cocking phase, with the American group generating 33% more torque. This greater varus torque may in part be due to maximum shoulder external rotation being 15° greater in the American group compared to the Korean group (Escamilla et al., 1999). Since varus torque is needed to resist elbow valgus stress, this stress may be greater in the American group. This can lead to an increased injury risk in the UCL. Radiocapitellar compression injuries are also at a higher risk, such as avascular necrosis, osteochondritis dissecans, and osteochondral chip fractures (Fleisig et al, 1995). Maximum elbow flexor torque occurred during the arm acceleration phase to help decelerate the rapid rate of elbow extension. This torque was 33% greater in the American pitchers. The elbow flexors, which help generate this torque, have shown moderate activity during the arm acceleration phase (DiGiovine et al., 1992). Hence, the elbow flexors may be more active in the American group compared to Korean group. The final significant differences were maximum elbow and shoulder proximal forces, which occurred during the arm deceleration phase. These forces, which were approximately 25-30% greater in the American group, are needed in order to help resist shoulder and elbow distraction. These were the largest forces generated during the pitch, being in excess of body weight. The greater shoulder and elbow forces and torques generated by the American group may predispose this group to a higher risk of injury to elbow and shoulder structures, such as rotator cuff tensile failure (Fleisig et al.,1995).

Since all kinetic parameters were quantified through inverse dynamics, the actual forces generated across the articulating surfaces of the shoulder and elbow still remain unknown. In order to accurately calculate these forces, shoulder and elbow muscle and ligamentous forces would need to be determined. Due to complexity of the elbow and shoulder joints, mathematical modeling and computer optimizations are needed to help estimate these articulating forces. There are currently no known modeling or optimization programs that have been employed to calculate these articulating forces during baseball pitching. This should be the focus of future baseball pitching studies.

REFERENCES

DiGiovine, N.M. et al. (1992). *J. Shoulder Elbow Surg.*, **1**, 15-25.

Escamilla, R.E. et al. (1999). *Med. Sci. Sports Exerc.*, **31**, S40.

Fleisig, G.S. et al. (1995). *Amer. J. Sports Med.*, **23**, 233-39.

Table 1. Mean (M±SD) max shoulder (Sh) and elbow (Elb) forces (N) and torques (N·m) between American and Korean pitchers.

	American (n = 11)	Korean (n = 7)
Arm-Cocking Phase		
Sh anterior force	360±70	350±75
Sh horiz adduction torque	98±15	86±21
Sh internal rotation torque*	**63±10**	**49±10**
Elb medial force	295±55	260±55
Elb varus torque**	**61±10**	**46±7**
Arm Acceleration Phase		
Elb flexor torque**	**56±12**	**42±6**
Arm Deceleration Phase		
Sh proximal force**	**1090±160**	**830±165**
Elb proximal force**	**900±125**	**725±135**
Sh adduction torque	87±31	81±15
Sh posterior force	340±120	315±85
Sh horiz abduction torque	77±35	68±17

*$p < 0.05$; **$p < 0.01$

SENSITIVITY ANALYSIS OF A GRAPHICS-BASED, ANATOMICALLY DETAILED, FORWARD DYNAMIC SIMULATION OF THE STANCE PHASE OF GAIT

S.I. Ringleb[1,2], H.J. Hillstrom[2]

[1] Department of Mechanical Engineering and Mechanics, Drexel University, Philadelphia, PA
[2]Gait Study Center, Temple University, Philadelphia, PA
Email: sringleb@tuspm.temple.edu

INTRODUCTION

An anatomically detailed model of the lower extremity capable of performing a forward dynamic simulation of stance phase under specific conditions has been developed (Ledoux et al.,1999). This unilateral model has eight degrees of freedom (i.e., pelvic height, tilt and translation; hip, knee, and ankle flexion/extension; subtalar joint pronation/ supination; and one metatarsophalangeal rotation representing all five toes). Quasi-linear viscoelastic models of the area beneath the five metatarsal heads (submetatarsal), the hallux (subhallucal), and the calcaneus (subcalcaneal), were also included (Ledoux et al., 1999). The emphisis of this simulation was the interaction between the foot and ground. Therefor, to avoid potential difficulties due to the motion of the pelvis, hip, and knee these joints were prescribed. The ankle, subtalar, and metatarsophalangeal joint motions were simulated.

Predicted vertical ground reaction forces (GRF) were compared with measured healthy asymptomatic data. The predicted vertical GRF estimates were excessive, however the temporal sequence of loading was similar to the healthy data. It has been shown that optimization of muscle parameters improves the accuracy of predicted outcomes (Anderson et al.,1999). It has been our laboratory's approach to improve the underlying structural components prior to performing optimization. The objective of this study was to use the sensitivity analysis as a means for identifying the areas within the model that are most in need of improvement.

METHODS

A sensitivity analysis was conducted on seven degrees of freedom of the first generation foot model. Pelvic translation was neglected. This analysis was performed using Simulation for Interactive Musculoskeletal Modeling or SIMM and Dynamics Pipeline (MusculoGraphics, Inc., Evanston, IL) in conjunction with SD/FAST (Symbolic Dynamics, Inc., Mountain View, CA). Data were collected in the gait lab, fit with a 5th order polynomial, and used to prescribe the motion of the pelvis, hip, and knee. Each DoF was modified incrementally and the resulting vertical GRFs were studied.

The prescribed motions were changed by incrementally modifying and refitting the collected data. For example, the pelvic height was modified in ±1% increments from –9% to +4%. One percent of the original data was added or subtracted to the original data set and fit to a 5th order polynomial (Figure 1). These simulations were stopped when the ground reaction forces were infinite or maximum joint torque within the joint definition was exceeded. The unprescribed DoF were modified by changing the initial kinematic conditions in ±10% increments until they were altered by ±100%.

Upon performing a re-simulation, the resulting vertical GRFs under each of the seven plantar soft tissue regions was compared to the original results. A ratio of the percent change in GRF to percent change in a given DoF translation or rotation was calculated.

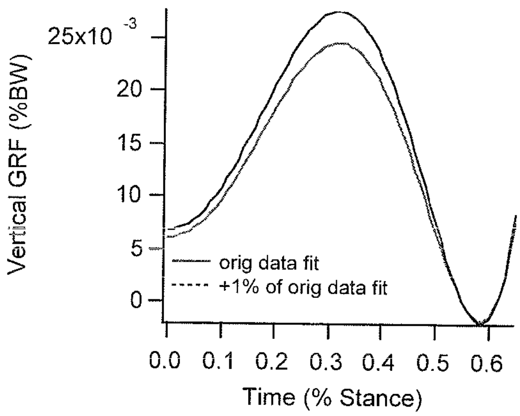

Figure 1. Example of shift in prescribed pelvic height motion. One percent of the original data was added to itself and curve fit to a 5th order polynomial

RESULTS AND DISCUSSION

As expected, the model was most sensitive to changes in the prescribed motions. Hip flexion produced the greatest ratio of percent change in GRFs to percent change in DoF for all plantar soft tissue areas. Comparatively, a small ratio was obtained when the initial kinematic conditions of the unprescribed DoF were changed (Table 1).

Because the model is most sensitive to changes in the prescribed motions, the original decision to constrain hip and knee motion in the model is being questioned. Optimization of the prescribed motions will be explored . Additionally, unconstraining the hip and knee by adding the pertinent muscle models will be considered.

SUMMARY

A sensitivity analysis was performed on an anatomically detailed model of the human lower extremity to determine which degree(s) of freedom was most sensitive to modifications. It was found that sagittal hip motion, one of the prescribed degrees of freedom, was most sensitive.

REFERENCES

Anderson F.C., Pandy M.G. (1999). *Computer Methods in Biomechanics and Biomedical Engineering,* **2,** 201-231.

Ledoux W.R., Hillstrom H.J. (1999). Proceedings International Society of Biomechanics

Ledoux W.R., Meaney D.F., Hillstrom H.J. (1999). Proceeding American Society of Biomechanics

Table 1: Ratio of Percent Change in Vertical GRF vs. Percent Change in DoF Position

	SUBCALC	SUBMET1	SUBMET2	SUBMET3	SUBMET4	SUBMET5	SUBHALL
pelvic height	6.22	1.35	1.03	0.70	0.21	0.35	1.27
pelvic tilt	0.81	0.20	1.54	1.38	1.52	1.66	0.65
hip flex/ext	25.74	3.93	11.15	11.64	12.15	12.27	18.48
knee flex/ext	2.30	1.40	4.93	5.70	5.49	6.20	6.72
Ankle flex/ext	0.42	0.03	0.01	0.01	0.01	0.01	0.05
STJ pro/sup	0.14	0.02	0.01	0.01	0.00	0.02	0.06
MTP flex/ext	0.02	0.00	0.01	0.01	0.01	0.02	0.06

EFFECTS OF NEURO-MUSCULAR TRAINING ON VERTICAL JUMP HEIGHT: A FORWARD-DYNAMICS SIMULATION STUDY

Akinori Nagano and Karin G. M. Gerritsen
Biomechanics Lab., Dept. of Exericise Science and Phys. Ed., Arizona State University
Email: akinori.nagano@asu.edu
Web: http://www.public.asu.edu/~nagano/

INTRODUCTION

In several sports, it is extremely important for athletes to be able to jump high. Athletes' jumping ability can be improved by training both muscular and neural factors of the neuro-muscular system. However, it is difficult to quantitatively analyze the effect of improving each parameter using experimental approaches, as there are many factors that are modified simultaneously during the course of a training program. One of the approaches to solve this problem is the forward-dynamics simulation method (Bobbert and van Soest, 1994). The purpose of this study was to systematically investigate the training effects of selected neuro-muscular parameters on vertical jumping performance using forward-dynamics method. Maximal isometric force (F_{max}), maximal shortening velocity (V_{max}), and maximal activation signal sent to muscles (ACT_{max}) were selected as trainable parameters.

METHODS

Neuro-musculo-skeletal model: A two-dimensional model consisted of four rigid segments connected to each other by three revolute joints. This musculo-skeletal model was actuated by six Hill-type muscle models (Fig. 1). The skeletal model was simulated using DADS 9.01 (LMS CADSI, Coralville, Iowa) linked together with FORTRAN code describing the neuro-musculo-skeletal properties (Gerritsen et al., 1998). All simulations were started from a squat position and were executed on an SGI workstation (Octane, Silicon Graphics Inc., Mountain View, CA).

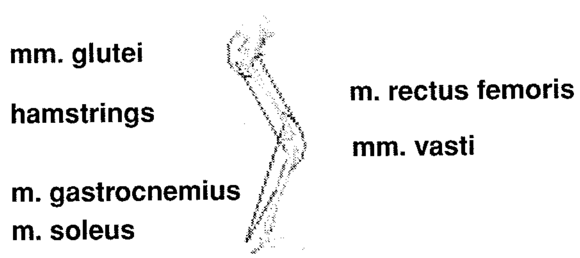

Fig. 1. The model consisted of four rigid segments, three hinge joints (with passive moments), and six lower extremity muscles.

Optimization of muscle activation pattern: Optimizations were executed with a modified version (J. M. Winters, personal communication) of the algorithm of Bremermann (1970) implemented in MATLAB (The Math Works Inc., Natick, MA). The objective of the optimization was to find the muscle activation patterns that make the model jump as high as possible (JH: jump height = maximal height of the body center of mass). Each muscle activation pattern was specified by three parameters (onset time, offset time, and amplitude).

Neuro-muscular training effects: The effects of strength training were simulated by systematically increasing three parameters of the neuro-muscular model: F_{max}, V_{max}, and ACT_{max} (up to +20%, +20%, and +10%, respectively: these numbers were derived from the literature), and re-optimizing the muscle activation patterns. These parameter manipulations were performed both individually and simultaneously. Intermediate increments were also investigated in order to test the linearity between the increase in parameter values and the increase in jump height. These manipulations were performed on (1) all muscles, and (2) individual muscle groups.

RESULTS AND DISCUSSION

The optimization processes all resulted in well-coordinated vertical jumping motions (Fig. 2). The optimized JH for the original (before training) model was 141.68 cm. Largest increase in jumping performance (ΔJH) was observed when F_{max} parameters were increased (Tab. 1), whereas the increase in V_{max} parameters produced the smallest effect. For all three parameters, the relationship between the increase in parameter value and ΔJH was linear (r^2>0.999). Increasing F_{max}, V_{max}, and ACT_{max} simultaneously for all muscles resulted in a large increase in jumping performance (+16.62 cm), which is greater than the sum of the ΔJH for individual factors.

When the three factors were manipulated simultaneously for ankle plantar flexors, knee extensors, and hip extensors, the largest ΔJH was found by manipulating the neuromuscular properties of knee extensors (+9.61 cm). The sum of ΔJH is smaller than the increase in jump height that was found when the manipulations were applied simultaneously to all the muscles. These results suggest that the model was able to make use of the improved neuro-muscular properties even more by combining the training effects in different parameters (F_{max}, V_{max}, and ACT_{max}) and different functional muscle groups (hip extensors, knee extensors, and plantar flexors). In all the cases of this study, re-optimization of the activation patterns was necessary after parameter modifications for the model to fully benefit from these modifications.

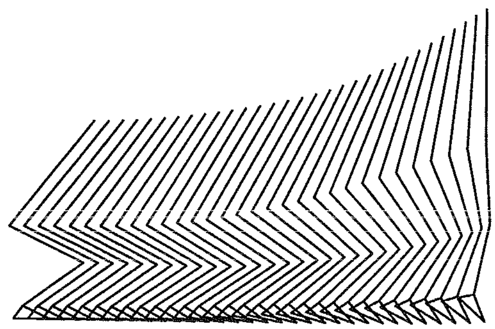

Fig. 2. An example of a simulated jumping movement.

REFERENCES

Bobbert, M.F. and van Soest, A.J. (1994). *Med. Sci. Sports Exerc.* **26**, 1012-1020.

Gerritsen K.G.M. et al. (1998). *Motor Control* **2**, 206-220.

Tab. 1. Effects of strengthening neuro-muscular parameters on vertical jumping performance.

Individual Parameters: All Muscles					
	Before Training	ΔF_{max} (+20%)	ΔV_{max} (+20%)	ΔACT_{max} (+10%)	$\Delta F_{max}+\Delta V_{max}+\Delta ACT_{max}$
JH (cm)	141.68	148.67	145.51	145.94	158.30
ΔJH (cm)	-	+6.99	+3.83	+4.26	+16.62

Individual Muscle Groups: ΔF_{max}(+20%) + ΔV_{max}(+20%) + ΔACT_{max}(+10%)					
	Before Training	Ankle P. Flexors	Knee Extensors	Hip Extensors	All Muscles
JH (cm)	141.68	144.83	151.29	143.36	158.30
ΔJH (cm)	-	+3.15	+9.61	+1.68	+16.62

CUP ANTEVERSION/TILT EFFECTS ON DISLOCATION PROPENSITY FOR SMALL-HEAD-SIZE TOTAL HIP REPLACEMENTS

M. E. Nadzadi, D. R. Pedersen, J. J. Callaghan, and T. D. Brown

Orthopaedic Biomechanics Laboratory, University of Iowa, Iowa City, Iowa 52242
Email: tom-brown@uiowa.edu

INTRODUCTION

Malposition of the acetabular component is a leading cause of dislocation in total hip arthroplasty (Woo, 1982). The two most influential surgeon-controlled variables are thought to be abduction (tilt) and anteversion of the cup. Empirically, while 30-50° of tilt and 5-25° of anteversion is felt to be a "safe-zone" (Morrey, 1992), dislocation nevertheless remains a disturbingly frequent occurrence.

To date, most research on the influence of surgical placement on dislocations has been done for large- or medium-diameter (32, 28, or 26mm) components. Some surgeons, however, are willing to accept the tradeoff of higher dislocation risk for small head size (22mm) implants, given the latter's recognized advantage of reduced polyethylene wear. We here report results from a physically validated finite element (FE) model of dislocation, examining the effects of tilt and anteversion on implant stability, specifically for the vulnerable situation of 22mm heads.

METHODS

A series of three-dimensional FE models of a widely utilized titanium-backed total hip implant system were developed from manufacturer IGES files, using Patran 8.5 pre-processing. Following an established formulation (Scifert, 1998), a non-linear, large displacement contact analysis was performed with Abaqus 5.8. The cup backing and liner (Duraloc 22-52mm, DePuy, Inc.) was modeled with 3920 continuum elements, while the proximal third of a femoral component (22mm Endurance std+3, DePuy, Inc.) was modeled with 4238 rigid body Bezier surface elements (Figure 1A). The polyethylene liner was characterized by a 4th order constitutive relationship between stress and tangent modulus (Cripton, 1993).

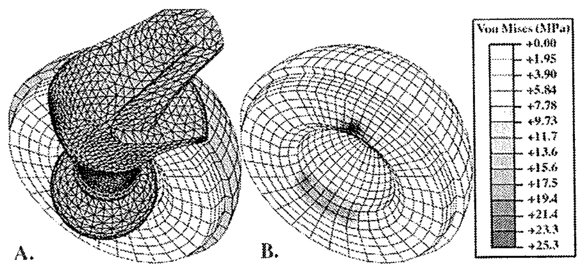

Figure 1: FE model (A) and typical Von Mises stress plot after impingement (B). Note high stress at the head egress site as well as at the neck impingement site.

Starting from 90° of femoral flexion, 0° adduction, and 0° endorotation, a seated leg cross maneuver was incrementally input to the femur ($\Delta\theta$ = 2:1:0 ratio of flexion to adduction to endorotation). A physiological load of 942N was used, based on optoelectronic motion analysis. The cup was studied in 10 distinct surgical positions: 50° of tilt with 0°, 5°, 10°, 20°, 30°, and 40° of anteversion, and then 20° of anteversion, varying tilt from 30° to 70° in 10° increments.

RESULTS AND DISCUSSION

As either tilt or anteversion was increased, the flexion angle at impingement, the maximum resisting moment, and the flexion angle at the onset of hooking increased in a nominally linear fashion (Figure 2).

(Hooking is when the upper collar surface of the skirted femoral component engages the metal backing of the cup at large flexion angles, causing an upward spike in resisting moment). This shift of motion range and resisting moment was much more sensitive to cup tilt than to anteversion, although "apparent stiffness" ($\Delta M/\Delta\theta$) was unaffected by the surgical positioning perturbations (Figure 3). For anteversion of 5° or less at 50° of tilt, and for tilt of 40° or less at 20° of anteverison, impingement occurred prior to 90° of flexion, which affectively constricted the envelope of the "safe zone". Subluxation initiated as the femur was flexed beyond the position of maximum resisting moment, and involved a gentler (downward) slope for increasing tilt than occurred for increasing anteversion. However, hooking ensued at an earlier flexion angle for the increased-tilt positions.

In an earlier FE study employing 26mm components (Scifert, 1998), impingement prior to 90° of flexion occurred at 45° of tilt and 15° of anteversion or less. Although the two series of specific tilt and anteversion angles are not identical, it appears that impingement angle was independent of head size. Due to hooking, frank dislocation was not observed in the present 22mm series, although comparable dislocation angles for the 26mm series were nearly identical. Very dissimilar maximum resisting moments were observed, however: the 22mm series had values nearly 25% lower than the 26mm series. The apparent stiffness was nearly uniform (2.8 Nm/deg) in both series. Both series also showed similar effects of tilt and anteversion on impingement and resisting moment, and both showed gentler $\Delta M/\Delta\theta$ slope in the subluxation regime.

SUMMARY

For 22mm head size, the dependence of resisting moment on cup tilt and anteversion showed similar trends as for larger head size, but with the important caveat of a smaller maximum resisting moment for the 22mm heads. Of course, while increased cup tilt or anteversion reduces the likelihood of posterior dislocation, a tradeoff is increased propensity for anterior dislocation.

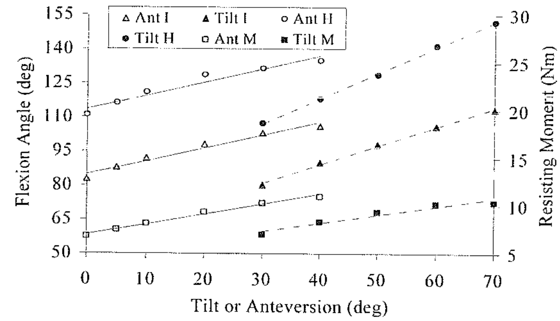

Figure 2: Impingement angle (I), hooking angle (H), and resisting moment (M) as functions of surgical positioning.

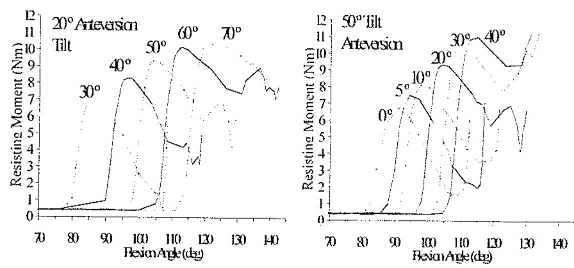

Figure 3: Tilt and anteversion influence on resisting moment (M) about cup center, versus flexion angle.

REFERENCES

Cripton, P.A. (1993). Thesis. Queen's University.

Morrey, B. (1992). *Ortho Clinics of N Am*, **23**, 237-48.

Scifert, C. et al. (1998). *Clin Ortho*, **355**, 152-62.

Woo, R. et al. (1982). *JBJS*, **64A**, 1295-306.

ACKNOWLEDGEMENTS

Financial support was provided by DePuy, Inc., and by a VA Merit Grant administered by the Iowa City VAMC.

THE USE OF WEIGHTS IN ARTIFICIAL NEURAL NETWORK FOR STUDYING HUMAN POSTURAL CONTROL — THEORETICAL CONSIDERATIONS

Gongbing Shan and Ge Wu
Department of Physical Therapy, University of Vermont, Burlington, VT, 05401

INTRODUCTION

It is still under exploration about how the central nervous system (CNS) utilizes sensory information in human postural control because of their overlapping characteristics [Rothwell, 1994]. Artificial Neural Network (ANN) models have been considered as a suitable tool for such exploration. However, when an ANN is trained with the same input and output multiple times, the weights do not maintain constant [Kemp et al., 1997]. This Study attempted to investigate whether or not it is possible to determine the input-output relation of the ANN with its weights in spite of the chaotic nature of training.

CONTROL POTENTIAL (CP)

The most popular ANN has one input layer of sigmoid neurons, followed by an output layer of linear neurons [Demuth, 1998].

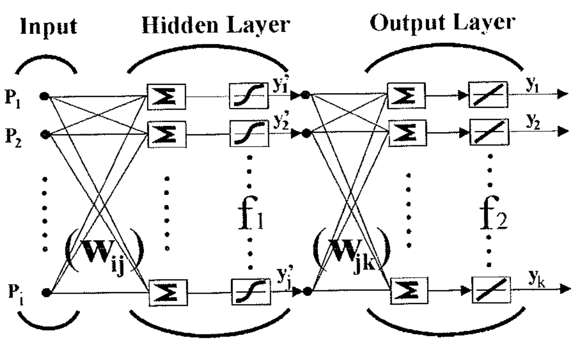

Figure 1. The model of ANN

Such a network is shown in Figure 1, in which $\{P_i\}$ is the input, $\{w_{ij}\}$ the weight between input and hidden layer, $\{W_{jk}\}$ the weight between hidden layer and output layer, $\{y_j'\}$ and $\{y_k\}$ the output from the hidden layer and the output layer, respectively, and f_1 and f_2 the function in the hidden layer and the output layer, respectively.

The output and input relation can be estimated using the first-order estimation in MacLauren series as:

$$y_k \approx \frac{1}{2}\sum_j W_{jk} + \frac{1}{2}\sum_i \sum_j W_{jk} w_{ij} P_i$$

Therefore, each output y_k is primarily related to an input by the first-order coefficient, or referred to as control potential (CP) as:

$$cp_{ki} = \sum_j W_{jk} w_{ij} \qquad (1)$$

For an ANN with a total of N_i inputs and N_k outputs, there are $N_k \times N_i$ CP components.

The principle of neural network training, in particular, the back-propagation algorithm, is to update each weight in the direction in which the error function E is minimized [Demuth, 1998]. That is,

$$\Delta W_{jk} = -\eta \frac{\partial E}{\partial W_{jk}} \text{ and } \Delta w_{ij} = -\eta \frac{\partial E}{\partial w_{ij}}$$

where η is the learning grade. These definitions establish the following relation between the two layer weight:

$$\Delta w_{ij} = -\eta C W_{jk} \qquad (2)$$

where C is related P_i, y_k and t_k.

Equation (2) indicates that the weight of the output layer W_{jk} is proportional to the change (or gradient) of the weight of the hidden layer w_{ij}. Substituting Eqn 2 into 1, cp_{ki} is now proportional to $\sum_j \Delta w_{ij} w_{ij}$,

which bears analogy to the concept of potential energy surface defined as the product of the position and its gradient. Thus, we may consider CP as a decision surface that describes the input-output relations. For a given set of input-output, although each individual weight may vary with multiple training, the input-output relation as described by the product of the weights in the input and output layers (or CP) should belong to one decision surface. As the input-output relation changes, the corresponding decision surface should become distinguishable, while the individual weights may or may not. To distinguish different decision surfaces, one can use their statistical characteristics such as the mean values of CPs.

SIMULATION EXPERIMENTS

A total of 23 numerical simulations were done to examine whether or not the control potential could be used to indicate and distinguish the known input-output relations. All neural network models were trained based on Back-Propagation training. For each case, a total of 120 training sessions with 10,000 epochs/training was done in order to determine the statistical characteristics of the CP. The training was done with the Neural Network Toolbox of Matlab software (MathWorks Inc., Natick, MA).

As examples, four simulation results were shown in Fig.2. The ANN model in the simulations had five inputs and two targets. In case 1, P_3 and t_1 were identical (except for noises). The CP component relating P_3 and t_1, or CP_{31}, was the largest among all other CPs. In case 2, t_1 was changed to t'_1 (i.e., reduced frequency by 2), resulting in a dramatic reduction in CP_{31}. In case 3, the magnitude of P_3 in case 1 was reduced by 5. Accordingly, CP_{31} was increased enormously. In case 4, P_3 in case 3 was reversed, resulting in the same CP_{31} as in case 3 but with a negative sign.

DISCUSSIONS AND CONCLUSION

All simulation results suggested that (1) CPs had better statistical characteristics than the individual weights; (2) given a known input-output relation, CPs in an ANN could be used to represent such relation; (3) when either input or output or both were changed, resulting in an altered input-output relation, the corresponding CP was distinguishable. Furthermore, the sign of the CPs could be used to identify the phase relation among inputs and outputs.

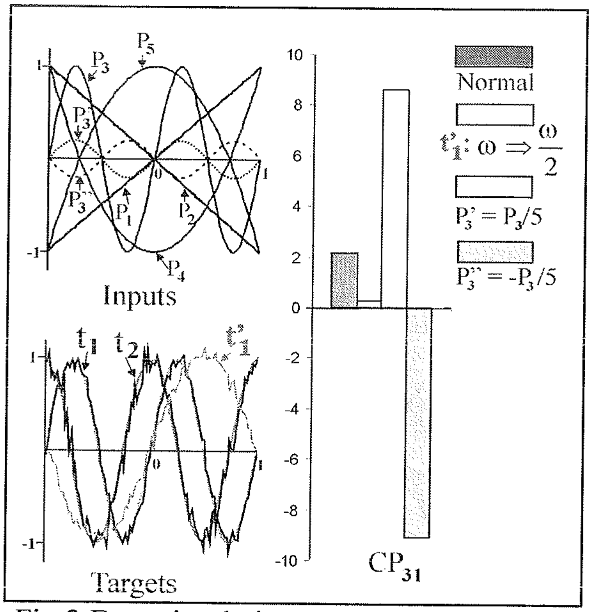

Fig.2 Four simulation examples (only CP_{31} was shown).

In conclusion, the control potential, defined as the product of the weights in ANN, has been shown to have the ability to identify the relation among inputs and outputs in non-linear, redundant systems. This concept may have the potential to study CNS mechanisms in human postural control.

REFERENCES

Demuth and Beale. Neural Network Toolbox. The MathWorks Inc., 1998

Kemp et al., Anal Cell Path, 14(1), 1997

Rothwell, Control of human voluntary movement. Chapman and Hall, 1994

ACKNOWLEDGEMENT: This work was supported by NIH grants No.1R29AG11602.

DEFORMATION AND SCALING OF MUSCULOSKELETAL MODELS: APPLICATION TO SURGICAL PLANNING

Allison S. Arnold and Scott L. Delp

Biomechanical Engineering Division, Mechanical Engineering Department
Stanford University, Stanford, CA

Email: *asarnold@stanford.edu* **Web:** *www.stanford.edu/group/biomech*

INTRODUCTION

The hamstrings and psoas muscles are often lengthened surgically in an effort to correct crouch gait and other movement abnormalities in persons with cerebral palsy. At present, it is difficult to predict which patients will benefit from these procedures. Several studies have suggested that analyses of the muscle-tendon lengths during crouch gait may help distinguish patients who have short muscles from those who do not have short muscles, and thus may provide a more effective means to identify appropriate candidates for surgery (e.g. Hoffinger *et al.* 1993, Delp *et al.* 1996). These studies have relied on "generic" models of the lower extremity with normal adult musculoskeletal geometry; however, many individuals who undergo these surgeries are children with femoral deformities. It is not known how variations in size, age, or femoral geometry affect the accuracy of muscle-tendon length calculations. Before generic models can be used to guide treatment decisions for specific patients, the models must be tested.

The purpose of this study was to determine if, and under what conditions, medial hamstrings and psoas lengths estimated with a "deformable" musculoskeletal model accurately characterize the lengths of the muscles in persons with cerebral palsy. Detailed models of four individuals with crouch gait (ages 7-27 yrs) were created from magnetic resonance (MR) images. These models were used in conjunction with joint kinematics obtained from gait analysis to calculate the muscle-tendon lengths at body positions corresponding to each subject's abnormal gait. The lengths calculated with the MRI-based models were normalized and were compared to the lengths estimated with a deformable generic model. The generic model was either left undeformed and unscaled, or was deformed or scaled to more closely approximate the femoral geometry or bone dimensions of each subject.

This work provides guidelines for interpreting the results of muscle length calculations and other biomechanical analyses based on generic musculoskeletal models.

METHODS

Muscle-tendon lengths calculated from MRI-based models of four subjects with crouch gait were used to examine the accuracy of the lengths estimated with a deformable generic model. These models describe the geometry of the pelvis, femur, and proximal tibia, the kinematics of the hip and tibiofemoral joints, and the paths of the medial hamstrings and psoas muscles (Arnold 1999). Ellipsoidal "wrapping surfaces" and via points (Delp *et al.* 1990) were used to represent underlying structures and other anatomical constraints. We modified the generic lower limb model defined by Delp *et al.* (1990) such that the moment arms of the muscles computed with the model are similar to the moment arms determined experimentally on cadavers with normal musculoskeletal geometry. We developed algorithms to deform the femur of the generic model, and we verified that these algorithms are consistent with the deformed femurs of the cerebral palsy subjects derived from MR images.

The gait kinematics of each subject were input into the subject's MRI-based model and into four variations of the deformable model: *(i)* the undeformed generic model, *(ii)* the generic model scaled to the subject along anatomical axes, *(iii)* the generic model deformed to match the subject's femoral anteversion angle, called Deformed Model A, and *(iv)* the generic model deformed to match the subject's anteversion and neck-shaft angles, called Deformed Model B. The medial hamstrings were not affected by our representation of femoral deformities, since the position of the knee center with respect to the hip center in the generic model was not changed.
The lengths of the muscles during crouch gait (L_i) were normalized at every two percent of the gait cycle based on the maximum averaged length (L_{max}) and the minimum averaged length (L_{min}) of the muscle during normal walking as follows:

$$\hat{L}_i = (L_i - L_{min}) / (L_{max} - L_{min}),$$

where $\hat{L}_i$ is the normalized length of the muscle at the *ith* point of the gait cycle. Values of L_{max} and L_{min} for each model were obtained from the gait kinematics of 18 unimpaired subjects. To make comparisons across models, the peak muscle-tendon lengths during crouch gait were expressed in standard deviations (SD) of the peak lengths during normal walking. For the medial hamstrings, the equivalent length of 1 SD ranged from 3-5 mm, as calculated with the different models. For the psoas, the length of 1 SD ranged from 2-3 mm.

RESULTS AND DISCUSSION

The peak medial hamstrings lengths computed with the undeformed generic model differed by at most 1 SD from the peak lengths computed with each MRI-based model, with the exception of the semitendinosus of Subject 4 (Table 1). The discrepancy for Subject 4 reflects the abnormally posterior path of the subject's semitendinosus in the popliteal region, which was evident in the MR images.

Errors in the peak psoas lengths computed with the undeformed model ranged from 0.5 to 1.8 SD (Table 2). Errors computed for Deformed Model A ranged from 0 to 0.9 SD; errors computed for Deformed Model B ranged from 0 to 0.6 SD. Hence, the deformable model was more accurate in predicting psoas lengths when subject-specific variations in femoral geometry were considered. Scaling the generic model to each subject along anatomical axes did not improve the accuracy of medial hamstrings or psoas lengths estimated with the model.

SUMMARY

Our analysis suggests that a deformable musculoskeletal model can provide reasonably accurate estimates of medial hamstrings and psoas lengths during crouch gait— *if* the model is appropriately deformed to represent the femoral anteversion angle of each subject. Whether such estimates can aid surgical decision-making for persons with cerebral palsy is the focus of ongoing work.

REFERENCES

Arnold (1999). Ph.D. Dissertation, BME Dept., Northwestern University

Delp et al. (1990). *IEEE Trans. Biomed. Eng.*, **37**, 757-767.

Delp et al. (1996). *J. Orthop. Res.*, **14**, 144-151.

Hoffinger et al. (1993). *J. Ped. Orthop.*, **13**, 722-726.

ACKNOWLEDGMENTS

Thanks to Pete Loan, Ken Smith, Deanna Asakawa, Silvia Salinas, and the staff of the Motion Analysis Center at the Children's Memorial Medical Center in Chicago. Supported by NIH R01 HD33929 and the United Cerebral Palsy Foundation.

Table 1. Errors† in Peak Medial Hamstrings Lengths

	Semimembranosus		*Semitendinosus*	
	Generic	**Scaled**	**Generic**	**Scaled**
Subject 1	−0.9	−1.0	−0.9	−1.0
Subject 2	−0.2	−1.0	+0.3	−0.6
Subject 3	+1.0	+1.2	+0.4	+0.6
Subject 4	+0.5	+0.7	+3.2	+3.3

Table 2. Errors† in Peak Psoas Lengths

	Generic	**Scaled**	**Deformed A**	**Deformed B**
Subject 1	−0.8	−0.7	+0.3	+0.3
Subject 2	+0.5	+0.6	0.0	0.0
Subject 3	−1.8	−1.8	−0.9	−0.3
Subject 4	−1.5	−1.8	−0.8	−0.6

† *error defined as the difference in peak muscle-tendon length during crouch gait calculated with the deformable and MRI-based models, expressed in standard deviations of the peak length during normal walking.*

+ *indicates length estimated with the deformable model is greater than length calculated with the MRI-based model.*

MECHANICAL ANISOTROPY OF ARTICULAR CARTILAGE IS ASSOCIATED WITH VARIATIONS IN MICROSTRUCTURES

John Z. Wu and Walter Herzog

Human Performance Lab., Faculty of Kinesiology
The University of Calgary, Calgary, Alberta, Canada
Email: wu@kin.ucalgary.ca

INTRODUCTION

Articular cartilage serves mainly as a load-bearing tissue in joints; thus, the structure of cartilage is "customarily designed" to carry high stresses. It is well accepted that the collagen fibers form a three-dimensional network that is adapted to the mechanical loading in the joint, while chondrocytes play an important role in cartilage adaptation and degeneration. The volumetric concentration of collagen fibers increases from the superficial (16-31%) to the deep zone (14-42%) (e.g., [3]). In normal cartilage, chondrocyte shapes and volumetric concentrations change across the thickness (e.g., [1]). Chondrocytes are flattened in the surface zone, spherical in the middle zone, and column-like in the deep zone. The average cell volumetric concentration increases from the deep zone to the surface zone by a factor of about three [6]. Because of the huge difference in material properties between matrix, cells and collagen fibers, the micro-structural variations influence the global material properties of the cartilage matrix. The purpose of the present study was to investigate theoretically the effects of variations in the collagen fiber-network and the shape and distribution of chondrocytes on the global material properties of articular cartilage.

METHODS

For convenience of numerical simulation, the heterogeneous, anisotropic cartilage was approximated as transversely isotropic in our model. Assuming axis 1 to be symmetric and plane 2-3 isotropic (Fig.1), a transversely isotropic relation using Hill's [2] notation is based on five material properties, *k, l, m, n, p*, which are related to the five conventional Young's moduli, E_{11}, E_{22}, Poisson's ratios, ν_{12}, ν_{23}, and shear modulus, μ_{12}.

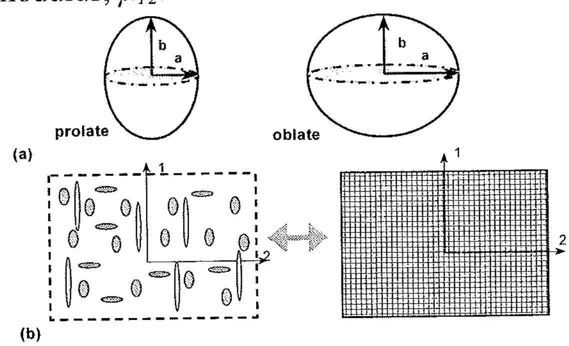

Figure 1: Cartilage modeled as a composite

We applied Qiu and Weng's [4] solution for n-phasic composite (Fig.1) (i.e., with one matrix and n-1 inclusions) to estimate the global effective material properties of the cartilage. Cartilage was represented by a four-phasic composite, comprised of one matrix, one cell inclusion, and two collagen fiber inclusions, i.e., vertical and horizontal fiber inclusions. The horizontal and vertical fiber inclusions were represented by changing the aspect ratio of the spheroidal inclusions to two extreme values, $\alpha(=b/a)=0$ and $\alpha\to\infty$, respectively. In the superficial layer, collagen fibers were assumed to be parallel to the contact surface, and the shape of the chondrocytes was assumed to change from flat to spherical. In the middle zone, 1/3 of the fibers were assumed vertical to the contact surface and 2/3 of the fibers were assumed parallel to the contact surface; the shape of the chondrocytes was assumed to vary around spherical. In the deep zone, collagen fibers were assumed to be vertical to the contact surface, and the shape of the chondrocytes was assumed to change from spherical to columnar. The effective elastic material properties in the superficial, middle, and deep layer of the articular cartilage were calculated.

RESULTS AND DISCUSSION

Our analysis suggests that the Young's modulus normal to the contact surface increases from the superficial to the deep zone by a factor of 10 to 60 (Figs. 2a and 2b). This prediction agrees well with experimental measurements [5] who reported that the compressive elastic modulus increases with depth in bovine articular cartilage, from 0.08 MPa at the surface layer to 2.10 MPa in the deep layer (i.e., by a factor of about 26).

According to our predictions, the tangential (in the direction parallel to the contact surface) Young's modulus for a typical articular cartilage increases from the deep to the surface zone by 50-100%.

Our simulation showed that the matrix is mechanically stable even when the volumetric concentration of chondrocytes reaches 20% in the surface zone; in the deep zone, the matrix becomes mechanically unstable when the volumetric concentration of chondrocytes is over 10%, i.e., Poisson's ratio becomes negative (results not shown). This result suggests that in order to maintain mechanical stability of the matrix, the volumetric concentration of chondrocytes should decrease from the surface to the deep zone, and should not exceed a certain limiting value. In general, we found that if cell shapes or cell volumetric fractions deviated too much from those observed experimentally, cartilage material properties exhibited unstable behaviour.

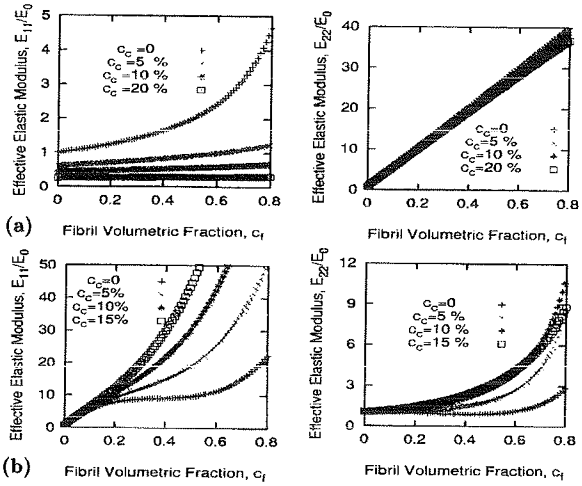

Figure 2: Predicted effective Young's modulus in the surface (α=0.1) **(a)** and deep zone (α=10) **(b)**. E_{11}, E_{22}, and E_0 are effective Young's moduli of cartilage in directions 1 and 2 and Young's modulus of the matrix, respectively.

SUMMARY

The results of this study suggest that the microstructure of collagen fibers and chondrocytes produces, at least to a certain extent, the variations in cartilage mechanical properties and the experimentally observed anisotropies. The results further suggest that collagen fiber orientation and volumetric fraction are intricately linked to chondrocyte shape and volumetric fraction to provide the tissue properties as observed in cartilage and to maintain the mechanical stability of the structure.

ACKNOWLEDGEMENTS

Alberta Heritage Foundation for Medical Research, the Medical Research Council of Canada, and the Arthritis Society of Canada

REFERENCES

[1] Guilak, F. et al. 1995. J. Orthop. Res., 13:410-421. **[2]** Hill, R. 1964. J. Mech. Phys. Solids, 12:199-212. **[3]** Langsjo, T. et al. 1999. J. Anat., 195:281-293. **[4]** Qiu, Y. and G. Weng .1990. Int. J. Eng. Sci., 28:1121-1137. **[5]** Schinagl, R. et al. 1997. J. Orthop. Res., 15: 499-506. **[6]** Wong et al. 1997. J. Orthop. Res., 15:189-198.

The Effect of Shoulder Translation and Forearm Pronation on Upper Extremity Loading During Side Air Bag Deployment

Stefan M. Duma, Brian M. Boggess, Edwin M. Sieveka, and Jeff R. Crandall
Automobile Safety Laboratory, University of Virginia, Charlottesville, Virginia
Email: duma@virginia.edu

INTRODUCTION

Although side air bags have been installed in only a limited number of vehicles to date, experimental studies with cadaveric subjects have elucidated the risk of upper extremity injury from side air bag deployment. Duma et al. (1998) found chondral and osteochondral fractures in the elbow joint in seven of the twelve upper extremities that had been loaded by a deploying side air bag. In similar tests by Jaffredo et al. (1998) and Kallieris et al. (1997), fractures of the trapezium and humerus were observed. In order to evaluate the injury potential of side air bags, automobile manufacturers utilize test dummies that currently do not include biofidelic shoulder and forearm kinematics. The purpose of this study was to investigate the effect of shoulder translation and forearm pronation on upper extremity loading during side air bag deployment.

METHODOLOGY

Simulations were conducted using the CVS/ATB multi-body modeling software. The air bag was represented as a multi-body system of ellipsoidal surfaces and validated against a production air bag system. Time-dependent functions were incorporated to control both the force of the simulated deployment of the bag from behind the seat, as well as the stiffness of each ellipsoid. Additional surfaces and ellipsoids were used to simulate the armrest and handgrip (Figure 1). All simulations were performed in a static test environment that was similar to the cadaveric experimental studies.

The occupant mass and geometric properties were based on a 5^{th} percentile female occupant in order to represent a higher risk segment of the adult population. The upper extremity was modeled using a total of 9 ellipsoids, including one each for the humerus and clavicle which allowed shoulder translation. To allow for pronation and supination of the forearm, the forearm was divided into two segments of equal length with longitudinal rotation the only degree of freedom allowed at the midpoint. To simulate the hand engaged in the handgrip, ellipsoids were added to model the wrist, fingers, and thumb. Joint segment dimensions, masses, moments of inertia, and moment versus angle joint properties were included in the model for the 5^{th} percentile female. While the loads and moments at each joint were recorded, the forearm axial force (FZ) was presented as the overall indicator of load severity.

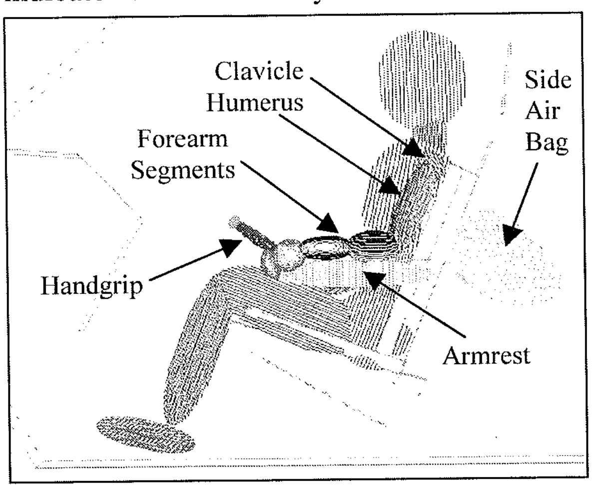

Figure 1: The side air bag, occupant, armrest, and handgrip as modeled in CVS/ATB simulation software.

RESULTS

Simulated air bag deployments were performed with the shoulder allowed to translate, labeled free clavicle, and with a rigid shoulder that was allowed only to rotate, labeled locked clavicle. The simulations revealed discrepancies in the forearm axial load (Figure 2). Although the inertial loads at the beginning of impact were the same, the momentum transfer was much greater in the free clavicle case. This discrepancy was due to a completely different interaction with the handgrip between the two cases. The shoulder translation allowed the forearm to translate further and interact more extensively with the handgrip compared to the locked clavicle case.

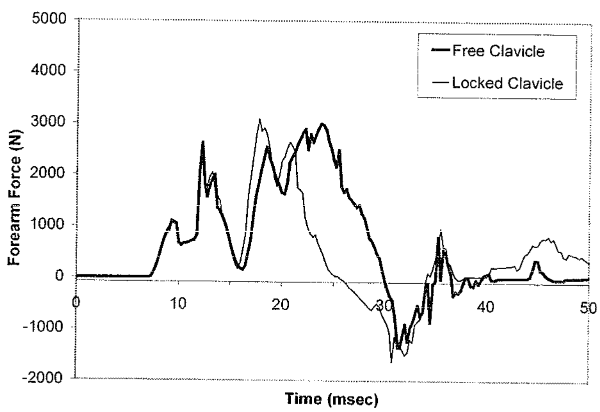

Figure 2: Forearm axial load (FZ) for a locked and free clavicle during side air bag loading with the forearm pronation permitted in both simulations.

Additional simulations were performed with forearm pronation allowed, labeled free forearm, and with forearm pronation prevented, labeled locked forearm. In contrast to the shoulder translation results, the inclusion of forearm pronation resulted in a lower peak force and momentum transfer compared to the locked forearm (Figure 3). Again, a different interaction pattern was observed with the door handgrip.

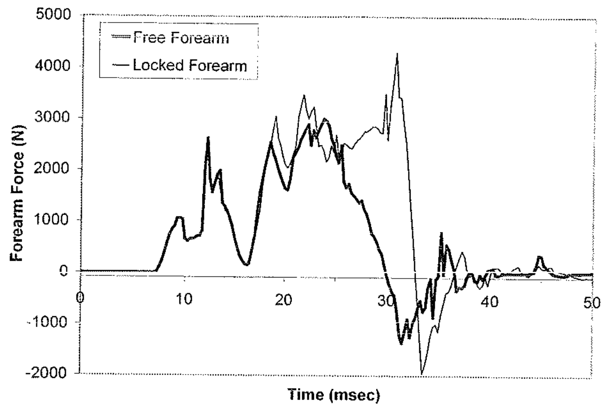

Figure 3: Forearm axial load (FZ) for a locked and free forearm during side air bag loading with the clavicle free in both simulations

DISCCUSION

The simulations suggest that preventing shoulder translation or forearm pronation will result in non-biofidelic interaction patterns. Given that there is no consistent interaction pattern between the simulations with the free and locked joints, it is impossible to develop a technique that could be used to scale the dummy response. It is suggested that in order to accurately predict the upper extremity loading, the shoulder translation and forearm pronation must be incorporated into the dummy design.

REFERENCES

Duma, S., Crandall, J., Hurwitz, S., Pilkey, W., (1998), Stapp International Car Crash Conference.

Jaffredo, A., Potier, P., Robin, S., Le Coz, J., Lassau, J., (1998) International Research Council on the Biomechanics of Impact.

Kallieris, D., Rizzetti, A., Mattern, R., Jost, S., Priemer, P., Unger, M., (1997) Stapp International Car Crash Conference.

FLOOR PLAN OF MEETING SPACE IN CHICAGO CIRCLE CENTER

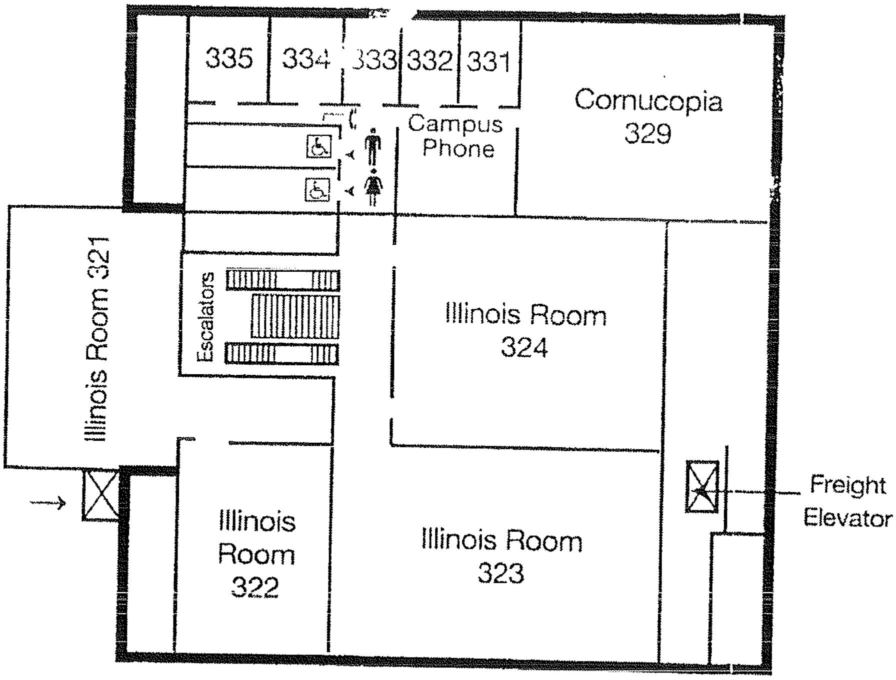

THIRD FLOOR (Meeting Rooms)

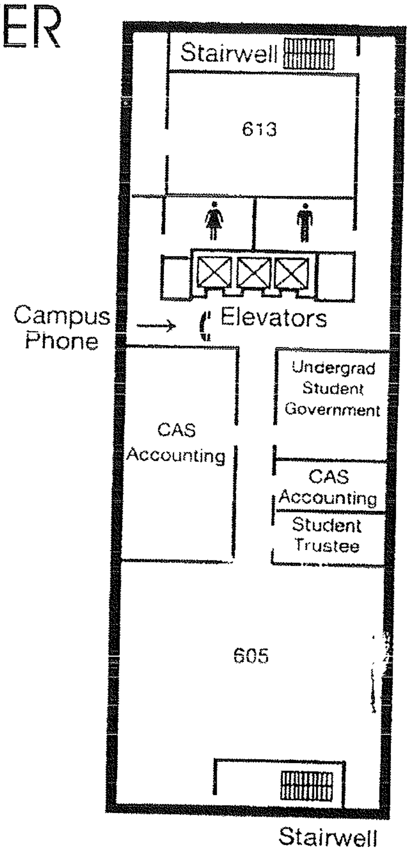

SIXTH FLOOR

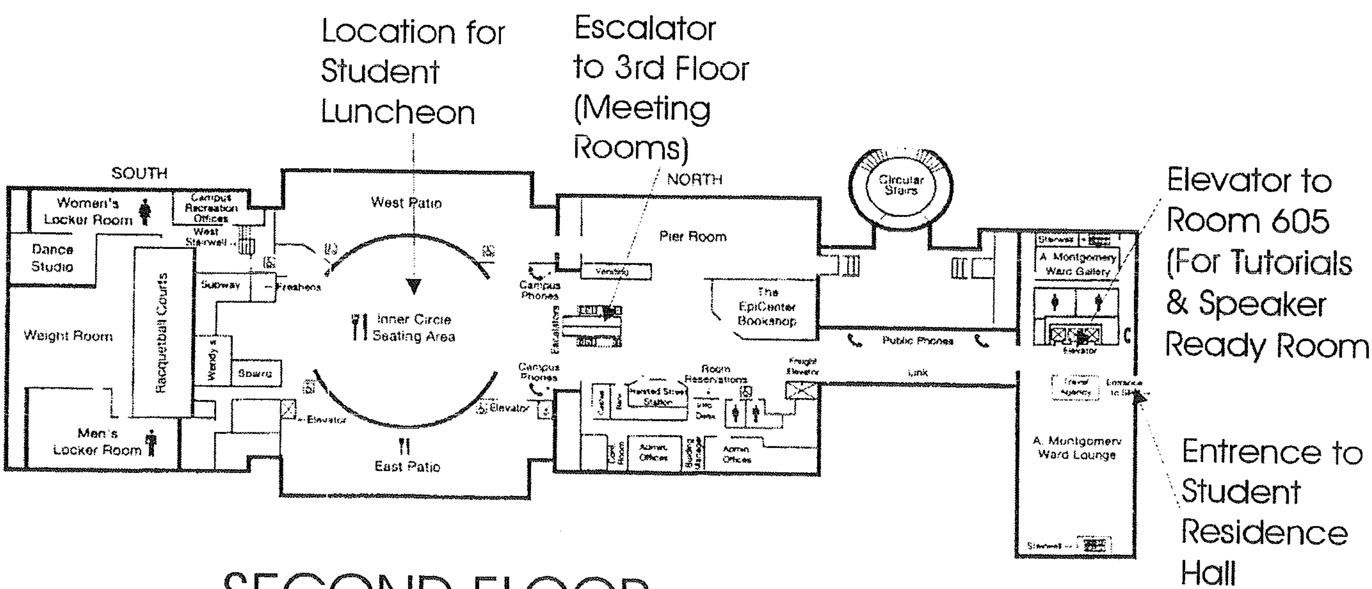

SECOND FLOOR

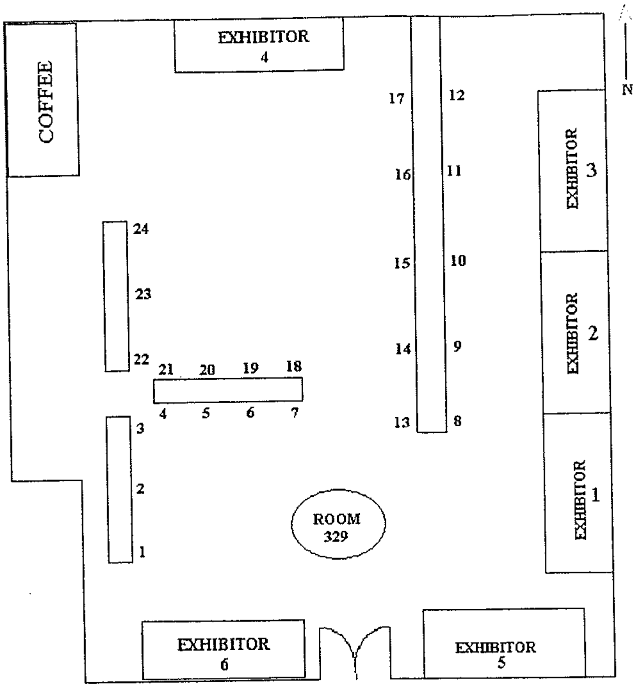

Poster and Exhibitor locations Room 329

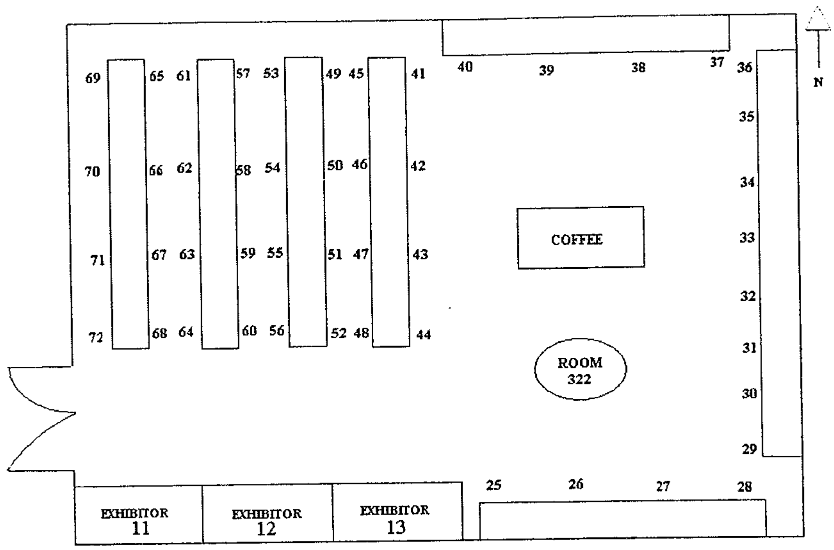

Poster and Exhibitor locations in Room 322

(1) Innovative Sports Training, Inc.
(4) Motion Analysis
(7) Novel Electronics
(10) HMA Technology Inc.
(13) Tekscan Inc.

(2) Bertec Corporation
(5) SIMI Reality Motion Systems
(8) Measurand Inc.
(11) Northern Digital Inc.

(3) Noraxon USA Inc.
(6) Peak Formance Tech. Inc
(9) Run Technologies
(12) Redlake Imaging Corporation

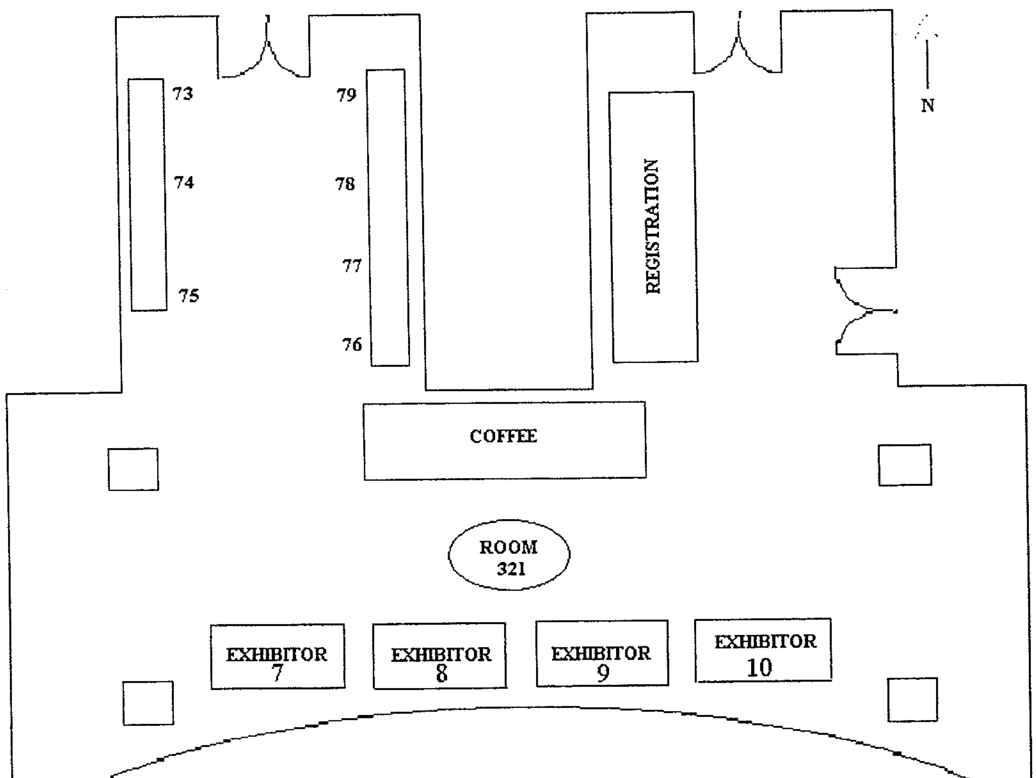

Poster and Exhibitor locations in Room 321

POSTER AND EXHIBITION LOCATIONS IN CHICAGO CIRCLE CENTER (UIC)

ASB Corporate Members

Aircast, Inc.

Depuy, Inc.

Orthofix

Tekscan, Inc.

MotionAnalysis

"True" 3D Real-Time for Sports, Animation, Ergonomics, Therapy and Biofeedback